Mario Lebrato

FROM ELEMENTAL PROCESS STUDIES TO ECOSYSTEM MODELS IN THE OCEAN BIOLOGICAL PUMP

GEOMAR
Helmholtz Centre for Ocean Research Kiel

From elemental process studies to ecosystem models in the ocean biological pump

Dissertation zur Erlangung des Doktorgrades der Mathematisch-Naturwissenschaftlichen Fakultät der Christian-Albrechts-Universität zu Kiel

vorgelegt von MARIO LEBRATO

Kiel 2012

Helmholtz Centre for Ocean Research Kiel

AVDENTES FORTVNA IVVAT

Vergil. Aen. 10, 284

Referent: ..... Prof. Dr. Andreas Oschlies

1. Koreferent: ..... Prof. Dr. Birgit Schneider
2. Koreferent: .....

Tag der mündlichen Prüfung: ...
Zum druck genehmigt: .....

Contents

List of figures 1
List of tables 8
Summary 13
Zusammenfassung 16

1. General introduction 19
1.1 Basic processes in the biological pump 19
1.2. Gaps in bentho-pelagic coupling 22
1.2.1. Organic carbon production and export 22
1.2.2. Inorganic carbon and elemental composition in the context of ocean acidification (OA) 25
1.3. Synopsis of the chapters 29

2. Jelly-falls historic and recent observations: a synthesis to drive future research directions 32

3. Jelly biomass sinking speed reveals a fast carbon export mechanism 53

4. Depth attenuation of organic matter export associated with jelly falls 72

5. Jelly biomass export follows regime shifts in a continental shelf 94

6. Proximate, elemental composition, and biometric relationships in gelatinous zooplankton 123

7. Removal of organic magnesium in coccolithophore carbonates 152

8. Coccolithophore carbonate ratios and elemental response to CO_2 and temperature 188

9. The future of marine calcification 240

10. Effect of nutrients availability on *Emiliania huxleyi* (NZEH) physiology in different CO_2 scenarios 253

11. The effect of artificial upwelling and in-situ ocean acidification on coccolithophore physiology 274

12. Susceptibility of echinoid larvae to artificially upwelled deep ocean waters 301

13. Ontogenesis Mg-calcite in echinoids reveals adaptation traits to climate change 316

14. Revisiting the modern echinoderms global carbonate budget 336

15. Seawater saturation state of Mg-calcite reveals imminent ocean acidification risks to marine ecosystems 396

16. European Project on Ocean Acidification: meta-analysis to guide future experiment and modeling 448

17. Conclusions and outlook 465

Authors contribution 467

Bibliography 473

Acknowledgements 523

Erklärung 524

List of figures

Fig. 1.1. Biological pump representation and processes studied 21
Fig. 1.2. Jelly-falls images 23
Fig. 1.3. Coccolithophore blooms 25
Fig. 1.4. Mg-calcite ecosystem images 27
Fig. 2.1. Conceptual model of a jelly-fall 36
Fig. 2.2. Global distribution of jelly-falls 47
Fig. 3.1. Empirically determined sinking speed of gelatinous biomass 61
Fig. 3.2. Sinking speed box plots of a wide range of marine particles 64
Fig. 3.3. Jelly-POM export ratio simulation using taxonomically separated sinking speeds at high, tropical, and temperate latitudes 65
Fig. 4.1. Parameterization of the jelly-POM decay rate and temperature 77
Fig. 4.2. Jelly-POM remineralization rate simulations in the Atlantic and Pacific Ocean 78
Fig. 4.3. Jelly-POM export ratio calculations as a function of latitude in the Atlantic and Pacific Ocean 82
Fig. 4.4. Jelly-POM export ratio calculations as a function of latitude varying the "death depth" and the sinking speed 83
Fig. 4.5. A comparison of the jelly-POM export ratio with the Martin Curve and a particle-based parameterization 84

Fig. 4.6. Photographic evidence of the decomposition, and disappearance of a *Pyrosoma atlanticum* carcass in the Madeira Abyssal Plain 88
Fig. 5.1. Map of the study region in the Mediterranean Sea 111
Fig. 5.2. Trends of *Pyrosoma atlanticum* biomass *vs.* trawl depth 113
Fig. 5.3. Satellite temperature and chlorophyll *a* mean monthly values from 1994 to 2005 115
Fig. 5.4. z-scores and moving variance of monthly temperature and chlorophyll *a* from 1994 to 2005 118
Fig. 5.5. Monthly hydroclimate first principal component (PC1) cumulative sum and quartile analysis of the z-scores of sea surface temperature (SST), chlorophyll *a*, and the normalized (per unit area) *Pyrosoma atlanticum* biomass from 1994 to 2005 121
Fig. 5.6. Monthly hydroclimate first principal Component (PC1) individual values extended from 1950 to 2011 126
Fig. 6.1. Gelatinous zooplankton and other marine organisms (for comparison) organic carbon, nitrogen, and C/N box plots 150
Fig. 6.2. Relationship of carbon and nitrogen in gelatinous zooplankton and other marine organisms (for comparison) 151
Fig. 7.1. Representation of two procedures used to harvest coccolithophore pellets to measure elemental composition 165
Fig. 7.2. Calcite elemental ratios (Mg/Ca, Sr/Ca, Fe/Ca, and P/Ca) measured in synthetic pellets cleaned with different protocols to remove organic-Mg 168
Fig. 7.3. Calcite Mg/Ca *vs.* contamination proxies (Fe/Ca an P/Ca) measured in synthetic pellets cleaned with different protocols to remove organic-Mg 169
Fig. 7.4. Cultured coccolithophore Mg/Ca and Sr/Ca and contamination proxies (Fe/Ca and P/Ca) 170
Fig. 7.5. Correlation of measured coccolithophores Mg/Ca with ambient seawater Mg/Ca 174

Fig. 7.6. Seawater Mg/Ca compilation in estuaries, shelves, and oceanic regions and also as a function of depth 180
Fig. 8.1. Summary of coccolithophore physiological parameters 224
Fig. 8.2. Summary of coccolithophore particulate matter elemental composition measured via ICP-AES 225
Fig. 8.3. Plots of organic and inorganic carbon measurements in various *Emiliania huxleyi* strains using the different analytical methods 226
Fig. 8.4. Relationship of coccolithophores Mg/Ca and Sr/Ca with seawater composition and also contamination proxies (P/Ca and Fe/Ca) 228
Fig. 8.5. Relationship of different parameters (growth rate, calcite Mg/Ca and Sr/Ca, D-Mg, D-Sr, and PIC production) with experimental temperature, salinity, and growth rate in coccolithophores 229
Fig. 8.6. Relationship of coccolithophore Mg/Ca ratios with organic-Mg contamination proxies (P/Ca and Fe/Ca) in coccolithophores 231
Fig. 8.7. Relationship of coccolithophore Mg/Ca with Chlorophyll *a* production and the PIC/POC 232
Fig. 8.8. Relationship of coccolithophore Sr/Ca and Mg/Ca ratios with temperature, pCO_2, and growth rate at present CO_2, and growth rate at increasing CO_2 234
Fig. 8.9. Relationship of *Gephyrocapsa oceanica* physiological parameters with incubation temperatures 236
Fig. 8.10. Relationship of *Gephyrocapsa oceanica* Mg/Ca with the contamination proxies for organic-Mg (P/Ca and Fe/Ca) 237
Fig. 8.11. Correlation of *Gephyrocapsa oceanica* Mg/Ca and Sr/Ca, contamination proxies (P/Ca and Fe/Ca), and diffraction coefficients (D-Mg and D-Sr) with incubation temperature 238
Fig. 8.12. Correlation of *Gephyrocapsa oceanica* Mg/Ca and Sr/Ca with the growth rate as a function of temperature 239

Fig. 9.1. Speciation of dissolved inorganic carbon in seawater as a function of increasing atmospheric pCO_2 243
Fig. 9.2. Models describing calcification mechanisms in organisms that calcify extracellularly (corals, foraminifera) and intracellularly (coccolithophores) 245
Fig. 9.3. Putative proton-pumping mechanism by which some marine calcifiers indirectly utilize HCO_3^- in the calcification process 247
Fig. 9.4. Coccolithophore calcification as a function of CO_3^{2-} and HCO_3^- concentrations 250
Fig. 10.1. The response of *Emiliania huxleyi* strain CAWPO6 (NZEH) to different nutrient levels under different CO_2 scenarios 264
Fig. 10.2. Enzymatic response of nitrate reductase (NRase) and alkaline phosphatase (APase) to different CO_2 and nutrient scenarios in *Emiliania huxleyi* strain CAWPO6 (NZEH) 266
Fig. 10.3. Correlation of POC with PON and NRase under nutrient replete conditions in *Emiliania huxleyi* strain CAWPO6 (NZEH) 267
Fig. 10.4. Correlation of APase with POC and PIC under phosphorus limited conditions 267
Fig. 11.1. Shipboard incubation system on the vessel deck 279
Fig. 11.2. The response of various *Emiliania huxleyi* strains to the seawater conditions from different depths from 30 to 5000 m, and thus a natural carbonate chemistry gradient 280
Fig. 12.1. The physiological response of echinoid larvae to the seawater conditions from different depths from 30 to 5000 m, and thus a natural carbonate chemistry gradient: fertilization success, larval morphology, particulate carbon [PIC (calcification) and POC (organic carbon)] 312
Fig. 12.2. PIC/POC values per echinoid larvae and variation in the medium carbonate/bicarbonate ratios 313

Fig. 12.3. Morphometrics and skeletal rods of *Psammechinus miliaris* larvae reared in seawater from different depths from 30 to 5000 m, and thus a natural carbonate chemistry gradient 314
Fig. 13.1. Elemental composition of the skeleton in 38 days *Psammechinus miliaris* larvae incubated at three temperatures and two CO_2 conditions 329
Fig. 13.2. changes in *Psammechinus miliaris* skeleton Mg-calcite [$CaCO_3$ %, $MgCO_3$ %, $SrCO_3$ %, total PIC dry weight % (dw), Mg/Ca (mol/mol), and Sr/Ca (mmol/mol)] cultured and collected at similar temperatures 330
Fig. 13.3. Saturation state with respect to the measured mol % $MgCO_3$ (ΩMg) in *Psammechinus miliaris* during ontogeny 331
Fig. 14.1. Global distribution of the samples used for carbonate analyses 342
Fig. 14.2. Correlation between $MgCO_3$ % and $SrCO_3$ % *vs.* $CaCO_3$ % and $SrCO_3$ *vs.* $MgCO_3$ for all samples 346
Fig. 14.3. Correlations between whole body $CaCO_3$, $MgCO_3$, $SrCO_3$ as well as Mg/Ca and Sr/Ca with dry weight (size estimation) 358
Fig. 14.4. Latitudinal patterns of echinoderms Mg-calcite composition 363
Fig. 14.5. Rare elements concentration in echinoderm whole body samples 390
Fig. 14.6. Rare elements concentration in echinoderms spines, plates, and calcareous ring samples 391
Fig. 14.7. Rare elements ratios normalized to Ca^{2+} in echinoderm whole body samples 392
Fig. 14.8. Rare elements ratios normalized to Ca^{2+} in echinoderm spines, plates, and calcareous ring samples 393
Fig. 14.9. Individual rare elemental ratios normalized to Ca^{2+} in echinoderm whole bodies *vs.* latitude 394
Fig. 14.10. Individual rare elemental ratios normalized to Ca^{2+} in echinoderm spines, plates, and calcareous ring *vs.* latitude 395
Fig. 15.1. Benthic samples global distribution and ambient seawater samples distribution (GLODAP) 417

Fig. 15.2. Box plots of skeletal mineralogy ($CaCO_3$ and $MgCO_3$ % dw and Mg/Ca) of all organisms used in this study 418
Fig. 15.3. Trends of organism mol % $MgCO_3$ and calculated saturation states (ΩCal., ΩArag., $\Omega Mg_{cleaned}$, and $\Omega Mg_{min.\ prep.}$) *vs.* latitude 419
Fig. 15.4. Trends of organism mol % $MgCO_3$ *vs.* calculated saturation states (ΩCal., ΩArag., $\Omega Mg_{cleaned}$, and $\Omega Mg_{min.\ prep.}$) at present CO_3^{2-} conditions 420
Fig. 15.5. Seasonal changes in the skeleton mol % $MgCO_3$ in the coralline algae *Corallina squamata* in the Dorset coast (Atlantic Ocean) 421
Fig. 15.6. Trends of "dissolution potential" (1 - ΩX) for calcite, aragonite, $Mg_{cleaned}$, and $Mg_{min.\ prep.}$ at present , and future conditions (reduction of CO_3^{2-} by 20 % and 50 %) *vs.* organism latitude 422
Fig. 15.7. Trends of "dissolution potential" (1 - ΩX) for calcite, aragonite, $Mg_{cleaned}$, and $Mg_{min.\ prep.}$ at present, and future conditions (reduction of CO_3^{2-} by 20 % and 50 %) *vs.* measured mol % $MgCO_3$ 423
Fig. 15.8. Trends of temperature, salinity, and CO_3^{2-} in present and future scenarios with latitude, and salinity *vs.* present CO_3^{2-} concentrations for each organism recovered from a NEAR 3D analysis 445
Fig. 15.9. Solubility curves of biogenic Mg-calcite *vs.* mol % $MgCO_3$ empirically obtained used in the calculation of the saturation states 446
Fig. 15.10. Corrections of the temperature and salinity effect on the Mg-calcite ion activity product (IAP) from the ΩCal.data 447
Fig. 16.1. The relationship between pCO_2, temperature, and salinity *vs.* time in mesocosms, the field, and laboratory experimental studies (including indoor mesocosms) 454
Fig. 16.2. The relationship between the PIC/POC ratio of coccolithophores and ΩCal. in laboratory experiments and mesocosms 458
Fig. 16.3. A selection of global model outputs and the way they selected the input data to work out $CaCO_3$ export 459

Fig. 16.4. Biogeographical distribution of the EPOCA meta-data from experimental and mesocosm work available in 2009 462

List of tables

Table 2.1. A compilation of naturally occurring jelly-falls 40
Table 2.2. Sampling techniques and initiatives that may be available to monitor jelly-falls 42
Table 2.3. Occurrences of jelly-falls and the associated megafaunal taxa feeding on them 44
Table 3.1. Organisms field meta-data and organic matter biochemistry 57
Table 3.2. Organisms sinking rate experiment summary 58
Table 3.3. Summary of field conditions used to work out the jelly-POM export ratio in the Atlantic Ocean 59
Table 3.4. A selection of sinking rates from published abiogenic an biogenic marine particles 68
Table 4.1. Jelly-POM decay rate data *vs.* experimental temperature 77
Table 4.2. Summary of field conditions used to work out the jelly-POM export ratio in the Atlantic and Pacific Ocean 80
Table 4.3. Difference in the export ratio between a particle-based and the jelly-POM model 86
Table 5.1. Summary of MEDITS-ES trawling catches of *Pyrosoma atlanticum* in the Mediterranean Sea from 1994 to 2005 100
Table 5.2. Complete MEDITS-ES trawling catches of *Pyrosoma atlanticum* in the Mediterranean Sea from 1994 to 2005 and associated calculations 101

Table 6.1. Summary of the proximate body composition of Thaliacea, Ctenophora and Cnidaria: DW %WW and AFDW %DW 133
Table 6.2. Summary of the proximate body composition of Thaliacea, Ctenophora and Cnidaria: C %DW, N %DW, P %DW, and C/N 134
Table 7.1. Culture conditions, medium chemistry and sample parameters of coccolithophores in experimental cultures 159
Table 7.2. Summary of protocols tested, elemental ratios, and cleaning efficiencies on *Chlorella autotrophica* and calcite pellets 161
Table 7.3. Comparison of the target elemental ratios measured in non-treated samples and samples cleaned with the final optimized cleaning protocol 166
Table 7.4. Properties of the synthetic pellets of the non-calcifying alga *Chlorella autotrophica* and the treatments used 176
Table 7.5. Carbonate P/Ca and Fe/Ca (contamination proxies), Mg/Ca and Sr/Ca from the *Chlorella autotrophica* + $CaCO_3$ pellets and the reference $CaCO_3$ material used 177
Table 7.6. Database to organize project coordination 185
Table 8.1. Coccolithophore species and strains details along with environmental parameters 194
Table 8.2. Coccolithophore species and strains medium carbonate chemistry and seawater elemental composition 196
Table 8.3. Coccolithophore species and strains physiological and biochemical measurements 198
Table 8.4. Coccolithophore species and strains elemental composition and data used from the literature 200
Table 8.5. Coccolithophore species and strains elemental composition and partitioning coefficients for carbonate Mg/Ca and Sr/Ca (also included contamination proxies P/Ca and Fe/Ca 202
Table 8.6. All phytoplankton species and strains elemental composition and partitioning coefficients for carbonate 205

Table 8.7. Summary of inorganic (PIC) and organic carbon (POC) estimations using inductive coupled plasma atomic emission spectroscopy (ICP-AES) and elemental analyzer (EA) 208
Table 8.8. Coccolithophores experimental conditions and medium carbonate system chemistry parameters from the batch and chemostat experiments 209
Table 8.9. Coccolithophores physiological and biochemical parameters 213
Table 8.10. Coccolithophores geochemistry 216
Table 8.11. Medium carbonate chemistry at the end of the experiment at the different temperatures 219
Table 8.12. Coccolithophores physiological and biochemical parameters at harvesting time at the different temperatures 220
Table 8.13. Coccolithophores geochemistry and medium elemental composition at the different temperatures 222
Table 10.1. Medium carbonate chemistry parameters at the beginning and end of the experiment 259
Table 10.2. Experimental sample properties of *Emiliania huxleyi* strain CAWPO6 (NZEH) at high CO_2 in combination with nutrient availability 263
Table 11.1. Strain details and experimental conditions in all incubations 281
Table 11.2. Oceanographic and experimental data from the shipboard incubation 1 with *Emiliania huxleyi* 282
Table 11.3. Oceanographic and experimental data from the shipboard incubation 2 with *Emiliania huxleyi* 285
Table 11.4. Experimental data at harvesting time from incubations with 5 *Emiliania huxleyi* strains with water from 38 m 288
Table 12.1. Carbonate chemistry, oceanographic experimental conditions and seawater elemental composition at the PAP site 306
Table 13.1. Medium chemistry used in incubations of *Psammechinus miliaris* larvae at three temperatures and two CO_2 conditions 322

Table 13.2. Dry (dw) and wet weight (wt) and the dw/wt percentage conversion ratio from the pellets of *Psammechinus miliaris* larvae in the temperature and CO_2 experiment and the juveniles/adults collected in the field 323
Table 13.3. Raw seawater chemistry used to calculate ΩCal. and ΩMg for the different input conditions in the experiment and field conditions 328
Table 13.4. Complete dataset of the elemental composition of *Psammechinus miliaris* larvae (pellets) in the temperature and CO_2 experiment and the juveniles/adults from the field 333
Table 14.1. Echinoderm samples used for carbonate analyses 349
Table 14.2. Echinoderm samples carbonate percentages and elemental ratios 352
Table 14.3. Echinoderm budget re-assessment data 356
Table 14.4. Echinoderm global carbonate production 357
Table 14.5. Raw data from all echinoderm species used in this study 375
Table 14.6. List of elements measured in echinoderms, atomic weights, units (of concentration and ratios), and ICP detection limits for each element 380
Table 14.7. Echinoderm whole body Mg-calcite trace and rare elemental geochemistry results classified using latitude and class 382
Table 14.8. Echinoderm spines Mg-calcite trace and rare elemental geochemistry results classified using latitude and class 385
Table 14.9. Echinoderm plates and calcareous ring Mg-calcite trace and rare elemental geochemistry results classified using latitude and class 387
Table 15.1. Details of taxa used, skeleton mineralogy, and biogeography 401
Table 15.2. Details of the ion activity products (IAPs) corrected for in situ salinity, temperature and pressure and the correspondent activity coefficients [$\gamma_T(i)$] 408
Table 15.3. Details of sample collection and material used 435
Table 15.4. Summary of skeleton mineralogy 442
Table 16.1. A selection of pelagic and benthic mesocosm studies testing the effects of pCO_2 on organisms in the EPOCA database 452

Table 16.2. A selection of meta-data used in parameterizations of the export ratio (PIC/POC) in biogeochemical models assimilating experimental, mesocosm, and field data 453
Table 16.3. Further considerations of the models and outputs selected 460

Summary

The biological pump controls the transport of particles from the ocean surface to the deep sea. Vertical fluxes govern chemical gradients, playing a fundamental role in the carbon dioxide (CO_2) ocean-atmosphere feedback, driving physicochemical properties of seawater, and providing resources for benthic ecosystems. Particles vary in size and composition, originating in every trophic level as detritus, fecal material, biogenic carbonates or the organisms biomass. A recent concern is that the concomitant increase in anthropogenic CO_2 and temperature, may alter carbon fluxes and atmospheric feedbacks, as well as ecosystem shifts driven by organisms' physiological and biogeochemical responses. This dissertation focused on poorly characterised biological pump compartments and processes that are central to assess potential implications of future climate scenarios. Essentially, this thesis tackles the export of gelatinous zooplankton biomass, the role of inorganic elements (Mg^{2+} and Sr^{2+}) on biogenic carbonate at high CO_2 and temperature, the combined effect of CO_2 and nutrient availability on calcifying phytoplankton, and the role of Mg-calcite benthic ecosystems on the global carbonate cycle. The first part of the thesis focuses on the organic carbon pump, describing historical gelatinous zooplankton biomass depositions at the seabed to assess particulate matter (jelly-POM) export and seasonality. A new parameterization (export ratio) of the depth attenuation of jelly-POM based on temperature and decay rate (k) is developed, for use in global models. We assessed remineralization differences between gelatinous taxa, namely jellyfish and pelagic tunicates, based on life-history and sinking speed. The later was empirically determined to provide taxonomic data on jelly carbon sequestration efficiencies. A biochemical analysis of published results was also conducted, providing the scientific community with a baseline information database. Eventually, a new gelatinous POM export event by pelagic tunicates was described from a shelf environment in the

Mediterranean Sea, and then correlated to environmental and atmospheric variables using time-series and principal component analysis.

The second part focuses on calcification processes in coccolithophores. Mg/Ca and Sr/Ca ratios were studied by developing a new organic-Mg cleaning protocol and using organic-Mg contamination proxies. We designed this protocol to further study coccolithophores as a paleoceanography tool but also to understand elemental composition response in the context of ocean acidification (OA). The protocol was tested on *Emiliania huxleyi* (13 strains), *Gephyrocapsa oceanica* (1 strain), and *Calcidiscus leptoporus* (1 strain). From here, we conducted experiments to assess inter species and strain variability, and then responses to high CO_2 and temperature. In brief: 1) We studied *Emiliania huxleyi* strain-specific elemental composition using 13 strains under identical environmental conditions. 2) We assessed the elemental response (calcite Mg/Ca and Sr/Ca) of *G. oceanica* to a gradient of 12 CO_2 levels and 3 temperatures (*E. huxleyi* and *C. leptoporus* were also used in combination with previous experiments). 3) We assessed the elemental response (calcite Mg/Ca and Sr/Ca) of *G. oceanica* to a temperature gradient using artificial seawater to calibrate a palaeoproxy.

The third part consists in collaborative experiments and field work to assess the physiological and biogeochemical response of *E. huxleyi* to CO_2 and nutrient co-limitation. *E. huxleyi* was exposed to 3 CO_2 levels and 3 nutrient conditions under nitrate and phosphate limitation to study physiology and nutrient use (by analyzing enzyme activities). A new method to study ocean acidification and artificial upwelling in the field was developed following a previous experiment (*see* also below). Using the increasing CO_2 gradient in the water column, seawater was retrieved with a CTD rosette from 30 to 5000 m, and then 3 *E. huxleyi* strains were incubated at 4 CO_2 concentrations resulting from the equilibration with surface temperature conditions.

The last part concentrates on a carbonate producing benthic phylum, the Echinodermata. We assess the effects of OA during echinoids ontogenesis on key physiological and geochemical parameters by conducting both laboratory and field incubations (using the CO_2 gradient in the water column). We also study ontogenetic changes at present CO_2 in echinoid skeleton Mg-calcite geochemistry from larvae to adults. Eventually, we provide a geochemical re-analysis of adult echinoderms from all latitudes to assess the global contribution to the marine carbon cycle diving the different carbonates ($CaCO_3$, $MgCO_3$, and $SrCO_3$). The latitudinal patterns help to understand carbonate export based elements and possible susceptibilities to OA. Using this dataset and a literature compilation, we provide a new set of calculations of the saturation state of Mg-calcite mineral phases (ΩMg) in benthic organisms using field data. We use a

geostatistical tool (NEAR 3D) analysis to retrieve field temperature, salinity, and CO_3^{2-} data near to our samples, and calculate the modern ocean species-specific ΩMg corrected for temperature, salinity, and pressure. We also do calculations for future ocean scenarios, decreasing CO_3^{2-} by 20 and 50 %. The limited information on several biological pump processes, especially those related to gelatinous biomass export and biogenic carbonates elemental composition impair an accurate assessment at present and in a high CO_2 world. Some of these caveats are addressed here, providing fundamental information to gain understanding on critical processes in biogeochemical cycles.

Zusammenfassung

Die biologische Pumpe steuert den Teilchentransport von der Meeresoberfläche bis in die Tiefsee. Dabei regulieren vertikale Flüsse den chemischen Gradienten und spielen eine wesentliche Rolle beim Kohlenstoffdioxid (CO_2) Ozean-Atmosphäre-Feedbackmechanismus. Sie beeinflussen die physikalisch-chemischen Eigenschaften des Meerwassers und stellen Ressourcen für benthische Ökosysteme bereit. Die Partikel, die in jeder trophischen Ebene als Detritus, biogene Karbonate oder neue Biomasse entstehen, unterscheiden sich in ihrer Größe und Zusammensetzung. Ein aktuelles Problem ist die gleichzeitige Zunahme des anthropogenen CO_2 sowie der Temperaturanstieg, welche im Verdacht stehen, die Kohlenstoffflüsse, sowie durch physiologische und biologische Reaktionen bestehende Ökosysteme zu verändern. Die vorliegende Dissertation konzentriert sich auf den bisher wenig beschriebene Aspekte der biologischen Pumpe sowie auf die Prozesse, die für die Einschätzung zentraler Veränderungen unter zukünftigen Klimaszenarien relevant sind. Im Wesentlichen befasst sich diese Arbeit mit dem Export von gelatinöser Zooplanktonbiomasse und der Rolle der anorganischen Elemente Mg^{2+} und Sr^{2+} auf Bildung und Löslichkeit biogener Karbonate bei hoher CO_2-Konzentration und Temperatur. Weitere Schwerpunkte liegen auf der kombinierten Wirkung von CO_2 und der Verfügbarkeit von Nährstoffen auf die Kalzifizierung von Phytoplankton sowie auf der Rolle der Mg-Calcit Anteile benthischer Ökosysteme im globalen Kohlenstoffkreislauf. Der erste Teil der Arbeit konzentriert sich auf die organische Kohlenstoff-Pumpe, wobei der Export und die Saisonalität historischer Ablagerungen gelatinöser Zooplanktonbiomasse am Meeresboden (jelly-POM) beurteilt werden. Eine neue Parametrierung des Remineralisierungsprofils von jelly-POM, der auf Temperatur und Zerfallsrate (k) basiert, wurde für den allgemeinen Einsatz in globalen Modellen entwickelt. Unterschiede in der Remineralisierung zwischen den gallertartigen Taxa Quallen und pelagischen Manteltieren, werden dabei aufgrund von Lebenszyklus und Sinkgeschwindigkeit beurteilt. Außerdem wurde der Kohlenstoffanteil aus

taxonomischen Daten empirisch ermittelt. Eine biochemische Analyse der veröffentlichten Ergebnisse wurde ebenfalls durchgeführt, die wissenschaftliche Gemeinsamkeiten mit einer Basis-Informations-Datenbank darstellt. Schließlich wurde der jelly-POM Export durch pelagische Manteltiere im Mittelmeer beschrieben und mit Hilfe von Zeitreihen- und Hauptkomponentenanalyse mit Umweltbedingungen und atmosphärischen Variablen korreliert.

Der zweite Teil der Arbeit konzentriert sich auf Verkalkungsprozesse in Coccolithophoriden. Mg/Ca- und Sr/Ca- Verhältnisse wurden durch die Entwicklung eines neuen Bio-Mg-Reinigungs-Protokolls und unter Verwendung von Proxies der organischen Mg-Verunreinigung untersucht. Das Protokoll wurde für weitere Studien an Coccolithophoriden als Paleoozeanographie-Tool zur Analyse von Veränderungen im Zusammenhang mit der Ozeanversauerung angewandt. Das Protokoll wurde an *Emiliania huxleyi* (13 Stämme), *Gephyrocapsa oceanica* (1 Stamm) und *Calcidiscus leptoporus* (1 Stamm) getestet. In weiteren Experimenten wurden die Variabilität innerhalb der einzelnen Arten und Stämme sowie die Reaktion auf hohe CO_2-Konzenrationen und Temperaturen bewertet. In Kürze: 1) Die Stamm-spezifische elementare Zusammensetzung von *Emiliania huxleyi* wurde unter identischen Umweltbedingungen in 13 Stämmen untersucht. 2) Die Elementverhältnisse (Calcit Mg/Ca und Sr/Ca) von *G. oceanica* wurden für 12 CO_2-Gehalte und 2 Temperaturen systematisch untersucht (*E. huxleyi* und *C. leptoporus* wurden auch in Kombination mit früheren Experimenten verwendet). 3) Die Elementverhältnisse (Calcit Mg/Ca und Sr/Ca) von *G. oceanica* wurden an einen Temperaturgradient wurde mit künstlichem Meerwasser analysiert, um ein Palaeoproxy zu kalibrieren.

Der dritte Teil der Arbeit besteht aus Ergebnissen gemeinschaftlicher Labor- und Feldexperimente. Er dient der Beurteilung der physiologischen und biochemischen Reaktion von *E. huxleyi* auf CO_2- und Nährstoff-Kolimitierung. Die Physiologie und Nährstoffnutzung von *E. huxleyi* wurde unter 3 verschiedenen CO_2- bzw. Nährstoffbedingungen, darunter Nitrat- und Phosphatlimitierung, untersucht (durch die Analyse von Enzymaktivitäten). Eine neue Methode zur Erforschung der Ozeanversauerung und des künstlichen Auftriebs im Feld wurde nach einem vorherigen Experiment (siehe unten) entwickelt. Dabei wurden 3 *E. huxleyi* Stämme unter 4 verschiedenen CO_2-Konzentrationen entsprechend Wasserproben von 30 bis 5000 m Tiefe inkubiert.

Der letzte Teil der Arbeit befasst sich mit dem kalkbildenden benthischen Stamm Echinodermata. Sowohl unter Labor- als auch Feldbedingungen (unter Verwendung des CO_2-Gradienten in der Wassersäule) wurden die Auswirkungen des OA während der Seeigel-

Ontogenese auf zentrale physiologische und geochemische Parameter beurteilt. Auch ontogenetische Veränderungen Mg-Calcit Geochemie im Skelett von Seeigel-Larven zu ausgewachsenen Tieren wurden unter diesen CO_2-Bedingungen untersucht. Schließlich wurde eine geochemische Re-Analyse von erwachsenen Stachelhäutern aus allen Breitengraden zur Beurteilung des globalen Beitrags zum marinen Kohlenstoffkreislauf verschiedener Kohlenstoffe ($CaCO_3$, $MgCO_3$, und $SrCO_3$) entwickelt. Die Breitenmuster helfen, den Karbonat-Export sowie die mögliche Anfälligkeit gegenüber Ozeanversauerung zu verstehen. Unter Nutzung dieses Datensatzes und der Literaturzusammenstellung wird eine neue Reihe von Berechnungen des Sättigungszustands von Mg-Calcit Mineralphasen (ΩMg) in benthischen Organismen mit Felddaten vorgestellt. Temperatur, Salzgehalt und CO_3^{2}-Daten in der Nähe der Proben wurden mit dem geostatistischen Analysentool (NEAR 3D) erfasst. Der um Temperatur, Salzgehalt und Druck korrigierte artspezifische ΩMg wurde für den heutigen Ozean berechnet. Außerdem wurden zukünftige Ozeanszenarien unter 20 bis 50 % verringerter CO_3^{2-} Konzentration kalkuliert. Die begrenzte Informationen über verschiedene biologische Pumpprozesse, insbesondere jene aus dem Export gallertartiger Biomasse und biogenen Karbonaten unterschiedlicher elementarer Zusammensetzung, erschwert eine realistische Einschätzung ihrer Bedeutung in der Gegenwart und unter höheren CO_2-Konzentrationen. Dieser Einschränkungen werden hier diskutiert, um ein grundlegendes Verständnis wesentlicher Prozesse biogeochemischer Kreisläufe der Ozeane herzustellen.

1.

General introduction

1.1. Basic processes in the biological pump

The oceans cover the majority of the Earth's surface (~ 70 %), playing a preponderant role in regulating climate patterns, temperature, and atmospheric gases. They harbour a large portion of the world's biodiversity. The average depth is roughly 4 kilometres; however, the majority of the biological and chemical processes that we study take place in the first kilometre. The deep ocean remains largely unexplored, and challenges, as the last frontier, the scientific community. Over the last 40 years we have studied in detail the biogeochemical processes occurring in these first 1000 m, and especially in the so-called euphotic zone (~ 200 m), where the waters are exposed to sunlight that can support photosynthesis. This photochemical process mediates primary production by forming organic material using dissolved carbon dioxide (CO_2) as a substrate (Fig. 1.1). The majority of life in the oceans directly or indirectly depends on primary production, which forms the base of trophic webs.

The biological pump addresses biogeochemical processes that transfer and transform these materials created by primary production at the sea surface to the ocean's interior (Fig. 1.1). The material exported is known as particulate matter, and can be of organic or inorganic origin depending on the ecosystem compartment. It includes the continuous downward flux of autochthonous particles, pulses of organic-rich material derived from phytodetritus blooms (Beaulieu 2002; Smith et al. 2008), carbonate sinking following pelagic calcification (Schiebel

2002; Stoll et al. 2007), zooplankton faecal material (Turner 2002), gelatinous biomass (Billett et al. 2006), and large food falls in fish and whale carcasses (Smith et al. 1989; Smith and Baco 2003). Carbonate production also takes place in benthic ecosystems (Smith 1972), mainly as Mg-calcite (Chave 1954) that can be incorporated into the biochemical cycling in sediments (Fig. 1.1).

Primary producers use dissolved inorganic carbon (DIC) during photosynthesis, thus they provide the main feedback to atmospheric carbon dioxide (CO_2), consuming it and building up organic carbon and then removing it out from the euphotic zone (Buesseler and Boyd 2009). All sinking particulate organic material (POM) removes net CO_2 from the upper ocean, but it releases it back to water column or the seabed during remineralization. This rises the dissolved inorganic carbon (DIC) to total alkalinity (TA) ratios (DIC/TA) as the water masses age, leaving a respiration signal that can be tracked along the conveyor belt from the North Atlantic to Pacific Ocean (Feely et al. 2004). The contrary occurs with sinking pelagic carbonates, which dissolution below the lysocline increases TA, decreasing DIC, counteracting the CO_2 increase. Seemingly, Mg-calcites play an important role in all benthic ecosystems, since their susceptibility to dissolution above a certain mol % $MgCO_3$ is higher than pelagic calcite or aragonite alone (Morse et al. 2006). Therefore, the balance between organic and inorganic matter production, export, and dissolution governs the net CO_2 balance from the atmosphere to the ocean´s interior and its feedbacks (Gehlen et al. 2007). The significance and magnitude of the biological pump is primarily assessed using a variety of indirect techniques (Buesseler et al. 1992). They include satellite-based algorythms (Behrenfeld and Falkowski 1997), surface-tethered and neutrally-buoyant sediment traps (Honjo et al. 2008) and acoustic backscatter profiling sensors (ABS and ADCP) to study particles and biomass in the water column (Jiang et al. 2007). Sediment traps are by far the most used device, however, they can underestimate the contribution of large particles and detritus (Rowe and Staresinic 1979), particulate matter sources such as gelatinous zooplankton carcasses forming jelly-falls (Billett et al. 2006; Lebrato and Jones 2009) as well as mucous sheets (Robison et al. 2005) and large faecal pellets (Fortier et al. 1994; Gonzalez et al. 2000). The same occurs for benthic production and large particles, which can only be sampled in situ using visual or trawling techniques.

In the biological pump compartments scientific study, many elemental processes are used across disciplines to understand organism-level roles in ecosystems, responses to ambient variables to understand the past (geological record and paleo proxies) and the future (climate change, ocean acidification), or simply to constraint fluxes in marine cycles. Yet, there are still numerous caveats that have either been poorly addressed and explored at a fundamental level, or that have been so far overlooked. This prevents an complete scientific understanding to use this information to advance the specific research field.

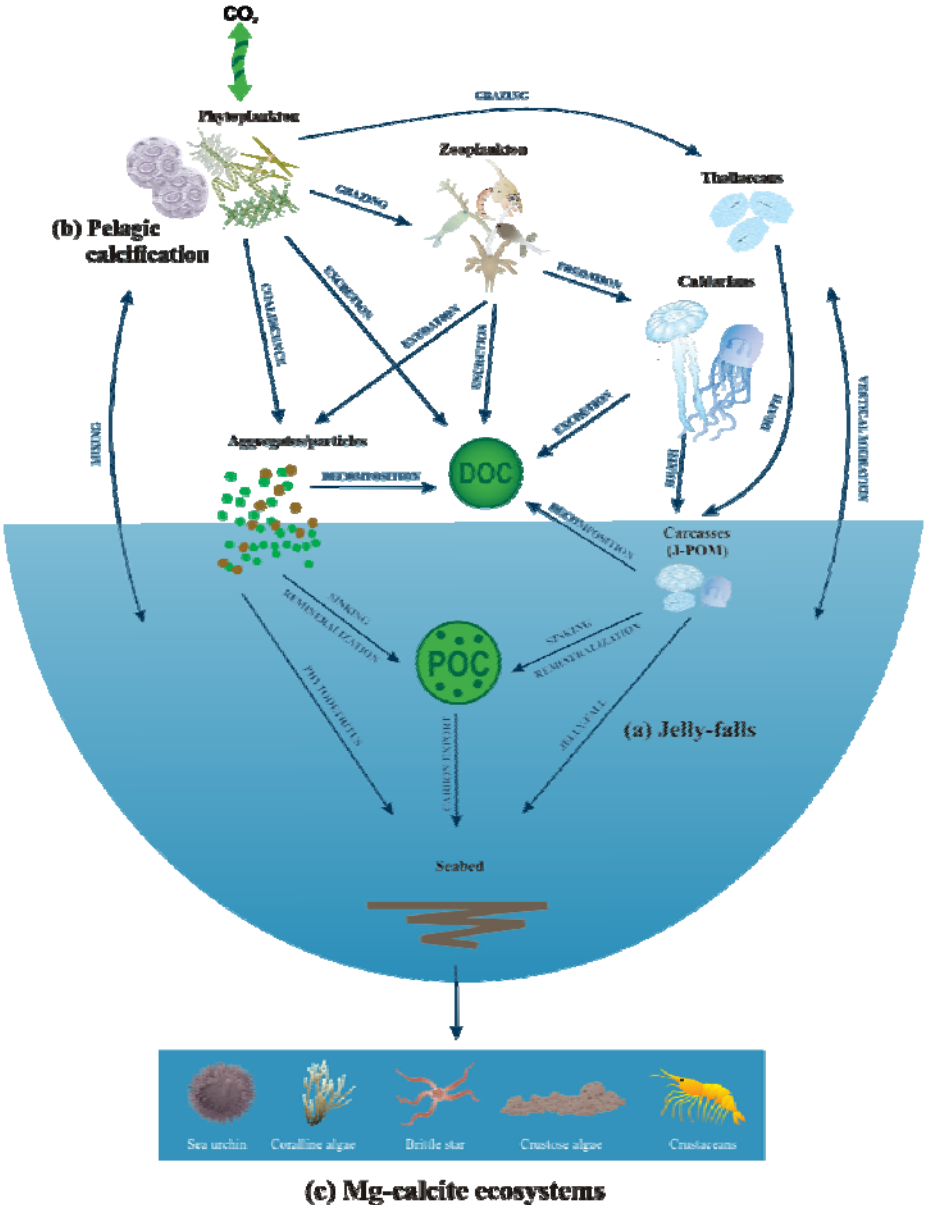

Fig. 1.1. A representation of the biological pump and the biogeochemical processes that remove elements from the surface ocean by sinking biogenic particles. The diagram is adapted from a JGOFS US cartoon to accommodate the main topics described in this thesis: jelly-falls, Mg-calcite benthic systems and pelagic calcification. Symbols are courtesy of the Integration and Application Network (http://ian.umces.edu/symbols/). (a), (b), and (c) are exemplified in the next figures with images.

1.2. Gaps in bentho-pelagic coupling

1.2.1. Organic carbon production and export

Marine gelatinous organisms with a pelagic life style are often termed "gelatinous zooplankton", highlighting convergent evolution traits such as planktonic life history, a transparent structure, and a fragile body mainly composed of water (Haddock 2004). The term "gelata" describes other planktonic gelatinous organisms beyond jellyfish (Cnidaria) and pelagic tunicates (Thaliacea), such as siphonophores, ctenophores, pelagic worms and molluscs. For the purpose of this thesis we refer to "gelatinous biomass" (J-POM and jelly-falls; Fig. 1.1, 1.2) as dead and sinking biomass (as carcasses/bodies) originating in Cnidaria, Thaliacea, and Ctenophora. Blooms of these organisms occur periodically in the oceans, and can extend for thousands of square kilometers (Madin et al. 2006). The complex spatiotemporal distribution of the biomass, and the existence of large deep-sea gelatinous populations (beyond 1000 m), makes it difficult to understand the fate of the gelatinous biomass after blooms crash and die. The biomass cannot just vanish, and the most reasonable assumption is that it sinks, while remineralizing, and in some cases sedimenting out at the seabed (Billett et al. 2006; Lebrato and Jones 2009; Fig. 1.2). Jelly-falls are not only a feature of the present ocean, but they left behind evidence in rocks and sediments as fossil depositions (see Young and Hagadorn 2010 for a review). Jelly-falls were first described in the Cambrian (~ 500 ma) as circular impressions (Cnidaria-like) found in sedimentary layers and specimens accumulated in sedimentary horizons (Gaillard et al. 2006).

In the modern ocean, since the late 1950's there are several field reports of jelly-falls occurring at the seabed (see Chapter 2). Jelly-falls of thaliaceans (pyrosomids and salps) have been described in New England (US), New Zealand, Tasman Sea, Australia, Madeira, Mediterranean Sea, and Gulf of Guinea. Other jelly-falls associated with scyphozoans (Cnidaria) have also been observed in the Japan Sea, Red Sea, Pakistan Margin, Chesapeake Bay (US), and the Arabian Sea. The jelly-fall in the Gulf of Guinea (Ivory Coast) was studied in detail (Lebrato and Jones 2009) (Fig. 1.2). Decomposing *Pyrosoma atlanticum* carcasses were observed from the continental shelf (< 200 m) to the deep slope (> 1000 m) using ROV surveys in collaboration with the oil industry (SERPENT project, http://www.serpentproject.com/). Carcasses were observed in large patches at the seabed, accumulating in channels and also being transported by the bottom current. Organic carbon contribution was estimated to be one order of magnitude

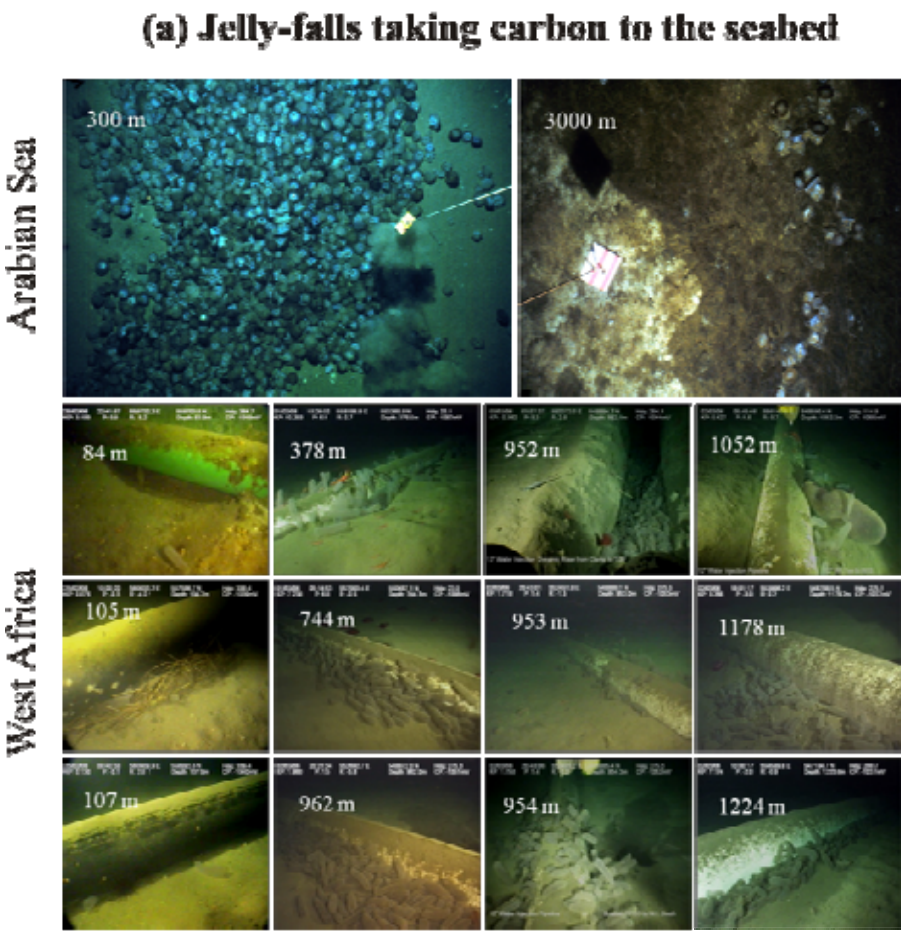

Fig. 1.2. Jelly-falls in the Arabian Sea and west Africa (Billett et al. 2006; Lebrato and Jones 2009).

above sediment trap data in the area. Benthic animals were observed periodically feeding on the decaying material, thus indicating that jelly-falls have an active role in benthic food webs. This means that apart from bacterial decay (Titelman et al. 2006; Frost et al. 2012), large organisms (mega- and macro-fauna) play an important role in consuming jelly biomass. Another large jelly-fall was also studied in the Arabian Sea (Billett et al. 2006) (Fig. 1.2). Thousands of *Crambionella orsini* carcasses were surveyed with a towed camera and found to form large patches at the seabed on the continental shelf (~ 300 m), canyons, and the continental rise (~ 3000 m). Organic carbon was estimated to be several orders of magnitude above sediment trap data. In many cases, the patches were so densely packed that they completely carpeted the seabed with a "fluffy" material. Yet, no major study on the processes behind these observations or the actual remineralization dynamics were conducted to date (*see* Chapter 3, 4, and 5).

The baseline information obtained from jelly-falls observations is a sudden, large pulse of organic carbon (J-POM) reaching the seabed. Yet, the origin in time and space is unclear (*see* Chapter 5). Current oceanographic techniques (sediment traps, remote sensing, acoustic backscatter) do not accurately assess the flux of J-POM. A jelly-fall can start at any point in the water column from the euphotic zone (0-200 m) to near the seabed (> 1000 m) depending on the

life history and the vertical migration patterns of the organisms involved. This starting point is called the "death depth" or an exiting depth (E*z*) (*see* Chapter 4), similar to other pelagic particles (small size) exiting the euphotic zone (Buesseler and Boyd 2009). The actual exiting depth of particles governs the strenght of the biological pump and the carbon sequestration dynamics. Gelatinous biomass sinks by density changes and as it sinks it starts decomposing (also being consumed by planktonic scavengers). Dissolved carbon components (DOC) leach and contribute to the total carbon pool (the so-called jelly-pump, Condon and Steinberg 2008), thus fuelling the pelagic microbial loop (Fig. 1.1). The combination of material lability (the ease of assimilation e.g. stoichiometric ratios), sinking rate (*see* Chapter 4), E*z*, and remineralization rates determinate the extent of recycling in the water column *vs.* at the seabed (Lebrato et al. 2011; *see* Chapter 3 and 5). At the seafloor, J-POM is a source of labile food for benthic communities (as with phytodetritus) (Sweetman et al. 2011) thus it is a further factor promoting organisms patchiness. J-POM is widely known to be an important component in the diet of scavengers (Fanelli et al. 2011), and at certain times of the year when gelatinous biomass is available it could be the dominant resource (Duggins 1981).

Jelly-falls as a post-bloom process have been poorly explored in oceanography. We do not even have good understanding of what triggers death or how this relates to the environment and climate variables (*see* Chapter 5). Much research has focused on life cycles and the biology surrounding the start of blooms with a growing interest to manage populations from a socioeconomic perspective (Purcell 2011), but now is time to move on to assess processes at the end of the bloom and explore the fate of the biomass. Quantification of the regional and global gelatinous biomass [e.g. Jellyfish Database Initiative, JEDI (http://www.jellywatch.org/blooms)] (Condon et al. 2012) is a key step towards integrating these elemental fluxes into models and thus broadening the understanding of the biological pump. Jelly-falls exemplify a fundamental vector of rapid carbon transport to the deep waters that has been overlooked in field studies and in models (*see* Chapter 3). This is particularly important because the role gelatinous zooplankton plays in bottom-up and top-down processes, as well as in ecological stoichiometry in pelagic food webs.

1.2.2. Inorganic carbon and elemental composition in the context of ocean acidification (OA)

Calcification is a pivotal process in the Earth's carbon cycle (Ridgwell 2005), being central to biomineralization of skeletons made of metastable carbonate: low-Mg calcite (< 4% $MgCO_3$), high-Mg calcite (> 4% $MgCO_3$), and aragonite (Morse et al. 2006). Numerous marine organisms produce calcite on its different mineralogies in pelagic and benthic ecosystems. A recent concern following anthropogenic emissions of greenhouse gases is that the oceans will become enriched in CO_2, while carbonate ions (CO_3^{2-}) and thus the calcite saturation state (Ω) will decrease, termed ocean acidification (OA) (Caldeira and Wickett 2003).

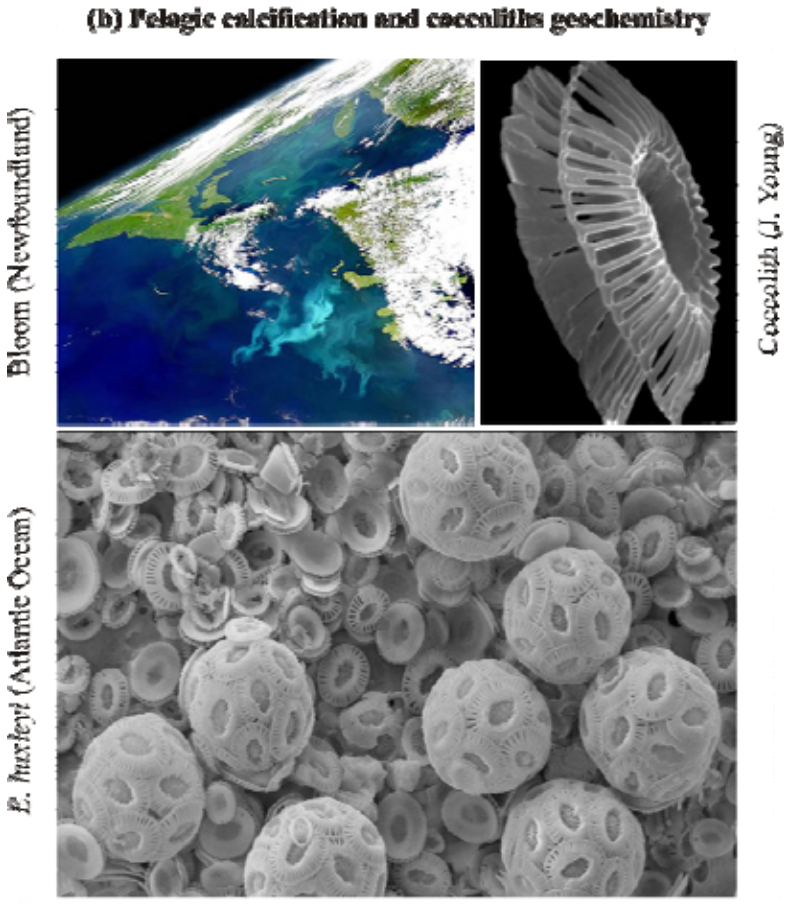

Fig. 1.3. *Emiliania huxleyi* bloom, and details of coccoliths and liths. Images: SeaWiFS, J. Young, and S. Blanco-Ameijeiras.

Pelagic organisms tend to secrete low Mg-calcite (except some foraminifera, Vinogradov 1953), especially coccolithophores (Fig. 1.3). Coccolithophores are ubiquitous in the modern ocean (Beaufort et al. 2011) and through their production of calcite, create around half of the carbonate that is ultimately buried in sediments (Schiebel 2002). The calcite secreted by coccolithophores (and foraminifera) plays a wide variety of roles in modulating atmospheric pCO_2 (Ridgwell et al. 2007) and setting the efficiency of the biological pump (Armstrong et al. 2002). Various calcified species and strains are distributed in the ocean according to carbonate chemistry, but calcification responses of natural assemblages as a whole to OA and warming are currently far from clear (Langer et al. 2009b; Ridgwell et al. 2009; *see* Chapter 8, 9, 10, and 11). In particular, the effect of rising CO_2 on

coccolithophores has been on the spotlight because while most studies indicate a negative effect on calcification, there is still substantial species and strains variability (Riebesell et al. 2000; Langer et al. 2006; Iglesias-Rodriguez et al. 2008a; Langer et al. 2009b; Shi et al. 2009; Bach et al. 2011; Fiorini et al. 2011; Krug et al. 2011; *see* Chapter 8, 9, 10, and 11). A study by Beaufort et al. (2011) exemplified the complexity of coccolithophore responses to CO_2 levels in the field. Highly calcified cells of the coccolithophore *E. huxleyi* were observed in CO_2-rich waters. Seeminlgy three recent studies combining CO_2 and nutrient limitation (Borchard et al. 2011; Langer et al. 2012; Müller et al. 2012) found again contrasting physiological and morphometric responses (*see* also Chapter 10). This new evidence indicates that predicting individual organism responses in the context of OA is unlikely to be as simple as previously though.

Beyond $CaCO_3$ production, coccolithophores incorporate other elements in the carbonate, mainly Mg^{2+} and Sr^{2+}, that have not been assessed in the context of OA and that also have applications in paleoceanography. The calcite Mg/Ca in coccolithophores has so far limited use since major issues in removing organic-Mg phases avoid a widespread characterization (Stoll et al. 2001; *see* Chapter 7). Organic-Mg is present in all biomolecules and a robust protocol has not been developed yet to routinely apply it in experimental and field work (*see* Chapter 7). So far, two experiments have correlated Mg/Ca with temperature (using < 3 data points) with limited success (Stoll et al. 2001; Ra et al. 2010; *see* Chapter 8). Conversely, the calcite Sr/Ca is widely used to assess paleo productivity regimes (Stoll et al. 2007) since this ratio correlates well with the phytoplankton growth rate (*see* Chapter 8).

In benthic ecosystems, many organisms such as echinoderms, coralline algae, or bryozoans secrete calcite with high Mg-calcite between 4 and 30 mol % $MgCO_3$ (Vinogradov 1953; Chave 1954; Weber 1973). They have colonized the deep-sea, the shelf intertidal/subtidal, and the high latitudes, where carbonate chemistry conditions are naturally more corrosive to carbonates than at low latitudes or the open ocean (Feely et al. 2004; Orr et al. 2005; Borges et al. 2006). For organisms bearing high Mg-calcite, rising CO_2 levels might come at a cost of increasing skeleton dissolution, driven by the increasing solubility of Mg-calcite with a certain mol % $MgCO_3$ (Morse et al. 2006) (*see* Chapter 8, 13, 14, and 15). Despite the threat of OA to Mg-calcites, there is still a poor understanding of basic controls on Mg^{2+} skeletal content both in benthic and pelagic organisms. Detailed knowledge is essential to assess if benthic organisms

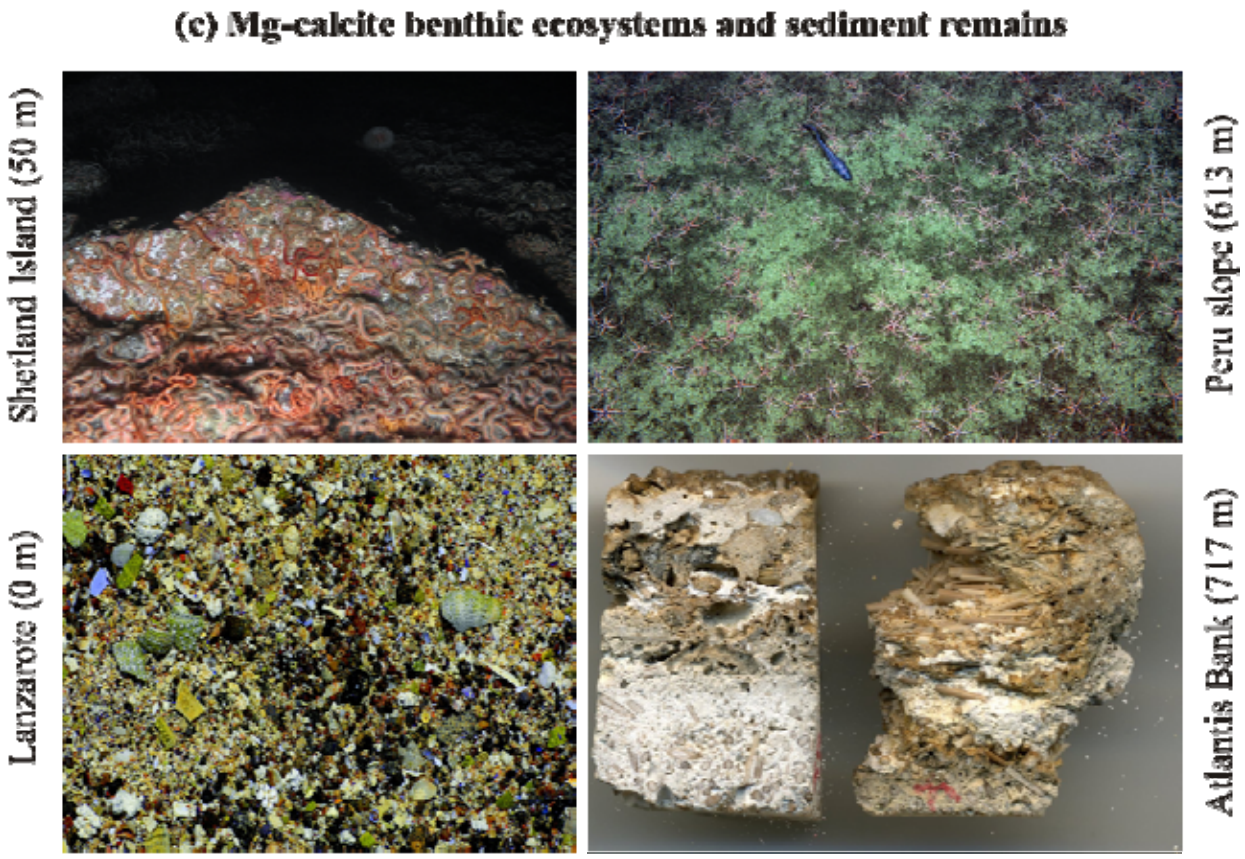

Fig. 1.4. High Mg-calcite benthic ecosystems dominated by echinoderms. Images taken Lebrato et al. (2010).

will be the first responders to OA, to which extent dissolution of metastable Mg-calcite might affecttheir life cycles, and which life stages are most sensitive to OA in terms of skeletal mineralogy.

In this thesis, I present two fundamental views of how major calcite ion contents (Ca^{2+}, Mg^{2+}, and Sr^{2+}) are regulated by pelagic and benthic organisms, which then are assessed in the context of OA:

(1) "**Proximate control factors (PCF)**": An abiotic/biotic effect on elemental composition in short time-scales, from weeks to months, such as changes in Mg/Ca and Sr/Ca ratios, and $MgCO_3$ and $SrCO_3$ content in newly accreted skeleton material owing to seasonal temperature, salinity, and carbonate chemistry cycles. This involves phenotypical plasticity controlled within a range. The main PCF driving biogenic Mg^{2+} in the long-term is seawater composition, namely the [Ca^{2+}], [Mg^{2+}] and the $Mg/Ca_{seawater}$ ratio (reviewed by Ries 2010). The $Mg/Ca_{seawater}$ has oscillated over geological times, from ~ 1-2 around the Cretaceous to ~ 5.10 in the modern ocean (Hardie 1996; Demicco et al. 2005). At present, it is accepted that the $Mg/Ca_{seawater}$

exhibits a conservative behavior, Marcet's principle *sensu* Culkin and Cox (1966). However, there is evidence of variability from ~ 4.50 mol/mol in estuaries (Zang et al. 2003), to ~ 5.20 in the open ocean (Fabricand et al. 1967), to 5.40-5.90 mol/mol in shelves (Blanco-Ameijeiras et al. in press; *see* Chapter 7), and enclosed seas. This suggests that pelagic and benthic organisms calcify in slightly different seawater conditions owing to biogeography and spatial separation in the water column. In benthic and pelagic organisms, the $Mg/Ca_{calcite}$ increases linearly with increasing $Mg/Ca_{seawater}$, including modern ocean waters in the ~ 4 to 6 mol/mol range (Ries 2010). Other PCFs include temperature and growth rate (μ). In adult echinoderms, $MgCO_3$ content is driven by temperature (reviewed by Kroh and Nebelsick 2010) and salinity (Borremans et al. 2009), while in molluscs, seasonal variability induces shell $MgCO_3$ changes, with no correlation to seawater temperature or salinity, but to μ (via food supply) (Lorrain et al. 2005). A higher μ may decrease the ability to discriminate against Mg^{2+} ions, owing to a deregulation across the Ca^{2+} channels. Ambient carbonate chemistry (namely CO_2) drives $MgCO_3$ variability in benthic organisms following a physiological species-specific fingerprint and environmental control (Mackenzie et al. 1983). The CO_2 effect on coccolithophore Mg/Ca and Sr/Ca ratios has not been assessed so far (*see* Chapter 8). The $MgCO_3$ content of coralline algae correlates negatively to increasing CO_2 (Ries 2011), while opposite trends occur in echinoid larvae (*see* Chapter 13).

(2) "**Ultimate control factors (UCF)**": A biological trait controlling elemental composition driven by life-history, which should bear a genetic component that evolved from PCFs over time. The evidence appears at the onset of skeleton deposition in calcifying eukaryotes. The $MgCO_3$ (and possibly $SrCO_3$) content is likely a phenotypically plastic trait (Ries 2011), established during early life stages. During ontogenesis, some benthic organisms produce amorphous calcium carbonate (ACC) as a precursor (Echinoids - Politi et al. 2004; Molluscs - Weiner et al. 2003). It is unclear if the ultimate crystalline form and the $MgCO_3$ are defined at the ACC stage, if different PFCs can modulate the end-mineral product, or if there is a synergistic effect. Larvae and juveniles from benthic organisms grow much faster than adults, and thus Mg^{2+} incorporation increases with μ (Lorens 1981). However, there are no data on how mineralogy evolves during ontogeny, and how CO_2 changes could affect this process (*see* Chapter 13).

1.3. Synopsis of the chapters

This PhD thesis aims at describing numerous processes covering a wide range of disciplines that belong fundamentally to poorly addressed compartments in the carbon cycle. The results will be therefore for interest to experimentalists, modellers and paleoceanographers. Each chapter address a specific topic, and constitute therefore to some extent an independent piece of work, although they are divided in four major parts.

The first part of the thesis focuses on a newly described aspect of the organic carbon pump: inputs of gelatinous zooplankton biomass to the seabed known as "jelly-falls" that can sequester large amounts of carbon. We describe historical gelatinous zooplankton biomass depositions at the seabed to assess particulate matter export and seasonality. A new parameterization (export ratio) of the depth attenuation of gelatinous biomass based on temperature and decay rate (k) is developed, for use in global models. We conclude that the export ratio below 500 m is 20-45 % larger in subpolar and temperate areas than in the tropics, therefore high latitudes are an important corridor for jelly carbon sequestration. Vertical migration leads to a variable biological "death depth" in various water layers, governing the start of remineralization, and ultimately the biomass fate. This formulation questions the use of other model particle-based formulations that do not have a temperature component in the remineralization process. The gelatinous biomass sinking rate was estimated in the laboratory and in the field by mimicking field density measurements with sinking rates between 400 and 1800 m day^{-1} depending on taxa. The high sinking speed provides robust evidence of the high carbon sequestration capabilities of gelatinous biomass. We also studied a new jelly carbon export deposition event from 1994 to 2005 in the Mediterranean Sea at shelf and slopes depths using catches from benthic trawls. The biomass seasonality was linked to hydroclimate and ocean colour data (temperature and chlorophyll) using principal component analysis. We found a robust pelagic-benthic coupling after a major climate regime shift as well as seawater properties partly driving the biomass export to the seabed. This is the first evidence of jelly carbon export occurring across an entire shelf area, which corresponds with modifications of Mediterranean Sea hydroclimate parameters.

The second part focus on inorganic carbon (calcite) processes in coccolithophores. Namely, we decided to study Mg incorporation owing to its diverse applications and a basic lack of

understanding of the processes controlling it in coccolithophores. Mg/Ca and Sr/Ca ratios, and coccoliths elemental composition were measured by developing a new organic-Mg cleaning protocol using reductive and oxidative steps. Organic contamination proxies were also used to assess cleaning level (P/Ca and Fe/Ca ratios). The protocol was first optimized in non-calcifying algae mixed with reagent grade calcite, and then it was tested on *Emiliania huxleyi* (13 strains), *Gephyrocapsa oceanica* (1 strain), and *Calcidiscus leptoporus* (1 strain). Using this protocol, we conducted several experiments to assess inter species and strain Mg/Ca and Sr/Ca variability, and responses to ocean acidification and temperature. The response to high CO_2 (increase in calcite Mg/Ca and Sr/Ca) can be interpreted as a physiological deregulation of the calcifying mechanism, avoiding a tight control of the element incorporation through Ca^{2+} channels. The pelagic calcite Mg/Ca increase also suggests a higher $MgCO_3$ % in skeletons and thus a possible shallowing of the remineralization horizon in the future ocean through preferential dissolution of calcite with a higher Mg content. We also found a decrease of the Mg/Ca with temperature but an increase of Sr/Ca, both highly correlated to growth rate, which could be used as a temperature proxy. Lastly, we describe how different water sources from coastal to the offshore had slightly different elemental composition (mainly seawater Mg/Ca) deviating from the Marcett constant proportions principle. We speculate that this may influence coccoliths calcite ratios in the modern ocean and thus carbonate export and paleoceanography applications. This finding needs to be expanded to pelagic and benthic ecosystems to truly understand modern ocean controls on calcite mineralogy and elemental composition.

The third part consists in a series of collaborative laboratory and field studies to understand the physiological and biogeochemical response of *E. huxleyi* to CO_2 and nutrient co-limitation. In the laboratory, contrasting responses were found in physiological parameters (μ, PIC/POC, calcification) depending on the CO_2 and nutrient condition, which suggests an alteration on the phytoplankton competitive ability for nutrient uptake in a high CO_2 ocean. A new method to study ocean acidification and artificial upwelling was developed in the field using the increasing CO_2 gradient in the water column. Seawater was retrieved with a CTD rosette from 30 to 5000 m, and then 3 *E. huxleyi* strains were incubated at 4 CO_2 concentrations resulting from the natural equilibration with surface temperature conditions. The method worked well and it may be an additional tool to study ocean acidification (OA) in the field beyond natural CO_2 volcanic vents. It can also be used with the correct set-up to study artificial upwelling (geo-engineering) from different depth levels.

The last parts concentrate on a carbonate producing benthic taxa, the Echinodermata. Specifically, we assessed the effect of ocean acidification during echinoid ontogenesis on physiological and skeleton geochemical parameters, by conducting laboratory and field incubations (using the water column CO_2 gradient method). Fertilization success and calcification decrease at high CO_2, with no effect on organic matter build-up and skeleton carbonate ($MgCO_3$, $SrCO_3$, Mg/Ca, and Sr/Ca). When growing larvae at present CO_2 conditions during ontogeny, we observe that juvenile and adult's $MgCO_3$ and $SrCO_3$ levels are established much earlier than $CaCO_3$. This provides a biological advantage to stabilize the calcite and reduce dissolution potential and it may also relate to the swimming abilities. Adults have a higher skeleton mol % $MgCO_3$ than larvae, which means that from the mineralogy point of view they are more susceptible to OA. This implicates that larvae are more tolerant to dissolution by maintaining a lower Mg-calcite until they metamorphosize at the seabed. A global geochemical re-analysis of juvenile and adult echinoderms from all latitudes revealed that calcite export remained between 0.113 and 0.853 Pg C yr^{-1}, depending on the calculation method, which is near to pelagic-based estimations. The $MgCO_3$ contribution alone was > 12 % of the total. The latitudinal patterns help to understand carbonate export production based on specific elements and possible susceptibilities to OA based on skeleton mineralogy. Using the measured mol % $MgCO_3$ data and literature values for other taxa (pelagic and benthic), we calculate saturation states for the Mg-calcite (ΩMg) both in modern ocean conditions and decreasing CO_3^{2-} by 20 and 50 %. We find that numerous benthic ecosystems are already close to seawater undersaturation (ΩMg = 1), and that the generalized use of ΩCal. and ΩArag. in experiment and modeling work may become irrelevant when considering the species-specific ΩMg. This is particularly true when using outcomes that intend to assess the future of marine ecosystems in the context of OA.

In brief, the multi-processes approach used in this PhD thesis, going from the atomic and elemental level to the large scale dimension can help to reduce uncertainties in the study of the biological pump organic and inorganic processes. It also paves the way to understand elemental processes that may become relevant in the context of global change and OA. However, as noted in many chapters, these datasets should just be the start of further investigations, so topics that today are poorly addressed, can be well described in the near future. This PhD thesis eventually provides the baseline data for this to be a reality.

2.

Jelly-falls historic and recent observations: a synthesis to drive future research directions

Abstract

The biological pump describes the transport of particulate matter from the sea surface to the ocean's interior including the seabed. This downward flux affects the distribution of chemical properties in the water column and it also governs the resources available for benthic ecosystems. The contribution by gelatinous zooplankton bodies as Particulate Organic Matter (POM) vectors ("jelly-falls") has been neglected owing to technical and spatiotemporal sampling limitations. In this paper, we compile and assess the existing evidence on jelly-falls from early ocean observations to present times. The seasonality of jelly-falls indicates that they mostly occur after periods of strong upwelling and/or spring blooms in temperate/subpolar zones (thus at high chlorophyll/suspended organic matter levels) and during late spring/early summer. Our conceptual model helps to define a jelly-fall based on empirical and field observations of the biogeochemical and ecological processes encountered during sedimentation. We then compile and discuss existing strategic and observational oceanographic techniques and others that could be implemented to further jelly-falls research. Seabed video- and photography-based studies deliver the best results at a local scale, but the correct use of fishing techniques, such as trawling, could provide comprehensive regional datasets in the future. We conclude by considering the possibility of increased gelatinous biomasses in the future ocean induced by upper ocean processes favouring their populations, thus increasing the jelly-POM downward

transport. We suggest that this could provide a "natural compensation" for predicted losses in pelagic POM with respect to fuelling benthic ecosystems.

This chapter is based on:

Lebrato, M., Pitt, K. A., Sweetman, A. K., Jones, D. O. B., Cartes, J. E. ,Oschlies, A., Condon, R. H., Molinero, J. C., Adler, L., Gaillard, C., Lloris, D. and Billett, D. S. M. 2012. Jelly-falls historic and recent observations: a synthesis to drive future research directions. In: *Hydrobiologia* DOI: 10.1007/s10750-012-1046-8.

Acknowledgements: Thanks to the SERPENT project for enabling access to benthic data. We also thank the following contributions: L. Gil de Sola and C. Garcia from the E.G.O (Fuengirola Oceanographic Center, Spain) for providing MEDITS-ES data, Brian J. Bett and Richard S. Lampitt from the National Oceanograhy Center Southampton, UK provided data of *Crambionella orsini* from Billett et al. (2006) and from Roe et al. (1990). This work was also supported by the "European Project on Ocean Acidification" (EPOCA), which is funded from the European Community's Seventh Framework Programme (FP7/2007-2013) under grant agreement n° 211384. This work was also funded by the Kiel Cluster of Excellence "The Future Ocean" (D1067/87).

2.1. Introduction: particulate organic matter (POM) and jelly-falls

The input of particulate organic material (POM) drives secondary production and most benthic ecosystem processes in the deep sea (Ruhl et al. 2008; Smith et al. 2008). POM inputs mainly include autochthonous particles from the euphotic zone, ranging in increasing size from phytodetritus (organic-rich material derived from phytoplankton blooms) (Beaulieu 2002; Smith et al. 2008), marine snow (Caron et al. 1986; Alldredge and Silver 1988), mucilaginous aggregates (Cartes et al. 2007; Martin and Miquel 2010), mucous sheets from zooplankton (Robison et al. 2005; Lombard et al. 2010), faecal pellets (reviewed by Turner 2002), wood particles (Turner 1973), and macrophyte detritus (Vetter and Dayton 1998, 1999; Cartes et al. 2010) to fish and whale carcasses (Soltwedel et al. 2003; Smith and Baco 2003; Gooday et al. 2010). Jelly-falls can be defined as point source organic matter inputs (as corpses/carcasses) that sink through the water column (remineralizing as dissolved organic/inorganic components), eventually causing an accumulation of jelly-POM (J-POM) at the seabed (Fig. 2.1). Numerous gelatinous zooplankton groups have been shown to accumulate at the ocean floor including the Cnidaria (Scyphozoa), and Thaliacea (Pyrosomida, Doliolida, and Salpida) (Table 2.1). The significance and magnitude of sinking material in the biological pump is primarily assessed by a variety of indirect techniques (Buesseler et al. 1992; Jahnke 1996; Marchant et al. 1999) that cannot target the J-POM associated with jelly-falls. They include remote sensing algorithms (Behrenfeld and Falkowski 1997; Balch et al. 2007), surface-tethered and neutrally-buoyant sediment traps (Lampitt et al. 2001; Buesseler et al. 2007), and acoustic backscatter profiling sensors (ABS and ADCP) to study particles and biomass in the water column (Merckelbach and Ridderinkhof 2005; Jiang et al. 2007). Sediment traps are the most used device, but they often underestimate the contribution of large particles and detritus (e.g. Rowe and Staresinic 1979; but *see* Conte et al. 2003; Buesseler et al. 2007). Jelly-falls can only be sampled directly using techniques such as video (Wiebe et al. 1979; Lebrato and Jones 2009), towed/still photography (Roe et al. 1990; Billett et al. 2006; Sweetman and Chapman 2011), or benthic trawling (Sartor et al. 2003) (*see* Table 2.1 for other techniques/strategies). Therefore, although many sources of organic material have been widely studied and POM/DOM remineralization dynamics considered in biogeochemical models as a result (e.g. Burd et al. 2010), jelly-falls are relatively unexplored sources of POM, despite a significant fraction of the pelagic biomass being sequestered in the bodies of gelatinous zooplankton.

The study of jelly-falls represents a major challenge in the understanding of the biological pump mainly due to technical/sampling hurdles, and although there is no consensus that the oceans will turn into a "jelly-slime" ecosystem (e.g. Jackson 2008), gelatinous zooplankton biomass appears to be increasing in certain areas of the world's oceans (Mills 2001; Richardson et al. 2009; Purcell 2011). As such, increased gelatinous biomass may translate into increased transfer of this material to the ocean floor and thus enhancing the magnitude and importance of the biogeochemical and ecological processes associated with jelly-falls. Thus, there is a pressing need for research on gelatinous zooplankton post-bloom processes. Our primary objective is to provide a qualitative overview of historical and present records of jelly-falls, as well as the environmental context in which they were studied. Secondly, we define and conceptually model a general jelly-fall within the biological pump, including a synthesis of the factors triggering these events. We also assess the seasonality of jelly-falls from the available data and the benthic organisms that were observed feeding on the material. Our third objective is to discuss the possible consequences of increased gelatinous biomasses in the future ocean and provide a summary of the observational techniques and platforms that are, or could be used to study jelly-falls and their biogeochemical feedbacks.

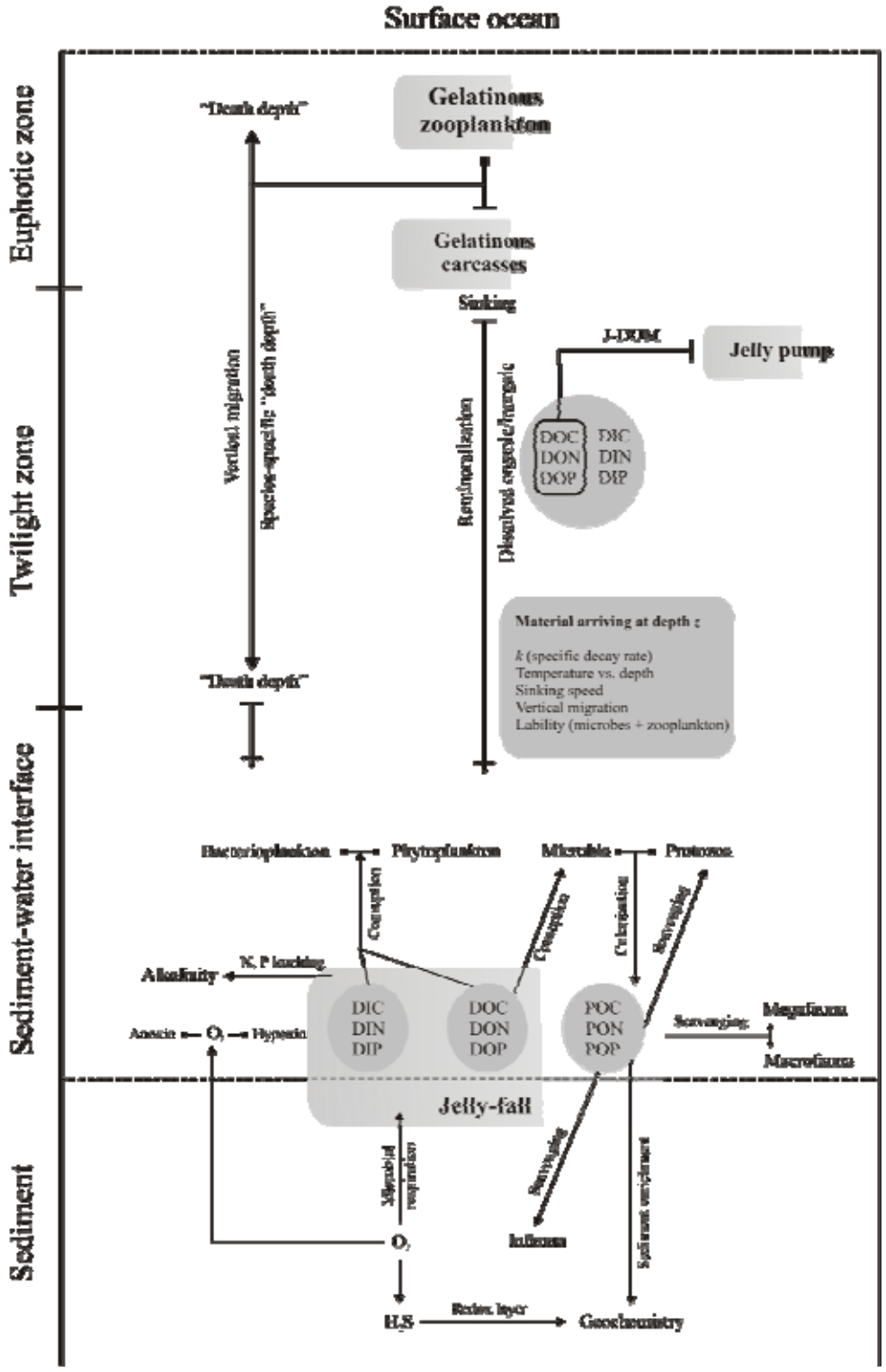

Fig. 2.1. Conceptual model of common processes beginning with sinking and the start of remineralization in the euphotic and twilight zones to deposition at the seabed followed by decomposition and scavenging. Under "material arriving at depth *z*", we have identified five critical factors that determine the amount of material reaching the seabed. The links to "bacterioplankton" and "phytoplankton" only proceed in the euphotic/twilight zone. Jelly-falls are linked to the "jelly-pump" concept (Condon and Steinberg 2008; Condon et al. 2010) through the production of Dissolved Organic Matter (J-DOM) in the water column and at the seabed. J-DOM is organic matter that fuels other trophic levels, which can occur while the organisms are still alive (e.g. Condon et al. 2011) or when dead (Hansson and Norrman, 1995).

2.2. Jelly-fall observations in the field

2.2.1. Thaliaceans

During the 1872-1876 H. M. S. Challenger expeditions, Moseley (1892) realized the potential importance of jellyfish in the biological pump by experimentally assessing the time it took a dead salp to sink 20 cm in a cylinder. He then left the carcass in the cylinder for 1 month and noticed that it did not decompose completely. He subsequently wrote: "the deep-sea has to derive food for its inhabitants entirely from debris of animals and plants falling to the bottom from the water above them. The dead pelagic animals must fall as a constant rain of food. It might be supposed that the animal carcasses would consume so long a time in dropping to the seabed that their soft tissues would be decomposed" (Mosely 1892). This is, to the best of our knowledge, the first mention of jelly-falls in the literature. A number of both quantitative and qualitative studies have followed since then (Table 1), but they remain scarce when compared with studies that have assessed the importance of other POM vectors (Turner 2002).

Hurley and McKnight (1959) were the first to report on a natural jelly-fall when they found the thaliacean *Pyrosoma atlanticum* Peron 1804 on the seabed off New Zealand. The organisms were sampled with a bottom trawl between 160 and 170 m depth (bottom temperature (BT) ~ 9 °C) during spring and were described as “resting” on the seabed. Their observations are further supported by reports from the same area of seabed being covered in *P. atlanticum* carcasses in 1952 (H. B. Fell pers. obs. reported to Hurley and McKnight 1959) and reports that local fishermen frequently trapped large quantities of moribund carcasses. Similar fishermen’s reports occur in the Mediterranean Sea (e.g. Sartor et al. 2003). Later, in the Tasman Sea, Cowper (1960) found that the stomachs of freshly caught carangid fish were full of *P. atlanticum* carcasses during winter. All fish were caught close to the bottom (BT ~ 7 °C); therefore, the authors concluded that they were feeding either on recently-settled carcasses or on moribund individuals near the seabed. A further analysis of stomach contents from the same fish species in the Tasman Sea from January to October revealed that the carcasses were most abundant in stomachs in January and March (Cowper 1960). There are other observations in New South Wales, Australia of the giant pyrosomid *Pyrosoma spinosum* Herdman 1888 near to or deposited on rocky bottoms, and also portions of salps being recovered from stomachs of carangid fish feeding at the seabed (Griffin and Yaldwyn 1970).

A considerable number of more recent studies document pyrosome falls. In the tropical Atlantic (off Cape Verde), Monniot and Monniot (1966) recorded moribund *P. atlanticum* at the seabed. In the deep Atlantic Madeira Abyssal Plain, high densities of pyrosomids were observed in the first 800 m of the water column (Roe et al. 1990). A survey using a fixed camera photographed a single carcass in an advanced state of decomposition at 5433 m depth (BT 2.2°C). A starfish and a crustacean scavenged the carcass, which took > 16 days to decompose completely. Recently, Lebrato and Jones (2009) reported a vast jelly-fall of *P. atlanticum* off the Ivory Coast, West Africa during ROV (remotely operated vehicle) surveys. Decomposing carcasses formed large patches (~ 1 to 20 m^2) and accumulated in troughs and channels (to a thickness of at least 0.5 m) from the shelf (< 200 m) to the deep slope (> 1200 m) (BT ~ 4 °C). The organic carbon contribution was estimated to be more than 20 g C m^{-1} in some areas, which is almost 10-times the annual fluxes in the area, as measured by sediment traps (Wefer and Fischer 1993). Carcasses were very abundant (707 individuals 100 m^{-2}) at the maximum depth surveyed (1275 m) and the maximum depth of the deposit could not be determined. Megafauna (including echinoderms and crustaceans) were observed 63 times directly feeding on the material (Lebrato and Jones, 2009). In the Mediterranean Sea (Alboran Sea to the Catalan Sea), jelly-falls of *P. atlanticum* were identified and sampled from 1994 to 2005 (spring and summer) during bottom trawling down to 800 m (average BT ~ 13 °C) in the MEDITS-ES surveys (Bertrand et al. 2002) (Fig. 2.2b). The catch often exceeded 300 carcasses per haul. This dataset provided the first evidence of jelly-falls along entire shelves during a period of 12 years (Fig. 2.2b). Living *P. atlanticum* were recovered from benthic trawls in canyon heads and walls (Ramirez-Llodra et al. 2009) near the wind-driven upwelling region of the Gulf of Lions (Johns et al. 1992). Sartor et al. (2003) reported catches in benthic trawls from 1995-1999 in the Mediterranean Sea (Tyrrhenian Sea) with numerous *P. atlanticum* occurring at the seafloor (100-500 g h^{-1} during > 500 h over several km^2) at 300 and 650 m (BT ~ 12 °C) (Fig. 2.2b). In the Mediterranean Sea, benthic deposits of *P. atlanticum* seem to be a common feature that are generally unnoticed.

Thaliaceans other than *P. atlanticum* have also been recorded at the seabed. Cacchione et al. (1978) described sinking living/moribound *Salpa aspera* Chamisso 1819 in the water column from a series of ROV observations below 2500 m (BT ~ 3 °C) in the Hudson Canyon, northwest Atlantic, over 30 days during summer. Salp bodies were observed rolling down the canyon. In the same area, Wiebe et al. (1979) observed a jelly-fall of *S. aspera* at > 2000 m (BT ~ 3 °C). The carcasses accumulated in channels and furrows and formed string-like aggregations at the

seabed (*see* Grassle and Morse-Porteous 1987; Grassle and Grassle 1994). In the Pacific Ocean, Duggins (1981) reported thousands of *Salpa fusiformis* Cuvier 1804 in the intertidal/subtidal environment (BT ~ 4 °C) of the Alaska Gulf over several months. Echinoderms fed preferentially on the gelatinous resource as soon as it was available. Recently, in the Red Sea, salps have formed jelly-falls during spring and after upwelling (20 m, BT ~ 23 °C) although these observations were not quantified (A. Alamaru pers. comm). In the Sea of Japan, a doliolid jelly-fall was studied in the water column by means of a sediment trap below 150 m (temperature ~ 12 °C) (Takahashi et al. 2010).

2.2.2. Cnidarians

For Cnidaria, the first natural jelly-fall recorded was in a photographic survey (Jumars 1976) below 1000 m (BT ~ 4 °C), where ophiuroids congregated around a *Pelagia* sp. carcass in the Santa Catalina basin (northeast Pacific). Recently, jelly-falls of *Aurelia limbata* Brandt 1835, *Parumbrosa polylobata* Kishinouye 1910, and *Nemopilema nomurai* Kishinouye 1922 were reported on the seafloor at 400 m depth (BT ~ 2.2-10 °C) in the Sea of Japan during summer and autumn (Miyake et al. 2002, 2005; Yamamoto et al. 2008, respectively). Thousands of *Crambionella orsini* Vanhöffen 1888 carcasses were photographed using a towed camera after seasonal upwelling in the Arabian Sea (Billett et al. 2006). Carcasses were recorded as freshly deposited on the shelf, while "jelly-lakes" of decomposing detritus were observed on the continental rise deeper than 3000 m (BT ~ 2 °C). White bacterial mats decomposing the organic material, covered the detritus. A scyphozoan jelly-fall (probably *C. orsini*) was reported near the Pakistan Margin at 900 m (BT ~ 9.5 °C) also after seasonal upwelling (Murty et al. 2009). A large gelatinous mat covering the seabed, presumably scyphozoans in a very advanced state of decomposition, was surveyed for 7 days with a ROV in the Norwegian Sea at 1380 m (BT ~ -1 °C) during summer and (Jones et al. 2010). A jelly-fall of *Periphylla periphylla* Peron and Lesueur 1810 was studied in spring 2011 in the Lurefjorden, Norway between 396 and 443 m (BT ~ 7 °C) (Sweetman and Chapman 2011). Carcasses were documented with a camera in two different areas in 7 transects at low densities (0.01 carcass m^{-2}), estimated to contribute < 1% to the annual organic matter flux in the area. Numerous jelly-falls of *Aurelia aurita* Linnaeus 1758 occurred during spring and after upwelling events at 20 m depth in the Red Sea (BT ~ 23 °C) (Alamaru et al. 2009). Sexton et al. (2010) reported a jelly-fall of *Chrysaora quinquecirrha* Desor 1848 medusae in a shallow sub-estuary of Chesapeake Bay during autum

Table 2.1. A compilation of naturally occurring jelly-falls.

Location	Origin	Species	Material state [a]	Latitude (range) [b]	Longitude (range) [b]	Depth (m) [b]*	Survey device	Duration [c]	Reference
Norwegian Sea (Atlantic Ocean)	Likely Scyphozoa	pending DNA analysis [d]	Det.	66.14°N	3.94°E	1380 (8.3/-1)	ROV (video)	7 days (S)	Jones et al. (2010)
Norwegian Sea (Atlantic Ocean)	Scyphozoa	*Periphylla periphylla*	F/Dec.	60.40°N-60.41°N	5.09°E-5.10°E	396-443 (-/7)	Yo-Yo (towed camera)	1 day (Spr.)	Sweetman and Chapman (2011)
Japan Sea (Pacific Ocean)	Scyphozoa	*Aurelia limbata*	F	42.58°N	143.96°E	320 (17/2.2)	ROV (video)	Unknown (S)	Miyake et al. (2002)
Chesapeake Bay (Atlantic Ocean)	Scyphozoa	*Chrysaora quinquecirrha*	F	38.59°N	76.12 °W	1.5 - 3 (15/14)	Visual (observers)	90 days (S)	Sexton et al. (2010) [e]
Japan Sea (Pacific Ocean)	Scyphozoa	*Nemopilema nomurai*	F	35.8°N-36.3°N	136°E-135.5°E	146-354 (22/10)	VTR system (towed camera)	35 days (S-A)	Yamamoto et al. (2008)
Japan Sea (Pacific Ocean)	Scyphozoa	*Parumbrosa polylobata*	F	34.91°N	138.65°E	453 (16/8)	ROV (video)	unknown (S)	Miyake et al. (2005)
Santa Catalina Basin (Pacific Ocean)	Scyphozoa	*Pelagia* sp.	Unk.	32.46°N	117.49°W	>1000 (17/4)	Photographs	unknown (N)	Jumars (1976)
Bermuda (Atlantic Ocean)	Scyphozoa	*Cassiopeia xamachana*	F/Dec./Det.	32.34°N	64.70°W	3 (25-25)	Photographs (quadrats)	unknown (S)	M. Lebrato (unpublished)
Gulf of Aqaba (Red Sea)	Scyphozoa	*Aurelia aurita*	F	29.50°N	34.91°E	20 (25-23)	Photographs (scuba diver)	unknown (Sp. #)	Alamaru et al. (2009)
Arabian Sea (Indian Ocean)	Scyphozoa	probably *Crambionella orsini*	F	22.95°N	66.61°E	900 (25/9.5)	WASP (towed camera)	1 day (S #)	Murty et al. (2009)
Arabian Sea (Indian Ocean)	Scyphozoa	*Crambionella orsini*	F/Dec./Det.	22.58°N-23.50°N	60.65°E-59.04°E	304 -3299 (25/2)	SHRIMP (towed camera)	17 days (W #)	Billett et al. (2006)
Japan Sea (Pacific Ocean)	Thaliacean (Doliolidae)	Not identified	F	34.40°N	150°E	150 (16/12)	Sediment trap	5 days (Sp.)	Takahashi et al. (2010) [f]
Tyrrhenian Sea (Mediterranean Sea)	Thaliacean (Pyrosomatidae)	*Pyrosoma atlanticum*	F/Dec.	42.30°N	10.60°E	300-650 (25/12)	Bottom trawling	1995-1999 (Sp. S)	Sartor et al. (2003) [g]
Mediterranean Sea	Thaliacean (Pyrosomatidae)	*Pyrosoma atlanticum*	F/Dec.	36.24°N-42.39°N	5.20°W-3.63°W	43 - 791 (18/13)	Bottom trawling (GOC 73)	1994-2005 (Sp. #)	Bertrand et al. (2002), MEDITS-ES [h]
Madeira Abyssal (Atlantic Ocean)	Thaliacean (Pyrosomatidae)	*Pyrosoma atlanticum*	F/Dec.	31.28°N	25.40°W	5433 (20/2.2)	BATHYSNAP (fixed camera)	16 days (S)	Roe et al. (1990)

Cape Verde (Atlantic Ocean)	Thaliacean (Pyrosomatidae)	*Pyrosoma atlanticum*	F	15.80°N	23.50°W	unknown (26/-)	unknown	Unknown (N)	Monniot and Monniot (1966)
Ivory Coast (Atlantic Ocean)	Thaliacean (Pyrosomatidae)	*Pyrosoma atlanticum*	F/Dec.	5.15°N-4.94°N	4.51°W-4.49°W	26-1275 (25/4)	ROV (video)	60 days (W #)	Lebrato and Jones (2009)
Cook Strait (Pacific Ocean)	Thaliacean (Pyrosomatidae)	*Pyrosoma atlanticum*	Dec.	41.73°S	174.3°E	100 (15/9)	Bottom trawling	unknown (Sp.)	Hurley and McKnight (1959)
Tasman Sea (Pacific Ocean)	Thaliacean (Pyrosomatidae)	*Pyrosoma atlanticum*	Unk.	42°S	148°E	330-640 (14/7)	Stomach content	unknown (W)	Cowper (1960)
Gulf of Alaska (Pacific Ocean)	Thaliacean (Salpidae)	*Salpa fusiformis*	F	58.33°N	136.83°W	1-10 (7/4)	Visual (scuba diver)	120 days (Sp.)	Duggins (1981)
Sargasso Sea (Atlantic Ocean)	Thaliacean (Salpidae)	*Salpa aspera*	F/Dec.	38.60°N-39°N	71.4°E-71.1°E	2500-3000 (19/3)	ROV (video)	4 days (S)	Cacchione et al. (1978)
Sargasso Sea (Atlantic Ocean)	Thaliacean (Salpidae)	*Salpa aspera*	F/Dec.	38°N-40°N	72.5°E-70°E	2000-3000 (19/3)	ROV (video)	30 days (S)	Wiebe et al. (1979)
Gulf of Aqaba (Red Sea)	Thaliacean (Salpidae)	Not identified	F	34.90°N	29.50°E	20 (25/23)	Photographs (scuba diver)	unknown (Sp. #)	Alamaru et al. (unpublished) [i]

[a] Material state refers to the condition in which the material was found: Dec. = decomposing, Det. = detritus, F = fresh, unk. = unknown (if not stated).

[b] Range for latitude, longitude and depth indicates that in some cases the material was retrieved along a gradient of depths and not in isolation (*see* reference paper for additional information).

[b*] *In situ* surface and bottom temperature (°C) are included in () when available in the original study or otherwise compiled from the GLODAP database (Key et al. 2004) and the World Ocean Atlas (http://odv.awi.de/en/data/ocean) in the nearest place available at the same depth.

[c] Duration only indicates the time that the material was observed or surveyed at the seabed and does not indicate annual events; otherwise the time-series is given for annual depositions. The season is indicated as: not available = N ; Spring = Sp. Summer = S, Autumn = A, Winter = W. # indicated when the event happened after seasonal upwelling and/or monsoon winds (e.g. tropical latitudes or specific cases like the Mediterranean Sea).

[d] Jelly material was unidentifiable to species level. Bar-coding with mtDNA and 18S rDNA ITS regions in progress to determine the affiliation.

[e] The authors do not show seabed evidence. The potential POC flux to the sediments was relatively small (12.5 to 72.5 mg C m^{-2} yr^{-1}) in comparison with the total annual flux to the sediments in the area (61.2 g C m^{-2} yr^{-1} Kemp et al. 1997).

[f] Carcasses recorded in sediment traps (export flux = 1.05 mg C m^{-2} d^{-1}, sinking speed = 4000 m d^{-1}, small degradation observed).

[g] The data used for *Pyrosoma atlanticum* correspond to the trawling catch from the seabed. The carcasses were dead at the seabed and decomposing.

[h] The data were in the MEDITS-ES project (International bottom trawl survey in the Mediterranean) (http://www.sibm.it/SITO%20MEDITS/). The data for *Pyrosoma atlanticum* correspond to the trawling catch from the seabed.

[i] A. Alamaru also reports on the presence of salps at the seabed in the same area as *Aurelia aurita*.

Table 2.2. Sampling techniques and initiatives that may be available to monitor jelly-falls.

Study method	Description	Advantages	Disadvantages
		Large scale (regional)	
1) Deep ocean observatories network (e.g. EUR-OCEANS, OceanSITES, ESONET) and offshore scientific platforms (e.g. PLOCAN)	Long-term reference network stations could be used to monitor seabed processes associated with jelly-falls. They could be used to study the organisms and carcasses in the water column and their arrival at the seabed by use of camera arrays.	The moorings and cruises are in place so it is a matter of adapting the strategy. Camera systems throughout the year with periodic recoveries. In situ and real time monitoring.	Challenging to study the jellies in the water column with camera devices. Possibility that jelly-falls do not occur near the stations and/or the seabed may too deep for jelly-falls to be observed).
2) Collaborations with industry (e.g. SERPENT project and similar)	The offshore oil and gas industry has regular access to expensive equipment (e.g. ROVs, camera systems) used in monitoring their own infrastructures. This equipment is not routinely used in scientific studies, but through collaboration it could be used to study jelly-falls at specific times of the year.	Access to state-of-the-art expensive equipment to study the seabed in deep waters. ROVs used in industry operations follow paths, allowing transect study. They cover a larger seabed area than normal in a scientific study.	Obtaining agreements with key industry personnel with access to the facilities. Confidentially and data release may take time to arrange. Surveys are confined to where the infrastructure exists. Cannot deviate greatly from established survey lines.
		Medium scale (local)	
3) Scientific ROV surveys	Used at known sites of jelly-falls to monitor the depositions in transects.	Real time monitoring and quantitative or qualitative data available at the seabed.	Time available to conduct the survey. Total area covered. Exclude water column processes. Expensive.
4) Towed and drop cameras from a vessel	Either used at known sites of jelly-falls or use to search for depositions in transects/specific locations.	Real time monitoring and quantitative or qualitative data available at the seabed. Can cover a relatively large area.	Time available to conduct the survey. Camera angle of view much less than ROV camera. Exclude water column processes.
5) Time lapse cameras (e.g. BATHYSNAP and benthic landers)	Used at known sites of jelly-falls to study the evolution of the material over time. A network of time lapse cameras also feasible at specific locations.	Real time monitoring and qualitative data available at the seabed. Time component of the jelly-falls.	Limited area covered. No biomass data. Jelly-fall may not occur where cameras are installed. Camera angle of view restricted. Exclude water column processes.
6) Trawling (from fisheries)	The fishery industry and other commercial species surveys (e.g. MEDITS) have records of bycatch organisms trawled at the seabed, including jelly-falls (carcasses)	Quantitative or qualitative data available at the seabed. Large areas covered over bathymetric gradients. Time component often available.	Obtaining agreements with industry personnel that have access to the facility. Surveys confined to the industry study of commercial species. Excludes water column processes. Environmentally destructive.

7) Acoustic/electronic tagging studies	Living individuals in large blooms could be acoustically/electronically tagged to follow their fate.	Real time study of individuals in a jelly-fall. Time component of sinking and deposition.	Difficulty of tag attachment to gelatinous body. Premature release of the tag. Limited information.
	Small scale (local)		
8) Large sediment traps (+5 m)	If a neutrally-buoyant sediment trap is developed to follow blooms it may deliver data on the associated sinking material.	Quantitative data in the water column. Possible to combine with a method at the seabed.	Probably unable to catch much of the sinking jelly-fall. Problems with organisms that vertically migrate and are mistakenly trapped alive. Cost-effective problems.
9) Moored and free drifting profilers	Some in development to measure water column properties over time (McLane labs, SeaCycler). If installed with a camera, study could cover the entire water column to the seabed.	Possible to monitor entire water problem over time. Quantitative data. Possible to relate camera data and water column properties.	Camera installation problems. Jelly-fall may not occur where the profilers are installed. Sinking speed of carcasses not tracked by profiler.
10) Genetic tools in sediments	Sediment proxy on freshly deposited gelatinous material can be tested using mtDNA and nuclear DNA.	Possible to obtain an ID from jelly-falls in the sediment. Possible to combine with camera studies. Time component may be available.	Limited to very fresh depositions. DNA contamination problems. Limited area covered.

Table 2.3. Occurrences of jelly-falls and the megafaunal taxa feeding on them.

Year	Depth (m)	Taxon	Timing [a]	Duration	Units	Feeding taxa	Reference
2011	396-443	*Periphylla periphylla*	Mar - Sp.	1	days	None [b]	Sweetman and Chapman (2011)
2010	150	Doliolids	May - Sp.	5	-	none	Takahashi et al. (2010)
2009	20	Salps	Post-upwelling	-	-	Anthozoans	Alamaru et al. (unpublished)
2009	20	*Aurelia aurita*	Post-upwelling	-	-	Anthozoans	Alamaru et al. (2009)
2009	900	*Crambionella orsini*	Post-upwelling	-	-	none	Murty et al. (2009)
2009	1380	Scyphozoans	Jun - S	7	days	none	Jones et al. (2010)
2007	3	*Cassiopeia xamachana*	Sep - S	-	-	none	M. Lebrato (unpublished)
2006	146-354	*Nemopilema nomurai*	Sep/Oct - S/A	30	days	Crustaceans, echinoderms	Yamamoto et al. (2008)
2006	26-1275	*Pyrosoma atlanticum*	Post-upwelling	60	days	Several [c]	Lebrato and Jones (2009)
2005	1.5 -3	*Chrysaora quinquecirrha*	Jun/Sep - S	90	days	none	Sexton et al. (2010)
2003	304-3299	*Crambionella orsini*	Post-upwelling	17	-	Crustaceans, echinoderms	Billett et al. (2006)
2002	453	*Parumbrosa polylobata*	Sep - S	-	-	Echinoderms	Miyake et al. (2005)
2001	320	*Aurelia limbata*	Aug - S	-	-	Echinoderms	Miyake et al. (2002)
1999	300-650	*Pyrosoma atlanticum*	Sp./S	3	months	none	Sartor et al. (2003)
1998	300-650	*Pyrosoma atlanticum*	Sp./S	3	months	none	Sartor et al. (2003)
1997	300-650	*Pyrosoma atlanticum*	Sp./S	3	months	none	Sartor et al. (2003)
1996	300-650	*Pyrosoma atlanticum*	Sp./S	3	months	none	Sartor et al. (2003)
1995	300-650	*Pyrosoma atlanticum*	Sp./Sum	3	months	none	Sartor et al. (2003)
1985	5433	*Pyrosoma atlanticum*	Jun/Jul - S	17	days	Crustaceans, echinoderms	Roe et al. (1990)
1978	1-10	*Salpa fusiformis*	Mar/Jun - Sp./S	3	months	Echinoderms	Duggins (1981)
1975	2500-3000	*Salpa aspera*	Aug - S	-	-	none	Cacchione et al. (1978)
1975	2000-3000	*Salpa aspera*	Aug - S	4	days	none	Wiebe et al. (1979)
1955	330-640	*Pyrosoma atlanticum*	Jun/Jul - S	-	-	Fish	Cowper (1960)
1952	100	*Pyrosoma atlanticum*	Oct - Sp.	-	-	Fish	Hurley and McKnight (1959)

[a] The month is abbreviated (when available), and the season is indicated as: Spring = Sp. Summer = S, Autumn = A, Winter = W.

[b] Caridean shrimps and galatheid crabs observed near carcasses, but no grazing directly observed.

[c] Anthozoans, crustaceans, echinoderms, fish, arthropods, polychaetes

2.3. Jelly-falls conceptualization

2.3.1. Processes from the euphotic zone to the seabed

A jelly-fall (Fig. 2.1) starts when gelatinous organisms die and sink from a so-called "death depth" subject to the organisms' vertical migration. Because gelatinous detritus is denser than the surrounding seawater, the corpses sink through the water column at a rate determined by the material's size and excess density (Stokes´ Law) (Yamamoto et al. 2008). The organisms can settle at the seabed while still alive (Wiebe et al. 1979; Gili et al. 2006) and then die, thus remineralization can start on the seabed. As it sinks, the material is consumed by scavengers and return to the faunal food web or remineralized by bacteria (bacterioplankton), entering the microbial loop (Hansson and Norrman 1995). Dissolved Organic Matter (DOM) leaching from living or dead organisms provides a link to the "jelly-pump" concept (J-DOM) of microbial communities being fuelled by DOM excretion (Condon and Steinberg 2008; Niggl et al. 2010; Condon et al. 2011) (Fig. 2.1). Microzooplankton and small zooplankton may also consume J-DOM (Iguchi et al. 2006; Titelman et al. 2006; West et al. 2009a). Laboratory incubations of scyphozoan material using deep (334 m) and shallow water (< 10 m) differed in the remineralization time (Iguchi et al. 2006), which was attributed to the microbial community as well as temperature in situ. Differences in the lability of gelatinous tissues (C:N ratios; Larson, 1986), the various rates at which the different materials sink (Apstein 1910; Mills 1981), and rates of scavenging and bacterial mineralization (which may vary with temperature and depth) greatly influence the extent to which the jelly-fall is recycled within the water column *vs.* at the seabed (Fig. 2.1). Jelly-falls that reach the seafloor may be transported elsewhere (e.g. along geomorphological features) (Billett et al. 2006), or retained in situ and consumed by the local faunal and microbial community (Lebrato and Jones 2009). Leaching of dissolved compounds fuels production in higher trophic levels (West et al. 2009a) and biogeochemical processes such as oxygen consumption in the water and in the sediment proceed during the organic enrichment (West et al. 2009b; Sexton et al. 2010). Associated Total Alkalinity changes from excess DOM (Hansson and Norrman, 1995; Hoppe et al. 2010) and the non-Redfield stoichiometry of nitrogen and phosphorus leaching from the corpses (Pitt et al. 2009; Condon et al. 2010; Tinta et al. 2010) should also be considered. The decomposition dynamics has been the focus of several papers targeting a variety of species at different temperatures, thus decay rates (k) are available (e.g. Titelman et al. 2006). The turnover of jelly-POM is rapid during the first few days

(Sempere et al. 2000) and then slows down, but it is highly dependent on temperature (Iguchi et al. 2006). These quantitative data on decomposition dynamics have enabled remineralization of sinking carcasses to be modelled in open ocean conditions (Lebrato et al. 2011). They provided a new metrics based on decay rate, temperature fields, "death depth", and sinking speed that helps to understand why different gelatinous zooplankton groups transfer organic carbon to the seabed (e.g. scyphozoans and thaliaceans), while others may be completely remineralized in the water column.

The transport to the seafloor of jelly-POM is an important source of labile material to the whole size-spectrum of benthic communities in continental margins and the deep-sea (Table 2.1; Fig. 2.1). Evidence of organisms consuming jelly-POM at the seabed has accumulated slowly from photographs and videos (Table 2.1; Fig. 2.2a). Gelatinous material has a low energy content (0.5-6 gross energy kJ g dry mass^{-1}) compared to other types of carrion such as fish (5-22 gross energy kJ g dry mass^{-1}) or algae (> 10 gross energy kJ g dry mass^{-1}) (Doyle et al. 2007). Among gelatinous species, the energy content is highest in salps and pyrosomids (4-6 gross energy kJ g dry mass^{-1}) (Davenport and Balazs 1991; Clarke et al. 1992), which are important parts of the diets of numerous benthic organisms (Table 2.3). Although high energy resources are readily available on continental margins, food is a limiting factor in the deep-sea (Gage and Tyler 1991). Thus, jelly-falls represent a valuable nutritional input at certain times of the year (Table 2.3).

Unlike other large food falls, which are usually sparsely scattered over the sea floor, gelatinous corpses accumulate in large patches (Billet et al. 2006; Lebrato and Jones, 2009) making it easier for scavengers to locate; however, scavengers traditionally observed around fish falls (such as isopods or fish), have not been observed around jelly-falls (Sweetman and Chapman 2011). The reduced energy spent searching for food, and the lability of the gelatinous carrion relative to other sources of detritus, may compensate for the reduced energy density of the jelly falls at least for some scavenger species (Doyle et al. 2007). Additionally, jelly-falls may provide an environment for macrofauna/microbial communities to proliferate, which, in turn, may be preyed upon by other taxa (Sweetman and Chapman 2011). Sessile organisms (anthozoans, including hexacorallians, octocorallians, and scleractians) also consume jelly-POM (Gili et al. 2006; Alamaru et al. 2009; Lebrato and Jones 2009). Echinoderms dominate scavenging observations at any depth, followed by crustaceans and fish (Table 2.3). Remains of

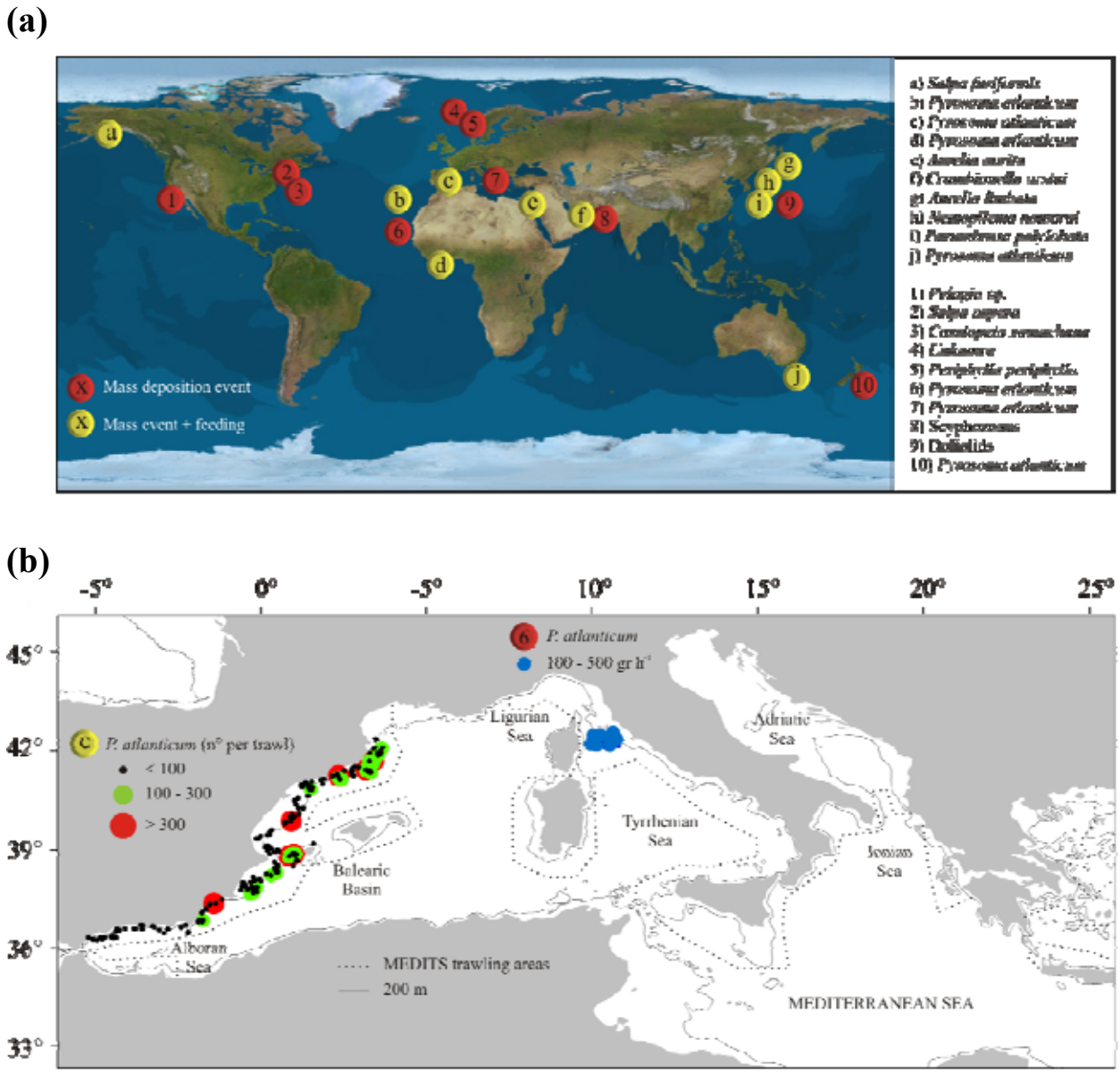

Fig. 2.2. (A) Global distribution of reported jelly-falls. Also included are the species that were recorded in each individual event (see Table 1 for detailed information). (B) Observations of *Pyrosoma atlanticum* jelly-falls at the seabed in the Mediterranean Sea (from the MEDITS-ES project) (Bertrand et al. 2002). Numerous jelly-falls occur along the whole western Iberian Margin. The legend shows the average number of carcasses observed at each station from 1994 to 2005. Also included are observations of *P. atlanticum* in the Tyrrhenian Sea (northwest Mediterranean Sea) (Sartor et al. 2003). The bathymetric line (200 m) are from the general bathymetric chart of the oceans (GEBCO) Digital Atlas (IOC et al. 2003). The dotted line indicates the zones trawled in the MEDITS project that can be used to study jelly-falls from trawling data, as proposed in section 3.2.

jelly-POM (e.g. *Cymbulia peroni* De Blainbille 1810) are commonly found in gut of numerous bnethic decapods, such as the Norway lobster *Nephrops norvegicus* Linnaeus 1758, the crab *Geryon longipes* Milne-Edwards 1882 (in Cartes 1993a), and the squat lobster *Munida tenuimana* Sars 1872 (in Cartes 1993b). Jelly-POM (*Iasis zonaria* Pallas 1774, *Pyrosoma atlanticum*, *Periphylla periphylla*) is also found in the guts of deep shrimps, such as *Plesionika*

martia Milne-Edwards 1883 (in Fanelli and Cartes 2008) or fish (Carrasson and Cartes 2002; Drazen et al. 2008; Goldman and Sedberry 2010). Any remaining material that is not channelled through macro-/megafaunal scavenging will eventually be respired by microbial communities (Fig. 2.1). The build-up of impermeable gelatinous material (as in Billett et al. 2006) on the seafloor leads to reductions in O_2 flux into sediments (West et al. 2009b). This would favour microbial over metazoan biomass and remineralization processes, although low seawater O_2 combined with no light slows microbial decomposition of settling organic matter (Gooday et al. 2010), and toxic remineralization products (e.g. ammonium and free sulphides) could accumulate and seriously impact sediment biota as well as pelagic ecosystems (Titelman et al. 2006; Pitt et al. 2009) (Fig. 2.1). Ultimately, jelly-falls could induce spatial heterogeneity in the biodiversity of benthic communities (Gooday et al. 2010) as a consequence of the mass accumulation of undegraded labile material.

2.4. Causes and seasonality of jelly-falls

Factors driving the onset of jelly-falls are mostly linked to the ageing and end of a bloom (Purcell et al. 2001) and a long-term cumulative effect of negative factors, such as parasitism, starvation, infection, and predation (Mills 1993), with subsequent deposition at the seabed if the material is not completely remineralized while sinking. In other cases, the material floats and it is washed ashore (e.g. Pakhomov et al. 2003; Houghton et al. 2007). The life history of individual species dictates their fate, although some generalities apply to all groups, such as seasonal disappearance from the waters (Mills 1993). Life cycles are often completed within a year or a few months, with subsequent death (Franqueville 1971; Mills 1993). For thaliaceans, there is evidence that high concentrations of particles and suspended organic matter [e.g. chlorophyll *a* > 1 mg m^{-3}; Perissinotto and Pakhomov (1998)] clog their feeding apparatus causing death (Acuña 2001) despite food being abundant (Harbison et al. 1986; Zeldis et al. 1995). This explains the salp jelly-fall studied by Duggins (1981) in the subtidal zone in Alaska and the beaching of salps reported by Pakhomov et al. (2003) in the Southern Ocean. Thaliacean jelly-falls tend to appear at the seabed after strong periods of upwelling (Lebrato and Jones, 2009) or after the spring bloom months when chlorophyll *a* levels are high (Wiebe et al. 1979; Duggins 1981; Roe et al. 1990) (Table 2.3). Re-assessment of the season (n = 24) when carcasses of all groups arrive at the seabed indicates that > 75% of jelly-falls occur after the spring bloom in temperate/subpolar areas and > 25% in post-upwelling periods in the tropics.

This happens irrespectively of the depth at which they are deposited. It remains unclear for thaliaceans if the concentration or particles per se causes clogging and subsequent death, or if the biological composition of the particles and autotroph community play a role. Potential connections between climate and gelatinous zooplankton populations in the water column and the jelly-falls at the seabed have not yet been investigated. In tropical areas, monsoon patterns trigger upwelling events that alter water column properties (e.g. lower temperature, high nutrients and chlorophyll a, high DOM levels, higher POM export) (Coble et al. 1998; Honjo et al. 1999), thus forcing in these zones is different than in temperate/subpolar latitudes.

In the Cnidaria, several variables may trigger the onset of jelly-falls, including sudden or sustained changes in temperature exceeding physiological performance (Gatz et al. 1973) (relevant in upwelling systems where organisms can experience rapid changes in the water mass properties due to physical forcing), ageing of the bloom followed by food depletion (causing starvation and poor nutrition) (Mills 1993; Purcell et al. 2001; Sexton et al. 2010). The latter cause may have relevance for the *C. orsini* carcasses studied by Billett et al. (2006) and the depositions of *N. nomurai* observed by Yamamoto et al. (2008). The food exhaustion hypothesis would explain why we often observe scyphozoan jelly-falls after the spring bloom but predominantly in the late spring/early summer months (Table 2.3). Other factors include grazing damage (Arai 2005), parasitism/injury/viral infections (Mills 1993), senescence (Sexton et al. 2010), extreme weather events triggering large changes in physical properties of water (Cargo 1976), and sinking driven by low temperatures and inducing deposition and later death owing to temperature changes (Sexton et al. 2010).

2.5. Operational oceanography and exploration techniques

The jelly-fall concept originates from a handful of studies undertaken in the field that either described accidental encounters or, in few cases, targeted known gelatinous depositions. In > 80% of the cases (n = 22), ROV video and/or towed/still cameras were used as the sampling technique (Table 2.1). Unless a large area was covered and transects used to count individual carcasses (Billett et al. 2006; Lebrato and Jones 2009), these techniques remain qualitative (Roe et al. 1990; Miyake et al. 2002, 2005; Yamamoto et al. 2008). Other techniques, including scuba diving and sediment traps account for < 5% of the observations. Trawling is the only other technique that allows large quantitative studies (MEDITS-ES dataset; Sartor et al. 2003). Field

work has been accompanied by a series of laboratory or mesocosm studies that target associated biogeochemical processes (e.g. Sempere et al. 2000; Pitt et al. 2009; Tinta et al. 2010). Although we now have important information about the occurrence of jelly-falls and their potential influence on elemental cycling, we still lack combined effort and large-scale projects on this topic. Temporal monitoring can be addressed by "ocean observatories" (Table 2.2; Claustre et al. 2010; Send et al. 2010). From these ocean observatory initiatives (e.g. EUR-OCEANS, OceanSITES, ESONET) and scientific projects that collaborate with offshore industries (e.g. SERPENT (Jones, 2009), DELOS (http://www.delos-project.org/), and HAUSGARTEN (Soltwedel et al. 2005), regular access to the deep-sea will increase our chances of making informative observations. We need to move beyond the present semi-empirical state of understanding to local or regional monitoring and quantification of jelly-falls. ROVs, AUVs (autonomous underwater vehicles), benthic landers, and towed, drop, and time-lapse cameras should be used (Table 2.2). In particular, the use of repeated AUV surveys or a network of time-lapse cameras strategically placed at the seabed in areas where jelly-falls have been observed could provide insights into seasonality and decomposition at the seabed. Benthic crawlers (Karpen et al. 2007) can survey inaccessible areas where jelly falls have been observed via a optical cable from a shore-based station for long periods of time.

For large-scale quantification of jelly-falls, logbooks of bottom-trawling surveys from historical to present times are a unique tool that have not fully utilized. They mainly target commercial demersal fish and crustaceans species, but non-commercial or "discarded" (bycatch) species, including gelatinous zooplankton, are sometimes consistently recorded (e.g. Sartor et al. 2003; Sanchez et al. 2004; Bastian et al. 2011). Data from jelly-falls have been collected in this way (Fig. 2.2b) and also data on living biomass (Bastian et al. 2011). Many benthic trawling programmes exist worldwide [e.g. MEDITS (International bottom trawl survey in the Mediterranean Sea) (Bertrand et al. 2002); Relini (2000) (Italian Seas); Sartor et al. (2003) (Tyrrhenian Sea); ITBS (International Bottom Trawl Survey); NOAA Gulf of Alaska bottom trawl survey; NEFSC bottom trawl survey (Gulf of Maine Area); Wilkins et al. (1995) (The 1995 Pacific West Coast bottom trawl survey); Bastian et al. (2011) (North Atlantic Ocean)]. Information could also be retrieved from fisheries information networks [e.g. PacFIN (http://pacfin.psmfc.org/index.php); AKFIN (http://www.akfin.org)]; and from state and wildlife agencies and fishery management councils (e.g. http://pacfin.psmfc.org/pacfin_pub/links.php)]. Trawling surveys normally cover specific depth ranges in so-called "trawlable" areas in the

shelves and slopes. The surveys do not normally work beyond the continental slope [(e.g. 0-800 m in the MEDITS-ES, 250-800 m in Sartor et al. (2003)] (Fig. 2.2b), but effectively sample the shelves consistently and repeatedly. The problem often is that to reduce cost and effort and increase efficiency, the size, weights, and numbers only of commercial species are recorded in logbooks, and the living and dead gelatinous component, if present, is overlooked. This issue was discovered in the MEDITS-ES project, where certain partners recorded the same data for commercial and for non-commercial species (jelly-fall data used in Fig. 2.2b), while the majority did not. Only through effective science-industry communication and collaboration can we make use of their potential to quantify jelly-falls and living biomass (Bastian et al. 2011).

At local scales, we suggest use of acoustic/electronic tagging (e.g. Seymour et al. 2004; Gordon and Seymour, 2008; Hays et al. 2008) on individuals found in blooms to discover their fate (Table 2.2). Tags can be mechanically secured in cnidarians in the bell area and peduncle, or using setting glue. Large neutrally-buoyant sediment traps also could be used (Lampitt et al. 2008) that could drift under blooms, as well as free-drifting profilers with mounted cameras to investigate the water column. Genetic tools (e.g. Reusch et al. 2010) could be also used to characterize a jelly-fall signature in the sediment. Further research should quantify and study the diversity of the scavenging communities attracted to an “artificial” jelly-fall (e.g. Yamamoto et al. 2008). This has traditionally been done with a bait in the field of view of a still camera (reviewed by Bailey et al. 2007). This can be combined with labelling studies to assess the fate of jelly-derived organic material, as for phytodetritus (Middelburg et al. 2000; Witte et al. 2003; Franco et al. 2008).

2.6. Can jelly-falls provide ecosystem services in the future?

The future ocean is expected to be a warmer, more-stratified, acidic, and oxygen-poor system characterized by reduced upwelling (Cox et al. 2000; Gregg et al. 2003). As a result, production exported to depth is expected to be reduced as phytoplankton communities shift from large diatom-based assemblages to picoplankton with lower export efficiency (Buesseler et al. 2007; Smith et al. 2008). Reduced export production and changes in community structure are expected to result in reduced delivery to, and an overall change in the composition of organic material reaching the abyssal ocean floor (Laws 2004; Smith et al. 2008). This is expected to reduce food availability to the already food-limited deep-sea floor, causing a decline in deep-sea

biomass and ecosystem changes (e.g. in faunal behaviour (Kaufmann and Smith 1997; Wigham et al. 2003), bioturbation (Smith et al. 2008; Vardaro et al. 2009), faunal densities (Ruhl and Smith 2004; Ruhl 2007, 2008; Smith et al. 2008), reproductive traits (Tyler 1988; Young 2003; Ramirez-Llodra et al. 2005), faunal diversity (Levin et al. 2001), body size (McClain et al. 2005), taxonomic composition (Ruhl and Smith 2004), sediment infaunal response (Sweetman and Witte 2008a, b), and dominance (Cosson et al. 1997; Sweetman and Witte 2008b). Reduced carbon export may also inhibit the ocean's ability to sequester carbon (Smith et al. 2008). The potential consequences of the combination of altered food inputs to the benthos and increased CO_2 content of seawater on ecosystem functioning and services (e.g. nutrient regeneration, energy transfer to higher trophic levels) could have large implications because recent studies suggest that an organism's ability to cope with acidification and elevated water temperatures may be regulated by food supply (Wood et al. 2008; Gooding et al. 2009).

Gelatinous zooplankton populations, on the other hand, may benefit from anthropogenic impacts on the marine environment (Purcell et al. 2007; Purcell 2011). There is evidence of some populations increasing during the last decades, such as thaliaceans in the Southern Ocean (Loeb et al. 1997; Atkinson et al. 2004) and jellyfish in the Mediterranean Sea (Molinero et al. 2008). It has been suggested that jelly-biomass will become an increasingly important component in the future ocean (Purcell et al. 2007; Jackson 2008; Richardson et al. 2009; Purcell 2011). Therefore, if classic POM vectors (e.g. phytodetritus) become less important in the future ocean, an increased amount of jelly-POM sinking to the seabed could mitigate some of the losses of carbon from phytoplanktonic carbon sources, although it is likely to be much more heterogeneous at the seafloor (Gooday et al. 2010). Because the majority of jelly-falls deposits are located in deep, cold (< 10 °C) marine environments (Table 2.1), we hypothesize that jelly-POM:phytodetrital-POM flux ratios are likely to be higher in deep-sea and polar settings (Lebrato et al. 2011). This may maintain certain ecosystem functions in some areas (dependent on the threshold POM flux) by ensuring a continued minimum POM flux from the surface to the seafloor. It is also likely to have drastic implications for benthic community composition just as changes in surface phytoplankton community composition can substantially modify abyssal community composition.

3.

Jelly biomass sinking speed reveals a fast carbon export mechanism

Abstract

Large gelatinous particles sink as carcasses when gelatinous zooplankton populations collapse in post-bloom processes known as jelly-falls. Jellyfish (scyphozoans, hydrozoans), ctenophores, and thaliaceans (pyrosomes, salps, and doliolids) contribute to this organic matter (jelly-POM) export to the seabed in shelves and slopes. However, the jelly carbon export efficiency has not been assessed in a global context yet. To this end, the inclusion of jelly-POM compartments in models needs basic data, e.g. sinking speed, which were absent. Here, we conducted field and laboratory experiments at in situ density to assess the sinking rate of schyphozoans (n = 3 species), ctenopores (n = 2 species), thaliaceans (n = 2 species), and also pteropods (n = 2 species) for comparison. Jelly-POM sinked on average between 400 and 1500 m day^{-1} (salps: 800-1700 m day^{-1}, ctenophores: 500-1800 m day^{-1}, scyphozoans: 1000-1100 m day^{-1}, pyrosomes: 1200-1300 m day^{-1}), and e.g. salps were well correlated with biovolume. Combining the taxonomic sinking speed separation with an export ratio calculation for jelly-POM, we calculated the export efficiency based on decay rates and water column temperature profiles. We used two scenarios with jelly-POM sinking from 200 and 600 m to represent different life styles, and we used water column data at temperate, tropical, and polar areas in the Atlantic Ocean. There was a general remineralization profile for all jelly-POM except in the poles. High latitudes provide a fast-sinking/low remineralization corridor for jelly-POM, where material is

quickly exported to depth, while in tropical and temperate settings major remineralization takes place in the first 1500 m, unless biomass starts sinking below the thermocline. The export efficiency based on sinking speed indicates that jelly-POM needs to be urgently incorporated in models to realistically assess the oceanic carbon export efficiency at regional and global scales.

This chapter is based on:

Lebrato, M., de Jesus Mendes, P., Steinberg, D. K., Cartes, J. E., Jones, B. M., Birsa, L., Benavides, R. and Oschlies, A. in preparation. Jelly biomass sinking speed reveals a fast carbon export mechanism. To be submitted: *Geophysical Research Letters*.

Acknowledgements: We thank Kerstin Nachtigall for biochemical analayses. We are also grateful to Captain Joseph Abshire and the officers of the ASRV Laurence M. Gould for their support during LTER1101. We would also like to thank the Raytheon Polar Services contractors who assisted us with zooplankton collection during this cruise This work was supported by the "European Project on Ocean Acidification" (EPOCA), which is funded from the European Community's Seventh Framework Programme (FP7/2007-2013) under grant agreement n° 211384. This work was also funded by the Kiel Cluster of Excellence "The Future Ocean" (D1067/87).

3.1. Introduction

Marine particles are a size continuum ranging from individual cells and exudates to assemblages of degraded biogenic detritus, also including the biomass of gelatinous zooplankton. The sedimentation of particles to the ocean's interior is central to the biological pump concept (Buesseler et al. 2007), re-distributing elements (e.g. C, N, P, Si) in the water column (Lee and Fisher 1993). Particle sinking rate tends to increase with individual size and length (Shanks and Trent 1980), and sedimentation with depth is modelled in different ways based on theory and observations: increasing sinking speed with depth (Schmittner et al. 2005), constant rate (Fasham et al. 1990), variable according to size (Kriest and Evans 1999), or ballasted by $CaCO_3$ biominerals (Armstrong et al. 2002). In the field, particles from any origin with size fractions small enough to be collected by sediment traps (Madin; 1982; Fowler and Knauer 1986; Asper 1987) or visible from cameras (Jackson et al. 1997) (from < 1 mm to ~ 50 mm) comprise the present knowledge, while in the laboratory phytoplankton and zooplankton derived material (e.g. marine snow and faecal pellets) from 0.5 to 1000 μm have been commonly studied (Apstein 1910; Smayda 1969; Shanks and Trent 1980; Walsby and Holland 2006; Ploug et al. 2008). However, the study of larger particles from millimeters to meters originating in gelatinous zooplankton has received little attention beyond faecal pellets (Turner 2002). Sinking gelatinous biomass starts as a post-bloom process following seasonal population collapse, when the organisms die (*see* Lebrato et al. 2012), being referred to as jelly-falls and jelly-POM (Lebrato et al. 2011). The main contributors are jellyfish (Scyphozoa and Hydrozoa) (Billett et al. 2006), but also pelagic tunicates (Salpa and Pyrosomida) (Wiebe et al. 1979; Lebrato and Jones 2009). The bloom biomass is occasionally exported and deposited at the seafloor sequestering large amounts of organic carbon and providing labile food for benthic communities (Sweetman et al. 2011), but it normally decomposes while sinking (Lebrato et al. 2011). While sinking, it releases large amounts of nutrients (Pitt et al. 2009; Tinta et al. 2010; Frost et al. 2012), providing labile resources for bacterioplankton and microzooplankton (Titelman et al. 2006). Recent work at the Jellyfish Database Initiative (JEDI) highlighted in a snapshot the global gelatinous biomass distribution from surface to mesopelagic and deep waters (Condon et al. 2012). These data will allow in the future to study jelly-POM transfer efficiency, and subsequent incorporation in models to assess the strength of the biological pump. While the first parameterization using the ocean vertical thermal gradient was recently developed (Lebrato et al. 2011), we still lack fundamental data to separate taxonomically the carbon export. This paper

provides the first set of laboratory and field observations on jelly-POM sinking rates in scyphozoans, salps, pyrosomes, and ctenophores. Using these data, we present a jelly-POM export ratio taxonomic separation as defined in Lebrato et al. (2011) by using water column temperature data from three stations at polar, temperate, and tropical latitudes.

3.2. Methods

3.2.1. Sinking field experiments

The field experiments were conducted onboard ASRV Laurence M. Gould in the research cruise LTER1101 in the western Antarctic Peninsula in January/February 2011. Salps (*Salpa thompsoni*) (n = 15), ctenophores (lobate) (n = 13), and also pteropods (*Limacina helicina*) (n = 8) (used for comparison), were collected with a plankton net (700 µm Metro net) between 0 and 100 m (temperature = 0.50-1.50 °C, salinity = 33-34 and density = 1026.43-1027.29 kg m^{-3}) between 63 °S and 70 °S (Table 3.1). They were subsequently submerged in hot water for a few minutes until death. Salps were placed in a 20 ml beaker to measure biovolume (displacement volume), while for ctenophores this was not possible because they broke down in pieces. Pteropods were directly frozen and sent to OceanLab, Jacobs University (Germany). In Antarctica, salps (whole bodies) and ctenophores (whole bodies and small pieces) were sunk individually in a clear plexiglass column 57 cm tall, with a diameter of 12.5 cm. The column was filled with surface seawater (to mimic field density values) to roughly 6 cm below the top, and animals were released just below the water surface in a pre-known 30 cm interval to assess the sinking time. The experiment was conducted in a temperature-controlled enclosure at 0 °C. Once concluded, the 15 salps and 13 ctenophores were sent frozen to OceanLab, Jacobs University (Germany) to re-assess the sinking speed in the laboratory.

3.2.2. Sinking laboratory experiments

The laboratory experiments were conducted at OceanLab, Jacobs University (Germany) in April 2011 in two separate days. Apart from the Antarctic samples described above, we obtained scyphozoans [*Cyanea* sp. (n = 2) - Baltic Sea, *Periphylla periphylla* (n = 2) - Mediterranean Sea, and *Pelagia noctiluca* (n = 5) - Mediterranean Sea], ctenophores [*Mnemiopsis leidyi* (n = 2) - Atlantic Ocean], pyrosomes [*Pyrosoma atlanticum* (n = 2) - Mediterranean Sea] and pteropods

Table 3.1. Organisms field meta-data and organic matter biochemistry.

		Field meta-data						Material composition				
Organism	**Species**	***n*** [a]	**Origin**	**Depth (m)** [b]	**T (°C)** [c]	**Sal.** [c]	**Den. (kg m^3)**	***n*** [d]	**Dry wt (mg)** [e]	**C % dry wt**	**N % dry wt**	**C/N (mol/mol)**
Scyphozoan	*Cyanea* sp.	2	Baltic Sea	0-10	15.50	14.00	1011.69	2	1.055 ± 0.062	42.750 ± 0.448	13.644 ± 0.382	2.686 ± 0.103
Ctenophore	*Mnemiopsis leidyi*	2	Atlantic Ocean	0-10	16.50	16.50	1011.50	2	1.110 ± 0.002	non-detectable [f]	non-detectable [f]	n/a [g]
Thaliacean	*Salpa thompsoni*	15	Antarctica	0-100	1.50-0.50	33.00-34.00	1026.43-1027.29	16	1.126 ± 0.058	14.322 ± 6.877	2.262 ± 1.242	5.923 ± 2.576
Ctenophore	Lobate ctenophore	13	Antarctica	0-100	1.50-0.50	33.00-34.00	1026.43-1027.29	6	1.127 ± 0.041	1.403 ± 0.978	0.542 ± 0.255	2.060 ± 0.449
Pteropod	*Limacina helicina*	8	Antarctica	0-100	1.50-0.50	33.00-34.00	1026.43-1027.29	8	1.113 ± 0.042	34.488 ± 1.995	7.190 ± 0.908	4.172 ± 0.622
Thaliacean	*Pyrosoma atlanticum*	2	Mediterranean Sea	0-1500	24.49-13.07	37.75-38.48	1025.60-1029.10	4	1.046 ± 0.037	20.083 ± 5.418	3.351 ± 0.864	5.123 ± 0.150
Scyphozoan	*Periphylla periphylla*	2	Mediterranean Sea	0-674	26.34-13.06	37.75-38.48	1025.03-1029.10	4	1.145 ± 0.045	27.111± 11.423	5.420 ± 2.220	4.330 ± 0.657
Pteropod	*Cymbulia peroni*	7	Mediterranean Sea	0-1000	25.45-13.23	37.75-38.48	1025.31-1029.07	4	1.051 ± 0.036	27.817 ± 4.150	7.522 ± 1.152	3.170 ± 0.103
Scyphozoan	*Pelagia noctiluca*	5	Mediterranean Sea	0-1000	25.45-13.23	37.97-38.48	1025.47-1029.07	3	1.123 ± 0.057	11.063 ± 5.703	3.828 ± 1.846	2.429 ± 0.147

[a] Number of individual organisms collected in the field.

[b] Depth range were organisms were collected by plankton net.

[c] Temperature and salinity in situ at collection place or the range measured at initial and final depth by CTD or probe.

[d] Number of replicate measurements. Note that not all organisms collected were analyzed, but replicates were measured for a subset in duplicates (e.g. *Salpa thompsoni*: 8 organisms used, then split in half, thus $n = 16$).

[e] Dry weight of the material measured to work out percentages.

Table 3.2. Organisms sinking rate experiment summary.

Organism	Species	Water height (cm)	*n***n*-sink [a]	T (°C) [b]	Sal. [b]	Den. (kg m^3)	Den.$_{field}$/Den.$_{lab.}$ [c]	Material sunk	Exp.	Sinking rate (m day^{-1})	Shape	Sinking orient.
Scyphozoan	*Cyanea* sp.	97.50	2/1	6.10	13.70	1010.78	1.000	All body	Lab.	1018 ± 175	Ovoid	Horizontal
Ctenophore	*Mnemiopsis leidyi*	107.60	1/3	5.30	24.20	1019.12	0.992	Pieces	Lab.	1487 ± 1126	Ovoid	Vertical
Thaliacean	*Salpa thompsoni* 1	107.60	10/1	4.50	33.90	1026.88	0.999	All body	Lab.	868 ± 489	Elongated	Vertical
Thaliacean	*Salpa thompsoni* 2	57.00	15/1	-0.16	33.50	1026.92	0.999	All body	Field	1150 ± 401	Elongated	Horizontal
Ctenophore	Lobate ctenophore 1	-	-	-	-	-	-	-	Lab.	-	-	-
Ctenophore	Lobate ctenophore 2	57.00	6/1	1.30	33.50	1026.84	1.000	All body	Field	424 ± 228	Elongated	Vertical
Ctenophore	Lobate ctenophore 3	57.00	7/1	1.30	33.50	1026.84	1.000	Pieces	Field	1175 ± 250	Elongated	Vertical
Pteropod	*Limacina helicina*	100.00	7/1	11.30	34.20	1026.12	1.000	All body	Lab.	1681 ± 149	Sphere	-
Thaliacean	*Pyrosoma atlanticum*	100.00	2/3	11.50	37.80	1028.89	0.998	All body	Lab.	1278 ± 133	Cylinder	Horizontal
Scyphozoan	*Periphylla periphylla*	100.00	2/1	11.50	37.80	1028.89	0.998	All body	Lab.	3892 ± 3005	Sphere	-
Pteropod	*Cymbulia peroni*	100.00	4/1	11.30	34.20	1026.12	1.001	All body	Lab.	2183 ± 548	Sphere	-
Scyphozoan	*Pelagia noctiluca*	100.00	3/1	11.50	37.80	1028.89	0.998	All body	Lab.	1102 ± 311	Ovoid	Vertical

[a] *n* indicates the number of individual carcasses sunk and *n*-sink how many times the carcasses were sunk. By multiplying *n* by *n*-sink we get the total number of sinking events done. For example, *Pyrosoma atlanticum* *n***n*-sink = 2*3 means that we sunk 2 different carcasses, 3 times each, while *Salpa thompsoni* *n***n*-sink = 15*1 means that we sunk 15 different carcasses, 1 time each.

[b] Air temperature in the laboratory was maintained at 10 °C, while in the field (Antarctica) it was between -0.16 and 1.30 °C. Salinity in the laboratory was established by adding NaCl to tap water starting at the lowest density, while in the field (Antarctica) we used in situ water.

[c] This is the field to laboratory density ratio to check that we mimicked closely field densities to avoid major deviations from reality by using artificial seawater.

Table 3.3. Summary of the temperatures [$T(z)$] and thermal gradients ($-K_T$) used to work out the jelly-POM export ratio $M(z_R):M(z_D)$ in three areas of the Atlantic Ocean.

Area	z_D = 200 m z_D = 600 m	200-400 m		400-600 m		600-800 m		800-1000 m		1000-1500 m		1500-2000 m		2000-2500 m		2500-3000 m	
	$T(z_D)$	$T(z_R)$	$-K_T$ [a]	$T(z_R)$	$-K_T$	$T(z_R)$	$-K_T$	$T(z_R)$	$-K_T$	$T(z_R)$	$-K_T$	$T(z_R)$	$-K_T$	$T(z_R)$	$-K_T$	$T(z_R)$	$-K_T$
Tropical	13.89	9.30	-0.0229	5.89	-0.0107	4.74	-0.0057	4.49	-0.0013	4.15	-0.0007	3.54	-0.0012	2.90	-0.0013	2.66	-0.0005
(9.63 °N - 52.36 °W)	5.89																
Temperate	17.19	15.05	-0.0107	11.99	-0.0153	8.02	-0.0199	6.07	-0.0097	4.11	-0.0039	3.69	-0.0008	3.51	-0.0004	3.04	-0.0009
(42.02 °N - 41.99 °W	11.99																
Polar (Antarctic)	-1.09	1.56	-0.013	1.36	-0.0010	1.23	-0.0007	1.037	-0.0010	0.77	-0.0005	0.62	-0.0003	0.38	-0.0005	0.27	-0.0002
(70.50 °S - 50.01 °W	1.36																

[a] $-K_T$ represents the thermal gradient coefficient of each interval *i* from one depth to the next (*see* text).

[*Cymbulia peroni* (*n* = 7) - Mediterranean Sea] (*see* Table 3.1 for seawater field conditions). All organisms were collected by plankton net, then frozen at - 20 °C and sent frozen to OceanLab, Jacobs University (Germany). We thawed organisms for 24 h at 5 °C (to prevent degradation) in a temperature-controlled room in the same water used in the column before each experimental day. All organisms were sunk as whole bodies (except *M. leidyi* that was sunk in small pieces) in a clear acrylic column 118.50 cm tall, with a diameter of 19 cm (volume = 30 L) in a temperature-controlled enclosure at 10 °C. The column was filled with freshwater at the beginning of each experimental day, and the salinity was established by adding NaCl to the lowest value resembling the field samples and then progressively increased to the highest value (*see* Table 3.1, 3.2). Corrections on density were made for temperature changes. At any field temperature, laboratory and field density values remained within 0.5 % (Table 3.2). Using this procedure we managed to mimic closely the field density conditions independently of seawater temperature. The water in the column was always left stabilizing between 15 and 30 minutes to avoid turbulence and eddies between different species sinking runs. However, owing to the high sinking speed observed in all cases, turbulence was not a major issue. In the case the same organism was sunk several times (*see* Table 3.2), we used a small net mounted on a metal frame to recover the material once arriving at the column base. We placed a 1 m ruler inside the column to have a dimension reference for post-video analyses. We also measured the exact water column height before each sinking event (Table 3.2). We recorded all sinking events with a video camera Canon Legria HF R16 mounted on an Erno P-55 tripod placed 1 m away from the column. All videos were analyzed with video software during terminal velocity on a straight line to assess sinking rate.

3.2.3. Material biochemical analyses

Immediately after the experiments concluded, we froze all organisms at -20 °C for 12 h inside Petri dishes and then freeze dried them continuously for 24 h at 60 °C. The samples were sent to the Helmholtz Centre for Ocean Research Kiel (GEOMAR) (Germany). Once there, two sub-samples from each organism were cut and dry weighted in a precision balance (*see* Table 3.1). The samples were then carefully introduced in tin vessels and closed for analysis. Organic carbon and nitrogen were measured in a Euro EA 3000 elemental analyzer with acetanilide standards at GEOMAR (Germany).

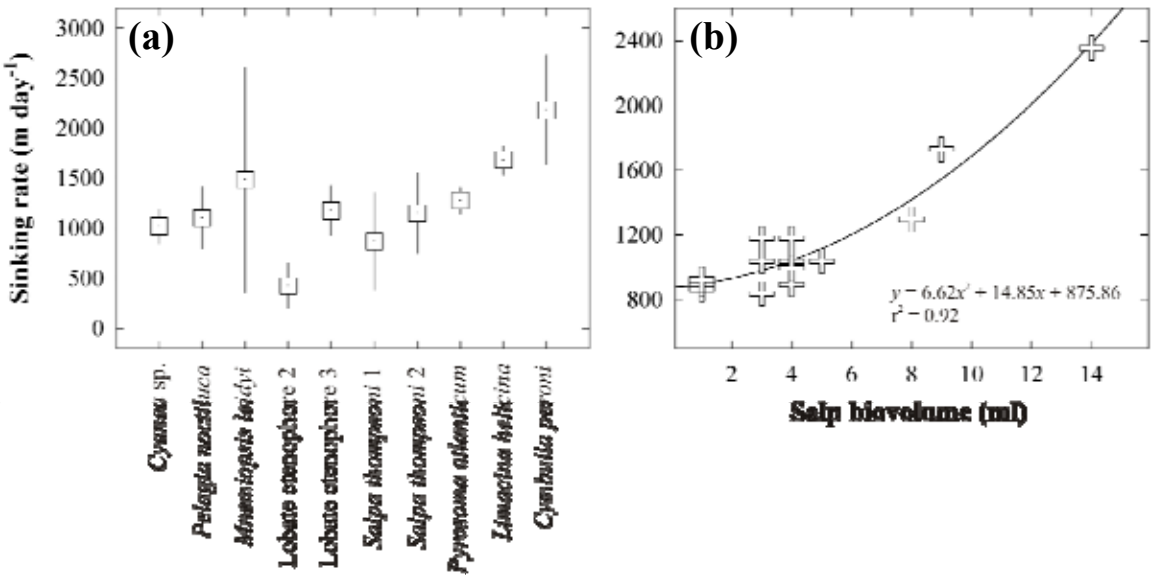

Fig. 3.1. (a) Sinking rate of all species studied except *Periphylla periphylla* (*see* Table 3.2). (b) Correlation of Antarctic salps (*Salpa thompsoni*) biovolume and sinking rate.

3.2.4. Taxonomic separation of the jelly-POM export ratio

In order to assess the jelly-POM export potential (thus organic carbon) using measured sedimentation rates, we used a newly developed export ratio calculation for gelatinous zooplankton biomass (Lebrato et al. 2011). In brief, jelly-POM remineralization can be explained by a first order kinetic decay constant as a function of temperature, independently of the material size (*see* Lebrato et al. 2011; Frost et al. 2012). This was used to develop a jelly-POM export ratio [$M(z_R)$:$M(z_D)$] relating an initial biomass [$M(z_D)$] sinking from a given depth z_D (called "death depth") with temperature $T(z_D)$, to a final proportion [$M(z_R)$] arriving at depth z_R with temperature $T(z_R)$. The terms z_R and $T(z_R)$ are the reference depth (or seabed) and temperature in the water column. The vertical position of z_D is driven by the population vertical migration and the organism life-history, which is species-specific (Franqueville 1971). Here, we chose two death depths (z_D) at 200 m (euphotic zone base) and 600 m (mesopelagic zone) following zooplankton biomass vertical migration distribution profiles in the north Atlantic (Roe et al. 1990). The jelly-POM export ratio was calculated by using a piecewise linear function dividing the depth ranges used (200-3000 m and 600-3000 m) into n discrete intervals (i = 200 m from 200 to 1000 m, and i = 500 m from 1000 to 3000 m) using the parameterization described in Lebrato et al. (2011) (*see* Table 3.3 for input data):

$$M(z_i):M(z_{i-1}) = e^{\left[\frac{-0.140\, e^{0.165\, T(z_{i-1})}}{0.145\, K_T(i)\, C}\left(e^{0.145\, K_T(i)\Delta z C} - 1\right)\right]} \quad (1)$$

The export ratio was calculated as the product of the individual decay ratios of all linear sections i:

$$M(z_R):M(z_D) = \prod_{i=1}^{n} M(z_i):M(z_{i-1}) \quad (2)$$

Raw temperature data were obtained from transects in the Atlantic Oceans from 0 to 3000 m [World Ocean Circulation Experiment data accessed at the Climate Variability and Predictability, and Carbon Hydrographic Data office from cruise line A16N (04 June-11 August 2003) and A16S (11 January-24 February 2005) in the Atlantic Ocean. We chose a temperate, tropical, and polar (Antarctic) area to divide the jelly-POM export ratio based on sinking speed taxonomic differences (Table 3.2) and the specific temperature profiles (Table 3.3).

3.3. Jelly-POM sinking speed and export

Large particles associated with blooms and jelly-falls have been rarely studied to date, and sinking rate data were scarce [salps: ~ 100 - 800 m day^{-1} (Moseley 1892, Apstein 1910), siphonophores: ~ 200 m day^{-1} (Apstein 1910)] (Table 3.4). The passive sinking rate of living (motionless) hydromedusae was also studied (Mills 1981) with rates between 500 and 1700 m day^{-1}, although the dynamics of dead carcasses are different from living biomass. Therefore, our study is the first comprehensive dataset on sinking speed that can be used in models to understand the jelly-POM carbon export efficiency. Jelly biomass sinks on average between 400 and 1500 m day^{-1} (Salps: 800-1700 m day^{-1}, Ctenophores: 500-1800 m day^{-1}, Scyphozoans: 1000-1100 m day^{-1}, Pyrosomes: 1200-1300 m day^{-1}) (Table 3.2; Fig. 3.1a). Exceptionally, they may sink much faster such as in the case of *Periphylla periphylla* (> 3500 m day^{-1}). In the case of Ctenophores, we found a large difference between sinking small pieces and the whole body (from 400 to > 1100 m day^{-1}), which is a consequence of the size per se. Seemingly, for the Antarctic *Salpa thompsoni*, biovolume correlates positively with sinking rate ($P < 0.01$, $r^2 = 0.92$) (Fig. 3.1b). This biovolume (thus size) effect on sinking rate is well known for faecal pellets (Bruland and Silver 1981) and it is applicable to other carcasses of increasing sizes.

However, the specific organism material density (Yamamoto et al. 2008), influenced by composition (*see* Table 3.1) may also influence the sinking speed. Another important factor is the carcass geometry and orientation adopted while sinking. The drag coefficient changes with material shape, therefore, carcasses resembling a sphere or an ovoid (scyphozoans and pyrosomes) tend to sink faster than those with an elongated shape that in many cases bears a mucous tail (ctenophores and salps). This causes an increasing drag that reduces the overall sinking rate. The shape concept is well known for phytoplankton cells, where deviations from an ideal sphere increase the drag coefficient (e.g. elongated, with spicules), and thus delay sedimentation (Walsby and Xypolyta 1977; Berelson 2002; De La Rocha et al. 2008). In faecal pellets, model formulations of spherical (standard Stokes' Law) *vs.* cylindrical particles (Komar 1980 equation at low Reynolds number) explain differences in sinking rates in the field (McDonnell and Buesseler 2010). This applies to gelatinous zooplankton carcasses of contrasting shape (a ~ spherical scyphozoan *vs.* an ~ elliptical pyrosomid) (*see* Table 3.2). The increasing shape complexity affecting fluid dynamics has been studied in gelatinous zooplankton during vertical displacement (Katija and Dabiri 2009). Liquid displacement and resistance are not analogous to sinking carcasses (mainly driven by gravity and density rather than by muscular propulsion), but the shape complexity reveals a negative correlation in drift volume from a sphere (e.g. ~ scyphozoan) to an ellipsoid (e.g. ~ pyrosomid). Changes induced during remineralization (C/N ratio) can also affect the sinking rate as a consequence of decay rate (*see* also chapter 4). Salp faecal material incubated at 22 °C for 1 day and then at 5 °C for 9 days (resembling a transition from the euphotic to the bathypelagic zone) experienced sinking rate changes between 11 and 46 % of the initial one (decrease of sinking speed with depth) (Caron et al. 1989). During jelly-POM decay incubations, the biomass C/N ratio quickly increases during the first 3 to 5 days (Titelman et al. 2006) owing to a preferential hydrolysis of N-compounds with respect to C (Thomas et al. 1999; Anderson and Pondaven 2003; Pitt et al. 2009) as in marine snow (Smith et al. 1992). After a few days, the C/N ratio decreases as C-compounds are hydrolysed, while the whole process is temperature dependant following total biomass decay (Lebrato et al. 2011). This could slightly decrease the sinking rate with depth, although the overall large speeds observed here for some species prevent major remineralization until biomass reaches the seabed. Field evidence suggest that jelly-POM reaches the seabed in shelves and slopes from 200 to > 3000 m (*see* Lebrato et al. 2012 for a review).

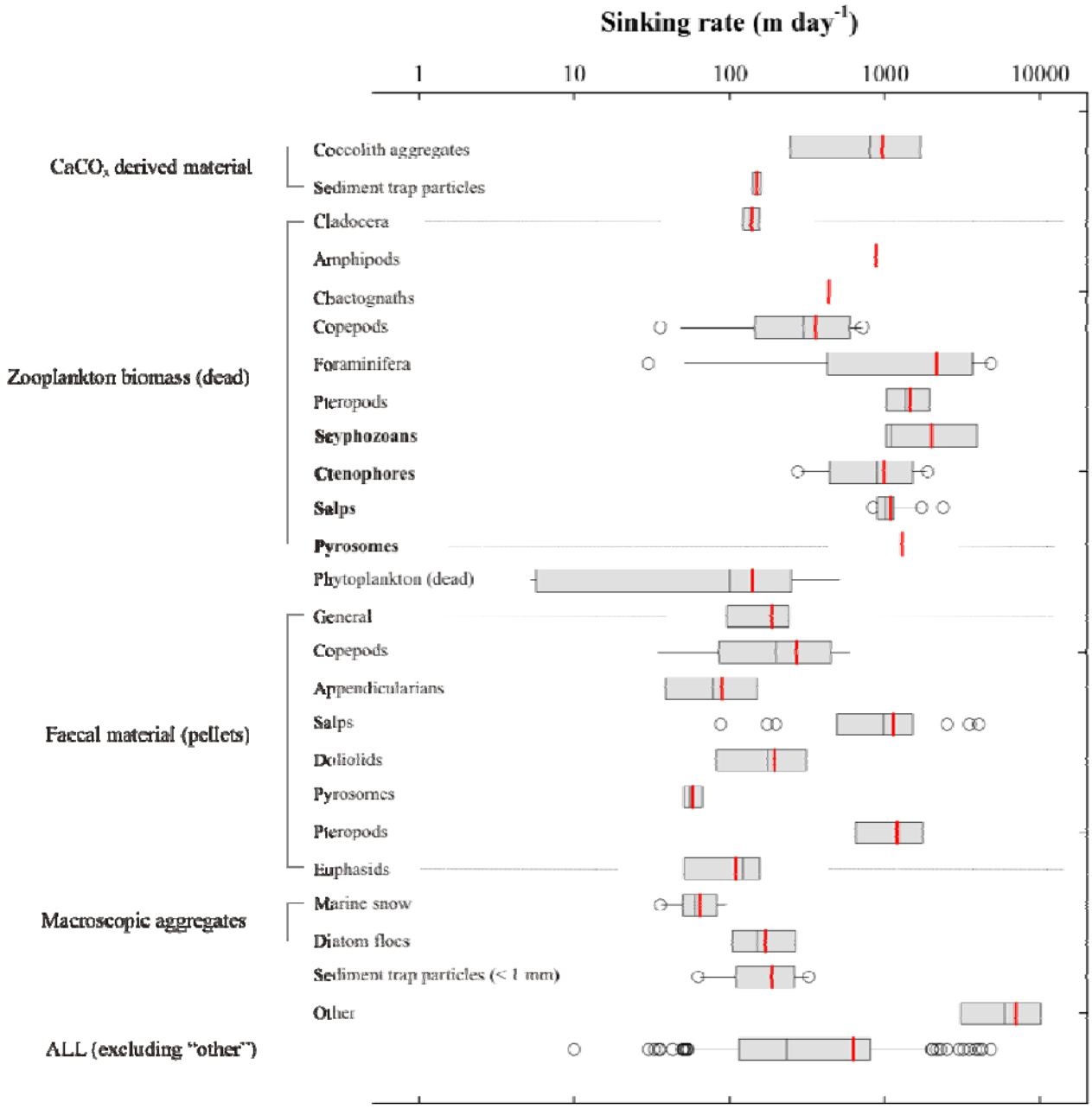

Fig. 3.2. Box and whisker plots of a selection of sinking rates for different marine materials/organisms (*see* Table 3.4 for details). The ends of each bar represent the 5th and 95th percentiles for all the data analyzed. The ends of each box represent the lower and upper median while the solid line in the box represents the main median. The red line indicates the grand mean. The data points outside the 5th and 95th percentile are plotted as empty circles.

Phytoplankton cells (except coccolithophores) and marine snow/aggregates sink in many cases much slower than jelly-POM (near one order of magnitude) (Fig. 3.2). Carcasses from other organisms sink slower than gelatinous zooplankton [cladocerans: ~ 140 m day^{-1}, amphipods: ~ 900 m day^{-1}, chaetognaths: ~ 400 m day^{-1}, copepods: 30 - 700 m day^{-1} (Apstein 1910; Kuenen 1950)] (*see* Table 3.4; Fig. 3.2). The pellets from the living gelatinous organisms sink in some cases faster than their own carcasses, but in others not (*Salpa fusiformis*: 500 - 4000 m d^{-1},

Pegea socia: > 2000 m d^{-1}, *Salpa maxima*: > 1700 m d^{-1}, *Salpa thompsoni*: 200 - 1400 m d^{-1}, *Iasis zonaria*: > 900 m d^{-1}) (Bruland and Silver 1981; Madin 1982; Phillips et al. 2009).

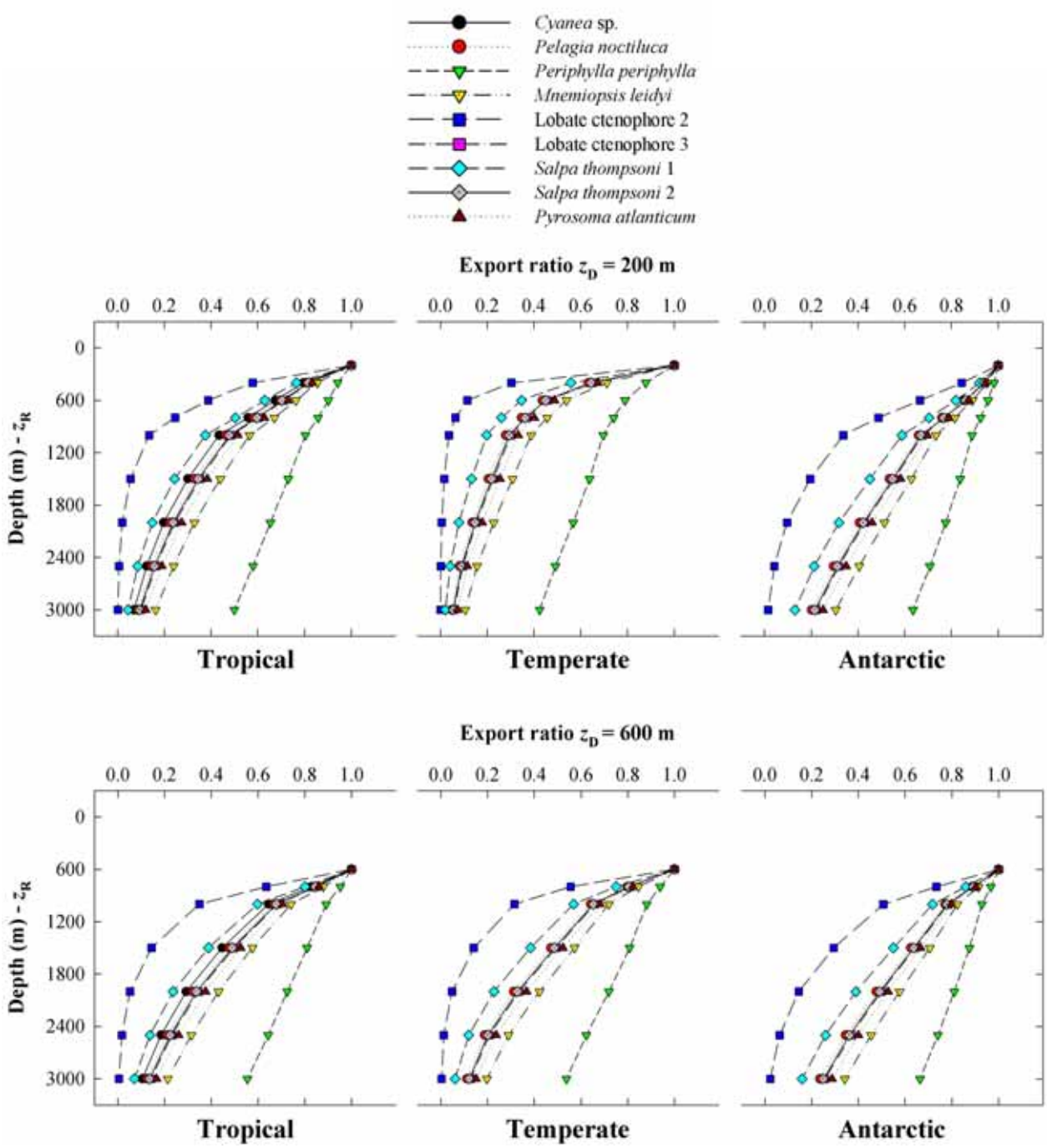

Fig. 3.3. Results from the simulation of the jelly-POM export ratio $M(z_R)$:$M(z_D)$ for three major areas in tropical, temperate and polar (Antarctic) latitudes. A matrix of 6 and 8 depth intervals between the sinking depth (z_D = 200 and 600 m) and the reference depth (z_R = 100, 200, 500, 1000, 3000, and 5000 m) and 5 sinking velocities (C) (100, 300, 500, 800, and 1500 m day^{-1}) was used.

The sinking rates described here can be used to constraint the jelly-POM formulation of the export ratio proposed by Lebrato et al. (2011) using a correlation of decay rate and temperature. This allows to differentiate taxonomically the carbon export capabilities. In general, jelly-POM

has a lower C/N ratio than other zooplankton groups (C and N are ~ 20 % lower on average), below 5 mol/mol (Table 3.1) (*see* Lucas et al. 2011). There are exceptions though, such as in thaliaceans and some scyphozoans, where the C/N remains between 5 and 6 mol/mol and organic carbon can vary from 15 to ~ 30 %. Sinking speed exerts a major control on jelly-POM and carbon export to depth owing to the quick decay of the material following temperature gradients above the thermocline (Lebrato et al. 2011). In their study, simulations using a death depth (z_D) = 0 m and reference depth (z_R) = 1000 m in the temperate Atlantic Ocean, and an increasing sinking speed matrix, increased the jelly-POM export ratio at 1000 m from 0.05 using 100 m day^{-1} to 0.65 using 1500 m day^{-1}. Using the sinking rate divided by taxa described here, we compared export to z_R = 3000 m by using a z_D = 200 and 600 m. Overall, we found that except in extreme cases [very low or high sinking speed: Lobate ctenophore 2 (whole body) = 424 m day^{-1}, and *P. periphylla* = 3892 m day^{-1}], there was a general remineralization profile for all gelatinous zooplankton species at any latitude (tropical, temperate or polar) (Fig. 3.3). Using z_D = 200 m, in tropical and temperate latitudes, the major remineralization occurred down to 1500 m where the export ratio was 0.25-0.44, and 0.14-0.31 respectively (range including all species). It then decreased at 3000 m to 0.05-0.17, and 0.02-0.11 respectively. In polar latitudes (Antarctic), the export ratio remained above 0.45 in any species at 1500 m, and above 0.13 at 3000 m. When using z_D = 600 m, the tropical and temperate latitudes export ratio at 1500 m increased to 0.39-0.58 and 0.38-0.57 respectively, and at 3000 m it increased to 0.07-0.21 and 0.06-0.19 respectively. In Antarctic conditions, it increased to 0.55-0.70 at 1500 m and to 0.15-0.34 at 3000 m. For comparison, sediment trap POC fluxes normalized to 150 m (export ratio) in the tropical and sub-arctic Pacific were ~ 0.35 and 0.70 at 300 m and 0.25 and 0.50 at 500 m respectively (Buesseler et al. 2007). These remineralization profiles were similar to our tropical and temperate jelly-POM export ratios for the same depths (*see* Fig. 3.3). Conversely, our polar estimations (0.93-0.95 at 400 m and 0.81-0.89 at 600 m) were above sediment trap estimations. This means, that at least in polar latitudes, the strength of the jelly-mediated carbon export is higher than smaller particles, sequestering carbon to deeper water layers. High latitudes provide a fast-sinking corridor for jelly-POM, where material may be quickly exported to depth, while in tropical and temperate settings major remineralization takes place in the first 1500 m, unless biomass starts sinking from below the thermocline. The biomass vertical distribution exerts a major control beyond sinking speed, governing the start of remineralization and therefore driving the thermal gradient encountered. This information in combination with taxa-specific sinking speed, global biomass biogeography (Condon et al. 2012), and the export ratio (Lebrato

et al. 2011), should be used to assess the strength of the biological pump (Buesseler and Boyd 2009) including jelly-POM. This will certainly enhance carbon export predictions from the upper ocean derived from biogeochemical models that expand to gelatinous zooplankton compartments.

Table 3.4. A selection of sinking rates from published abiogenic an biogenic material used in Fig. 3.2.

Material	Organism/description [a]	Size (mm) [b]	Sinking rate (m day^{-1}) [c]	Temp. (°C)	Location	Reference
			$CaCO_3$-derived material n = 5			
Coccolith aggregates	*Emiliania huxleyi*	-	432 - 2160	17	north Atlantic)	Biermann and Engel 2010
Coccolith aggregates	*Emiliania huxleyi*	1.67	246	15	-	Ploug et al. 2008
Coccolith aggregates	Aggregate of *S. costatum/E. huxleyi*	2.02	125	15	North Sea	Ploug et al. 2008
Sediment trap particles	Coccolithophores faecal pellets	-	150	-	east Pacific Ocean	Honjo 1976
Sediment trap particles	*Syracosphaera pulchra*	-	137 - 162	-	north Atlantic Ocean	Knappertsbusch and Brummer 1995
			Dead/carcasses zooplankton n = 15			
Dead cladocera	-	-	120 - 160	16.40	-	Apstein 1910
Dead amphipoda	-	-	875	16.40	-	Apstein 1910
Dead chaetognatha	-	-	435	16.40	-	Apstein 1910
Dead copepoda	-	-	36 - 720	-	-	Apstein 1910
Dead copepoda	*Temora* sp.	-	257.91	16.40	-	Apstein 1910
Dead copepoda	*Pseudocalanus* sp.	-	144.06	16.40	-	Apstein 1910
Dead foraminifera	-	0.50	30 - 4800	-	-	Kuenen 1950
Dead larvacean	*Oikopleura* sp.	-	32.91	16.40	-	Apstein 1910
Dead pteropoda	-	-	760 - 2270	-	-	Vinogradov 1961
Dead pteropoda	*Limacina* sp.	-	1100	-	-	Vinogradov 1961
Dead radiolarians	-	0.50	350	-	-	Kuenen 1950
Dead salpa	-	10	165 - 263	16.40	-	Apstein 1910
Dead salpa	-	76.20	864	-	-	Moseley 1892
Dead salpa	*Salpa mucronata*	-	124.67	16.40	-	Apstein 1910
Dead siphonophora	-	-	240	16.40	-	Apstein 1910
			Dead phytoplankton n = 5			
Phytoplankton	-	-	1 - 510	-	-	Smayda 1969
Phytoplankton	*Planktothrix* sp.	1.74×10^{-4}	5.90	-	lab (isolated in a lake)	Walsby and Holland 2006
Phytoplankton	*Planktothrix* sp.	1.64×10^{-4}	5.42	-	lab (isolated in a lake)	Walsby and Holland 2006
Phytoplankton	*Planktothrix* sp.	1.73×10^{-4}	5.18	-	lab (isolated in a lake)	Walsby and Holland 2006
Phytoplankton	*Skeletonema costatum*	2.51	113	15	-	Ploug et al. 2008

			Faecal material n = 39			
Faecal pellets	-	1.06×10^{-4}	80	15	north Atlantic Ocean	Smayda 1970
Faecal pellets	-	1.2×10^{-4}	96	15	north Atlantic Ocean	Smayda 1970
Faecal pellets	-	1.33×10^{-4}	140	15	north Atlantic Ocean	Smayda 1970
Faecal pellets	-	1.46×10^{-4}	189	15	north Atlantic Ocean	Smayda 1970
Faecal pellets	-	1.60×10^{-4}	189	15	north Atlantic Ocean	Smayda 1970
Faecal pellets	-	1.73×10^{-4}	240	15	north Atlantic Ocean	Smayda 1970
Faecal pellets	Copepod (fed *Rhodomonas* sp.)	-	35	16	North Sea	Ploug et al. 2008
Faecal pellets	Copepod (fed *T. weissfloggi*)	-	322	17	North Sea	Ploug et al. 2008
Faecal pellets	Copepod (fed *E. huxleyi*)	-	200	18	North Sea	Ploug et al. 2008
Faecal pellet and houses	*Oikopleura dioica*	8×10^{-4}	30	4	Mediterranean Sea	Gorsky et al. 1984
Faecal pellet and houses	*Oikopleura dioica*	8×10^{-4}	90	15	Mediterranean Sea	Gorsky et al. 1984
Faecal pellet and houses	*Oikopleura dioica*	8×10^{-4}	170	24	Mediterranean Sea	Gorsky et al. 1984
Faecal pellet and houses	*Oikopleura dioica*	8×10^{-4}	65	14	Mediterranean Sea	Gorsky et al. 1984
Faecal pellets	Copepods	-	100 - 600	-	Mediterranean Sea	Small et al. 1979
Faecal pellets	*Salpa fusiformis/Pegea socia*	-	500 - 4000	-	north Pacific Ocean	Bruland and Silver 1981
Faecal pellets	*Corolla spectabilis*	-	500 - 2000	-	north Pacific Ocean	Bruland and Silver 1981
Faecal pellets	*Dolioletta gegenbaurii*	-	50 - 200	-	north Pacific Ocean	Bruland and Silver 1981
Faecal pellets	*Dolioletta gegenbaurii*	-	59 - 405	18	north Atlantic Ocean	Deibel 1990
Faecal pellets	*Pegea socia* (solitary)	2 - 2.20	2022	25	north Atlantic Ocean	Madin 1982
Faecal pellets	*Cyclosalpa pinnata* (aggregation)	1- 3	588	25	north Atlantic Ocean	Madin 1982
Faecal pellets	*Pegea socia* (aggregation)	0.30 - 1	850	25	north Atlantic Ocean	Madin 1982
Faecal pellets	*Salpa maxima* (aggregation)	3 - 7	1702	25	north Atlantic Ocean	Madin 1982
Faecal pellets	*Salpa thompsoni*	0.50 - 3.50	200 - 1400	-0.6 - 3.4	Southern Ocean	Phililips et al. 2009
Faecal pellets	*Pyrosoma atlanticum*	50 - 65	70	23	east Atlantic Ocean	Drits et al. 1992
Faecal pellets	*Pyrosoma atlanticum*	50 - 65	57.20	23	east Atlantic Ocean	Drits et al. 1992
Faecal pellets	*Pyrosoma atlanticum*	50 - 65	54	8	east Atlantic Ocean	Drits et al. 1992
Faecal pellets	*Pyrosoma atlanticum*	50 - 65	49.40	8	east Atlantic Ocean	Drits et al. 1992
Faecal pellets	Copepoda	0.35	69.90	18	east Atlantic Ocean	Yoon et al. 2001
Faecal pellets	Euphasiacea	1.33	50.80	18	east Atlantic Ocean	Yoon et al. 2001
Faecal pellets	Euphasiacea	1.51	122.30	18	east Atlantic Ocean	Yoon et al. 2001
Faecal pellets	Euphasiacea	1.48	155.20	18	east Atlantic Ocean	Yoon et al. 2001

Faecal pellets	*Carinaria* sp.	-	231.10	18	east Atlantic Ocean	Yoon et al. 2001
Faecal pellets	*Clio* sp.	1.10	119.30	18	east Atlantic Ocean	Yoon et al. 2001
Faecal pellets	*Salpa fusiformis*	0.61	87.10	18	east Atlantic Ocean	Yoon et al. 2001
Faecal pellets	*Cyclosalpa affinis*	2.27	356.60	18	east Atlantic Ocean	Yoon et al. 2001
Faecal pellets	Salp	1.17	173.30	18	east Atlantic Ocean	Yoon et al. 2001
Faecal pellets	Salp	1.04	383.50	18	east Atlantic Ocean	Yoon et al. 2001
Faecal pellets	*Iasis zonaria*	1.58	992.60	18	east Atlantic Ocean	Yoon et al. 2001
Faecal pellets	*Salpa maxima*	1 - 4	950	22	north Atlantic Ocean	Caron et al. 1989
Faecal pellets	*Salpa maxima*	1 - 4	2470	22	north Atlantic Ocean	Caron et al. 1989
Faecal pellets	*Salpa maxima*	1 - 4	2170	22	north Atlantic Ocean	Caron et al. 1989
Faecal pellets	*Salpa cylindrica*	1 - 4	490	22	north Atlantic Ocean	Caron et al. 1989
Faecal pellets	*Pegea socia*	1 - 4	460	22	north Atlantic Ocean	Caron et al. 1989
Faecal pellets	*Pegea socia*	1 - 4	460	22	north Atlantic Ocean	Caron et al. 1989
Faecal pellets	*Pegea socia*	1 - 4	980	22	north Atlantic Ocean	Caron et al. 1989
Faecal pellets	*Pegea socia*	1 - 4	1670	22	north Atlantic Ocean	Caron et al. 1989
Faecal pellets	*Pegea bicaudata*	1 - 4	650	22	north Atlantic Ocean	Caron et al. 1989
Faecal pellets	*Pegea bicaudata*	1 - 4	1410	22	north Atlantic Ocean	Caron et al. 1989
Faecal pellets	*Pegea bicaudata*	1 - 4	1500	22	north Atlantic Ocean	Caron et al. 1989
Faecal pellets	*Pegea confoederata*	1 - 4	300	22	north Atlantic Ocean	Caron et al. 1989
Faecal pellets	*Pegea confoederata*	1 - 4	1040	22	north Atlantic Ocean	Caron et al. 1989
Faecal pellets	*Cyclosalpa affinis*	1 - 4	650	22	north Atlantic Ocean	Caron et al. 1989
Faecal pellets	*Cyclosalpa affinis*	1 - 4	570		north Atlantic Ocean	Caron et al. 1989
Faecal pellets	*Cyclosalpa affinis*	1 - 4	1290		north Atlantic Ocean	Caron et al. 1989
Faecal pellets	*Brooksia rostrata*	1 - 4	1040	22	north Atlantic Ocean	Caron et al. 1989
Faecal pellets	*Ihlea punctata*	1 - 4	530	22	north Atlantic Ocean	Caron et al. 1989
			Aggregates $n = 15$			
Macroscopic aggregates	Marine snow	2	53	-	north Pacific Ocean	Shanks and Trent 1980
Macroscopic aggregates	Marine snow	3	60	-	north Pacific Ocean	Shanks and Trent 1980
Macroscopic aggregates	Marine snow	3	52	-	north Pacific Ocean	Shanks and Trent 1980
Macroscopic aggregates	Marine snow	4	95	-	north Pacific Ocean	Shanks and Trent 1980
Macroscopic aggregates	Marine snow	5	78	-	north Pacific Ocean	Shanks and Trent 1980

Macroscopic aggregates	Marine snow	17	95	-	north Pacific Ocean	Shanks and Trent 1980
Macroscopic aggregates	Marine snow	11	43	-	north Pacific Ocean	Shanks and Trent 1980
Macroscopic aggregates	Marine snow	1	78	-	north Pacific Ocean	Shanks and Trent 1980
Macroscopic aggregates	Marine snow	4	60	-	north Pacific Ocean	Shanks and Trent 1980
Macroscopic aggregates	Marine snow	4 - 5	1	-	east Pacific Ocean	Asper 1987
Macroscopic aggregates	Marine snow	1 - 2.50	36	-	east Pacific Ocean	Asper 1987
Macroscopic aggregates	Diatom aggregates	-	100 - 150	-	north Atlantic Ocean	Billett et al. 1983
Macroscopic aggregates	Diatom flocs	-	117	-	east Pacific Ocean	Alldredge and Gotschalk 1989
Macroscopic aggregates	Diatom aggregates	-	288	-	Southern Ocean	Asper and Smith 2003
Macroscopic aggregates	Diatoms-Flagellates aggregates	2 - 16	0 - 300	-	North Sea	Riebesell 1992
			Sediment traps $n = 10$			
Sediment trap (< 1 mm)	All (mean)	-	326	-	north Atlantic Ocean	Fischer and Karakas 2009
Sediment trap (< 1 mm)	All (mean)	-	299	-	east Atlantic Ocean	Fischer and Karakas 2009
Sediment trap (< 1 mm)	All (mean)	-	211	-	west Atlantic Ocean	Fischer and Karakas 2009
Sediment trap (< 1 mm)	All (mean)	-	117	-	south Atlantic Ocean	Fischer and Karakas 2009
Sediment trap (< 1 mm)	All (mean)	-	157	-	Southern Ocean	Fischer and Karakas 2009
Sediment trap (< 1 mm)	All (mean)	-	235	-	east Atlantic Ocean	Fischer and Karakas 2009
Sediment trap (< 1 mm)	All (winter-spring)	-	63	-	east Atlantic Ocean	Fischer and Karakas 2009
Sediment trap (< 1 mm)	All (summer)	-	250	-	east Atlantic Ocean	Fischer and Karakas 2009
Sediment trap (< 1 mm)	All (winter spring)	-	90	-	east Atlantic Ocean	Fischer and Karakas 2009
Sediment trap (< 1 mm)	All (summer)	-	120	-	east Atlantic Ocean	Fischer and Karakas 2009
			Other $n = 6$			
Synthetic	Mineral (anthracite)	1.32	4752	-	laboratory	Baldock et al. 2004
Particle	Beach sand grain	0.22	1987	-	laboratory	Baldock et al. 2004
Particle	Beach sand grain	0.32	3456	-	laboratory	Baldock et al. 2004
Particle	Filter sand	0.66	7171	-	laboratory	Baldock et al. 2004
Particle	Filter sand	0.78	8121	-	laboratory	Baldock et al. 2004
Particle	Gravel	2.42	16243	-	laboratory	Baldock et al. 2004

[a] Detailed description of the material and data used. When nothing stated should refer to the original citation or otherwise the description in the 1st column applies.

[b] Size only indicates a representative measurement of width/length and in some cases diameter (when applicable) for comparison. It does not allow to study sinking rate vs. size (it would need a normalization to volume according to shape. Additionally, all types of material are not comparable based only on size) (*see* Bruland and Silver 1981, Deibel 1990, Fortier et al. 1994 for analysis of sinking velocity vs. volume).

[c] Sinking rates were retrieved in some cases directly from a graph or a range. In many cases they have been normalized from other units (e.g. cm s^{-1}, m s^{-1}) to m day^{-1} to allow for broad comparisons.

4.

Depth attenuation of organic matter export associated with jelly falls

Abstract

We explore the attenuation in the export ratio of jelly-POM (particulate organic matter) with depth as a function of the decay rate, temperature, and sedimentation rate. Using data from the Vertical Transport In the Global Ocean project (VERTIGO) we compare ratios computed with the Martin-curve, with a particle-based parameterization, and with sediment trap data. Owing to the temperature dependence of the decay rate (Q_{10} = 4.28), the jelly-POM export ratio below 500 m is 20-45% larger in subpolar and temperate areas than in the tropics. Vertical migration of gelatinous zooplankton leads to a variable starting depth of a jelly fall (death depth), which governs the start of remineralization, and the fate of the biomass. Owing to the absence of observations, we employ a sinking speed matrix ranging from 100 to 1500 m day^{-1} to represent slow and fast sinking carcasses. The assumption of a constant decay rate k independent of temperature in other particle-based models may not be appropriate. These results provide information for including jelly-POM in global biogeochemical model formulations.

This chapter is based on:

Lebrato, M., Pahlow, M., Oschlies, A., Pitt, K. W., Jones, D. O. B., Molinero, J-C. and Condon, R. H. 2011. Depth attenuation of organic matter export associated with jelly-falls. In: *Limnology and Oceanography* 56: 1917-1928.

Acknowledgements: This work was funded by the Kiel Cluster of Excellence 'The Future Ocean' (D1067/87), and also by the 'European project on Ocean Acidification' (which received funding from the European Community's Seventh Framework Programme (FP7/2007-2013) under grant agreement 211384) to ML. We thank anonymous reviewers for their comments, which improved the final version of this paper.

4.1. Introduction

4.1.1. Particulate and gelatinous material export

Vertical fluxes of biogenic and particulate organic matter (POM) govern chemical gradients and thus drive the ocean's biological carbon pump. Sinking POM varies in size and composition, originating in every trophic level as exudates, detritus, fecal material, aggregates, biogenic carbonates or the carcasses of the organisms themselves (Turner 2002). The remineralization profile of POM generally depends on the sinking speed (McDonnell and Buesseler 2010) and the decay rate (Martin et al. 1987). The contribution of gelatinous zooplankton to POM export has been assessed for detrital particles and fecal pellets (Turner 2002). The fate of the biomass of gelatinous organisms (jelly-POM), mainly from Cnidaria and Thaliacea, however, has been rarely assessed and thus not included in biogeochemical models. Yet, there is substantial evidence of sedimentation events in the last decades, so called ‘jelly falls’, that can deposit large amounts of biomass on the seafloor (Lebrato and Jones 2009). Remineralization of gelatinous material releases dissolved organic matter (jelly-DOM), creating a ‘jelly carbon shunt’ (Condon et al. 2011). Inorganic nutrients are also released (Pitt et al. 2009) and oxygen is consumed (West et al. 2009b). Thus, remineralization of jelly falls has broad biogeochemical implications, similar to other sinking particles, although the different biochemical composition (C/N/P) and the absence of mineral ballast imply different stoichiometric relationships.

4.1.2. Jelly-POM representation in biogeochemical models

The parameterisation of sinking organic matter in regional and large-scale biogeochemical models has evolved from the early use of static remineralization profiles, and the depth dependence of the flux of sinking particles. Recent work on sinking particles, covering a size range of about 1-1000 μm, is not truly applicable for the size spectrum of particles found in jelly falls (millimeters to meters). The sedimentation of POM has been modeled using constant rates or an acceleration with depth, which can be related to the Martin et al. (1987) formulation. Observations of sinking material are limited to particles whose size fractions are small enough (< 1 mm to ~ 50 mm) to be collected by sediment traps. However, larger particles (such as those associated with jelly falls) have rarely been investigated [salps: ~ 100-800 m d^{-1}, siphonophores: ~ 200 m d^{-1} (Apstein 1910)]. Information on carcasses from other organisms could give an

indication of jelly-POM sinking rates [e.g. cladocerans: ~ 140 m d^{-1}, amphipods: ~ 900 m d^{-1}, chaetognaths: ~ 400 m d^{-1}, copepods: 30-700 m d^{-1} (Kuenen 1950)]. The sedimentation rate of jelly-POM is governed by a combination of size, diameter, biovolume, and geometry (Walsby and Xypolyta 1977), material density (Yamamoto et al. 2008), and drag coefficients (McDonnell and Buesseler 2010). For large gelatinous carcasses (e.g. 100-200 kg *Nemopilema nomurai* carcasses) the weight per se dominates over any other forcing. Owing to their size, gelatinous carcasses sink individually, and do not coagulate as smaller particles do. Coagulation may occur during decomposition, however, when the material accumulates in high densities, forming mats at the seabed (Billett et al. 2006).

Although scyphozoans and thaliaceans sometimes occur on the seabed in enormous numbers, other gelatinous taxa, such as ctenophores and hydrozoans have never been observed. This implies that the transfer efficiency of gelatinous biomass varies among taxa. The attenuation concept (Buesseler and Boyd 2009) motivated the current study. Here we examine the remineralization of gelatinous biomass to assess the fraction arriving at a given reference depth and/or at the seafloor (jelly-POM export ratio). In the following, we present a model parameterization describing two processes: The relationship between water column temperature and decay rate [$k_{(T)}$] for gelatinous material, and hence a temperature-dependent remineralization time scale (referred to as $t_{0.01}$), and a jelly-POM export ratio [$M(z_R)$:$M(z_D)$], e.g. the proportion of jelly-POM originating from a death depth z_D and arriving at a reference depth z_R while sinking at constant velocity. Owing to the lack of empirical data, we consider a spectrum of sinking rates from 100 to 1500 m day^{-1}, representing different jelly-POM functional groups and size classes. A novel aspect is the use of POM remineralization profiles as a function of the vertical thermal gradient, which can be expanded to other kinds of particles. We also extend the parameterization of Kriest and Oschlies (2008) by varying the decay rate (k), and examining a sinking speed matrix of 20 to 2000 m day^{-1} to represent gelatinous biomass. The modeled jelly-POM export ratio is compared with that predicted by the Martin curve (Martin et al. 1987) using field data from the Vertical Transport In the Global Ocean (VERTIGO) project (Buesseler et al. 2007). Model-data and model-model differences are analysed to establish the theoretical grounds for further exploration of the jelly-POM remineralization concept.

4.2. Methods

4.2.1. Decay rate (k) and remineralization times scale ($t_{0.01}$)

At any given temperature the initial decomposition of thaliacean and cnidarian carcasses by bacteria is followed by a progressive decrease in the remineralization rate attributed to a loss in lability of the jelly-material. During experimental work, > 80% of the carbon and nitrogen are remineralized within 5 to 8 days (Titelman et al. 2006). This indicates the lack of a refractory organic matter pool (negligible contribution) that would justify the use of a second order kinetic decay constant. Salps have a larger C/N than scyphozoans (Lucas et al. 2011) that could delay remineralization, but the decay rate seems to be comparable across groups as a function of temperature (Q_{10} = 4.28 using experimental initial and final temperatures) (Table 1). Therefore, the assumption of a single first order kinetic decay constant for all gelatinous biomass may be justified (Table 4.1; Fig. 4.1a). In this model, the decay rate at time t is the product of mass and the first-order decay constant k, which is a function of temperature. A second assumption owing to the lack of empirical data is a size-independent decay rate of jelly-POM as observed for macroaggregates (Ploug and Grossart 2000) and assumed in other models. The differential equation for jelly-POM biomass M is:

$$dM/dt = -M\, k_{(T)} \tag{1}$$

with

$$k_{(T)} = 0.140 \text{ day}^{-1}\, e^{0.145T(z)} \tag{2}$$

where M is the jelly-POM at time t, $k_{(T)}$ is the temperature-dependent decay rate (in day^{-1}), and $T(z)$ is temperature in °C at depth z. The coefficients in Eq. 2 were obtained from empirical observations (Fig. 4.1a). For constant temperature (T) Eq. 1 has the following solution:

$$M_1 = M_0\, e^{-k_{(T)}t} \tag{3}$$

where M_0 and M_1 are initial and final biomass at time t.

Table 4.1. Data for the decay rate (k) *vs.* temperature relationship used in Eq. 2.

Organism	Species	Weight (g)	Depth (m)	Exp. temp. (°C)	k [a]	Reference
Scyphozoan	*N. nomurai*	955	2.5	8	0.513	Iguchi et al. 2006 [c]
Scyphozoan	*N. nomurai*	884	10 [b]	2.7 [b]	0.215	Iguchi et al. 2006 [c]
Scyphozoan	*P. periphylla*	300	8	12.5	0.844	Titelman et al. 2006
Scyphozoan	*P. periphylla*	223	1	10.1	0.666	Titelman et al. 2006
Scyphozoan	*P. periphylla*	121	1	10	0.716	Titelman et al. 2006
Salpa	*T. democratica*	-	1	16.5	1.600	Sempere et al. 2000

[a] The temperature coefficient Q_{10} [$Q_{10} = (R_2/R_1)^{(10/T2-T1)}$], where R is reaction rate, and T is temperature, varies between 4 and 5.20 depending on the pairs used. $Q_{10} = 4.28$ using the initial (2.7°C) and final temperature (16.5°C).
[b] Intake water from 334 m into a tank at 10 m depth (therefore microbial population retained).
[c] Full citation in http://jsnfri.fra.affrc.go.jp/Kurage/kurage_hp18/Sado_bunkai.pdf

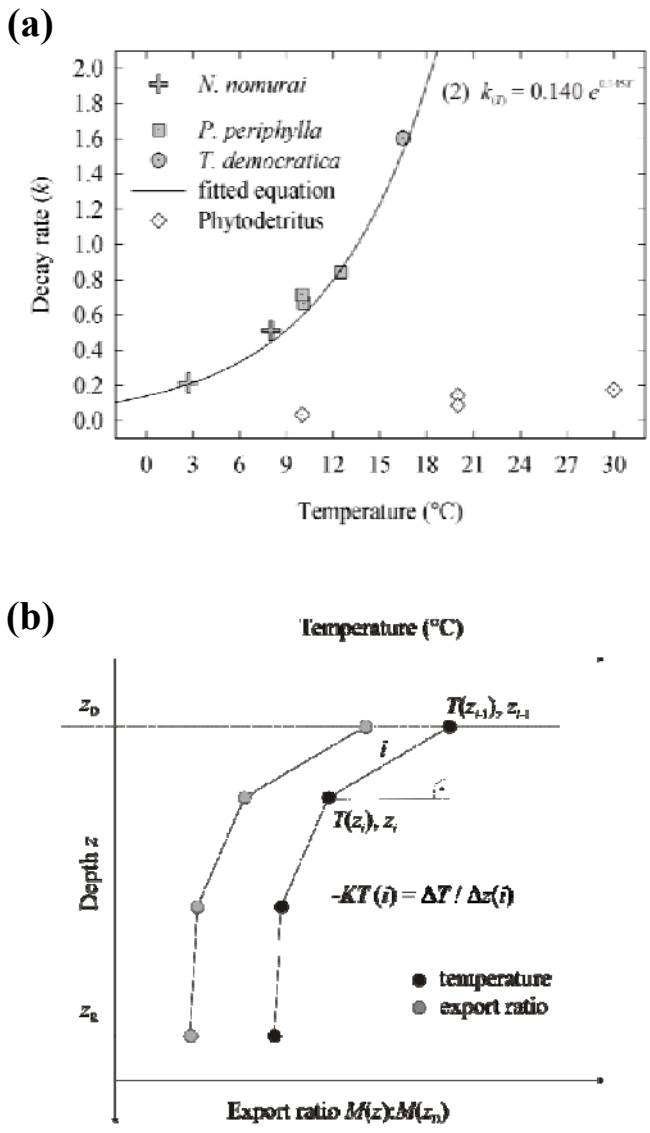

Fig. 4.1. (a) Parameterization of the decay rate [$k_{(T)}$] of jelly-POM and temperature. Also, k data of phytodetritus (Sudo et al. 1978; Fujii et al. 2002)]. (b) Piecewise linear calculation of the export ratio. The depth range between z_D and z_R is divided into intervals bounded by z_{i-1} and z_i, within which a linear thermal gradient $K_T(i)$ is assumed.

We define the remineralization time scale $t_{0.01}$ (in days) as the time takes for 99% of the initial biomass to decompose at a specific temperature:

$$t_{0.01} = -\ln (0.01) / k_{(T)} \quad (4)$$

with $k_{(T)}$ given by Eq. 2, we obtain:

$$t_{0.01} = -\ln (0.01) / (0.140\ \text{day}^{-1}\ e^{0.145T_{(z)}}) \quad (5)$$

Temperature data were obtained from transects in the Atlantic and Pacific Oceans from 0 to 6000 m [World Ocean Circulation Experiment data accessed at the Climate Variability and Predictability, and Carbon Hydrographic Data office from cruise line A16N (04 June-11 August 2003) and A16S (11 January-24 February 2005) in the Atlantic and P16N (13 February to 29 March 2006) and P16S (09 January to 19 February 2005) in the Pacific]. Data were gridded using a

minimum curvature method with 62 field lines in the x-axis (latitude) and 129 field lines in the z-axis (depth) from 60°N to 60°S and from 0 to 6000 m. Data were treated in the software Surfer v8 ™ (Golden Software 2002).

4.2.2. Jelly-POM export ratio [M(z_R):M(z_D)]

4.2.2.1. Ecological considerations

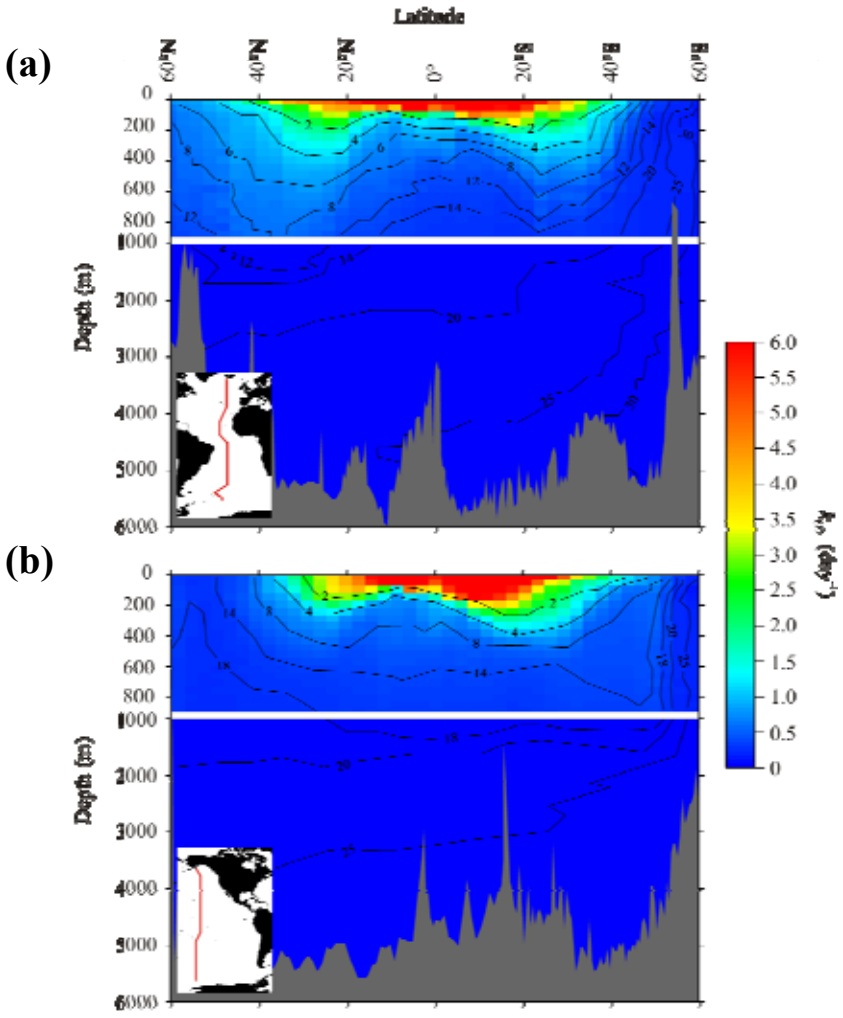

Fig. 4.2. The modeled $k_{(T)}$ as function of temperature in (A) Atlantic Ocean and (B) Pacific Ocean based on temperature fields from hydrographic transects from 0 to 6000 m. Overlaid are contours of the $t_{0.01}$ (in days). From 0 to 900 m the scale is spaced at intervals of 200 m (for magnification), while from 1000 to 6000 m it is spaced at 1000 m intervals. Note that there are no k data on the tropics to verify $k > 2$, thus results are calculated from Eq. 2.

The downward transfer of gelatinous material starts from the depth where gelatinous zooplankton die [death depth (z_D) in the following]. Our model uses the export ratio [$M(z_R):M(z_D)$], relating an initial biomass [$M(z_D)$] sinking from a depth z_D with temperature $T(z_D)$, to a final amount [$M(z_R)$] at depth z_R with temperature $T(z_R)$. The parameters z_R and $T(z_R)$ represent any reference depth in the water column (or seabed) (Fig. 4.1b). The use of z_D is similar to the euphotic zone depth concept (Ez) (Buesseler and Boyd 2009). In contrast to Ez, z_D variability is governed by the organisms' vertical migration distributing the biomass. Therefore, values

for z_D vary between the euphotic zone and the lower level of the migratory range (taxon and species-specific). Pyrosomids migrate to near the seabed (Andersen and Sardou 1994). Salps migrate from the euphotic zone down to 400-800 m and in some cases to 1200-1800 m (Franqueville 1971). Living salps have been observed resting on the seabed (Gili et al. 2006). Cnidaria generally remain in the upper water column although this is not always the case (e.g. hydrozoans), and large populations exist in the mesopelagic and bathypelagic zone. Ctenophores remain in the upper water column (0-80 m) with migration amplitudes between 20 and 30 m (Huwer et al. 2008), but in some cases 250-600 m (Roe et al. 1984), or even down to the seabed. Therefore, we defined two scenarios for z_D: A general case applicable for sinking from the top of the euphotic zone between 0 and 20 m (z_D) down to 100-5000 m (z_R), and a case taking into account vertical migration using a z_D between 100 and 1000 m and a z_R of 1000 or 3000 m.

4.2.3. Calculations of the export ratio [$M(z_R):M(z_D)$]

We approximate the temperature profile in the ocean by a piecewise linear function dividing the depth range between z_D and z_R into n discrete intervals (Fig. 4.1b). We used thermocline data at large scale (Table 4.2), thus at local and regional scales in situ temperature data could be resolved by smaller depth intervals. For each depth interval i, a linear temperature gradient was assumed between depths z_{i-1} and z_i ($i \in [1;n]$, $z_0 = z_D$, $z_n = z_R$). The corresponding temperatures $T(z_{i-1})$ and $T(z_i)$ were obtained from transect observations and averaged for each latitude band from the corresponding depths using a search window of ±20 m for 0-500 m, and ±200 m for 1000-5000 m (Table 2). For $z_D = 0$ m we used data only from 0 to 20 m. Temperature data points $T(z)$ were calculated as the average of all data points within each search window (Table 2). For each linear section, the vertical temperature gradient z_{i-1} and z_i is represented by $K_T(i)$ (Fig. 4.1b; Table 4.2):

$$T(z_i) = T(z_{i-1}) + K_T(i)(z_i - z_{i-1}) \quad (6)$$

and

$$K_T(i) = \Delta T(i) / \Delta z(i) \quad (7)$$

Table 4.2. Summary of the temperatures [$T(z)$] and thermal gradients ($-K_T$) used to work out the jelly-POM export ratio $M(z_R):M(z_D)$.

Latitude interval	z_D = 0 m		0-100 m			100-200 m			200-500 m			500-1000 m			1000-3000 m			3000-5000 m		
	$T(z_D)$	n [a]	$T(z)$	n	$-K_T$	$T(z)$	n	$-K_T$	$T(z)$	n	$-K_T$	$T(z)$	n	$-K_T$	$T(z)$	n	$-K_T$	$T(z)$	n	$-K_T$
Atlantic Ocean																				
60 °N - 40 °N	12.14	34	10.44	27	0.0170	9.50	43	0.0094	8.95	34	0.0018	5.87	25	0.0062	2.79	23	0.0015	2.57	9	0.00011
40 °N - 20 °N	22.08	35	17.96	31	0.0412	16.02	41	0.0194	12.31	29	0.0124	8.29	31	0.0080	2.81	25	0.0027	2.45	11	0.00018
20 °N - 0°	26.22	41	17.87	32	0.0835	13.12	49	0.0475	8.92	28	0.0140	5.27	33	0.0073	2.75	34	0.0013	2.32	13	0.00022
0° - 20 °S	26.76	42	18.61	45	0.0815	12.97	34	0.0564	6.90	45	0.0202	4.16	40	0.0055	2.69	39	0.0007	0.90	12	0.00090
20 °S - 40 °S	23.45	54	19.33	49	0.0412	15.91	29	0.0342	9.92	53	0.0200	6.35	28	0.0071	3.76	41	0.0013	0.99	14	0.00139
40 °S - 60 °S	9.20	28	6.63	31	0.0257	4.99	27	0.0164	3.03	30	0.0065	2.18	22	0.0017	1.11	33	0.0005	0.21	8	0.00045
Pacific Ocean																				
60 °N - 40 °N	5.78	22	5.35	25	0.0043	5.30	34	0.0005	4.13	41	0.0039	2.95	29	0.0024	1.59	22	0.0007	1.55	11	0.00002
40 °N - 20 °N	18.09	35	17.64	36	0.0045	13.31	36	0.0433	6.87	39	0.0215	3.61	31	0.0065	1.57	25	0.0010	1.51	12	0.00003
20 °N - 0°	26.01	40	25.89	31	0.0012	19.43	41	0.0646	7.68	36	0.0392	4.60	41	0.0062	1.70	24	0.0015	1.41	15	0.00015
0° - 20 °S	27.97	31	25.58	40	0.0239	18.45	35	0.0713	7.86	27	0.0353	4.39	35	0.0069	1.70	23	0.0013	1.37	11	0.00017
20 °S - 40 °S	24.08	32	19.63	28	0.0445	16.02	33	0.0361	8.71	35	0.0244	4.30	28	0.0088	1.72	18	0.0013	1.25	9	0.00024
40 °S - 60 °S	10.27	29	7.23	30	0.0304	7.03	29	0.0020	6.10	31	0.0031	3.80	26	0.0046	1.65	15	0.0011	1.18	7	0.00024
VERTIGO site (Aloha Station)																				
	z_D = 20 m		20-150 m			150-300 m			300-500 m			500-1000 m			1000-4000 m					
22.75 °N	26.10	-	21.93	-	0.0321	13.55	-	0.0559	7.62	-	0.0297	3.94	-	0.0074	1.52	-	0.0003			

[a] n = number of data points retrieved from the datasets to work out the grand averages.

where $\Delta T(i) = T(z_i) - T(z_{i-1})$ and $\Delta z(i) = z_i - z_{i-1}$. Within the linear section and for constant sinking speed C, the temperature can now be written as a function of time:

$$T(z_i) = T(z_{i-1}) + K_T(i)\,\Delta t\,C \tag{8}$$

where Δt is the time it takes the particle to sink from depth z_{i-1} to depth z_i.

The decay rate of jelly-POM over the linear section i is obtained by substituting Eq. 8 into Eq. 2 and integrating (*see* Web Appendix: www.aslo.org/lo/toc/vol_xx/issue_x/xxxxa.pdf for full solutions):

$$M(z_i):M(z_{i-1}) = e^{\left[\frac{-0.140\,e^{0.145\,T(z_{i-1})}}{0.145\,K_T(i)\,C}\left(e^{0.145\,K_T(i)\Delta t\,C} - 1\right)\right]} \tag{9}$$

The export ratio is then calculated as the product of the individual decay ratios of all linear sections i:

$$M(z_R):M(z_D) = \prod_{i=1}^{n} M(z_i):M(z_{i-1}) \tag{10}$$

Owing to the absence of sinking speed observations, we chose 5 (depth invariant) sinking speeds (C) from 100 to 1500 m day^{-1} [100 m day^{-1} for ctenophores and hydromedusae, 300 and 500 m day^{-1} for increasing size classes and some scyphomedusae, 800 m day^{-1} for scyphomedusae and thaliaceans, and 1500 m day^{-1} for fast sinking material]. In order to compare jelly-POM to particle-based export ratios, we extended the matrix (below 100 and above 1500 m day^{-1}) using VERTIGO project data (*see* below).

4.2.4. Comparison with a particle-based parameterization and the Martin curve

We compare the jelly-POM export ratios with a particle-based formulation for particles of a single size class (Kriest and Oschlies 2008):

$$M(z_R):M(z_D) = e^{-k\,(z_R - z_D)\,/\,C} \tag{11}$$

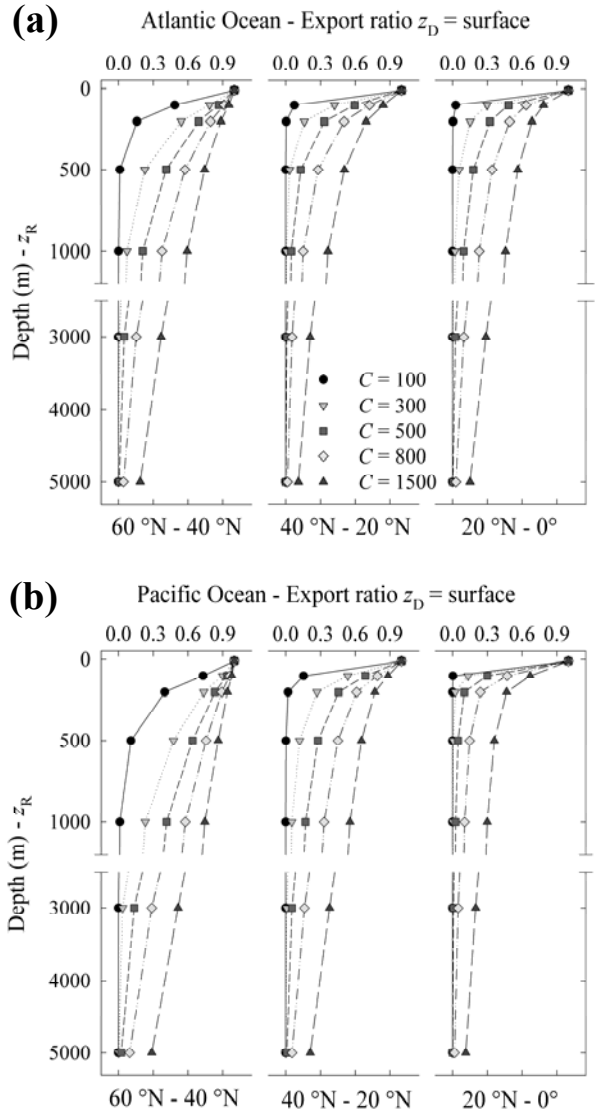

Fig. 4.3. Results from the simulation of the jelly-POM export ratio $M(z_R):M(z_D)$ divided in latitudinal ranges (60 °N to 0° shown, and 0° to 60 °S described in results). Temperature divisions are averaged over latitudinal ranges and depth intervals: (a) in the Atlantic Ocean, and (b) in the Pacific Ocean (Table 2). A matrix of 6 depth intervals between the surface (z_D = 0) and the reference depth (z_R = 100, 200, 500, 1000, 3000, and 5000 m) and 5 sinking velocities (C) (100, 300, 500, 800, and 1500 m day^{-1}) was used.

where k is the remineralization rate (set to 0.03 day^{-1}, varied from 0.01 to 0.05 day^{-1}, and assumed to be independent of size and temperature), z_D and z_R are initial and reference depth, and C is the sinking speed for an individual size class (originally set to < 0.05 m day^{-1}). To make this formulation comparable to the jelly-POM model, we used a 10 x 10 matrix of k (0.05 to 5 day^{-1}) and C (20 to 2000 m day^{-1}) (Table 3). We also compared the jelly-POM export ratio to the Martin curve formulation (Martin et al. 1987), which for a constant remineralization rate implies a POM sinking velocity increasing linearly with depth:

$$M(z_R):M(z_D) = (z_R/z_D)^{-k:a} \quad (12)$$

where k:a (set at 0.858) is a ratio of a constant remineralization rate (k) over a coefficient a derived from fitting to field data. We used temperature data from the VERTIGO project at the ALOHA station (22° 45' N, 158° W) in the Pacific Ocean (Buesseler et al. 2007) at depths of 20, 150, 300, 500, 1000, and 4000 m. We also used sediment trap data (at 150, 300, 500, and 4000 m) from the station to compare in situ data with the jelly-POM attenuation with depth and the results using both the single-size-class constant-sinking model and the Martin curve formulations.

4.3. Results

4.3.1. Atlantic and Pacific Ocean $k_{(T)}$ and $t_{0.01}$

In the following we consider an idealized water column of varying depth according to real bottom topography, neglecting horizontal processes, vertical mixing, or seasonal variability. In the tropical regions of the Atlantic and Pacific Oceans from 30 °N to 30 °S and from 0 to 100 m, decay rates $k_{(T)}$ are high (> 4 day^{-1}), and decrease towards higher latitudes and greater depths, concomitant with lower temperatures to < 1 day^{-1} (Fig. 4.2). $k_{(T)}$ is relatively high (0.5 to 1 day^{-1}) in the subarctic North Atlantic compared to the other high-latitudes (Fig. 4.2). Below 1000 m, $k_{(T)}$ remains roughly constant (between < 0.1 and 0.3 day^{-1}) owing to the uniform temperature of the deep sea (Fig. 4.2b). Decay time scale ($t_{0.01}$) varies inversely to decay rate and ranges from <2 days in the tropical surface ocean to about 25 days below 1000 m. The asymmetry in $k_{(T)}$ between the subarctic North Atlantic and other high-latitude regions is also reflected in $t_{0.01}$ (Fig. 4.2).

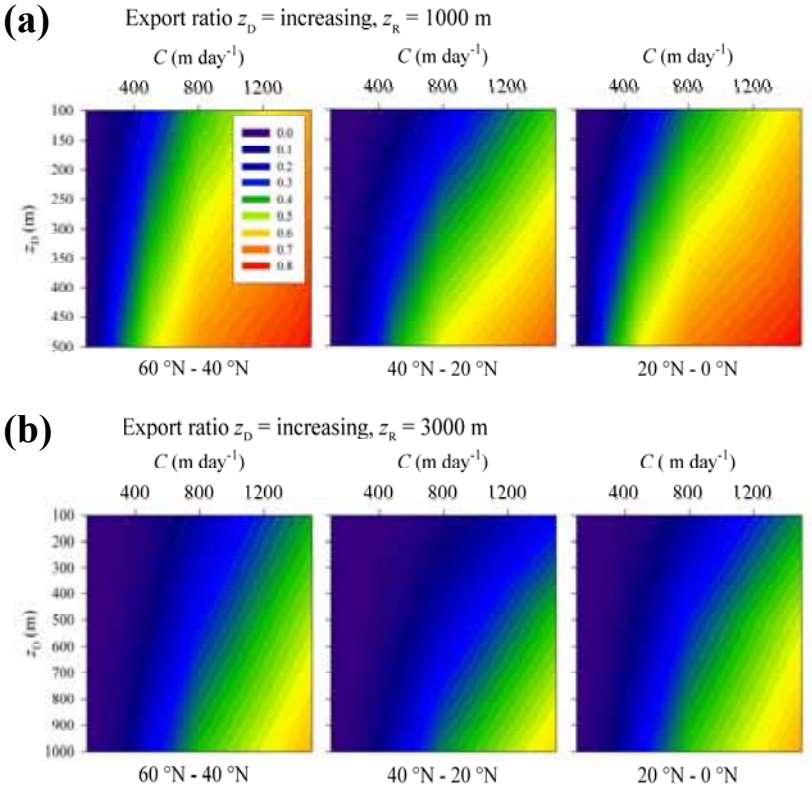

Fig. 4.4. Results from the simulation of the jelly-POM export ratio $M(z_R)$:$M(z_D)$: (A) Reference depth z_R = 1000 m (death depth z_D = 100 and 500 m) and (B) reference depth z_R = 3000 m (death depth z_D = 100, 500, and 1000 m) using an increasing sinking speed from 100 to 1500 m day^{-1}. Data are divided in three major latitudinal intervals only for the northern hemisphere in the Atlantic Ocean.

4.3.2. Model estimates of the jelly-POM export ratio

For scenario 1 (z_D = 0 m), results for the export ratios $M(z_R)$:$M(z_D)$ (Fig. 4.3) are similar in the Atlantic and Pacific Oceans at all depth intervals (from 0-100 to 0-5000 m) at all latitudinal bands (with proportional changes based on C from 100 to 1500 m day^{-1}), except in the 20 °N-20 °S where there is a ~ 10-20% difference between the Atlantic and the Pacific (e.g.

100 m = 63% in the Atlantic *vs.* 100 m = 47% in the Pacific). Less than 30% of the material arrives at 5000 m, and only in 40-60 °N and 40-60 °S significant amounts of material arrive below 3000 m (< 20% elsewhere). For C < 500 m day^{-1}, < 20% of the material arrives below 500 m (except 40-60 °N and 40-60 °S). The following trend emerges: in the Atlantic (Fig. 4.3a), within 60-40 °N between 28% and 85% of the sinking material arrives at 500 m (between 54% and 90% in the Pacific) using a C between 300 and 1500 m day^{-1}. At 5000 m and for C = 800 m day^{-1} 6% is left in the Atlantic (18% in the Pacific), while for C = 1500 m day^{-1} 23% and 32% are left respectively in both oceans. For any depth the $M(z_R)$:$M(z_D)$ estimates in the 60-40 °N and 40-60 °S latitude bands suggest a smaller percentage of jelly-POM reaching the deep North Atlantic compared to the deep South Atlantic, while in the Pacific (Fig. 4.3b) the inter-hemispheric trend is reversed. A sinking speed of 1500 m day^{-1} does not guarantee a large jelly-POM export ratio below 1000 m at any latitude (< 35% in both oceans), except in the subpolar and polar areas (< 60%).

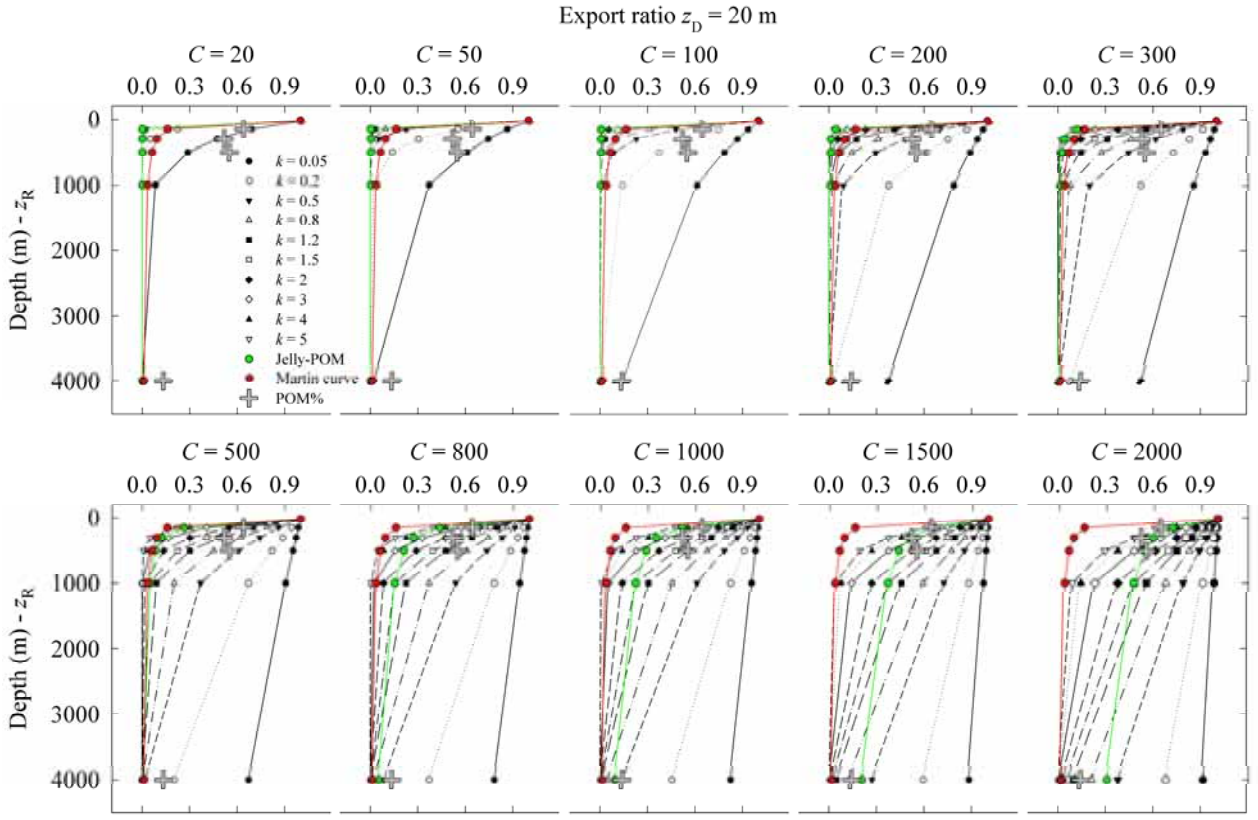

Fig. 4.5. A comparison of the jelly-POM export ratio $M(z_R)$:$M(z_D)$ with the Martin curve (Martin et al. 1987) and a particle-based parameterization (Kriest and Oschlies 2008). Results are presented for 5 depths with the export ratio normalized to 20 m. 10 sinking rates are used ranging from 20 to 2000 m day^{-1}. Temperature data [$T(z)$] are from the Vertical Transport In the Global Ocean (VERTIGO) project at the ALOHA station (22.75 N°, 158° W) (Table 2). The POM% data originate from neutrally buoyant sediment traps (Buesseler et al. 2007).

For scenario 2 (z_D determined by vertical migration), the $M(z_R)$:$M(z_D)$ reveals similar trends as in the first case study (shown only for the Atlantic Ocean, Fig. 4). However, higher percentages of jelly-POM reach z_R owing to an increasing (deeper) z_D used in this second case, and the thermal gradient approaching linearity below the thermocline. In all simulations (z_D = 100, 500, or 1000 m), the percentage change at any z_R within its corresponding latitude is similar (< 20% variability), because of smaller latitudinal thermal variations below the euphotic zone. For any of the depth ranges used, a sinking velocity of C = 100 m day^{-1} delivers < 1% of the material at z_R exceeding 3000 m. Using the deepest z_D (500 and 1000 m), the portion of jelly-POM reaching 3000 m is largest. Using C = 1500 m day^{-1} for any z_D, more than 20% of the jelly-POM reaches z_R at any latitude. For a z_D of 500 m or deeper, > 50% of the jelly-POM arrives at z_R at any latitude at fast sinking rates (C = 1500 m day^{-1}).

A comparison with the VERTIGO data from the ALOHA station and the Martin curve illustrates the dependence of the jelly-POM export ratio and the particle-based formulation on the sinking rate (Fig. 4.5). The jelly-POM export ratio remains below the Martin curve estimates up to C = 300 m day^{-1} and exceeds it in all cases for C > 300 m day^{-1} (Fig. 4.5). The particle-based estimates remain below the Martin curve predictions for all k (except for 0.05 day^{-1}) only for C = 20 m day^{-1}. Particle-based calculations of the export ratio exceed the Martin curve only for sinking speeds of 1000 m day^{-1} or larger (Fig. 4.5). The largest differences between the jelly-POM formulation and the particle-based export model are encountered in the export ratio between 150 and 300 m for k < 1.2 day^{-1} (Table 4.3). Deeper, the differences become smaller as k increases from 0.05 to 5 day^{-1}. Differences between the two models are smaller for single-particle decay rates closer to those predicted by the temperature-dependent $k_{(T)}$ in the jelly-POM formulation. The particle-based model can reproduce measured POM% from ALOHA station sediment trap data within 20% for C = 20-50 m day^{-1} and a decay rate of k = 0.05 day^{-1} and similarly well if both sinking velocity and decay rate increase by the same factor (Fig. 4.5). For ratios predicted by the jelly-POM export ratio model, observed POM% can be reproduced at all depths within ~ 5% using C = 1500 m day^{-1}, and within ~ 20% using C = 1000 and 2000 m day^{-1}, while the model underestimates the observed export ratio for lower sinking velocities.

Table 4.3. Difference in export ratio $M(z_R):M(z_D)$ between a particle-based and the jelly-POM model at 5 depths and 10 sinking speeds (C) normalized to 20 m.

k [a]	Depth (m)	Model difference % = (Particle$_{[\text{Export ratio}]}$ - Jelly$_{[\text{Export ratio}]}$) x 100 [b] C (m d^{-1})									
		20	50	100	200	300	500	800	1000	1500	2000
0.05	150	68.73	86.07	92.65	92.73	86.65	72.08	55.54	47.85	35.33	27.93
0.2	150	**22.31**	54.88	73.95	82.48	79.60	67.75	52.79	45.64	33.85	26.81
0.5	150	**2.35**	**22.31**	47.11	65.14	67.00	59.64	47.52	41.37	30.95	**24.62**
0.8	150	**0.25**	**9.07**	29.99	51.29	56.15	52.24	42.54	37.29	28.14	**22.48**
1.2	150	**0.01**	**2.73**	**16.40**	37.07	44.00	43.34	36.32	32.12	**24.52**	**19.69**
1.5	150	**0.00**	**1.11**	**10.41**	28.88	36.35	37.34	31.96	28.44	**21.90**	**17.66**
2	150	**0.00**	**0.25**	**4.85**	**18.72**	25.91	28.45	25.20	**22.67**	**17.70**	**14.37**
3	150	**0.00**	**0.01**	**0.98**	**6.95**	**11.43**	**14.23**	**13.45**	**12.36**	**9.91**	**8.15**
4	150	**0.00**	**0.00**	**0.12**	**1.39**	**2.65**	**3.69**	**3.71**	**3.47**	**2.86**	**2.38**
5	150	**0.00**	**0.00**	**-0.07**	**-1.24**	**-2.67**	**-4.11**	**-4.37**	**-4.17**	**-3.52**	**-2.97**
0.05	300	47.24	74.08	86.07	92.23	92.05	84.66	71.04	63.32	49.16	39.93
0.2	300	**4.98**	30.12	54.88	73.54	78.80	76.31	65.67	58.98	46.23	37.72
0.5	300	**0.06**	**4.98**	**22.31**	46.70	57.58	61.70	55.80	50.88	40.64	33.45
0.8	300	**0.00**	**0.82**	**9.07**	29.58	41.86	49.49	46.98	43.47	35.37	29.37
1.2	300	**0.00**	**0.07**	**2.73**	**15.99**	27.04	36.29	36.66	34.58	28.82	**24.20**
1.5	300	**0.00**	**0.01**	**1.11**	**10.00**	**19.24**	28.27	29.87	28.57	**24.24**	**20.53**
2	300	**0.00**	**0.00**	**0.24**	**4.44**	**10.46**	**17.73**	**20.13**	**19.69**	**17.19**	**14.76**
3	300	**0.00**	**0.00**	**0.01**	**0.57**	**1.90**	**4.15**	**5.36**	**5.46**	**5.04**	**4.44**
4	300	**0.00**	**0.00**	**0.00**	**-0.29**	**-1.25**	**-3.31**	**-4.79**	**-5.07**	**-4.91**	**-4.44**
5	300	**0.00**	**0.00**	**0.00**	**-0.48**	**-2.40**	**-7.41**	**-11.77**	**-12.88**	**-13.06**	**-12.09**
0.05	500	28.65	60.65	77.88	88.06	90.45	86.91	75.95	68.87	54.87	45.22
0.2	500	**0.67**	**13.53**	36.79	60.46	70.10	73.66	67.28	61.82	50.08	41.59
0.5	500	**0.00**	**0.67**	**8.21**	28.46	41.91	52.44	52.19	49.22	41.18	34.71
0.8	500	**0.00**	**0.03**	**1.83**	**13.34**	**24.81**	36.72	39.68	38.37	33.12	28.34
1.2	500	**0.00**	**0.00**	**0.25**	**4.79**	**11.98**	**21.90**	26.26	26.22	**23.56**	**20.54**
1.5	500	**0.00**	**0.00**	**0.05**	**2.16**	**6.66**	**14.10**	**18.19**	**18.57**	**17.18**	**15.19**
2	500	**0.00**	**0.00**	**0.00**	**0.48**	**2.01**	**5.32**	**7.68**	**8.12**	**7.87**	**7.12**
3	500	**0.00**	**0.00**	**0.00**	**-0.14**	**-0.88**	**-3.24**	**-5.64**	**-6.35**	**-6.68**	**-6.30**
4	500	**0.00**	**0.00**	**0.00**	**-0.19**	**-1.43**	**-6.38**	**-12.76**	**-15.13**	**-17.11**	**-16.75**
5	500	**0.00**	**0.00**	**0.00**	**-0.19**	**-1.53**	**-7.54**	**-16.58**	**-20.45**	**-24.58**	**-24.89**
0.05	1000	**8.21**	36.79	60.65	77.83	84.00	85.60	78.78	73.02	60.16	50.52
0.2	1000	**0.00**	**1.83**	**13.53**	36.74	50.69	62.15	62.72	59.77	50.96	43.47
0.5	1000	**0.00**	**0.00**	**0.67**	**8.16**	**18.23**	31.90	38.37	38.55	35.09	30.86
0.8	1000	**0.00**	**0.00**	**0.03**	**1.78**	**6.30**	**15.30**	**21.63**	**22.83**	**22.11**	**20.02**
1.2	1000	**0.00**	**0.00**	**0.00**	**0.20**	**1.18**	**4.19**	**7.16**	**8.01**	**8.37**	**7.87**
1.5	1000	**0.00**	**0.00**	**0.00**	**0.00**	**0.02**	**0.09**	**0.18**	**0.21**	**0.23**	**0.22**
2	1000	**0.00**	**0.00**	**0.00**	**-0.05**	**-0.53**	**-3.05**	**-6.95**	**-8.57**	**-10.20**	**-10.23**
3	1000	**0.00**	**0.00**	**0.00**	**-0.05**	**-0.65**	**-4.64**	**-12.81**	**-17.13**	**-23.03**	**-24.70**
4	1000	**0.00**	**0.00**	**0.00**	**-0.05**	**-0.65**	**-4.85**	**-14.48**	**-20.27**	-29.61	-33.48
5	1000	**0.00**	**0.00**	**0.00**	**-0.05**	**-0.65**	**-4.88**	**-14.96**	**-21.43**	-32.99	-38.81
0.05	4000	**0.00**	**1.83**	**13.53**	36.79	51.34	67.03	77.88	81.87	87.52	90.48
0.2	4000	**0.00**	**0.00**	**0.03**	**1.83**	**6.95**	**20.19**	36.79	44.93	58.66	67.03
0.5	4000	**0.00**	**0.00**	**0.00**	**0.00**	**0.13**	**1.83**	**8.21**	**13.53**	26.36	36.79
0.8	4000	**0.00**	**0.00**	**0.00**	**0.00**	**0.00**	**0.17**	**1.83**	**4.08**	**11.84**	**20.19**
1.2	4000	**0.00**	**0.00**	**0.00**	**0.00**	**0.00**	**0.01**	**0.25**	**0.82**	**4.08**	**9.07**
1.5	4000	**0.00**	**0.00**	**0.00**	**0.00**	**0.00**	**0.00**	**0.06**	**0.25**	**1.83**	**4.98**
2	4000	**0.00**	**0.00**	**0.00**	**0.00**	**0.00**	**0.00**	**0.00**	**0.03**	**0.48**	**1.83**
3	4000	**0.00**	**0.00**	**0.00**	**0.00**	**0.00**	**0.00**	**0.00**	**0.00**	**0.03**	**0.25**
4	4000	**0.00**	**0.00**	**0.00**	**0.00**	**0.00**	**0.00**	**0.00**	**0.00**	**0.00**	**0.03**
5	4000	**0.00**	**0.00**	**0.00**	**0.00**	**0.00**	**0.00**	**0.00**	**0.00**	**0.00**	**0.00**

[a] k data were increased from 0.05 to 5 to approximate the variability modeled as a function of jelly-POM decomposition (Fig. 4.2).

[b] Data calculated as the difference between $M(z_R):M(z_D)$ from Kriest and Oschlies (2008) particle-based parameterization and the jelly-POM parameterization presented in this paper. Bold cells show values within a 25% of the jelly-POM model. Positive and negative values are over and underestimations from the particle-based model in relation to the jelly-POM model.

4.4. Discussion

The active transport of living gelatinous material caused by vertical migration affects the death depth z_D and determinates the temperature at which export and decomposition commence. The complex migratory response (governing z_D) is not included in particle-based export formulations, but similar considerations are needed for other migratory taxa enhancing POC export at depth (Steinberg et al. 2007). Variability in the depth of the euphotic zone may have to be considered to explain confounding effects of particle fluxes measured at the same depth but originating at different depths (Buesseler and Boyd 2009). Similarly, information about the patterns of z_D is required to constrain regional and latitudinal estimates of jelly-POM export. The scarcity of field data on the organisms' z_D prevents an accurate parameterisation in the model. However, z_D must lie within the vertical migration range (likely near the lower limit), which may be close to the seabed in the case of salps and pyrosomids (Wiebe et al. 1979). The four death depths considered here (z_D = 20, 100, 500, 1000 m) correspond to the depths at which different taxa occur and migrate (Fig. 4.3, 4.4). The actual distribution of the start of jelly falls in space and time is complex. Other death depths (z_D = 1000 m) apply to situations where animals die on the deeper range of their vertical migration (e.g. *Pyrosoma atlanticum* in Roe et al. 1990 migrating down to 800 m and below). As a generalization (including Cnidaria) several variables trigger the onset of jelly falls: High levels of primary production clogging the feeding apparatus of thaliaceans (Perissinotto and Pakhomov 1998), changes in temperature (Gatz et al. 1973), ageing of blooms and food exhaustion (Purcell et al. 2001), grazing and predation damage (Arai 2005), and parasitism (injury and viral) infections during ageing blooms (Mills 1993). We do not include biological controls on jelly falls in the model, as we are concerned only with the subsequent fate of the jelly-POM.

Our model assumes that the amount of gelatinous material arriving at z_R is mainly controlled by the temperature dependence of remineralization (Q_{10} = 4.28) (Table 4.2) and the sinking speed. The temperature at z_D is important in the euphotic zone (Fig. 4.4), but, at high sinking velocities (above 500 m day^{-1}), jelly-POM can reach lower temperatures below the thermocline relatively fast, which reduces the overall remineralization rate. The interaction among the three parameters death depth, temperature dependence, and sinking speed is thus fundamental in predicting the jelly-POM export ratio. According to our model, gelatinous material sinking from the euphotic zone (z_D < 100 m) is likely to reach the seabed at temperate and high latitudes (poleward of 40

°N and 40 °S) (Fig. 4.2, 4.3), while in tropical and subtropical areas, the material is not likely to sink below 500 m before being completely remineralized (except at sinking speeds above 800 m day^{-1}). Greater death depths (z_D = 500-1000 m), representative of deep migratory species, allow significant amounts of jelly-POM to reach 3000 m (and below) at any latitude for sinking speeds above 500 m day^{-1} (jelly-POM = 20-87%, Fig. 4.4). This prediction is concomitant to visual observations of living and moribund salps close to the seabed in the North Atlantic and deposition of dead corpses (Cacchione et al. 1978). Living salp chains were observed off the

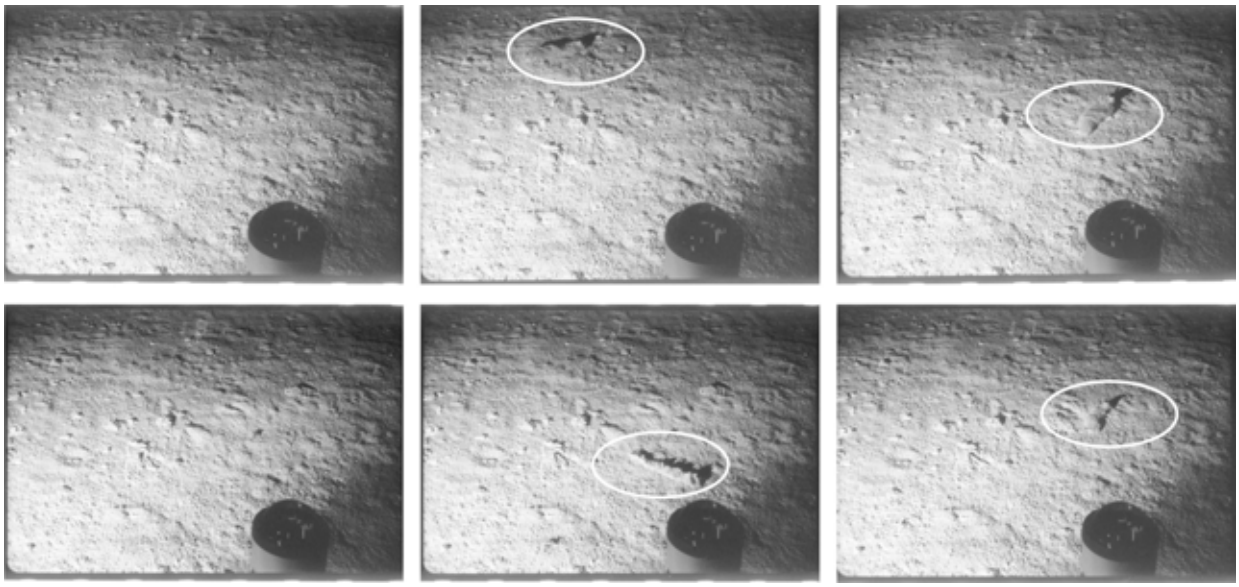

Fig. 4.6. A photographic sequence showing the settlement, decomposition, and disappearance of a *Pyrosoma atlanticum* carcass in the Madeira Abyssal Plain (northeast Atlantic) at 5433 m. The images were obtained with an instrument called 'Bathysnap' (time lapse photography) in a deployment at 31.26 N°, 25.42 W°, from 19 July to 19 November 1985 (123 days). Each frame interval equals 512 minutes, and the area of each image is 2 m^2. Circles in red show the carcass. (a) Initial view of the seabed with no carcass on frame 133 (04 September 1985), (b) settlement of carcass on frame 134 (04 September 1985), (c) start of decomposition of carcass on frame 161 (13 September 1985), (d) carcass showing clear signs of degradation on frame 176 (19 September 1985), (e) carcass completely degraded on frame 179 (20 September 1985), and (f) carcass disappear or completely decomposed on frame 180 (21 September 1985). The residence time of the carcass was 16.71±0.35 days, with the error indicating the time interval for which there is no data. Degradation can be visually confirmed over time. Images courtesy of R. S. Lampitt.

Antarctic Peninsula on the seabed at 800 m (Gili et al. 2006), thus it is plausible that they die and decompose in the vicinity. Remineralization would start on the seabed itself (at low temperatures (< 2-4°C), therefore delaying decomposition (Fig. 4.2). The observations of *P. atlanticum* carcasses on the seabed below 5000 m (likely sinking from 500-800 m) further confirms our model results (Fig. 4.6). A deep z_D combined with fast sinking rates allows transfer to the seabed, although in a decaying state. The observed carcasses stayed 17 days at the seabed

before being completely decomposed (Fig. 4.6), in agreement with our model giving $k_{(T)} \approx 0.2$, $t_{0.01} \approx 22$ days (Fig. 4.2).

The depth of the seabed relative to the remineralization depth eventually determines the amount and the state of the material found. The two major jelly falls studied to date were sampled in tropical areas below 1000 m (Arabian Sea: Billett et al. 2006; Gulf of Guinea: Lebrato and Jones 2009), while no other major deposition has been recorded in the tropics (M. Lebrato unpubl.). A deep z_D linked to a wide vertical migration range and fast sinking rates (> 800 m day^{-1}) might allow the material to arrive at the seabed. If z_D is located within a few meters of the seabed, decomposition starts at the seabed itself. In oxygen deficient areas of the Arabian Sea and the Gulf of Guinea, oxygen could limit remineralization in the first 1000 m. Temperature drops below 10-12°C below the sharp thermocline in these tropical areas (Table 4.2), keeping decay rates [$k_{(T)}$] small (< 0.8 day^{-1}). Jelly falls are studied by visual surveys using video and photography, which does not allow estimation of the gelatinous POM% (to compare with living biomass). Visual observation of a jelly fall also cannot provide information on its stoichiometry, which prevents comparisons with model export predictions. Based on our model, the most likely material to arrive at the seabed is therefore from taxa that perform large vertical migrations (salps and pyrosomids) and whose z_D is below the thermocline and/or very close to the bottom. The decay time scale ($t_{0.01}$) at depths below 1000 m amount to 15-30 days (Fig. 4.2) across the studied transects, providing a reasonable time window to encounter this material.

Besides variations in z_D and sedimentation rates, differences in stoichiometry and body size may explain why thaliaceans and scyphozoans accumulate on the sea floor and hydrozoans and ctenophores do not. Hydrozoans and ctenophores typically have a lower C/N than thaliaceans and scyphozoans (Lucas et al. 2011) and the greater lability of the hydrozoans and ctenophore tissues facilitates a rapid remineralization. Most hydrozoans and many ctenophores are smaller than thaliaceans (especially pyrosomids) and scyphozoans, which may reduce the sinking rate. Jelly-POM should normally reach the seafloor on temperate and sub-polar shelves and continental slopes, but is also consumed by macro and megafauna in the benthic communities (Yamamoto et al. 2008).

4.4.1. Model limitations: Factors governing jelly-POM remineralization

Gelatinous material is remineralized by microzooplankton (Titelman et al. 2006) and by microbial action (Condon and Steinberg 2008). Hence, differences in rates of remineralization of gelatinous material in deep and shallow waters are not only attributable to temperature but also to the in situ microbial community. Thus, while jelly-POM remineralization is certainly more complex than presented here, the model provides the theoretical grounds for an objective assessment of gelatinous biomass contribution to POM export and its incorporation in biogeochemical models. Additional factors governing the export ratio, beyond $k_{(T)}$, temperature and sinking rate are pressure, non-Redfield stoichiometry (Frost et al. 2002), oxygen concentration, the abundance and biomass of large pelagic fauna (Arai 2005), physical forcing, and the microbial community (Titelman et al. 2006). Our model parameterizes the temperature effect, assuming that the microbial activity and pressure effects are included in this formulation. Improved formulations will requiere quantification of gelatinous material decomposition under different temperature and pressure regimes, with different microbial communities.

4.4.2. Treatment in biogeochemical models

Jelly falls and their biogeochemical feedbacks differ from other POM sources because of their episodic nature, their initiation from below the euphotic zone, and the size classes involved. In contrast to fecal pellets and mucilaginous detritus, which provide an almost continuous small flux (Robison et al. 2005), jelly falls deliver a large and sudden pulse of material after their demise (Lebrato and Jones 2009). This is analogous to phytodetritus pulses after the spring bloom in temperate latitudes. By changing the sinking velocity and the decay rate (k) we can simulate the export ratio for ALOHA at depth by both the particle-based (Kriest and Oschlies 2008) and the jelly-POM model. The Martin curve can simulate jelly-POM remineralization and/or the particle-based model for sinking velocities smaller than C = 200 m day^{-1} and remineralisation rates larger than k = 0.5 day^{-1}. The particle-based model uses a constant decay rate with varying sinking speed, which we applied to a wide k spectrum (0.05 to 5 day^{-1}) to mimic the $k_{(T)}$ dependency (Table 4.2; Fig. 4.5). Inter model differences (Table 4.2) in the export ratio decrease with depth (150 to 4000 m) because of the lower temperature variability. This reduces the difference between the $k_{(T)}$ of the jelly-POM model and the k of the particle-based model.

In principle, it should be relatively straightforward to augment parameterizations of POM export and remineralization used in current three-dimensional marine biogeochemical models. This could be done by an extra (large-size) detritus compartment, representing jelly-POM. The typical sinking speeds (5-50 m day^{-1}) applied in numerical model formulations to represent the sinking of 'ordinary' detritus (Oschlies and Garcon 1999) and remineralization rates (0.1-0.3 day^{-1}, *see* Fig. 1A), do not generally apply to jelly-POM. Remineralization rates of ordinary detritus are used as functions of ambient temperature in some models (Schmittner et al. 2008), and this could be expanded to jelly-POM. The jelly-POM parameterization format could also be applied to describe other POM compartments, provided that the temperature dependence of *k* (Fig. 4.1a) is known. Some formulations of organic matter export suggest using constant decay rates as a function of depth, with an exponential attenuation of the flux (Lutz et al. 2002). This assumption induces a large flux attenuation in the upper ocean in models, not representing sediment trap data. This occurs for jelly-POM export when not using appropiate sinking speeds, and/or *k* data (Table 4.3; Fig. 4.5). We propose that the use of *k* should include a temperature dependency for any particle to mimic vertical profiles accounting for different starting depths. The POM size spectrum is much larger than we currently measure in sediment traps. The use of our formulations might enable the application of the same metrics with different parameters to a much wider range of particles. For jelly-POM, robust hypotheses about what triggers jelly blooms, death, and falls await development. They should eventually be combined with the theory presented here about the fate of jelly-POM to reach a better understanding of the role of gelatinous zooplankton in marine biogeochemical cycles.

4.5. Web appendix

4.5.1. Full equation descriptions and solutions for the jelly-POM export ratio [$M(z_D)$:$M(z_R)$]

The novelty of our parameterization is a temperature dependence of the jelly-POM decay rate based on experimental observations (Table 4.1) from ~ 2 °C to 16 °C using surface and deep water experiments. Therefore, the equation assumes that remineralization only depends on temperature (*T*) at any depth (*z*) and it does not take into account differences in microbial communities and other water mass properties:

$$k_{(T)} = 0.140 \text{ day}^{-1}\ e^{0.145T(z)} \quad \text{(A1)}$$

The behavior of the system above the experimental temperatures (tropical latitudes) should be considered tentative. Eq. A1 determines the behavior of k_T as a function of temperature. Assuming a linear temperature gradient k_T with depth within linear section i, we have:

$$T(z_i) = T(z_{i\text{-}1}) + K_T(i)\ (z_i - z_{i\text{-}1}) \quad \text{(A2)}$$

where $K_T(i)$ describes the local temperature gradient between depths $z_{i\text{-}1}$ and z_i with corresponding temperatures [$T(z_{i\text{-}1})$ and $T(z_i)$, Table 4.2, and Fig. 4.3, 4.4] as:

$$K_T(i) = \Delta T / \Delta z(i) \quad \text{(A3)}$$

where $\Delta T = T(z_i) - T(z_{i-1})$, and $\Delta z(i) = z_i - z_{i\text{-}1}$

We calculate specific $K_T(i)$ for each scenario (Table 4.2). We introduce a time interval ($\Delta t = t_1 - t_0$), which is the time it takes for the material to sink from $z_{i\text{-}1}$ to z_i at a sinking rate C (in m d^{-1}):

$$\Delta t = \Delta z(i) / C \quad \text{(A4)}$$

the final depth z_i is written as function of Δt and C:

$$\Delta z(i) = \Delta t\, C \quad \text{(A5)}$$

which is substituted into Eq. A2 to provide the temperature as a function of time and sinking rate:

$$T(z_i) = T(z_{i\text{-}1}) + K_T(i)\ \Delta t\ C \quad \text{(A6)}$$

The temperature dependent (thus depth-dependent) decay of particle mass over time (independent of size and time) is then:

$$dM/dt = -M\, k_{(T)} \quad \text{(A7)}$$

where $k_{(T)}$ is the decay coefficient given by Eq. A1 as function of temperature.

Substituting Eq. A1 into Eq. A7 for an arbitrary depth z between z_{i-1} and z_i:

$$dM/dt = -M\, k_{(T)} = -0.140\, M\, e^{0.145T(z)} \tag{A8}$$

Here we substitute $T(z)$ with the solution of Eq. A6 for time t ($0 \le t \le \Delta t$) corresponding to depth z within depth interval i:

$$dM/dt = -0.140\, M\, e^{0.145T(z)} = -0.140\, M\, e^{0.145\,[T(z_{i-1}) + K_T(i)\, t\, C]} \tag{A9}$$

and integrate:

$$\int_{M_{(zi-1)}}^{M_{(zi)}} dM = \int_0^{\Delta t} -0.140 M \mathrm{e}^{0.145[T(z_{i-1})+K_T(i)tC]} dt = -0.140 M \mathrm{e}^{0.145T(z_{i-1})} \int_0^{\Delta t} \mathrm{e}^{0.145 K_T(i)tC}\, dt \tag{A10}$$

We calculate the definite integral between time 0 and Δt:

$$[\ln(M)]_{zi-1}^{zi} = -0.140\, e^{0.145\, T(z_{i-1})} \left[\frac{1}{0.145\, K_T(i)\, C}\, e^{0.145\, K_T(i)\, t\, C} \right]_0^{\Delta t} - \frac{-0.140\, e^{0.145\, T(z_{i-1})}}{0.145\, K_T(i)\, C} \left[e^{0.145\, K_T(i)\, t\, C} \right]_0^{\Delta t} \tag{A11}$$

$$\ln M_{zi} - \ln M_{zi-1} = \ln(M_{zi}/M_{zi-1}) = \frac{-0.140\, e^{0.145\, T(z_{i-1})}}{0.145\, K_T(i)\, C} \left(e^{0.145\, K_T(i)\, \Delta t\, C} - 1 \right) \tag{A12}$$

and thus the solution for $M(z_i):M(z_{i-1})$:

$$M(z_i):M(z_{i-1}) = e^{\left[\frac{-0.140\, e^{0.145\, T(z_{i-1})}}{0.145\, K_T(i)\, C} \left(e^{0.145\, K_T(i)\, \Delta t\, C} - 1 \right) \right]} \tag{A13}$$

The export ratio is then the product of the individual decay ratios:

$$M(z_R):M(z_D) = \prod_{i=1}^{n} M(z_i):M(z_{i-1}) \tag{A14}$$

5.

Jelly biomass export follows regime shifts in a continental shelf

Abstract

Particulate matter export fuels benthic ecosystems in continental margins and the deep ocean, also removing carbon from the upper ocean. The biomass originating in gelatinous zooplankton (jelly-falls) provides a fast carbon export vector that has recently been adequately described. The pelagic tunicate *Pyrosome atlanticum* forms large blooms following phytoplankton production, which then collapse and die, quickly sinking to the shelves and slopes seafloor. The observation of a large and continuous benthic trawling catch of *P. atlanticum* carcasses on the western Mediterranean Sea from 1994 to 2005 provided a unique opportunity to quantify for the first time jelly-falls on an entire continental margin. We sampled thousands of carcasses from the Alboran Sea to the Gulf of Lions between 40 and 800 m with biomass and carbon peaks (60 mg m^2 and 2 mg C m^2 respectively) in the first 200 m after trawling between 30,000 and 175,000 m^2 of seabed. Biomass accumulated in the shelf and was evenly distributed in slopes, suggesting initial shallow deposition following quick sinking rates (1200 m day^{-1}), and then a benthic transport pathway through cascading events in canyons. Anomalies of sea surface temperature (SST), chlorophyll a (Chla) and hydroclimate (sea surface temperature, precipitation rate, outgoing long- wave radiation and 500 mb geopotential height monthly time series) were used to assess the spatiotemporal relations of the jelly-falls with environmental variables. The long term trend of hydroclimate was extracted from a principal component analysis (PCA). We show that

large changes in STT, Chla, and hydroclimate in the late 1990s may have caused a jelly-falls increase after 2001, enhancing regional jelly carbon export. This is part of an ecosystem-wide modification in the western Mediterranean Sea, where jelly-falls may play a more conspicuous role than previously thought in biomass and carbon export to the ocean's interior.

This chapter is based on:

Lebrato, M., Molinero, J-C., Cartes, J., Lloris, D., Beni-Casadella, L. and Melin, F. in preparation. Jelly biomass export follows regime shifts in a continental shelf. To be submitted: *PLoS ONE*.

Acknowledgements: Thanks for Pedro de Jesus Mendes for providing laboratory facilities and expertise in assessing jelly-POM sinking speed. This work was also supported by the "European Project on Ocean Acidification" (EPOCA), which is funded from the European Community's Seventh Framework Programme (FP7/2007-2013) under grant agreement n° 211384. This work was also funded by the Kiel Cluster of Excellence “The Future Ocean” (D1067/87).

5.1. Introduction

The biogenic production of organic matter and its remineralization when sinking from the upper ocean constitute the basis of the biological pump (Behrenfeld and Falkowski 1997; Buesseler et al. 2007). The input of particulate organic matter (POM) also fuels benthic ecosystems in continental margins and the deep ocean (Gooday and Turley 1990). POM export is dominated by biogenic particles originating in the euphotic and mesopelagic zone (0-1000 m), including phytodetritus (Smith et al. 2008), marine snow (Alldredge and Silver 1988), zooplankton mucous sheets (Robison et al. 2005), faecal pellets (Turner 2002), and gelatinous zooplankton biomass (Billett et al. 2006). In particular, the export of gelatinous zooplankton biomass [Cnidaria (Scyphozoa and Hydrozoa), Thaliacea (Pyrosomida, Doliolida, Salpida) and Ctenophora] has recently gained considerable attention owing the potential importance as non-minor carbon source for benthic communities, the so-called "jelly-falls" (Lebrato et al. 2011; Sweetman and Chapman 2011). This is important because during jelly-falls biomass decomposition, dissolved organic carbon (DOC) (Hansson and Norrman 1995) and nutrients (Pitt et al. 2009) are released, while large amounts of oxygen are consumed (West et al. 2009b). Furthermore, carcasses enter the trophic web (consumed by macro- and mega-fauna) at or near benthic ecosystems (Lebrato and Jones 2009; Carrasson and Cartes 2002; Fanelli et al. 2011) or are channelled through pelagic bacteria (Tinta et al. 2010; Condon et al. 2011). Growing evidence of post-bloom processes in continental margins, showing that fast-sinking carcasses of scyphozoans and thaliaceans (pyrosomes and salps) sink *en masse* (Lebrato et al. 2012), delivering at times more carbon to the seafloor than phytoplankton-base export (Billett et al. 2006; Lebrato and Jones 2009). Other gelatinous carcasses (e.g. Hydrozoa and Ctenophora) however, do not reach the seabed due to low sinking speeds and (high) temperature-dependant decay rates (Lebrato et al. 2011), and they remineralize in the first 500-1000 m boosting microbial processes in the water column (Frost et al. 2012).

Historically, the Thaliacea (pelagic tunicates) account for the majority of the jelly-falls in the Atlantic and Pacific Ocean, and particularly the genus Pyrosomida (*Pyrosoma atlanticum*) (Lebrato et al. 2012). Pyrosomes are free-floating colonial tunicates, brightly bioluminescent and cylindrical in shape, taxonomically more related to humans than to true jellyfish. They inhabit the mesopelagic and near-benthic ecosystems, displaying vertical migrations at night ranging from 300 to 700 m (Franqueville 1970, 1971; Andersen et al. 1992). In the

Mediterranean Sea, *P. atlanticum* is abundant in the Balearic Sea (Casanova 1961), the Ligurian and Tyrrhenian Sea (Andersen and Sardou 1994; Sartor et al. 2003), the Adriatic Sea (Godeaux 1976), the Catalan Sea and the Alboran Sea (Madin 1991). They are present but less abundant (likely driven by low productivity regimes) in the eastern Mediterranean Sea (Galil and Goren 1994) and Levantine Sea (Weikert and Godeaux 2008). Their distribution and abundance peak coincides with wind- and front-induced upwelling systems, where high biological productivity is enhanced by deep cold and nutrient-loaded waters (Johns et al. 1992; Sarhan et al. 2000; Granata et al. 2004). However, little is known on how *P. atlanticum* populations are influenced by natural variability in ocean properties, large-scale climate oscillations, anthropogenic forcing or their synergies. Factors driving post-bloom death and onset of a jelly-fall in pelagic tunicates may be linked to ageing of a bloom (Purcell et al. 2001) and cumulative negative circumstances, such as starvation, parasitism, infection, and predation (Mills 1993). Life cycles are normally completed within a year or a few months, with subsequent death (Franqueville 1971). For pelagic tunicates, there is evidence that high concentrations of particles/material clog their feeding apparatus causing death (Madin 1972; Harbison et al. 1986; Reinke 1987; Acuña 2001) despite food being abundant (Zeldis et al. 1995). Salp blooms collapse was thought to be driven by chlorophyll *a* in the Southern Ocean, starting at a threshold of ~ 1 mg m^{-3} (Perissinotto and Pakhomov 1998). The physiological mechanisms underpinning this observation include a lack of lipid reserves, which constrains pelagic tunicates to feed continuously, otherwise they starve. Such continuous feeding mode can be counterproductive when the mucus sheet used to trap particles is clogged, causing it to break away, leading to the formation of a bolus in the oesophagus (Harbison et al. 1986). The reduction in the feeding efficiency is lethal if organisms are exposed for long periods of time (Fortier et al. 1994).

To the best of our knowledge, in the Mediterranean Sea the only evidence of a *P. atlanticum* jelly-fall event was reported by Sartor et al. (2003) during a benthic trawl survey targeting shrimps in the Tyrrhenian Sea from 1995 to 1999. They caught as by-catch between 0.2 and 0.5 kg h^{-1} of dead *P. atlanticum* carcasses between 300 and 650 m depth during 500 h of trawling effort. The only comparable *P. atlanticum* jelly-fall took place in the Atlantic Ocean, off Ivory Coast, where thousands of carcasses were surveyed with remote operated vehicle (ROV) video from ~ 200 m to ~ 1300 m (Lebrato and Jones 2009). The average organic carbon associated with the carcasses was 5 g C m^2 in the slope, with values as high as 22 g C m^2 in certain trough areas, although this was heavily driven my accumulation in channels. They observed eight

megafaunal species from three different phyla scavenging on the material, which provided robust direct evidence on the active trophic role of gelatinous depositions in the seabed. Other *P. atlanticum* jelly-falls have been described elsewhere: Off New Zealand between 160 and 170 m (Hurley and McKnight 1959), in the mid slope of the Tasman Sea (Cowper 1960), in New South Wales in the shelf (Griffin and Yaldwyn 1970), off Cape Verde (Monniot and Monniot 1966), in the Madeira Abyssal Plain at 5433 m (Roe et al. 1990)

The observation of a continuous benthic trawling bycatch of *P. atlanticum* carcasses on the western Mediterranean margin from 1994 to 2005 during spring and summer opened a new and unique opportunity to study mass deposition events of gelatinous biomass. Carcasses were sampled from the Alboran Sea to the Gulf of Lions between 40 and 800 m in the shelf and slope, providing the first evidence to date of jelly-falls carbon export along entire continental margins. A combined approach using ocean climate and satellite sea surface colour data was used to reconstruct hydroclimate scenarios concurrent with the deposition of *P. atlanticum* carcasses. The results provide new evidence of bentho-pelagic coupling and the contribution of gelatinous zooplankton biomass to the organic carbon export that sequesters CO_2 in the biological pump.

5.2. Supplementary material: methods

5.2.1. The MEDITS survey programme

The International bottom trawl survey in the Mediterranean Sea (MEDITS programme) was designed to produce scientific data on benthic and demersal species to study biomass distribution and population structure. This was carried out in seasonal bottom trawl surveys (Bertrand et al. 2000), including the majority of the trawlable areas in shelves and slopes (10 to 800 m) of all Mediterranean partners. A standardized sampling methodology for all surveys was set-up to allow inter-site comparison (Anonymous 1998). In some partner programmes such as MEDITS-ES (e.g. Abello et al. 2002) along the Iberian Peninsula, additional data of non-commercial species such as *P. atlanticum* (traditionally catalogued as bycatch) was recorded in the 1994-2005 period following the same protocol as for the commercial species. The availability of these data opened a new and unique opportunity to study mass deposition events of gelatinous biomass in a time-series.

5.2.2. The trawl system: Sampling strategy and details

The trawling gear was operated in the *R/V Cornide de Saavedra* with a towing power of a minimum of 368 kW and 4.5 tons of bollard pull. The same vessel and crew were used every year to minimize uncertainty in sampling effort between years. The standard sampling device used in all surveys was a bottom trawl with a GOC 73 net designed for experimental fishing (Fiorentini et al. 1999). The use of a device to control trawl geometry was implemented, resulting in a vertical opening of 2.75 ±0.52 m and a horizontal opening of 19.30 ±2.47 m (calculated for each individual haul from 1994 to 2005, n = 247 hauls) (*see* Table 5.2). The cod end mesh size was 20 mm. The fishing speed was 2.89 ±0.23 knots (5.12 ±1.16 km h^{-1}) on the ground (n = 247 hauls). The haul duration was fixed at 30 minutes on depths less than 200 m (n = 81 hauls) and at 60 minutes at depths more than 200 m (n = 166 hauls), which resulted in trawled distances of 2736 ±164 m and 4941 ±912 m respectively (Table 5.1, 5.2). This translates into trawled areas (T_{AREA}) of 47,137 ±5,412 m^2 and 100,499 ±21,834 m^2 depending on depth strata (*see* Table 5.1, 5.2 for individual trawl areas and volumes), assuming the front of the GOC 73 trawl was an elliptical cylinder, and then:

$$T_{AREA}\ (m^2) = b\ h \tag{1}$$

$$T_{VOLUME}\ (m^3) = \pi\ a\ b\ h \tag{2}$$

where π = phi, a = vertical opening, b = horizontal opening, and h = cylinder height, which in this case is the distance travelled by the haul.

The explored area was divided into three geographical sectors for the purpose of trawling and to facilitate data analysis and interpretation (Fig. 5.1): Sector 1 - from Tarifa (36.00 °N/5.59 °W) to Cape Palos (37.62 °N/0.60 °W), Sector 2 - from Cape Palos (37.62 °N/0.60 °W) to Sagunto (39.64 °N/0.19 °W), and Sector 3 - from Sagunto (39.64 °N/0.19 °W) to Cape Creus (42.27 °N/3.30 °E). The trawling stations were distributed according a stratified sampling scheme following depth with random hauls inside each stratum. The bathymetric limits used were: 10-50 m, 50-100 m, 100-200 m, 200-500 m and 500-800 m. The hauls were conducted at a constant depth not exceeding 5 % the initial depth in straight lines (Table 5.2). Each position was selected randomly in small sub-areas. Sampling was performed during spring, from April to July, always

Table 5.1. Summary of MEDITS-ES trawling catches of *Pyrosoma atlanticum* carcasses from 1994 to 2005.

Year/Month	**Latitude** Start End	**Longitude** Start End	**Depth** (m) (Min-Max)	**Trawl speed** (knots)	***h*** (m) (Min-Max)	T_{AREA} (m^2) (Min-Max)	T_{VOLUME} (m^3) (Min-Max)	**Carcass** (n°) (Min-Max)	**Wet wt** (gr) (Min-Max)	$T_{BIOMASS}$ (mg m^2) (Min-Max)	T_{POC} (mg C m^2) (Min-Max)	T_{PON} (mg C m^2) (Min-Max)
1994/June	41.9443 °N 41.9757 °N	3.5512 °E 3.5928 °E	564-690	2.80 ± 0.84	4015-6348	86724-139656	980825-1228477	2-2	8-11	0.050-0.120	0.001-0.003	0.000-0.001
1995/April - May	36.6137 °N 40.8718 °N	0.2413 °W 4.3492 °W	122-591	2.80 ± 0.00	2575-5395	38764-121927	231383-900939	1-12	4-96	0.048-0.915	0.001-0.022	0.000-0.004
1996/May	36.3230 °N 41.9847 °N	0.1297 °W 4.4587 °W	73-780	2.92 ± 0.20	2673-6514	37460-141053	170765-1203302	1-471	1-2500	0.020-49.75	0.001-1.204	0.000-0.201
1997/May - June	38.8393 °N 42.3940 °N	0.4885 °E 3.5417 °E	134-692	2.65 ± 0.19	2650-5002	47700-103371	534121-1215085	1-18	2-51	0.021-0.536	0.001-0.013	0.000-0.002
1998/May	36.2770 °N 38.4723 °N	0.4687 °E 5.0687 °W	311-671	2.81 ± 0.53	4062-6968	77418-140057	340502-1027780	1-5	8-242	0.057-2.349	0.001-0.057	0.001-0.009
1999/May	36.8240 °N 42.1233 °N	0.4943 °W 3.3762 °E	92-295	3.00 ± 0.39	2323-5786	34380-100098	911952-864252	1-1	2-84	0.087-1.589	0.001-0.038	0.000-0.006
2000/May - June	36.3435 °N 42.4005 °N	1.7772 °W 5.2102 °W	41-428	2.75 ± 0.10	2496-5224	42731-104717	410314-1008333	1-2	3-56	0.030-1.476	0.001-0.036	0.000-0.006
2001/May - June	36.2612 °N 41.4673 °N	0.2453 °W 4.9417 °W	173-750	2.75 ± 0.14	2603-5777	44251-128369	816546-1375411	1-24	1-35	0.010-0.380	0.000-0.009	0.000-0.002
2002/May - June	36.3503 °N 41.9795 °N	0.1488 °W 5.2088 °W	34-770	2.90 ± 0.25	2404-5591	30050-132086	330417-1059819	1-1164	1-3200	0.011-56.01	0.001-1.355	0.000-0.226
2003/April - May	36.2820 °N 42.3935 °N	0.0037 °W 5.2080 °W	35-774	2.89 ± 0.23	1846-7792	33412-175320	290857-1432037	1-308	1-1000	0.009-18.890	0.000-0.457	0.000-0.076
2004/May - June	36.5042 °N 42.1297 °N	0.0053 °W 3.8338 °W	59-724	2.97 ± 0.09	2646-5763	34398-121022	216128-1135494	1-906	2-1450	0.020-11.981	0.000-0.290	0.000-0.048
2005/May	37.7958 °N 41.2802 °N	0.6240 °W 2.7827 °E	44-636	2.97 ± 0.05	2704-5549	41912-123743	368677-971872	1-10	2-206	0.032-4.915	0.001-0.119	0.000-0.020

Table 5.2. Complete MEDITS-ES trawling catches of *Pyrosoma atlanticum carcasses* from 1994 to 2005 with additional meta-data and calculations.

Cast	Date	Time		Latitude		Longitude		Depth (m)		Trawl speed	*a*	*b*	*h*	T_{AREA}	T_{VOLUME}	Carcass	Wet wt	$T_{BIOMASS}$	T_{POC}	T_{PON}
(n°)	(trawl)	Start	End	(Start	End)	(Start	End)	(Start	End)	(knots)	(m)	(m)	(m)	(m^2)	(m^3)	(n°)	(gr)	(mg m^2)	(mg C m^2)	(mg C m^2)
81	19.06.1994	15.18	15.18	41.976°N	41.932°N	3.551°E	3.554°E	570	564	2.2	3.6	21.6	4015	86724	980825	2	11	0.127	0.003	0.001
82	19.06.1994	17.35	17.35	41.944	41.912	3.593°E	3.530°E	682	690	3.4	2.8	22.0	6348	139656	1228477	2	8	0.057	0.001	0.000
2	22.04.1995	11.30	11.30	36.614	36.598	4.349°W	4.371°W	122	130	2.9	1.9	14.7	2637	38764	231383	1	31	0.800	0.019	0.003
30	30.04.1995	8.50	8.50	37.748	37.701	0.241°W	0.255°W	387	390	2.9	2.2	20.9	5392	112693	778876	2	9	0.080	0.002	0.000
36	01.05.1995	12.33	12.33	38.027	38.048	0.322°W	0.306°W	139	139	2.9	1.9	19.0	2740	52060	310747	1	4	0.077	0.002	0.000
38	02.05.1995	6.24	6.24	38.354	38.395	0.487°E	0.520°E	577	576	2.9	2.1	22.6	5395	121927	804394	2	8	0.066	0.002	0.000
39	02.05.1995	8.46	8.46	38.473	38.451	0.424°E	0.413°E	171	180	2.9	2.1	20.2	2697	54479	359419	4	24	0.441	0.011	0.002
48	04.05.1995	13.05	13.05	38.484	38.440	0.477°E	0.450°E	310	309	2.9	2.3	18.9	5389	101852	735948	6	27	0.265	0.006	0.001
50	05.05.1995	6.25	6.25	38.863	38.908	1.026°E	1.012°E	269	269	2.8	2.6	20.6	5091	104875	856630	12	96	0.915	0.022	0.004
51	05.05.1995	8.28	8.28	38.892	38.850	0.969°E	0.980°E	453	461	2.6	2.9	21.0	4709	98889	900939	2	20	0.202	0.005	0.001
53	05.05.1995	14.17	14.17	38.894	38.943	0.921°E	0.933°E	591	589	3.0	2.1	20.8	5561	115669	763106	7	32	0.277	0.007	0.001
54	06.05.1995	6.33	6.33	38.690	38.667	1.084°E	1.084°E	124	124	2.8	2.4	14.4	2575	37080	279576	1	17	0.458	0.011	0.002
55	06.05.1995	10.37	10.37	38.529	38.566	0.956°E	0.920°E	523	520	2.9	2.3	16.2	5226	84661	611733	2	28	0.331	0.008	0.001
70	11.05.1995	7.21	7.21	40.666	40.620	1.403°E	1.394°E	406	398	2.8	2.3	21.0	5113	107373	775840	2	16	0.149	0.004	0.001
71	11.05.1995	11.15	11.15	40.872	40.903	1.449°E	1.496°E	529	521	2.8	2.3	16.1	5205	83801	605514	1	4	0.048	0.001	0.000
12	04.05.1996	14.00	14.00	36.323	36.325	4.459°W	4.389°W	780	771	3.4	2.7	22.5	6269	141053	1196449	1	7	0.050	0.001	0.000
18	06.05.1996	8.37	8.37	36.617	36.610	3.814°W	3.876°W	530	540	3.1	2.3	21.8	5616	122429	884629	1	10	0.082	0.002	0.000
20	06.05.1996	13.58	13.58	36.661	36.658	3.230°W	3.175°W	624	634	2.7	2.7	21.3	4914	104668	887826	1	5	0.048	0.001	0.000
24	07.05.1996	12.11	12.11	36.595	36.589	2.806°W	2.776°W	165	170	3.0	2.3	21.6	2771	59854	432482	1	5	0.084	0.002	0.000
31	09.05.1996	6.24	6.24	36.846	36.886	1.869°W	1.834°W	315	320	3.0	2.3	18.0	5458	98244	709877	1	7	0.071	0.002	0.000
32	09.05.1996	9.05	9.05	37.096	37.143	1.791°W	1.764°W	277	282	3.1	1.4	19.4	5806	112636	495400	26	69	0.613	0.015	0.002
33	09.05.1996	12.05	12.05	37.200	37.254	1.661°W	1.632°W	620	611	2.6	2.8	21.0	6514	136794	1203302	26	76	0.556	0.013	0.002
34	09.05.1996	15.30	15.30	37.379	37.376	1.380°W	1.446°W	415	420	2.7	1.2	18.5	5821	107689	405976	47	250	2.322	0.056	0.009
35	10.05.1996	6.23	6.23	38.072	38.095	0.228°W	0.173°W	232	242	3.0	2.5	22.0	5486	120692	947912	47	781	6.471	0.157	0.026

36	10.05.1996	8.38	8.38	38.033	38.015	0.311°W	0.331°W	156	147	2.9	1.8	15.1	2705	40846	230976	15	131	3.207	0.078	0.013
37	10.05.1996	11.21	11.21	37.870	37.892	0.130°W	0.185°W	467	481	3.0	2.3	16.0	5404	86464	624759	41	236	2.729	0.066	0.011
38	10.05.1996	14.18	14.18	37.734	37.755	0.134°W	0.082°W	533	529	2.8	2.4	20.9	5122	107050	807136	5	9	0.084	0.002	0.000
39	11.05.1996	6.15	6.15	37.817	37.792	0.412°W	0.415°W	159	159	3.0	1.2	16.4	2762	45297	170765	32	803	17.728	0.429	0.072
41	11.05.1996	10.01	10.01	37.903	37.929	0.586°W	0.578°W	66	72	3.2	2.9	17.3	2966	51312	467482	3	31	0.604	0.015	0.002
42	11.05.1996	11.29	11.29	37.963	37.984	0.514°W	0.498°W	94	94	3.0	2.3	18.4	2706	49790	359768	1	15	0.301	0.007	0.001
43	11.05.1996	13.53	13.53	38.191	38.215	0.240°W	0.238°W	88	84	2.9	2.8	17.6	2673	47045	413827	1	5	0.106	0.003	0.000
50	13.05.1996	12.51	12.51	38.493	38.448	0.478°E	0.457°E	296	313	2.9	2.6	21.1	5299	111809	913270	2	25	0.224	0.005	0.001
52	14.05.1996	6.32	6.32	38.830	38.872	0.841°E	0.852°E	668	676	2.6	2.6	22.0	4681	102982	841171	467	900	8.739	0.211	0.035
53	14.05.1996	8.46	8.46	38.883	38.928	0.922°E	0.930°E	600	595	2.8	2.6	21.7	5125	111213	908399	174	574	5.161	0.125	0.021
54	14.05.1996	11.25	11.25	38.882	38.840	0.971°E	0.984°E	467	471	2.6	2.3	18.0	4787	86166	622606	85	590	6.847	0.166	0.028
55	14.05.1996	13.09	13.09	38.858	38.906	1.026°E	1.012°E	281	275	3.0	2.6	18.3	5427	99314	811211	36	170	1.712	0.041	0.007
56	15.05.1996	6.14	6.14	39.896	39.914	0.894°E	0.914°E	144	146	3.0	2.4	18.4	2731	50250	378879	449	2500	49.751	1.204	0.201
57	15.05.1996	8.05	8.05	39.852	39.836	0.737°E	0.712°E	93	90	3.0	2.8	16.0	2730	43680	384229	44	285	6.525	0.158	0.026
58	15.05.1996	10.25	10.25	40.022	40.042	0.889°E	0.910°E	88	90	3.2	2.8	15.7	2916	45781	402712	2	5	0.109	0.003	0.000
59	15.05.1996	11.41	11.41	40.035	40.037	0.984°E	1.021°E	106	106	3.0	2.7	17.5	2761	48318	409843	23	261	5.402	0.131	0.022
60	15.05.1996	13.00	13.00	40.099	40.098	0.921°E	0.887°E	90	91	3.2	2.6	14.5	2947	42732	349037	4	18	0.421	0.010	0.002
62	16.05.1996	6.23	6.23	40.670	40.627	1.397°E	1.385°E	369	370	2.8	2.7	21.8	4954	107997	916064	56	220	2.037	0.049	0.008
63	16.05.1996	10.12	10.12	40.875	40.907	1.456°E	1.507°E	533	523	3.1	1.7	17.2	5559	95615	510650	17	48	0.502	0.012	0.002
64	16.05.1996	12.50	12.50	40.892	40.875	1.536°E	1.483°E	610	611	2.7	2.8	22.7	4855	110209	969444	49	126	1.143	0.028	0.005
67	17.05.1996	16.28	16.28	41.104	41.103	1.520°E	1.551°E	73	79	2.9	2.6	14.2	2638	37460	305975	1	7	0.187	0.005	0.001
73	19.05.1996	6.25	6.25	41.985	41.948	3.510°E	3.476°E	302	301	2.7	2.1	17.3	4979	86137	568273	9	38	0.441	0.011	0.002
74	19.05.1996	8.43	8.43	41.960	41.914	3.523°E	3.509°E	430	433	2.8	1.7	22.2	5211	115684	617835	102	307	2.654	0.064	0.011
75	19.05.1996	12.01	12.01	41.971	41.931	3.571°E	3.549°E	704	702	2.8	2.4	23.1	4809	111088	837582	11	25	0.225	0.005	0.001
76	19.05.1996	14.58	14.58	41.735	41.717	3.379°E	3.357°E	178	172	2.9	2.6	18.3	2689	49209	401943	471	151	3.069	0.074	0.012
78	20.05.1996	6.31	6.31	41.393	41.396	3.270°E	3.211°E	589	571	2.7	2.6	18.1	4931	89251	729015	51	180	2.017	0.049	0.008
79	20.05.1996	8.37	8.37	41.418	41.448	3.259°E	3.298°E	542	550	2.8	2.4	18.0	4688	84384	636240	25	97	1.150	0.028	0.005
80	20.05.1996	11.12	11.12	41.469	41.494	3.149°E	3.089°E	345	352	3.1	2.4	17.8	5659	100730	759487	34	127	1.261	0.031	0.005
83	21.05.1996	6.27	6.27	41.298	41.297	2.729°E	2.693°E	653	661	3.3	2.0	17.0	3047	51799	325462	5	15	0.290	0.007	0.001
105	27.05.1996	5.37	5.37	39.001	38.968	0.500°E	0.538°E	791	798	2.6	2.4	20.2	4935	99687	751622	19	65	0.652	0.016	0.003
106	27.05.1996	9.00	9.00	38.991	39.021	0.189°E	0.184°E	113	116	3.1	2.3	17.9	2832	50693	366289	1	1	0.020	0.000	0.000

53	24.05.1997	6.43	6.43	38.839	38.879	0.845°E	0.868°E	657	663	2.7	2.5	21.2	4876	103371	811875	7	12	0.116	0.003	0.000
54	24.05.1997	10.32	10.32	38.891	38.933	0.924°E	0.929°E	589	585	2.5	3.9	21.3	4656	99173	1215085	18	35	0.353	0.009	0.001
56	24.05.1997	15.19	15.19	38.901	38.859	1.010°E	1.028°E	293	253	2.7	3.5	20.0	4937	98740	1085702	2	6	0.061	0.001	0.000
68	27.05.1997	10.00	10.00	42.394	42.387	3.432°E	3.400°E	141	136	3.0	3.5	17.6	2760	48576	534121	1	6	0.124	0.003	0.000
73	28.05.1997	6.02	6.02	41.921	41.945	3.542°E	3.582°E	682	692	2.4	3.1	22.6	4236	95734	932343	1	2	0.021	0.001	0.000
74	28.05.1997	8.22	8.22	41.953	41.912	3.522°E	3.502°E	409	416	2.6	3.2	17.5	4794	83895	843404	4	6	0.072	0.002	0.000
75	28.05.1997	11.14	11.14	41.981	41.943	3.502°E	3.471°E	316	302	2.7	2.7	15.8	5002	79032	670369	1	3	0.038	0.001	0.000
78	26.05.1997	6.35	6.35	41.554	41.533	2.804°E	2.788°E	158	134	2.9	3.8	18.0	2650	47700	569445	1	25	0.524	0.013	0.002
81	29.05.1997	14.44	14.44	41.395	41.394	3.220°E	3.272°E	580	590	2.4	3.5	22.0	4321	95062	1045260	15	51	0.536	0.013	0.002
102	03.06.1997	13.19	13.19	39.001	38.969	0.489°E	0.522°E	737	785	2.6	2.7	19.7	4838	95309	808435	1	5	0.052	0.001	0.000
6	05.05.1998	10.26	10.26	36.277	36.316	5.069°W	5.033°W	367	365	2.9	2.0	19.2	5366	103027	647338	4	242	2.349	0.057	0.009
11	07.05.1998	5.34	5.34	36.395	36.389	4.478°W	4.530°W	562	570	2.6	1.4	16.5	4692	77418	340502	1	73	0.943	0.023	0.004
12	07.05.1998	8.19	8.19	36.364	36.359	4.422°W	4.344°W	660	671	3.8	2.2	20.1	6968	140057	968002	1	8	0.057	0.001	0.000
14	07.05.1998	14.36	14.36	36.354	36.364	4.720°W	4.676°W	558	559	2.2	2.5	22.2	4062	90176	708243	1	56	0.621	0.015	0.003
19	09.05.1998	3.15	3.15	36.569	36.540	3.072°W	3.032°W	584	579	2.6	2.5	22.4	4807	107677	845691	1	32	0.297	0.007	0.001
48	18.05.1998	15.05	15.05	38.472	38.430	0.469°E	0.442°E	301	311	2.8	3.4	18.3	5258	96221	1027780	5	13	0.135	0.003	0.001
32	12.05.1999	10.06	10.06	36.824	36.850	1.901°W	1.852°W	263	272	2.8	2.9	18.1	5241	94862	864252	1	2	0.021	0.001	0.000
47	16.05.1999	13.27	13.27	37.990	37.972	0.494°W	0.509°W	92	93	2.6	4.0	14.8	2323	34380	432036	1	3	0.087	0.002	0.000
56	19.05.1999	10.05	10.05	38.542	38.594	0.497°E	0.503°E	295	290	3.1	2.9	17.3	5786	100098	911952	1	48	0.480	0.012	0.002
81	25.05.1999	8.30	8.30	42.123	42.104	3.376°E	3.356°E	123	120	3.5	2.9	16.7	3166	52872	481698	1	84	1.589	0.038	0.006
6	23.05.2000	13.21	13.21	36.344	36.358	4.830°W	4.779°W	428	422	2.6	1.8	21.6	4848	104717	592159	1	20	0.191	0.005	0.001
10	24.05.2000	14.05	14.05	36.348	36.369	5.210°W	5.201°W	48	41	2.7	3.3	15.2	2496	37939	393325	1	56	1.476	0.036	0.006
19	26.05.2000	15.10	15.10	36.719	36.710	3.623°W	3.594°W	83	75	2.9	2.9	16.3	2763	45037	410314	1	9	0.200	0.005	0.001
36	31.05.2000	10.25	10.25	37.106	37.145	1.777°W	1.747°W	370	375	2.8	3.2	19.6	5170	101332	1018700	2	14	0.138	0.003	0.001
84	16.06.2000	13.35	13.35	42.401	42.395	3.437°E	3.408°E	139	134	2.7	3.3	17.3	2470	42731	443003	1	6	0.140	0.003	0.001
91	18.06.2000	13.08	13.08	41.413	41.393	2.749°E	2.692°E	269	273	2.8	3.2	19.2	5224	100301	1008333	1	3	0.030	0.001	0.000

5	13.05.2001	8.10	8.10	36.261	36.236	4.942°W	4.993°W	631	652	2.9	3.1	21.6	5374	116078	1130479	1	13	0.112	0.003	0.000
11	14.05.2001	11.55	11.55	36.368	36.370	4.516°W	4.461°W	652	651	2.7	3.2	22.6	4984	112638	1132364	1	1	0.009	0.000	0.000
18	17.05.2001	6.30	6.30	36.601	36.605	3.590°W	3.540°W	535	541	2.5	2.5	22.9	4540	103966	816546	1	4	0.038	0.001	0.000
30	20.05.2001	6.35	6.35	36.505	36.522	2.199°W	2.150°W	566	564	2.6	3.9	22.4	4789	107274	1314338	1	3	0.028	0.001	0.000
32	20.05.2001	12.54	12.54	36.824	36.860	1.784°W	1.753°W	725	715	2.6	4.0	22.6	4843	109452	1375411	1	1	0.009	0.000	0.000
41	23.05.2001	6.37	6.37	37.704	37.747	0.245°W	0.229°W	419	411	2.7	3.6	19.5	4971	96935	1096302	10	22	0.227	0.005	0.001
42	23.05.2001	8.35	8.35	37.732	37.747	0.152°W	0.099°W	523	528	2.7	3.3	22.4	4980	111552	1156487	9	18	0.161	0.004	0.001
43	23.05.2001	11.28	11.28	37.872	37.888	0.150°W	0.201°W	459	468	2.6	3.7	19.1	4793	91546	1064123	3	1	0.011	0.000	0.000
44	23.05.2001	13.33	13.33	37.875	37.909	0.287°W	0.321°W	403	393	2.6	3.5	18.6	4811	89485	983934	22	34	0.380	0.009	0.002
51	25.05.2001	5.29	5.29	38.336	38.373	0.470°E	0.502°E	576	569	2.6	3.8	21.1	4936	104150	1243342	2	6	0.058	0.001	0.000
55	27.05.2001	6.16	6.16	38.449	38.469	0.408°E	0.421°E	178	173	2.8	3.5	17.0	2603	44251	486565	1	4	0.090	0.002	0.000
63	28.05.2001	10.23	10.23	39.047	39.085	0.308°E	0.270°E	291	306	2.9	3.0	18.1	5381	97396	917936	1	1	0.010	0.000	0.000
64	28.05.2001	13.35	13.35	39.006	38.972	0.478°E	0.582°E	740	750	2.9	3.3	24.6	5339	131339	1361628	12	35	0.266	0.006	0.001
69	30.05.2001	7.54	7.54	38.693	38.641	1.063°E	1.068°E	214	216	3.0	3.5	19.2	5777	110918	1219610	1	4	0.036	0.001	0.000
71	01.06.2001	10.35	10.35	39.212	39.207	1.575°E	1.513°E	309	315	2.9	3.4	20.7	5367	111097	1186671	1	2	0.018	0.000	0.000
85	04.06.2001	8.51	8.51	40.908	40.877	1.509°E	1.462°E	524	532	2.8	3.0	21.9	5227	114471	1078866	3	2	0.017	0.000	0.000
86	04.06.2001	11.36	11.36	40.943	40.916	1.539°E	1.492°E	460	470	2.7	3.2	21.6	5002	108043	1086168	2	2	0.019	0.000	0.000
106	10.06.2001	6.42	6.42	41.392	41.391	3.297°E	3.230°E	612	616	3.0	3.0	22.7	5655	128369	1209844	1	1	0.008	0.000	0.000
107	10.06.2001	10.29	10.29	41.416	41.447	3.251°E	3.295°E	481	471	2.7	2.9	20.9	5068	105921	965007	24	10	0.094	0.002	0.000
108	10.06.2001	12.22	12.22	41.467	41.482	3.158°E	3.098°E	348	341	2.8	3.0	20.2	5269	106434	1003114	2	4	0.038	0.001	0.000
10	14.05.2002	6.15	6.15	36.350	36.371	5.209°W	5.200°W	50	34	2.4	3.5	12.5	2404	30050	330417	1	141	4.692	0.114	0.019
21	16.05.2002	11.24	11.24	36.706	36.719	3.583°W	3.608°W	67	68	2.8	2.9	16.8	2637	44302	403615	3	180	4.063	0.098	0.016
22	16.05.2002	13.54	13.54	36.683	36.688	3.275°W	3.217°W	371	386	2.8	2.4	20.3	5170	104951	791311	2	135	1.286	0.031	0.005
23	16.05.2002	15.35	15.35	36.663	36.663	3.216°W	3.159°W	638	592	2.8	2.1	23.2	5155	119596	789015	1	29	0.242	0.006	0.001
24	17.05.2002	6.26	6.26	36.595	36.591	2.817°W	2.788°W	178	181	2.9	2.4	18.8	2687	50516	380878	1	7	0.139	0.003	0.001
34	19.05.2002	13.56	13.56	36.484	36.479	2.926°W	2.983°W	602	622	2.8	2.6	22.5	5125	115313	941888	2	35	0.304	0.007	0.001
50	23.05.2002	15.22	15.22	37.875	37.895	0.283°W	0.313°W	414	330	2.9	1.9	20.0	4691	93820	560014	1	1	0.011	0.000	0.000
58	26.05.2002	11.37	11.37	38.070	38.099	0.225°W	0.172°W	208	220	3.0	2.9	16.4	5591	91692	835374	2	14	0.153	0.004	0.001
62	27.05.2002	11.40	11.40	38.337	38.374	0.470°E	0.504°E	545	576	2.7	2.8	22.7	5053	114703	1008980	3	6	0.052	0.001	0.000
63	27.05.2002	13.46	13.46	38.440	38.484	0.447°E	0.477°E	302	311	3.0	2.4	21.5	5538	119067	897743	1	2	0.017	0.000	0.000

72	29.05.2002	8.30	8.30	38.880	38.834	0.973°E	0.986°E	468	463	2.8	2.9	22.2	5240	116328	1059819	2	3	0.026	0.001	0.000
73	29.05.2002	12.00	12.00	38.833	38.879	0.838°E	0.853°E	662	704	2.8	2.4	23.4	5241	122639	924679	1	3	0.024	0.001	0.000
75	30.05.2002	6.29	6.29	39.630	39.591	0.320°E	0.281°E	305	329	2.9	2.9	20.6	5377	110766	1009148	1	2	0.018	0.000	0.000
78	30.05.2002	13.08	13.08	39.365	39.373	0.149°W	0.180°W	73	64	3.2	3.2	15.9	2826	44933	451719	1	4	0.089	0.002	0.000
98	04.06.2002	13.34	13.34	40.966	40.948	1.433°E	1.409°E	283	286	3.0	2.8	21.6	2840	61344	539610	5	5	0.082	0.002	0.000
100	05.06.2002	6.32	6.32	41.041	41.033	1.844°E	1.780°E	418	412	3.0	2.9	20.8	5481	114005	1038653	51	61	0.535	0.013	0.002
103	06.06.2002	8.43	8.43	41.297	41.306	2.261°E	2.294°E	154	151	3.4	3.2	17.6	2957	52043	523195	86	60	1.153	0.028	0.005
104	06.06.2002	11.35	11.35	41.283	41.291	2.320°E	2.351°E	224	227	2.8	3.1	19.0	2725	51775	504233	492	361	6.972	0.169	0.028
105	06.06.2002	13.17	13.17	41.218	41.211	2.326°E	2.300°E	402	398	2.4	1.2	23.6	4475	105610	398140	210	631	5.975	0.145	0.024
106	06.06.2002	15.40	15.40	41.169	41.176	2.413°E	2.440°E	702	770	2.6	3.0	23.1	4780	110418	1040664	175	233	2.110	0.051	0.009
108	07.06.2002	11.20	11.20	41.491	41.506	2.712°E	2.739°E	139	141	3.0	3.0	17.2	2809	48315	455356	1	2	0.041	0.001	0.000
110	08.06.2002	8.38	8.38	41.725	41.701	3.248°E	3.234°E	129	130	3.3	3.2	18.4	2961	54482	547716	271	407	7.470	0.181	0.030
111	08.06.2002	11.25	11.25	41.676	41.695	3.369°E	3.386°E	226	230	2.9	3.1	18.5	2616	48396	471325	299	1090	22.523	0.545	0.091
114	09.06.2002	11.15	11.15	41.980	41.958	3.273°E	3.280°E	112	131	2.7	3.4	18.6	2494	46388	495493	83	110	2.371	0.057	0.010
115	09.06.2002	13.26	13.26	41.947	41.966	3.471°E	3.494°E	293	314	3.2	2.6	19.8	5746	113771	929295	151	181	1.591	0.038	0.006
116	09.06.2002	15.28	15.28	41.949	41.900	3.526°E	3.514°E	430	480	2.9	2.5	20.3	5457	110777	870041	51	48	0.433	0.010	0.002
117	10.06.2002	6.31	6.31	41.388	41.390	3.301°E	3.232°E	638	617	3.1	2.5	23.1	5718	132086	1037399	121	149	1.128	0.027	0.005
118	10.06.2002	8.45	8.45	41.413	41.441	3.244°E	3.288°E	486	468	2.5	2.7	19.9	4762	94764	803814	159	317	3.345	0.081	0.014
119	10.06.2002	11.34	11.34	41.460	41.470	3.153°E	3.122°E	356	346	3.3	2.7	20.2	2828	57126	484556	1164	3200	56.017	1.355	0.226
120	10.06.2002	13.24	13.24	41.540	41.552	2.933°E	2.901°E	104	108	3.3	3.2	18.7	2994	55988	562850	52	50	0.893	0.022	0.004
4	27.04.2003	6.08	6.08	36.351	36.367	5.208°W	5.183°W	47	35	3.1	3.6	16.8	2800	47040	532009	3	394	8.376	0.203	0.034
6	27.04.2003	10.14	10.14	36.282	36.318	5.063°W	5.022°W	365	335	3.0	3.2	21.6	5376	116122	1167381	2	235	2.024	0.049	0.008
8	27.04.2003	15.00	15.00	36.289	36.299	4.791°W	4.741°W	753	761	2.5	3.1	24.2	4637	112215	1092858	1	4	0.036	0.001	0.000
10	28.04.2003	8.35	8.35	36.338	36.337	4.355°W	4.303°W	719	720	2.5	3.1	23.8	4655	110789	1078966	1	1	0.009	0.000	0.000
11	28.04.2003	11.53	11.53	36.528	36.553	4.388°W	4.340°W	257	252	2.8	3.1	20.1	5059	101686	990312	1	157	1.544	0.037	0.006
12	28.04.2003	13.43	13.43	36.565	36.588	4.267°W	4.218°W	304	308	2.7	2.9	20.2	5052	102050	929741	6	730	7.153	0.173	0.029
13	29.04.2003	7.43	7.43	36.616	36.628	4.095°W	4.041°W	341	346	2.7	3.2	21.6	4993	107849	1084213	2	209	1.938	0.047	0.008
15	29.04.2003	12.55	12.55	36.616	36.606	3.770°W	3.717°W	504	518	2.6	2.8	20.7	4807	99505	875290	1	206	2.070	0.050	0.008
18	30.04.2003	7.40	7.40	36.680	36.688	3.280°W	3.222°W	387	392	2.8	3.0	21.2	5217	110600	1042383	1	3	0.027	0.001	0.000
23	01.05.2003	7.25	7.25	36.718	36.714	2.277°W	2.306°W	251	216	2.8	3.4	17.6	2606	45866	489909	2	2	0.044	0.001	0.000

24	01.05.2003	9.11	9.11	36.651	36.640	2.414°W	2.471°W	331	321	2.8	3.4	20.2	5230	105646	1128448	17	145	1.373	0.033	0.006
26	01.05.2003	15.20	15.20	36.502	36.519	2.208°W	2.157°W	514	605	2.7	3.3	23.4	4917	115058	1192833	2	7	0.061	0.001	0.000
27	02.05.2003	6.22	6.22	36.838	36.856	1.888°W	1.870°W	269	292	2.7	2.9	20.2	2566	51833	472232	3	5	0.096	0.002	0.000
28	02.05.2003	8.39	8.39	36.863	36.825	1.750°W	1.784°W	707	730	2.8	3.1	23.5	5191	121989	1188037	7	11	0.090	0.002	0.000
44	05.05.2003	13.27	13.27	38.077	38.101	0.004°W	0.049°E	610	600	2.9	2.9	22.8	4764	108619	989587	7	73	0.672	0.016	0.003
45	06.05.2003	6.12	6.12	38.277	38.293	0.156°E	0.180°E	151	149	3.0	3.2	18.5	2736	50616	508847	2	10	0.198	0.005	0.001
46	06.05.2003	8.01	8.01	38.241	38.281	0.293°E	0.330°E	449	457	3.0	2.0	21.8	5545	120881	759517	1	3	0.025	0.001	0.000
47	06.05.2003	11.10	11.10	38.337	38.371	0.465°E	0.511°E	537	603	3.0	2.9	23.0	5474	125902	1147044	66	324	2.573	0.062	0.010
48	06.05.2003	13.36	13.36	38.447	38.491	0.451°E	0.479°E	296	305	2.9	2.9	22.2	5431	120568	1098450	30	163	1.352	0.033	0.005
49	06.05.2003	15.42	15.42	38.461	38.441	0.417°E	0.401°E	176	177	2.9	3.2	18.2	2671	48612	488703	7	65	1.337	0.032	0.005
50	07.05.2003	6.14	6.14	39.109	39.127	0.113°E	0.096°E	122	124	2.9	3.4	17.0	2533	43061	459952	3	2	0.046	0.001	0.000
51	07.05.2003	7.50	7.50	39.144	39.116	0.180°E	0.232°E	308	332	3.0	3.1	20.8	5448	113318	1103600	2	7	0.062	0.001	0.000
52	07.05.2003	10.54	10.54	39.014	38.980	0.480°E	0.522°E	748	774	2.9	3.4	17.0	5336	90712	968932	11	27	0.298	0.007	0.001
53	07.05.2003	14.04	14.04	38.932	38.951	0.374°E	0.357°E	188	186	2.8	3.1	17.5	2595	45413	442269	31	119	2.620	0.063	0.011
54	07.05.2003	16.00	16.00	38.898	38.916	0.222°E	0.200°E	99	98	2.9	3.6	16.9	2731	46154	521988	1	24	0.520	0.013	0.002
55	08.05.2003	6.19	6.19	39.610	39.571	0.301°E	0.261°E	235	279	3.0	3.2	21.3	5562	118471	1190995	40	198	1.671	0.040	0.007
56	08.05.2003	8.50	8.50	39.498	39.451	0.256°E	0.190°E	556	612	4.0	2.6	22.5	7792	175320	1432037	63	345	1.968	0.048	0.008
57	08.05.2003	11.34	11.34	39.434	39.412	0.020°W	0.033°W	115	113	2.9	3.0	17.9	2682	48008	452462	6	20	0.417	0.010	0.002
58	08.05.2003	12.56	12.56	39.367	39.390	0.092°W	0.102°W	89	86	3.0	3.3	16.0	2784	44544	461799	1	4	0.090	0.002	0.000
68	11.05.2003	6.14	6.14	39.829	39.845	0.702°E	0.727°E	95	96	3.0	3.1	16.7	2777	46376	451652	2	8	0.173	0.004	0.001
69	11.05.2003	7.54	7.54	39.894	39.912	0.889°E	0.913°E	144	151	3.0	3.0	18.1	2820	51042	481059	21	64	1.254	0.030	0.005
70	11.05.2003	9.53	9.53	40.012	40.031	0.874°E	0.897°E	92	94	3.2	3.2	16.2	2935	47547	477994	58	367	7.719	0.187	0.031
71	11.05.2003	11.22	11.22	40.037	40.069	0.995°E	1.021°E	125	115	3.0	3.1	17.0	2820	47940	466884	12	53	1.106	0.027	0.004
72	11.05.2003	12.56	12.56	40.107	40.129	1.134°E	1.152°E	175	180	3.0	2.9	17.5	2814	49245	448652	8	21	0.426	0.010	0.002
73	12.05.2003	6.13	6.13	40.310	40.285	1.269°E	1.263°E	137	140	3.0	2.9	17.3	2799	48423	441160	33	160	3.304	0.080	0.013
74	12.05.2003	7.50	7.50	40.300	40.323	1.121°E	1.133°E	96	96	3.0	3.1	18.4	2797	51465	501212	8	28	0.544	0.013	0.002
75	12.05.2003	9.51	9.51	40.412	40.436	1.045°E	1.057°E	88	86	3.1	3.1	17.9	2866	51301	499621	6	10	0.195	0.005	0.001
76	12.05.2003	11.20	11.20	40.531	40.544	1.014°E	1.040°E	78	79	2.9	3.2	17.5	2681	46918	471666	1	27	0.575	0.014	0.002
77	12.05.2003	12.38	12.38	40.606	40.630	1.108°E	1.107°E	85	87	2.8	3.2	17.6	2650	46640	468876	18	133	2.852	0.069	0.012
78	12.05.2003	15.15	15.15	40.924	40.949	1.229°E	1.223°E	89	86	3.0	3.1	17.5	2821	49368	480787	47	248	5.024	0.122	0.020
79	13.05.2003	7.01	7.01	41.085	41.083	1.334°E	1.367°E	67	71	3.0	3.2	16.6	2756	45750	459925	4	15	0.328	0.008	0.001

80	13.05.2003	8.18	8.18	41.023	41.006	1.376°E	1.352°E	141	143	2.9	3.1	19.2	2799	53741	523378	73	356	6.624	0.160	0.027
81	13.05.2003	10.34	10.34	40.935	40.918	1.424°E	1.404°E	336	338	2.7	3.1	19.2	2536	48691	474200	58	108	2.218	0.054	0.009
82	13.05.2003	12.16	12.16	40.876	40.896	1.489°E	1.541°E	587	607	2.7	2.1	23.6	4918	116065	765719	165	65	0.560	0.014	0.002
83	13.05.2003	14.44	14.44	40.862	40.849	1.520°E	1.468°E	684	690	2.5	2.5	23.2	4578	106210	834168	61	130	1.224	0.030	0.005
84	14.05.2003	6.30	6.30	41.161	41.172	2.366°E	2.429°E	661	735	2.9	2.7	24.3	5427	131876	1118612	57	171	1.297	0.031	0.005
86	14.05.2003	11.07	11.07	41.283	41.289	2.312°E	2.346°E	221	230	3.1	3.0	19.8	2844	56311	530720	44	8	0.142	0.003	0.001
87	14.05.2003	12.32	12.32	41.306	41.298	2.293°E	2.260°E	151	150	3.1	2.9	19.1	2874	54893	500112	4	33	0.601	0.015	0.002
89	15.05.2003	9.14	9.14	41.429	41.430	2.499°E	2.532°E	84	94	2.9	3.1	16.6	2696	44754	435852	11	55	1.229	0.030	0.005
90	15.05.2003	11.09	11.09	41.398	41.420	2.702°E	2.765°E	275	275	3.1	2.7	22.0	5828	128216	1087566	23	99	0.772	0.019	0.003
91	15.05.2003	13.54	13.54	41.302	41.282	2.728°E	2.778°E	624	650	2.5	2.2	22.8	4741	108095	747097	9	31	0.287	0.007	0.001
92	16.05.2003	6.24	6.24	42.005	41.981	3.597°E	3.596°E	621	657	2.6	2.8	23.1	2791	64472	567126	31	84	1.303	0.032	0.005
93	16.05.2003	8.46	8.46	41.906	41.952	3.516°E	3.526°E	475	424	2.8	2.6	21.8	5162	112532	919173	300	700	6.220	0.151	0.025
94	16.05.2003	11.31	11.31	42.126	42.170	3.625°E	3.641°E	539	529	2.8	2.6	21.3	5153	109759	896525	200	600	5.467	0.132	0.022
95	16.05.2003	13.43	13.43	42.109	42.088	3.593°E	3.577°E	465	435	2.8	2.9	20.8	2657	55266	503503	232	800	14.476	0.350	0.058
96	16.05.2003	15.45	15.45	42.128	42.107	3.385°E	3.366°E	125	123	3.0	3.1	18.2	2757	50177	488674	54	124	2.471	0.060	0.010
97	17.05.2003	6.15	6.15	42.394	42.387	3.430°E	3.397°E	140	137	3.0	3.0	18.6	2805	52173	491719	6	30	0.575	0.014	0.002
100	17.05.2003	11.15	11.15	41.977	41.952	3.271°E	3.280°E	112	142	3.1	2.9	18.2	2894	52671	479863	2	31	0.589	0.014	0.002
101	17.05.2003	13.44	13.44	41.700	41.680	3.394°E	3.374°E	236	228	3.0	3.0	18.9	2801	52939	498937	308	1000	18.890	0.457	0.076
104	18.05.2003	9.04	9.04	41.729	41.706	3.252°E	3.237°E	129	129	3.0	3.1	18.8	2764	51963	506066	19	94	1.809	0.044	0.007
105	18.05.2003	11.40	11.40	41.434	41.419	3.277°E	3.255°E	466	475	2.7	1.8	20.9	2461	51435	290857	27	109	2.119	0.051	0.009
106	18.05.2003	13.21	13.21	41.460	41.472	3.147°E	3.117°E	357	344	3.0	2.9	21.3	2813	59917	545880	114	496	8.278	0.200	0.033
107	18.05.2003	15.10	15.10	41.536	41.546	2.942°E	2.911°E	104	106	3.0	3.1	16.7	2728	45558	443682	25	162	3.556	0.086	0.014
108	19.05.2003	6.15	6.15	41.143	41.141	1.782°E	1.815°E	63	69	3.0	3.2	14.6	2768	40413	406273	1	5	0.124	0.003	0.000
109	19.05.2003	7.37	7.37	41.183	41.173	1.891°E	1.862°E	43	41	2.9	3.4	14.8	2711	40123	428568	1	3	0.075	0.002	0.000
111	20.05.2003	7.06	7.06	41.262	41.247	2.142°E	2.132°E	76	75	2.0	3.1	18.1	1846	33413	325403	13	73	2.185	0.053	0.009
114	20.05.2003	13.39	13.39	41.006	40.981	1.260°E	1.261°E	82	95	3.0	3.2	18.3	2687	49172	494331	4	20	0.407	0.010	0.002
115	20.05.2003	14.57	14.57	40.990	40.965	1.187°E	1.190°E	74	79	3.0	3.2	18.0	2787	50166	504323	2	16	0.319	0.008	0.001
15	09.05.2004	11.49	11.49	36.616	36.600	3.834°W	3.883°W	530	534	3.0	2.1	21.1	4760	100436	662610	1	2	0.020	0.000	0.000
23	11.05.2004	8.33	8.33	36.719	36.713	2.283°W	2.313°W	251	246	2.9	2.6	16.2	2735	44307	361906	11	30	0.677	0.016	0.003
27	12.05.2004	6.10	6.10	36.878	36.837	1.845°W	1.879°W	327	309	2.9	2.7	11.2	5380	60256	511109	2	10	0.166	0.004	0.001

28	12.05.2004	8.48	8.48	36.863	36.895	1.750°W	1.742°W	706	698	2.9	3.4	17.5	4562	79835	852750	188	419	5.248	0.127	0.021
29	12.05.2004	11.30	11.30	37.112	37.158	1.779°W	1.756°W	300	293	3.0	2.4	15.5	5553	86072	648963	20	41	0.476	0.012	0.002
30	12.05.2004	13.45	13.45	37.225	37.262	1.667°W	1.635°W	501	547	2.9	2.4	18.3	5015	91775	691963	6	20	0.218	0.005	0.001
32	13.05.2004	7.44	7.44	37.359	37.347	1.557°W	1.584°W	150	157	3.0	2.4	16.2	2747	44501	335532	2	5	0.112	0.003	0.000
33	13.05.2004	9.37	9.37	37.381	37.389	1.433°W	1.372°W	490	414	2.9	2.2	22.3	5427	121022	836444	906	1450	11.981	0.290	0.048
34	13.05.2004	12.13	12.13	37.508	37.512	1.180°W	1.150°W	178	185	3.0	2.5	18.1	2735	49504	388799	12	15	0.303	0.007	0.001
37	14.05.2004	5.56	5.56	37.686	37.729	0.335°W	0.309°W	256	250	2.8	2.4	16.1	5284	85072	641430	234	748	8.793	0.213	0.035
38	14.05.2004	8.07	8.07	37.716	37.760	0.245°W	0.226°W	406	398	2.8	2.3	19.4	5192	100725	727803	107	203	2.015	0.049	0.008
39	14.05.2004	10.28	10.28	37.729	37.747	0.157°W	0.098°W	520	521	3.0	2.4	20.4	5511	112424	847659	43	101	0.898	0.022	0.004
40	14.05.2004	13.05	13.05	37.871	37.892	0.136°W	0.195°W	458	500	3.1	2.4	21.2	5650	119780	903119	112	341	2.847	0.069	0.011
43	15.05.2004	9.07	9.07	37.927	37.950	0.472°W	0.457°W	110	110	3.0	3.6	18.1	2835	51314	580342	19	76	1.481	0.036	0.006
44	15.05.2004	10.59	10.59	38.006	38.030	0.577°W	0.566°W	59	59	3.0	3.4	17.3	2789	48250	515375	5	8	0.166	0.004	0.001
47	16.05.2004	10.55	10.55	38.121	38.112	0.064°W	0.094°W	272	279	2.9	3.5	18.8	5493	103268	1135494	7	26	0.252	0.006	0.001
48	16.05.2004	12.26	12.26	38.101	38.086	0.172°W	0.197°W	222	217	3.0	3.4	19.3	2783	53712	573719	9	35	0.652	0.016	0.003
49	16.05.2004	14.45	14.45	38.075	38.101	0.005°W	0.052°E	609	602	3.1	2.3	17.8	5014	89249	644884	33	133	1.490	0.036	0.006
51	17.05.2004	8.00	8.00	38.243	38.284	0.294°E	0.330°E	448	454	3.0	2.4	18.8	5509	103569	780893	244	440	4.248	0.103	0.017
52	17.05.2004	10.29	10.29	38.333	38.372	0.463°E	0.504°E	539	578	3.1	2.4	18.7	5621	105113	792530	242	774	7.364	0.178	0.030
53	17.05.2004	12.53	12.53	38.451	38.472	0.408°E	0.423°E	174	172	3.0	2.4	19.0	2735	51965	391807	99	296	5.696	0.138	0.023
54	17.05.2004	14.46	14.46	38.641	38.665	0.404°E	0.396°E	118	115	3.0	2.5	17.4	2813	48946	384422	10	25	0.511	0.012	0.002
55	18.05.2004	6.43	6.43	38.828	38.875	0.830°E	0.850°E	677	701	3.0	2.3	19.6	5516	108114	781192	320	400	3.700	0.090	0.015
56	18.05.2004	9.13	9.13	38.900	38.951	0.925°E	0.935°E	577	601	3.1	2.3	18.7	5669	106010	765994	303	979	9.235	0.223	0.037
57	18.05.2004	11.39	11.39	38.882	38.835	0.972°E	0.988°E	463	460	2.9	2.2	19.2	5446	104563	722688	551	1013	9.688	0.234	0.039
58	18.05.2004	14.08	14.08	38.894	38.869	1.017°E	1.022°E	266	282	3.0	2.4	18.3	2793	51112	385374	152	394	7.709	0.187	0.031
60	19.05.2004	6.44	6.44	38.984	39.022	0.500°E	0.455°E	740	730	3.1	2.3	21.2	5702	120882	873455	31	110	0.910	0.022	0.004
61	19.05.2004	9.36	9.36	39.111	39.124	0.243°E	0.216°E	341	322	3.0	2.3	19.2	2805	53856	389145	14	40	0.743	0.018	0.003
67	20.05.2004	12.55	12.55	39.458	39.482	0.189°E	0.241°E	600	580	2.8	2.4	18.9	5237	98979	746286	47	66	0.667	0.016	0.003
68	20.05.2004	15.13	15.13	39.566	39.588	0.255°E	0.275°E	282	282	3.1	2.3	18.6	2893	53810	388811	46	66	1.227	0.030	0.005
70	21.05.2004	7.57	7.57	39.899	39.916	0.898°E	0.922°E	147	167	3.1	2.3	18.2	2839	51670	373348	34	40	0.774	0.019	0.003
75	22.05.2004	6.17	6.17	40.293	40.316	1.263°E	1.268°E	135	130	2.8	2.0	13.0	2646	34398	216129	3	9	0.262	0.006	0.001
76	22.05.2004	8.18	8.18	40.302	40.324	1.120°E	1.133°E	95	95	3.0	2.3	17.2	2716	46715	337548	17	53	1.135	0.027	0.005
84	23.05.2004	14.19	14.19	40.862	40.851	1.520°E	1.455°E	684	684	3.0	2.3	20.1	5572	111997	809253	3	5	0.045	0.001	0.000

85	24.05.2004	6.35	6.35	41.162	41.176	2.371°E	2.430°E	661	724	2.9	2.2	18.8	5203	97816	676058	20	15	0.153	0.004	0.001
86	24.05.2004	8.57	8.57	41.221	41.207	2.348°E	2.288°E	403	398	2.8	1.9	16.0	5283	84528	504549	1	2	0.024	0.001	0.000
89	25.05.2004	6.45	6.45	41.387	41.392	3.297°E	3.231°E	639	606	3.0	2.2	20.6	5512	113547	784781	6	7	0.062	0.001	0.000
90	25.05.2004	9.10	9.10	41.420	41.454	3.247°E	3.292°E	568	540	3.0	2.3	20.1	5270	105927	765392	11	15	0.142	0.003	0.001
100	28.05.2004	6.34	6.34	42.130	42.176	3.625°E	3.645°E	538	534	3.0	2.5	20.1	5423	109002	856101	3	6	0.055	0.001	0.000
107	29.05.2004	12.32	12.32	41.912	41.959	3.513°E	3.525°E	452	409	2.9	2.5	19.3	5386	103950	816419	30	6	0.058	0.001	0.000
108	29.05.2004	15.00	15.00	41.969	42.014	3.576°E	3.612°E	695	631	3.1	2.7	17.8	5763	102581	870125	3	5	0.049	0.001	0.000
122	02.06.2004	7.32	7.32	36.504	36.528	2.201°W	2.148°W	500	448	3.0	2.4	20.3	5437	110371	832178	1	4	0.036	0.001	0.000
36	18.05.2005	5.59	5.59	37.796	37.820	0.624°W	0.935°E	47	44	3.0	2.9	16.0	2841	45456	414132	1	2	0.044	0.001	0.000
54	22.05.2005	10.26	10.26	38.898	38.946	0.925°E	0.733°E	577	590	2.9	2.0	18.1	5333	96527	606498	2	26	0.269	0.007	0.001
67	25.05.2005	6.11	6.11	39.833	39.849	0.709°E	0.919°E	95	97	3.0	2.8	18.3	2790	51057	449120	4	86	1.684	0.041	0.007
68	25.05.2005	7.51	7.51	39.900	39.918	0.896°E	1.133°E	142	153	3.0	2.6	19.1	2751	52544	429187	3	53	1.009	0.024	0.004
74	26.05.2005	7.04	7.04	40.300	40.322	1.120°E	2.723°E	96	95	2.9	2.8	15.5	2704	41912	368677	10	206	4.915	0.119	0.020
89	30.05.2005	12.13	12.13	41.280	41.303	2.783°E	3.554°E	636	628	3.0	2.5	22.3	5549	123743	971872	1	4	0.032	0.001	0.000

in the same stations. Hence, the consistency of the sampling protocol make *P. atlanticum* catches comparable through time (Table 5.1, 5.2). Once onboard, trawls were split into five categories: (A) Fish, (B) Crustaceans Decapoda and Stomatopoda, (C) Cephalopods, (D) Other commercial species, (E) Other non-commercial animal species (e.g. *P. atlanticum* carcasses). For each species (including *P. atlanticum* carcasses) the total weight (individual) in grams and number of individuals was recorded (*see* Table 5.1, 5.2). The material was not frozen for further analysis because the MEDITS-ES original surveys did not intend to assess gelatinous depositions.

5.2.3. *Pyrosoma atlanticum* biochemistry and field estimations

Pyrosoma atlanticum carcasses were collected in 2010 by means of trawling surveys at 1226 m in the Catalan Sea (Expedition Antromare). (Fig. 5.1), to measure organic carbon, nitrogen and the C/N. We used a similar sampling protocol as for the samples collected during the 1994-2005 period to have a conservative assessment of carcasses biochemistry since measurements from old carcasses could bias analytical results. In brief, four carcasses were measured (n = 4 - 5.45 ±0.22 cm), then frozen at -20 °C and dried for 48 h at 60 °C, and weighted (n = 4 - 2.092 ±0.065 mg dry weight). A sub-sample from each carcass was cut and re-weighted (n = 4 - 1.037 ±0.027 mg dry weight). The four samples were then carefully introduced in tin vessels and closed for analysis. Organic carbon and nitrogen were measured in a Euro EA 3000 elemental analyzer with acetanilide standards at the Helmholtz Centre for Ocean Research Kiel (GEOMAR) (Germany). The mean carcass organic carbon and nitrogen dry weight % was 20.08 ±5.41 and 3.35 ±0.86 respectively, while the C/N (mol/mol) was 5.12 ±0.15. These conversion factors were used to assess the organic carbon and nitrogen based on the wet weights recorded in trawls. Wet weight conversion (wt/dwt %) were done using published data (Lebrato and Jones 2009) from samples collected in the same area in the spring of 2007 (wt/dwt % = 12.05 ±1.17). Using the total number of carcasses and the wet weight from each trawl, we computed estimations of dry weight, and then to organic carbon and nitrogen percentages using the values from the elemental analyzer. The trawled (T) biomass, POC and PON in mg per m^2 per haul were calculated using the individual trawl biomass ($T_{BIOMASS}$) using the T_{AREA} from Eq. 1 (*see* Table 5.1, 5.2) along with the trawl POC (T_{POC}) and PON (T_{PON}) from individual hauls as follows:

$$T_{BIOMASS}\ (\text{mg m}^2) = (\text{wt} / T_{AREA}) * 1000 \quad (3)$$

$$T_{POC}\ (\text{mg C m}^2) = T_{BIOMASS} * \text{dw/dwt \%} * \text{POC \%} \quad (4)$$

$$T_{PON}\ (\text{mg N m}^2) = T_{BIOMASS} * \text{dw/dwt \%} * \text{PON \%} \quad (5)$$

where wt = wet weight, $T_{AREA} = b$ h (*see* Eq. 1), dw/dwt % = 12.05, POC % = 20.08, and PON % = 3.35. POC and PON %s were used directly from the dry weight (elemental analyzer).

Note that the trawling method in combination with the area estimation does not distinguish biomass spatial distribution. Thus we cannot assess if carcasses accumulated in certain areas (as previously done using video or towed photography), increasing the local particulate matter export.

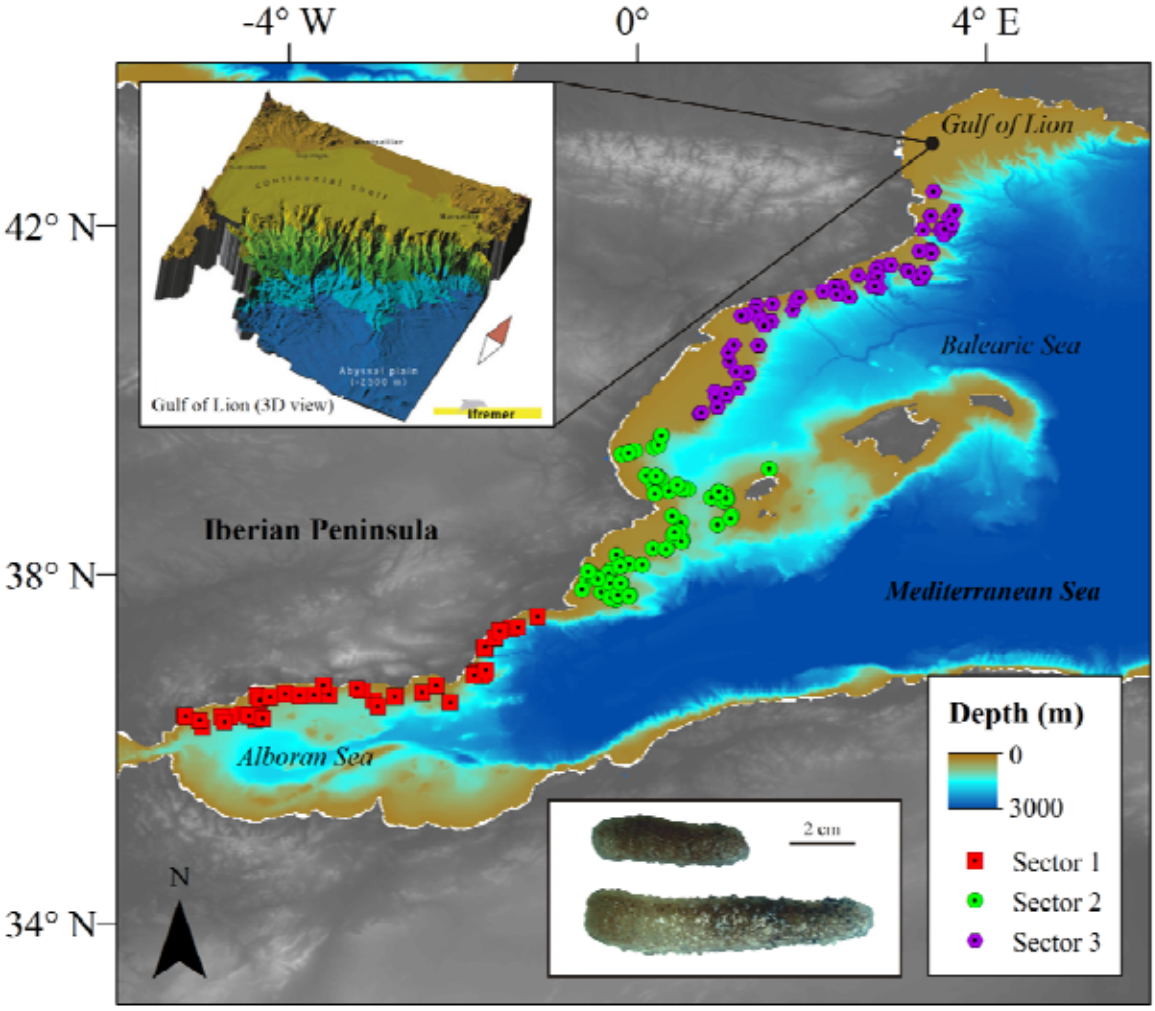

Fig. 5.1. Study region in the western Mediterranean Sea margin showing sampling sites (trawls) separated by sector. Also included is a detailed 3D bathymetry display (copyright by Ifremer) of the canyon complexity in the north of sector 3 and a photo of freshly caught *Pyrosoma atlanticum* carcasses. General bathymetry map data taken from the General Bathymetric Chart of the Oceans (GEBCO) digital atlas (IOC et al. 2003).

5.2.4. *Pyrosoma atlanticum* sinking speed

Two extra *Pyrosoma atlanticum* carcasses collected in 2010 (section 5.2.3) were used to measure biomass sinking rate in the laboratory. These estimates are the first for gelatinous zooplankton biomass. In brief, we used laboratory facilities at OceanLab, Jacobs University (Germany) in April 2011 in two separate days. Pyrosome samples were collected in the Catalan Sea by plankton net (CTD field surface temperature = 24.49 °C, salinity = 37.75, density = 1025.60 kg m^{-3}), then frozen at - 20 °C and sent frozen to OceanLab, Jacobs University (Germany). Organisms were thawed for 24 h at 5 °C (to prevent degradation) in a temperature-controlled room in the same water used in the column before each experimental day. Pyrosomes were sunk as whole bodies in a clear acrylic column 118.50 cm tall, with a diameter of 19 cm (volume = 30 L) in a temperature-controlled enclosure at 10 °C. The acrylic column was filled with freshwater at the beginning of each experimental day, and the salinity was established by adding NaCl. Two carcasses were sunk 3 times each under similar conditions as in the field, i.e. temperature = 11.50 °C, salinity = 37.80, and density = 1028.89 kg m^{-3}. We placed a 1 m ruler inside the column to have a dimension reference for post-video analyses. The exact water column height before each sinking event (100 cm) and the actual sinking events were recorded with a video camera Canon Legria HF R16 mounted on an Erno P-55 tripod placed 1 m away from the column. All videos were analyzed using video software during terminal velocity on a straight line to assess sinking rate. The final averaged sinking rate of two carcasses sunk three times each was 1278 ±133 m day^{-1}.

5.2.5. Acquisition of satellite temperature and chlorophyll *a* data

Chlorophyll *a* data were derived from the Sea-viewing Wide Field-of-view Sensor (SeaWiFS) and the Moderate Resolution Imaging Spectroradiometer (MODIS, on-board Aqua) missions. We used as Chla (and also SST) locations the coordinates given where trawls started, assuming that Pyrosomes inhabited water masses in the vicinity (search radius of ±1 km). The Chla data processing followed the new methods presented by Mélin et al. (2011) extended to the entire Mediterranean basin. First, the remote sensing reflectance data from the 2 satellite missions were merged through an optically-based merging technique. Then, Chla was computed with two algorithms, one proposed for the open Mediterranean waters (Volpe et al. 2007) and one developed for coastal regions (D'Alimonte and Zibordi 2003). Note that in the coastal area we

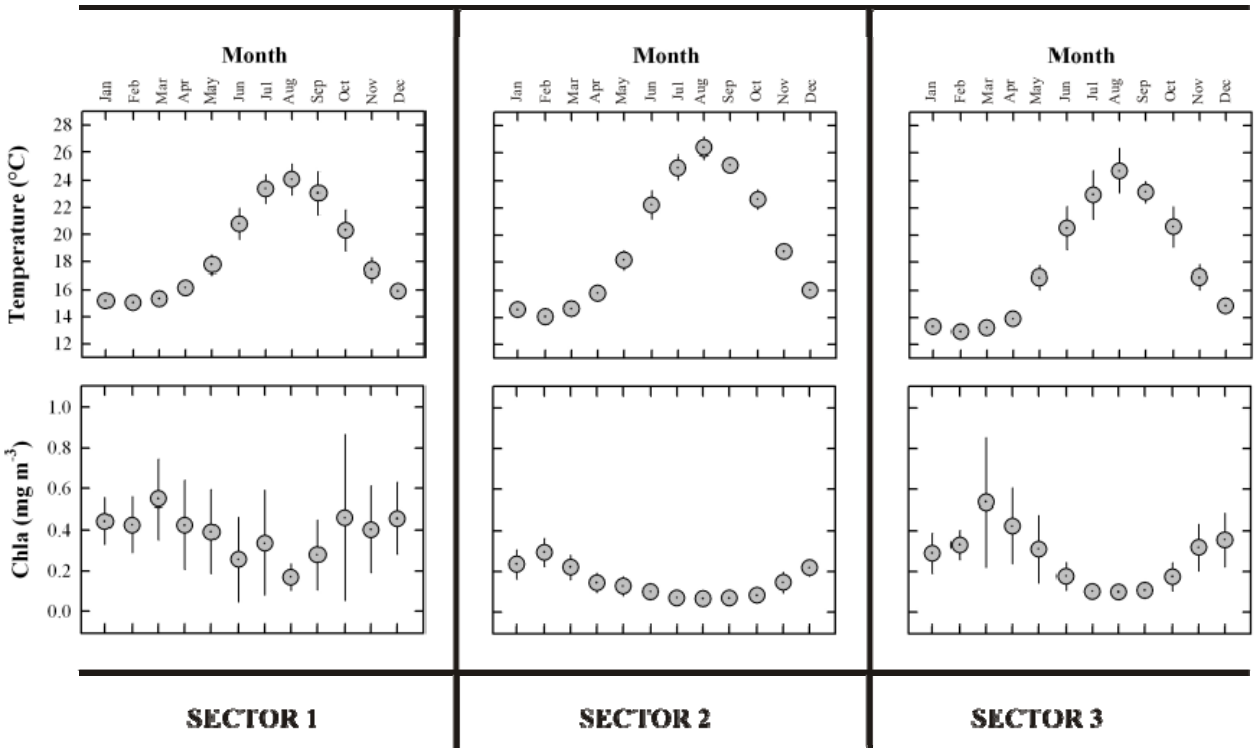

Fig. 5.2. Temperature and chlorophyll *a* (Chla) mean monthly values from 1994 to 2005 at each sector. Standard deviations show the time-series variability per month.

did not include high Chla levels of e.g. local upwelling events. The domain of applicability of each algorithm was determined through a novel detection approach (D'Alimonte et al. 2003) by computing the probability of each input reflectance spectrum belonging to the optical class associated with open sea or coastal waters. The final Chla values were a weighted average with weights defined by these probabilities. Time composites were then generated from the daily maps. Satellite values were extracted from an equidistant grid with a 2-km spatial resolution for the location and time of interest. We divided the Chla data in two parts: 1) Specific 1-day, 8-day and 1-month composites (depending on availability) at the exact site of the jelly-fall from April to June, and 2) monthly composites for each year at each location. Chla data however did not cover the years 1994 to 1997, available data existed from late 1997 (data summary in Fig. 5.2). For the series of SST we used the Pathfinder data set (v.5, Vázquez-Cuervo et al. 2010) obtained from the Physical Oceanography Distributed Active Archive Center (PODAAC, NASA). The data were mapped on a 4.8-km equidistant global grid. Only the grid points with the highest level of quality flags were considered in the analysis. We divided the SST database in the same way as Chla. In this case, SST data were available from 1994 to 2005 in 1-day composites in part 1 (thus we did not use 8-day and 1-month data), and from 1998 to 2005 in part 2. For

analysis, we only used data from 1997 to 2005 to match the Chla time series (data summary in Fig. 5.2). For both Chla and SST, the extracted satellite values were obtained by bi-linear interpolation of the four satellite data around the location of interest (Table 5.1, 5.2). The result was considered valid only if 4 satellite retrievals were available.

Hydroclimate data were obtained from the NCEP/NCAR re-analysis of monthly series from the Earth System Research Laboratory of the National Oceanic and Atmospheric Administration (NOAA) (http://www.esrl.noaa.gov/psd/data/timeseries/). The long term trend of hydroclimatic forcing was extracted by applying a principal component analysis (PCA) on the sea surface temperature, precipitation rate, outgoing long- wave radiation and 500 mb geopotential height monthly time series. Only the first component (PC1) was subsequently used for analysis.

5.2.6. Time-series analyses and statistics

Before analyzing the hydroclimate, data were seasonally detrended by subtracting the monthly average to each individual value. Principal component analysis (PCA) was applied to the hydroclimate matrix (year * month). The first component resulting from this analysis (PC1 capturing 63 % of the total variance) was subsequently used to investigate structural environmental changes. Structural changes in the hydroclimate long term trend were addressed using Cumulative Sum of Ordinary Least Square residuals (CUSUM-OLS) (Ploberger and Krämer 1992). The method is an extension of the classical CUSUM analysis using Ordinary Least Squares (OLS) residuals instead of recursive residuals. OLS residuals were obtained from fitting the PC1 scores to a linear regression with time as covariate, and CUSUM-OLS was used to calculate the empirical fluctuation process. To identify significant changes in the structure of the empirical fluctuation process along time a boundary limit was calculated using a generalized fluctuation test, establishing as the model null hypothesis that the fluctuation process remains constant with a 0.95 confidence limit. Analyses were done in Matlab Software (The MathWorks, Inc. UK)

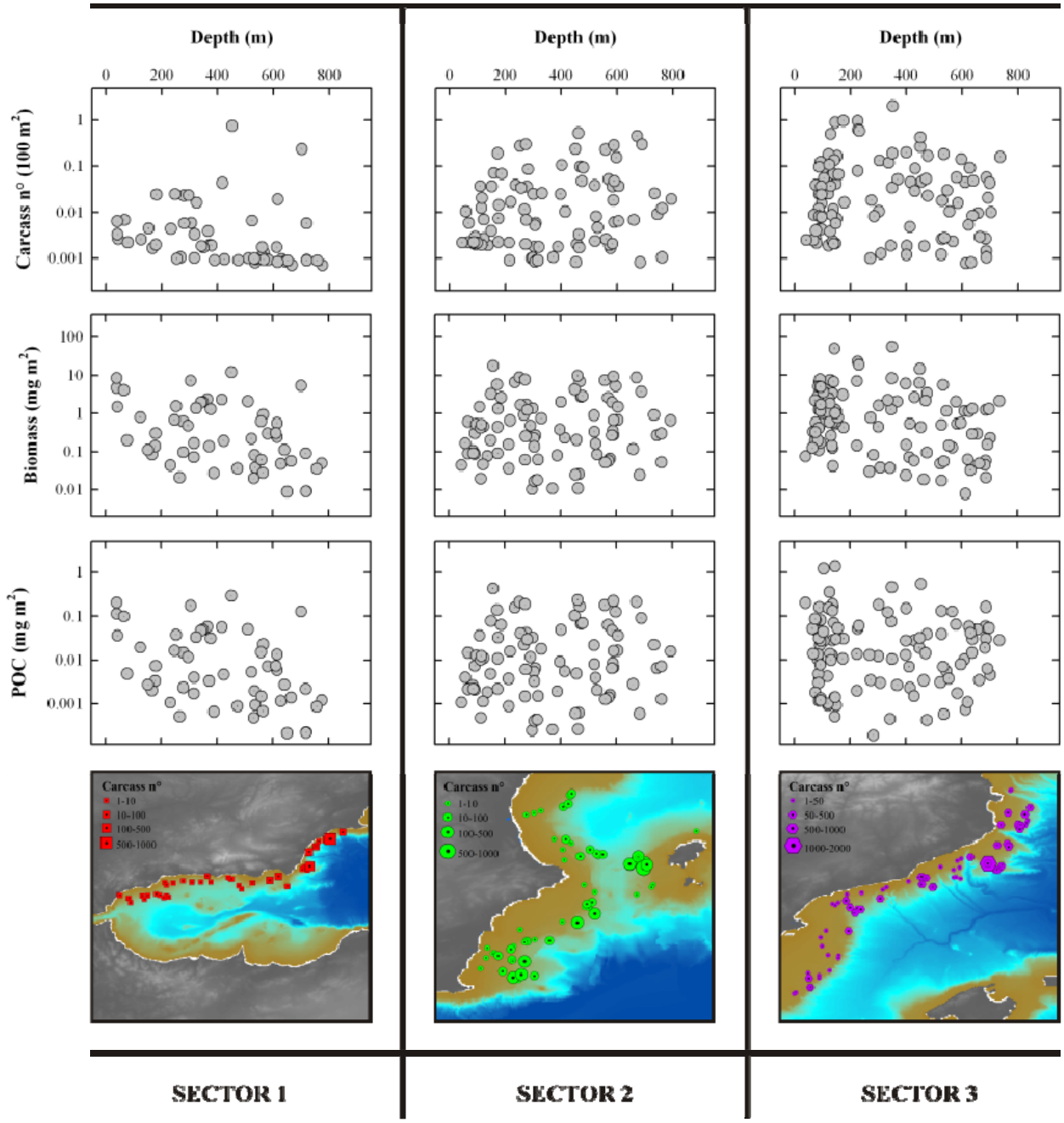

Fig. 5.3. Trends of *Pyrosoma atlanticum* carcass n°, total biomass and total particulate organic carbon (POC) *vs.* depth normalized to unit area using the total trawled area per haul at each sector. Also included are total carcass n° raw data displayed in maps and spatial distribution per sector.

5.3. Results and Discussion

Low biomass of Pyrosome jelly-falls was found from 1994 to 2001. On average a number < 30 carcasses per trawl was sampled, except in 1996 when the number reach up to 471 carcasses per

trawl (biomass = 49.75 mg m^2) (Table 5.1). Successful trawls at these low densities varied from 2 to 20 depending on the year (Table 5.2). From 2002 to 2004, however, a noticeable increase in biomass was observed with a maxima of carcasses per trawl of 1164 (biomass = 56.01 mg m^2), 308 (biomass = 18.89 mg m^2), and 906 (biomass = 11.98 mg m^2), respectively, and a total of carcasses varying from 1000 to > 3000 gr of wet material. During the period 2002-2004 the number of successful trawls ranged from 30 to 68 depending on year (Table 5.2). The total biomass (60 mg C m2) and carbon export (POC: 2 mg C m^2) in any trawl (Table 5.1; Fig. 5.3) remained , relatively low compared to the 22 g C m^2 observed also for Pyrosomes off Ivory Coast (Lebrato and Jones 2009). Our observations however, should be considered cautiously due to the large area integrated (30,050 to 175,320 m^2), which likely mask local accumulations that can drastically increase the POC per unit area. Moreover, such large explored area impairs a direct comparison with other estimates (e.g. video or photography; reviewed by Lebrato et al. 2012) due to the consideration of only the visible sampling seabed to quantify biomass deposition, however it provides the first evidence of jelly-falls over a wide area in the Mediterranean Sea and shows a conspicuous increase after the 2000.

Jelly-falls are extremely patchy events, and logistically difficult to quantify. Local POC input can reach high values (10 to 70 g C m^2), e.g. in the Arabian Sea (Billett et al. 2006) and off Ivory Coast (Lebrato and Jones 2009), although we might expect generally lower values in the Mediterranean Sea due to the relative lower biological production compared to the above areas. We observed that the Pyrosome biomass was evenly distributed over the range 0 - 800 m depth except in sector 1 (Alboran Sea), where a decrease with depth was observed. Overall, biomass patchiness was noticed at any depth, suggesting that Pyrosome blooms occupy large areas in the western Mediterranean shelf where they sink from different depths (section 5.2.4) or sink from the Benthic Boundary Layer (BBL). Such hypothesis further suggests that in the area explored, Pyrosome carcasses reach the shelf and slope seabed within a low time window after blooms collapse, allowing low remineralization in the water column (Lebrato et al. 2011). Carcasses reach the seabed at different depth bands (average sinking rate > 1200 m day^{-1}) and are transported at varying rates down slope, accumulating along geomorphological bottom features.

In particular, the area investigated in sector 3 was characterised by extensive continental shelves (60-120 km wide) facing the Gulf of Lion and the Ebro river, but a narrow shelf in the Balearic Islands (20 km). In the Gulf of Lion, the shelf is dissected by large canyons that extend down to

the Catalan Sea (Fig. 5.1). Along the Ebro slope and Catalan margin are mainly short canyons, and no canyons exist along Mallorca and Minorca. This suggests that organic matter associated with Pyrosomes originally sinks in the shelf as suggested by the large accumulation from 0 to 200 m (Fig. 5.3), and then progressively moves down canyons to slope depths. The largest accumulation was observed at the edge of the shelf and in canyon mouths. A similar phenomena has been observed for phytodetritus (Danovaro et al. 1999), and is probably related to the transport of particulate organic matter associated with cascading events extending from the Gulf of Lions along and across the continental slope reported by Company et al. (2008). The cascading process enhances the recruitment of deep-sea living communities. This reinforces the notion of a Pyrosome benthic transport pathway redistributing the biomass and not an in situ sinking event. Whether accumulation and final decomposition takes place in the shelf or deep slope remains unknown, although the deep slope decomposition hypothesis looks most likely at least in sector 2 and 3. Western Mediterranean Sea margins and probably others in all oceans harbour these Pyrosome and other jelly-falls on a seasonal basis or during the whole year, with biomass export peaks depending on productivity regimes (*see* time-series results below). These inputs provide additional food for the impoverished deep-sea sediments, where organisms may scavenge on the jelly-falls (Lebrato and Jones 2009; Sweetman and Chapman 2011). Their abundance and distribution could also be potentially driven by jelly material at least in areas where biomass accumulates (such as shelf breaks, Fig. 5.3) along with other sinking particles, aggregates, and phytodetritus (Gooday and Turley 1990).

The correlation of the Pyrosome depositions and the sea surface temperature and Chla proved complicated. Sector 1 (Alboran Sea) is characterized by turbulent mixing governed by the opposing flows of the Mediterranean and the Atlantic which enhance productivity year round (*see* Fig. 5.2). High Chla levels remain through the year following eddy features, large water exchange regimes, frontal instabilities causing vertical mixing and bringing cold and nutrient-rich waters to the surface (Boucher et al. 1987; Fig. 5.2). The Alboran Sea is dominated by small-size fractions: nanoflagellates (2-10 μm), diatoms, and coccolithophores. Early diatom blooms happen as soon as January, while the late bloom is in April (Delgado 1990). This coincides with the period when Pyrosome blooms likely collapse and die, probably in March and April following the highest Chla concentrations (in all sectors). This contrasts with sector 2, where Chla remains much stable year-round, following only seasonal oscillations (Fig. 5.2). In sector 3, the localized upwelling events in the Gulf of Lions and the influence of the Ebro Delta

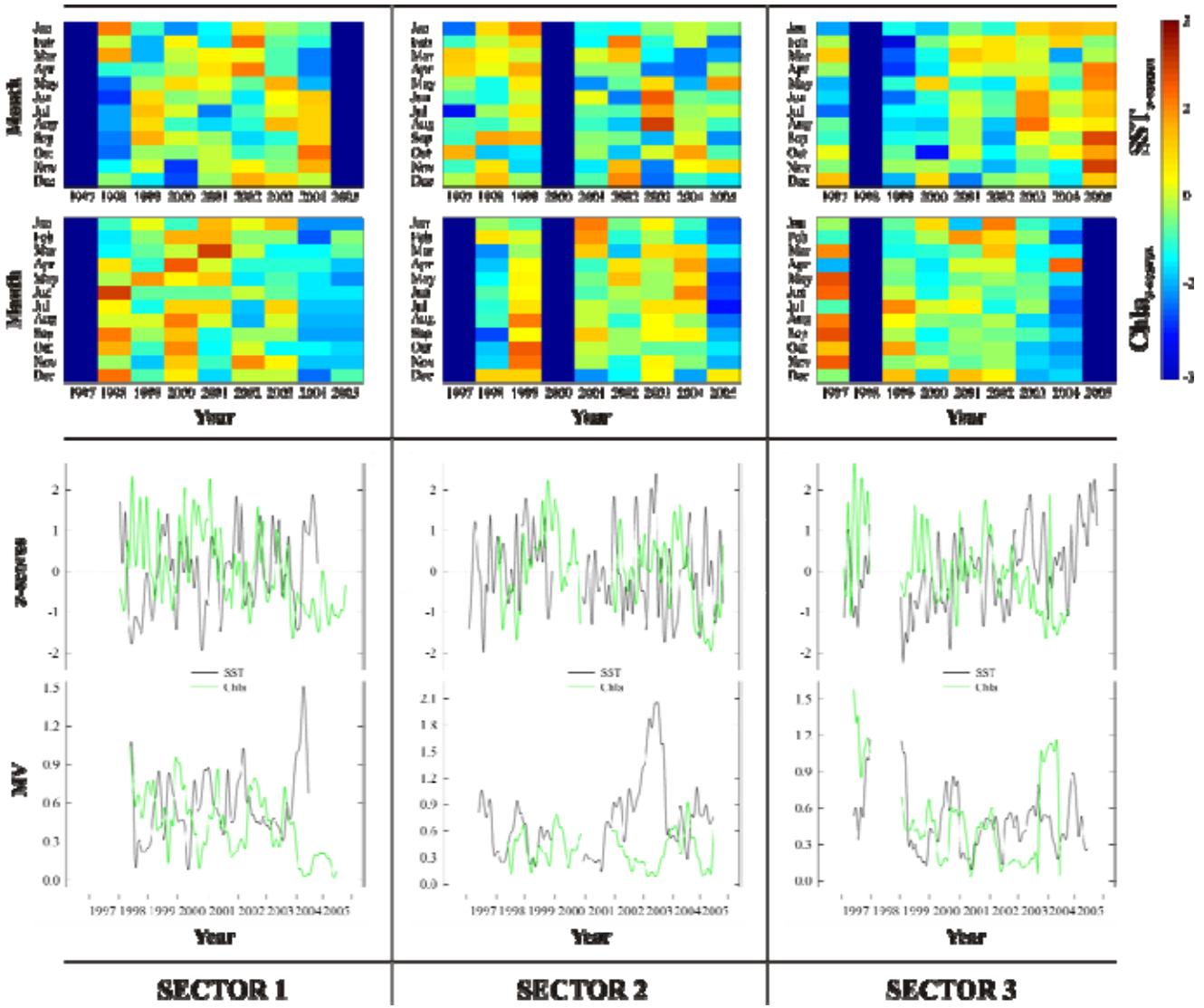

Fig. 5.4. z-scores and moving variance (MV) of monthly sea surface temperature (SST) and chlorophyll *a* (Chla) from 1994 to 2005 divided per sector.

cause large variability around monthly Chla means (Fig. 5.2). We suggest that this increases the Pyrosome biomass export locally, following upwelling-induced blooms collapse. Chla large spatiotemporal variability (Velasquez 1997) in this sector creates large Chla patchiness. This can be explained by the "chimneys", where mixing can reach the seabed and is associated with high productivity (Lefevre et al. 1997). The Catalan Front also contributes to the high productivity regimes (Estrada and Salat 1989). Chla biomass tends to concentrate in the first 50 km from shore (Estrada et al. 1999) within the shelf, which suggests that Pyrosomes bloom and collapse there and are then are transported to deeper areas directly at the seabed. Isolated upwelling events exist in the area, highly related to the shape and processes of the local coastline (Millot and Wald 1981). We suggest that these regional features could explain the complexity and patchiness of the Pyrosome depositions especially on the upper part of sector 3 (Fig. 5.3). In sector 2 we found considerably less Pyrosome biomass than in sector 3, which may be associated to low productivity regimes (Fig. 5.2), which are known to occur in the Balearic basin (Estrada et al. 1999).

Our results further point out a conspicuous change in SST, Chla, and hydroclimate conditions in the western Mediterranean that occurred in the late 1990s (*see* Fig. 5.4, 5.5, 5.6), with increasing SST and Chla anomalies after 2002 (Fig. 5.4). Such environmental modification agree with a manifested change in the thermal gradient between surface and 75 m depth around 1999 recently reported in the Balearic Archipelago (Fernandez de Puelles and Molinero in review). Whilst sea surface temperature and summer stratification revealed a noticeable increase after the late 1990s, winters appear colder and salinity increase as well. In turn, such changes appeared related with modification in plankton communities, in particular with an increase of gelatinous zooplankton, as well as the length of the peak of maximum abundance. This translated into a higher jelly biomass export following hydroclimate, and SST and Chla anomalies (Fig. 5.5) that enhanced regionally the carbon flux. Similar changes in the structure of plankton communities have been observed in the Mediterranean basin, as shown by the increase in jellyfish blooms intensity (Molinero et al. in review). Our observations allow suggesting that the greater Pyrosomes biomass depositions after 2000 are likely part of an ecosystem-wide modification in the western Mediterranean in which the role of jelly-falls coupling bentho-pelagic systems is naturally enhanced. We also suggest that the increase in jelly-falls biomass is a cyclical phenomenon following productivity regimes coupled to hydroclimate (Fig. 5.5, 5.6). If increased jelly carbon export continues in the future remains speculative, but if it happens, it becomes relevant in the

context of global change to mitigate losses of carbon from phytoplankton (Buesseler et al. 2007) that regulate the strength of the biological pump.

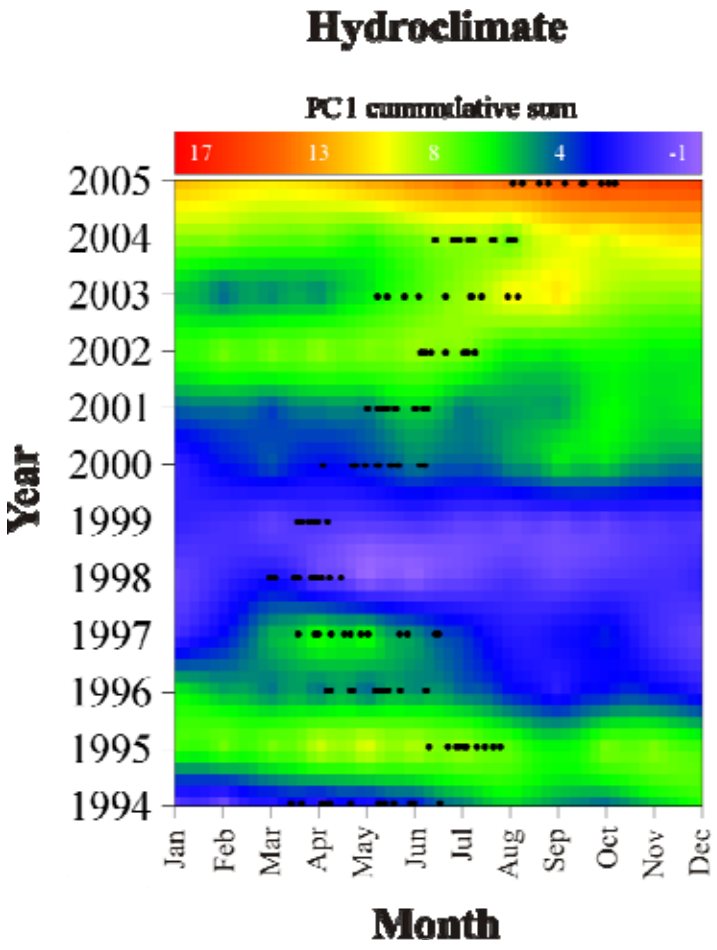

Seawater and biomass

SST	Chla	Bio	SST	Chla	Bio	SST	Chla	Bio	SST	Chla	Bio
1.46	0.61	-0.69	-0.27		-0.65	0.42	-3.76	-0.61	0.72	0.06	-1.05
-1.37	0.02	2.41	-1.84	0.51	1.45	-1.72	1.66	-0.76	-1.76	1.10	-0.30
1.83	1.28	1.48	1.48	0.72	-0.13	1.51	-0.49	-0.05	1.79	0.86	0.01
-0.25	1.30	0.52	-0.13	0.05	-0.68	-0.08	-0.96	1.43	-0.18	0.43	1.34
0.94	-0.26	-0.67	0.66	0.41	-0.63	0.44	0.21	-0.80	0.78	-0.04	-1.25
0.06	-0.50	-0.31	1.17	0.90	-0.71	1.59	1.00	-0.80	0.90	0.37	-1.21
0.47	-1.24	-0.69	-0.43	-1.95	-0.60	-0.21	-0.83	-0.74	0.02	-2.04	-1.19
-0.87	-1.21	-0.09	-0.09	-4.89	-0.68	-0.24		-0.81	-0.50	-0.75	-1.17
-0.06		-0.69	1.34		-0.63	0.71		-0.79	0.62		-1.24
-0.77		-0.09	-0.59		-0.71	-0.64		-0.81	-0.74		-1.18
-0.87		-0.49	-1.09		-0.51	-1.26		-0.80	-1.15		-1.20
-0.57		-0.69	-0.21		-0.71	-0.52		-0.80	-0.49		-1.27
SECTOR 1			SECTOR 2			SECTOR 3			ALL sectors		

Fig. 5.5. Monthly hydroclimate first principal Component (PC1) cumulative sum data from 1994 to 2005. Also included is a quartile analysis of the z-scores of sea surface temperature (SST), chlorophyll *a* (Chla), and the normalized (per unit area) *Pyrosoma atlanticum* biomass from 1994 to 2005 separately for each sector and then for all sectors.

Appendix A

Fig. 5.6. Monthly hydroclimate first principal Component (PC1) individual values extended from 1950 to 2011 and then amplified for the study period from 1994 to 2005.

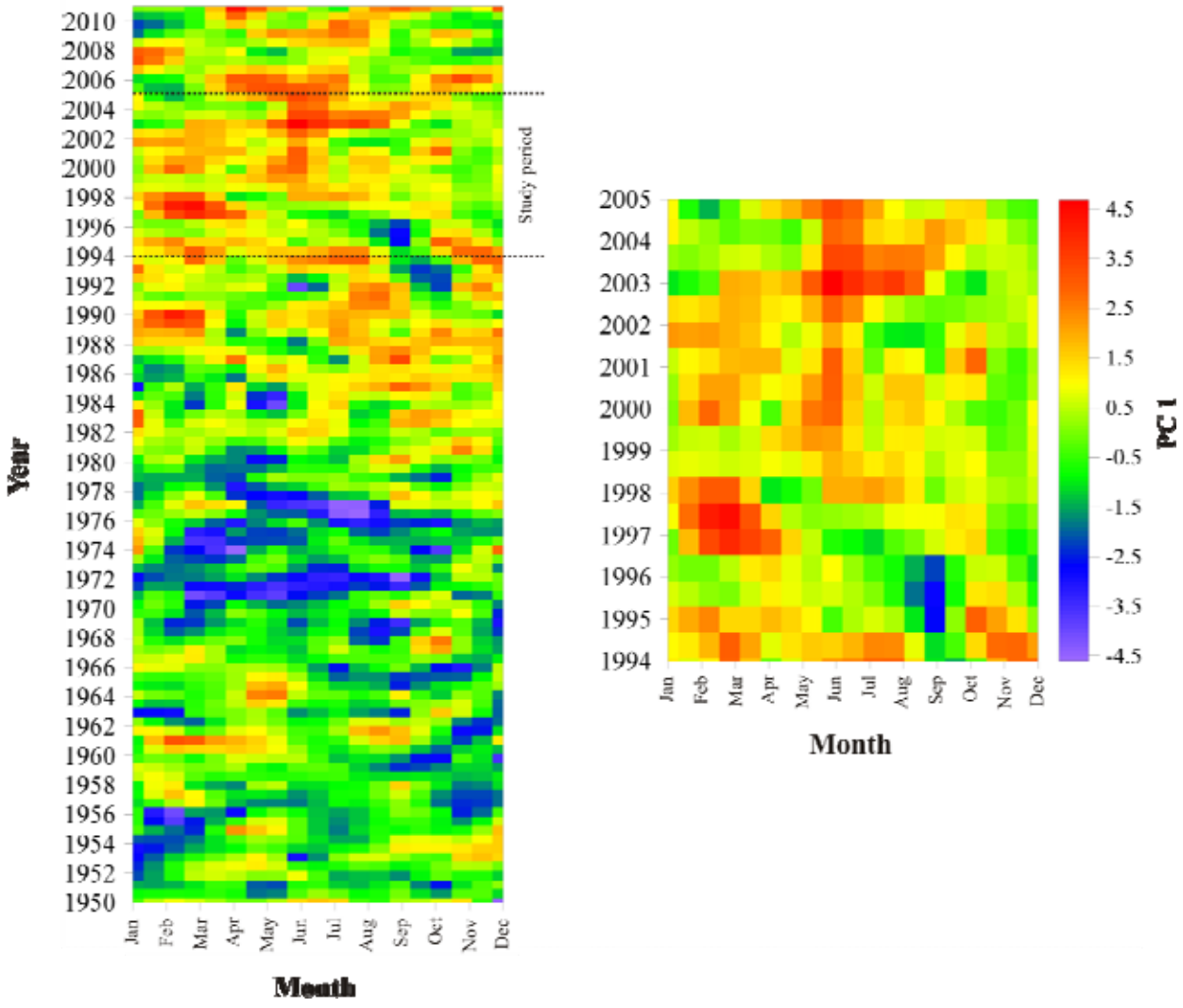

6.

Proximate, elemental composition, and biometric relationships in gelatinous zooplankton

Abstract

A wide range of marine organisms have a gelatinous body, but the extent is greatest in the medusae (phylum Cnidaria), ctenophores (phylum Ctenophora) and the pelagic tunicates (phylum Chordata, class Thaliacea). Although there are taxonomic and trophic differences between the thaliaceans and the other two closely-related phyla, the collective term "jellyfish" is used in this article. Because of the apparent increase in bloom events, jellyfish are receiving attention from the wider marine science community. Questions being posed include: 1) what is the role of jellyfish in pelagic food webs in a changing environment, and 2) what is the role of jellyfish in large-scale biogeochemical processes such as the biological carbon pump? In order to answer such questions fundamental data on body composition and biomass are required. The purpose of this dataset was to compile proximate and elemental body composition and length-weight and weight-weight regressions for jellyfish (medusae, siphonophores, ctenophores, salps, doliolids and pyrosomes) to serve as a baseline, informing biogeochemistry studies, food web dynamics, ecosystem modeling, as well as physiology. Using published data from 1932 to 2010, we assembled three data sets: 1) body composition (wet, dry and ash-free dry weights, C, N, P as a percentage of wet and dry weights, and C/N), 2) length-weight biometric equations, and 3) weight-weight biometric equations. The datasets represent a total of 102 species from 6 classes (20 Thaliacea, 2 Cubozoa, 33 Hydrozoa, 26 Scyphozoa, 17 Tentaculata, 4 Nuda) in 3 phyla. We

have included supplementary data on location, salinity, whole animal or tissue type, size range, and where appropriate, the regression type with values of sample size, correlation coefficients (r, r^2) and level of significance for the relationship. In addition to the raw unpublished data, we have provided summary tables of mean (± sd) body composition for the main taxonomic groups.

This chapter is based on:

Lucas, C. H., Pitt, K. A., Purcell, J. E., **Lebrato, M.** and Condon, R. H. 2011. What's in a jellyfish? Proximate and elemental composition and biometric relationships for use in biogeochemical studies. In: *ESA Ecology* 92: 1704-1704. *ESA Ecological Archives* E092-144.

Acknowledgements: The work was funded by the "*Global Expansion of Jellyfish Blooms: Magnitude, Causes and Consequences*" Working Group, supported by the National Center for Ecological Analysis and Synthesis (NCEAS) and by NSF (Grant #DEB-94-21535), the University of California at Santa Barbara, and the State of California. This work was also funded by the Kiel Cluster of Excellence "The Future Ocean" (D1067/87).

6.1. Introduction

Several marine taxa have a gelatinous body, in particular the medusae and siphonophores (phylum Cnidaria), ctenophores (phylum Ctenophora) and the pelagic tunicates - salps, doliolids and pyrosomes (phylum Chordata, sub-phylum Thaliacea). While it is known that the thaliaceans are rather different from the cnidarians and ctenophores which are closely-related in taxonomic and trophic terms, there is scope for them to be included in the collective terms "jellies", "jellyfish" or "gelatinous zooplankton", due to their watery bodies, low carbon content, ability to reproduce rapidly and form extensive bloom populations, and potential impact on marine plankton communities and biogeochemical cycling. Within the framework of this article the collective term "jellyfish" will be used.

Jellyfish are found throughout the world's oceans, from the surface to great depths, and from estuaries to the open ocean. In the short term, numbers can increase rapidly in a matter of weeks or months under conditions that favour rapid growth and reproduction (Lucas 2001; Madin et al. 2006). Over longer time-scales outbreaks can become more frequent or persistent in response to large-scale variability in climate (e.g. North Atlantic Oscillation, El Niño) (Kogovšek et al. 2010; Licandro et al. 2010) and oceanic (Lynam et al. 2010) influences; or they can in fact decline (Brodeur et al. 2008). Locally, these naturally occurring episodic bloom events can be exacerbated by anthropogenic impacts such as overfishing, translocations, eutrophication, alterations to coastal geomorphology and climate warming (Mills 2001; Lynam et al. 2006; Purcell et al. 2007; Richardson et al. 2009; Dong et al. 2010; Reusch et al. 2010).

Medusae and ctenophores are voracious predators, consuming a wide range of zooplankton prey, and in some ecosystems acting as important 'keystone' species (Pauly et al. 2009). Many species consume fish eggs and larvae and/or are competitors with fish larvae for the same food resources. Thus, in some regions of the world's oceans, jellyfish and fish stocks have been inextricably linked, for example, the Benguela (Lynam et al. 2006), southeast Asia (Uye 2008; Dong et al. 2010), and Bering Sea (Brodeur et al. 2008). Pelagic tunicates (e.g. salps) are efficient filter-feeders, removing small particles such as bacteria and phytoplankton (Madin et al. 2006). At times they can contribute significantly to the cycling of organic matter in the oceans, packaging and exporting primary organic carbon principally out of the euphotic zone via the production of large and rapidly sinking faecal pellets (Wiebe et al. 1979; Madin and Deibel

1998; Phillips et al. 2009). Thus, it is believed that jellyfish populations play an important role in ecosystem diversity and function and in biogeochemical cycling. Bloom populations could potentially alter trophic pathways in the following ways. Firstly, increased conversion of primary and secondary production into gelatinous biomass (Condon and Steinberg 2008; Pitt et al. 2009) may limit carbon bioavailability to higher trophic levels, including fish, and promote a microbially-dominated food web through release of labile organic matter (Condon et al. in press). Increased carbon export and transfer efficiency of the biological carbon pump through sinking of carcasses and faecal pellet production (Billett et al. 2006; Madin et al. 2006; Lebrato and Jones 2009; Pitt et al. 2009) would supply the benthos with an increased food supply. This is particularly important in the deep-sea, which by definition is a food-limited environment (Gage and Tyler 1991). However, large accumulations of dead jellyfish (e.g. Billett et al. 2006) could potentially cause hypoxic events and alter the oxygen exchange flux with sediments as a result of the high oxygen demand for the mineralisation of carbon during decomposition (West et al. 2009b; Sexton et al. 2010). Finally, blooms can cause trophic cascades in estuarine and coastal systems (Purcell and Decker 2005; Pitt et al. 2007), altering ecosystem services in unknown ways.

Apparent increases in jellyfish bloom events in several regions of the world (e.g. the Giant jellyfish *Nemopilema nomurai* in the Sea of Japan (Uye 2008), the ctenophore *Mnemiopsis leidyi* in the Black Sea (Kovalev and Piontkovski 1998), *Chrysaora hysoscella* and *Aequorea forskalea* in the Benguela upwelling (Lynam et al. 2006) and the Mauve stinger *Pelagia noctiluca* in the Mediterranean (Licandro et al. 2010), has resulted in jellyfish receiving increased attention from the wider marine science community, including biogeochemists, fisheries scientists and ecosystem modellers (Daskalov et al. 2007; Pauly et al. 2009). Ecosystems experiencing shifting baselines or alternative stable states may result in jellyfish having greater influence on ecosystem function. Thus, the need to understand and quantify the role of jellyfish in pelagic and benthic food webs and in biogeochemical cycling in these changing environments gains prominence.

In order to answer such questions we require data on the spatial and temporal extent of populations, knowledge of trophic ecology and metabolic processes, as well as fundamental data on body composition size to weight conversions. Two commonly applied measures of biomass and production are dry weight (DW) and ash-free dry weight (AFDW), as both these weight

types are relatively simple to determine. However, neither DW nor AFDW truly reflect jellyfish biomass when compared with non-gelatinous groups. In the latter group, carbon (C) accounts for 30-60% of DW (Harris et al. 2000), whereas in jellyfish it is typically <15% (Larson 1986). As part of a multinational project studying the magnitude, causes and consequences of jellyfish blooms globally, data of body composition and biometric equations have been assembled for salps, pyrosomes, doliolids, medusae (including siphonophores) and ctenophores. Data have been compiled primarily from the peer-reviewed literature, spanning the period 1932 to the end of 2010, and covering a wide range of marine ecosystems (e.g. estuaries, coastal seas, oceanic) from the poles to the subtropics. In addition, summary tables have also been compiled using the data set. Where available, data on the salinity of the sample location have been included. It is well established that values of DW and AFDW are affected by 'water of hydration', e.g. bound water that is not removed during the drying process at 50-70^{o}C, but which is driven off during the ashing process at 500-600^{o}C, and which is influenced by the ambient salinity and body size (Larson 1986; Hirst and Lucas 1998). Detailed analyses of the effects of salinity and body size on body composition in the ubiquitous scyphozoan *Aurelia* are given in Hirst and Lucas (1998).

The data sets provide easy access to the most comprehensive compilation of published data of proximate and elemental body composition, and size-weight and weight-weight regression equations in jellyfish. It will serve as a baseline data set for use in a wide range of subject areas, including biogeochemical cycling, food web dynamics, population ecology, ecosystem modelling, as well as rate measurements of feeding, metabolism and growth.

6.2. Metadata class I. data set descriptors

6.2.1. Data set identity: What's in a jellyfish? Proximate and elemental composition and biometric relationships for use in biogeochemical studies.

6.2.2. Data set identification code: Jellyfish_body_composition_and_biometry

6.3. Class II. Research origin descriptors

6.3.1. Overall project description

Identity: Global expansion of jellyfish blooms: magnitude, causes and consequences.

Originators: Robert H. Condon, Dauphin Island Sea Lab, Dauphin Island, AL, 36528, USA.

Carlos M. Duarte, Department of Global Change Research, IMEDEA (UIB-CSIC), Instituto Mediterráneo de Estudios Avanzados, Esporles, 07190, Spain.

William M Graham, Dauphin Island Sea Lab, Dauphin Island, AL, 36528, USA.

Period of Study: 2009 - due to end late 2011.

Objectives: To provide a global synthesis of reports of jellyfish abundance to achieve four main objectives: (1) to examine the hypothesis of a global expansion of jellyfish blooms, and to explore the possible drivers for this expansion; (2) to examine the effects of jellyfish blooms on the ecosystem, addressing in particular, carbon cycling, and food webs; (3) to identify current and future consequences of jellyfish blooms for tourism, industry and fisheries, including ecosystem-based management on regional and global scales; and (4) to inform the public at large of the project results. The centrepiece of this project is a scientifically-coordinated global jellyfish and environmental database (JEDI, JEllyfish Database Initiative) based on published and un-published datasets from coastal, estuarine and open-ocean regions.

Abstract: Jellyfish are an important and often conspicuous component of oceanic food webs. During the past several decades, dramatic spatial increases and temporal shifts in jellyfish distributions have been reported around the world. Undoubtedly there are associated ecological ramifications such as food web and biogeochemical pathway alterations. Moreover, socio-economic impacts include damage to fisheries, industry and tourism. However, reports have remained local in scope, and scientists agree that a composite understanding of the extent of the problem is still lacking. The bottle-neck is the lack of synthetic analyses across marine ecosystems, due to the present fragmentation of data sources. In 2009, a research project entitled "Global expansion of jellyfish blooms: magnitude, causes and consequences" started with the aim of providing a global synthesis of jellyfish abundance to achieve the objectives outlined above.

Source(s) of funding: National Center for Ecological Analysis and Synthesis (NCEAS), a Center supported by NSF (Grant #DEB-94-21535), the University of California at Santa Barbara, and the State of California. Parts of the dataset on elemental composition and global biomass were provided by M. Lebrato while working on a GEOMAR-funded project: Kiel Cluster of Excellence 'The Future Ocean' (D1067/87)

6.3.2. Specific subproject description

Study Region: Data of body composition and biometric relationships were obtained for a wide range of marine ecosystems, including estuaries, coastal lagoons and fjords, hyposaline seas, coastal and shelf seas, open oceans and the mesopelagic. In terms of climate, data were obtained from polar (e.g. sub-Arctic Pacific, Antarctic Peninsula, Southern Ocean), temperate (e.g. coastal and shelf Europe, North America, Australia) and some subtropic (e.g. Caribbean, Australia, SE Asia) regions. Although this is a global database, entries are most comprehensive for Europe, North America, the North Atlantic, and the Antarctic, reflecting where most of the research has been conducted over the last ~70 years.

Experimental or sampling design: Most data have been compiled, as published, from the primary articles in the peer-review literature. In a few cases where the primary article could not be accessed, we have cited the primary and secondary source. Shin-Ichi Uye, Kylie Pitt and Cathy Lucas have provided unpublished data (unpubl. data) or data from a PhD thesis.

Research Methods:

Collation of data sets:

Data on body composition and biometric relationships were collected by the authors, primarily from the peer-reviewed literature. Where possible we have used the primary literature source so that as much detail and ancillary information can be gathered. In some instances the primary source could not be accessed, so we have cited both the primary and secondary source. The data collated and stored in the ESA Ecological Archives (http://esapubs.org/archive) are as published (e.g. we have not carried out any data transformations). A total of 29 terms have been collated. Detailed information on the analytical methods used to determine size and weight can be found

in the original publications, but brief summaries of the most common methods are included in the list of definitions of each term and how they were collected as set out below.

Phylum: The taxonomic phylum to which the animal belongs.

Class: The taxonomic class to which the animal belongs.

Order: The taxonomic order to which the animal belongs.

Genus: The taxonomic genus to which the animal belongs as published in the source reference.

Species: The taxonomic species that identifies the animal as published in the source reference.

Location: The location where the species was collected according to the source reference. This varies in resolution and detail from, for example, 'Australia' or 'Southern Ocean' to named bays and estuaries such as 'Southampton Water' or 'Kiel Bight'.

Salinity: The salinity of the water from which the species was collected, as published in the source reference. The majority of salinity measurements are made using a CTD (Conductivity, Temperature, Density) sensor, YSI multi-parameter probe, or refractometer. Although salinity is known to affect dry weight and ash free dry weight values due to the effects of bound 'water of hydration' (Larson 1986, Hirst and Lucas 1998), we have not attempted to approximate salinity from other literature sources for those records where salinity has not been included in the primary source material.

Life stage: Where it has been stated, the life stage of the sampled animals has been included. Thaliaceans are classified as either solitary or aggregate, oozoids or blastozooids. The life stages of hydrozoans and scyphozoans are rarely described other than as, rather arbitrarily, medusae, immature, ephyrae, juveniles, adults, adults with gonads, and eudoxies (immature or mature males or females) in siphonophores. Similarly ctenophores may be described as larvae, young or mature. In all groups, nd (no data) indicates where no life stage has been recorded.

Tissue type: The great majority of body composition and biometric data are for whole animals. In the cnidarians (principally the scyphozoans) there are some data for separate tissues – umbrella, gonad, oral arm, or tentacle.

Size: (Body composition) The size of individuals used in the analyses of body composition, if available. Sizes are published as either the minimum to maximum range, range (and average), mean ± standard deviation, and less than (<) or more than (>) a numeric value. Most sizes are expressed as linear measures, but some entries have reported weight or biovolume.

Size range: (Biometric equations) The size range of individuals used in the analysis of size-weight and weight-weight regressions. Most sizes are expressed as linear measures, but some entries have reported weight or biovolume.

Units: Standard SI units used to measure size (as length, height, weight, volume, age), as published in the source material. Size definitions are as follows: Thaliaceans – mm^3 or ml biovolume, length defined as either oral-aboral (O-A) length or just length, individual wet weight or dry weight; Cnidarians – bell diameter (BD), coronal diameter (CD) for coronate scyphozoans, diameter, disc diameter, interradalia diameter, arm tips, bell height, individual wet weight or dry weight, age in days; Ctenophores – length, oral-apical (O-A) length, gut length, individual wet weight or dry weight.

DW (%WW): Dry weight as a percentage of wet weight. Samples are typically rinsed with distilled water to remove excess salt and gently blotted to remove excess water prior to wet weighing. Dry weight is measured following oven drying at between 50 and 70^{o}C for between 1 and 7 days or until a constant weight is achieved. The overall temperature range used is 50-110^{o}C and the duration of drying range is 5 hours to 3 weeks. Some data are derived from samples that have been freeze-dried.

AFDW (%DW): Ash free dry weight as a percentage of dry weight. Following oven drying, samples are incinerated at 400-600^{o}C for between 2 and 24 hours or until a constant weight is achieved.

C (%WW): Carbon as a percentage of wet weight. Carbon is measured using CHN elemental analysers.

N (%WW): Nitrogen as a percentage of wet weight. Nitrogen is measured using CHN elemental analysers.

C (%DW): Carbon as a percentage of dry weight. Carbon is measured using CHN elemental analysers.

N (%WW): Nitrogen as a percentage of dry weight. Nitrogen is measured using CHN elemental analysers.

P (%DW): Phosphorous as a percentage of dry weight. Phosphorous is typically measured as phosphate following chemical procedures (*see* Malej et al. 1993; Iguchi and Ikeda 2004).

C/N (by wt): The ratio of carbon to nitrogen by weight. Only published ratios have been included.

Equation: The regression equation used to predict the dependent variable (weight) from the measured independent variable (size or weight). The regression equations have been listed exactly as published. These may be power or linear functions using untransformed or ($\log_{10}$ or ln)-transformed data.

Measured size (units): The independent variable and unit of measure (*see* Units for definitions).

Measured wt (units): The independent variable and unit of measure (*see* Units for definitions).

Unknown wt (units): The dependent variable and unit of measure (*see* Units for definitions).

a: The intercept of the regression line.

b: The slope of the regression line.

n: The number of data points used to form the regression equation.

r^2, r*: The correlation coefficient of the regression, published as either r^2 or r (r values are indicated by *).

P: The level of significance of the correlation coefficient.

Source: The source where the entry was obtained. These are either primary sources, or secondary sources as indicated by the phrase 'cited in', e.g. Madin and Harbison (1978) Bull Mar Sci, 28: 335-344. (cited in Madin *et al*. (1981) Mar Biol, 63: 217-226). unpubl. data = unpublished data.

Summary (descriptive) statistics:
Using the data collated for this study, summary statistics have been carried out using MS Excel to produce Phylum-, Class-, and Order-specific averages for proximate and elemental body composition (Tables 1 and 2).

Table 6.1. Summary of the proximate body composition of Thaliacea, Ctenophora and Cnidaria. Values are mean (± standard deviation, sample number), calculated using published averages in each study. WW = wet weight, DW = dry weight, AFDW = ash free dry weight. nd = no data in the literature.

Classification Level	Taxon	DW %WW	AFDW %DW
CLASS	THALIACEA	5.50 (2.47, 12)	33.35 (10.33, 14)
Order	Doliolida	nd	nd
Order	Pyrosoma	7.18 (3.59, 3)	45.90 (21.07, 2)
Order	Salpidae	4.94 (1.93, 9)	31.26 (7.23, 12)
PHYLUM	**CTENOPHORA**	**3.53 (0.92, 27)**	**26.85 (6.45, 15)**
Order	Beroida	3.28 (0.95, 8)	29.71 (0.58, 3)
Order	Cestida	nd	20.20 (0, 1)
Order	Cydippida	4.01 (0.78, 9)	32.14 (3.90, 5)
Order	Lobata	3.43 (1.01, 10)	20.59 (2.62, 6)
PHYLUM	**CNIDARIA**	**4.07 (1.23, 71)**	**34.24 (10.92, 50)**
CLASS	HYDROZOA	3.93 (0.98, 30)	36.47 (12.89, 22)
Order	Hydroida	3.90 (1.01, 28)	36.31 (13.19, 21)
Order	Siphonophora	4.43 (0.18, 2)	39.96 (0, 1)
CLASS	SCYPHOZOA	4.17 (1.39, 41)	32.46 (8.92, 28)
Order	Coronatae	4.48 (0.87, 5)	31.57 (2.20, 2)
Order	Rhizostomeae	4.90 (0.75, 10)	34.76 (16.21, 5)
Order	Semaeostomeae	3.84 (1.56, 26)	32.02 (7.33, 21)

Table 6.2. Summary of the elemental body composition of Thaliacea, Ctenophora and Cnidaria. Values are mean (± standard deviation, sample number), calculated using published averages in each study. DW = dry weight, C = carbon, N = nitrogen, P = phosphorous, C/N ratio by weight as published only (e.g. not derived from separate C and N values). nd = no data in the literature.

Classification Level	Taxon	C %DW	N %DW	P %DW	C/N
CLASS	THALIACEA	10.58 (9.26, 26)	1.70 (1.17, 24)	0.16 (0.05, 6)	4.62 (1.05, 39)
Order	Doliolida	0.67 (0, 1)	0.15 (0, 1)	nd	4.5 (0, 1)
Order	Pyrosoma	23.71 (15.54, 4)	2.20 (1.63, 3)	nd	4.0 (0, 1)
Order	Salpidae	8.55 (5.22, 21)	1.70 (1.17, 20)	0.16 (0.05, 6)	4.64 (1.08, 37)
PHYLUM	**CTENOPHORA**	**4.73 (3.78, 41)**	**0.96 (0.70, 29)**	**0.13 (0.07, 5)**	**4.29 (0.46, 12)**
Order	Beroida	6.90 (1.91, 8)	1.56 (0.53, 7)	0.13 (0.05, 2)	3.9 (0, 1)
Order	Cestida	3.0 (0, 1)	0.70 (0, 1)	nd	4.4 (0, 1)
Order	Cydippida	6.15 (5.24, 10)	1.33 (0.69, 8)	0.23 (0, 1)	4.77 (0.36, 3)
Order	Lobata	3.37 (3.13, 22)	0.43 (0.32, 13)	0.08 (0.06, 2)	4.13 (0.42, 7)
PHYLUM	**CNIDARIA**	**11.73 (7.42, 74)**	**3.36 (3.49, 71)**	**0.39 (0.60, 10)**	**4.53 (1.44, 22)**
CLASS	HYDROZOA	13.10 (8.56, 41)	3.95 (4.38, 41)	1.0 (1.38, 2)	4.97 (1.65, 14)
Order	Hydroida	13.93 (9.92, 28)	4.64 (5.07, 28)	1.0 (1.38, 2)	3.76 (0.39, 5)
Order	Siphonophora	11.38 (4.96, 13)	2.47 (1.60, 13)	nd	5.65 (1.71, 9)
CLASS	SCYPHOZOA	10.03 (5.33, 33)	2.48 (1.27, 30)	0.22 (0.06, 8)	3.75 (0.31, 8)
Order	Coronatae	15.66 (3.90, 3)	3.45 (0.78, 2)	nd	nd
Order	Rhizostomeae	13.39 (4.91, 7)	3.15 (1.04, 6)	nd	nd
Order	Semaeostomeae	8.32 (4.87, 23)	2.21 (1.28, 22)	0.22 (0.06, 8)	3.75 (0.31, 8)

6.4. Class III. Data set status and accessibility

6.4.1. Status

Latest Update: The data are collated from published articles spanning the period 1938 – end of 2010.

Latest Archive date: 24 April 2011

Metadata status: The metadata are complete and up-to-date.

Data verification: The majority of the data entered have been sourced from the peer-reviewed literature. Unpublished data have been obtained from members of the NCEAS Global Jellyfish Blooms Working Group (*see* Class II-B Research Origin Descriptors). All data entries have been

double-checked by the authors against the original data sets as published or provided to the first author.

6.4.2. Accessibility

Storage location and medium: Ecological Society of America data archives, http://esapubs.org/archive, the URL is published in each issue of its journals. The original data files exist on the primary author's personal computer in MS Excel format.

Copyright restrictions: None

Proprietary restrictions: None

Costs: None

6.5. Class IV. Data structural descriptors

6.5.1. Body composition

6.5.1.1. Data Set File

Identity: body_composition

Size: 239 records, not including header rows.

Format and Storage mode: ASCII (comma-delimited), compressed and ZIP.

Header information: The first row of the file name contains the variable names (*see* Class IV-B Data structural descriptors).

Alphanumeric attributes: Mixed.

Special characters/fields: -999 denotes lack of information in numeric fields, nd denotes lack of information in character fields.

Authentication procedures: n/a

6.5.1.2. Variable Information

Variable name	Variable definition	Units	Storage type	Range	Missing value codes
Phylum	Taxonomic phylum to which the species belongs.	N/A	Character	N/A	N/A
Class	Taxonomic class to which the species belongs.	N/A	Character	N/A	N/A
Order	Taxonomic order to which the species belongs.	N/A	Character	N/A	N/A
Genus	Genus designation for the species.	N/A	Character	N/A	N/A
Species	Species designation.	N/A	Character	N/A	N/A
Location	Geographic location from where the species was collected.	N/A	Character	N/A	nd
Salinity	Salinity of the water from where the species was collected. Mostly numeric values, but some descriptive terms used where this may help identify approximate salinity range.	N/A (but most published in ‰ or psu.)	Floating point Character	6 – 38.52	-999
Life stage	Descriptions of life stages as described in source material. Taxa specific descriptions are: Thaliaceans – solitary, aggregates, oozoids, blastozooids, fresh carcasses. Cnidarians – x mm height, x cm diameter, immature, ephyrae, juveniles, medusae,	N/A	Character	N/A	nd
Tissue type	Type of tissues used in analysis. Whole – whole animal or mixed tissue if subsample used. In scyphozoans, there are also separate analyses of tissues from the gonad, umbrella, tentacle, oral arm. In siphonophores, there are also separate analyses of tissues from the swim bell, and cormidia + stem.	N/A	Character	N/A	nd

Size	Size of individuals used in the analyses of body composition. Published as either the minimum to maximum size range, range (and average), mean ± standard deviation, and less than (<) or more than (>) a numeric value. Mostly linear measures, but some entries weight or biovolume.	N/A	Floating point	0.0021 – 8488 (note variable units)	-999
Units	Units of size (as length, height, weight, volume, age). Size units are as follows: Thaliaceans – mm^3 or ml biovolume, length defined as oral-aboral (O-A) length or 'length', wet weight (WW) or dry weight (DW). Cnidarians – bell diameter (BD), coronal diameter (CD), diameter, disc diameter, interradalia diameter, arm tips, bell height, wet weight or dry weight, age in days. Ctenophores – length, oral-apical (O-A) length, gut length, individual wet weight or dry weight.	mm, cm, mm^3, µm, mg, g, kg, days	Character	N/A	nd
DW (%WW)	Dry weight as a percentage of wet weight, as published. Majority are average values. Some min to max ranges included, with average (avg) in parentheses.	Percentage	Floating point	0.95 – 8.9	-999
±sd	The standard deviation of the average DW (%WW), as published.	Percentage	Floating point	0.1 – 2.2	-999
AFDW (%DW)	Ash free dry weight as a percentage of dry weight, as published. Majority are average values. Some min to max ranges included, with average (avg) in parentheses.	Percentage	Floating point	10.9 – 92.0	-999
±sd	The standard deviation of the average AFDW (%DW), as published.	Percentage	Floating point	0.1 – 18.97	-999
C (%WW)	Carbon as a percentage of wet weight, as published.	Percentage	Floating point	0.02 – 5.6	-999
±sd	The standard deviation of the average C (%WW), as published.	Percentage	Floating point	0.005 – 1.1	-999
N (%WW)	Nitrogen as a percentage of wet weight, as published.	Percentage	Floating point	0.004 – 0.53	-999
±sd	The standard deviation of the average N (%WW), as published.	Percentage	Floating point	0.002 – 0.05	-999

C (%DW)	Carbon as a percentage of dry weight, as published. Majority are average values. Some min to max ranges included.	Percentage	Floating point	0.67 – 43.0	-999
±sd	The standard deviation of the average C (%DW), as published.	Percentage	Floating point	0.0 – 5.94	-999
N (%DW)	Nitrogen as a percentage of dry weight, as published. Majority are average values. Some min to max ranges included.	Percentage	Floating point	0.15 – 24.73	-999
±sd	The standard deviation of the average N (%DW), as published.	Percentage	Floating point	0.06 – 3.02	-999
P (%DW)	Phosphorous as a percentage of dry weight, as published.	Percentage	Floating point	0.0 – 1.97	-999
±sd	The standard deviation of the average P (%DW), as published.	Percentage	Floating point	0.03 – 0.25	-999
C:N (by wt)	Ratio of carbon to nitrogen by weight, as published. Majority are average values. Some min to max ranges included.	Number	Floating point	3.3 – 9.67	-999
±sd	The standard deviation of the average C:N ratio, as published.	Number	Floating point	0.0 – 3.48	-999
Source	Source material from where the data were obtained. Mainly primary source, but secondary sources identified by xxx (‘cited in xxx’)	N/A	Character	N/A	N/A

6.5.2. Size to weight biometric equations

6.5.2.1. Data Set File

Identity: size_to_weight_biometric_equations

Size: 199 records, not including header rows.
Format and Storage mode: ASCII (comma-delimited), compressed and ZIP .

Header information: The first row of the file name contains the variable names (*see* Class IV-B Data structural descriptors).

Alphanumeric attributes: Mixed.

Special characters/fields: -999 denotes lack of information in numeric fields, nd denotes lack of information in character fields.

Authentication procedures: n/a

6.5.2.2. Variable Information

Variable name	Variable definition	Units	Storage type	Range	Missing value codes
Phylum	Taxonomic phylum to which the species belongs.	N/A	Character	N/A	N/A
Class	Taxonomic class to which the species belongs.	N/A	Character	N/A	N/A
Order	Taxonomic order to which the species belongs.	N/A	Character	N/A	N/A
Genus	Genus designation for the species.	N/A	Character	N/A	N/A
Species	Species designation.	N/A	Character	N/A	N/A
Location	Geographic location from where the species was collected.	N/A	Character	N/A	nd
Salinity	Salinity of the water from where the species was collected. Mostly numeric values, but some descriptive terms used where this may help identify approximate salinity range.	N/A (but most published in ‰ or psu.)	Floating point Character	6 - 37	-999
Life stage	Descriptions of life stages as described in source material. Taxa specific descriptions are: Thaliaceans – solitary, aggregates, gonozoids. Cnidarians – immature, ephyrae, juveniles, medusae, mature + gonads, eudoxies. Ctenophores – larvae, adults.	N/A	Character	N/A	nd

Tissue type	Type of tissues used in analysis. Whole – whole animal or mixed tissue if subsample used. Part umbrella has been indicated. Assume that unpreserved tissue used unless indicated otherwise.	N/A	Character	N/A	nd
Size range	Size range of individuals used in biometric analyses. Published as the minimum to maximum size range, or range (and average). Mostly linear measures, but some are weights or descriptive terms.	N/A	Floating point	0.38 – 5456.4 (note variable units)	-999
Units	Units of size (as length, weight). Size units are as follows: Thaliaceans – length defined as oral-aboral (O-A) length or 'length', wet weight (WW) or dry weight (DW). Cnidarians – bell diameter (BD), coronal diameter (CD), diameter, disc diameter, interradalia diameter, arm tips, bell height, wet weight or dry weight, age in days, displacement volume. Ctenophores – length, oral-apical (O-A) length, diameter.	mm, cm, ml, µm, mg, g, days	Character	N/A	nd
Equation	Regression equation used to predict the dependent variable (weight) from the measured independent variable (size or weight). The regression equations have been listed exactly as published. These may be power or linear functions using untransformed or (log_{10} or ln)-transformed data.	N/A	Character	N/A	N/A
Measured size (units) [Size-weight biometry]	Independent variable (measured as length, diameter, height, volume) and unit of measure.	N/A (various units in parentheses)	Character	N/A	N/A
Measured wt (units) [Weight-weight biometry]	Independent variable (measured as weight) and unit of measure.	N/A (various units in parentheses)	Character	N/A	N/A
Unknown wt (units)	Dependent variable (weight) and unit of measure.	N/A (various units in	Character	N/A	N/A

		parentheses)			
a	Intercept of the regression line.	N/A	Floating point	-4.796 – 317.67 (note change of scale and units)	N/A
b	Slope of the regression line.	N/A	Floating point	0.054 – 71.3 (note change of regression type)	N/A
n	Number of data points used to form the regression equation.	Number of individuals	Floating point	3 – 2475	-999
r^2, r*	Correlation coefficient of the regression equation, published as either r^2 or r (indicated by *).	N/A	Floating point	0.608 – 0.999	-999
P	The level of significance of the correlation coefficient.	Between 0.000 and 0.999	Floating point	0.0001 – 0.05	-999
Source	Source material from where the data were obtained. Mainly primary source, but secondary sources identified by xxx ("cited in xxx")	N/A	Character	N/A	N/A

6.5.3. Weight to weight biometric equations

6.5.3.1. Data Set File

Identity: weight_to_weight_biometric_equations

Size: 66 records, not including header rows.

Format and Storage mode: ASCII (comma-delimited), compressed and ZIP.
Header information: The first row of the file name contains the variable names (*see* Class IV-B Data structural descriptors).

Alphanumeric attributes: Mixed.

Special characters/fields: -999 denotes lack of information in numeric fields, nd denotes lack of information in character fields.

Authentication procedures: n/a

6.5.3.2. Variable Information

As for Class IV-B: Size to Weight Biometric Equations.

6.6. Class V. Supplemental descriptors

6.6.1. Data acquisition

Data forms: n/a

Location of completed data forms: n/a

6.6.2. Quality assurance / quality control procedures: Data were entered directly from source material into the computer file. Values have been double-checked by the authors.

6.6.3. Related material: Several publications contain data on biochemical composition (e.g. proteins, lipids and carbohydrates), but these have not been archived in this study.

Displayed below is the complete list of 113 source references used in the compilation of the three data sets: 1) body composition, 2) size-weight biometric equations, and 3) weight-weight biometric equations.

6.6.4. Complete list of source references

1) Anninsky, B.E. G.A. Finenko, G.I. Abolmasova, and Z.A. Romanova. 2007. Somatic organic content of the ctenophores *Mnemiopsis leidyi* (Ctenophora: Lobata) and *Beroe ovata* (Ctenophora: Beroida) in early ontogenetic stages. Russian Journal of Marine Biology 33:417-424.
2) Bailey, T.G. M.J. Youngbluth, and G.P. Owen. 1994. Chemical composition and oxygen consumption rates of the ctenophore *Bolinopsis infundibulum* from the Gulf of Maine. Journal of Plankton Research 16:673-689.
3) Bailey, T.G. M.J. Youngbluth, and G.P. Owen. 1995. Chemical composition and metabolic rates of gelatinous zooplankton from midwater and benthic boundary layer environments off Cape Hatteras, North Carolina, USA. Marine Ecology Progress Series 122:121-134.
4) Båmstedt, U. 1981. Water and organic content of boreal macroplankton and their significance for the energy content. Sarsia 66:59-66.
5) Båmstedt, U. 1990. Trophodynamics of the scyphomedusae *Aurelia aurita*. Predation rate in relation to abundance, size and type of prey organism. Journal of Plankton Research 12:215-229.
6) Båmstedt, U. M.B. Martinussen, and S. Matsakis. 1994. Trophodynamics of the two scyphozoan jellyfishes, *Aurelia aurita* and *Cyanea capillata*, in western Norway. ICES (International Council for the Exploration of the Sea) Journal of Marine Science 51:369-382.
7) Båmstedt, U. J. Lane, and M.B. Martinussen. 1999. Bioenergetics of ephyra larvae of the scyphozoan jellyfish *Aurelia aurita* in relation to temperature and salinity. Marine Biology 135:89-98.
8) Buecher, E. C. Sparks, A. Brierley, H. Boyer, and M. Gibbons. 2001. Biometry and size distribution of *Chrysaora hysoscella* (Cnidaria, Scyphozoa) and *Aequorea aequorea* (Cnidaria, Hydrozoa) off Namibia with some notes on their parasite *Hyperia medusarum*. Journal of Plankton Research 23:1073-1080.
9) Ceccaldi, H.J. A. Kanazawa, and S-I. Teshima. 1976. Chemical composition of some Mediterranean macroplanktonic organisms. 1. Proximate analysis. Tethys 8:295-298.
10) Cetta, C.M. L.P. Madin, and P. Kremer. 1986. Respiration and excretion by oceanic salps. Marine Biology 91:529-537.
11) Clarke, A. L.J. Holmes, and D.J. Gore. 1992. Proximate and elemental composition of gelatinous zooplankton from the Southern Ocean. Journal of Experimental Marine Biology and Ecology 155:55-68.
12) Cooper, L.H.N. 1939. Phosphorous, nitrogen, iron and manganese in marine zooplankton. Journal of the Marine Biological Association of the United Kingdom 23:387-390.
13) Costello, J. 1991. Complete carbon and nitrogen budgets for the hydromedusa *Cladonema californicum* (Anthomedusa: Cladonemidae). Marine Biology 108:119-128.
14) Curl, H. 1962. Standing crops of carbon, nitrogen, and phosphorous and transfer between trophic levels, in continental shelf waters south of New York. Rapports et Proces-verbaux des Réunions Conseil international pour l'Exploration de la Mer 153:183-189.
15) Daan, R. 1986. Food intake and growth of *Sarsia tubulosa* (Sars, 1835) with quantitative estimates of predation on copepod populations. Netherlands Journal of Sea Research 20:67-74.
16) Daan, R. 1989. Factors controlling the summer development of copepod populations in the Southern Bight of the North Sea. Netherlands Journal of Sea Research 23:305-322.
17) Davenport, J. and G.H. Balazs. 1991. 'Fiery pyrosomas': Are Pyrosomas an important items in the diet of leatherback turtles? British Herpetological Society Bulletin 37: 33-38.

18) Davenport, J. and E.R. Trueman. 1985. Oxygen uptake and buoyancy in zooplankton organisms from the tropical eastern Atlantic. Comparative Biochemistry and Physiology 18A:857-863.

19) Deibel, D. 1985 Clearance rates of the salp *Thalia democratica* fed naturally occurring particles. Marine Biology 86:47-54.

20) Doyle, T.K. J.D.R. Houghton, R. McDevitt, J. Davenport, and G.C. Hays. 2007. The energy density of jellyfish: Estimates from bomb-calorimetry and proximate-composition. Journal of Experimental Marine Biology and Ecology 343:239-252.

21) Dubischar, C.D. and U.V. Bathmann. 1997. Grazing impact of copepods and salps on phytoplankton in the Atlantic sector of the Southern Ocean. Deep-Sea Research II 44:415-433.

22) Dubischar, C.D. E.A. Pakhomov, and U.V. Bathmann. 2006. The tunicate *Salpa thompsoni* ecology in the southern ocean. II. Proximate and elemental composition. Marine Biology 149:625-632.

23) Finenko, G.A. G.I. Abolmasova, and Z.A. Romanova. 1995. Feeding, respiration, and growth of the ctenophore *Mnemiopsis mccradyi* in relation to grazing conditions. Russian Journal of Marine Biology 21:283-287.

24) Finenko, G.A. B.E. Anninsky, Z.A. Romanova, G.I. Abolmasova, and Kideys A.E. 2001. Chemical composition, respiration and feeding rates of the new alien ctenophore, *Beroe ovata*, in the Black Sea. Hydrobiologia 451:177-186.

25) Finenko, G.A. Z.A. Romanova, G.I. Abolmasova, B.E. Anninsky, L.S. Svetlichny, E.S. Hubareva, L. Bat, and A.E. Kideys. 2003. Population dynamics, ingestion, growth and reproduction rates of the invader *Beroe ovata* and its impact on plankton community in Sevastopol Bay, the Black Sea. Journal of Plankton Research 25:539-549.

26) Fosså, J.H. 1992. Mass occurrence of *Periphylla periphylla* (Scyphozoa, Coronatae) in a Norwegian fjord. Sarsia 77:237-251.

27) Garcia, J.R. 1990 Population dynamics and production of *Phyllorhiza punctata* (Cnidaria: Scyphozoa) in Laguna Joyuda, Puerto Rico. Marine Ecology Progress Series 64:243-251.

28) Gibson, D.M. and G-A. Paffenhöfer. 2000. Feeding and growth rates of the doliolid, *Dolioletta gegenbauri* Uljanin (Tunicata, Thaliacea). Journal of Plankton Research 22:1485-1500.

29) Gorsky, G. S. Dallot, J. Sardou, R. Fenaux, C. Carré, and I. Palazzoli. 1988. C and N composition of some northwestern Mediterranean zooplankton and micronekton species. Journal of Experimental Marine Biology and Ecology 124:133-144.

30) Haddad, M.A. and M. Nogueira Jr. 2006. Reappearance and seasonality of *Phyllorhiza punctata* von Ledenfeld (Cnidaria, Scyphozoa, Rhizostomeae) medusae in southern Brazil. Revista Brasileira de Zoologia 23:824-831.

31) Harbison, G.R. and R.W. Gilmer. 1976. The feeding rates of the pelagic tunicate *Pegea confoederata* and two other salps. Limnology and Oceanography 21:517-528.

32) Hay, S. J.R.G. Hislop, and A.M. Shanks. 1990. North Sea scyphomedusae: summer distribution, estimated biomass and significance particularly for 0-group Gadoid fish. Netherlands Journal of Sea Research. 25:113-130.

33) Heron, A.C. P.S. McWilliam, and G. Dalpont. 1988. Length-weight relation in the salp *Thalia democratica* and potential of salps as a source of food. Marine Ecology Progress Series 42:125-132.

34) Hirota, J. 1972. Laboratory culture and metabolism of the planktonic ctenophore, *Pleurobrachia bachei* A. Agassiz. In: Takenouti, A.Y. (ed) Biological oceanography of the northern North Pacific. Idemitsu Shoten, Tokyo, pp. 465-484.

35) Hirst, A.G. and C.H. Lucas. 1998. Salinity influences body weight quantification in the scyphomedusa *Aurelia aurita*: important implications for body weight determination in gelatinous zooplankton. Marine Ecology Progress Series 165:259-269.

36) Hoeger, U. 1983. Biochemical composition of ctenophores. Journal of Experimental Marine Biology and Ecology 72:251-261.

37) Huntley, M.E. P.F. Sykes, and V. Marin. 1989. Biometry and trophodynamics of *Salpa thompsoni* Foxton (Tunicata: Thaliacea) near the Antarctic Peninsula in Austral summer 1983 – 1984. Polar Biology 10:59-70.

38) Hyman, L.H. 1938. The water content of medusae. Science 87:166-167.

39) Hyman, L.H. 1940 Observations and experiments on the physiology of medusae. Biological Bulletin (Woods Hole, Mass.) 79:282-296.

40) Iguchi, N. and T. Ikeda. 2004. Metabolism and elemental composition of aggregate and solitary forms of *Salpa thompsoni* (Tunicata: Thaliacea) in waters off the Antarctic Peninsula during austral summer 1999. Journal of Plankton Research 26:1025-1037.

41) Ikeda, T. 1972. Chemical composition and nutrition of zooplankton in the Bering Sea. In: Takenouti, A.Y. (ed) Biological oceanography of the northern North Pacific. Idemitsu Shoten, Tokyo, pp. 432-442.

42) Ikeda, T. and B. Bruce. 1986. Metabolic activity and elemental composition of krill and other zooplankton from Prydz Bay, Antarctica, during early summer (November-December). Marine Biology 92:545-555.

43) Ikeda, T. and A.W. Mitchell. 1982. Oxygen uptake, ammonia excretion and phosphate excretion by krill and other Antarctic zooplankton in relation to their body size and chemical composition. Marine Biology 71:283-298.

44) Ivleva, I.V. and T.I. Litovchenko. 1978. Respiration of coelenterata and ctenophore depending on the habitat temperature. Biologiya Morya (Kiev) 46: 3-25. In Russian; English abstract.

45) Jankowski, T. 2000. Chemical composition and biomass parameters of a population of *Craspedacusta sowerbii* Lank 1880 (Cnidaria: Limnomedusa). Journal of Plankton Research 22:1329-1340.

46) Katechakis, A. H. Stirbor, U. Sommer, and T. Hansen. 2004. Feeding selectivities and food niche separation of *Acartia clausi*, *Penilia avirostris* (Crustacea) and *Doliolum denticulatum* (Thaliacea) in Blanes Bay (Catalan Sea, NW Mediterranean). Journal of Plankton Research 26:589-603.

47) Kideys, A.E. and M. Moghim. 2003. Distribution of the alien ctenophore *Mnemiopsis leidyi* in the Caspian Sea in August 2001. Marine Biology 142:163-171.

48) Kideys, A.E. G. Shahram, G. Davood, A. Roohi, and S. Bagheri. 2001. Strategy for combating *Mnemiopsis* in the Caspian waters of Iran. Final report, July 2001, prepared for the Caspian Environment Programme, Baku, Azerbaijan.

49) Kikinger, R. 1992. *Cotylorhiza tuberculata* (Cnidaria: Scyphozoa) - life history of a stationary population. P.S.Z.N.I. Marine Ecology (Berlin) 13:333-362.

50) Kraeuter, J.N. and E.M. Setzler. 1975. The seasonal cycle of scyphozoa and cubozoa in Georgia estuaries. Bulletin of Marine Science 25:66-74.

51) Kremer, P. 1975. Excretion and body composition of the ctenophore *Mnemiopsis leidyi* (A. Agassiz): comparisons and consequences. 10th European Marine Biology Symposium on Marine Biology, Ostend, Belgium. Sept 17-23, 1975, Volume 2: 351-362.

52) Kremer, P. and S.W. Nixon. 1976. Distribution and abundance of the ctenophore, *Mnemiopsis leidyi*, in Narragansett Bay. Estuarine and Coastal Marine Science 4:627-629.

53) Kremer, P. M.F. Canino, and R.W. Gilmer. 1986a. Metabolism of epipelagic tropical ctenophores. Marine Biology 90:403-412.

54) Kremer, P. M.R. Reeve, and M.A. Syms. 1986b. The nutritional ecology of the ctenophore *Bolinopsis vitrea*: comparisons with *Mnemiopsis mccradyi* from the same region. Journal of Plankton Research 8:1197-1208.

55) Kremer, P. J. Costello, J. Kremer, and M. Canino. 1990. Significance of photosynthetic endosymbionts to the carbon budget of the scyphomedusa *Linuche unguiculata*. Limnology and Oceanography 35:609-624.

56) Larson, R.J. 1986. Water content, organic content, and carbon and nitrogen composition of medusae from the Northeast Pacific. Journal of Experimental Marine Biology and Ecology 99:107-120.

57) Larson, R.J. 1991. Diet, prey selection and daily ration of *Stomolophus meleagris*, a filter-feeding scyphomedusa from the NE Gulf of Mexico. Estuarine and Coastal Shelf Science 32:511-525.

58) Le Borgne, R. 1982. Zooplankton production in the eastern tropical Atlantic Ocean, net growth efficiency and P:B in terms of carbon, nitrogen, and phosphorus. Limnology and Oceanography 27:681-698.

59) Lebrato, M. and D.O.B. Jones. 2009. Mass deposition event of *Pyrosoma atlanticum* carcasses off Ivory Coast (West Africa). Limnology and Oceanography 54:1197-1209.

60) Lucas, C.H. 1993. The biology of gelatinous predators and their impact on the mesozooplankton community of Southampton Water. PhD Thesis, University of Southampton, UK

61) Lucas, C.H. 1994. Biochemical composition of *Aurelia aurita* in relation to age and sexual maturity. Journal of Experimental Marine Biology and Ecology 183:179-192.

62) Lucas, C.H. 1996. Population dynamics of *Aurelia aurita* (Scyphozoa) from an isolated brackish lake, with particular reference to sexual reproduction. Journal of Plankton Research 18:987-1007.

63) Lucas, C.H. 2009. Biochemical composition of the mesopelagic coronate jellyfish *Periphylla periphylla* from the Gulf of Mexico. Journal of the Marine Biological Association of the United Kingdom 89:77-81.

64) Lucas, C.H. and J.A. Williams. 1994. Population dynamics of the scyphomedusa *Aurelia aurita* in Southampton Water. Journal of Plankton Research 16:879-895.

65) Lutcavage, M. and P.L. Lutz. 1986. Metabolic rate and food energy requirements of the leatherback sea turtle, *Dermochelys coriacea*. Copeia 1986:796-798.

66) Madin, L.P. and D. Deibel. 1998. Feeding and energetics of Thaliacea. In: Bone, Q. (ed) The Biology of Pelagic Tunicates. Oxford University Press, Oxford, pp. 81-103.

67) Madin, L.P. and G.R. Harbison. 1978. Salps of the genus *Pegea* Savigny 1816 (Tunicata: Thaliacea). Bulletin of Marine Science 28:335-344.

68) Madin, L.P. and J.E. Purcell.1992. Feeding, metabolism and growth of *Cyclosalpa bakeri* in the subarctic Pacific. Limnology and Oceanography 37:1236-1251.

69) Madin, C.P. C.M. Cetta, and V.L. 1981 Elemental and biochemical composition of salps (Tunicata: Thaliacea). Marine Biology 63:217-226.

70) Malej, A. J. Faganeli, and J. Pezdič. 1993. Stable isotope and biochemical fractionation in the marine pelagic food chain: the jellyfish *Pelagia noctiluca* and net zooplankton. Marine Biology 116:565-570.

71) Martinussen, M.B. and U. Båmstedt. 1999. Nutritional ecology of gelatinous planktonic predators. Digestion rate in relation to type and amount of prey. Journal of Experimental Marine Biology and Ecology, 232: 61-84.

72) Matsakis, S. and R.J. Conover. 1991. Abundance and feeding of medusae and their potential impact as predators on other zooplankton in Bedford Basin (Nova Scotia, Canada). Canadian Journal of Fisheries and Aquatic Science 48:1419-1430.

73) Matsakis, S. and P. Nival. 1989. Elemental composition and food intake of *Phialidium* hydromedusae in the laboratory. Journal of Experimental Marine Biology and Ecology 130:277-290.

74) Matthews, J.B.L. and L. Hestad. 1977. Ecological studies on the deep-water pelagic community of Korsfjorden, Western Norway. Sarsia 63:57-63.

75) Mayzaud, P. M. Boutonte, R. Perissinotto, and P. Nichols. 2007. Polar and neutral lipid composition in the pelagic tunicate *Pyrosoma atlanticum*. Lipids 42:647-657.

76) Møller, L.F. and H.U. Riisgård. 2007. Feeding, bioenergetics and growth in the common jellyfish *Aurelia aurita* and two hydromedusae, *Sarsia tubulosa* and *Aequorea vitrina*. Marine Ecology Progress Series 346:167-177.

77) Morand, P. C. Carré, and D.C. Biggs. 1987. Feeding and metabolism of the jellyfish *Pelagia noctiluca* (Scyphomedusae, Semaeostomeae). Journal of Plankton Research 9:651-665.

78) Morris, R.J. M.J. McCartney, and A. Schulze-Röbbecke. 1983. *Bolinopsis infundibulum* (O.F. Müller): biochemical composition in relation to diet. Journal of Experimental Marine Biology and Ecology 67:149-157.

79) Mutlu, E. 1999. Distribution and abundance of ctenophores and their zooplankton food in the Black Sea. II. *Mnemiopsis leidyi*. Marine Biology 135:603-613.

80) Mutlu, E. and F. Bingel. 1999. Distribution and abundance of ctenophores and their zooplankton food in the Black Sea. I. *Pleurobrachia pileus*. Marine Biology 135:589-601.

81) Nemazie, D.A. J.E. Purcell, and P.M. Gilbert. 1993. Ammonium excretion by gelatinous zooplankton and their contribution to the ammonium requirements of microplankton in Chesapeake Bay. Marine Biology 116:451-458.

82) Nogueira Jr M. and M.A. Haddad. 2006. Relações de tamanho e peso das grandes medusas (Cnidaria) do litoraldo Paraná, Sul do Brasil. Revista Brasileira de Zoologia 23:1231-1234.

83) Olesen, N.J. K. Frandsen, and H.U. Riisgård. 1994. Population dynamics, growth and energetics of jellyfish *Aurelia aurita* in a shallow fjord. Marine Ecology Progress Series 105:9-18.

84) Olesen, N.J. J.E. Purcell, and D.K. Stoecker. 1996. Feeding and growth by ephyrae of scyphomedusae *Chrysaora quinquecirrha*. Marine Ecology Progress Series 137:149-159.

85) Percy, J.A. and F.J. Fife. 1981. The biochemical composition and energy content of Arctic marine macrozooplankton. Arctic 34:307-313.

86) Persad, G. R.R. Hopcroft, M.K. Webber, and J.C. Roff. 2003. Abundance, biomass and production of ctenophores and medusae off Kingston, Jamaica. Bulletin of Marine Science 73:379-396.

87) Pertsova, N.M. K.N. Kosobokova, and A.A. Prudkovsky. 2006. Population size structure, spatial distribution, and life cycle of the hydromedusa *Aglantha digitale* (O.F. Müller, 1766) in the White Sea. Oceanology 46:228-237.

88) Pitt, K.A. and M.J. Kingsford. 2003. Temporal variation in the virgin biomass of the edible jellyfish, *Catostylus mosaicus* (Scyphozoa, Rhizostomeae). Fisheries Research 63:303-313.

89) Purcell, J.E. 1982. Feeding and growth of the siphonophore *Muggiaea atlantica* (Cunningham 1893). Journal of Experimental Marine Biology and Ecology 62:339-354.

90) Purcell, J.E. 1992. Effects of predation by the scyphomedusan *Chrysaora quinquecirrha* on zooplankton populations in Chesapeake Bay, USA. Marine Ecology Progress Series 87:65-76

91) Purcell, J.E. and P. Kremer. 1983. Feeding and metabolism of the siphonophore *Sphaeronectes gracilis*. Journal of Plankton Research 5:95-106.

92) Purcell, J.E. V. Fuentes, D. Atienza, U. Tilves, D. Astorga, M. Kawahara, and G.C. Hays. 2010. Use of respiration rates of scyphozoan jellyfish to estimate their effects on the food web. Hydrobiologia 645:35-152.

93) Reinke, M. 1987. On the feeding and locomotory physiology of *Salpa thompsoni* and *Salpa fusiformis*. Berichte zur Polarforschung 36:1-89.

94) Reeve, M.R. 1980. Comparative experimental studies on the feeding of chaetognaths and ctenophores. Journal of Plankton Research 2:381-393.

95) Reeve, M.R. and L.D. Baker. 1975. Production of two planktonic carnivores (Chaetognath and Ctenophore) in South Florida inshore waters. Fisheries Bulletin US 73:238-248.

96) Reeve, M.R. and M.A. Walter. 1976. A large-scale experiment on the growth and predation potential of ctenophore populations. In: Mackie, G. (ed) Coelenterate Ecology and Behaviour. Plenum Press, New York, pp. 187-199.

97) Reeve, M.R. M.A. Walter, and T. Ikeda. 1978. Laboratory studies of ingestion and food utilization in lobate and tentaculate ctenophores. Limnology and Oceanography 23:740-751.

98) Reeve, M.R. M.A. Syms, and P. Kremer. 1989. Growth dynamics of a ctenophore (*Mnemiopsis*) in relation to variable food supply. I. Carbon biomass, feeding, egg production, growth and assimilation efficiency. Journal of Plankton Research 11:535-552.

99) Schneider, G. 1988. Chemische Zusammensetzung und Biomasseparameter der Ohrenqualle *Aurelia aurita*. Helgoländer Meeresuntersuchungen 42:319-327.

100) Schneider, G. 1989. Zur chemischen Zusammensetzung der ctenophore *Pleurobrachia pileus* in der Kieler Bucht. Helgoländer Meeresuntersuchungen 43:67-76.

101) Scolardi, K.M. K.L. Daly, E.A. Pakhomov, and J.T. Torres. 2006. Feeding ecology and metabolism of the Antarctic cydippid ctenophores *Callianira antarctica*. Marine Ecology Progress Series 317:111-126.

102) Shenker, J.M. 1985. Carbon content of the neritic scyphomedusa *Chrysaora fuscescens*. Journal of Plankton Research 7:169-173.

103) Shiganova, T.A. Y.V. Bulgakova, S.P. Volovik, Z.A. Mirzoyan, and S.I. Dudkin. 2001. The new invader *Beroe ovata* Mayer 1912 and its effect on the ecosystem of the northeastern Black Sea. Hydrobiologia 451:187-197.

104) Shushkina, E.A. E.I. Musaeva, L.L. Anokhina, and T.L. Lukasheva. 2000. The role of gelatinous macroplankton, jellyfish *Aurelia*, and ctenophores *Mnemiopsis* and *Beroe* in the planktonic communities of the Black Sea. Russian Academy of Sciences. Oceanology 40:809-816.

105) Small, L.F. S.W. Fowler, S.A. Moore, and J. La Rosa. 1983. Dissolved and fecal pellet carbon and nitrogen release by zooplankton in tropical waters. Deep-Sea Research 30 (Part 12A):1199-1220.

106) Uye, S. and H. Shimauchi. 2005. Population biomass, feeding, respiration and growth rates, and carbon budget of the scyphomedusa *Aurelia aurita* in the Inland Sea of Japan. Journal of Plankton Research 27:237-248.

107) van Soest, R.W.M. 1973. The genus *Thalia* Blumenbach 1798 (Tunicata, Thaliacea), with descriptions of two new species. Beaufortia 20:193-212.

108) van Soest, R.W.M. 1974a. Taxonomy of the subfamily Cyclosalpinae Yount, 1954 (Tunicata, Thaliacea) with descriptions of two new species. Beaufortia 22:17-55.

109) van Soest, R.W.M. 1974b. A revision of the genera *Salpa* Forskal 1775, *Pegea* Savigny 1816, and *Ritteriella* Metcalf, 1919 (Tunicata, Thaliacea). Beaufortia 22:153-191.

110) Weisse, T. and M-T. Gomiou. 2000. Biomass and size structure of the scyphomedusa *Aurelia aurita* in the northwestern Black Sea during spring and summer. Journal of Plankton Research 22:223-239.

111) Youngbluth, M.J. and U. Båmstedt. .2001. Distribution, abundance, behavior and metabolism of *Periphylla periphylla*, a mesopelagic coronate medusa in a Norwegian fjord. Hydrobiologia 451:321-333.

112) Youngbluth, M.J. P. Kremer, T.G. Bailey, and C.A. Jacoby. 1988. Chemical composition, metabolic rates and feeding behaviour of the midwater ctenophore *Bathocyroe fosteri*. Marine Biology 98:87-94.

113) Yousefian, M. and A.E. Kideys. 2003. Biochemical composition of *Mnemiopsis leidyi* in the southern Caspian Sea. Fish Physiology and Biochemistry 29:127-131.

6.6.5. Computer programs and data processing algorithms: Means and standard deviations were calculated using the “average” and “stdev” functions in MS Excel.

6.6.6. Archiving: n/a

6.6.7. Publications using the data set: n/a

6.6.8. Publications using the same sites: n/a

6.7. Addendum: Gelatinous zooplankton biochemistry comparison

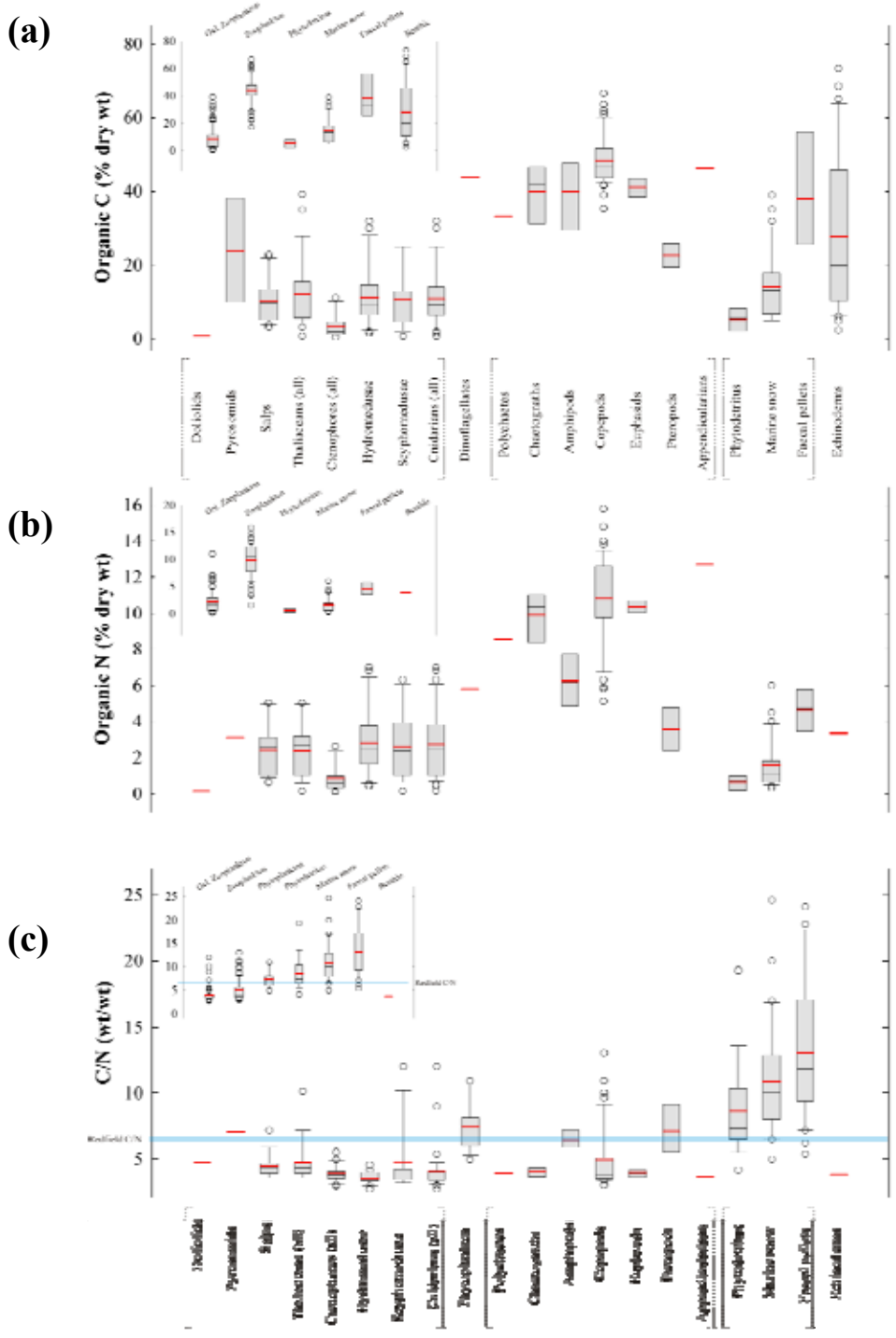

Fig. 6.1. Box and whisker plots of organic carbon (a), nitrogen (b), and C/N (wt/wt) (c) for the major groups of gelatinous zooplankton, for other zooplanktonic organisms, and for biogenic materials found in the ocean (phytodetritus, marine snow, and faecal pellets) (inner plots show major divisions). A benthic taxa (echinoderms) is also shown for comparison. For phytoplankton only C/N is used (c) [blue line represents the Redfield ratio by weight which is 5.71 (Redfield 1934)]. The ends of each bar represent the 5th and 95th percentiles for all the data analyzed. The ends of each box represent the lower and upper median while the solid line within the box represents the main median. The red line indicates the grand mean. The data points outside the 5th and 95th percentile are plotted as empty circles. For some groups few data were available so only the mean or the medians are plotted.

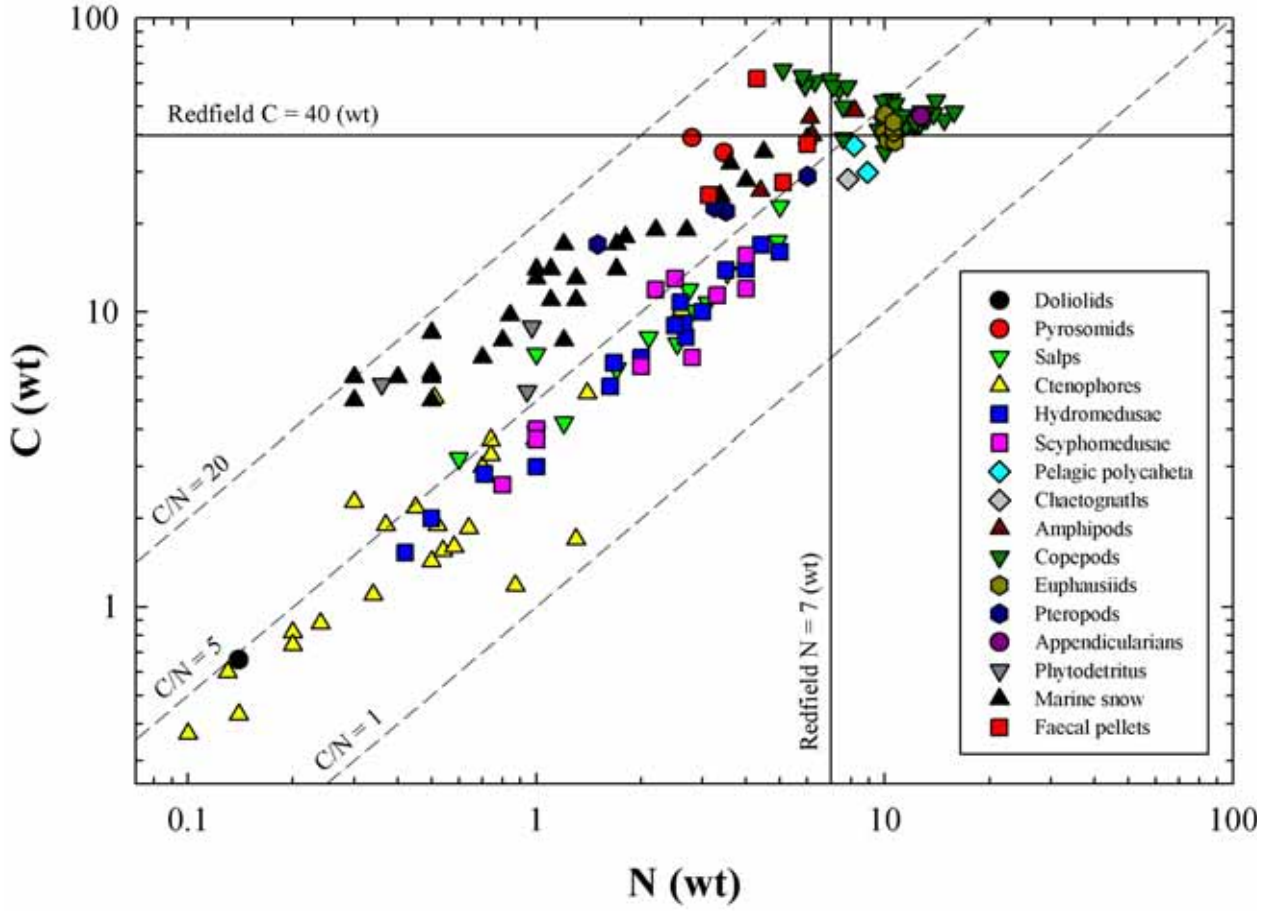

Fig. 6.2. (a) The relationship between carbon and nitrogen (by weight) on major groups of gelatinous zooplankton, on other zooplanktonic organisms, and on biogenic materials found in the ocean (phytodetritus, marine snow, and faecal pellets). A benthic taxa (echinoderms) is also shown for comparison. The Redfield ratio values by weight are also included (C/N = 40/7 = 5.71).

7.

Removal of organic magnesium in coccolithophore carbonates

Abstract

Coccolithophores carbonate refers to the plates of calcite produced by calcifying phytoplankton. The empirical study of the elemental composition has a big potential in the development of paleoproxies. Yet, the difficulties to separate coccolithophore carbonates from organic phases avoid the study of coccoliths magnesium/calcium (Mg/Ca). Magnesium is concentrated in cellular organic molecules up to 400 times higher than in inorganically precipitated calcite in modern seawater. This study aimed to optimize a reliable procedure for organic Mg removal from coccolithophore samples to ensure reproducibility in measurements of inorganic Mg. Two baseline methods comprising organic matter oxidations with (1) bleach and (2) hydrogen peroxide (H_2O_2) were tested on synthetic pellets, prepared by mixing pure reagent calcium carbonate ($CaCO_3$) with organic matter from the non-calcifying marine algae *Chlorella autotrophica* and measured *via* ICP-AES (inductively coupled plasma-atomic emission spectrometry). Our results show that treatments with a reductive solution [hydroxylamine-hydrochloride ($NH_2OH{\cdot}HCl$ + NH_4OH)] followed by three consecutive oxidations (H_2O_2) yielded the best cleaning efficiencies, removing > 99% of organic Mg in 24 h, with no alteration of the Mg/Ca and Sr/Ca of reagent $CaCO_3$. P/Ca and Fe/Ca were used as indicators of organic contamination. The optimized protocol was tested in dried coccolithophore pellets from batch cultures of *Emiliania huxleyi*, *Calcidiscus leptoporus* and *Gephyrocapsa oceanica*. Mg/Ca of

treated coccoliths were 0.151 ±0.018, 0.220 ±0.040, and 0.064 ±0.023 mmol/mol. Comparison with literature values suggests a tight dependence on seawater Mg/Ca, which changes as a consequence of different origins (< 10%). The reliable determination of Mg/Ca and Sr/Ca, and the low levels of organic contamination (Fe/Ca and P/Ca) make this protocol applicable to field and laboratory studies of elemental composition in coccolithophore calcite.

This chapter is based on:

Blanco-Ameijeiras, S., **Lebrato, M** (shared 1st authorship with S.B.A)., Stoll, H. M., Iglesias-Rodriguez, M. D., Mendez-Vicente, A., Sett, S., Müller, M. N., Oschlies, A. and Schulz, K. G. 2012. Removal of organic magnesium in coccolithophore carbonates. *Geochimica et Cosmochimica Acta* DOI http://dx.doi.org/10.1016/j.gca.2012.04.043

Acknowledgements: We thank Ian Probert for providing *Calcidiscus leptoporus* and culture advice, and Stephen Widdicombe for assisting in seawater collection. We are also grateful to Tanja Klüver for laboratory assistance, and Julie LaRoche and Ulf Riebesell for laboratory permission at GEOMAR. This work was funded by the "European Project on Ocean Acidification" (EPOCA) under grant agreement n° 211384 for the PhD of ML and Abbey-Santander Internationalization Fund to SBA, and ERC-STG-240222PACE for funding HMS and AMV.

7.1. Introduction

Coccolithophores are marine calcifying phytoplanktonic organisms that play a pivotal role by contributing to the particulate matter production and export *via* the biological carbon pump (Francois et al. 2002; Gehlen et al. 2007; Ridgwell et al. 2009). The export of inorganic carbon takes place in the form of coccoliths, which are composed of calcium carbonate ($CaCO_3$), with minor proportions of magnesium carbonate ($MgCO_3$) and strontium carbonate ($SrCO_3$) in bloom-forming species such as *Emiliania huxleyi* and *Gephyrocapsa oceanica* (Siesser 1977; Stoll et al. 2001; Stoll et al. 2007; Ra et al. 2010; Müller et al. 2011). Mass accumulation of coccolithophore carbonates has been taking place since coccolithophores first appeared in the sediment record of the Permian/Triassic (P/T) boundary, ca. 250 million years ago (Bown et al. 2004; de Vargas et al. 2004). Sedimentation of inorganic material that has not been dissolved during sinking and accumulated on the seabed (Feely et al. 2004; Berelson et al. 2007) has thus formed an extensive stratigraphical fossil record that is available for geochemical analysis in paleoceanographic studies.

The rate of trace elements incorporation (e.g. Mg, Sr and Ba) in coccolithophore carbonates depends largely on their concentration in seawater (Langer et al. 2006a; Ries 2009; Langer et al. 2009a), but it also depends on thermodynamic, kinetic (Morse and Bender 1990), and biological discrimination imposed by the organisms (Stoll and Schrag 2000) that modulates calcite composition. Experimental data (Stoll et al. 2001; Ra et al. 2010) suggest that temperature also exerts a control on the Mg/Ca as in abiogenic calcites (Mucci and Morse 1987; Tesoriero and Pankow 1996), foraminifera (reviewed by Barker et al. 2005) echinoderms (reviewed by Kroh and Nebelsick 2010). Mg/Ca has, therefore, been used as a paleothermometry proxy, although "cleaning issues" in removing organic Mg have precluded a widespread implementation in coccolithophore carbonates (Stoll et al. 2001; Stoll and Ziveri 2004; Ra et al. 2010; Müller et al. 2011). An understanding of the Mg contribution and composition in sinking carbonates also allows to assess susceptibilities to dissolution [e.g. the biomineral saturation state with respect to Mg phases (Andersson et al. 2008)]. However, this is more relevant in high magnesium (> 4 % $MgCO_3$) carbonates (e.g. Morse et al. 2006; Kuffner et al. 2008).

Magnesium is abundant in the organic fraction of coccolithophores. This element is present in biomolecules, such as chlorophyll, where Mg is a central ion in the porphyrin ring (e.g. Mg-

protoporphyrin and Mg -2, 4-diviniyl pheoporphyrin a_5) (Stanier and Smith 1959; Chereskin et al. 1982). Magnesium also binds to cellular polyphosphate compounds such as RNA and DNA (Lusk et al. 1968), and adenosine triphosphate (ATP), which is the main energetic molecule for cellular metabolism (Leroy 1926). Furthermore, magnesium also acts as a cofactor to activate multiple enzymes in the cell (Legong et al. 2001). Therefore, studies based on the Mg/Ca in biogenic calcites (e.g. laboratory incubations, sediment traps, and sediment cores) require removal of Mg associated to organic phases in order to prevent contamination of the inorganic phases (Stoll et al. 2001; Barker et al. 2003). The major limitations in cleaning procedures are the small size of the individual coccoliths that complicate individual manipulation, and the low Mg content in calcite (< 0.1 mmol/mol) (Stoll et al. 2001, Stoll et al. 2007; Ra et al. 2010; Müller et al. 2011).

In this study we optimized cleaning methods using synthetic samples of non calcite-bearing marine organic matter and abiogenic reagent calcite whose Mg/Ca was independently measured. The effectiveness of the cleaning protocols and uncertainties can therefore be assessed. The optimization procedure focused on two baseline methods consisting in organic matter oxidations with (1) bleach, and (2) hydrogen peroxide. The protocol that yielded the highest cleaning efficiency with respect to reagent calcite (> 99%), and the lowest P and Fe contamination levels, requiring less time of incubation (~ 24 h) was applied to dry pellets of three coccolithophore species used in this study (*Emiliania huxleyi*, *Gephyrocapsa oceanica*, and *Calcidiscus leptoporus*). Carbonate elemental ratios (Mg/Ca and Sr/Ca) and organic phases and Fe oxides (Tang and Morel, 2006) contamination indicators (P/Ca and Fe/Ca, respectively) of synthetic and coccolithophore pellets were determined via inductively coupled plasma-atomic emission spectrometry (ICP-AES). Additionally, we report the culture media conditions (abiotic factors, seawater carbonate chemistry and Mg/Ca ratios) as well as physiological parameters: particulate carbon production and organic C/N. The protocol optimized and tested here considerably reduces the uncertainties in the study of Mg/Ca in coccolithophore calcite and monitors organic matter contamination through P/Ca and Fe/Ca. This will allow expanding the use of Mg/Ca as a proxy and also to measure/calibrate data from laboratory experiments to assess responses of coccolith chemistry to different environmental conditions.

7.2. Methods

7.2.1. Culture methods

Monoclonal cultures of two species of coccolithophore *Emiliania huxleyi* CAWPO6 and *Calcidiscus leptoporus* RCC1169 and a green alga *Chlorella autotrophica* CCMP243 were grown at the National Oceanography Center, Southampton (United Kingdom). Cultures were incubated at 19.3 ±0.8 ºC in a light:dark cycle of 12:12 hours. The photosynthetically active radiation (PAR) was 125 ±10 µmol quanta m^{-2} s^{-1}, provided by cool-white fluorescent lamps (Osram LUMILUX), and salinity was 35 ±1 (culture conditions are summarized in Table 1). The culture medium was prepared using filter-sterilized (0.22 µm) seawater from the Celtic Sea, offshore Plymouth (UK), and enriched with 100 µM sodium nitrate ($NaNO_3$) and 6.4 µM sodium di-hydrogen phosphate (NaH_2PO_4), and trace metals and vitamins were added following the f/2 medium recipe (Guillard and Ryther 1962; Guillard 1975).

Chlorella autotrophica was grown in triplicates using 12 L of culture medium in sterilized 20 L polycarbonate culture vessels under similar environmental conditions to the coccolithophores (Table 7.1). *Emiliania huxleyi* and *C. leptoporus* were cultured in duplicate, using 3 L of culture medium, in sterile 5 L borosilicate Erlenmeyer flasks. The carbonate chemistry system of the medium reflected the original coastal water at present-day conditions (pH_{total} = 7.82 and 7.94, respectively), and it was left equilibrating with the atmosphere in the chambers (*see* Table 1 for initial and final values). At the start of all experiments the carbonate chemistry of the medium was in the range of present-day observations (Key et al. 2004), but at the time of harvest (as a consequence of high biomass) *C. leptoporus* had consumed 28.3% of the dissolved inorganic carbon (DIC). Particulate organic and inorganic carbon measurements (cell quota and production rates) were in agreement ($PIC/POC_{E.\ huxleyi}$ = 0.81, $PIC/POC_{C.\ leptoporus}$ = 2.18) with published datasets at present-day carbonate chemistry conditions (e.g. Langer et al. 2006b; Iglesias-Rodriguez et al. 2008a) (*see* Table 7.1). *Gephyrocapsa oceanica* (RCC1303) was cultured at the GEOMAR (Germany) in a climate chamber at 20 ºC (Table 7.1) with a 16:8 L:D cycle using 150 µmol quanta m^{-2} s^{-1}. Cultures were grown in individual 2.5 L polycarbonate bottles (closed system) in artificial seawater (Kester et al. 1967) enriched with 64 µM of $NaNO_3$ and 4 µM of $NaH_2PO_4 \cdot H_2O$ and trace metals and vitamins according to f/8 medium recipe (Guillard and Ryther 1962; Guillard 1975). Carbonate chemistry was adjusted to present-day

conditions (pH_{total} = 8.03) by combined additions of Na_2CO_3 and HCl as described in the EPOCA Guide to best practices in ocean acidification research and data reporting (Gattuso et al. 2010). Parameters of carbonate chemistry system and determination for each culture are summarized in Table 7.1. All experimental cultures (for the three species) were inoculated from cultures pre-acclimated to experimental conditions for at least eight generations, in exponential growth phase.

7.2.2. Pellet preparation

7.2.2.1. Synthetic pellets

Synthetic pellets were prepared by mixing 5 mL of a suspension of 10 g L^{-1} of reagent grade $CaCO_3$ powder, with 5 mL of a suspension of the non-calcifying marine microalgae *Chlorella autotrophica* (~1.5×10^6 cell mL^{-1}) (Appendix A1 - Table 7.4). The mixture was centrifuged with a relative centrifuge force (RCF) of 1970 g for 20 minutes at 4 ºC in a Hettich ROTANTA 460RS Centrifuge. After discarding the supernatant, the synthetic pellets were frozen at -80 ºC, freeze-dried for 48 h in Falcon tubes (Harris 1954), and kept at room temperature until analysis. Additionally, control samples were prepared with a suspension of 10 g L^{-1} of reagent-grade $CaCO_3$ (without algal addition) following the same protocol as for the preparation of synthetic pellets (Table 7.4). The pellets were produced in a single batch, with similar weights and $CaCO_3$/organic matter ratios (Table 7.4), then freeze-dried for 48 h, and stored at room temperature for two weeks before analysis. Thus, differences among the individual pellets as well as the bacterial oxidation effect (Stoll et al. 2001) were minimized to asses the net organic Mg removal achieved purely by chemical treatment (protocol). Stoll et al. (2001) reported that synthetic pellets of untreated *C. autotrophica* + $CaCO_3$ had similar Mg/Ca as those from samples extracted from coccolithophore cultures with high organic content (0.5-300 mmol/mol). Therefore, we assume that our synthetic pellets also reproduce the properties of coccolithophore material to test the organic Mg removal protocols.

8.2.2.2. Coccolithophore pellets

Cultures of coccolithophores were concentrated into cellular pellets (one pellet per replicate bottle) by centrifugation. Since the culture experiments were conducted at different laboratories,

the facilities available conditioned the application of two different procedures of centrifugation (Fig. 7.1). A Hettich ROTANTA 460RS Centrifuge was used at the National Oceanography Centre Southampton (it only takes conic-bottom tubes), and a Beckman AVANTI^{TM} J-25 Centrifuge was used at the GEOMAR (it only takes flat-bottom tubes). The two separation techniques used to harvest coccolithophore pellets were as follows (Fig. 7.1): (1) *Gephyrocapsa oceanica* was centrifuged in flat-bottom tubes, where the calcite forms a characteristic rim around the organic matter (free coccoliths), and (2) *Emiliania huxleyi* and *Calcidiscus leptoporus* were centrifuged in conical-bottom tubes, where all the material was mixed. In the first procedure, calcite was selected by pipetting from the rim around the organic matter, which allows performing several initial manual discriminations of organic matter. In the second one, this was not possible, and all material remained mixed until cleaning protocols were applied (Fig. 7.1).

Table 7.1. Culture conditions, medium chemistry and sample parameters of coccolithophores in experimental cultures.

Species	***Chlorella autotrophica*** [a]	***Emiliania huxleyi*** [b]		***Calcidiscus leptoporus*** [b]		***Gephyrocapsa oceanica*** [c]	
Strain	CCMP243	CAWPO6 (NZEH)		RCC1169		RCC1303	
Location	North Atlantic	New Zealand		Mediterranean Sea		North Atlantic	
Latitude	43.41 °N	46.58 °S		43.41 °N		44.60 °N	
Longitude	73.10 °W	168.05 °E		7.19 °E		1.5 °W	
		Culture conditions [d]					
Temperature (°C)	19.90 ± 0.18	18.45 ± 0.11		20.09 ± 0.10		20.00 ± 0.00	
PAR (µmol quanta m^{-2} s^{-1})	130.57 ± 2.71	120.94 ± 4.35		134.59 ± 3.97		150.00 ± 0.00	
Salinity	35 ± 0.00	35.27 ± 0.11		35.03 ± 0.14		35.00 ± 0.10	
Nitrate (µM)	100 ± 0.00	95.25 ± 0.00		94.33 ± 0.00		58.80 ± 3.09	
Phosphate (µM)	6.40 ± 0.00	4.88 ± 0.00		2.82 ± 0.00		6.28 ± 0.21	
		Medium carbonate chemistry [d]					
		t*0*	t*n*	t*0*	t*n*	t*0*	t*n*
TA (µmol kg^{-1})	-	2272.72 [e]	2242.74 ± 1.66	2294.85 [e]	1573.60 ± 8.08	2343.49 ± 1.88 [f]	2236.40 ± 0.01
DIC (µmol kg^{-1})	-	2131.06 [e]	2046.52 ± 3.67	2202.70 [e]	1503.06 ± 58.53	2081.69 ± 10.81 [g]	1970.18 ± 90.09
pH_{total}	8.13 ± 0.04	7.82	7.95 ± 0.01	7.66	7.66 ± 0.22	8.05 ± 0.02	8.06 ± 0.17
pCO_2 (µatm)	-	721.96	505.07 ± 6.57	1087.00	389.04 ± 03.29	408.37 ± 26,78	388.69 ± 174.92
HCO_3^- (µmol kg^{-1})	-	1994.25	1885.7 ± 4.62	2080.00	1415.96 ± 72.35	1880.05 ± 18.58	1782.77 ± 160.29
CO_3^{2-} (µmol kg^{-1})	-	112.49	143.78 ± 1.17	86.92	60.96 ± 26.53	188.44 ± 8.64	188.35 ± 56.76
CO_2 (µmol kg^{-1})	-	24.32	17.01 ± 0.22	35.04	26.15 ± 13.71	13.18 ± 0.88	12.56 ± 5.65
Ω-Cal.	-	2.68	3.43 ± 0.03	2.08	1.46 ± 0.63	4.51 ± 0.21	4.51 ± 1.36
$Mg/Ca_{seawater}$ (mol/mol) [j]		5.665 ± 0.025	5.670 ± 0.025	5.396 ± 0.032	5.827 ± 0.043	-	5.632 ± 0.019
$Sr/Ca_{seawater}$ (mmol/mol) [j]		8.589 ± 0.044	8.607 ± 0.066	8.721 ± 0.055	8.871 ± 0.053	-	7.946 ± 0.081
		Sample parameters [d]					
Cell density (cell ml^{-1})	$1.51 \cdot 10^6 \pm 5.08 \cdot 10^5$	33890 ± 2009		9066 ± 945		24793 ± 2283	
Growth rate (µ)	0.73 ± 0.042	1.45 ± 0.015		0.37 ± 0.009		0.91 ± 0.120	
PIC quota (pg C $cell^{-1}$)	-	6.42 ± 0.89 [h]		433.87 ± 49.48 [h]		28.00 ± 2.80 [i]	
PIC prod. (pg C $cell^{-1}$ d^{-1})	-	9.35 ± 1.25 [h]		162.56 ± 14.58 [h]		25.31 ± 1.02 [i]	

POC quota (pg C $cell^{-1}$)	-	7.96 ± 1.04	198.71 ± 1.77	26.85 ± 0.49
POC prod. (pg C $cell^{-1}$ d^{-1})	-	11.59 ± 1.41	74.57 ± 1.31	11.14 ± 0.34
PIC/POC (wt/wt)	-	0.81 ± 0.07	2.18 ± 0.23	1.92 ± 0.14
C/N (wt/wt)	-	8.28 ± 0.92	13.58 ± 0.93	5.15 ± 1.97

[a] Non-calcifying algae used for synthetic pellet preparation along with pure calcite. Medium chemistry only recorded as pH_{total}.

[b] Strains cultured in natural seawater.

[c] Strain cultured in artificial seawater (*see* main text for details). Sampling of medium carbonate chemistry at final time (t_n) was performed 2-12 hours before the harvesting for pellet production. The head-space effect in the bottle during this period may have biased these values.

[d] Medium carbonate chemistry was determined at time zero of the experiment (t*0*) and at harvesting time (t*n*) with the software CO2SYS (Pierrot et al. 2006) using TA and DIC as imput data. Data of *C. autotrophica*, *E. huxleyi*, *C. leptoporus* cultures at tn are calculated form duplicates. *Gephyrocapsa oceanica* values are the average from two CO_2 conditions (381 and 496 µatm) sampled one day before harvesting the pellets. Initial and final conditions are presented as an average of both replicates.

[e] Measured with a VINDTA instrument (Mintrop 2006). TA and DIC at harvesting (final) were extremely low probably as a consequence of high densities of *C. leptoporus* consuming the medium chemistry. To confirm measured samples, DIC was re-calculated using TPC build-up: $DIC_{final} = DIC_{initial}$ - TPC, and then TA re-calculated using measured pH_{total} values. The re-calculated conditions were: TA_{final} = 1666.40 ± 111.21, DIC_{final} = 1500.76 ± 100.72. These conditions do not affect the work on the cleaning of organic Mg and the subsequent ICP-AES measurements.

[f] TA measured in a Metrohm Basic Titrino 794 titration device.

[g] DIC measured photometrically in a QUAATRO analyzer (Stoll et al. 2001) .

[h] PIC measured as calcite with an ICP-AES and obtained values where corrected for contribution of seawater salts (*see* main text for details).

[i] PIC measured from: PIC = TPC - POC, with an elemental analyzer Euro EA (Sharp 1974).

[j] Standard error calculated form duplicate measurements of the same sample analysed with ICP-AES.

Table 7.2. A summary of protocols tested, elemental ratios, and cleaning efficiencies on *Chlorella autotrophica* and calcite pellets.

Protocol code	**A**	**B**	**C**	**D**	**E**	**F**	**G**	**H** [d]
Cleaning protocol	Bleach[a]	Bleach	Red.[b] Bleach	Oxid.[c]	Red. Oxid.	Oxid.	Red. Oxid.	Red. Oxid.
Pellet n°	(1-6)	(1-6)	(7-8)	(9-11)	(12-14)	(12-14)	(15)	(16)
Pre-treatment								
Rinses DI [e]	-	-	-	-	-	x6	x5	x3
Volume (ml)	-	-	-	-	-	2	2	2
Reduction + Oxidation								
Reduction	-	-	Red.	-	Red.	-	Red.	Red.
Volume (ml)	-	-	1	-	0.350	-	0.750	0.750
Sonication (min.)	-	-	15	-	15	-	20	20
Incubation (h)	-	-	24	-	24	-	24	24
Temperature (°C)	-	-	22	-	22	-	22	22
Rinse DI	-	-	x2	-	x4	-	x4	x4
Volume (ml)	-	-	2	-	2	-	2	2
1st Oxidation	Bleach	Bleach	Bleach	Oxid.	Oxid.	Oxid.	Oxid.	Oxid.
Volume (ml)	2	2	2	3	3	3	2	2
Sonication (min)	15	15	15	10	10	10	10	10
Incubation	24 h	24 h	24 h	10 min	10 min	10 min	10 min	10 min
Temperature (°C)	22	22	22	100	100	100	100	100
Rinse DI	x2	x2	x2	x3	x3	x3	x2	x2
Volume (ml)	2	2	2	2	2	2	2	1
2nd Oxidation	Bleach	Bleach	Bleach	Oxid.	Oxid.	Oxid.	Oxid.	Oxid.
Volume (ml)	2	2	2	3	3	3	1	1
Sonication (min)	15	15	15	10	10	10	10	10
Incubation	24 h	24 h	24 h	10 min	10 min	10 min	10 min	10 min
Temperature (°C)	22	22	22	100	100	100	100	100
Rinse DI	x2	x2	x2	x3	x3	x3	x2	x2
Volume (ml)	2	2	2	2	2	2	2	1
3rd Oxidation	Bleach	Bleach	Bleach	Oxid.	Oxid.	Oxid.	Oxid.	Oxid.
Volume (ml)	2	2	2	1.5	1.5	1.5	1	1
Sonication (min)	15	15	15	10	10	10	10	10
Incubation	24 h	24 h	24 h	10 min	10 min	10 min	10 min	10 min
Temperature (°C)	22	22	22	100	100	100	100	100
Rinse DI	x2	x2	x2	x3	x3	x3	x2	x2
Volume (ml)	2	2	2	2	2	2	2	1
4th Oxidation	Bleach	Bleach	Bleach	Oxid.	Oxid.	Oxid.	Oxid.	-
Volume (ml)	2	2	2	0.5	0.5	0.5	1	-
Sonication (min)	15	15	15	10	10	10	10	-
Incubation	24 h	24 h	24 h	10 min	10 min	10 min	10 min	-
Temperature (°C)	22	22	22	100	100	100	100	-
Rinse DI	x4	x2	x4	x4	x4	x4	x4	-
Volume (ml)	2	2	2	1	1	1	1	-
5th Oxidation	-	Bleach	-	-	-	-	-	-

Volume (ml)	-	2	-	-	-	-	-	-
Sonication (min)	-	15	-	-	-	-	-	-
Incubation	-	24 h	-	-	-	-	-	-
Temperature (°C)	-	22	-	-	-	-	-	-
Rinse DI	-	x4	-	-	-	-	-	-
Volume (ml)	-	2	-	-	-	-	-	-
Protocol time [f]	96 h	120 h	120 h	40 min	24.6 h	40 min	24.6 h	24.5 h

[a] Oxidation solution: 10% NaClO (v/v).
[b] Reduction solution: 4.76% (v/v) Hydroxylamine-hydrochloride $NH_2OH{\cdot}HCl$ + 38% (v/v) NH_4OH.
[c] Oxidation solution: 0.33% (v/v) H_2O_2 + 0.98% (v/v) NaOH.
[d] Protocol H was used to treat all coccolith samples.
[e] DI stands for alkaline deionised water rinses, which pH_{total} was adjusted between 9 and 10 with NH_4OH to avoid carbonate dissolution. After the rinses all pellets were centrifuged at 3000 rpm for 10 minutes and the supernatant was removed. Time for incubations only. This excludes handling and preparation for ICP-AES.
[f] Time of incubations only. This excludes handling and preparation for ICP-AES analyzes.

7.2.3. Cleaning protocols

Two different oxidation procedures were applied during the protocol optimization. The first one was a bleach-based method consisting of consecutive oxidations with a solution of sodium hypochlorite (10% NaClO v/v) for 24 h at room temperature (Table 7.2). The second one involved an oxidizing solution of alkaline hydrogen peroxide [0.33% (v/v) H_2O_2 + 0.98% (v/v) NaOH], based on a method originally developed by Boyle (1983) and widely used for Mg/Ca in sediment samples of foraminifera (e.g. Martin and Lea 2002; Barker et al. 2003; Barker et al. 2005). For foraminifera samples rich in organic phases from cultures (Russell et al. 2004) and sediment traps (Anand et al. 2003; Pak et al. 2004) this solution was applied in higher concentrations for longer time periods (Table 2). In the present study, the oxidative incubations started with pellet immersion in the alkaline H_2O_2 solution (inside 15 mL tubes) during 10-15 min (Table 7.2) in an ultrasonic bath at room temperature, which disrupts organic matter and enhances the oxidative action. Afterwards, the temperature was raised to ~100 ºC in a "warm bath", to break down the residual H_2O_2, removing it from the solution. Any associated impurities are brought into suspension, and then removed in subsequent rinses with deionized water (Table 7.2). Several variations were introduced in the original protocol to achieve the most effective and rapid treatment (Table 7.2): (1) Rinses with deionized water (DI) and manual removal of organic matter by pipetting before the oxidative incubations (treatments F-H), (2) reductive incubation using a solution of 4.76% (v/v) $NH_2OH{\cdot}HCl$ + 38% (v/v) NH_4OH (Boyle 1981) before oxidation (treatments C, E, G, H), (3) increase in the number of oxidizing incubations (treatment B), and (4) modifications in the volume of reactive solution and DI water

according to sample size. All the reagent solutions used were alkaline to avoid carbonate dissolution. The efficiency in removing organic Mg phases was assessed by comparison with elemental ratios measured on reagent-grade $CaCO_3$. Phosphorus and iron (P/Ca and Fe/Ca) were used as indicators of contamination by organic material and Fe oxyhydroxides, respectively.

7.2.4. Measurements of elemental ratios via ICP-AES

Treated pellets were transferred to clean microfuge tubes (15 mL), dissolved in 250 µL of ultra-pure 2% HNO_3 and diluted in 750 µL of DI water. Elemental analysis was performed in an ICP-AES, using the Thermo *i*CAP 6300 Series ICP Spectrometer (installed in the Department of Geology, University of Oviedo, Spain). To improve precision by minimizing matrix effects, all samples were diluted to similar Ca concentrations for final analysis of trace metal/Ca ratios. To this end, an aliquot of 50 µL of dissolved material was analyzed for Ca concentrations. Based on the measured Ca, the other samples were diluted to a common Ca level, seeking the highest possible Ca concentration within the range of standard calibration solutions (15, 50, 100 ppm Ca). For trace element ratios, we measured in both radial and axial mode: P (177 nm axial), Fe (259 nm radial), Ca (315 nm radial) and Sr (407 nm radial). Calibrations were performed with multi-element standards offline using the intensity ratio method of de Villiers et al. (2002).

Elemental ratios of non-treated coccolithophore samples (only for *E. huxleyi* and *C. leptoporus*) were obtained as a by-product from the measurements of Ca concentration for determination of particulate inorganic carbon (PIC). These samples were obtained by filtering 200 mL of culture medium at harvesting time through a 0.22 µm Cyclopore polycarbonate membrane and rinsed with buffered Milli-Q water (pH ~ 9). Samples were stored at -20 ºC until analysis. Before analysis the samples were dried for 24 h at 60 ºC, dissolved in ultra-pure 2% HNO_3 and analyzed using the ICP-AES, Thermo *i*CAP 6300 Series ICP Spectrometer. Mg/Ca and Sr/Ca in seawater were determined separately by the method of standards addition in culture medium samples (0.22 µm filtered) diluted to 1/200 and 1/10 respectively, and measured with a Thermo *i*Cap 6300 Series ICP Spectrometer as described above. The partition coefficients of Mg (D_{Mg}) and Sr (D_{Sr}) between coccoliths' calcite and seawater were calculated as elemental ratios of coccolithophore calcite divided by the same elemental ratio obtained for the seawater [$D_x = (x/Ca)_{calcite}/(x/Ca)_{seawater}$; where x is the trace element of interest].

7.2.5. Protocol assessment criteria

P/Ca and Fe/Ca were used as indicators of organic contamination and hydroxide coatings, respectively (Table 7.3). The P/Ca was selected because phosphorus is an essential component of biomolecules in the cell metabolism such as nucleotides [structural units of DNA and RNA, and energetic molecules like ATP] and phospholipids (essential constituents of cellular membranes) (Chu 1946). Fe/Ca was selected because iron is generally a major compound in the trace metals stock solution added to culture medium (e.g. Guillard and Ryther 1962). It can be deposited on the cell surface as Fe-oxides and bind organic molecules (Ho et al. 2003; Tang and Morel 2006), which have high affinity to bind organic ligands (Wu and Luther 1995; Rue and Bruland 1997; Barker et al. 2003).

The efficiency of the protocols was assessed by comparing different elemental ratios (Mg/Ca, Fe/Ca) measured in treated synthetic pellets with the same elemental ratios measured in samples of reagent-grade $CaCO_3$ in the same analysis (Fig. 7.2). In this study, elemental ratios of non-treated synthetic pellets were not determined. Therefore, removal efficiency of organic Mg cannot be accurately calculated with respect to synthetic pellets (*Chlorella* + $CaCO_3$), but it can be done with respect to the original $CaCO_3$ sample. Since all the synthetic pellets were produced with similar proportions of organic/inorganic material (Table 7.4), the relative amount of organic Mg and Fe removed after the treatment was estimated by comparison with the reagent-grade $CaCO_3$ following the equation: % organic contamination removed = $[(1 - ratio_{sample}) \times 100]/(1 - ratio_{reagent\ CaCO3})$ (Fig. 7.2). For the coccolith samples, subsequently cleaned with the optimized protocol, we cannot calculate the cleaning efficiency since we did not independently determine the elemental ratios in the coccolith calcite. We estimated the percentage of organic Mg removed during the cleaning treatment comparing with the elemental ratios determined in non-treated samples (*Emiliania huxleyi* and *Calcidiscus leptoporus*) (Table 7.3).

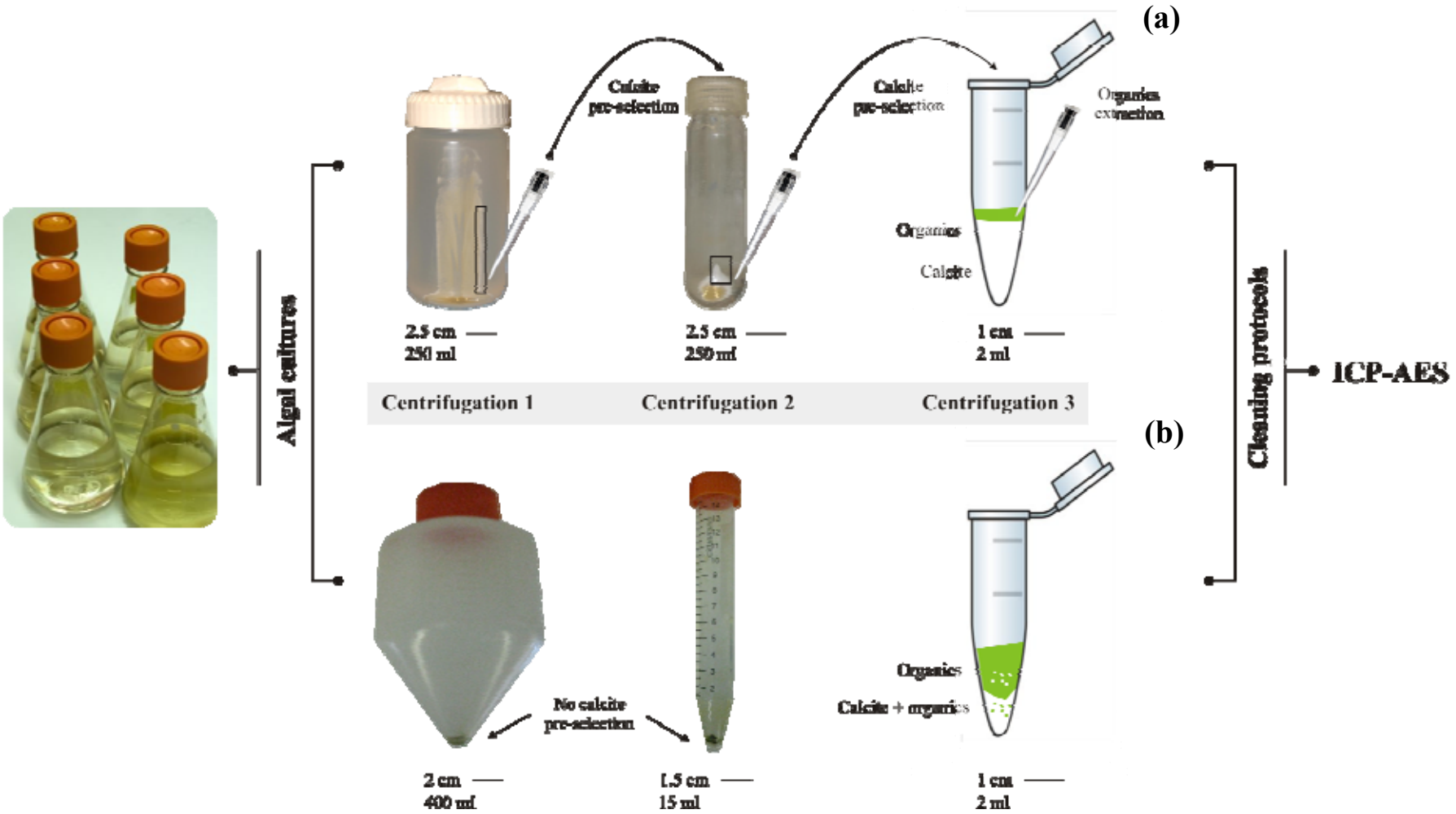

Fig. 7.1. Schematic representation of two procedures to harvest coccolithophore pellets using different centrifugation devices: (a) Using a Hettich ROTANTA 460RS Centrifuge and flat-bottom tubes allowing the manual pre-selection of $CaCO_3$ in samples before applying cleaning protocols and measuring in the ICP-AES. (b) Using a Beckman AVANTI^{TM} J-25 Centrifuge and conical-bottom tubes; the initial separation between calcite and organic matter is not obvious as in procedure (a). Images taken by S. B. A and M. L and courtesy of the "Integration and Application Network" (http://ian.umces.edu/).

Table 7.3. Comparison of the target elemental ratios measured in non-treated samples and samples cleaned with the optimized cleaning protocol H.

	Non-treated Average [a]	**Cleaned pellets** Average	**% removal** [b]
	E. huxleyi NZEH [c]		
Mg/Ca (mmol/mol)	47.996 ± 3.821	0.151 ± 0.018	99.69
Sr/Ca (mmol/mol)	3.530 ± 0.019	2.731 ± 0.218	22.63
P/Ca (mmol/mol)	99.508 ± 4.644	0.750 ± 0.243	99.25
Fe/Ca (mmol/mol)	392.734 ± 31.094	7.613 ± 6.246	98.06
	C. leptoporus RCC1169 [c]		
Mg/Ca (mmol/mol)	4.217 ± 0.385	0.220 ± 0.039	94.79
Sr/Ca (mmol/mol)	3.273 ± 0.041	3.048 ± 0.008	6.87
P/Ca (mmol/mol)	5.987 ± 0.949	0.398 ± 0.313	93.35
Fe/Ca (mmol/mol)	27.630 ± 3.475	5.631 ± 5.419	79.62

[a] Elemental ratios obtained as a by-product in measurements of calcite (PIC) samples (from the same strain) where no cleaning procedure is applied. Measurements include elements in salt, organic, and carbonate phases. PIC data is shown in Table 7.1.
[b] The percentage of element removal during the cleaning process. Calculated as: [(non-treated samples – treated pellets) × 100] / non-treated samples.
[c] Elemental ratios from PIC samples (non-treated) measured via ICP-AES are only available for these two strains and not for *G. oceanica*, where PIC was measured via Elemental Analyzer (*see* Table 7.1 for details)].

7.3. Results

7.3.1. Protocol optimization on synthetic pellets

Mg/Ca measured in synthetic pellets treated with bleach [treatments A-C (Table 7.2, Fig. 7.2)] ranged from 0.335 to 0.545 mmol/mol, which were higher than 0.136 ± 0.008 mmol/mol measured in the samples of certified $CaCO_3$ used as a control (Appendix A2 - Table 7.5). The estimated percentage of organic Mg removed was < 80% in all the bleach-based treatments (A-C) (Fig. 7.2a). These protocols were effective removing P (average P/Ca = 0.072 mmol/mol) (Fig. 3b). However, Fe/Ca was still high, > 2 mmol/mol (Fig. 7.3a). The Sr/Ca was 0.043 ± 0.002 in the bleach-based treatments (A-C) and the values measured in the reagent grade $CaCO_3$ samples were 0.042 ± 0.002. The introduction of an additional oxidation step in treatment B (Table 7.2), after four oxidations with bleach (24 h each incubation), did not decrease the Mg/Ca (0.415 mmol/mol), even though the P/Ca decreased from 0.042 to 0.012 mmol/mol. In treatment C, the introduction of an initial reductive incubation (Table 7.2) decreased the Fe/Ca from 4.808 mmol/mol (in treatment A) to 0.157 mmol/mol. However, the Mg/Ca was similar to previous treatments (0.429 mmol/mol). Total time of incubation required in the bleach-based treatments

was 96 h for treatment A, and 120 h for treatments B and C. Treatments D-H were based on oxidations with H_2O_2 and were in general more efficient in decreasing Fe/Ca, although Mg/Ca and P/Ca did not behave equally (Fig. 7.3). Treatment D, consisting in four consecutive oxidations with H_2O_2, removed only a small percentage of organic Mg (5.21%), yet, this method decreased the Fe/Ca by ~ 60% in less than 1 h after the start of the incubation, compared with treatments A-C (Fig. 7.2). Treatment E, which introduced a reductive incubation before the oxidations, raised the percentage of Mg removed up to 87.72% and the P/Ca decreased a further 43%. When DI water rinses were applied as the pre-treatment prior to the oxidation steps (treatment F), the P/Ca and Fe/Ca decreased by 40% and 66% respectively, in comparison with treatment E, and the removal of organic Mg increased to 94%. Therefore, a combination of initial DI water rinses, reductive and oxidative incubations was applied in treatment G (Table 7.2) and the Mg removal raised to 98%. Treatment G retrieved the highest values removing organic Mg, P and Fe (Fig. 7.2, 7.3). Before applying this protocol to the coccolithophore samples, minor adjustments in the number of DI water rinses, oxidation steps, and volumes applied were introduced in treatment H to prevent carbonate loss during samples cleaning (previously observed in other treatments, with more reactive volume and more DI water rinses and oxidations). In a small amount of time [24.5 h of incubation (Table 7.2)], treatment H delivered the best results in removing organic Mg (> 99.9%) and was selected to apply to coccolithophore samples. The measurements of P/Ca and Fe/Ca (0.043 and 0.029 mmol/mol, respectively) after application of treatment H were still above measurements in reagent grade $CaCO_3$ samples (0.028 and 0.001 mmol/mol, respectively) (Fig. 7.2). The large standard deviation registered in the P/Ca in synthetic pellets may be attributed to the variability introduced by the cleaning protocol. When samples of reagent grade $CaCO_3$ were treated with the optimized protocol H, the Mg/Ca and Sr/Ca did not variate from those measured in non-treated $CaCO_3$ (Fig. 7.4).

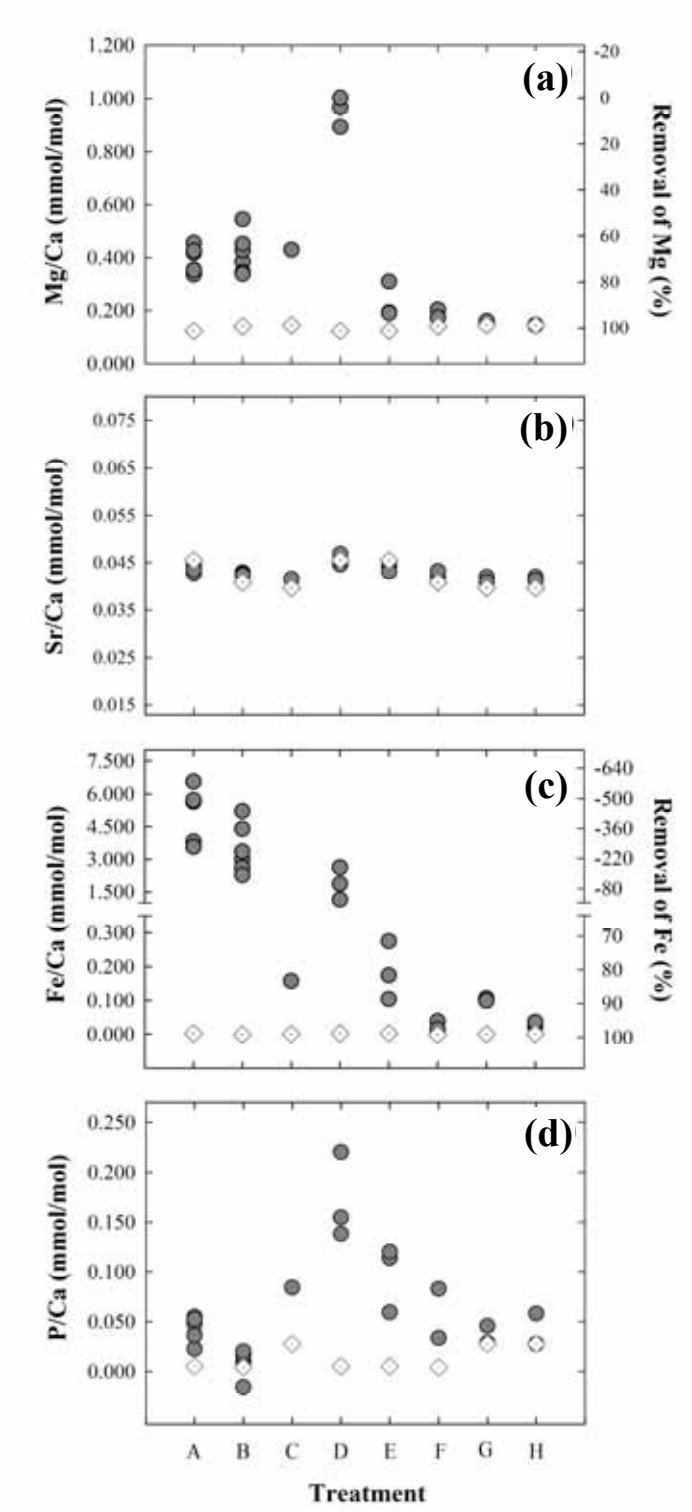

Fig. 7.2. Elemental ratios measured in synthetic pellets with reagent grade $CaCO_3$. Grey circles (●) are synthetic pellets treated with different protocols applied to coccolithophore samples from monoclonal cultures: (a) (Bleach oxidation), (b) (Bleach oxidation), (c) (Reductive incubation and bleach oxidation), (d) (H_2O_2 oxidation), (e) (Reductive incubation and H_2O_2 oxidation), (f) (H_2O_2 oxidation), (g) (Reductive incubation and H_2O_2 oxidation) and (h) (Reductive incubation and H_2O_2 oxidation). White diamonds (◊) are the reagent grade $CaCO_3$ measured in the same ICP-AES run. (a) Mg/Ca measured in reagent grade $CaCO_3$ and the synthetic pellets treated following the different protocols. (b) Sr/Ca. (c) Fe/ca. (d) P/Ca. The secondary axes of (a) and (c) represent an estimation of the percentage of Mg and Fe removed (calculated following the equation: [(reagent grade $CaCO_3$ - treated synthetic pellets) × 100] / reagent grade $CaCO_3$. This percentage cannot be plotted here for the Sr and P because of the values measured in $CaCO_3$ (reference). Details about each protocol are given in Table 7.2 and raw data of the measurements are given in Table 7.5.

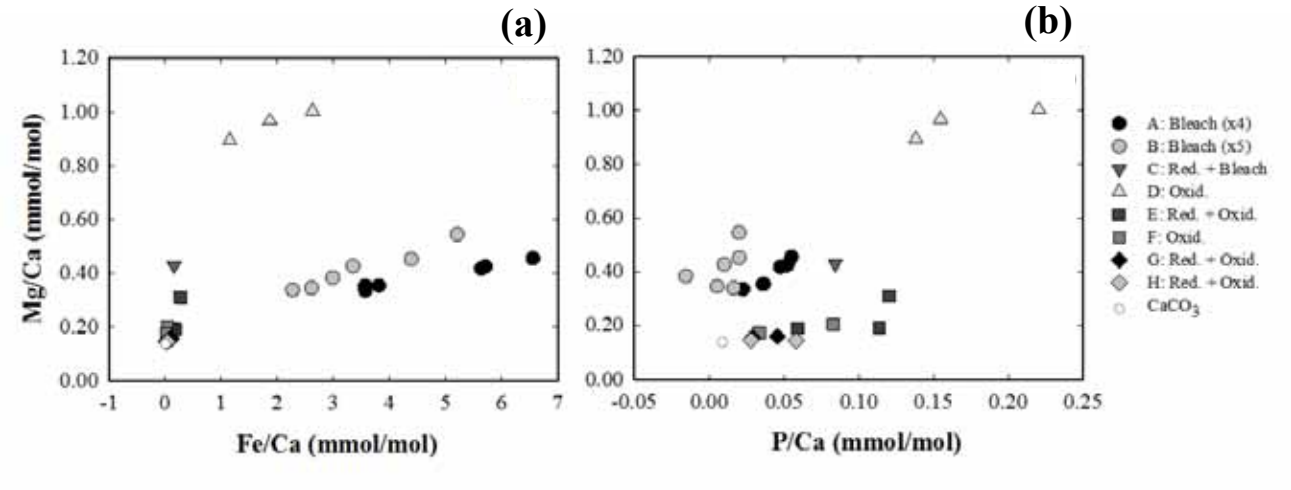

Fig. 7.3. Mg/Ca of synthetic pellets treated with individual protocols plotted against the corresponding Fe/Ca (a), and P/Ca (b), used as indicators of organic phases contamination in biogenic calcite.

8.3.2. Application of the optimized protocol to coccolithophore samples

The Mg/Ca determined in untreated culture samples of *Emiliania huxleyi* was 48 ± 3.82 mmol/mol (Table 7.3). After the implementation of protocol H, the Mg/Ca was 0.151 ± 0.018 mmol/mol (Fig. 7.4), and for treated *Gephyrocapsa oceanica* pellets it was 0.064 ± 0.023 mmol/mol (Fig. 7.4). The Mg/Ca determined for treated samples of *Calcidiscus leptoporus* was 0.220 ± 0.039 mmol/mol (Fig. 7.4), while for non-treated samples this ratio was 4.217 ± 0.385 mmol/mol (Table 7.3). In samples of *E. huxleyi* the cleaning treatment was estimated to remove 99.7% of Mg, 99.3% of P, and 98.1% of Fe associated with organic phases (Table 7.3). Just a 22.6% of the Sr was removed, which indicates that the contribution of organic phases to inorganic Sr are small. In samples of *Calcidiscus leptoporus* the estimated removal of Mg during cleaning was 94.8%, estimated Sr removal was 6.9%, and estimated phosphorus and iron removal were 93.4% and 79.6% respectively. The Fe/Ca determined in *E. huxleyi* and *C. leptoporus* (7.613 and 5.613 mmol/mol) was much higher than that in *G. oceanica* (0.0006 mmol/mol) (Fig. 7.4). The P/Ca was overall higher in *E. huxleyi* and *G. oceanica* (0.750 and 0.786 mmol/mol, respectively) compared to *C. leptoporus* (0.398 mmol/mol). Sr/Ca varied among the different species; the lowest ratio was observed in *E. huxleyi* (2.731 ± 0.218 mmol/mol), followed by *C. leptoporus* (3.048 ± 0.008 mmol/mol) and then *G. oceanica* (3.413 ± 0.098 mmol/mol). Since we used both artificial (laboratory) and natural seawater (coastal), the medium Mg/Ca varied (5.67 mol/mol in *E. huxleyi*, 5.83 mol/mol in *C. leptoporus* and 5.63 mol/mol in *G. oceanica* cultures at harvesting time). The variation in Mg/Ca of coccoliths from different species, all grown at similar temperatures (19.78 ± 0.26 ºC), was correlated with the

seawater Mg/Ca (R^2 = 0.8387; F = 140.398, P < 0.0001) (Fig. 5). Partition coefficients for Mg also varied among the different species from $1.1\times10^{-5} \pm 0.4\times10^{-5}$ in *G. oceanica*, and $2.7\times10^{-5} \pm 0.3\times10^{-5}$ in *E. huxleyi*, to $3.8\times10^{-5} \pm 0.7\times10^{-5}$ in C. *leptoporus*.

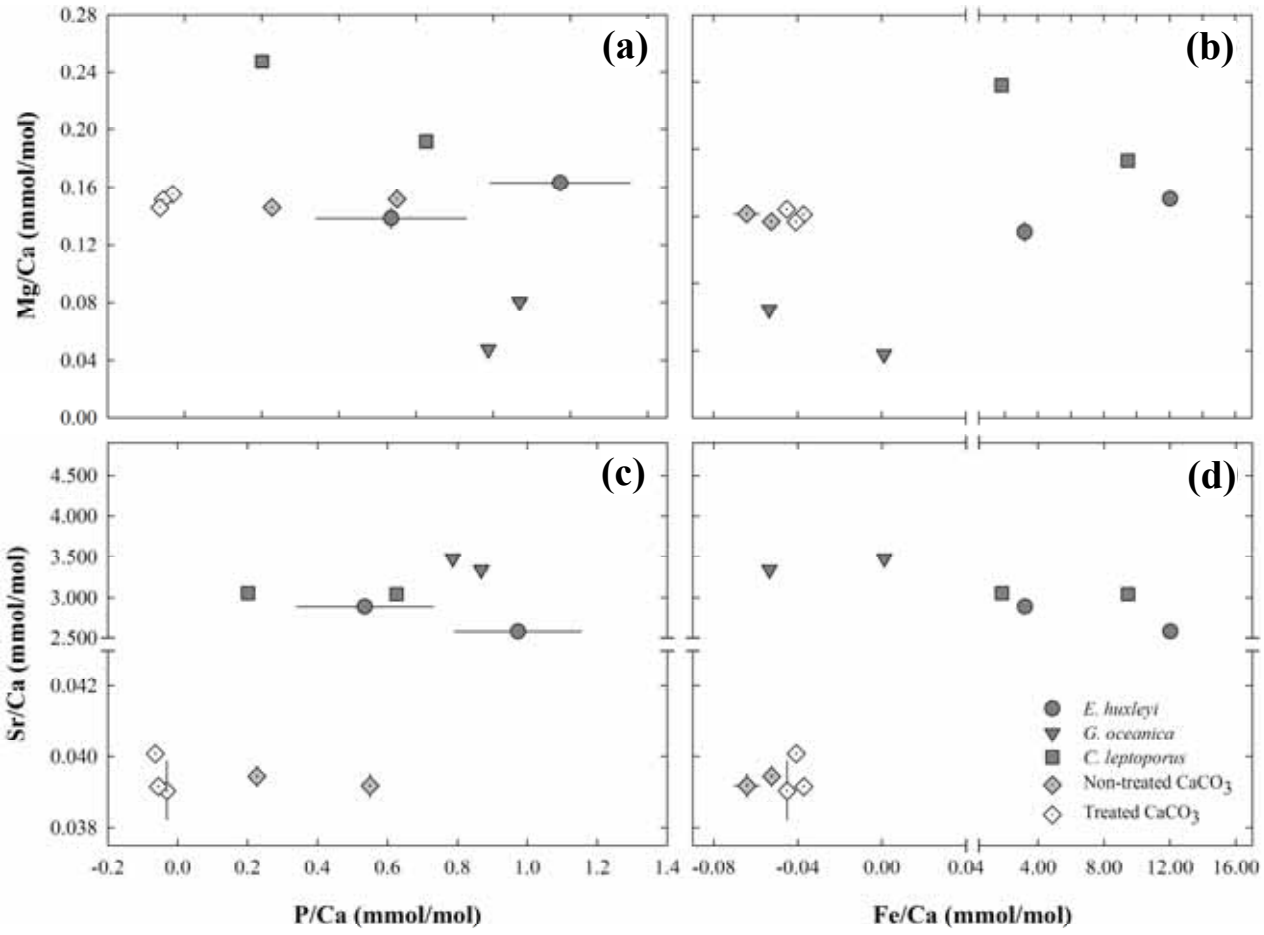

Fig. 7.4. Mg/Ca and Sr/Ca in *Emiliania huxleyi*, *Gephyrocapsa oceanica*, and *Calcidiscus leptoporus* cleaned with protocol H (DI + Red. + Oxid.). The relationship to the P/Ca is shown in the x-axis in (a), (c), and to the Fe/Ca in (b), (d). We also determined the same ratios in samples of treated and non-treated certified $CaCO_3$ to remove organic Mg following protocol H. Bidirectional error bars (standard deviation) from repeated measurements of each pellet represent the individual error of the analysis.

7.4. Discussion

7.4.1. The cleaning protocol

Because bleach-based cleaning treatments retrieved low percentage of organic Mg removal and the long period of incubations required, the optimization efforts were focused on H_2O_2-based treatments. Even though the decrease in Fe/Ca obtained with treatment C (Table 2) indicates that further optimization tests including initial rinses with DI water might improve the efficiency in

removing organic phases, the experimental matrix of this study was not completed. Pak et al. (2004) also implemented bleach- and H_2O_2-based protocols on sediment trap foraminiferal material (rich in organic phases). Their results concluded that Mg/Ca on samples treated with bleach were consistently higher and reproducibility was significantly lower than the samples treated with H_2O_2. Oxidizing reagents are effective in decomposing organic compounds into more hydrophilic groups, which was reflected in the removal of phosphorus (Fig. 7.2). However, in coccolithophore culture samples, a portion of the iron added to the culture medium (in the trace metals stock solution) forms ferric (oxyhydro-) and oxide (FeO_x) precipitates, which become associated with cell surfaces, and might adsorb other trace elements interfering with the elemental analysis (Ho et al. 2003; Tang and Morel 2006). Therefore, a reductive incubation with a solution of hydroxylamine-hydrochloride (Boyle 1981) was introduced as a previous step before the oxidative incubations to remove organic phases associated with metal oxides. The decrease in the Fe/Ca in coccolithophore samples was large, but a complete removal of iron was not achieved (Fig. 7.2). The values of Fe/Ca (0.0006 mmol/mol) in pellets of *G. oceanica* were lower than the Fe/Ca measured in *E. huxleyi* and *C. leptoporus* (Fig. 7.4). This could be attributed to the smaller addition of Fe in the culture medium ($2.93 \cdot 10^{-3}$ µM of $FeCl_3 \cdot 6H_2O$ for *G. oceanica*, compared to $11.7 \cdot 10^{-3}$ µM of $FeCl_3 \cdot 6H_2O$ added besides the natural values for *E. huxleyi* and *C. leptoporus*) (Boye and van der Berg 2000; Ho et al. 2003; Tang and Morel 2006). Results from Bian and Martin (2010) on foraminiferal $CaCO_3$ samples indicate that the use of reductive treatments may be acceptable for the Mg/Ca analysis even though there is a potential risk of sample partial dissolution, lowering the Mg/Ca (Barker et al. 2003; Yu et al. 2007). In the present study, Mg/Ca measured in treatments F and G [essentially identical except in the initial reductive cleaning in G (*see* Table 2)] indicated that the hydroxylamine-hydrochloride solution applied decreased the Mg/Ca by 0.030 mmol/mol (Fig. 7.2). Even though, the potential partial dissolution of carbonate phases was not directly assessed (no SEM images available), we suggest that this reduction is associated with removal of organic Mg rather than partial dissolution of the $CaCO_3$ (Barker et al. 2003; Yu et al. 2007; Bian and Martin 2010). This is because the Mg/Ca determined in samples of reagent grade $CaCO_3$ treated with the optimized protocol (treatment H) was equal to the Mg/Ca in non-treated reagent-grade $CaCO_3$ (0.149 mmol/mol in both cases). Identical results were obtained for the Sr/Ca determined in treated and non-treated reagent-grade $CaCO_3$ (0.039 mmol/mol) (Fig. 7.4). Thus, the optimized protocol does not alter Mg/Ca and Sr/Ca of reagent grade $CaCO_3$, and we assume the same occurs in coccolithophore calcite. However, distribution of Mg in coccolithophore plates is

still unknown, thus potential effects on partial dissolution remain open. Anand et al. (2003), Pak et al. (2004) and Russell et al. (2004) applied stronger concentrations of H_2O_2-based oxidizing solutions during longer periods of time in organic enriched foraminifera samples, which suggests that the optimization tests based on variations in reactives concentration and time of incubation should be performed to improve the organic removal efficiency. However, foraminifera tests are about 10 times thicker than coccoliths (Eggins et al. 2003; Young et al 2003). Therefore, potential higher dissolution susceptibilities of coccolithophore calcite should be kept in mind. In addition to the chemical treatment, previous manual separation and removal of organic material represents an important improvement in the final efficiency when removing organic Mg as demonstrated in treatment F (Fig. 7.1). Initial rinses with DI water (Boyle 1981) combined with an ultrasonic bath, and removal of visible organic phases by pipetting reduced the P/Ca, Fe/Ca, and Mg/Ca. Determination of Mg/Ca and Sr/Ca in this study were supported by the use of P/Ca and Fe/Ca (obtained simultaneously in the elemental analysis via ICP-AES for the same sample) as indicators of organic matter contamination. Its implementation does not require additional steps and we can establish an indirect method to assess the reliability of cleaning procedures in different laboratories. Fe/Ca and P/Ca should be provided in future geochemical studies as indicators of organic contamination to allow an accurate interpretation of the results. They should be carefully considered as indicators of organic matter, although, they may not have a unique correlation equation with cleaning efficiency. For example, iron concentration, which is not strictly associated with organic matter, greatly depends on the sample origin (cultures, sediment traps, natural community or sediment samples).

Sample properties such as the weight of material and the species used are two important factors that *a priori* might compromise the cleaning efficiency of organic Mg phases. The volume of reagent applied should be proportional to the sample size to avoid sample loss associated with pipetting during the intermediate rinses. Moreover, pellet weight should be kept within a small range of variation when the volume of reagents is constant, otherwise this would compromise reproducibility between samples. Additionally, the species-specific calcite/organic matter ratio (PIC/POC) of coccolithophores (e.g. Langer et al. 2009b) may also be affecting the efficiency of this protocol. For example, *Emiliania huxleyi* (PIC/POC ~ 0.8), unlike *C. leptoporus* (PIC/POC > 2), requires the removal of larger proportions of organic matter. The later has lower initial contribution of organic phases (relative to calcite), therefore, the fraction of elements removed during oxidative cleaning of organic phases was lower than in *E. huxleyi* (Table 7.3). The P/Ca

measured in *C. leptoporus* pellets (0.398 mmol/mol) was smaller that in *E. huxleyi* (0.750 mmol/mol), reflecting the greater ease to effectively clean this species with higher ratio of calcite/organics. Amongst the samples used in this study, *E. huxleyi*, with the lowest PIC/POC, and the smallest and most structurally complex coccoliths, requires a more effective removal of organic Mg than *C. leptoporus* and *G. oceanica*.

8.4.2. The elemental composition of coccolithophores

The Mg/Ca of *Emiliania huxleyi* and *Gephyrocapsa oceanica* (Fig. 4) obtained in this study were within the range of variation of previous data from batch cultures of the same species (Stoll et al. 2001), with data from coccoliths obtained from sediment traps (Stoll et al. 2007), and with cultured coccoliths cleaned with acetone and H_2O_2 (Ra et al. 2010). The much higher Mg/Ca (2.710 mmol/mol) measured in living cultures of *E. huxleyi* at present seawater conditions cleaned with a bleach-based protocol (Müller et al. 2011), or in coccoliths of other cultured species for which no cleaning is reported (Stanley et al. 2005) may be due to incomplete removal of organically sourced Mg. The lack of a robust and common cleaning protocol hampers inter-laboratory comparisons to bring together different datasets, and thus advance the use of Mg in coccoliths.

We suggest that the recorded variation in coccolithophore Mg/Ca in cleaned samples within the species concept can be attributed to natural seawater variability. Ra et al. (2010) report, for coccoliths treated with acetone/H_2O_2-based protocol, Mg/Ca between 0.029 and 0.051 mmol/mol in *E. huxleyi*, and between 0.011 and 0.025 mmol/mol in *G. oceanica*, grown in seawater with a Mg/Ca of 5.18 mol/mol. These data points fit on the regression implied by the Mg/Ca of our coccoliths cultured in coastal seawater with Mg/Ca of 5.670-5.827 mol/mol (Fig. 7.5). Wild samples of *E. huxleyi* obtained from the Bermuda Oceanic Flux Program (OFP) sediment traps, pre-treated with H_2O_2 and analyzed with ion probe yield comparable low values, although they are subjected to higher uncertainty depending on the Mg blank in the epoxy mounting resin (Stoll et al. 2007). Nonetheless, assuming oceanic waters in the North Atlantic Ocean have a Mg/Ca of 5.162 mol/mol (Fabricand et al. 1967), the sediment trap samples off Bermuda fit the regression well (Fig. 7.5). It reflects the variability of coccoliths Mg/Ca as a function of seawater Mg/Ca of different origins (e.g. coastal *vs.* oceanic). This has been observed in seawater Mg/Ca (Fabricand et al. 1967; Zang et al. 2003) and Sr/Ca (de Villiers 1999) showing latitudinal variability, which we propose can drive the wild

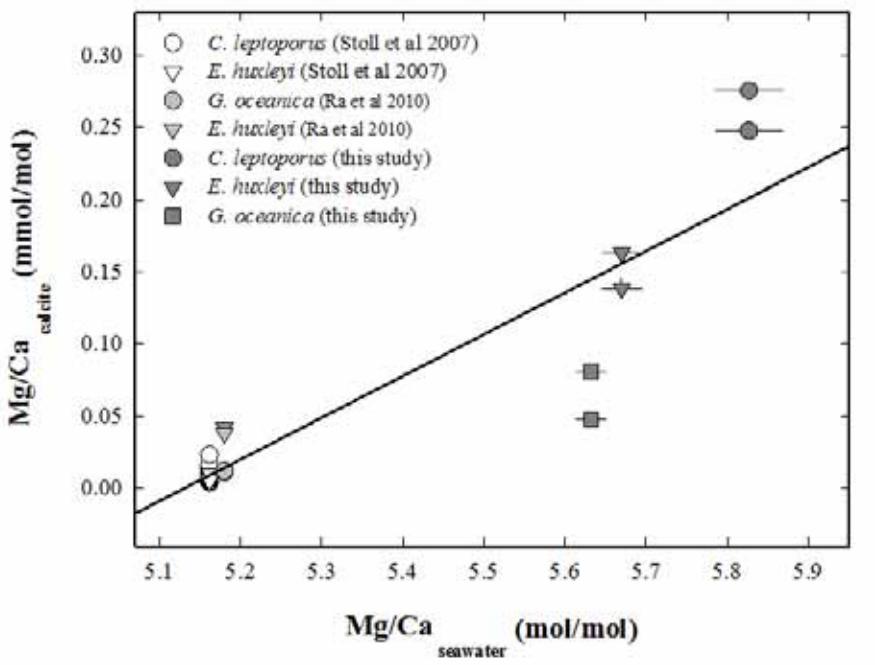

Fig. 7.5. Relationship of coccoliths Mg/Ca and seawater Mg/Ca in coccolithophores in this study and the literature. The data form the literature were selected including samples grown at ~20 ºC. The resulting linear equation is: $y = 0.289\ x - 1.485$; $R^2 = 0.838$; $F = 140.398$ and $P < 0.0001$. Bidirectional error bars represent the standard deviation from repeated measurements of each sample. Average North Atlantic Ocean seawater Mg/Ca used for the data set from Stoll et al. (2007) were taken from Fabricand et al. (1967).

coccoliths elemental composition and may have implications for the sinking carbonates and the dissolution at depth. Further investigation of deviations from the constant elemental proportions in seawater [Marcet's principle (1918)] should aim to understand natural variability as a control of Mg and Sr in coccolithophores. The number of coccolithophore samples and range of seawater Mg/Ca examined are relatively small, therefore, a broader comparison is required to fully test this relationship, expanding from de Villiers (1999) study on seawater Sr/Ca to Mg/Ca across large latitudinal gradients.

Interpretations of the Mg/Ca variability based on published data are currently limited by: (1) uncertainty in different organic Mg removal treatments applied, (2) variable medium conditions (carbonate chemistry, seawater Mg/Ca), and (3) biological effect on elemental partitioning imposed by the physiological fingerprint of species and strains used (Stanley et al. 2005; Müller et al. 2011). For Sr/Ca the situation is simpler because the organic contamination is minimal and Sr/Ca measured in the three species (Fig. 7.4) were in agreement with values measured in culture samples and sediment traps (Stoll et al. 2002; Stoll et al. 2007).

7.5. Conclusions

The Mg/Ca retrieved after organic phases removal are in accordance with bibliographic data and culture conditions. However, this study cannot guanratee that the removal of organic Mg was

truly complete. Further optimization work is needed, specially to work out the minimum amount of sample required, if the proportion of organic phases to calcite (PIC/POC) should be considered when optimizing protocols, and SEM images to asses partial dissolution. The protocol matrix could be extended by testing other organic removal methods such as combustion, and the combination of acetone treatments (Ra et al. 2010) with H_2O_2-based protocols. In order to improve the yield of our protocol, we recommend to introduce a manual separation of calcite (Fig. 7.1). This pre-selection before the chemical treatment enables to remove concentrated organic material on the coccolith surface [e.g. coccolith polysaccharides (Henriksen et al. 2004; Kayano and Shiraiwa 2009)]. While this technique prior to reduction and oxidation was not used before, it helps targeting selectively the calcite fraction from the beginning of the protocol. In addition, the trace metal concentration of the culture medium is an important factor in the formation of metal-oxides in samples from living cultures. Thus, it is recommended to adjust the amount of trace metals added to the minimum amount required without compromising phytoplankton growth rates (Boye and van der Berg 2000; Ho et al. 2003; Tang and Morel 2006), to increase the efficiency of oxidizing reagents. Additionally, in paleoceanographic applications it is better to target culture efforts on species with high PIC/POC such as *Calcidiscus* sp., which also can be individually extracted from sediments. Finally, to routinely measure Mg/Ca in living coccolithophore material from laboratory experiments and field samples, it is necessary to establish a series of baseline measures (quality control) to make datasets comparable. Environmental conditions of growth and carbonate chemistry in the culture media should always be provided because elemental partition (e. g. D_{Mg}) is affected by the carbonate chemistry (Ries 2011) and seawater elemental composition (Ries 2010; Müller et al. 2011). Values of Mg removal efficiency, associated to organic phases, and the P/Ca and Fe/Ca should be provided along with the Mg/Ca results to allow independent assessment and comparison of datasets. In the short term, we should aim to calibrate the coccolithophore Mg/Ca as a proxy for temperature and study relationships to carbonate chemistry parameters, contributing to the development of a coccolithophore multi-proxy approach. This will ease more accurate estimations by reducing biases originating in different habitats, ecophysiology and productivity regimes. We should also be able to understand coccolithophore Mg/Ca and Sr/Ca responses to environmental perturbations such as pCO_2 and temperature variability, and investigate other trace elements incorporated in the calcite and their potential biogeochemical applications.

7.6. Appendix A

7.6.1. A1

Table 7.4. Properties of the synthetic pellets of the non-calcifying alga *Chlorella autotrophica* and the treatments used.

Pellet n° [a]	Label [b]	Cell density (cell ml^{-1})	Total cells (in 50 ml) [c]	Pellet weight (mg) [d]	$CaCO_3$/organic (wt/wt) [e]	Protocol key [f]
1	a	1.93×10^6	2.316×10^9	64.50	0.775	A - B
2	a	1.93×10^6	2.316×10^9	64.20	0.778	A - B
3	b	1.66×10^6	1.992×10^9	65.50	0.763	A - B
4	b	1.66×10^6	1.992×10^9	68.30	0.732	A - B
5	c	9.45×10^5	1.134×10^9	62.40	0.801	A - B
6	c	9.45×10^5	1.134×10^9	62.00	0.806	A - B
7	a	1.93×10^6	2.316×10^9	64.60	0.773	C
8	a	1.93×10^6	2.316×10^9	65.30	0.765	C
9	a	1.93×10^6	2.316×10^9	70.40	0.710	D
10	b	1.66×10^6	1.992×10^9	64.70	0.772	D
11	c	9.45×10^5	1.134×10^9	61.00	0.819	D
12	a	1.93×10^6	2.316×10^9	65.20	0.778	E - F
13	b	1.66×10^6	1.992×10^9	64.70	0.772	E - F
14	c	9.45×10^5	1.134×10^9	62.40	0.801	E - F
15	b	1.66×10^6	1.992×10^9	64.50	0.775	G
16	b	1.66×10^6	1.992×10^9	65.50	0.763	H
17	- [g]	0	0	192.90	Pure calcite [h]	-
18	-	0	0	197.30	Pure calcite [h]	-

[a] Pellet code given for identification purposes for the different protocols.

[b] The label indicates the origin of the seawater batch with a different cell density for a, b, and c. *Chlorella autotrophica* were grown in each batch (12 L).

[c] Cell density in 50 ml aliquots. 5 ml were transferred from the re-suspended material to the final pellets.

[d] Dry weight only from the organic material.

[e] The $CaCO_3$ dry weight is 50 mg for all treatments. The ratio (by weight) varies depending on the amount of organic pellet centrifuged. It resembles the proportions found in pellets made from living *E. huxleyi* cells with a high calcite content.

[f] The code is used to identify the protocols applied to each pellet in Table 7.2.

[g] - indicates "not applicable" or "not given" in all tables.

[h] Only calcite re-suspended and centrifuged in the treatments.

7.6.2. A2

Table 7.5. Carbonate P/Ca and Fe/Ca (contamination proxies), Mg/Ca and Sr/Ca from the *Chlorella autotrophica* + $CaCO_3$ pellets and the reference $CaCO_3$ material used.

Protocol key	**A**	**B**	**C**	**D**	**E**	**F**	**G**	**H**
Cleaning protocol	Bleach	Bleach	Red. Bleach	Oxid.	Red. Oxid.	Oxid.	Red. Oxid.	Red. Oxid.
Pellet nº	(1-6)	(1-6)	(7-8)	(9-11)	(12-14)	(12-14)	(15)	(16)
Elemental ratios (mmol/mol)								
P/Ca	0.037	0.016	-	-	-	-	-	-
	0.048	0.010	-	-	-	-	-	-
	0.023	0.005	-	-	-	-	-	-
	0.036	0.016	-	0.138	0.114	-	-	-
	0.055	0.020	-	0.155	0.120	0.083	0.029	0.028
	0.052	0.020	0.084	0.220	0.059	0.034	0.046	0.058
Average	**0.042**	**0.009**	**0.084**	**0.171**	**0.098**	**0.058**	**0.037**	**0.043**
SD	0.012	0.014	0.000	0.043	0.033	0.035	0.012	0.022
Reagent $CaCO_3$	**0.005**	**0.004**	**0.028**	**0.005**	**0.005**	**0.004**	**0.028**	**0.028**
SD	0.001	0.004	0.008	0.001	0.001	0.004	0.008	0.008
Fe/Ca	3.811	2.987	-	-	-	-	-	-
	5.636	3.349	-	-	-	-	-	-
	3.568	2.609	-	-	-	-	-	-
	3.566	2.272	-	1.150	0.174	-	-	-
	6.559	4.388	-	1.867	0.275	0.039	0.107	0.022
	5.707	5.209	0.157	2.626	0.104	0.015	0.099	0.037
Average	**4.808**	**3.469**	**0.157**	**1.881**	**0.184**	**0.027**	**0.103**	**0.029**
SD	1.314	1.122	0.000	0.738	0.086	0.017	0.005	0.010
Reagent $CaCO_3$	**0.003**	**0.000**	**0.001**	**0.003**	**0.003**	**0.000**	**0.001**	**0.001**
SD	0.002	0.001	0.001	0.002	0.002	0.001	0.001	0.001
Mg/Ca	0.354	0.383	-	-	-	-	-	-
	0.417	0.427	-	-	-	-	-	-
	0.335	0.345	-	-	-	-	-	-
	0.353	0.338	-	0.893	0.193	-	-	-
	0.455	0.452	-	0.967	0.309	0.204	0.156	0.145
	0.425	0.545	0.429	1.003	0.190	0.173	0.160	0.144
Average	**0.390**	**0.415**	**0.429**	**0.954**	**0.230**	**0.188**	**0.158**	**145**
SD	0.049	0.078	0.000	0.056	0.068	0.021	0.003	0.001
Reagent $CaCO_3$	**0.123**	**0.140**	**0.144**	**0.123**	**0.123**	**0.140**	**0.144**	**0.144**
SD	0.007	0.001	0.000	0.007	0.007	0.001	0.000	0.000
Sr/Ca	0.044	0.043	-	-	-	-	-	-
	0.044	0.043	-	-	-	-	-	-
	0.043	0.043	-	-	-	-	-	-
	0.044	0.043	-	0.045	0.044	-	-	-

	0.045	0.043	-	0.045	0.045	0.042	0.042	0.042
	0.043	0.042	0.042	0.047	0.043	0.043	0.041	0.041
Average	**0.044**	**0.043**	**0.042**	**0.046**	**0.044**	**0.043**	**0.041**	**0.042**
SD	0.001	0.000	0.000	0.001	0.001	0.001	0.001	0.001
Reagent $CaCO_3$	**0.046**	**0.041**	**0.040**	**0.046**	**0.046**	**0.041**	**0.040**	**0.040**
SD	0.001	0.003	0.000	0.001	0.001	0.003	0.000	0.000

7.7. Addendum: On deviations from seawater constant element proportions (Marcet's principle) and roles in biogenic calcites

7.7.1. Justification for an "addendum"

Hereafter, I develop a brief contribution to section 8.4.2. (*The elemental composition of coccolithophores*) and Fig. 8.5 from a research project that started during 2011 and will continue in 2012. The laboratory findings (Fig. 8.5) during the PhD motivated the current study in 2011. I have spent a lot of time during the last stages of the PhD (2011) on the management and coordination of the project, also participating in 4 research cruises to recover samples (Mediterranean Sea, Gibraltar Strait, Cantabric Sea, and Porcupine Abyssal Plain - Atlantic Ocean). Therefore, I find pertinent to briefly extend on the project ideas and summary on the work done to date.

7.7.2. Project summary

This project re-assesses the Marcet's principle, which states that the concentration proportions among macro elements remains constant in seawater in the ocean. Although Marcet's rule is a good first approximation, there are numerous exceptions across latitudinal gradients, in semi-enclosed seas, continental margins and estuaries that challenge the principle (*see* Fig. 8.5, 8.6). Namely, the Mg/Ca and Sr/Ca vary as a function of depth induced by elemental depletion at the surface and dissolution at depth and also driven by freshwater inputs in shelf seas. Seawater Mg/Ca and Sr/Ca largely control biogenic incorporation of Mg and Sr during calcification in marine organisms, dominating above other factors (e.g. temperature and carbonate chemistry). The majority of benthic calcifying communities inhabit continental margins, and pelagic organisms (namely coccolithophores and foraminifera) typically populate waters at the shelf break and open ocean. A comprehensive field study of the seawater elemental composition that organisms naturally encounter during their life cycle is thus fundamental to assess the composition of the material exported. It is also important to validate Mg/Ca and Sr/Ca paleo records in continental shelves where river discharges alter seawater composition, and temperature proxies based on foraminifera and coccolith records have been used. Changes in the Mg and Sr composition across latitudinal or biogeographical gradients are relevant for biogeochemical cycles because a higher Mg content in the calcite exported facilitates dissolution

at shallower depths, while Sr is a very soluble element itself. For Mg/Ca and Sr/Ca, modern open ocean values remain ~ 5.10-5.20 mol/mol and ~ 8.40-8.60 mmol/mol respectively, but there are notable exceptions in ecosystems where pelagic and benthic calcifyers live, challenging our understanding of biomineralization and carbonate dissolution at a regional scale. Using radial surveys in 59 research cruises from coastal to offshore waters (perpendicular), parallel to the coast, and in enclosed and open water bodies, we collected seawater samples measured via ICP-OES and chelation chromatography (to produce two independent datasets), to study the Marcet's principle focussing on the Mg/Ca and Sr/Ca. We propose that changes in seawater Mg/Ca and Sr/Ca (natural variability) in the present ocean could drive the elemental ratios in biogenic calcites driven by biogeography, and thus water mass origin. This is important to understand natural variability in calcite dissolution in the present ocean and paleo records in continental margins (influenced by river discharges) based e.g. on temperature reconstructions. Our results will deliver new information relevant for experimentalists, modellers, and paleoceanographers to better understand the effect of enviromental variables on calcification, carbonate dissolution and proxy development.

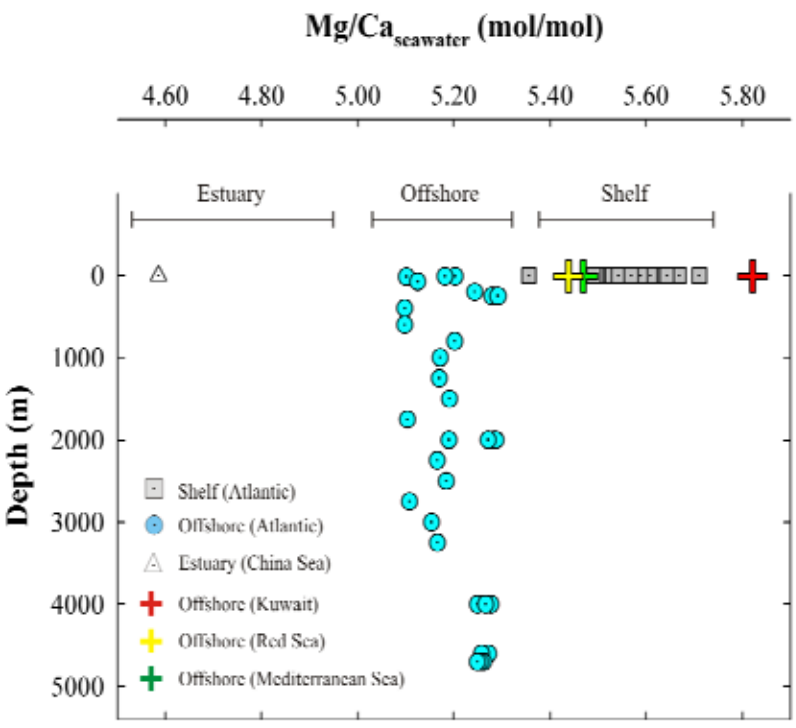

Fig. 7.6. Seawater Mg/Ca in estuaries, shelves, and oceanic environments and depth (only oceanic). Data from Zang et al. 2003, Fabricand et al. 1967, Blanco-Ameijeiras et al. in press, and Lenntech (http://www.lenntech.com/) routine measurements on intake water of desalination plants.

7.7.3. Introduction

Trace elements (e.g. Mg, Sr and Ba) are incorporated in biogenic carbonates (e.g. coccoliths, foraminifera) depending on the seawater concetration (Ries 2010; Langer et al. 2009a), thermodynamic and kinetic factors (Morse and Bender 1990). Physiological discrimination (Stoll and Schrag 2000) also controls the calcite composition. The effect of the seawater composition on biogenic calcite Mg/Ca is

ignored in the modern ocean as major ions are conservative (Tyrrell and Zeebe 2004). It is thus accepted that seawater composition behaves conservatively, which is known as the Marcet's principle (Marcet 1918; Culkin and Cox 1966; Millero et al. 2008). Variability from this rule is attributed to precipitation, evaporation, freshwater inputs, ice, and calcite dissolution. During the last 3 years, we conducted laboratory incubations at the GEOMAR using coccolithophores, and we noticed that the calcite Mg/Ca (measured via ICP-MES, Blanco-Ameijeiras et al. in press) changes as a function of seawater Mg/Ca [correlation only derived for benthic organisms (Ries 2010)]. The seawater used was natural, but it had different origins, from coastal (Mg/Ca ~ 5.70 mol/mol) to open ocean (Mg/Ca ~ 5.10 mol/mol) settings (Fig. 7.5, 7.6).

Depth also exerts a control on elemental composition as found by Brewer et al. (1975) in the Pacific Ocean, where the top 500-800 m are depleted in Ca ~ 1% relative to the deep waters, while in the Atlantic the contrary is found both for Ca and Mg (*see* Fabricand et al. 1967; Fig. 7.6). In the Pacific Ocean the same happens with Sr, and surface waters are depleted by ~ 1-3 % compared to deep waters (Bernstein et al. 1987, 1992; de Villiers 1999). This can be attributed to pelagic consumption at the surface (coccolithophores $SrCO_3$ and acantharians $SrSO_4$), and quick dissolution at depth (Martin et al. 2010). Across large Atlantic and Pacific Ocean latitudinal gradients in the open ocean, Sr/Ca exhibits spatial changes of 2-3 %, with the largest values at high latitudes near upwelling areas (de Villiers 1999). Although variability remains small, it questions the validity of paleo records where Sr/Ca is assumed to be conservative (Beck et al. 1992, 1997; Guilderson et al. 1994). In other cases, the freshwater input e.g. on esturies, modifies the water composition (as a consequence of large salinity changes) (Zang et al. 2003). This suggests that a combination of biological and physical processes are behind the observed deviations from Marcet's principle in the modern ocean.

In laboratory work it is generally assumed that the Marcet's principle (Marcet 1918) should apply to seawater used in culture stocks, incubations, indoor mesocosms, or other preparations. The same is assumed in paleo reconstructions of e.g. shelf and open ocean waters. We suggest that deviations from the Marcet's principle with respect to Mg and Ca could explain the small differences found in Mg/Ca in coccoliths in the modern ocean along with a species-specific physiological fingerprint. For coccoliths, Ra et al. (2010) report Mg/Ca ratios between 0.029 and 0.051 mmol/mol in *Emiliania huxleyi*, and between 0.011 and 0.025 mmol/mol in *Gephyrocapsa oceanica*, grown in seawater with a Mg/Ca of 5.18 mmol/mol. These data points fit well on a regression implied by the Mg/Ca of our coccoliths cultured in coastal seawater of

5.491-5.640 mmol/mol (Fig. 7.5). Wild samples of *E. huxleyi* obtained from the Bermuda Oceanic Flux Program (OFP) sediment traps, yield comparably low values (Stoll et al. 2007). Nonetheless, if oceanic waters in the North Atlantic Ocean have a Mg/Ca of 5.101-5.210 mmol/mol (Fabricand et al. 1967), the sediment trap samples off Bermuda fit the regression well (Fig. 7.5). If this regression is a robust indicator of the Mg/Ca in coccoliths calcite, the partitioning coefficient of Mg varies as a function of seawater Mg/Ca of different origins (coastal *vs.* oceanic). This has important implications for sinking and subsequent dissolution of pelagic calcite (and probably benthic sources) from shelf to oceanic regions. Seemingly, this natural variability in seawater elemental ratios, questions the assumption of seawater conservative behaviour e.g. in palae reconstructions in the vicinity of shelf and slope environments.

7.7.4. Project strategy and methods

We re-assess the Marcet paradigm in the global ocean by undertaking 59 surveys from pole to pole in the three major ocean basins at all possible latitudes and collecting seawater samples with the same method (*see* below). The following type of surveys were conducted (Table 7.6):

1) *Meridional transect - large vessels*: Some cruises collected water in large transects carried out from 5° to 20° latitude/longitude, parallel or perpendicular to the coast (*see* Table 7.6 for classification). This was done in the Atlantic, Pacific Ocean and Arctic Ocean. The majority of these large scale surveys delivered high quality CTD surface and depth readings attached to the samples. All surveys conducted perpendicularly to the coastline, had a clearly defined sampling strategy to target the subtidal, the main shelf, the slope, the slope break and the open ocean at different depths. In other cases, we just adapted to the official cruise track.

2) *Regional transect - medium/small vessels*: The majority of the samples originated in smaller transects at a regional scale (e.g. Peru upwelling, Canadian Arctic, Iceland, Beaufort and Bering Sea, Gibraltar Strait, Mozambique Channel, Gulf of Mexico) (*see* Table 7.6). Here, quality CTD readings were not available in all cases, as in some remote locations the cruise was from a private charter (only agreed to recover water sample following a specific procedure).

3) *Local transect - small boat/coastal*: Some samples were collected by partners near their working place in the coast or with the help of a zodiac. This results in qualitative surface samples from a few places, rather than a complete transect, and no depth samples (e.g. New Zealand, Durban, Vancouver, Kiel Bight, Fram Strait, Prince William Sounds - Alaska, Bay of Bizerte - Mediterranean Sea) (*see* Table 7.6). CTD readings were absent in these cases, and manual probes with a calibrated temperature and salinity sensor (e.g. YSI) were used.

4) *Permanent station - all size vessels*: In a few cases, samples were obtained from permanent/fix stations were there was a temporal component or a historical time series (BATS - Bermuda, Hydrostation S - Bermuda, Terceira Island - Azores, Papa Station - Pacific Ocean, Porcupine Abyssal Plain - Atlantic Ocean) (*see* Table 7.6). These datasets have the highest quality CTD and depth readings along with other measurements (e.g. carbonate chemistry, nutrients, chlorophyll) routinely taken by the institution managing them.

The coordination efforts in the project comprised:

1) *Cruise search, contact, and strategy*: This was established between the project leader (myself) and various research-cruise PIs to collect seawater samples and provide meta-data. The decision to choose a specific cruise was based on the location, cruise track, and the availability of personnel to collect the samples and the meta-data. The minimum meta-data requirements from samples to be acceptable and quality controlled were: "Survey name and label", "sample depth (m)", "date", "latitude", "longitude", "salinity", and "temperature". Additional information was collated where applicable. We used two communication methods: a) Direct contact by email in existing projects and surveys; b) Posting announcements in group emails. We identified and contacted with 45 research cruise PIs and individuals at 59 different scenarios (Table 7.6). The common strategy discussed with the research-cruise PIs aimed to obtain samples from the euphotic zone to the deep waters where possible, and assess horizontal (subsurface) and vertical (CTD casts) variability. We had positive replies in 100% of the cases, and we have received samples from 18 cruises so far.

2) *Gear and sampling material*: We sent to all cruise PIs sampling material and gear. They also instructed us on the available CTD or probe devices to obtain the meta-data. After collection,

samples were sent back to the GEOMAR. The original protocol sent to all participants along with the sampling gear was as follows:

- Ziploc plastic bags with all necessary equipment (sterile): 15 ml falcon tubes, 50 ml syringes, 0.22 um filters (to retain particles and bacteria), and parafilm to seal the tubes, avoiding leaking or sample contamination.
- Participants identified each tube with a code that was then linked to a spreadsheet with the available meta-data. CTD or probe sensor details were also provided.
- To obtain a sample, participants got a volume of water onboard with a bucket or from a Niskin bottle, and attached to a syringe a 0.22 um sterilized filter (different one used at each station). Then, the water was poured in the syringe, and gently filtered. A few millilitres were discarded and between 12 and 14 ml were poured in the falcon tube, which was closed tightly and the cap was sealed with parafilm.
- Samples were stored at 4°C until they were sent to the GEOMAR.

3) *Database*: We constructed a comprehensive spreadsheet to keep track of research cruises, contact person, dates, modifications, meta-data, and the incoming samples (Table 7.6). Analytic results of the seawater samples are kept separately.

4) *Samples storage*: Samples were kept in the fridge onboard at 4°C, and then sent in "cooled" ice packs to the GEOMAR, and stored at 4°C until analysis.

5) *Sample analysis*: Seawater composition analyses are only finished for two cruises (*see* Table 7.6). We are still in the process to measure the rest of the samples at two locations: a) Canada, with a Varian/Agilent 735 ICP-OES at "Activation Laboratories Ltd" (http://www.actlabs.com/); b) Tasmania, using a new chelation chromatography method (Nesterenko and Jones 2007) being developed at the Institute for Marine and Antarctic Studies (UTAS) by the analytical chemistry department (http://www.imas.utas.edu.au/). We will have two datasets from the same samples to compare both the ICP-OES and the chelation chromatography method.

Table 7.6. Database to organize project coordination, cruises, and data entry.

Cruise n°	Year	Cruise status [a]	Meta-data [b]	Seawater data [c]	Ocean	Location	Geographical data	PI - name	Survey type
1	2009	Finished	Ready	Ready	North Atlantic	Porcupine Abyssal Plain	49.02°N / 15.17°W	Nadia Suarez-Bosche	4) Permanent station
2	2009	Finished	Ready	Ready	North Atlantic	English Channel	50.28°N / 4.14°S	Sonia Blanco-Ameijeiras	3) Local transect
3	2010	Finished	Ready	Not ready	North Atlantic	Porcupine Abyssal Plain	49°N / 16.45°W	Debora Iglesias-Rodriguez	4) Permanent station
4	2011	Finished	Ready	Not ready	North Atlantic	Spain	43°N-43°N/7°W-5°W	Mario Lebrato	2) Regional transect
5	2011	Finished	Ready	Not ready	North Pacific	North American coast	48°N-32°N 127°W-118°W	Richard Feely Dana Greely	1) Meridional transect
6	2011	Finished	Ready	Not ready	South Pacific	Otago Harbour	45.82°S / 170.64°W	Miles Lamare	
7	2011	Finished	Ready	Not ready	South Pacific	Doubtful Sound, Fiordland	45.34°S / 167.04°W	Miles Lamare	
8	2011	Finished	Ready	Not ready	South Pacific	Stewart Island	46.90°S / 168.12°W	Miles Lamare	3) Local transect
9	2011	Finished	Ready	Not ready	South Pacific	Coastal Otago	45.77°S / 170.72°W	Miles Lamare	
10	2011	In preparation	Ready	Not ready	Southern Ocean	Antarctica	-	Miles Lamare	
11	2011	Finished	Not ready	Not ready	South Pacific	Tasman Sea	-	Marius Müller	
12	2012	In preparation	Not ready	Not ready	Indian Ocean	Durban-Australia	-		1) Meridional transect
13	2012	In preparation	Not ready	Not ready	Antarctica	Antarctica	34.82°S-65.41°S 115°E-112.94°E	Karen Westwodd	
14	2011	Pending	Not ready	Not ready	Tropical Atlantic	BATS (Bermuda)	31.40°N / 64.10°W	Rod Johnson	4) Permanent station
15	2011	Pending	Not ready	Not ready	Tropical Atlantic	Hydrostation S (Bermuda)	32.10°N / 64.30°W	Rod Johnson	
16	2011	Finished	Not ready	Not ready	South Indian	Richards Bay - Inhaca Island	-	Dylan Banwell	
17	2011	Finished	Not ready	Not ready	South Indian	Richards Bay	28°S / 32°W	Dylan Banwell	
18	2011	Finished	Not ready	Not ready	South Indian	Inhaca	26°S / 32°W	Dylan Banwell	3) Local transect
19	2011	Finished	Not ready	Not ready	South Indian	Cape Vidal	28°S / 32°W	Dylan Banwell	
20	2011	Finished	Not ready	Not ready	South Indian	Mission Rocks	28°S / 32°W	Dylan Banwell	
21	2011	Finished	Not ready	Not ready	South Indian	Margate	30°S / 30°W	Dylan Banwell	

22	2011	Finished	Ready	Not ready	South Pacific	Peru (OMZ)	12°S / 77.4°W	Aurelien Paulmier	2) Regional transect
23	2011	In preparation	Not ready	Not ready	South Pacific	Mexico (OMZ)	-	Aurelien Paulmier	
24	2011	Finished	Ready	Not ready	East Atlantic	Charleston Bump	31.05°N -32.05°N 79.37°W-82.01°W	Laura Birsa Christy Pavel	3) Local transect
25	2011	Finished	Ready	Not ready	East Atlantic	Savannah River	32.02°N / 80.55°W		
26	2011	Finished	Ready	Not ready	Mediterranean Sea	offshore Ebro Delta	40.93°N / 1.86°E	Joan Cartes	2) Regional transect
27	2011	Finished	Ready	Not ready	Atlantic Ocean	Terceira Island (Azores)	38.45°N / 27.23°W	Joana Barcelos Ramos	4) Permanent station
28	2011	Finished	Not ready	Not ready		-	-	Tiberius Csernok	2) Regional transect
29	2011	Finished	Ready	Not ready	North Pacific	Saanicht Inlet (Vancouver)	48.59°N / 123.50°W	Chris Payne	1) Meridional transect
30	2011	Finished	Ready	Not ready	North Pacific	Vancouver - Papa Station	48.60°N-50°N 126°W-145°W		
31	2011	Pending	Not ready	Not ready	North Atlantic	UK-Porcupine Abyssal Plain	-	Henry Ruhl	1) Meridional transect
32	2011	Pending	Not ready	Not ready	South Atlantic	off Cape Town	40°S-45°S 4°W-17°E	Reinhard Werner	1) Meridional transect
33	2011	Finished	Not ready	Not ready	North Atlantic	Vigo-Brest	42.17°N-48.17°N 9.01°W-4.74°W	Sascha Flögel	1) Meridional transect
34	2011	Finished	Ready	Not ready	Iceland	Faxafloi Siglunes Langanes Stokksnes	64.20°N-68°N 12.67°W-27.97°W	Solveig Olafsdottir	2) Regional transect
35	2011	Finished	Ready	Not ready	Gulf of Mexico	Alabama	29.81°N-30.40°N 88.02°W-88.21°W	Kelly Robinson	3) Local transect
36	2011	Finished	Not ready	Not ready	Arctic Ocean	Beaufort Sea	-	Zachary Tait	2) Regional transect
37	2011	Finished	Not ready	Not ready	Arctic Ocean	Chuckchi sea	-	Marc Frischer	
38	2012	Pending	Not ready	Not ready	Arctic Ocean	Barents Sea	-		
39	2011	Finished	Not ready	Not ready	Baltic Sea	Kiel Bight	-	Mario Lebrato	3) Local transect
40	2011	Finished	Not ready	Not ready	Arctic	Canadian Archipelago	69°N-76.34°N 70.10°W-106.60°W	Liisa Jantunen	2) Regional transect
41	2011	Finished	Not ready	Not ready	Arctic	Resolute Bay, Nuvanut	-	Christopher Mundy	3) Local transect

42	2011	Finished	Not ready	Not ready	Arctic	Fram Strait	-	Mats Granskog	3) Local transect
43	2011	Finished	Ready	Not ready	Greenland Sea	Sermilik Fjord	65.70°N / 37.60°W	Alexander Korablev Sara de la Rosa	3) Local transect
44	2011	Finished	Not ready	Not ready	Arctic	Newfoundland to Cambridge Bay	-	Adrianne Ativy	3) Local transect
45	2011	Finished	Ready	Not ready	North Pole	Resolute Bay to North Pole	74.72°N-77.56°N 93.32°W-96.95°W	Richard Webster	3) Local transect
46	2011	Pending	Not ready	Not ready	Pacific sub Arctic	Kamchatka	-	Ezra Zubrow	3) Local transect
47	2011	Pending	Not ready	Not ready	sub Arctic	Chukchi Sea, Beaufort Sea	-	Russell Hopcroft	2) Regional transect
48	2011	Finished	Not ready	Not ready	Greenland Sea	Hochstetter	-	Olivier Gilg	3) Local transect
49	2011	Finished	Ready	Not ready	north Pacific	Prince William Sound	59.05°N-60.08°N 145.01°W-145.96°W	Laurel McFadden	3) Local transect
50	2011	Finished	Not ready	Not ready	Arctic	Svalvard	70°N-80°N 5°E-20°E	Jacek Beldowski	1) Meridional transect
51	2011	Finished	Not ready	Not ready	Norwegian Sea	Bodo	-	Morten Krogstad	3) Local transect
52	2011	Pending	Not ready	Not ready	Arctic	Nuuk to Svalbard	-	Frida Bengtsson (Greenpeace)	3) Local transect
53	2011	Finished	Not ready	Not ready	Canadian Archipelago	Newfoundland to Iqaluit	-	Janelle Kennedy	3) Local transect
54	2011	Finished	Not ready	Not ready	Bering Sea Chukchi Sea	-	-	Carin Ashjian	2) Regional transect
55	2011	Finished	Not ready	Not ready	Mediterranean Sea	Bay of Bizerte (north Tunisia)	-	Nejib Daly	3) Local transect
56	2011	Finished	Not ready	Not ready	Mediterranean Sea	Aegean Sea	-	Soultana Zervoudaki (Tanya)	3) Local transect
57	2012	Pending	Not ready	Not ready	North Pole	Ellesmere Island - North Pole	-	Bill Smethie	3) Local transect
58	2011	Pending	Not ready	Not ready	Mediterranean Sea	Villefranche	-	Tsuneo Tanaka	3) Local transect
59	2011	Finished	Ready	Not ready	Atlantic Mediterranean	Strait of Gibraltar Alboran Sea	35.79°N-36.67°N 5.25°W-6.97°W	Mario Lebrato	2) Regional transect

[a] Cruise status means if the research vessel has concluded the surveys ("Finished" = about to conclude, "In preparation" = to go to sea soon, and "Pending" = still in discussion with PI.

[b] Meta-data refers to complementary information about the seawater samples: date, latitude, longitude, temperature, salinity, CTD sensor. "Ready" indicates that meta-data are already in the database, and "not ready" that the PI has not sent them yet.

[c] Seawater data mean if elemental composition data are already available. In some cases there are ("Ready"), and in the majority are still missing ("Not ready").

8.

Coccolithophore carbonate ratios and elemental response to CO_2 and temperature

Abstract

Pelagic calcification is mainly driven by coccolithophores and foraminifera, producing $CaCO_3$ and exporting it to depth. Both groups are used following their elemental composition (mainly Mg^{2+} and Sr^{2+}) to develop paleo proxies, although coccolithophores are more problematic owing to their small size and issues in removing organic matter fractions associated with inorganic elements. In particular, processes around the magnesium element are poorly understood in modern ocean conditions or in the future ocean with rising CO_2 and temperature levels. Changes in elemental composition can ultimately alter fluxes and change dissolution dynamics. Following the development of a new organic-Mg cleaning protocol, we run three major experiments to understand elemental composition in coccolithophores: (1) Strain-specific response (physiology and elemental organic and inorganic composition) of 13 strains of *Emiliania huxleyi* to constant conditions to assess genetic-based variability. (2) The response of various coccolithophores to a CO_2 range to assess elemental composition in the future ocean. (3) The calibration of a temperature paleo proxy culturing *Gephyrocapsa oceanica* at 6 temperature levels. In brief, we found a strain-specific response that can complicate the interpretation of samples from sediment cores since strains cannot be separated at the species level. Seemingly, it is very problematic to clean *Emiliania huxleyi* from organic-Mg, thus we suggest that other species should be used to calibrate proxies or understand environmental vairability.

Coccolithophores increase the Mg/Ca and Sr/Ca with rising CO_2 levels, while contrasting trends appear under rising temperature. We suggest that this could change elemental fluxes in pelagic calcites in the future ocean, also increasing dissolution, and that the correct use of species such as *G. oceanica* can pave the way for new paleo proxies development.

This chapter is based on:

Blanco-Ameijeiras, S., **Lebrato, M** (shared 1st authorship with S.B.A)., Stoll, H. M., Iglesias-Rodriguez, M. D., Mendez-Vicente, A. and Oschlies, A. in preparation. Coccolithophores carbonate ratios within the concept of species. To be submitted: *ESA Ecology*.

Müller, N. M., **Lebrato, M** (shared 1st authorship with M. N. M)., Blanco-Ameijeiras, S., Stoll, H. M., Mendez-Vicente, A. Sett, S., Schulz, K. G. and Oschlies, A. in preparation. Coccolithophores carbonate ratios in a high CO_2 world. To be submitted: *Nature Geosciences*.

Blanco-Ameijeiras, S., **Lebrato, M** (shared 1st authorship with S. B. A)., Stoll, H. M., Mendez-Vicente, A. Schulz, K. G. and Oschlies, A. in preparation. Coccolithophores Sr/Ca and Mg/Ca temperature proxy optimization and development. To be submitted: *Geochemistry Geophysics Geosystems*.

Acknowledgements: We are grateful to Tanja Klüver for laboratory assistance, and Julie LaRoche and Ulf Riebesell for enabling the use of laboratory facilities at GEOMAR. This work was funded by the "European Project on Ocean Acidification" (EPOCA) under grant agreement n° 211384 for the PhD of ML and Abbey-Santander Internationalization Fund to SBA, and ERC-STG-240222PACE for funding HS and AMV.

8.1. Introduction

Pelagic calcification is mainly dominated by coccolithophores and foraminifera. Coccolithophores are distinguishable by the presence of a cell wall covered with elaborated platelets of calcite ($CaCO_3$) in the majority of the strains (there are also naked cells). *Emiliania huxleyi* typically lives in upper stratified semi-oligotrophic waters from cold temperate to tropical regions with relatively high incident irradiance (Paasche 2001). It is a cosmopolitan species occurring in all ocean basins with exception of polar waters and forms extensive seasonal blooms in subpolar regions during the summer months, covering up to several hundreds of square kilometres (Iglesias-Rodriguez et al. 2002). Although there are numerous extant coccolithophore species, *Emiliania huxleyi* has been a subject of interest in many ecological, oceanographic, and paleoceanographic studies. This is because it exports large amounts of particulate carbon that regulate the strength of the biological pump. Thus, coccolithophores are a key compartment in studies of the earth's climate system, biogeochemical cycles and the role of calcification (Gehlen et al. 2007; Ridgwell et al. 2009). Mass burial of coccolithophorid carbonates on seabed sediments throughout the Mesozoic-Cenozoic (Bown et al. 2004) produced an abundant fossil record. The present biogeography, organic/inorganic composition, and diversity, provide a valuable proxy for the reconstruction of past oceanographic and environmental conditions (Stoll et al. 2000, 2002).

Increasing atmospheric CO_2 concentrations are expected to impact pelagic ecosystem functioning and elemental cycling in the near future by intensifying ocean acidification (OA) and rising global average temperatures. OA describes the decrease in carbonate ions (CO_3^{2-}), increase in bicarbonate ions (HCO_3^-), and in dissolved inorganic carbon (DIC) (Caldeira and Wickett 2003). Predicted changes in ocean surface temperatures will further reduce the CO_2 uptake capacity by > 10 % by the end of the century. Impacts of increasing temperature in the ocean, range from changes in phytoplankton assemblages (Rost et al. 2003; Hare et al. 2007), to productivity (Rose and Caron 2007; Buitenhuis et al. 2008), and export production (Laws et al. 2000; Buesseler et al. 2007). Previous studies on coccolithophorid sensitivity to OA show variable results, with a genaral trend of decreasing calcification to increasing CO_2 (Riebesell et al. 2000; Zondervan et al. 2001, 2002; Delille et al. 2005; Engel et al. 2005; Langer et al. 2006) with some exceptions (Iglesias-Rodriguez et al. 2008a; Langer et al. 2009b; Shi et al. 2009). Few studies have assessed the response of coccolithophores to CO_2 and temperature (Feng et al.

2008; De Bodt et al. 2010). Despite this high interest in calcification, no study has addressed to date changes in elemental composition (namely Mg/Ca and Sr/Ca) of coccolithophore calcite (except for boron, B/Ca - Stoll et al. 2012) at high CO_2 (only for benthic organisms - Ries 2011) and a few in a temperature range (Stoll et al. 2001; Ra et al. 2010). Changes in the incorporation of these elements could potentially alter fluxes when calcite is exported, and in the case of Mg^{2+} it could change dissolution dynamics (Andersson et al. 2008).

These elements (Mg^{2+} and Sr^{2+}) are incorporated in the calcite during crystallization. The processes is controlled by the concentration of elements in the seawater from which the carbonate is produced (Ries 2010), and the partitioning of the element between seawater and carbonate which depends on thermodynamic, kinetic and biological conditions (Stoll and Schrag 2000; Stoll and Ziveri 2004). Coccolith Sr/Ca has been used as an indicator of coccolithophores productivity (Stoll et al. 2000) and can be used to reconstruct past variations in the organic to inorganic carbon ratio. Stoll et al. (2002) suggested that the Sr/Ca might be applied to correct growth rates effects on carbon isotope fractionation in coccolithophorid biomarkers, to improve estimations of past dissolved CO_2 concentrations in surface waters (Stoll et al. 2002). Other potential useful tool is the Mg/Ca ratio. It has been used as a paleothermomether in foraminifera because it is mainly affected by temperature (Barker et al. 2005). However, the efforts required to remove non-carbonate sources of Mg (organic) from coccolithophore calcite limits present applications (Stoll et al. 2001; Stoll and Ziveri 2004).

In this chapter, I put together physiological and geochemical results from experiments in modern and future ocean seawater conditions (high CO_2 and temperature) with applications in bigeochemical cycling and paleoceanography. We measured carbonate elemental ratios in coccolithophores following the development of a novel organic-Mg cleaning protocol described in Chapter 7, where contamination indicators were used to assess cleaning efficiency. I summarize datasets from three main experiments on coccolithophores:

(1) Strain- (*E. huxleyi*) and species-specific (other) physiological (growth rate and particulate matter) and calcite geochemical measurements (calcite Mg/Ca and Sr/Ca and other organic + inorganic ratios) in modern ocean carbonate chemistry at constant temperature.

(2) The physiological (growth rate and particulate matter) and geochemical (calcite Mg/Ca and Sr/Ca) response of *Gephyrocapsa ocenica* to 12 pCO_2 levels and 2 temperatures.

(3) The physiological (growth rate and particulate matter) and geochemical (calcite Mg/Ca and Sr/Ca) response of *Gephyrocapsa ocenica* to 6 temperature levels in modern ocean carbonate chemistry conditions.

8.2. Supplementary information: methods summary

8.2.1. Laboratory incubations: strain-specific

8.2.1.1. *Emiliania huxleyi* and *Calcidiscus leptoporus* cultures

We conducted several experiments with coccolithophores under constant environmental conditions to evaluate intraspecific variability in physiological and geochemical parameters minimizing medium variability. In this way we could be sure that genetic variability was reflected in the measurements. The incubations were conducted at the National Oceanography Center (Southampton, UK) as part of the master thesis of Blanco-Ameijeiras et al. (2010). Here, I summarize the physiological results only for context and I present the new geochemical data analyzed thereafter. Clonal cultures of thirteen strains of *Emiliania huxleyi* isolated at different latitudes in different ocean basins (*see* Table 8.1 for details) were grown under constant controlled medium chemistry, temperature, salinity, nutrient, and light conditions. We used nine coccolith-bearing and four naked strains, including representatives of three different morphotypes). Additionally, one strain of *Calcidiscus leptoporus* was included for comparison.

Growth medium was prepared from natural seawater (two different batches), with salinity 35, collected off Plymouth in the English Channel. Immediately after water collection, it was filtered with 47 mm filter paper glass microfiber MF 300 (Fisherbrand) to retain particles > 0.7 µm, and stored at 4 ºC in the dark. Seawater was filtered-sterilized with 0.22 µm with a vacuum filter unit Stericup sterile polyethersulfone (PES) membrane (Millopore) and enriched with nitrate and phosphate to a final concentration of 100 µM and 6.24 µM, respectively, following the modified f/25 medium (Guillard 1975), and with metals and vitamins according to f/2 medium (Guillard and Ryther 1962). Incubations were conducted in a growth chamber at 19 ºC with a 12:12 light:dark (LD) cycle. Illumination was provided by cool-white fluorescent lamps giving a photon flux density (400-700 nm) of ~ 124 ±6 µm quanta m^{-2} s^{-1} PAR (*see* Table 8.1). Experiments were carried out in diluted batch cultures. Each strain was grown in triplicates in 3

L of seawater medium in sterile 5 L conical Erlenmeyer flasks of borosilicate glass with a narrow neck covered by a layer of aluminium foil. Additionally, we set up a fourth flask as a blank, which contained medium with no cells growing. Flasks were inoculated from cultures in exponential growth, pre-adapted to experimental conditions for at least eight generations, and synchronized to the 12:12 LD cycle. Cells were always inoculated at low concentrations (~ 100 cell ml^{-1}) and harvested at ~ 28000 ±5000 cell ml^{-1} to prevent large changes in the medium carbonate chemistry. Sampling was conducted at the same time of the day within a 3 to 5 h interval after the light phase started. Cell density and medium parameters such as temperature, pH, salinity and irradiance were monitored daily removing 10 ml with a sterile pipette. For in situ pH and temperature we used a pH-meter with a temperature probe (EUTECH EcoScan - pH/mV/ºC). Salinity was measured with a portable salinity refractometer and Photosynthetically Active Radiation (PAR) was measured using a LI-COR (LI-189) Quantum Sensor (Q 39308) (*see* Table 8.1). Samples were collected for total alkalinity (TA) and dissolved inorganic carbon (DIC) (Table 8.2), Particulate organic Nitrogen (PON) and Particulate Organic Carbon (POC), Total Particulate Nitrogen (TPN) and Total Particulate Carbon (TPC), Particulate Inorganic Carbon (PIC) (to measure via ICP-AES), medium elemental composition (ICP-AES), and inorganic nutrients [nitrate (NO_3) and phosphate (PO_3^{4-})]. The remaining suspension was concentrated by centrifugation to produce calcite pellets

8.2.1.2. *Emiliania huxleyi* and *Calcidiscus leptoporus* sample analytics

For growth rates, cells were counted under a ZEIS Axioskop 40 light microscope with a x20 phase objective in a Neubauer haemocytometer (Table 8.3). Generally, counting was done 2 h after sampling. As a general rule, cell concentration were reported based on counts of a minimum of 100 cells per sample. In most cultures, the logarithmic phase started on day 3. At this point, cell concentration was at least 2000 cell ml^{-1}. Growth rates (μ) were calculated as: $\mu = (\ln c1 - \ln c0)/\Delta t$, where c0 and c1 are the cell concentrations at the beginning and at the end of the experiment, respectively, and Δt is the duration of the incubation in days.

For particulate matter (Table 8.3), two samples of 200 ml from each flask were filtered onto pre-combusted (500 ºC, 12 h) 25 mm filter paper glass microfibre MF 300 (Fisherbrand), saved in plastic Petri dishes and frozen at -20 ºC, for POC, PON, TPC and TPN analysis. Filters for POC and PON analyses were fumed over HCl for 48 h with sulphurous acid under vacuum and dried

Table 8.1. Species and strains details along with environmental parameters.

Study	Species	Strain	Strain synonims	Latitude	Longitude	Medium chemistry	Temp. (°C)	Salinity	NO_3^- (µM)	PO_4^{3-} (µM)	Light	Irradiance (µmol m^{-2} s^{-1})	Cell density (cell ml^{-1})
THIS STUDY - *E. huxleyi*													
This study	*E. huxleyi*	NZEH	CAWPO6, PLY M219	-46.96	168.08	NSW	18.45 ±0.12	35.27 ±0.12	95.50	3.94	12-12	120.94 ±4.36	33890 ±2009
This study	*E. huxleyi*	M181CCMP88E	CCMP 378	43.00	-68.00	NSW	19.44 ±0.11	35.69 ±0.21	92.00	3.79	12-12	125.86 ±6.94	29323 ±5218
This study	*E. huxleyi*	M184CCMP1A1	CCMP372	32.00	-62.00	NSW	19.49 ±0.20	36.33 ±0.08	89.50	3.26	12-12	124.50 ±5.56	24433 ±751
This study	*E. huxleyi*	B92/11	PLY B92/11A	46.96	5.28	NSW	18.51 ±0.09	36.47 ±0.12	93.50	4.09	12-12	119.86 ±1.99	28567 ±3557
This study	*E. huxleyi*	South Africa	N/A	-29.85	31.05	NSW	19.21 ±0.14	35.00 ±0.00	98.60	4.27	12-12	121.02 ±5.91	26080 ±1344
This study	*E. huxleyi*	CCMP2758	CCMP1742C, NEPCC55A	50.30	-145.58	NSW	19.39 ±0.11	35.00 ±0.00	97.85	4.19	12-12	127.29 ±6.99	26517 ±6952
This study	*E. huxleyi*	CCMP1280	N/A	-12.00	-35.00	NSW	18.88 ±0.11	34.94 ±0.05	94.55	4.05	12-12	120.12 ±3.75	22167 ±1465
This study	*E. huxleyi*	CCMP370	451B, F451	59.83	10.00	NSW	19.61 ±0.14	35.00 ±0.00	89.60	4.12	12-12	122.40 ±5.83	26667 ±3372
This study	*E. huxleyi*	CCMP2090	CCMP1516	-2.82	-83.01	NSW	19.48 ±0.18	34.92 ±0.07	90.05	4.12	12-12	118.78 ±4.85	25000 ±4015
This study	*E. huxleyi*	AC472	TQ26, RCC1216	-48.30	169.83	NSW	19.90 ±0.09	35.10 ±0.08	89.15	6.31	12-12	120.55 ±4.77	31557 ±2502
This study	*E. huxleyi*	AC474	TW1	41.10	3.38	NSW	19.60 ±0.01	35.13 ±0.13	91.10	4.71	12-12	117.08 ±5.94	25667 ±3538
This study	*E. huxleyi*	RCC1212	AC477, NS10Y	-34.46	17.30	NSW	19.69 ±0.03	35.04 ±0.06	90.10	1.75	12-12	134.99 ±1.63	22667 ±643
This study	*E. huxleyi*	RCC1258	AC441, PC101	40.58	-10.00	NSW	19.56 ±0.05	35.05 ±0.08	97.30	2.30	12-12	127.85 ±3.63	28333 ±1553
LITERATURE - *E. huxleyi*													
Langer et al. 2009b	*E. huxleyi*	RCC1238	EHJG	34.00	139.83	HCl and NaOH	20.00 ±0.00	32.00 ±0.00	100.00	6.25	16-8	400.00 ±0.00	-
Langer et al. 2009b	*E. huxleyi*	AC472	TQ26, RCC1216	-48.30	169.83	HCl and NaOH	17.00 ±0.00	32.00 ±0.00	100.00	6.25	16-8	400.00 ±0.00	-
Langer et al. 2009b	*E. huxleyi*	RCC1256	BP91	63.45	-20.23	HCl and NaOH	17.00 ±0.00	32.00 ±0.00	100.00	6.25	16-8	400.00 ±0.00	-
Langer et al. 2009b	*E. huxleyi*	RCC1212	AC477, NS10Y	-34.46	17.30	HCl and NaOH	20.00 ±0.00	32.00 ±0.00	100.00	6.25	16-8	400.00 ±0.00	-
Iglesias-Rodriguez et al. 2008	*E. huxleyi*	NZEH	CAWPO6, PLY M219	-46.96	168.08	Bubbling	19.00 ±0.50	34.00 ±0.00	100.00	6.24	12-12	150.00 ±0.00	-
Feng et al. 2008	*E. huxleyi*	CCMP371	12-1	32.00	-62.00	Bubbling	20.00 ±0.00	32.00 ±0.00	100.00	6.25	12-12	50.00 ±0.00	-
Feng et al. 2008	*E. huxleyi*	CCMP371	12-1	32.00	-62.00	Bubbling	20.00 ±0.00	32.00 ±0.00	100.00	6.25	12-12	400.00 ±0.00	-
Feng et al. 2008	*E. huxleyi*	CCMP371	12-1	32.00	-62.00	Bubbling	24.00 ±0.00	32.00 ±0.00	100.00	6.25	12-12	50.00 ±0.00	-
Feng et al. 2008	*E. huxleyi*	CCMP371	12-1	32.00	-62.00	Bubbling	24.00 ±0.00	32.00 ±0.00	100.00	6.25	12-12	400.00 ±0.00	-
Zondervan et al. 2002	*E. huxleyi*	B92/11	PLY B92/11A	60.26	5.40	HCl and NaOH	15.00 ±0.00	32.00 ±0.00	100.00	6.25	24-0	15.00 ±0.00	-
Zondervan et al. 2002	*E. huxleyi*	B92/11	PLY B92/11A	60.26	5.40	HCl and NaOH	15.00 ±0.00	32.00 ±0.00	100.00	6.25	16-8	30.00 ±0.00	-
Zondervan et al. 2002	*E. huxleyi*	B92/11	PLY B92/11A	60.26	5.40	HCl and NaOH	15.00 ±0.00	32.00 ±0.00	100.00	6.25	16-8	80.00 ±0.00	-
Zondervan et al. 2002	*E. huxleyi*	B92/11	PLY B92/11A	60.26	5.40	HCl and NaOH	15.00 ±0.00	32.00 ±0.00	100.00	6.25	24-0	150.00 ±0.00	-
Sciandra et al. 2003	*E. huxleyi*	AC474	TW1	41.10	3.38	Bubbling	17.00 ±0.10	38.20 ±0.00	14.75	5.00	14-1	575.00 ±0.00	-
Fiorini et al. 2011	*E. huxleyi*	AC472	TQ26, RCC1216	-48.30	169.83	Bubbling	19.00 ±0.00	33.00 ±0.00	160.00	10.00	12-12	160.00 ±0.00	-

Gao et al. 2009	*E. huxleyi*	CS369	n/a	-42.98	-147.55	Bubbling	18.00 ±0.00	31.00 ±0.00	-	-	14-1	425.00 ±0.00	-
Shi et al. 2009	*E. huxleyi*	CCMP374	89E, CCMP1949	42.50	-69.00	Bubbling +acid/base	20.00 ±0.00	35.00 ±0.00	100.00	6.00	n/a	150.00 ±0.00	-
Shi et al. 2009	*E. huxleyi*	NZEH	CAWPO6, PLY M219	-46.96	168.08	Bubbling +acid/base	20.00 ±0.00	35.00 ±0.00	100.00	6.00	n/a	150.00 ±0.00	-
de Bodt et al. 2010	*E. huxleyi*	AC481	n/a	49.20	-1.08	Bubbling	18.00 ±0.00	35.60 ±0.00	32.00	1.00	14-1	150.00 ±0.00	-
Bergen 2003 (0-8 days)	*E. huxleyi*	Norwegian mix	n/a	60.30	5.20	Bubbling	10.01 ±0.38	31.15 ±0.04	8.60	0.38	n/a	716.73 ±0.00	-
Bergen 2003 (8-16 days)	*E. huxleyi*	Norwegian mix	n/a	60.30	5.20	Bubbling	11.98 ±0.70	31.04 ±0.12	8.60	0.38	n/a	1007.41 ±0.00	-
Bergen 2003 (16-23 days)	*E. huxleyi*	Norwegian mix	n/a	60.30	5.20	Bubbling	12.74 ±0.87	30.85 ±0.13	8.60	0.38	n/a	1094.74 ±0.00	-
THIS STUDY + LITERATURE - Other coccolithophore species													
This study	*C. leptoporus*	RCC1169	VF27	43.68	169.83	NSW	20.09 ±0.10	35.03 ±0.14	86.10	0.66	12-12	134.59 ±3.98	-
Langer et al. 2006	*C. quadriperforatus*	AC365	RCC1135, NS6-1	-36.40	16.46	HCl and NaOH	20.00 ±0.00	- -	100.00	6.25	16-8	350.00 ±0.00	-
Fiorini et al. 2011	*C. leptoporus*	AC370	RCC1130, NS10-2	-34.28	17.18	Bubbling	19.00 ±0.00	33.00 ±0.00	160.00	10.00	12-12	160.00 ±0.00	-
Sett et al. in preparation	*G. oceanica*	RCC1303	AC300	45.00	-1.20	ASW	15.00 ±0.00	35.00 ±0.00	59.41	3.31	16-8	150.00 ±0.00	-
Sett et al. in preparation	*G. oceanica*	RCC1303	AC300	45.00	-1.20	ASW	20.00 ±0.00	35.00 ±0.00	58.80	6.28	16-8	150.00 ±0.00	-
Sett et al. in preparation	*G. oceanica*	RCC1303	AC300	45.00	-1.20	ASW	25.00 ±0.00	35.00 ±0.00	60.42	3.65	16-8	150.00 ±0.00	-
Zondervan et al. 2001	*G. oceanica*	PC7-1	AC296, RCC1304	38.12	-9.38	HCl and NaOH	15.00 ±0.00	32.00 ±0.00	100.00	6.25	16-8	150.00 ±0.00	-
Rickaby et al. 2010	*G. oceanica*	PZ3-1	AC645, RCC1300	26.23	-110.00	NSW	18.00 ±0.00	-	100.00	6.25	16-8	200.00 ±0.00	-
Langer et al. 2006	*C. braarudii*	AC400	N476-2, RCC1200	-20	12	HCl and NaOH	17.00 ±0.00	-	100.00	6.25	16-8	350.00 ±0.00	-
Rickaby et al. 2010	*C. braarudii*	N476-2	AC400, RCC1200	-20	12	NSW	18.00 ±0.00	-	100.00	6.25	16-8	200.00 ±0.00	-
Krug et al. 2011	*C. braarudii*	RCC1200	N476-2, AC400	-20	12	ASW	17.00 ±0.00	34.00 ±0.00	80.00	5.00	16-8	130.00 ±0.00	-

Table 8.2. Species and strains medium carbonate chemistry and seawater elemental composition.

Species	Strain	TA (µmol kg^{-1})	DIC (µmol kg^{-1})	pH_{total}	pCO_2 (µatm)	HCO_3^- (µmol kg^{-1})	CO_3^{2-} (µmol kg^{-1})	ΩCal.	Mg/Ca_{SW} (mol/mol)	Sr/Ca_{SW} (mmol/mol)
THIS STUDY - *E. huxleyi*										
E. huxleyi	NZEH	2251.3 ±14.88	2051.99 ±9.84	7.95 ±0.01	499.92 ±9.82	1889.88 ±7.01	145.27 ±3.70	3.46 ±0.09	5.52 ±0.01	7.65 ±0.07
E. huxleyi	M181CCMP88E	2279.01 ±29.50	2065.46 ±13.03	7.95 ±0.01	497.55 ±41.73	1894.24 ±9.16	154.95 ±12.47	3.68 ±0.30	5.58 ±0.05	7.71 ±0.13
E. huxleyi	M184CCMP1A1	2266.52 ±2.24	2061.59 ±9.40	7.93 ±0.02	525.14 ±32.73	1895.64 ±14.20	148.87 ±5.89	3.52 ±0.14	5.61 ±0.13	7.73 ±0.03
E. huxleyi	B92/11	2283.04 ±24.36	2065.16 ±3.75	7.96 ±0.04	479.40 ±42.87	1892.27 ±8.35	156.86 ±13.38	3.70 ±0.31	5.58 ±0.07	7.68 ±0.32
E. huxleyi	South Africa	2266.49 ±0.64	2060.16 ±13.71	7.95 ±0.03	498.72 ±37.67	1893.19 ±21.00	150.50 ±8.61	3.59 ±0.21	5.59 ±0.09	7.84 ±0.09
E. huxleyi	CCMP2758	2288.60 ±4.36	2048.95 ±4.10	8.01 ±0.01	425.08 ±12.37	1863.12 ±7.59	171.85 ±4.41	4.10 ±0.11	-	-
E. huxleyi	CCMP1280	2286.66 ±2.87	2045.05 ±28.58	8.02 ±0.05	414.52 ±60.58	1858.26 ±43.06	172.97 ±16.57	4.13 ±0.40	-	-
E. huxleyi	CCMP370	2284.27 ±4.00	2037.34 ±3.01	8.02 ±0.05	413.50 ±2.77	1847.96 ±3.58	175.80 ±0.70	4.20 ±0.02	-	-
E. huxleyi	CCMP2090	2295.35 ±3.16	2081.97 ±12.78	8.03 ±0.00	493.93 ±33.27	1909.85 ±19.13	155.91 ±7.61	3.73 ±0.18	-	-
E. huxleyi	AC472	2276.81 ±3.36	2055.38 ±12.94	7.96 ±0.02	475.52 ±23.63	1879.72 ±17.98	160.26 ±5.86	3.82 ±0.14	5.62 ±0.06	7.86 ±0.04
E. huxleyi	AC474	2280.74 ±3.73	2067.18 ±4.21	7.97 ±0.02	492.30 ±7.29	1895.71 ±4.97	155.40 ±1.65	3.71 ±0.04	5.62 ±0.02	7.81 ±0.10
E. huxleyi	RCC1212	2235.51 ±4.00	2037.75 ±9.84	7.96 ±0.01	520.56 ±28.78	1876.34 ±14.32	144.45 ±5.72	3.45 ±0.14	5.59 ±0.07	8.03 ±0.06
E. huxleyi	RCC1258	2246.86 ±29.34	2042.05 ±27.66	7.93 ±0.02	501.44 ±14.60	1876.64 ±25.80	149.01 ±3.30	3.56 ±0.08	5.57 ±0.01	7.74 ±0.14
LITERATURE - *E. huxleyi*										
E. huxleyi	RCC1238	2243.01 ±83.44	2044.50 ±7.78	7.95 ±0.16	534.04 ±199.89	1882.50 ±34.65	144.50 ±48.79	3.55 ±1.20	-	-
E. huxleyi	AC472	2229.01 ±73.54	2063.50 ±4.95	7.92 ±0.16	573.02 ±216.30	1919.50 ±30.41	123.00 ±42.43	3.00 ±0.99	-	-
E. huxleyi	RCC1256	2188.01 ±73.54	2007.50 ±20.51	7.96 ±0.12	493.00 ±132.94	1859.00 ±8.49	130.50 ±34.65	3.20 ±0.85	-	-
E. huxleyi	RCC1212	2313.01 ±0.00	2066.00 ±0.00	8.05 ±0.00	407.00 ±0.00	1877.00 ±0.00	176.00 ±0.00	4.30 ±0.00	-	-
E. huxleyi	NZEH	2192.12 ±33.52	1975.33 ±6.10	7.97 ±0.07	469.28 ±88.30	1799.24 ±29.01	160.37 ±25.90	3.85 ±0.62	-	-
E. huxleyi	CCMP371	1892.40 ±0.00	1701.64 ±0.00	8.00 ±0.00	375.00 ±0.00	1557.59 ±0.00	131.73 ±0.00	3.22 ±0.00	-	-
E. huxleyi	CCMP371	1892.40 ±0.00	1701.64 ±0.00	8.00 ±0.00	375.00 ±0.00	1557.59 ±0.00	131.73 ±0.00	3.22 ±0.00	-	-
E. huxleyi	CCMP371	1901.55 ±0.00	1684.18 ±0.00	8.00 ±0.00	375.00 ±0.00	1523.92 ±0.00	149.21 ±0.00	3.67 ±0.00	-	-
E. huxleyi	CCMP371	1901.55 ±0.00	1684.18 ±0.00	8.00 ±0.00	375.00 ±0.00	1523.92 ±0.00	149.21 ±0.00	3.67 ±0.00	-	-
E. huxleyi	B92/11	2268.10 ±50.75	2120.56 ±6.05	7.92 ±0.00	419.99 ±86.72	1909.84 ±22.43	145.79 ±30.35	3.54 ±0.73	-	-
E. huxleyi	B92/11	2157.51 ±61.33	2052.63 ±40.65	7.81 ±0.00	508.58 ±103.32	1870.06 ±36.25	115.82 ±22.21	2.81 ±0.53	-	-
E. huxleyi	B92/11	2174.31 ±62.78	2057.65 ±55.32	7.85 ±0.00	483.57 ±123.77	1868.17 ±61.49	123.53 ±27.75	3.00 ±0.67	-	-
E. huxleyi	B92/11	2216.03 ±59.71	2082.41 ±23.36	7.89 ±0.00	442.10 ±86.77	1882.25 ±20.89	135.23 ±28.29	3.28 ±0.68	-	-
E. huxleyi	AC474	2506.01 ±17.00	2224.00 ±18.22	8.07 ±0.02	404.40 ±16.53	2008.31 ±20.01	202.10 ±5.59	4.71 ±0.13	-	-
E. huxleyi	AC472	2231.01 ±0.00	1984.00 ±0.00	8.04 ±0.00	403.00 ±0.00	1790.00 ±0.00	181.00 ±0.00	4.41 ±0.00	-	-

E. huxleyi	CS369	2118.31 ±0.00	1883.80 ±0.00	8.11 ±0.00	319.00 ±0.00	1738.00 ±0.00	176.00 ±0.00	4.32 ±0.00	-	-
E. huxleyi	CCMP374	2260.01 ±10.00	1980.00 ±50.00	8.08 ±0.02	345.19 ±0.00	1772.34 ±0.00	196.51 ±0.00	4.71 ±0.00	-	-
E. huxleyi	NZEH	2260.01 ±10.00	1980.00 ±50.00	8.08 ±0.02	345.19 ±0.00	1772.34 ±0.00	196.51 ±0.00	4.71 ±0.00	-	-
E. huxleyi	AC481	2057.11 ±17.11	1863.25 ±28.07	7.95 ±0.07	464.10 ±37.48	1863.25 ±28.07	139.80 ±5.94	3.31 ±0.14	-	-
E. huxleyi	Norwegian mix	2138.01 ±7.58	1989.84 ±10.63	8.02 ±0.00	397.99 ±9.00	1861.08 ±12.09	110.97 ±2.31	2.71 ±0.06	-	-
E. huxleyi	Norwegian mix	2085.01 ±61.63	1873.98 ±88.39	8.15 ±0.00	284.68 ±64.30	1713.37 ±102.19	148.71 ±18.97	3.63 ±0.47	-	-
E. huxleyi	Norwegian mix	1858.14 ±45.05	1649.39 ±32.47	8.17 ±0.00	232.31 ±17.71	1499.62 ±25.48	140.29 ±11.25	3.43 ±0.27	-	-
THIS STUDY + LITERATURE - Other coccolithophore species										
C. leptoporus	RCC1169	1563.33 ±18.71	1485.52 ±51.33	7.66 ±0.15	762.74 ±310.74	1400.71 ±57.07	60.26 ±16.29	1.44 ±0.39	5.59 ±0.07	8.03 ±0.06
C. quadriperforatus	AC365	2364.50 ±40.31	2115.50 ±0.71	8.20 ±0.10	411.00 ±93.34	1921.00 ±28.28	181.50 ±30.41	4.45 ±0.78	-	-
C. leptoporus	AC370	2221.00 ±0.00	1967.00 ±0.00	8.05 ±0.00	390.00 ±0.00	1774.86 ±0.00	180.48 ±0.00	4.38 ±0.00	-	-
G. oceanica	RCC1303	2291.27 ±41.97	2005.46 ±30.65	8.14 ±0.15	408.66 ±165.46	1791.89 ±125.82	201.45 ±49.78	4.80 ±1.19	-	-
G. oceanica	RCC1303	2289.25 ±76.74	2025.93 ±78.85	8.02 ±0.06	438.50 ±81.32	1822.52 ±61.00	189.55 ±24.03	4.53 ±0.57	-	-
G. oceanica	RCC1303	2279.00 ±68.76	2005.83 ±52.95	8.00 ±0.10	458.98 ±147.52	1757.81 ±111.04	212.66 ±42.38	5.11 ±1.02	-	-
G. oceanica	PC7-1	2084.14 ±38.75	1910.64 ±8.10	8.01 ±0.00	452.83 ±111.12	1767.92 ±30.79	126.25 ±29.26	3.06 ±0.00	-	-
G. oceanica	PZ3-1	2268.60 ±10.61	2074.94 ±0.52	7.98 ±0.02	474.35 ±27.08	1923.63 ±17.93	147.40 ±6.75	3.59 ±0.16	-	-
C. braarudii	AC400	2234.00 ±0.00	1994.00 ±0.00	8.22 ±0.00	345.00 ±0.00	1813.00 ±0.00	169.00 ±0.00	4.10 ±0.00	-	-
C. braarudii	N476-2	2246.37 ±8.90	2070.49 ±0.09	7.95 ±0.02	518.45 ±24.48	1938.73 ±4.71	136.25 ±5.54	3.32 ±0.14	-	-
C. braarudii	RCC1200	2242.33 ±5.86	2056.00 ±7.21	7.94 ±0.02	524.00 ±27.07	1898.60 ±11.01	138.96 ±5.52	3.33 ±0.12	-	-

Table 8.3. Species and strains physiological and biochemical measurements.

Species	Strain	GR (day^{-1})	SIZE (μm^3 $cell^{-1}$)		CELL QUOTA (pg C $cell^{-1}$)					CELL PRODUCTION (pg C $cell^{-1}$ day^{-1})					CELL RATIOS (mol/mol)	
			Coccosphere	Protoplasm	TPC	PIC	POC	TPN	PON	TPC	PIC	POC	TPN	PON	PIC/POC	C/N
THIS STUDY - *E. huxleyi*																
E. huxleyi	NZEH	1.45 ±0.01	53.10 ±1.97	50.88 ±0.00	10.50 ±0.78	2.42 ±1.81	8.07 ±1.05	1.32 ±0.32	1.36 ±0.06	15.30 ±1.29	5.061 ±0.61	11.75 ±1.42	1.92 ±0.45	1.98 ±0.07	0.43 ±0.05	6.90 ±0.55
E. huxleyi	M181CCMP88E	1.13 ±0.03	46.77 ±6.26	43.86 ±2.22	12.21 ±2.68	4.09 ±2.23	8.12 ±1.03	1.35 ±0.19	1.27 ±0.21	13.80 ±2.70	4.61 ±2.42	9.19 ±0.94	1.53 ±0.19	1.44 ±0.20	0.50 ±0.25	7.46 ±0.63
E. huxleyi	M184CCMP1A1	0.78 ±0.01	46.18 ±3.58	37.78 ±0.93	7.85 ±2.16	0.59 ±0.64	7.25 ±1.54	0.85 ±0.15	1.16 ±0.14	6.16 ±1.68	0.69 ±0.45	5.69 ±1.19	0.66 ±0.12	0.91 ±0.10	0.12 ±0.05	7.25 ±0.87
E. huxleyi	B92/11	1.12 ±0.03	46.82 ±0.00	34.12 ±0.00	12.36 ±2.21	2.38 ±0.43	9.97 ±1.78	1.27 ±0.26	1.25 ±0.19	13.93 ±2.16	2.69 ±0.42	11.24 ±1.73	1.43 ±0.26	1.41 ±0.18	0.23 ±0.01	9.26 ±0.64
E. huxleyi	South Africa	0.79 ±0.01	50.08 ±4.93	47.30 ±0.00	7.56 ±1.52	3.00 ±1.69	4.56 ±0.28	0.70 ±0.06	0.73 ±0.03	6.02 ±1.26	2.39 ±1.37	3.62 ±0.22	0.56 ±0.04	0.58 ±0.01	0.66 ±0.40	7.22 ±0.67
E. huxleyi	CCMP2758	0.61 ±0.03	75.27 ±14.86	57.48 ±0.45	9.97 ±0.00	-	11.13 ±0.78	1.57 ±0.24	1.46 ±0.20	5.97 ±0.00	-	6.86 ±0.20	0.96 ±0.11	0.89 ±0.09	-	8.95 ±0.64
E. huxleyi	CCMP1280	0.53 ±0.01	59.35 ±1.53	85.28 ±0.00	15.64 ±1.45	-	13.94 ±2.10	1.59 ±0.32	1.50 ±0.14	8.44 ±0.69	-	7.52 ±1.05	0.85 ±0.16	0.81 ±0.06	-	10.76 ±0.84
E. huxleyi	CCMP370	0.93 ±0.02	48.23 ±6.55	45.23 ±2.63	11.52 ±1.02	-	15.38 ±2.12	1.56 ±0.09	1.73 ±0.15	10.70 ±0.80	-	14.27 ±1.61	1.45 ±0.07	1.61 ±0.10	-	10.29 ±0.62
E. huxleyi	CCMP2090	0.78 ±0.02	45.31 ±2.40	37.27 ±0.00	7.18 ±2.46	-	7.66 ±0.41	0.96 ±0.22	1.06 ±0.15	5.64 ±1.86	-	6.02 ±0.17	0.75 ±0.17	0.83 ±0.09	-	8.50 ±0.89
E. huxleyi	AC472	0.95 ±0.01	67.34 ±4.71	52.48 ±0.00	14.11 ±3.66	2.42 ±1.89	11.69 ±1.95	1.37 ±0.31	1.28 ±0.18	13.52 ±3.45	2.31 ±1.78	11.21 ±1.88	1.32 ±0.30	1.23 ±0.16	0.20 ±0.14	10.60 ±0.38
E. huxleyi	AC474	0.79 ±0.02	48.81 ±6.48	43.20 ±0.00	10.27 ±1.46	4.06 ±1.99	6.20 ±0.69	0.83 ±0.12	0.62 ±0.21	8.12 ±1.09	3.20 ±1.52	4.92 ±0.66	0.66 ±0.10	0.49 ±0.18	0.65 ±0.40	12.09 ±0.11
E. huxleyi	RCC1212	0.67 ±0.01	121.45 ±25.82	92.17 ±12.47	35.53 ±0.58	12.49 ±1.22	23.04 ±1.80	2.55 ±0.13	2.42 ±0.23	24.09 ±0.44	8.46 ±0.81	15.62 ±1.25	1.72 ±0.09	1.64 ±0.15	0.54 ±0.10	11.08 ±0.44
E. huxleyi	RCC1258	0.70 ±0.01	89.90 ±5.12	74.82 ±8.09	24.88 ±1.21	11.91 ±0.40	12.63 ±0.82	1.41 ±0.17	1.30 ±0.23	17.53 ±0.61	8.39 ±0.16	8.91 ±0.50	0.99 ±0.10	0.92 ±0.15	0.94 ±0.02	11.39 ±1.17
LITERATURE - *E. huxleyi*																
E. huxleyi	RCC1238	1.65 ±0.02	-	-	-	7.99 ±0.41	10.99 ±0.82	-	-	-	13.23 ±0.48	18.21 ±1.66	-	-	0.72 ±0.09	-
E. huxleyi	AC472	1.12 ±0.02	-	-	-	10.33 ±0.48	11.90 ±0.60	-	-	-	11.56 ±0.69	13.30 ±0.51	-	-	0.86 ±0.08	-
E. huxleyi	RCC1256	1.21 ±0.09	-	-	-	11.49 ±0.81	14.95 ±2.28	-	-	-	14.15 ±0.28	17.94 ±1.29	-	-	0.78 ±0.06	-
E. huxleyi	RCC1212	0.98 ±0.01	-	-	-	9.35 ±0.51	11.41 ±1.12	-	-	-	9.18 ±0.55	11.21 ±1.14	-	-	0.81 ±0.04	-
E. huxleyi	NZEH	0.61 ±0.13	55.43 ±9.59	-	-	-	11.34 ±5.81	-	-	-	-	6.79 ±3.30	-	-	-	7.29 ±0.41
E. huxleyi	CCMP371	0.38 ±0.02	-	-	-	4.51 ±1.90	8.30 ±2.10	-	-	-	1.71 ±0.72	3.15 ±0.79	-	-	0.54 ±0.06	6.69 ±0.21
E. huxleyi	CCMP371	0.58 ±0.04	-	-	-	2.20 ±0.20	7.80 ±2.00	-	-	-	1.27 ±0.11	4.524 ±1.16	-	-	0.28 ±0.09	6.11 ±0.82
E. huxleyi	CCMP371	0.605 ±0.01	-	-	-	3.80 ±0.40	6.15 ±0.200	-	-	-	2.29 ±0.24	3.72 ±0.12	-	-	0.61 ±0.08	6.86 ±0.21
E. huxleyi	CCMP371	0.62 ±0.01	-	-	-	2.50 ±1.60	8.08 ±0.16	-	-	-	1.55 ±0.99	5.00 ±0.09	-	-	0.30 ±0.10	5.83 ±0.68
E. huxleyi	B92/11	0.53 ±0.01	-	-	-	2.83 ±0.15	6.67 ±0.06	-	-	-	1.51 ±0.07	3.56 ±0.06	-	-	0.42 ±0.02	-
E. huxleyi	B92/11	0.77 ±0.06	-	-	-	5.10 ±0.73	8.33 ±1.50	-	-	-	3.95 ±0.77	6.45 ±1.43	-	-	0.61 ±0.06	-
E. huxleyi	B92/11	1.04 ±0.06	-	-	-	8.43 ±0.32	11.98 ±1.57	-	-	-	8.76 ±0.39	12.42 ±1.38	-	-	0.70 ±0.07	-
E. huxleyi	B92/11	1.10 ±0.06	-	-	-	7.97 ±0.42	10.43 ±1.79	-	-	-	8.74 ±0.69	11.40 ±1.78	-	-	0.76 ±0.11	-
E. huxleyi	AC474	-	-	-	-	-	-	-	-	-	2.31 ±0.12	2.62 ±0.12	-	-	0.88 ±0.01	-
E. huxleyi	AC472	0.92 ±0.01	65.43 ±0.00	-	-	9.00 ±0.20	16.00 ±0.40	-	3.00 ±0.10	-	8.00 ±0.30	15.00 ±0.60	-	2.76 ±0.09	0.53 ±0.21	7.10 ±0.20

E. huxleyi	CS369	0.90 ±0.00	248.41 ±0.00	-	-	-	-	-	-	-	4.56 ±0.00	-	-	-	-	-
E. huxleyi	CCMP374	1.34 ±0.01	-	-												
E. huxleyi	NZEH	1.35 ±0.00	-	-	-	5.76 ±0.24	7.08 ±0.48	-	-	-	7.80 ±0.24	9.72 ±0.24	-	-	0.80 ±0.03	8.60 ±0.00
E. huxleyi	AC481	0.13 ±0.02	61.58 ±0.00	-	-	-	-	-	-	-	1.20 ±0.00	1.62 ±0.42	-	-	0.74 ±0.16	-
E. huxleyi	Norwegian mix	-	-	-	-	-	-	-	-	-	-	-	-	-	0.31 ±0.23	-
E. huxleyi	Norwegian mix	-	-	-	-	-	-	-	-	-	-	-	-	-	0.31 ±0.58	-
E. huxleyi	Norwegian mix	-	-	-	-	-	-	-	-	-	-	-	-	-	0.52 ±0.84	-
THIS STUDY + LITERATURE - Other coccolithophore species																
C. leptoporus	RCC1169	0.37 ±0.01	-	-	717.06 ±219.54	530.18 ±219.30	205.75 ±2.44	31.77 ±5.93	16.23 ±1.34	267.81 ±74.83	197.67 ±76.44	77.21 ±1.09	11.89 ±1.91	6.08 ±0.35	2.56 ±1.03	12.72 ±0.86
C. quadriperforatus	AC365	0.63 ±0.01	1662.81 ±0.00	-	-	138.00 ±11.31	64.50 ±2.12	-	-	-	87.00 ±9.89	40.50 ±2.12	-	-	2.14 ±0.12	-
C. leptoporus	AC370	0.33 ±0.01	904.55 ±0.00	-	-	113.00 ±15.20	82.00 ±9.10	-	16.00 ±1.20	-	37.00 ±6.60	27.00 ±4.10	-	5.28 ±0.39	1.37 ±0.28	5.90 ±0.40
G. oceanica	RCC1303	0.61 ±0.04	-	-	36.85 ±1.60	22.87 ±1.25	13.98 ±1.45	-	-	22.73 ±2.12	14.14 ±1.77	8.59 ±0.80	-	-	1.64 ±0.23	6.56 ±0.52
G. oceanica	RCC1303	0.91 ±0.12	-	-	42.60 ±3.16	19.55 ±0.36	11.81 ±0.46	-	-	26.85 ±0.49	20.63 ±0.52	12.46 ±0.40	-	-	1.65 ±0.09	5.15 ±1.97
G. oceanica	RCC1303	1.11 ±0.01	-	-		35.69 ±9.92	18.80 ±5.81	-	-		39.64 ±10.55	20.87 ±6.21	-	-	1.89 ±0.08	
G. oceanica	PC7-1	-	-	-	-	24.92 ±4.69	34.25 ±3.08	-	-	-	19.11 ±2.78	26.50 ±3.30	-	-	0.72 ±0.16	-
G. oceanica	PZ3-1	0.90 ±0.05	87.09 ±0.00	-	70.92 ±22.66	26.96 ±8.90	43.96 ±13.98	4.31 ±1.25	3.83 ±0.95	63.53 ±17.87	24.15 ±7.06	39.39 ±11.02	3.86 ±0.97	3.44 ±0.72	0.61 ±0.05	11.32 ±0.84
C. braarudii	AC400	0.73 ±0.00	-	-	-	338.00 ±0.00	198.00 ±0.00	-	-	-	245.00 ±0.00	144.00 ±0.00	-	-	1.70 ±0.00	-
C. braarudii	N476-2	0.63 ±0.01	696.73 ±0.00	-	453.43 ±39.89	170.66 ±20.08	282.77 ±20.92	28.00 ±2.96	36.12 ±9.05	301.01 ±24.13	106.82 ±11.33	177.03 ±10.69	-	23.96 ±5.85	0.60 ±0.03	7.62 ±1.43
C. braarudii	RCC1200	0.70 ±0.10	3941.47 ±0.00	-	-	490.00 ±74.80	313.33 ±32.73	-	-	-	343.00 ±52.36	219.33 ±22.91	-	-	1.56 ±0.04	7.03 ±0.25

Table 8.4. Species and strains elemental composition and data used from the literature (organic + inorganic matter).

Study	Species	Strain	Culture condition [a]	ELEMENTAL RATIOS (organic + inorganic) (mmol/mol)													
				Ba/Ca	Cd/Ca	Co/Ca	Cr/Ca	Fe/Ca	K/Ca	Mg/Ca	Mn/Ca	Ni/Ca	P/Ca	S/Ca	Sr/Ca	Zn/Ca	Mo/Ca	Cu/Ca
THIS STUDY - *E. huxleyi*																	
This study	*E. huxleyi*	NZEH	2	0.029	0.000	0.006	0.962	359.082	4.316	45.360	0.406	0.019	107.376	4.413	3.535	0.340	-	0.032
This study	*E. huxleyi*	M181CCMP88E	2	0.039	-0.002	0.008	1.702	593.508	4.751	81.773	0.714	0.050	172.436	5.169	4.036	0.577	-	0.103
This study	*E. huxleyi*	M184CCMP1A1	2	0.083	0.003	0.078	3.507	637.417	6.461	83.020	0.976	0.067	318.657	103.488	3.695	10.055	-	0.087
This study	*E. huxleyi*	B92/11	2	0.034	-0.002	0.007	1.657	512.257	6.710	64.982	0.464	0.035	161.885	7.001	3.914	0.599	-	0.052
This study	*E. huxleyi*	South Africa	2	0.039	0.000	0.012	5.040	561.763	9.580	68.813	0.570	0.102	150.766	6.740	3.729	1.042	-	0.072
This study	*E. huxleyi*	CCMP2758	2	0.376	0.001	0.078	43.991	6395.606	81.917	1114.730	5.755	1.190	1955.321	44.512	14.713	8.625	-	2.001
This study	*E. huxleyi*	CCMP1280	2	0.546	-0.004	0.081	66.963	5827.392	358.871	1731.584	6.716	1.340	1916.152	106.442	13.515	8.826	-	1.430
This study	*E. huxleyi*	CCMP370	2	0.447	-0.002	0.153	68.734	7653.964	121.996	889.707	7.543	1.701	2385.433	44.224	15.189	8.482	-	2.026
This study	*E. huxleyi*	CCMP2090	2	0.608	-0.019	0.084	53.103	7389.678	179.006	1120.967	6.436	0.970	2338.426	55.480	15.541	23.614	-	0.659
This study	*E. huxleyi*	AC472	2	0.045	0.000	0.012	6.522	478.979	12.624	69.817	0.464	0.113	179.188	6.008	4.005	0.578	-	0.123
This study	*E. huxleyi*	AC474	2	0.046	-0.001	0.014	7.785	537.025	13.417	72.316	0.558	0.145	178.803	6.538	3.668	0.597	-	0.217
This study	*E. huxleyi*	RCC1212	2	0.054	0.001	0.010	2.760	270.457	10.777	28.747	0.475	0.053	66.388	7.603	3.473	0.701	-	0.138
This study	*E. huxleyi*	RCC1258	2	0.033	0.001	0.008	3.729	299.906	8.864	27.519	0.434	0.077	69.538	4.552	3.375	0.358	-	0.069
THIS STUDY + LITERATURE - Coccolithophores																	
This study	*C. leptoporus*	RCC1169	2	0.004	0.000	0.001	0.238	25.418	1.106	4.217	0.098	0.005	6.843	3.193	3.273	0.032	-	0.008
Ho et al. 2003	*G. oceanica*	-	1	-	0.003	0.003	-	0.031	0.007	0.001	0.056	-	0.008	0.008	2.189	0.003	0.000	0.001
Ho et al. 2003	*E. huxleyi*	-	1	-	0.002	0.002	-	0.025	0.006	0.001	0.050	-	0.007	0.005	2.366	0.003	0.000	0.000
LITERATURE - Natural plankton assemblage																	
Martin and Knauer 1973	Coastal upwelling water	-	-	-	0.105	-	-	11.385	2.308	4.308	0.600	-	-	-	9.846	1.323	-	0.277
Martin et al. 1976	Oligotrophic open ocean water	-	-	-	0.294	-	-	2.000	0.506	0.778	0.200	-	-	-	137.222	1.033	-	0.211
Collier and Edmond 1984	Oligotrophic open ocean water	-	-	-	0.106	-	-	0.902	-	-	15.000	-	-	-	-	0.594	-	0.102
Kuss and Kremling 1999	Oligotrophic open ocean water	-	-	-	0.094	0.035	-	0.852	-	-	0.296	-	-	-	-	0.352	-	0.069
Ho et al. 2003	All phytoplankton species	-	1	-	0.404	0.731	-	14.423	3.269	1.077	7.308	-	-	-	9.615	1.538	0.058	0.731
LITERATURE - Green algae																	
Ho et al. 2003	*Dunaliella tertiolecta*	-	1	-	5.263	0.526	-	594.737	18.947	19.474	100.000	-	52.632	14.737	4.263	78.421	0.579	35.263
Ho et al. 2003	*Pyramimonas parkeae*	-	1	-	0.385	0.142	-	9.112	0.503	-	4.556	-	0.592	0.852	7.101	0.870	0.021	0.367
Ho et al. 2003	*Nannochloris atomus*	-	1	-	0.250	2.893	-	485.714	34.643	8.571	42.857	-	35.714	12.857	1.643	60.357	0.321	8.214
Ho et al. 2003	*Pycnococcus provasoli*	-	1	-	0.527	1.636	-	229.091	0.045	4.909	38.182	-	18.182	19.455	2.000	16.727	0.309	9.636
Ho et al. 2003	*Tetraselmis sp.*	-	1	-	0.174	0.130	-	4.535	0.585	0.267	4.651	-	1.163	1.547	29.070	0.512	0.033	0.593

LITERATURE - Red dinoflagelates																	
Ho et al. 2003	*Prorocentrum mimimum*	-	1	-	0.316	1.211	-	17.895	3.395	2.605	16.053	-	2.632	5.737	7.632	2.342	0.066	0.737
Ho et al. 2003	*Amphidinium carterae*	-	1	-	2.704	1.296	-	49.259	0.556	2.111	18.889	-	3.704	4.963	4.444	4.667	0.407	2.000
Ho et al. 2003	*Thoracosphaera heimii*	-	1	-	0.002	0.002	-	0.040	44.554	0.011	0.029	-	0.022	0.029	1.756	0.002	0.001	0.001
LITERATURE - Diatoms																		
Ho et al. 2003	*Ditylum brightwellii*	-	1	-	0.171	0.162	-	0.286	3.152	-	1.810	-	0.952	2.686	6.476	0.067	0.013	0.057
Ho et al. 2003	*Thalassiosira weissflogii*	-	1	-	0.165	0.270	-	4.250	13.250	-	13.250	-	2.500	3.350	5.500	1.875	0.500	0.425
Ho et al. 2003	*Nitzschia brevirostris*	-	1	-	0.070	0.207	-	11.481	9.000	2.222	8.519	-	3.704	4.259	4.815	1.000	0.052	0.667
Ho et al. 2003	*Thalassiosira eccentrica*	-	1	-	0.231	0.369	-	10.308	5.000	3.292	3.231	-	1.538	2.985	6.000	1.538	0.031	0.431

[a] We only used data from phytoplankton species collected or cultured at very similar conditions to ours for comparison. Condition 1: Temp. = 19 ±1 °C, Light = 12:12 h, Light intensity = 250 µmol m^{-2} s^{-1}. Condition 2: Temp = 19 ±1 °C, Light = 12:12 h, Light intensity = 120 µmol m^{-2} s^{-1}.

Table 8.5. Species and strains elemental composition and partitioning coefficients (only carbonate Mg/Ca and Sr/Ca). Also included contamination proxies (P/Ca and Fe/Ca).

Study	Species	Strain	ELEMENTAL RATIOS (carbonate) (mmol/mol)		PARTITIONING COEFFICIENT (carbonate)		ELEMENTAL RATIOS (contamination proxy) (mmol/mol)	
			Mg/Ca	Sr/Ca	D-Mg	D-Sr	P/Ca	Fe/Ca
THIS STUDY - *E. huxleyi*								
This study	*E. huxleyi*	NZEH	0.15 ±0.01	2.86 ±0.03	0.027 ±0.01	0.36 ±0.02	0.75 ±0.31	7.61 ±6.25
This study	*E. huxleyi*	M181CCMP88E	20.93 ±0.52	3.15 ±0.78	3.74 ±0.09	0.40 ±0.10	302.16 ±135.49	1090.90 ±120.46
This study	*E. huxleyi*	M184CCMP1A1	12.42 ±2.79	3.56 ±0.40	2.21 ±0.49	0.42 ±0.07	171.17 ±39.27	527.22 ±129.81
This study	*E. huxleyi*	B92/11	8.16 ±2.66	3.29 ±0.23	1.46 ±0.47	0.44 ±0.03	234.08 ±39.90	685.50 ±159.77
This study	*E. huxleyi*	South Africa	0.55 ±0.00	2.74 ±0.06	0.09 ±0.00	0.35 ±0.01	3.84 ±2.27	25.82 ±2.40
This study	*E. huxleyi*	AC472	5.52 ±0.83	3.37 ±0.06	0.98 ±0.14	0.45 ±0.05	111.50 ±16.96	177.15 ±3.51
This study	*E. huxleyi*	AC474	5.37 ±0.00	3.70 ±0.03	0.95 ±0.00	0.43 ±0.07	32.21 ±0.00	165.35 ±0.00
This study	*E. huxleyi*	RCC1212	0.45 ±0.16	3.16 ±0.06	0.08 ±0.02	0.39 ±0.01	1.14 ±0.08	36.74 ±5.30
This study	*E. huxleyi*	RCC1258	5.96 ±0.31	3.26 ±0.04	1.06 ±0.05	0.42 ±0.01	39.86 ±12.75	202.93 ±74.23
THIS STUDY - Other coccolithophore species								
This study	*C. leptoporus*	RCC1169	0.21 ±0.03	3.05 ±0.01	0.03 ±0.01	0.38 ±0.01	0.41 ±0.30	5.63 ±5.42

at 60 ºC for 48 h to remove inorganic carbon. All the samples were packed in pre-combusted aluminium foil and measured with an elemental analyser. The inorganic carbon (PIC) was calculated as the difference betwee TPC and POC. Inorganic and organic carbon/nitrogen production (pg C $cell^{-1}$ day^{-1}) were calculated according to: $P = \mu \times$ cellular carbon content. We also measured PIC using a different method, analyzing the Ca^{2+} via ICP-AES and extrapolating to total PIC. To this end, one aliquot of 200 ml from each flask was filtered through 47 mm hydrophilic polycarbonate filters (0.2 µm pore size) Whatman, washed with alkaline milli-Q water (pH ~ 9), made basic adding NH_4OH and stored at -20 ºC in 50 ml sterile Falcon tubes. Before measurements, 3 ml of ultra pure nitric acid (HNO_3) were added to previously dried filters (60 ºC, 24 h), to dissolve the sample. After 6 h in HNO_3, filters were removed from the tube and the HNO_3 dissolution was measured via the ICP-AES Thermo *i*CAP 6300 Series ICP Spectrometer (installed in the Department of Geology, University of Oviedo, Spain) (*see* Chapter 7 for full analytical methods and precission details).

Samples for nutrients (Table 8.1) were taken as one triplicate (20 ml each) from the blank flask at time zero and at the end of the incubations and from the culture flasks. All samples were filtered with a syringe filter Millex disposable sterile polyethersulphone (PES) membrane (0.22 µm pore size) Millipore, and kept in plastic pots, in the dark, at 4 ºC until analysis. Phosphate and nitrate were analyzed according to Hansen and Koroleff (1999) in a HITACHI U-2000 Spectrophotometer. 10 ml for phosphate and 20 ml for nitrate were used and nitrate was measured in duplicates. Calibrations were done with known concentrations of N and P in reference material.

Calcite pellets were produced in a Hettich ROTANTA 460R centrifuge. Aliquots of 400 ml were centrifuged (3600 rpm, 4 ºC, 20 min) until a single pellet was obtained. Pellets were frozen at -80 ºC, freeze-dried for 48 h and preserved at room temperature. Calcite Mg/Ca and Sr/Ca and the contamination proxies (P/Ca and Fe/Ca) and seawater Mg/Ca and Sr/Ca (Table 8.2, 8.4, 8.5) were determined with a Thermo *i*Cap 6300 Series ICP Spectrometer (installed in the Department of Geology, University of Oviedo, Spain) (*see* Chapter 7 for full analytical methods and precission). All other trace elements were determined using the same method (Table 8.4). The organic-Mg in the coccoliths calcite was cleaned using a newly developed protocol described in full in Chapter 7 using reductive and oxidizing steps. We provide resuls for coccolith pellets

prior to cleaning (full organic + inorganic composition) and after cleaning (only calcite) (Table 8.4, 8.5)

For medium carbonate chemistry all samples were preserved with 750 µl 3.5 % $HgCl_2$ solution to prevent microbial growth during storage. Samples were analysed for TA and DIC using a Versatile Instrument for the Determination of Titration Alkalinity (VINDTA) at the National Oceanography Centre (Southampton, UK). Certified reference materials (CR) to calibrate and establish correction factors for VINDTA measurements were obtained from Dr. Andrew Dickson at the Marine Physics Laboratory of the Scripps Institute of Oceanography, University of California San Diego, USA. VINDTA-derived values for TA and DIC were corrected for various parameters including titration acid density, nutrient concentration of the sample, temperature, salinity and CRM values using a MatLab R2010b (The MathWorks, Inc. UK) script obtained from Mrs Sue Hartman at the National Oceanography Centre, Southampton, UK. Carbonate chemistry parameters were calculated from *in-situ* (incubations) temperature, salinity, DIC, TA and nutrients using the "CO2SYS" macro (Lewis and Wallace 1998). The equilibrium constants were from Mehrbach et al. (1973), refitted by Dickson and Millero (1987), the KSO_4 constants were from Dickson (1990), and the total pH scale was used.

8.2.1.3. Other coccolithophore datasets

Other *E. huxleyi* measurements were retrieved from the literature (n = 13 strains, Table 8.1) cultured at similar conditions from 17 to 25 °C (except mesocosm samples between 10 and 12 °C) for comparison of the physiological parameters (*see* Table 8.1 for all details). Furthermore, five other coccolithophore species were used (*Calcidiscus leptoporus*, *Gephyrocapsa oceanica*, *Calcidiscus quadriperforatus*, *Coccolithus pelagicus*, and *Coccolithus braarudii*) for a broader comparison at similar temperatures (15 to 25 °C, Table 8.1). All the data from these species and strains was retrieved from experiments with a CO_2 gradient (*see* Table 8.1 for the method used), thus we only collected the modern ocean values. However, this gives a small range of initial conditions for all strains that allows a broad comparison of the genetic component attributed to their physiological parameters.

For comparison of organic + inorganic elemental composition (ratios) we collected data from other coccolithophores (*C. leptoporus*, *G. oceanica*, and *E. huxleyi* from Ho et al. 2003) and also

Table 8.6. Species and strains elemental composition and partitioning coefficients (only carbonate).

			MEDIUM CONDITIONS							MEASUREMENTS			SEAWATER		CALCITE (mmol/mol)		D-X	
Study	**Species**	**Strain**	**Temp. (°C)**	**Seawater**	**Sal.**	**pH**	**Nutrients**	**Light**	**Irradiance**	**GR** (day^{-1})	**PIC quota** (pg C $cell^{-1}$)	**PIC rate** (pg C $cell^{-1}$ d^{-1})	**Mg/Ca** (mol/mol)	**Sr/Ca** (mmol/mol)	**Mg/Ca**	**Sr/Ca**	**D-Mg**	**D-Sr**
Coccolithophores																		
Langer et al 2006	*E. huxleyi*	PML B92/11	15.00	artificial	35.00	-	replete	16-8	100.00	0.86	2.37	2.76	-	9.00	-	5.44	-	0.60
Langer et al 2006	*E. huxleyi*	PML B92/11	15.00	artificial	35.00	-	replete	16-8	300.00	0.85	2.65	3.12	-	9.00	-	5.48	-	0.61
Langer et al 2006	*E. huxleyi*	PML B92/11	15.00	artificial	35.00	-	replete	16-8	500.00	0.89	2.78	3.12	-	9.00	-	5.63	-	0.63
Langer et al 2006	*E. huxleyi*	PML B92/11	15.00	artificial	35.00	-	replete	16-8	800.00	0.87	2.61	3.00	-	9.00	-	5.32	-	0.59
Langer et al 2009	*E. huxleyi*	PML B92/11	17.00	natural	-	-	replete	16-8	270.00	1.10	-	-	-	8.16	-	3.10	-	0.38
Langer et al 2009	*E. huxleyi*	PML B92/11	17.00	artificial	35.00	8.20	replete	16-8	270.00	0.92	3.76	4.08	-	11.69	-	4.26	-	0.36
Langer et al 2009	*E. huxleyi*	PML B92/11	17.00	artificial	35.00	8.20	replete	16-8	270.00	0.93	3.68	3.96	-	11.69	-	3.55	-	0.30
Stoll et al 2002b	*E. huxleyi*	CCMP 374	18.00	natural	31.00	-	replete	24-0	123.00	1.16	4.08	4.80	-	-	-	3.01	-	-
Stoll et al 2002b	*E. huxleyi*	CCMP 374	18.00	natural	31.00	-	replete	24-0	123.00	1.19	4.68	5.52	-	-	-	3.03	-	-
Stoll et al 2002b	*E. huxleyi*	CCMP 374	18.00	natural	31.00	-	replete	24-0	144.00	1.42	3.84	5.52	-	-	-	3.05	-	-
Stoll et al 2002b	*E. huxleyi*	CCMP 374	18.00	natural	31.00	-	replete	24-0	144.00	1.48	4.32	5.88	-	-	-	3.01	-	-
Stoll et al 2002b	*E. huxleyi*	CCMP 374	18.00	natural	31.00	-	replete	24-0	265.00	1.58	3.12	4.92	-	-	-	2.84	-	-
Stoll et al 2007	*E. huxleyi*	AC284	24.00	natural	-	-	replete	24-0	117.00	0.52	-	-	-	-	-	3.06	-	-
Stoll et al 2007	*E. huxleyi*	AC320	24.00	natural	-	-	replete	24-0	117.00	0.52	-	-	-	-	-	3.27	-	-
Stoll et al 2007	*E. huxleyi*	NAP4	24.00	natural	-	-	replete	24-0	117.00	0.95	-	-	-	-	-	3.33	-	-
Ra et al 2010	*E. huxleyi*	-	15.00	artificial	-	8.20	replete	16-8	100.00	-	-	-	5.18	-	0.03	-	5.60	-
Ra et al 2010	*E. huxleyi*	-	15.00	artificial	-	8.20	stationary phase	16-8	100.00	-	-	-	5.18	-	0.03	-	5.79	-
Ra et al 2010	*E. huxleyi*	-	20.00	artificial	-	8.20	replete	16-8	100.00	0.39	-	-	5.18	-	0.04	-	8.11	-
Ra et al 2010	*E. huxleyi*	-	20.00	artificial	-	8.20	stationary phase	16-8	100.00	0.39	-	-	5.18	-	0.04	-	7.34	-
Ra et al 2010	*E. huxleyi*	-	25.00	artificial	-	8.20	replete	16-8	100.00	-	-	-	5.18	-	0.05	-	9.65	-
Ra et al 2010	*E. huxleyi*	-	25.00	artificial	-	8.20	stationary phase	16-8	100.00	-	-	-	5.18	-	0.05	-	9.85	-
Stoll et al 2002a	*G. oceanica*	A4727	21.20	natural	-	-	replete	14-10	175.00	-	-	-	-	8.59	-	2.84	-	0.33
Stoll et al 2002c	*G. oceanica*	-	17.00	natural	-	7.80	replete	14-10	137.00	1.89	136.13	72.03	-	-	-	2.50	-	-
Stoll et al 2002c	*G. oceanica*	-	17.00	natural	-	7.77	replete	14-10	137.00	1.74	131.93	75.82	-	-	-	2.47	-	-
Stoll et al 2002c	*G. oceanica*	-	17.00	natural	-	7.99	replete	14-10	137.00	0.68	23.20	34.12	-	-	-	2.44	-	-
Stoll et al 2002c	*G. oceanica*	-	17.00	natural	-	7.99	replete	14-10	137.00	1.73	59.03	34.12	-	-	-	2.38	-	-

Ra et al 2010	*G. oceanica*	-	20.00	artificial	-	8.20	replete	16-8	100.00	0.26	-	-	5.18	-	0.01	-	2.12	-
Ra et al 2010	*G. oceanica*	-	20.00	artificial	-	8.20	stationary phase	16-8	100.00	-	-	-	5.18	-	0.01	-	2.32	-
Ra et al 2010	*G. oceanica*	-	25.00	artificial	-	8.20	replete	16-8	100.00	-	-	-	5.18	-	0.03	-	4.83	-
Ra et al 2010	*G. oceanica*	-	25.00	artificial	-	8.20	stationary phase	16-8	100.00	-	-	-	5.18	-	0.02	-	4.05	-
Stoll et al 2002a	*C. leptoporus*	PCIIM2	17.00	natural	-	-	replete	14-10	175.00	-	192.08	-	-	8.65	-	3.08	-	0.36
Stoll et al 2002c	*C. leptoporus*	-	17.00	natural	-	-	replete	14-10	137.00	0.62	138.46	222.95	-	-	-	2.90	-	-
Stoll et al 2002c	*C. leptoporus*	-	17.00	natural	-	-	replete	14-10	137.00	0.61	198.94	325.84	-	-	-	2.88	-	-
Stoll et al 2002c	*C. leptoporus*	-	17.00	natural	-	-	replete	14-10	137.00	0.64	105.40	164.15	-	-	-	2.70	-	-
Stoll et al 2002c	*C. leptoporus*	-	17.00	natural	-	-	replete	14-10	137.00	0.67	130.39	193.55	-	-	-	2.68	-	-
Stoll et al 2002a	*C. leptoporus*	PCIIM2	17.00	natural	-	-	replete	14-10	175.00	-	192.08	-	-	8.67	-	3.09	-	0.36
Stoll et al 2002a	*C. leptoporus*	PC11M3B	17.00	natural	-	-	replete	14-10	175.00	-	-	-	-	8.63	-	2.74	-	0.32
Müller et al 2011	*C. braarudii*	Riebesell et al 2008	15.00	artificial	36.00	8.20	replete	14-10	125 – 200	0.70	92.40	132.00	5.00	9.40	0.86	3.24	172.00	0.34
Stoll et al 2002a	*C. pelagicus*	KL2	17.00	natural	-	-	replete	14-10	175.00	-	100.36	-	-	8.57	-	2.91	-	0.34
Stoll et al 2002a	*U. sibogae sibogae*	ASM36	17.00	natural	-	-	replete	14-10	175.00	-	30.25	-	-	8.55	-	2.42	-	0.28
Stoll et al 2002a	*U. sibogae foliosa*	ESP6M1	17.00	natural	-	-	replete	14-10	175.00	-	47.78	-	-	8.59	-	2.50	-	0.29
Stoll et al 2002c	*H. carteri*	-	19.26	natural	-	-	replete	14-10	137.00	0.33	-	-	-	-	-	3.08	-	-
Stoll et al 2002c	*H. carteri*	-	16.67	natural	-	-	replete	14-10	137.00	0.25	-	-	-	-	-	2.96	-	-
Stoll et al 2002c	*H. carteri*	-	15.56	natural	-	-	replete	14-10	137.00	0.14	-	-	-	-	-	2.87	-	-
Stoll et al 2002c	*S. pulchra*	GK17	19.35	natural	-	-	replete	14-10	137.00	0.26	-	-	-	-	-	2.43	-	-
Stoll et al 2002c	*S. pulchra*	GK17	16.77	natural	-	-	replete	14-10	137.00	0.25	-	-	-	-	-	2.41	-	-
Stoll et al 2002c	*S. pulchra*	GK7	19.35	natural	-	-	replete	14-10	137.00	0.22	-	-	-	-	-	2.38	-	-
Stoll et al 2002c	*S. pulchra*	GK7	16.77	natural	-	-	replete	14-10	137.00	0.16	-	-	-	-	-	2.32	-	-
Stoll et al 2002c	*S. pulchra*	GK7	15.48	natural	-	-	replete	14-10	137.00	0.16	-	-	-	-	-	2.29	-	-
							Dynoflagellates											
Gussone et al 2009	*T. heimii*	GeoB 92 – Ecuatorial Atlantic	27.50	natural	37.90	7.95	replete	12-12	100.00	-	-	-	-	-	4.37	2.47	2.47	-
Gussone et al 2009	*T. heimii*	GeoB 92 – Ecuatorial Atlantic	25.50	natural	38.10	7.91	replete	12-12	100.00	-	-	-	-	-	3.39	2.44	2.44	-
Gussone et al 2009	*T. heimii*	GeoB 92 – Ecuatorial Atlantic	23.50	natural	37.40	8.09	replete	12-12	100.00	-	-	-	-	-	3.54	2.45	2.45	-
Gussone et al 2009	*T. heimii*	GeoB 92 – Ecuatorial Atlantic	21.50	natural	37.30	8.18	replete	12-12	100.00	-	-	-	-	-	3.76	2.36	2.36	-
Gussone et al 2009	*T. heimii*	GeoB 92 – Ecuatorial Atlantic	19.50	natural	37.40	8.22	replete	12-12	100.00	-	-	-	-	-	2.70	2.30	2.30	-
Gussone et al 2009	*T. heimii*	GeoB 92 – Ecuatorial Atlantic	17.50	natural	37.30	8.32	replete	12-12	100.00	-	-	-	-	-	3.78	2.31	2.31	-
Gussone et al 2009	*T. heimii*	GeoB 92 – Ecuatorial Atlantic	15.00	natural	37.50	8.33	replete	12-12	100.00	-	-	-	-	-	3.54	2.28	2.28	-
Gussone et al 2009	*T. heimii*	GeoB 92 – Ecuatorial Atlantic	12.00	natural	37.40	8.41	replete	12-12	100.00	-	-	-	-	-	3.82	2.25	2.25	-
Gussone et al 2009	*T. heimii*	GeoB 92 – Ecuatorial Atlantic	30.00	natural	38.50	8.02	replete	12-12	100.00	-	-	-	-	-	7.35	2.41	2.41	-

Gussone et al 2009	*T. heimii*	GeoB 92 – Ecuatorial Atlantic	27.50	natural	37.80	8.21	replete	12-12	100.00	-	-	-	-	-	4.76	2.49	2.49	-
Gussone et al 2009	*T. heimii*	GeoB 92 – Ecuatorial Atlantic	25.50	natural	37.70	8.10	replete	12-12	100.00	-	-	-	-	-	4.01	2.45	2.45	-
Gussone et al 2009	*T. heimii*	GeoB 92 – Ecuatorial Atlantic	23.50	natural	37.90	8.15	replete	12-12	100.00	-	-	-	-	-	3.45	2.43	2.43	-
Gussone et al 2009	*T. heimii*	GeoB 92 – Ecuatorial Atlantic	21.50	natural	37.40	8.21	replete	12-12	100.00	-	-	-	-	-	4.23	2.33	2.33	-
Gussone et al 2009	*T. heimii*	GeoB 92 – Ecuatorial Atlantic	19.50	natural	37.40	8.17	replete	12-12	100.00	-	-	-	-	-	3.36	2.33	2.33	-
Gussone et al 2009	*T. heimii*	GeoB 92 – Ecuatorial Atlantic	17.50	natural	37.30	8.28	replete	12-12	100.00	-	-	-	-	-	3.94	2.27	2.27	-
Gussone et al 2009	*T. heimii*	GeoB 92 – Ecuatorial Atlantic	15.00	natural	37.40	8.29	replete	12-12	100.00	-	-	-	-	-	3.60	2.27	2.27	-
Gussone et al 2009	*T. heimii*	GeoB 92 – Ecuatorial Atlantic	12.00	natural	36.40	8.38	replete	12-12	100.00	-	-	-	-	-	3.70	2.24	2.24	-
Gussone et al 2009	*T. heimii*	GeoB 116 – Mediterranean Sea	30.00	natural	36.50	7.98	replete	12 – 12	100.00	-	-	-	-	-	6.89	2.43	2.43	-
Gussone et al 2009	*T. heimii*	GeoB 116 – Mediterranean Sea	27.50	natural	38.20	7.96	replete	12 – 12	100.00	-	-	-	-	-	4.62	2.47	2.47	-
Gussone et al 2009	*T. heimii*	GeoB 116 – Mediterranean Sea	25.50	natural	37.10	8.13	replete	12 – 12	100.00	-	-	-	-	-	4.70	2.49	2.49	-
Gussone et al 2009	*T. heimii*	GeoB 116 – Mediterranean Sea	23.50	natural	37.20	8.17	replete	12 – 12	100.00	-	-	-	-	-	4.09	2.44	2.44	-
Gussone et al 2009	*T. heimii*	GeoB 116 – Mediterranean Sea	21.50	natural	37.40	8.27	replete	12 – 12	100.00	-	-	-	-	-	4.42	2.36	2.36	-
Gussone et al 2009	*T. heimii*	GeoB 116 – Mediterranean Sea	19.50	natural	37.60	8.13	replete	12 – 12	100.00	-	-	-	-	-	3.05	2.28	2.28	-
Gussone et al 2009	*T. heimii*	GeoB 116 – Mediterranean Sea	17.50	natural	37.40	8.08	replete	12 – 12	100.00	-	-	-	-	-	2.62	2.31	2.31	-
Gussone et al 2009	*T. heimii*	GeoB 116 – Mediterranean Sea	15.00	natural	36.90	8.28	replete	12 – 12	100.00	-	-	-	-	-	4.97	2.27	2.27	-
Gussone et al 2009	*T. heimii*	GeoB 116 – Mediterranean Sea	12.00	natural	37.00	8.43	replete	12 – 12	100.00	-	-	-	-	-	3.86	2.25	2.25	-

Table 8.7. Summary of inorganic (PIC) and organic carbon (POC) estimations using inductive coupled plasma atomic emission spectroscopy (ICP-AES) and elemental analyzer (EA).

Species	Strain	**ICP-AES derived** (pg C cell^{-1})		**EA derived** (pg C cell^{-1})		
		PIC_{ICP} (from Ca^{2+} alone)	**POC_{ICP}** (TPC_{EA} - PIC_{Ca2+})	**PIC_{EA}** (TPC_{EA} - POC_{EA})	**POC_{EA}** (from organic C)	**TPC** (from all C)
E. huxleyi	NZEH	6.27 ±0.88	4.22 ±1.50	2.42 ±1.81	8.07 ±1.05	10.50 ±0.78
E. huxleyi	M181CCMP88E	3.76 ±0.57	8.44 ±2.13	4.09 ±2.23	8.12 ±1.03	12.21 ±2.68
E. huxleyi	M184CCMP1A1	4.57 ±0.77	3.27 ±1.61	0.59 ±0.64	7.25 ±1.54	7.85 ±2.16
E. huxleyi	B92/11	4.91 ±1.12	7.45 ±1.09	2.38 ±0.43	9.97 ±1.78	12.36 ±2.21
E. huxleyi	South Africa	4.29 ±0.21	3.27 ±1.54	3.00 ±1.69	4.56 ±0.28	7.56 ±1.52
E. huxleyi	CCMP2758	0.09 ±0.08	9.81 ±0.00	-1.58 ±0.00	11.13 ±0.78	9.97 ±0.00
E. huxleyi	CCMP1280	-0.01 ±0.01	15.66 ±1.45	1.69 ±0.66	13.94 ±2.10	15.64 ±1.45
E. huxleyi	CCMP370	0.085 ±0.09	11.44 ±0.99	-3.86 ±1.47	15.38 ±2.12	11.52 ±1.02
E. huxleyi	CCMP2090	0.16 ±0.15	7.01 ±2.35	-0.47 ±2.44	7.66 ±0.41	7.18 ±2.46
E. huxleyi	AC472	4.95 ±0.58	9.15 ±3.10	2.42 ±1.89	11.69 ±1.95	14.11 ±3.66
E. huxleyi	AC474	4.24 ±0.33	6.03 ±1.14	4.06 ±1.99	6.20 ±0.69	10.27 ±1.46
E. huxleyi	RCC1212	15.67 ±1.54	19.86 ±0.97	12.49 ±1.22	23.04 ±1.80	35.53 ±0.58
E. huxleyi	RCC1258	9.22 ±0.62	15.62 ±0.33	11.91 ±0.40	12.63 ±0.82	24.88 ±1.21

from natural plantkon assemblages, green algae, red dinoflagellates, and diatoms (Table 8.4). These data were selected only a conditions similar to our *E. huxleyi* at 19 °C, 12:12 LD and a light intensity of 120-250 µmol m^{-2} s^{-1}. Eventually, to compare our cleaned coccolith calcite ratios (Mg/Ca and Sr/Ca) with literature data, we collected datasets from 9 coccolithophores (*E. huxleyi* - 5 strains, *G. oceanica* - 1 strain, *C. leptoporus* - 3 strains, *C. braarudii* - 1 strain, *C. pelagicus* - 1 strain, *U. sibogae sibogae* - 1 strain, *U. sibogae foliosa* - 1 strain, *H. carteri* - 1 strain, and *S. pulchra* - 1 strain) and 1 dinoflagellate (*T. heimii* - 1 strain) (Table 8.6). These data were from experiments between 15 and 30 °C.

8.2.2. Laboratory incubations: high CO_2 experiments

We conducted two experiments with the coccolithophore *Gephyrocapsa oceanica* RCC1303 at two temperatures (20 and 25 °C) and a range of 12 pCO_2 as part of the master thesis of Sett et al. (2010) to understand physiological and biogeochemical responses (Table 8.8). The experiments were performed at the Helmholtz Centre for Ocean Research Kiel (GEOMAR). Using the left-over volume (1 L), we produced calcite pellets to then measure the elemental composition and assess the Mg/Ca and Sr/Ca response to high CO_2 and temperature. Here, I summarize Sett et al. (2010) results only for context and provide the new set of geochemical measurements from the pellets (via ICP-AES). During the development of this project, M. N. Müller suggested the possibility to combine our results with his results from several experiments under different

Table 8.8. Coccolithophores experimental conditions and medium carbonate system chemistry parameters from the batch and chemostat experiments. Values from the batch cultures are expressed as mean values with standard deviations (SD) calculated from start and end of the experiments (except in Experiment 4, *see* text).

Species (strain)	Temp. (°C)	pCO_2 (µatm)	SD	TA (µmol kg^{-1})	SD	DIC (µmol kg^{-1})	SD	pH_{total}	SD	CO_2aq (µmol kg^{-1})	SD	HCO_3^- (µmol kg^{-1})	SD	CO_3^{2-} (µmol kg^{-1})	SD	Ω-Cal.	SD
Experiment 1: S = 34, light = 180 µmol photons m^{-2} s^{-1}, L:D = 14:10 h, replicates = 3, Sr/Ca_{SW} = 8.42 ±0.30 mmol/mol, Mg/Ca_{SW} = 5.29 ±0.15 mol/mol																	
C. braarudii (RC1200)	10	417	15	2322	9	2139	19	8.04	0.03	18	1	1984	33	137	16	3.29	0.38
C. braarudii (RC1200)	15	320	17	2393	5	2107	8	8.15	0.02	12	1	1887	15	208	8	5.00	0.18
C. braarudii (RC1200)	18	501	30	2408	7	2182	8	7.99	0.02	17	1	1993	13	172	7	4.12	0.17
C. quadriperforatus (RCC 1135)	15	308	2	2453	2	2149	2	8.17	0.00	12	0	1915	2	222	1	5.33	0.03
C. quadriperforatus (RCC 1135)	18	451	45	2478	7	2221	8	8.04	0.03	16	2	2012	17	194	10	4.66	0.24
C. quadriperforatus (RCC 1135)	20	316	46	2351	17	2115	7	8.15	0.03	14	1	1930	10	171	9	4.10	0.23
E. huxleyi (Bergen 2005)	10	276	6	2425	6	2151	13	8.21	0.01	12	0	1941	19	198	7	4.75	0.26
E. huxleyi (Bergen 2005)	15	306	5	2436	0	2133	3	8.17	0.01	12	0	1901	5	221	2	5.30	0.05
E. huxleyi (Bergen 2005)	20	400	41	2415	12	2126	5	8.07	0.03	13	1	1899	15	214	11	5.15	0.27
E. huxleyi (Bergen 2005)	25	427	30	2470	14	2140	10	8.05	0.03	12	1	1882	20	246	13	5.97	0.31
Experiment 2: S = 34, light = 130 µmol photons m^{-2} s^{-1}, L:D = 14:10 h, replicates = 2, Sr/Ca_{SW} = 8.42 ±0.30 mmol/mol, Mg/Ca_{SW} = 5.29 ±0.15 mol/mol																	
E. huxleyi (Bergen 2005)	10	193	3	2520	3	2150	1	8.35	0.01	9	0	1876	4	265	3	6.36	0.07
E. huxleyi (Bergen 2005)	10	467	9	2311	3	2148	0	7.99	0.01	21	0	2002	2	125	2	2.99	0.06
E. huxleyi (Bergen 2005)	10	699	5	2240	1	2143	0	7.82	0.00	31	0	2027	0	85	1	2.05	0.01
E. huxleyi (Bergen 2005)	10	898	24	2199	2	2138	1	7.72	0.01	39	1	2032	2	67	2	1.60	0.04
E. huxleyi (Bergen 2005)	10	1238	23	2150	2	2131	0	7.58	0.01	54	1	2028	0	48	1	1.16	0.02
E. huxleyi (Bergen 2005)	20	175	0	2689	0	2139	0	8.39	0.00	6	0	1728	0	405	0	9.76	0.01
E. huxleyi (Bergen 2005)	20	365	4	2449	3	2135	1	8.11	0.00	12	0	1891	1	232	2	5.60	0.05
E. huxleyi (Bergen 2005)	20	690	12	2305	3	2135	1	7.85	0.01	22	0	1978	2	135	2	3.24	0.04
E. huxleyi (Bergen 2005)	20	812	20	2257	1	2118	3	7.78	0.01	26	1	1978	5	114	2	2.76	0.05
E. huxleyi (Bergen 2005)	20	1106	12	2217	0	2128	2	7.65	0.00	36	0	2006	2	86	1	2.08	0.01
Experiment 3: S = 34, light = 130 µmol photons m^{-2} s^{-1}, L:D = 16:8 h, replicates = 3, Sr/Ca_{SW} = 8.42 ±0.30 mmol/mol, Mg/Ca_{SW} = 5.29 ±0.15 mol/mol																	
C. braarudii (RC1200)	17	524	27	2242	6	2056	7	7.95	0.02	18	1	1899	11	139	6	3.33	0.12
C. braarudii (RC1200)	17	1151	130	2105	29	2046	21	7.61	0.05	41	5	1939	19	66	8	1.57	0.21
C. braarudii (RC1200)	17	1799	257	2038	16	2037	28	7.42	0.06	63	9	1931	25	42	5	1.00	0.10
C. braarudii (RC1200)	17	2311	122	2021	12	2052	18	7.31	0.02	81	4	1938	15	33	1	0.80	0.00
C. braarudii (RC1200)	17	3508	172	1943	3	2034	8	7.12	0.02	123	6	1890	4	21	1	0.50	0.00
Experiment 4: S = 35, light = 150 µmol photons m^{-2} s^{-1}, L:D = 16:8 h, replicates = 1, Sr/Ca_{SW} = 9.66 ±0.21 mmol/mol, Mg/Ca_{SW} = 5.43 ±0.13 mol/mol																	
G. oceanica (RCC1303)	20	23		2340		1421		8.99		1		801		619		14.81	
G. oceanica (RCC1303)	20	55		2296		1581		8.75		2		1093		486		11.62	
G. oceanica (RCC1303)	20	101		2288		1719		8.57		4		1325		390		9.33	

G. oceanica (RCC1303)	20	260	2291	1942	8.26	9	1688	245	5.86
G. oceanica (RCC1303)	20	385	2280	2014	8.12	13	1810	191	4.57
G. oceanica (RCC1303)	20	536	2268	2065	8.00	19	1896	151	3.61
G. oceanica (RCC1303)	20	717	2278	2122	7.89	25	1975	123	2.93
G. oceanica (RCC1303)	20	885	2309	2182	7.82	31	2044	107	2.56
G. oceanica (RCC1303)	20	1154	2296	2209	7.72	40	2084	86	2.05
G. oceanica (RCC1303)	20	1409	2307	2246	7.64	48	2125	73	1.76
G. oceanica (RCC1303)	20	1712	2303	2268	7.56	58	2148	62	1.49
G. oceanica (RCC1303)	20	2034	2314	2301	7.50	68	2178	54	1.29
G. oceanica (RCC1303)	25	32	2262	1378	8.90	1	791	587	14.12
G. oceanica (RCC1303)	25	32	2262	1378	8.90	1	791	587	14.12
G. oceanica (RCC1303)	25	67	2385	1615	8.72	2	1083	530	12.75
G. oceanica (RCC1303)	25	67	2385	1615	8.72	2	1083	530	12.75
G. oceanica (RCC1303)	25	126	2268	1689	8.52	4	1288	397	9.56
G. oceanica (RCC1303)	25	126	2268	1689	8.52	4	1288	397	9.56
G. oceanica (RCC1303)	25	318	2267	1905	8.23	9	1640	255	6.15
G. oceanica (RCC1303)	25	318	2267	1905	8.23	9	1640	255	6.15
G. oceanica (RCC1303)	25	447	2290	1996	8.11	13	1772	212	5.10
G. oceanica (RCC1303)	25	447	2290	1996	8.11	13	1772	212	5.10
G. oceanica (RCC1303)	25	612	2279	2049	8.00	17	1861	171	4.11
G. oceanica (RCC1303)	25	612	2279	2049	8.00	17	1861	171	4.11
G. oceanica (RCC1303)	25	771	2293	2103	7.91	22	1934	146	3.52
G. oceanica (RCC1303)	25	771	2293	2103	7.91	22	1934	146	3.52
G. oceanica (RCC1303)	25	1014	2264	2123	7.80	29	1978	116	2.80
G. oceanica (RCC1303)	25	1014	2264	2123	7.80	29	1978	116	2.80
G. oceanica (RCC1303)	25	1202	2242	2129	7.73	34	1995	100	2.41
G. oceanica (RCC1303)	25	1202	2242	2129	7.73	34	1995	100	2.41
G. oceanica (RCC1303)	25	1419	2248	2159	7.67	40	2031	88	2.11
G. oceanica (RCC1303)	25	1419	2248	2159	7.67	40	2031	88	2.11
G. oceanica (RCC1303)	25	1396	2018	1946	7.63	39	1834	73	1.75
G. oceanica (RCC1303)	25	1396	2018	1946	7.63	39	1834	73	1.75
G. oceanica (RCC1303)	25	1600	2227	2157	7.62	45	2033	78	1.88
G. oceanica (RCC1303)	25	1600	2227	2157	7.62	45	2033	78	1.88

temperatures at constant CO_2 and same temperature at increasing CO_2, thus he waited for our datasets. He obtained his calite pellets from previous experiments by Wiebe (2008) and Krug et al. (2011), for which we also summarize here the results only for context. When we assessed Müller (2009) pellet Mg/Ca data, we decided to re-measure all his samples (Müller 2009; Müller et al. 2011) applying our newly developed cleaning protocol (*see* Chapter 7) owing to a likely organic-Mg contamination issue. Thus, the results presented here are different from those in Müller (2009). The experimental details and analytics are summarized below only for *G. oceanica* experiments (*see* the other references for appropiate details).

8.2.2.1. *Gephyrocapsa oceanica* cultures and set-up

The coccolithophore *Gephyrocapsa oceanica* (strain RCC 1303) was grown in dilute batch cultures in a broad range of CO_2 levels (12 from ~ 20 to 2000 µatm) at constant alkalinity (~ 2350 µmol kg^{-1}) and at two temperatures: 20 and 25 ºC (Table 8.8). Pre-cultures were grown in artificial seawater (ASW) in 0.5 L polycarbonate bottles (Nalgene™) for at least seven generations to pre-acclimate to the corresponding CO_2 level. Cultures for the main experiment were grown in ASW in 2 L polycarbonate bottles (Nalgene™) and grown for at least 7 generations. Cultures were grown in a climate chamber (RUMED Rubarth Apparate GmbH) adjusted to the desired temperature, a light:dark cycle of 16:8 and light intensity (PAR) of 150 µmol photon m^{-2} s^{-1}. In order to ensure a homogenous cell distribution, the bottles were rotated once a day. The experiments were finished before cell densities reached 35000 cells ml^{-1} to measure the physiological parameters to avoid carbonate system drifts of more than 10 %. However, since not enough volume was available at harvest time to produce a pellet, we left the cells growing between 2 and 5 days. This means that while we had accurate initial and final carbonate chemistry data, we did not have cell density or medium chemistry data at harvesting time of the pellets. We can assume that cell densities reached < 200000 cells ml^{-1} checking the final density and growth rates.

Artificial seawater (ASW) was prepared according to Kester et al. (1967) and nutrients adjusted to 64 µmol kg^{-1} nitrate [NO_3^-] and 4 µmol kg^{-1} phosphate [PO_4^{3-}] to prevent nutrient limitation. Selenium (Se) was also added (10 nmol kg^{-1}) to maximize growth rate of *G. oceanica*. Vitamins and trace metals were prepared according to Guillard and Ryther (1962) and added according to f/4 and f/8, respectively. Sterile filtered NSW (North Atlantic) was also added to provide the

natural trace element components which were not supplied by the vitamins and trace metal solutions. The ASW solution (with nutrients, vitamins, natural seawater and trace metals) was filtered through a 0.20 µm sterile filter (Whatman® Polycap ™ 75 AS) directly into experiment bottles, minimizing the headspace.

Inorganic carbonate system parameters (Table 8.8), total alkalinity (TA) and total dissolved inorganic carbon (DIC) were adjusted by appropriate additions of acid (certified HCl with a concentration of 3.571 M) and Na_2CO_3 (2 mmol kg^{-1} stock solution). The manipulation was conducted according to the EPOCA Guide for Best Practices for ocean acidification research (Riebesell et al. 2010). In order to calculate carbonate system parameters we used the program CO2SYS (Lewis and Wallace 1997). The dissociation constants used for carbonate system calculations were from Roy et al. (1993) for K1 and K2 for carbonic acid and from Dickson (1990) for K_{SO4}. The total pH scale was used.

Samples were collected (initial and final) for total alkalinity (TA) and dissolved inorganic carbon (DIC). Samples were collected at harvesting time for Chlorophyll *a* (Chla), Particulate organic Nitrogen (PON) and Particulate Organic Carbon (POC), Total Particulate Nitrogen (TPN) and Total Particulate Carbon (TPC), medium elemental composition (ICP-AES), and inorganic nutrients [nitrate (NO_3) and phosphate (PO_3^{4-})] (Table 8.9). The remaining suspension was concentrated by centrifugation to produce calcite pellets.

8.2.2.2. *Gephyrocapsa oceanica* sample analytics

For particulate matter measurements (Table 8.9), samples were filtered on GF/F filters (Whatmann, pre-combusted at 500 °C for 6 h) in duplicate and stored in glass petri dishes (pre-combusted at 500 °C for 6 h) at -20 °C. Sampling took place two hours after the start of light cycle and was carried out within two hours to ensure that cell density did not vary due to the 24 hours rhythm in cell division and cell enlargement (Müller et al. 2008). Filters for total particulate carbon and nitrogen (TPC and TPN) were dried overnight at 60 °C and measured with a Euro EA Elemental Analyzer according to Sharp (1974). Samples for particulate organic carbon and nitrogen (POC and PON) were placed in a dessicator above a 37 % HCl solution for two hours to remove all inorganic carbon and dried overnight at 60 °C following analysis of TPC according to Sharp (1974). PIC was calculated from measured TPC and POC according to PIC = TPC - POC.

Table 8.9. Coccolithophore physiological and biochemical parameters.

Species (strain)	Temp. (°C)	pCO_2 (µatm)	SD	Growth rate (d^{-1})	SD	POC prod. (pg C $cell^{-1}$ d^{-1})	SD	PIC prod. (pg C $cell^{-1}$ d^{-1})	SD	TPN prod. (pg N $cell^{-1}$ d^{-1})	SD	Chla prod. (pg Chla $cell^{-1}$ d^{-1})	SD	PIC/POC (mol/mol)	SD	C/N (mol/mol)	SD
Experiment 1: S = 34, light = 180 µmol photons m^{-2} s^{-1}, L:D = 14:10 h, replicates = 3, Sr/Ca_{SW} = 8.42 ±0.30 mmol/mol, Mg/Ca_{SW} = 5.29 ±0.15 mol/mol																	
C. braarudii (RC1200)	10	417	15	0.38	0.01	149	8	75	1	18.8	1.1	2.33	0.22	0.50	0.03	9.27	0.37
C. braarudii (RC1200)	15	320	17	0.52	0.01	155	6	120	10	16.0	0.1	4.07	0.42	0.78	0.09	11.25	0.45
C. braarudii (RC1200)	18	501	30	0.56	0.01	205	5	137	6	20.2	0.3	5.43	0.22	0.67	0.04	11.84	0.14
C. quadriperforatus (RCC 1135)	15	308	2	0.51	0.01	28.6	2.4	40.9	0.7	7.84	1.44	0.91	0.37	1.43	0.12	4.31	0.52
C. quadriperforatus (RCC 1135)	18	451	45	0.54	0.01	44.9	7.2	54.4	6.1	5.10	0.53	0.44	0.12	1.23	0.24	10.25	1.21
C. quadriperforatus (RCC 1135)	20	316	46	0.64	0.01	55.8	1.1	72.8	1.1	5.92	0.06	1.16	0.06	1.31	0.01	10.99	0.13
E. huxleyi (Bergen 2005)	10	276	6	0.53	0.01	12.19	0.52	5.81	0.17	2.21	0.13	0.59	0.02	0.48	0.01	6.43	0.09
E. huxleyi (Bergen 2005)	15	306	5	1.03	0.01	8.21	0.06	6.27	0.16	1.42	0.09	0.27	0.01	0.76	0.01	6.76	0.47
E. huxleyi (Bergen 2005)	20	400	41	1.24	0.01	5.56	0.04	5.05	0.04	0.96	0.01	0.22	0.01	0.91	0.01	6.75	0.07
E. huxleyi (Bergen 2005)	25	427	30	1.34	0.01	7.31	0.16	7.72	0.19	1.11	0.06	0.27	0.01	1.06	0.01	7.66	0.42
Experiment 2: S = 34, light = 130 µmol photons m^{-2} s^{-1}, L:D = 14:10 h, replicates = 2, Sr/Ca_{SW} = 8.42 ±0.30 mmol/mol, Mg/Ca_{SW} = 5.29 ±0.15 mol/mol																	
E. huxleyi (Bergen 2005)	10	193	3	0.64	0.01	5.78	0.53	8.10	0.70	0.87	0.06	0.07	0.01	1.40	0.01	7.81	1.27
E. huxleyi (Bergen 2005)	10	467	9	0.65	0.00	5.48	0.07	8.21	0.25	0.79	0.03	0.07	0.00	1.50	0.03	8.09	0.36
E. huxleyi (Bergen 2005)	10	699	5	0.63	0.01	5.33	0.65	7.72	0.04	0.79	0.06	0.07	0.01	1.46	0.17	7.90	0.40
E. huxleyi (Bergen 2005)	10	898	24	0.62	0.01	5.13	0.02	6.68	0.54	0.73	0.01	0.06	0.00	1.30	0.10	8.17	0.06
E. huxleyi (Bergen 2005)	10	1238	23	0.57	0.01	5.11	0.09	5.70	0.77	0.69	0.02	0.06	0.00	1.12	0.17	8.59	0.44
E. huxleyi (Bergen 2005)	20	175	0	1.34	0.00	8.03	1.21	7.50	0.71	1.26	0.13	0.10	0.00	1.02	0.14	6.85	0.45
E. huxleyi (Bergen 2005)	20	365	4	1.41	0.00	7.74	0.56	6.70	1.18	1.27	0.04	0.13	0.01	0.87	0.22	7.11	0.27
E. huxleyi (Bergen 2005)	20	690	12	1.35	0.01	7.61	0.30	6.08	0.18	1.32	0.12	0.13	0.01	0.80	0.06	6.74	0.33
E. huxleyi (Bergen 2005)	20	812	20	1.31	0.02	7.42	0.22	5.02	0.42	1.47	0.24	0.12	0.00	0.70	0.05	5.80	1.04
E. huxleyi (Bergen 2005)	20	1106	12	1.19	0.03	8.14	0.11	3.83	0.29	1.55	0.09	0.10	0.01	0.47	0.04	6.13	0.29
Experiment 3: S = 34, light = 130 µmol photons m^{-2} s^{-1}, L:D = 16:8 h, replicates = 3, Sr/Ca_{SW} = 8.42 ±0.30 mmol/mol, Mg/Ca_{SW} = 5.29 ±0.15 mol/mol																	
C. braarudii (RC1200)	17	524	27	0.63	0.06	215	14	335	24	24.5	1.8	nan	nan	1.60	0.17	8.33	0.46
C. braarudii (RC1200)	17	1151	130	0.57	0.06	289	94	346	115	25.8	9.2	nan	nan	1.37	0.70	7.80	0.78
C. braarudii (RC1200)	17	1799	257	0.43	0.06	140	6	82	39	5.6	2.8	nan	nan	0.57	0.31	9.40	0.20
C. braarudii (RC1200)	17	2311	122	0.13	0.06	89	17	22	16	1.5	1.4	nan	nan	0.27	0.29	7.10	0.70
C. braarudii (RC1200)	17	3508	172	0.13	0.06	90	54	17	11	1.3	0.8	nan	nan	0.20	0.00	7.67	0.57
Experiment 4: S = 35, light = 150 µmol photons m^{-2} s^{-1}, L:D = 16:8 h, replicates = 1, Sr/Ca_{SW} = 9.66 ±0.21 mmol/mol, Mg/Ca_{SW} = 5.43 ±0.13 mol/mol																	
G. oceanica (RCC1303)	20	23		0.29		5.6		6.6		1.38		0.06		1.18		4.73	
G. oceanica (RCC1303)	20	55		0.54		6.2		13.4		1.11		0.12		2.17		6.50	
G. oceanica (RCC1303)	20	101		0.82		12.2		24.6		3.24		0.23		2.02		4.38	
G. oceanica (RCC1303)	20	260		1.00		14.3		26.0		2.19		0.24		1.81		7.64	
G. oceanica (RCC1303)	20	385		1.06		12.2		21.0		2.00		0.23		1.73		7.11	

G. oceanica (RCC1303)	20	536	1.05	12.7	20.3	2.10	0.23	1.59	7.09
G. oceanica (RCC1303)	20	717	0.88	16.7	19.7	2.40	0.22	1.18	8.12
G. oceanica (RCC1303)	20	885	0.79	13.7	15.9	2.32	0.16	1.16	6.92
G. oceanica (RCC1303)	20	1154	0.58	9.0	9.0	1.63	0.08	1.00	6.41
G. oceanica (RCC1303)	20	1409	0.51	8.2	8.1	1.40	0.08	0.99	6.78
G. oceanica (RCC1303)	20	1712	0.44	7.1	6.0	1.22	0.05	0.84	6.84
G. oceanica (RCC1303)	20	2034	0.36	7.6	7.8	1.34	0.06	1.02	6.64
G. oceanica (RCC1303)	25	32	0.21	1.5	1.7	0.59	0.02	1.11	3.06
G. oceanica (RCC1303)	25	32	0.21	1.5	1.7	0.59	0.02	1.11	3.06
G. oceanica (RCC1303)	25	67	0.47	4.0	7.5	1.35	0.06	1.85	3.50
G. oceanica (RCC1303)	25	67	0.47	4.0	7.5	1.35	0.06	1.85	3.50
G. oceanica (RCC1303)	25	126	0.79	14.1	32.8	4.36	0.30	2.33	3.76
G. oceanica (RCC1303)	25	126	0.79	14.1	32.8	4.36	0.30	2.33	3.76
G. oceanica (RCC1303)	25	318	1.13	14.3	28.0	5.27	0.24	1.96	3.17
G. oceanica (RCC1303)	25	318	1.13	14.3	28.0	5.27	0.24	1.96	3.17
G. oceanica (RCC1303)	25	447	1.10	26.7	48.6	8.47	0.42	1.82	3.67
G. oceanica (RCC1303)	25	447	1.10	26.7	48.6	8.47	0.42	1.82	3.67
G. oceanica (RCC1303)	25	612	1.11	21.6	42.3	6.93	0.36	1.95	3.64
G. oceanica (RCC1303)	25	612	1.11	21.6	42.3	6.93	0.36	1.95	3.64
G. oceanica (RCC1303)	25	771	1.07	19.5	33.0	6.04	0.35	1.69	3.78
G. oceanica (RCC1303)	25	771	1.07	19.5	33.0	6.04	0.35	1.69	3.78
G. oceanica (RCC1303)	25	1014	1.15	12.2	18.4	3.75	0.18	1.51	3.79
G. oceanica (RCC1303)	25	1014	1.15	12.2	18.4	3.75	0.18	1.51	3.79
G. oceanica (RCC1303)	25	1202	0.99	14.5	19.0	4.48	0.22	1.31	3.78
G. oceanica (RCC1303)	25	1202	0.99	14.5	19.0	4.48	0.22	1.31	3.78
G. oceanica (RCC1303)	25	1419	0.85	11.3	12.0	3.57	0.15	1.07	3.68
G. oceanica (RCC1303)	25	1419	0.85	11.3	12.0	3.57	0.15	1.07	3.68
G. oceanica (RCC1303)	25	1396	0.69	10.4	10.6	3.46	0.12	1.02	3.52
G. oceanica (RCC1303)	25	1396	0.69	10.4	10.6	3.46	0.12	1.02	3.52
G. oceanica (RCC1303)	25	1600	0.61	11.0	10.4	3.56	0.10	0.95	3.59
G. oceanica (RCC1303)	25	1600	0.61	11.0	10.4	3.56	0.10	0.95	3.59

Chlorophyll *a* was extracted with 90 % acetone and measured fluorometrically according to Welschmeyer (1994). Measurements of cell densities were done at the end of the experiment (Beckman Z2 Coulter®Particle Count and Size Analyzer) and growth rate (μ) was calculated according to the following equation: $\mu = (\ln(t_{final}) - \ln(t_0)/d^{-1}$, where t_{final} represents cell densities at the end of the experiment, t_0 represents initial cell densities and d represents the days between t_0 and t_{final}.

Samples for nutrients and TA (Table 8.8) were taken from the filtrate of each bottle and kept at 4 ºC, and processed within 14 days. Otherwise nutrient samples were frozen (-20 ºC) and TA samples poisoned with $HgCl_2$. Nutrient and TA samples were taken at the beginning and at the end of the experiment to calculate nutrient draw-down and TA drift. As I mentioned, these measurements are available at cell densities below 35000 cell ml^{-1} but not when pellets were sampled, which was below 200000 cell ml^{-1} using the final density and growth rate (Table 8.9). pH was measured immediately at the corresponding experimental temperature in a Metrohm 713 pH Meter with a temperature sensor and pH and reference electrodes. Nitrate (NO_3^-) and Phosphate (PO_4^{3-}) were analysed according to Hansen and Koroleff (1999) and measured in duplicates. TA samples were measured in duplicates at 20 °C in a Metrohm Basic Titrino 794 titration device with a 0.05 M HCl according to Dickson et al. (2003). Since DIC was not directly measured, the start DIC concentration was calculated according to: $DIC_{start} = (TA - A)/2$, where TA refers to the measured total alkalinity and A refers to the acid concentration added for the inorganic carbon manipulation (Bach et al. 2011). The final DIC concentration was calculated as $DIC_{final} = DIC_{start} - TPC_{buildup}$.

Calcite pellets were centrifuged in a Beckman AVANTI^{TM} J-25 Centrifuge. Aliquots of 500 and 50 ml were consecutively centrifuged in flat-bottom tubes (*see* Chapter 7 for benefits and protocol optimization) (12000 rpm and 6000 rpm, 6 min each at 10 °C) until a single pellet was obtained. Pellets were frozen at -20 ºC, dried 48 h at 60 °C and preserved at room temperature. Calcite Mg/Ca and Sr/Ca and the contamination proxies (P/Ca and Fe/Ca) and seawater Mg/Ca and Sr/Ca (Table 8.10) were determined with a Thermo *i*Cap 6300 Series ICP Spectrometer (installed in the Department of Geology, University of Oviedo, Spain) (*see* Chapter 7 for full analytical methods and precission). The organic-Mg in the coccoliths calcite was cleaned using a newly developed protocol described in full in Chapter 7 using reductive and oxidizing steps.

Table 8.10. Coccolithophore geochemistry.

Species (stran)	Temp (°C)	pCO_2 (µatm)	SD	Sr/Ca_{cal} (mmol/mol)	D-Sr	Mg/Ca_{cal} (mmol/mol)	D-Mg	P/Ca_{cal} (mmol/mol)	Fe/Ca_{cal} (mmol/mol)	Sr/Ca_{SW} (mmol/mol)	SD	Mg/Ca_{SW} mol/mol	SD
Experiment 1: S = 34, light = 180 µmol photons m^{-2} s^{-1}, L:D = 14:10 h, replicates = 3, Sr/Ca_{SW} = 8.42 ±0.30 mmol/mol, Mg/Ca_{SW} = 5.29 ±0.15 mol/mol													
C. braarudii (RC1200)	10	417	15	2.40	0.28	1.44	0.27	1.65	1.92	8.42	0.30	5.29	0.15
C. braarudii (RC1200)	15	320	17	3.00	0.36	0.74	0.14	0.32	0.17	8.42	0.30	5.29	0.15
C. braarudii (RC1200)	18	501	30	2.86	0.34	1.04	0.20	0.46	0.93	8.42	0.30	5.29	0.15
C. quadriperforatus (RCC 1135)	15	308	2	2.67	0.32	1.54	0.29	2.48	2.33	8.42	0.30	5.29	0.15
C. quadriperforatus (RCC 1135)	18	451	45	2.79	0.33	1.70	0.32	0.39	0.54	8.42	0.30	5.29	0.15
C. quadriperforatus (RCC 1135)	20	316	46	3.10	0.37	0.62	0.12	3.41	0.22	8.42	0.30	5.29	0.15
E. huxleyi (Bergen 2005)	10	276	6	2.64	0.31	3.61	0.68	1.37	5.68	8.42	0.30	5.29	0.15
E. huxleyi (Bergen 2005)	15	306	5	2.93	0.35	1.61	0.30	1.32	0.93	8.42	0.30	5.29	0.15
E. huxleyi (Bergen 2005)	20	400	41	3.21	0.38	1.97	0.37	1.27	0.79	8.42	0.30	5.29	0.15
E. huxleyi (Bergen 2005)	25	427	30	3.34	0.40	4.59	0.87	1.03	3.52	8.42	0.30	5.29	0.15
Experiment 2: S = 34, light = 130 µmol photons m^{-2} s^{-1}, L:D = 14:10 h, replicates = 2, Sr/Ca_{SW} = 8.42 ±0.30 mmol/mol, Mg/Ca_{SW} = 5.29 ±0.15 mol/mol													
E. huxleyi (Bergen 2005)	10	193	3	2.60	0.31	73.53	13.91	2.04	22.33	8.42	0.30	5.29	0.15
E. huxleyi (Bergen 2005)	10	467	9	2.82	0.33	12.33	2.33	0.91	0.87	8.42	0.30	5.29	0.15
E. huxleyi (Bergen 2005)	10	699	5	2.75	0.33	13.21	2.50	1.90	2.61	8.42	0.30	5.29	0.15
E. huxleyi (Bergen 2005)	10	898	24	3.13	0.37	98.64	18.66	2.12	2.76	8.42	0.30	5.29	0.15
E. huxleyi (Bergen 2005)	10	1238	23	3.12	0.37	35.52	6.72	4.55	14.81	8.42	0.30	5.29	0.15
E. huxleyi (Bergen 2005)	20	175	0							8.42	0.30	5.29	0.15
E. huxleyi (Bergen 2005)	20	365	4	3.35	0.40					8.42	0.30	5.29	0.15
E. huxleyi (Bergen 2005)	20	690	12	3.26	0.39					8.42	0.30	5.29	0.15
E. huxleyi (Bergen 2005)	20	812	20	3.53	0.42					8.42	0.30	5.29	0.15
E. huxleyi (Bergen 2005)	20	1106	12	3.80	0.45					8.42	0.30	5.29	0.15
Experiment 3: S = 34, light = 130 µmol photons m^{-2} s^{-1}, L:D = 16:8 h, replicates = 3, Sr/Ca_{SW} = 8.42 ±0.30 mmol/mol, Mg/Ca_{SW} = 5.29 ±0.15 mol/mol													
C. braarudii (RC1200)	17	524	27	3.26	0.39	8.49	1.61	0.43	4.66	8.42	0.30	5.29	0.15
C. braarudii (RC1200)	17	1151	130	3.42	0.41	7.02	1.33	1.26	3.60	8.42	0.30	5.29	0.15
C. braarudii (RC1200)	17	1799	257	3.40	0.40	15.64	2.96	0.11	0.53	8.42	0.30	5.29	0.15
C. braarudii (RC1200)	17	2311	122	3.47	0.41					8.42	0.30	5.29	0.15
C. braarudii (RC1200)	17	3508	172	3.63	0.43	164.55	31.12	9.71	127.29	8.42	0.30	5.29	0.15
Experiment 4: S = 35, light = 150 µmol photons m^{-2} s^{-1}, L:D = 16:8 h, replicates = 1, Sr/Ca_{SW} = 9.66 ±0.21 mmol/mol, Mg/Ca_{SW} = 5.43 ±0.13 mol/mol													
G. oceanica (RCC1303)	20	23								9.66	0.22	5.43	0.14
G. oceanica (RCC1303)	20	55		3.28	0.34	0.09	0.016	0.50	0.87	9.66	0.22	5.43	0.14
G. oceanica (RCC1303)	20	101		3.38	0.35	0.07	0.012	0.73	0.01	9.66	0.22	5.43	0.14
G. oceanica (RCC1303)	20	260		3.47	0.36	0.08	0.015	0.66	0.05	9.66	0.22	5.43	0.14
G. oceanica (RCC1303)	20	385		3.51	0.36	0.08	0.015	1.01	-0.02	9.66	0.22	5.43	0.14

G. oceanica (RCC1303)	20	536	3.56	0.37	0.09	0.016	0.87	-0.01	9.66	0.22	5.43	0.14
G. oceanica (RCC1303)	20	717	3.64	0.38	0.09	0.017	1.22	0.00	9.66	0.22	5.43	0.14
G. oceanica (RCC1303)	20	885	3.65	0.38	0.10	0.018	1.12	0.00	9.66	0.22	5.43	0.14
G. oceanica (RCC1303)	20	1154	3.93	0.41	0.12	0.022	1.36	-0.01	9.66	0.22	5.43	0.14
G. oceanica (RCC1303)	20	1409	3.91	0.40	0.12	0.021	1.46	-0.01	9.66	0.22	5.43	0.14
G. oceanica (RCC1303)	20	1712	4.14	0.43	0.12	0.023	1.60	-0.01	9.66	0.22	5.43	0.14
G. oceanica (RCC1303)	20	2034	3.97	0.41	0.13	0.024	1.04	-0.03	9.66	0.22	5.43	0.14
G. oceanica (RCC1303)	25	32							9.66	0.22	5.43	0.14
G. oceanica (RCC1303)	25	32							9.66	0.22	5.43	0.14
G. oceanica (RCC1303)	25	67	4.15	0.43	0.32	0.06	1.81	0.16	9.66	0.22	5.43	0.14
G. oceanica (RCC1303)	25	67	4.16	0.43	0.24	0.04	1.77	0.10	9.66	0.22	5.43	0.14
G. oceanica (RCC1303)	25	126	4.14	0.43	0.19	0.04	1.68	0.02	9.66	0.22	5.43	0.14
G. oceanica (RCC1303)	25	126	4.17	0.43	0.16	0.03	1.45	0.02	9.66	0.22	5.43	0.14
G. oceanica (RCC1303)	25	318	4.26	0.44	0.21	0.04	1.45	0.02	9.66	0.22	5.43	0.14
G. oceanica (RCC1303)	25	318	4.19	0.43	0.21	0.04	1.90	0.05	9.66	0.22	5.43	0.14
G. oceanica (RCC1303)	25	447	4.38	0.45	0.45	0.08	1.61	0.04	9.66	0.22	5.43	0.14
G. oceanica (RCC1303)	25	447	4.37	0.45	0.21	0.04	2.95	0.09	9.66	0.22	5.43	0.14
G. oceanica (RCC1303)	25	612	4.37	0.45	0.28	0.05	2.38	0.05	9.66	0.22	5.43	0.14
G. oceanica (RCC1303)	25	612	4.37	0.45	0.28	0.05	2.30	0.04	9.66	0.22	5.43	0.14
G. oceanica (RCC1303)	25	771	4.34	0.45	0.25	0.05	2.27	0.03	9.66	0.22	5.43	0.14
G. oceanica (RCC1303)	25	771	4.35	0.45	0.21	0.04	2.45	0.19	9.66	0.22	5.43	0.14
G. oceanica (RCC1303)	25	1014	4.21	0.44	0.29	0.05	2.82	0.09	9.66	0.22	5.43	0.14
G. oceanica (RCC1303)	25	1014	4.15	0.43	0.56	0.10	8.95	0.58	9.66	0.22	5.43	0.14
G. oceanica (RCC1303)	25	1202	4.15	0.43	0.35	0.07	2.45	0.06	9.66	0.22	5.43	0.14
G. oceanica (RCC1303)	25	1202	4.24	0.44	0.46	0.09	20.60	1.12	9.66	0.22	5.43	0.14
G. oceanica (RCC1303)	25	1419	4.16	0.43	0.62	0.11	3.21	0.18	9.66	0.22	5.43	0.14
G. oceanica (RCC1303)	25	1419	4.18	0.43	0.60	0.11	10.69	0.43	9.66	0.22	5.43	0.14
G. oceanica (RCC1303)	25	1396	4.07	0.42	1.03	0.19	1.71	0.10	9.66	0.22	5.43	0.14
G. oceanica (RCC1303)	25	1396	4.07	0.42	0.63	0.12	2.32	0.11	9.66	0.22	5.43	0.14
G. oceanica (RCC1303)	25	1600	4.10	0.42	0.73	0.13	2.00	0.09	9.66	0.22	5.43	0.14
G. oceanica (RCC1303)	25	1600	4.26	0.44	0.97	0.18	1.39	0.04	9.66	0.22	5.43	0.14

8.2.3. Laboratory incubations: temperature proxy calibration

We conducted an experiment with *Gephyrocapsa oceanica* RCC1303 at 6 temperatures in modern ocean carbonate chemistry conditions to assess the physiological and geochemical response and calibrate a possible paleo temperature proxy. The decission to conduct this study and with this species was taken after assessing the results obtained with the newly develop protocol to clean organic-Mg (*see* Chapter 7). The incubations were conducted at the Helmholtz Centre for Ocean Research Kiel (GEOMAR). Here, I summarize all physiological and geochemical data.

8.2.3.1. *Gephyrocapsa oceanica* cultures and set-up

The coccolithophore *Gephyrocapsa oceanica* (strain RCC 1303) was grown in dilute batch cultures at constant CO_2 conditions for the modern ocean (~ 320 to 450 µatm) at constant alkalinity (~ 2140 µmol kg^{-1}, except at 12 °C that was 2316 µmol kg^{-1}) and at five temperatures: 12, 15, 18, 21, 24, and 27 ºC (Table 8.11). Pre-cultures were grown in artificial seawater (ASW) in 1 L polycarbonate bottles (Nalgene™) for at least eight generations to pre-acclimate to the corresponding temperature level. Cultures for the main experiment were grown in ASW in triplicate (for each temperature) 4 L polycarbonate bottles (Nalgene™) and grown for at least 8 generations. Cultures were grown in a climate chamber (RUMED Rubarth Apparate GmbH) adjusted to the desired calibration temperature, a light:dark cycle of 16:8 and light intensity (PAR) of 135 µmol photon m^{-2} s^{-1}. In order to ensure a homogenous cell distribution, the bottles were rotated once a day. All experiments were finished before cell densities reached 100000 cells ml^{-1} to avoid carbonate system drifts of more than 10 % (Table 8.12).

Artificial seawater (ASW) was prepared according to Kester et al. (1967) and nutrients adjusted to 64 µmol kg^{-1} nitrate [NO_3^-] and 4 µmol kg^{-1} phosphate [PO_4^{3-}] to prevent nutrient limitation (actually measured, *see* Table 8.11). Vitamins and trace metals were prepared according to Guillard and Ryther (1962) and added according to f/8. The ASW solution (with nutrients, vitamins, and trace metals) was filtered through a 0.20 µm sterile filter (Whatman® Polycap ™ 75 AS) directly into experiment bottles, minimizing the headspace.

Table 8.11. Medium carbonate chemistry at the end of the experiment. Values are triplicate averages (SD = standard deviation).

Temp. (°C) Sal. = 35.00	**12**	**15**	**18**	**21**	**24**	**27**
NO_3^- (µM)	-	56.40	57.60	53.09	48.31	61.18
SD	-	4.01	1.17	6.62	10.40	1.94
PO_4^{2-} (µM)	-	2.98	3.27	2.57	2.04	3.51
SD	-	0.69	0.47	0.27	1.15	0.85
Si (µM)	-	9.89	9.98	10.32	5.02	10.47
SD	-	0.32	0.23	0.12	4.32	0.08
TA (µmol kg^{-1})	2316.73	2154.10	2121.90	2134.18	2120.93	2181.98
SD	18.16	129.11	151.21	209.78	173.68	71.97
DIC (µmol kg^{-1})	2088.20	1912.82	1876.70	1913.10	1851.92	1904.25
SD	36.51	124.45	140.72	166.80	141.81	71.12
***p*CO_2** (µatm)	353.62	326.61	345.72	453.35	382.81	437.50
SD	70.66	72.74	41.75	51.05	7.98	44.98
CO_2 (µmol kg^{-1})	14.49	12.19	11.81	14.25	11.11	11.78
SD	2.89	2.72	1.43	1.60	0.23	1.21
pHtotal	8.09	8.10	8.06	7.97	8.02	7.98
SD	0.08	0.08	0.03	0.07	0.03	0.03
HCO_3^- (µmol kg^{-1})	1912.57	1735.87	1698.52	1744.33	1656.86	1700.90
SD	55.82	121.88	129.07	136.45	115.19	69.44
CO_3^{2-} (µmol kg^{-1})	161.15	164.76	166.37	154.52	183.95	191.57
SD	24.08	25.27	16.63	34.20	26.95	12.08
Ω-Cal.	3.84	3.93	3.97	3.70	4.42	4.63
SD	0.57	0.60	0.40	0.82	0.65	0.29

Inorganic carbonate system parameters (Table 8.11), total alkalinity (TA) and total dissolved inorganic carbon (DIC) were adjusted by appropriate additions of acid (certified HCl with a concentration of 3.571 M) and Na_2CO_3 (2 mmol kg^{-1} stock solution). Before the actual experiment set-up, we adjusted several 1 L ASW flasks to make sure the method was working and retrieving TA near the expected range. The manipulation was conducted according to the EPOCA Guide for Best Practices for ocean acidification research (Riebesell et al. 2010). In order to calculate carbonate system parameters we used the program CO2SYS (Lewis and Wallace 1997). The dissociation constants used for carbonate system calculations were from Roy et al. (1993) for K1 and K2 for carbonic acid and from Dickson (1990) for K_{SO4}. The total pH scale was used.

Samples were collected (initial and final) for total alkalinity (TA) and dissolved inorganic carbon (DIC) (here I only show final measurements). Samples were collected at harvesting time for Particulate organic Nitrogen (PON) and Particulate Organic Carbon (POC), Total Particulate Nitrogen (TPN) and Total Particulate Carbon (TPC), medium elemental composition (ICP-

AES), and inorganic nutrients [nitrate (NO_3) and phosphate (PO_3^{4-})] (Table 8.11). The remaining suspension was concentrated by centrifugation to produce calcite pellets.

Table 8.12. Coccolithophore physiological and biochemical parameters at harvesting time.

Temp. (°C) Sal. = 35.00	**12**	**15**	**18**	**21**	**24**	**27**
Cell density (cell ml^{-1})	-	58428.89	44732.00	94939.33	67982.67	31498.33
SD	-	12001.29	4279.29	41762.51	6040.36	2418.03
Growth rate (day^{-1})	-	0.58	0.95	1.09	1.01	0.97
SD	-	0.02	0.02	0.01	0.02	0.02
PON quota (pg N $cell^{-1}$)	-	3.07	3.34	2.12	2.74	2.88
SD	-	0.63	0.40	0.15	0.20	0.03
PON prod. (pg N $cell^{-1}$ d^{-1})	-	1.79	3.16	2.30	2.77	2.79
SD	-	0.32	0.33	0.14	0.22	0.04
POC quota (pg C $cell^{-1}$)	-	18.07	22.37	13.89	18.55	18.38
SD	-	3.58	2.65	1.26	0.83	0.44
POC prod. (pg C $cell^{-1}$ d^{-1})	-	10.52	21.20	15.08	18.77	17.84
SD	-	1.80	2.19	1.18	1.01	0.55
PIC quota (pg C $cell^{-1}$)	-	26.89	30.94	21.70	28.88	29.08
SD	-	2.61	5.13	1.32	3.61	2.61
PIC prod. (pg C $cell^{-1}$ d^{-1})	-	15.68	29.31	23.57	29.22	28.22
SD	-	1.11	4.37	1.40	3.79	2.51
PIC/POC (mol/mol)	-	1.51	1.38	1.57	1.55	1.58
SD	-	0.14	0.08	0.16	0.13	0.10
C/N (mol/mol)	-	5.05	5.74	5.60	5.81	5.47
SD	-	0.05	0.15	0.16	0.19	0.10

8.2.3.2. *Gephyrocapsa oceanica* samples analytics

For particulate matter measurements (Table 8.12), samples were filtered on GF/F filters (Whatmann, pre-combusted at 500 °C for 6 h) in duplicate and stored in glass petri dishes (pre-combusted at 500 °C for 6 h) at -20 °C. Sampling took place two hours after the start of light cycle and was carried out within two hours to ensure that cell density did not vary due to the 24 hours rhythm in cell division and cell enlargement (Müller et al. 2008). Filters for total particulate carbon and nitrogen (TPC and TPN) were dried overnight at 60 °C and measured with a Euro EA Elemental Analyzer according to Sharp (1974). Samples for particulate organic carbon and nitrogen (POC and PON) were placed in a dessicator above a 37 % HCl solution for two hours to remove all inorganic carbon and dried overnight at 60 °C following analysis of TPC according to Sharp (1974). PIC was calculated from measured TPC and POC according to PIC = TPC - POC.

Measurements of cell densities were done at the end of the experiment (Beckman Z2 Coulter®Particle Count and Size Analyzer) and growth rate (μ) was calculated according to the following equation: $\mu = (\ln(t_{final}) - \ln(t_0)/d^{-1}$, where t_{final} represents cell densities at the end of the experiment, t_0 represents initial cell densities and d represents the days between t_0 and t_{final}.

Samples for nutrients (50 ml in falcon tubes), TA and DIC (500 ml in borosilicate flasks) (Table 8.11) were taken from the filtrate of each bottle and kept at 6 ºC. TA/DIC samples were poisoned with $HgCl_2$. Nutrient, TA and DIC samples were taken at the beginning and at the end of the experiment to calculate nutrient draw-down and TA/DIC drift (I only present here the final TA/DIC dataset). pH was routinely checked to ensure that the ASW restoration was within expected ranges at the beginning of the experiment at the corresponding experimental temperature. We used a Metrohm 713 pH Meter with a temperature sensor and pH and reference electrodes. The medium nitrate (NO_3^-) and Phosphate (PO_4^{3-}) were analysed according to Hansen and Koroleff (1999).

TA and DIC samples were measured at the "Service National d'Anylse des Parametres Oceaniques du CO_2 (SNAPOCO2)" from the 500 ml borosilicate flasks. The method followed a potentiometric titration following d'Edmond (1970), and it had for these samples a TA and DIC reproducibility of 2.6 μmol kg^{-1} and 2.8 μmol kg^{-1} respectively after 350 h of measurements.

Calcite pellets were centrifuged in a Beckman AVANTI™ J-25 Centrifuge. Aliquots of 500 and 50 ml were consecutively centrifuged in flat-bottom tubes (*see* Chapter 7 for benefits and protocol optimization) (12000 rpm and 6000 rpm, 6 min each at 10 °C) until a single pellet was obtained. Pellets were frozen at -20 ºC, dried 48 h at 60 °C and preserved at room temperature. Calcite Mg/Ca and Sr/Ca and the contamination proxies (P/Ca and Fe/Ca) and seawater Mg/Ca and Sr/Ca (Table 8.13) were determined with a Thermo *i*Cap 6300 Series ICP Spectrometer (installed in the Department of Geology, University of Oviedo, Spain) (*see* Chapter 7 for full analytical methods and precission). The organic-Mg in the coccoliths calcite was cleaned using a newly developed protocol described in full in Chapter 7 using reductive and oxidizing steps.

Table 8.13. Coccolithophore geochemistry and medium elemental composition.

Temp. (°C) Sal. = 35.00	**12**	**15**	**18**	**21**	**24**	**27**
Ca^{2+} (ppm)	101.02	87.79	78.51	97.14	97.34	87.39
SD	36.97	28.02	29.90	22.66	22.04	27.32
Mg/Ca_{cal} (mmol/mol)	0.25	0.13	0.10	0.13	0.11	0.11
SD	0.06	0.04	0.06	0.08	0.03	0.03
Sr/Ca_{cal} (mmol/mol)	3.40	3.65	3.86	3.96	4.12	4.35
SD	0.01	0.09	0.02	0.02	0.02	0.14
P/Ca_{cal} (mmol/mol)	0.27	1.47	1.29	7.34	1.57	3.19
SD	0.07	1.55	1.13	-	1.48	2.53
Fe/Ca_{cal} (mmol/mol)	0.11	1.19	1.06	6.89	1.39	3.02
SD	0.26	1.45	1.01	-	1.45	2.39
Mg/Ca_{ASW}	-	5.66	5.65	5.66	5.65	5.66
SD	-	0.02	0.01	0.03	0.04	0.01
Sr/Ca_{ASW}	-	9.73	9.76	9.75	9.72	9.32
SD	-	0.04	0.01	0.06	0.01	0.29
D-Mg	-	0.023	0.017	0.023	0.020	0.020
SD	-	0.01	0.01	0.01	0.01	0.00
D-Sr	-	0.375	0.395	0.406	0.424	0.467
SD	-	0.01	0.00	0.00	0.00	0.00

8.3. Results and discussion: brief summary

8.3.1. Strain-specific physiology and elemental composition in the modern ocean

All species and strains included in this assessment were incubated at present CO_2 conditions (Fig. 8.1), but a range remained between 300 and 550 µmol kg^{-1}. However, the physiological variability can be attributed to the traits of each strain and species used. In particular, we tested 13 strains of *Emiliania huxleyi* at very similar conditions: 19.42 ±0.46 ºC, 12:12 L:D cycle, 123.63 ±5.78 µmol quanta m^{-2} s^{-1} and nutrient replete medium. Growth rates (GR) ranged from 0.54 to 1.46 d^{-1} (Fig. 8.1). Non-calcifying strains had a lower GR variability, between 0.54 and 0.93 d^{-1}, while calcifyers varied between 0.68 and 1.46 d^{-1}. Literature *E. huxleyi* GR also showed this large variability, although different temperatures influence the GR (Stoll et al. 2002). For comparison, other coccolithophore species had a lower GR than *E. huxleyi* (Fig. 8.1). *Emiliania huxleyi* particulate carbon production varied between 4.55 ±0.23 and 15.36 ±1.88 pg C $cell^{-1}$ day^{-1} for POC, and from near 0 to 10.65 ±1.05 pg C $cell^{-1}$ day^{-1} for PIC (Fig. 8.1). The highest growth rate registered was 1.46 day^{-1} in NZEH, followed by 1.13 day^{-1} in B11, and from the literature the highest was in RCC1238 near 1.80 day^{-1}. For *E. huxleyi*, the strains with growth rates above 1 (B11, 88E, NZEH and 472), exhibited larger PIC/POC ratios than the rest. PIC/POC and C/N variation per se were strain- and species-specific, and they varied near 50 % even within *E. huxleyi* cultured in the same conditions. When PIC was correlated to POC there is a well known linear increasing relationship (Armstrong et al. 2002), acting as a ballast for the organic carbon (Fig. 8.1). Even within *E. huxleyi* strains, the PIC *vs.* POC varies, suggesting different ballasting properties for the same species in the samle population. Coccolithophore species like *G. oceanica*, *C. leptoporus*, and *C. pelagicus* bear a much higher calcite proportion than *E. huxleyi*. This may drive different remineralization profiles owing to different PIC/POC ratios, even within blooms of a single species.

We found a problem with the different methods used to measure PIC that would need further asessment. Each of the 13 *E. huxleyi* strains was sampled for measuring PIC via TPC - POC in an elemental analyzer (EA) and Ca^{2+} in an ICP-AES (Table 8.7; Fig. 8.3). When POC_{ICP} *vs.* POC_{EA} was correlated the measurements deviated from a 1:1 line because the POC in both cases is derived from the TPC, subtracting the corresponding PIC. However, when PIC_{ICP} vs PIC_{EA}

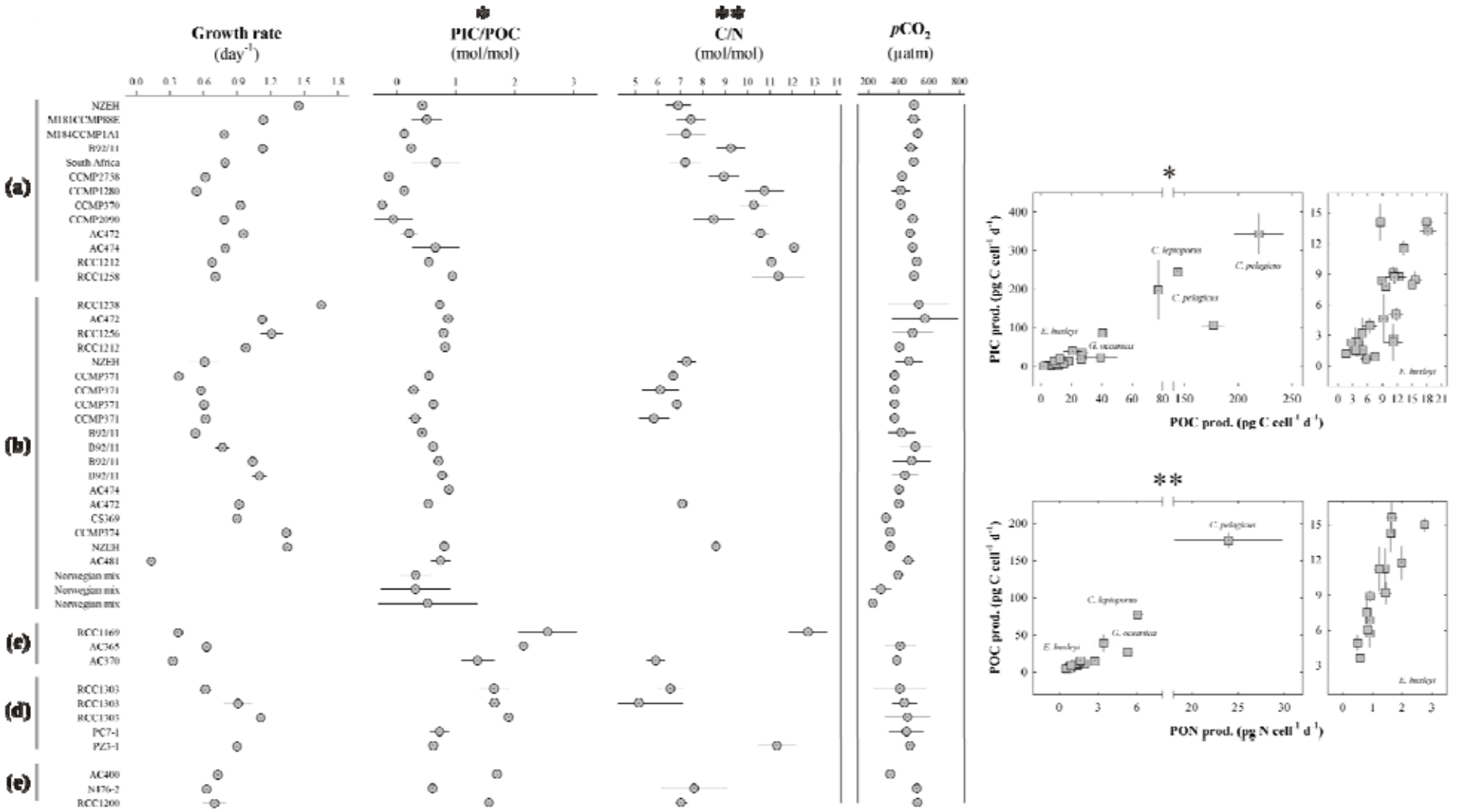

Fig. 8.1. Summary of growth rate, PIC/POC, C/N, and the pCO_2 level (experimental control) in all coccolithophore strains and species included: (a) THIS STUDY - *Emiliania huxleyi*, (b) LITERATURE - *Emiliania huxleyi*, (c) THIS STUDY AND LITERATURE - *Calcidiscus leptoporus*, (d) LITERATURE - *Gephyrocapsa oceanica*, and (e) LITERATURE - *Coccolithus pelagicus*. Also included are the correlations of PIC *vs.* POC (*) and POC *vs.* PON (**) for all species and strains with a zoom on *E. huxleyi*.

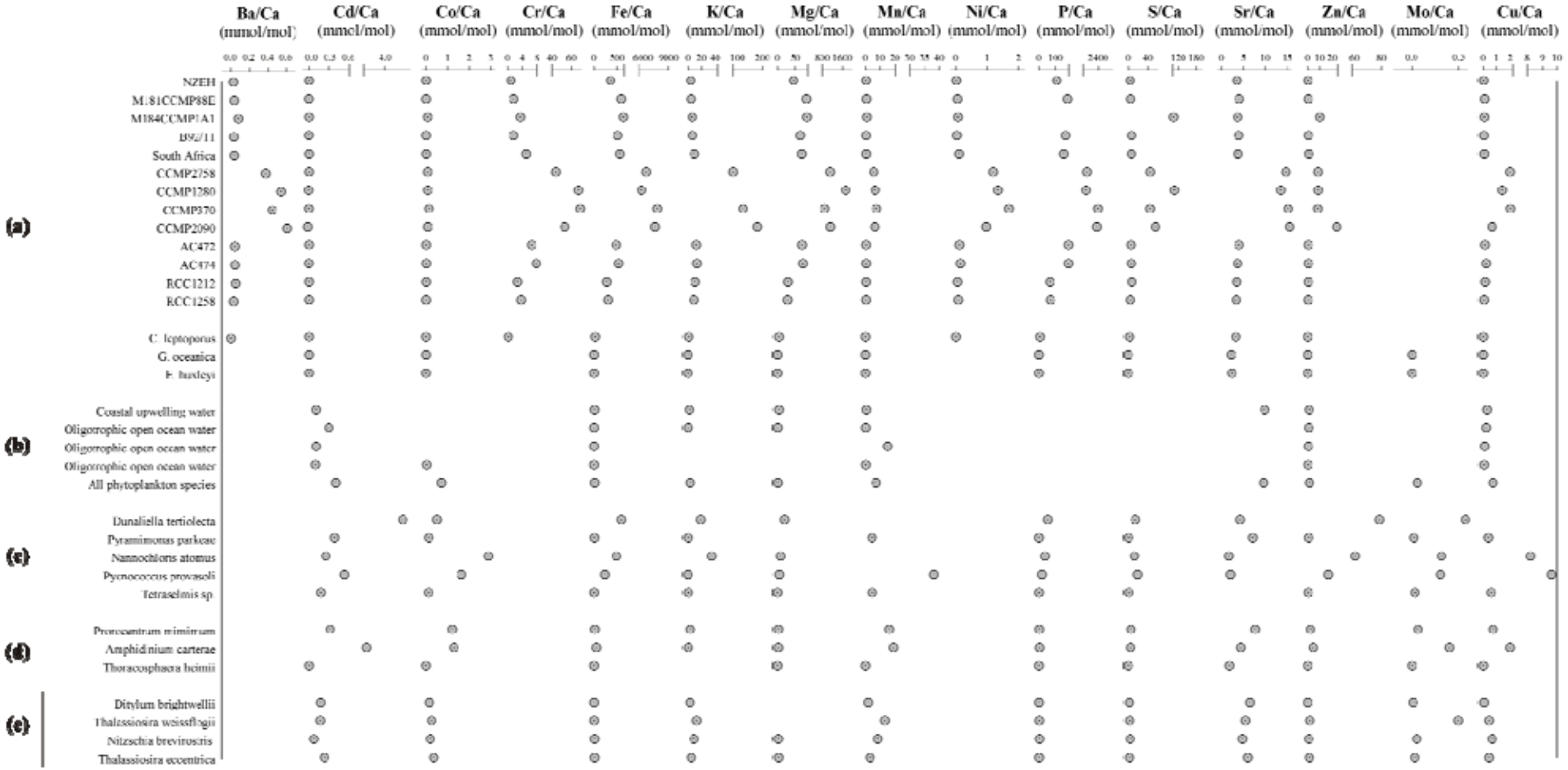

Fig. 8.2. Summary of organic + inorganic matter elemental composition in all coccolithophore strains and species included, and in other phytoplanton: (a) THIS STUDY AND LITERATURE - *Emiliania huxleyi* and other coccolithophore species, (b) LITERATURE - natural plankton assemblages, (c) LITERATURE - green algae, (d) LITERATURE - red dinoflagelates, and (e) LITERATURE - diatoms.

are correlated there is a better correlation around 1:1, but worryingly, the EA measures positive PIC concentrations in naked strains (presumably having no calcite). It is not clear what is the origin of these variability. These measurements indicate that the use of PIC and POC data from either an EA or an ICP or in combination can actually change the final dataset presented and analyzed.

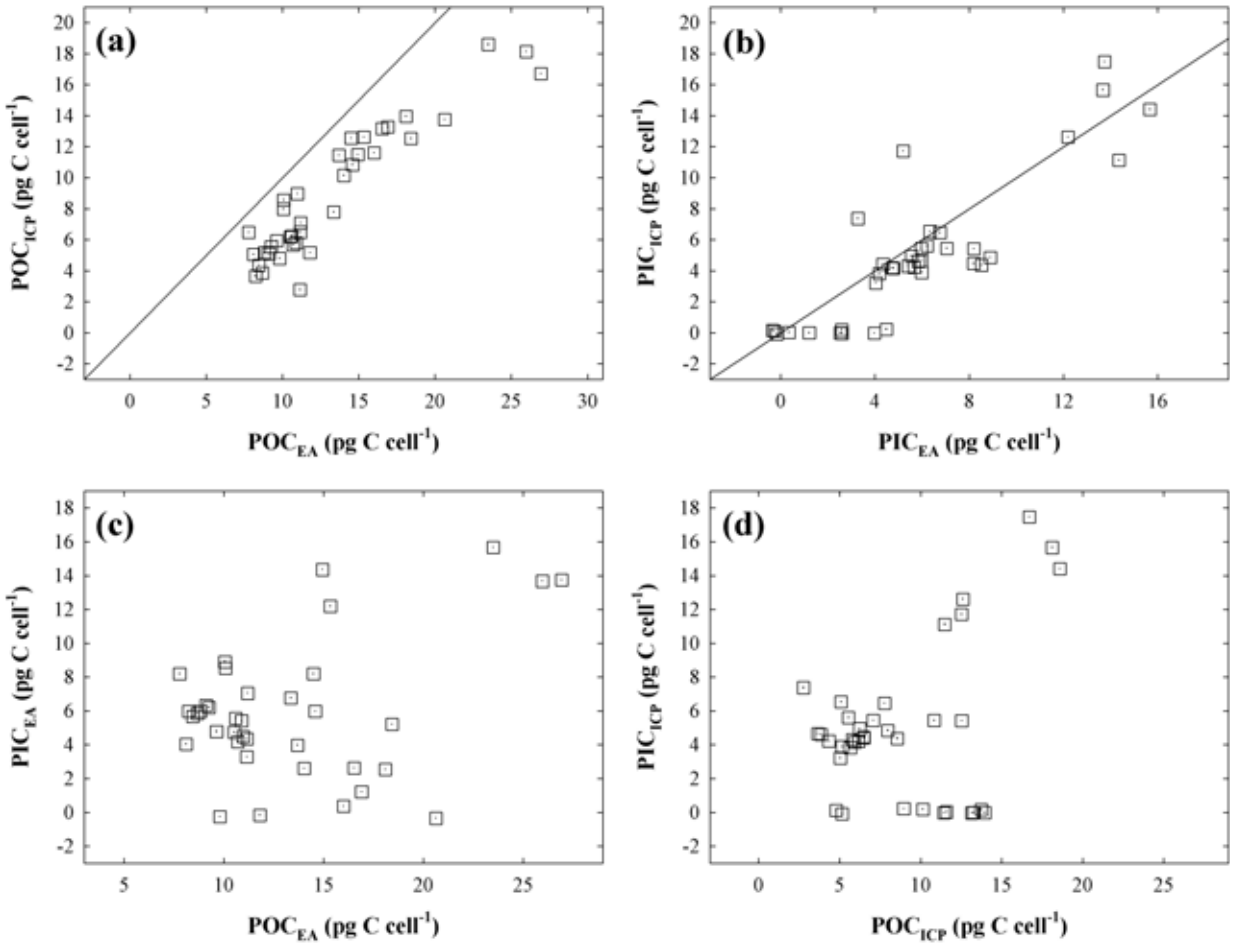

Fig. 8.3. Plots of organic (a) and inorganic (b) carbon measurements for all *Emiliania huxleyi* strains using the different analytical methods: $POC_{ICP} = TPC_{EA} - PIC_{ICP}$, $POC_{EA} = POC_{EA}$, $PIC_{ICP} = PIC_{Ca2+}$, $PIC_{EA} = TPC_{EA} - POC_{EA}$ (see text for details) Also included the PIC_{EA} vs. POC_{EA} (c) and the PIC_{ICP} vs. POC_{ICP} (d) trends for all strains. In (a) and (b) the line represent a 1:1 relationship if measurements were the same using the ICP or EA method.

The assessment of organic + inorganic material elemental ratios indicated that for *E. huxleyi*, those strains with low PIC/POC ratios, had larger ratios for certain elements (Ba/Ca, Sr/Ca, Fe/Ca, K/Ca, Mg/Ca, Ni/Ca, P/Ca, and S/Ca) (Fig. 8.2). In the case of P/Ca and Fe/Ca, they are used as organic matter contamination proxies for inorganic Mg^{2+} (*see* Chapter 7). Phosphorus is an essential component of biomolecules in the cell metabolism such as nucleotides [structural units of DNA and RNA, and energetic molecules like ATP] and phospholipids (essential constituents of cellular membranes) (Chu 1946). Iron is on the cell surface as Fe-oxides and

binds organic molecules (Tang and Morel 2006), which have high affinity to bind organic ligands (Rue and Bruland 1997). Magnesium is a central element of the chlorophyll molecule and other bio-molecules. The stoichiometry of some of the other elements in phytoplankton biomass have been previously investigated (*see* Ho et al. 2003). We propose that they may have applications to monitor organic matter contamination on Mg inorganic phases. Some of these elements (e.g. Ba/Ca, B/Ca) can also be used in their inorganic forms after appropiate cleaning to understand coccoliths physiology, calcification or to develop paleoproxies (Stoll et al. 2012).

We eventually measured inorganic Mg^{2+} and Sr^{2+} on *E. huxleyi* samples, previously cleaning them with the new protocol presented in Chapter 7. The relationship of the organic matter proxies (P/Ca and Fe/Ca) with the measured calcite Mg/Ca increased positively (Fig. 8.3) except in 3 strains (NZEH, South Africa, and RCC1212). The Mg/Ca for these strains varied from 0.15 to 0.55 mmol/mol, but Fe/Ca was also high from 7 to 36 mmol/mol. For *C. leptoporus*, the Mg/Ca was 0.21 mmol/mol with lower P/Ca and Fe/Ca (0.41 and 5.63 mmol/mol respectively). When we compared these data with the organic-Mg cleaned *G. oceanica* samples (*see* Chapter 7; Fig. 8.3), we suggest two possibilities: (1) different coccolithophore species and strains may have an acceptable P/Ca and Fe/Ca level that we can use to establish a cleaning threshold (lowest in *G. oceanica* and highest in *E. huxleyi*), (2) *E. huxleyi* cannot be used (with exceptions) to measure Mg/Ca owing to its relatively low PIC/POC ratio, thus high organic content, which difficulties the organic-Mg cleaning. The problem here is that in ocean there are mixed coccolithophore assemblages with many different strains. The strain-specific signature may prevent the generalized use of inorganic Mg/Ca. Furthermore, the variability in seawater composition from different origins (Fig. 8.3 and Chapter 7) indicates a positive relationship with coccolith Mg/Ca. This is a further source of uncertainty in present measurements. For Sr/Ca, we also find a strain-specific composition on *E. huxleyi*, which was unknown before (Fig. 8.3), apart from the species-specific variability. The Sr/Ca actually decreases with increasing seawater Sr/Ca (this is counterintuitive) and in this dataset it may relate to the actual growth rates, which correlate positively with Sr/Ca (Stoll et al. 2002).

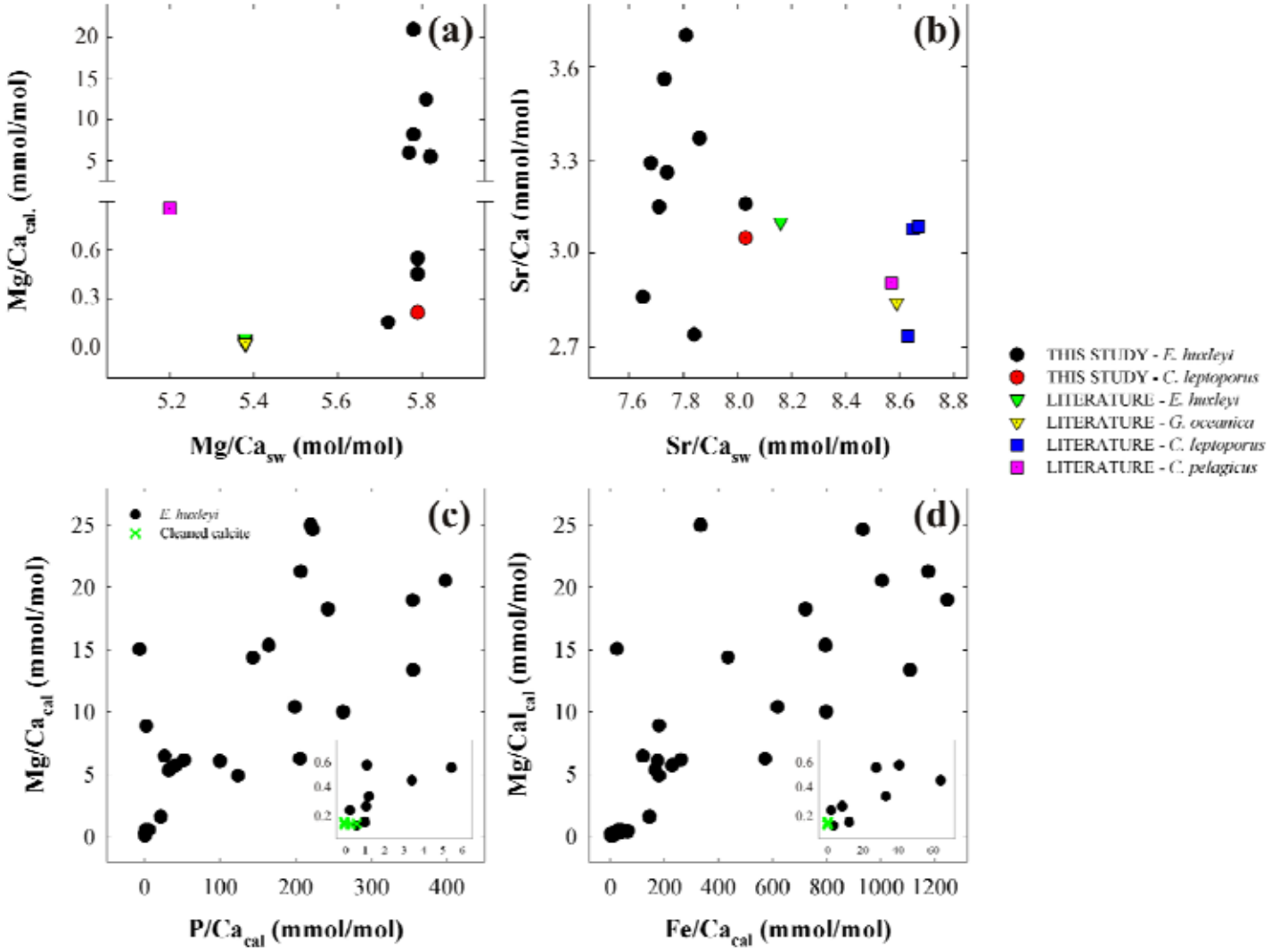

Fig. 8.4. Relationship of calcite Mg/Ca (a) and Sr/Ca (b) *vs.* seawater Mg/Ca and Sr/Ca in coccolitophores. Also included the relationship of the calcite Mg/Ca and the contamination proxies P/Ca (c) and Fe/Ca (d). The small graph in (c) and (d) zooms on the cleaned reagent grande calcite and the low Mg/Ca coccolith values.

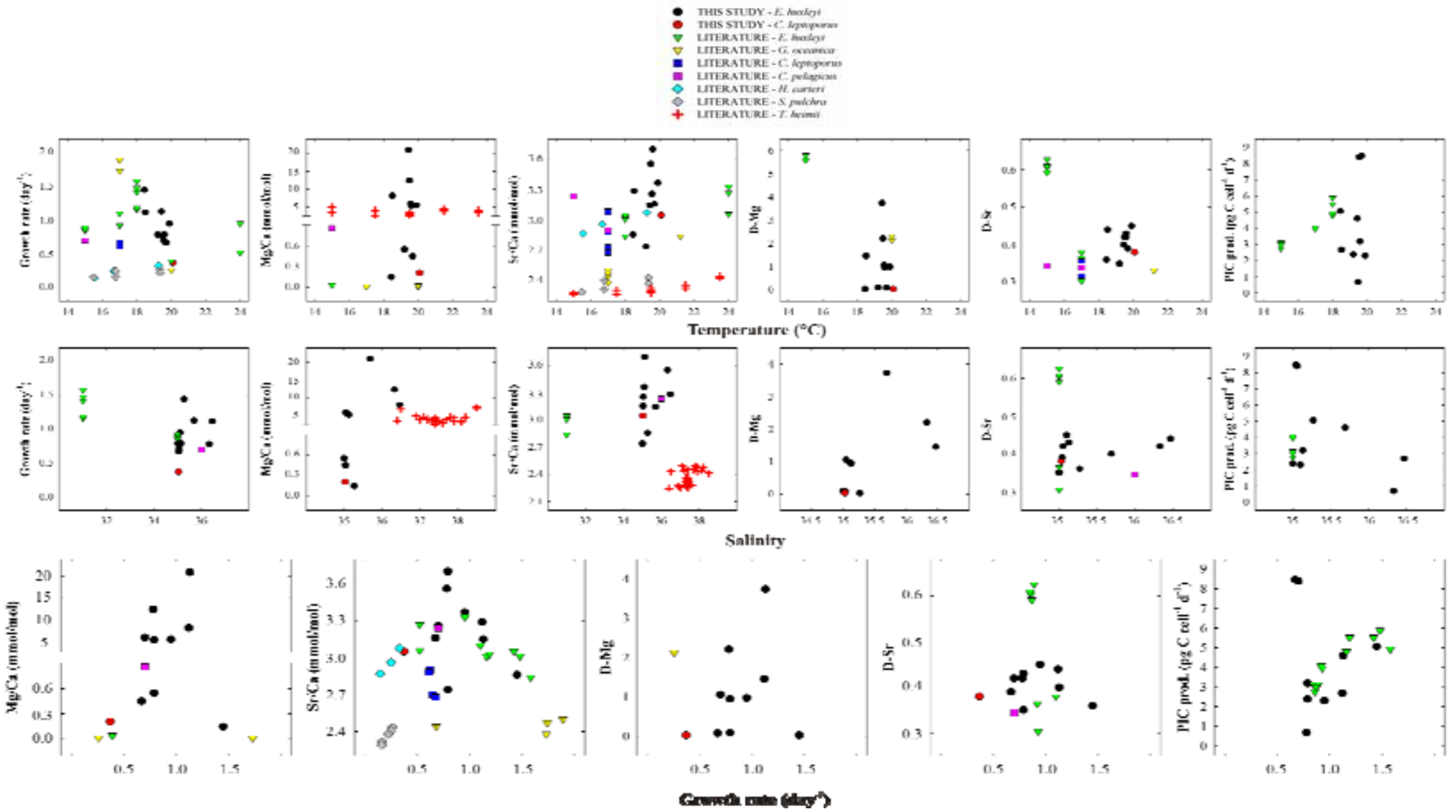

Fig. 8.5. Relationship of different parameters (growth rate, calcite Mg/Ca and Sr/Ca, D-Mg, D-Sr, and PIC production) with experimental temperature, salinity, and growth rate in the coccolithophores *Emiliania huxleyi*, *Calcidiscus leptoporus*, *Gephyrocapsa oceanica*, *Coccolithus pelagicus*, *Helicosphaera* carteri, *Syracosphaera* pulchra and in the dynophyte *Thoracosphaera heimii*.

Our results basically complicate the use of coccolithophore-based Mg/Ca and Sr/Ca proxies at all levels. We present the relationships of GR, Mg/Ca, Sr/Ca, D-Mg, D-Sr, and PIC production for all *E. huxleyi* strains and other coccolithophores from the literature *vs.* temperature and salinity (Fig. 8.4). Then we do the same for the above variables *vs.* GR. There is always some sort of correlation for GR, Mg/Ca, Sr/Ca and PIC production and the individual species (1 strain) following temperature and salinity. However, when considering a whole assemblage of coccoliths where the strains cannot be separated, we suggest that this physiological variability cannot be distinguished. Taking as an example the GR, it has been used as a paleo productivity proxy (Stoll and Ziveri 2004), but it also correlates with temperature for individual species and strains, and then it varies within strains. When the Sr/Ca is correlated with the GR, different increasing and parabolic patterns emerge for individual studies. However, our *E. huxleyi* cultured at the same conditions give scattered results at one single temperature. We suggest that acceptable calibrations can be developed in the laboratory by using a single species and strain (*see* this chapter section 8.3.3). But, the application of these correlations to field samples remains limited owing to the strain-specific variability observed for *E. huxleyi*. If this is not the case in other strains of *G. oceanica* and *C. leptoporus*, which are less problematic to remove organic-Mg remains to be studied.

8.3.2. Coccolithophores mineralogy in a high CO_2 world

In order to make decissions on which samples to use for analyses of trends in a CO_2 gradient, we assessed organic-Mg cleaning efficiency by plotting the P/Ca and the Fe/Ca *vs.* the Mg/Ca for all coccolithophore samples (Fig. 8.6a, b). Many *E. huxleyi* and *C. braarudii* samples had still high P/Ca and Fe/Ca levels above 4 and 2 mmol/mol respectively after cleaning. These results were not considered for further analyses. The *G. ocenica* samples had the lowest organic-Mg

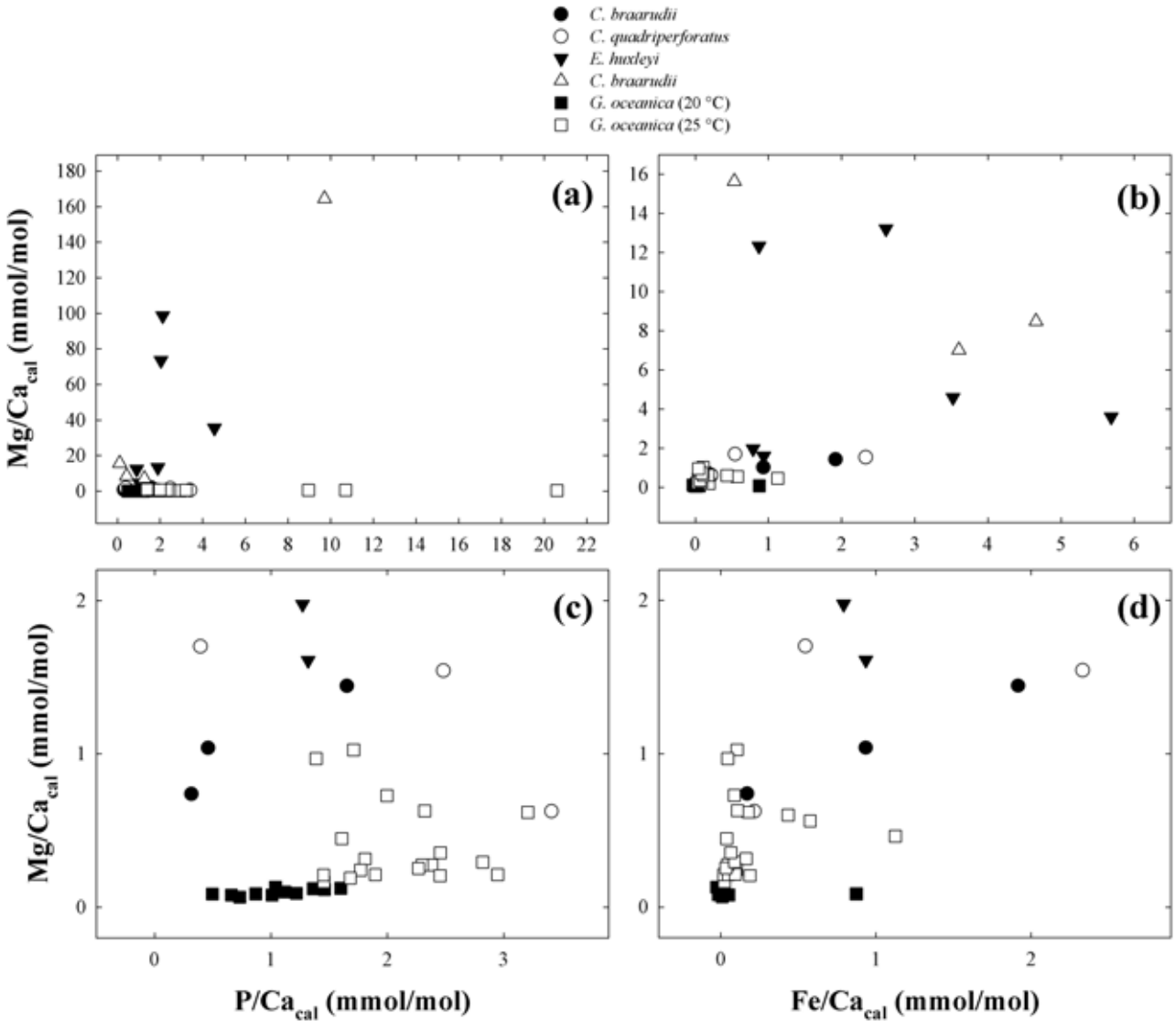

Fig. 8.6. Relationship of coccolithophore Mg/Ca_{cal} ratios with organic-Mg contamination proxies (P/Ca_{cal} and Fe/Ca_{cal}) for all coccolithophores (a, b) and then zoomed in for cleaned samples used in the CO_2 analyses (only *Gephyrocpsa oceanica*).

contamination levels, thus we used them to assess temperature, CO_2, and growth rate (GR) trends. A few *C. braarudii*, *C. quadriperforatus*, and *E. huxleyi* samples were reasonably

cleaned, but owing to the few data points we excluded them from further Mg/Ca *vs.* CO_2 analyses (Fig. 8.6c, d). The large number of well cleaned *G. oceanica* samples confirms the conclusion given in the previous section that this species may be the most adequate to study Mg/Ca responses and possible paleo proxies. To further study this issue, we plotted the calcite Mg/Ca *vs.* Cholophyll *a* (Chla) and the PIC/POC ratio (Fig. 8.7). The lowest Mg/Ca and thus P/Ca and Fe/Ca levels occur in species that have low Chla production such as *G. oceanica*. However, Chla production on *E. huxleyi* was also low, but Mg/Ca high, thus we suggest that the PIC/POC ratio also conditions this response. While both species may naturally have similar Mg/Ca ratios, during the cleaning process those species with a higher calcite proportion are better cleaned from organic-Mg. We suggest that only species with a relatively high PIC/POC such as *G. oceanica* or *C. quadriperforatus* can be used in experiments to measure the Mg/Ca.

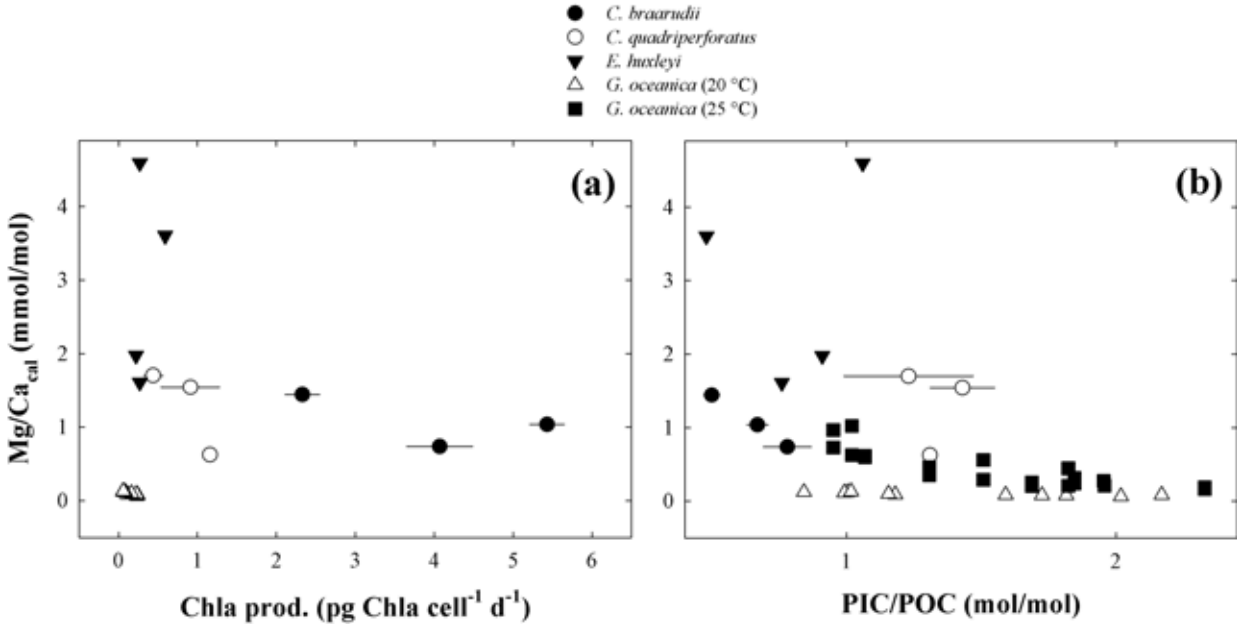

Fig. 8.7. Relationship of coccolithophore Mg/Ca_{cal} ratios with Chlorophyll a production (a) and the PIC/POC (b).

The coccoliths Sr/Ca response to temperature showed a positively increasing trend (from 2.5 to 4.5 mmol/mol) (Fig. 8.8a), which confirms that if using 1 strain of individual species a correlation could be derived. However, the inclusion of different strains at the same temperature can complicate this trend (*see* previous results section). The Sr/Ca response to a CO_2 gradient also showed an increase at all temperatures, except for *G. oceanica* at 25 °C, where there was a parabolic trend (Fig. 8.8b). The Sr/Ca at present CO_2 conditions increased with increasing GR also following the GR *vs.* temperature increase (Fig. 8.8c). Conversely, the Sr/Ca *vs.* GR at increasing CO_2 and constant temperature was constant (Fig. 8.8d). On the Mg/Ca response to

temperature, only two levels were available, thus a conclusion cannot be derived (Fig. 8.8e) but we observed a decrease, which then follows the decrease also observed for the GR at constant CO_2 (Fig. 8.8g). The Mg/Ca trend with increasing CO_2 was positive from 0.07 and 0.16 to 0.13 and 1.03 mmol/mol at 20 and 25 °C respectively (Fig. 8.8f). The Mg/Ca *vs.* GR at increasing CO_2 and constant temperature was also constant as for Sr/Ca (Fig. 8.8d). The main problem to interpret Sr/Ca and especially Mg/Ca responses is that many physiological processes are temperature-dependant, thus adding CO_2 complicates this even further. We suggest that these responses can be interpreted as a physiological deregulation of the calcifying mechanism, avoiding a tight control of elemental incorporation through Ca^{2+} channels. A temperature increase, increases the GR, which in turn relates to higher calcification rates. This can result in the lose of elemental discrimination ability resulting in higher Sr/Ca ratios. However, for Mg/Ca there is not relation with the GR, thus we suggest that this is either a mineral thermodynamic response (as observed for benthic organisms in Ries 2011 with various responses), a deregulation during calcification of the transport channels (Bentov and Erez 2006), an elevation of the Mg/Ca in the medium at the calcification site, or an actual mechanism to estabilize the calcite through inhibition of spontaneous crystallization (Raz et al. 2000; Weiner et al. 2003). This is despite a risk for increased dissolution owing to a higher Mg^{2+} percentage in the calcite (Morse et al. 2006). The pelagic calcite Mg/Ca increase may ultimately lead to a higher $MgCO_3$ % in skeletons and thus a possible shallowing of the remineralization horizon through preferential dissolution of calcites with a higher Mg content.

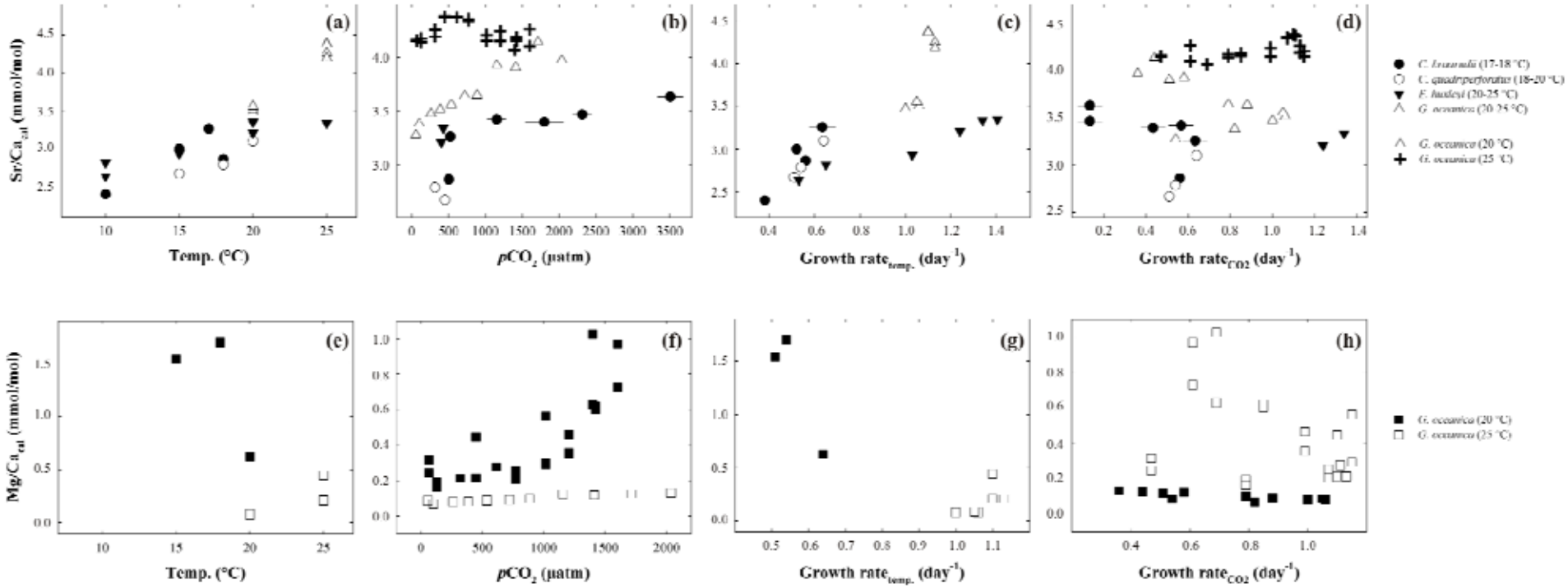

Fig. 8.8. Relationship of coccolithophore Sr/Ca$_{cal}$ and Mg/Ca$_{cal}$ ratios with temperature (a, e), pCO$_2$ (b, f), growth rate at present CO$_2$ (c, g), and growth rate at increasing CO$_2$. All data except in (a) was used from 17 to 25 °C. For Mg/Ca$_{cal}$ ratios only *Gephyrocapsa oceanica* data were used as they were completely cleeaned of organic-Mg (*see* Fig. 8.6).

8.3.3. Coccolithophores mineralogy proxy calibration

In this elemental composition temperature proxy calibration for *G. oceanica*, physiological parameters were measured to understand the response to increasing temperatures and the context of the calcite geochemical results. The growth rate (GR) displayed a parabolic response from 0.58 day^{-1} at 15 °C to 1.09 day^{-1} at 21 °C and 0.97 day^{-1} at 27 °C (there were no physiological data at 12 °C) (Fig. 8.9). The GR increase probably coincides with the optimum field temperature range for this strain. The temperature and GR gradient resulted in an increasing PON, POC, and PIC production that flattened out at 24 and 27 °C in all cases. The PIC/POC ratio increased up to 27 °C, and the C/N also showed a parabolic response. These results suggest that in a future warmer ocean, *G. oceanica* will presumably increase production and particulate matter export up to a limit, which could compensate for the effects of CO_2. Additionally, for this strain, a CO_2 gradient generates parabolic responses in the above measured parameters with optimum curves (Sett et al. 2010; Bach et al. 2011).

On the calcite geochemical measurements we found very low contamination levels except in a few cases with P/Ca and Fe/Ca above 4 mmol/mol (Fig. 8.10). This means that the Mg/Ca results can be considered robust. The Mg/Ca showed a decreasing trend with increasing temperature (12 to 27 °C) from 0.25 to 0.11 mmol/mol following the equation (Fig. 8.11):

$$Mg/Ca_{cal} = 0.0018\ T^2 - 0.0772\ T + 0.8915 \quad (1)$$

The Sr/Ca increased linearly from 3.40 to 4.35 mmol/mol following the equation (Fig. 8.11):

$$Sr/Ca_{cal} = 0.0582\ T + 2.759 \quad (2)$$

Using the contamination proxies P/Ca and Fe/Ca for organic-Mg divided per temperature we removed data points with values above 2 mmol/mol (Fig. 8.11). When we further correlated the calcite Mg/Ca *vs.* the GR we also found a decrease exactly as the temperature trend following the equation:

$$Mg/Ca_{cal} = 0.4218\ T^2 - 0.733\ T + 0.407 \quad (3)$$

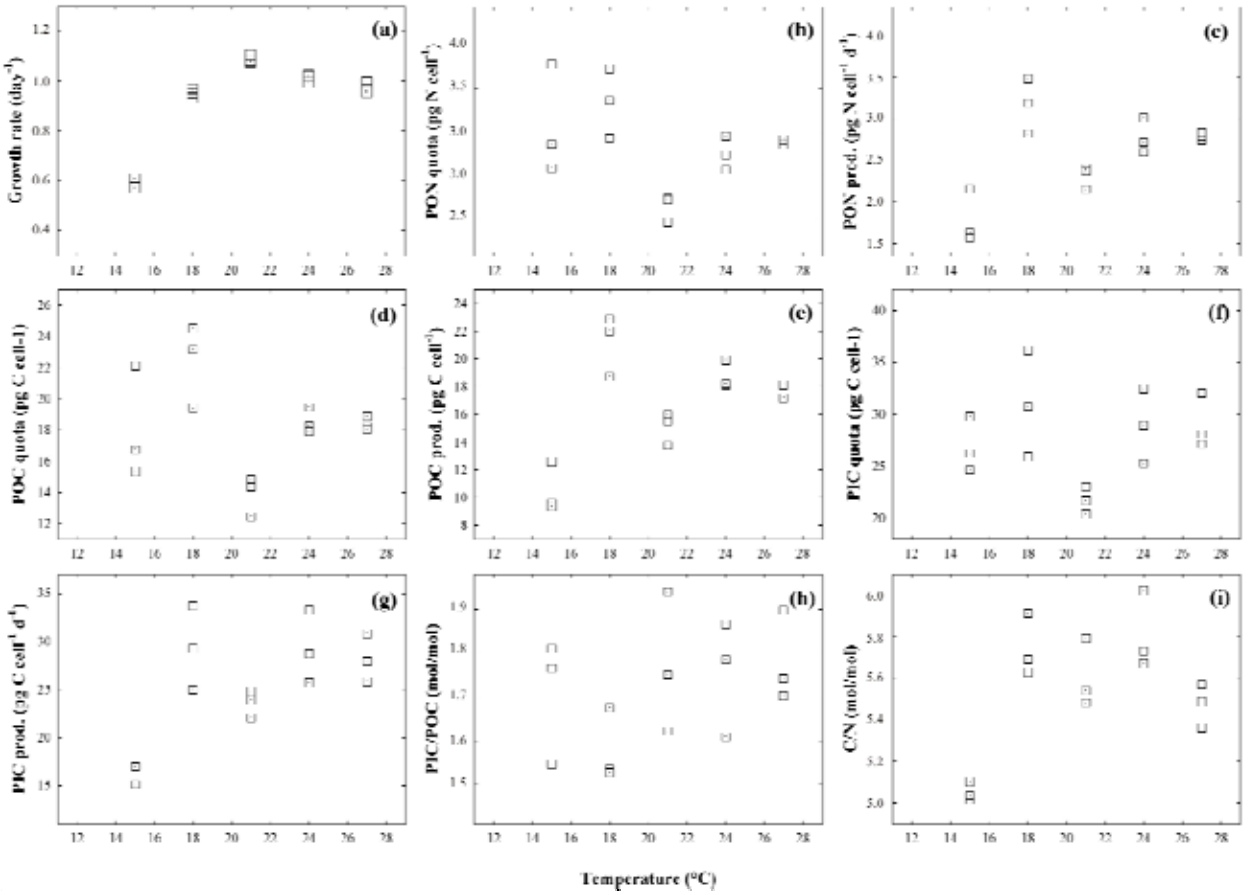

Fig. 8.9. Relationship of *Gephyrocapsa oceanica* physiological parameters with the incubation temperature: (a) growth rate, (b) PON quota, (c) PON production, (d) POC quota, (e) POC production, (f) PIC quota, (g) PIC production, (h) PIC/POC, and (i) C/N.

This means that the Mg/Ca incorporation may actually be controlled by the growth rate at least in *G. oceanica* as for Sr/Ca. For Sr/Ca there is a positive increasing correlation following the equation:

$$Sr/Ca_{cal} = 0.6845\ T^2 + 0.0037\ T + 0.3811 \quad (4)$$

Sr/Ca is tightly controlled by the GR, which is actually depends on the temperature (Eq. 2). Both Mg and Sr incorporation have a biological component but also that temperature regulates several physiological processes that depend on this variable. Our results suggest that using the species *G. oceanica* in combination with the new cleaning protocol presented in Chapter 7, we can for the first time derive a paleo temperature proxy and further constraint the paleo productivity proxy. This should be guaranteed by picking up the species in question from the sediments (Stoll et al. 2007; Stoll and Shimizu 2009). However, we suggest that problems may arise owing to the strain-specific responses presented in this chapter for *E. huxleyi*. It is therefore urgent to assess if

different strains of *G. oceanica* also respond different to the same temperature to start using general equations for the species.

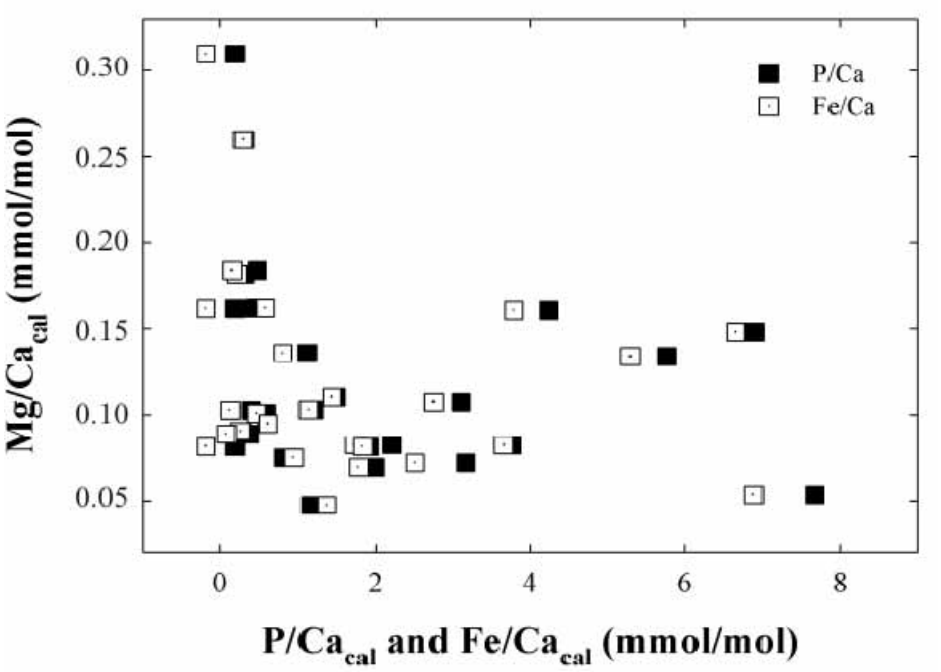

Fig. 8.10. Relationship of *Gephyrocapsa oceanica* Mg/Ca_{cal} with the contamination proxies for organic-Mg (P/Ca_{cal} and Fe/Ca_{cal}).

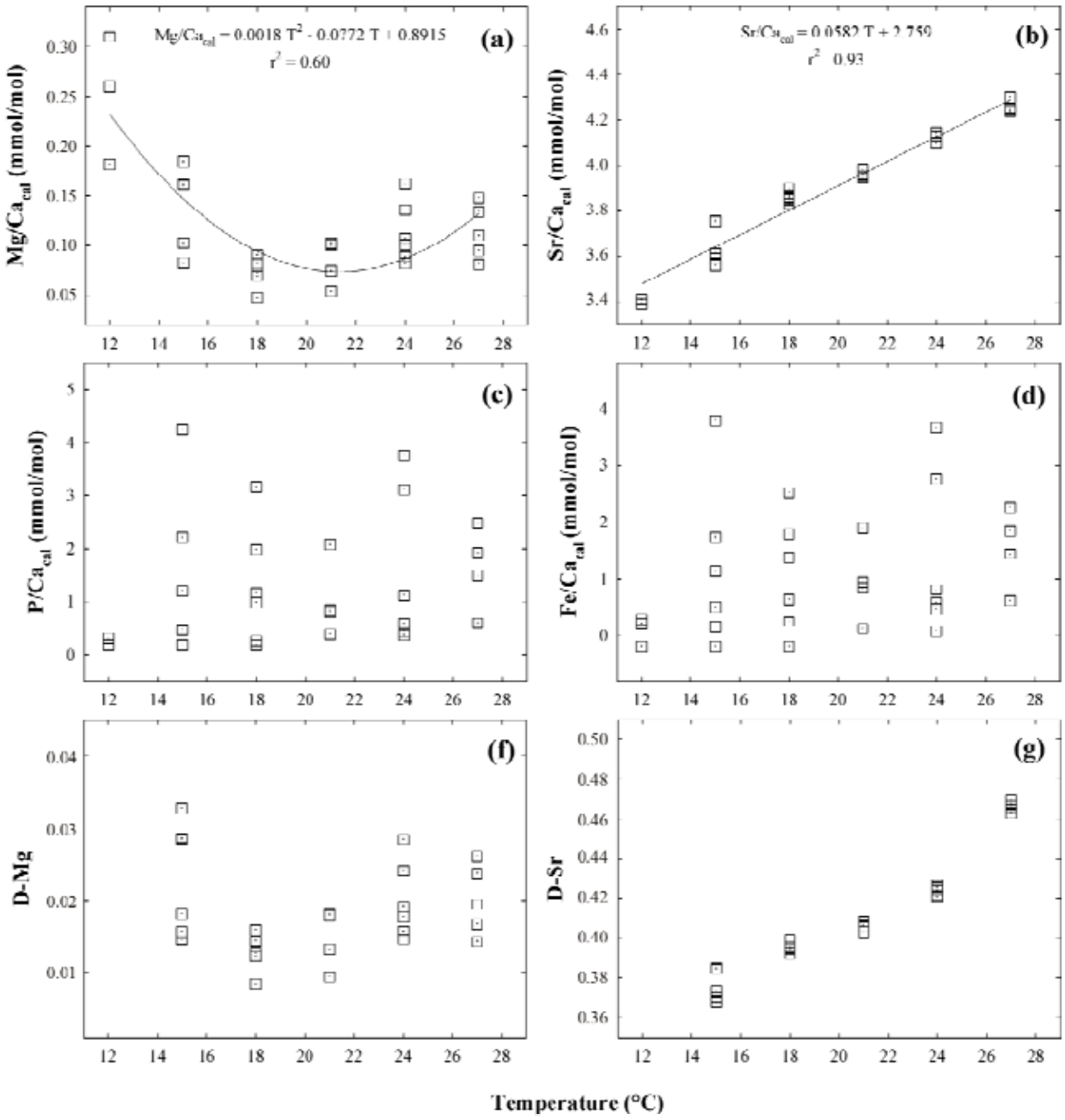

Fig. 8.11. Correlation of *Gephyrocapsa oceanica* Mg/Ca_{cal} and Sr/Ca_{cal} ratios (a, b), contamination proxies P/Ca_{cal} and Fe/Ca_{cal} (c, d), and diffraction coefficients (D-Mg and D-Sr) with incubation temperature.

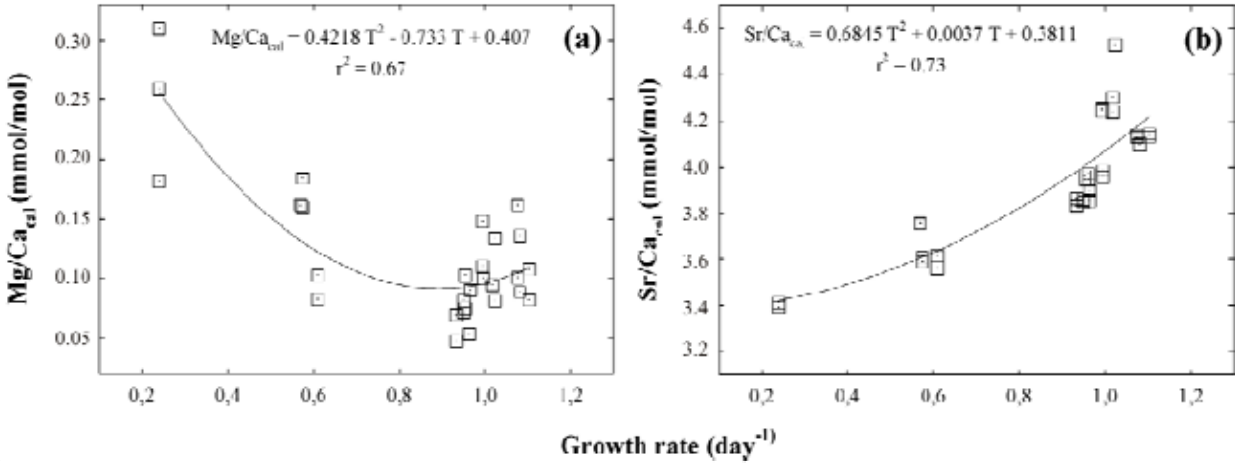

Fig. 8.12. Correlation of *Gephyrocapsa oceanica* Mg/Ca_{cal} and Sr/Ca_{cal} ratios (a, b) with the growth rate as a function of temperature

9.

The future of marine calcification

Abstract

The production of calcium carbonate ($CaCO_3$) or "calcification" is a critical process in biota and the Earth's carbon cycle. Marine calcifying organisms use calcium (Ca^{2+}) and carbonate ions (CO_3^{2-}) to form calcium carbonate ($CaCO_3$). A current concern is that anthropogenic carbon dioxide (CO_2) emissions have caused the oceans to become acidified, resulting in low levels of pH and CO_3^{2-} ions and high levels of CO_2 and bicarbonate ions (HCO_3^-) relative to pre-industrial conditions, a process we refer to as "ocean bicarbonation". The decline in CO_3^{2-} associated with "ocean bicarbonation" may negatively impact calcifiers that rely on the CO_3^{2-} ion for calcification. However, in some taxa, calcification increases when external HCO_3^- levels increase, and it is argued that these organisms can convert HCO_3^- to CO_3^{2-} for calcification by removing protons from the calcification reservoir, for which efficient proton pumps are needed. Here, we explore the effect of changes in bicarbonate ion concentration on calcification and assess coccolithophores as a case study in calcification responses to "bicarbonated oceans". We propose that in future "bicarbonated oceans", calcification will be controlled by organisms' ability to acquire HCO_3^- and convert it to CO_3^{2-} via efficient proton pumping.

This chapter is based on:

Iglesias-Rodriguez, M. D., **Lebrato, M.,** Buitenhuis, E., Ries, J., Gibbs, S. J., Schofield, O. M. and Lampitt, R. S. in review. The future of marine calcification. In: *Nature Climate Change*.

Acknowledgements: This work was supported by the "European Project on Ocean Acidification" (EPOCA) (FP7/2007-2013 under grant agreement n° 211384) for MDI-R and the PhD of ML. We thank Kate Davis for technical help with illustrations.

9.1. Introduction

In the marine environment, a wide range of planktonic (e.g., coccolithophores, foraminifera, pteropods, fish) and benthic groups (e.g., green and red algae, bivalves, gastropods, corals, echinoderms, crustacea, foraminifera, serpulid worms, bryozoa, sponges) produce the mineral calcium carbonate ($CaCO_3$) in the form of one of its polymorphs, calcite, aragonite or 'high-Mg calcite' (mol % $MgCO_3 > 4$), each with distinct susceptibilities to dissolution (Morse et al. 2006; Lebrato et al. 2010). In these organisms, the substrate of carbon for calcification is the carbonate ion (CO_3^{2-}) but this may be limiting for calcification because (a) CO_3^{2-} represents only 15% of the total dissolved inorganic carbon (DIC) species, and (b) CO_3^{2-} ions do not go through cellular membranes and therefore an alternative source of DIC species must be imported into the calcification reservoir to maintain calcification.

Carbon dioxide (CO_2)-induced ocean acidification will lead to "bicarbonated oceans", with high concentrations of CO_2 and bicarbonate ions [HCO_3^-] and low pH and CO_3^{2-} ion concentrations, relative to pre-industrial conditions (Fig. 9.1). The extent to which organisms can maintain calcification rates inside their calcification reservoir will be largely dependent upon the efficiency of trans-membrane ion-pumps that maintain pH, [CO_2], [CO_3^{2-}], [HCO_3^-] and [Ca^{2+}] at levels conducive to calcification. However, there is still considerable uncertainty as to (a) the effect of changes in seawater chemistry on the delivery of substrates for calcification, namely DIC species and Ca^{2+}, to the biomineralization compartment and (b) the mechanisms controlling changes in the ratios of carbon species (CO_2, HCO_3^-, CO_3^{2-}) within these compartments.

Different methods of manipulating seawater pH (bubbling with CO_2 enriched air *vs.* acid/base addition) yield different inorganic carbon species in seawater (Iglesias-Rodriguez et al. 2008a; Hurd et al. 2009; Gattuso et al. 2010), although a comparison of some of these methods has revealed similar responses in some coccolithophore species (Shi et al. 2009; Hoppe et al. 2011). Cellular models of calcification based on physiological experimentation suggest that CO_2 and HCO_3^- are the only DIC species that can be transported into the calcification reservoir (Fig. 9.2). However, the extent to which changes in inorganic carbon species in seawater affect the carbon chemistry of the calcification fluid remains largely unexplored. Although CO_3^{2-} is the carbon substrate for calcification ($Ca^{2+} + CO_3^{2-} \rightarrow CaCO_3$), increases in CO_2 and particularly HCO_3^- outside the calcification compartment are known to promote calcification in several calcifying taxa (Marubini and Thake 1999; Bentov et al. 2009; Jury et al. 2010). Under current seawater

conditions, the concentration of bicarbonate ions represents > 85 % of the DIC and in "bicarbonated oceans", its contribution to DIC will be even higher. Calcification responses to changing concentrations of DIC species in seawater are however typically reported as a function of pH, CO_2 and CO_3^{2-} levels and the role of HCO_3^- has generally been overlooked. This is also important because DIC speciation can vary significantly across different methods of manipulating pH (e.g., CO_2-bubbling *vs.* HCl acid addition[5]). In what follows, we present a brief account of the effects of changing carbon chemistry on marine calcification, and re-analyze data from experiments using different coccolithophore species and strains to reveal that some variability in calcification responses to ocean acidification may be explained by changes in seawater HCO_3^- concentrations.

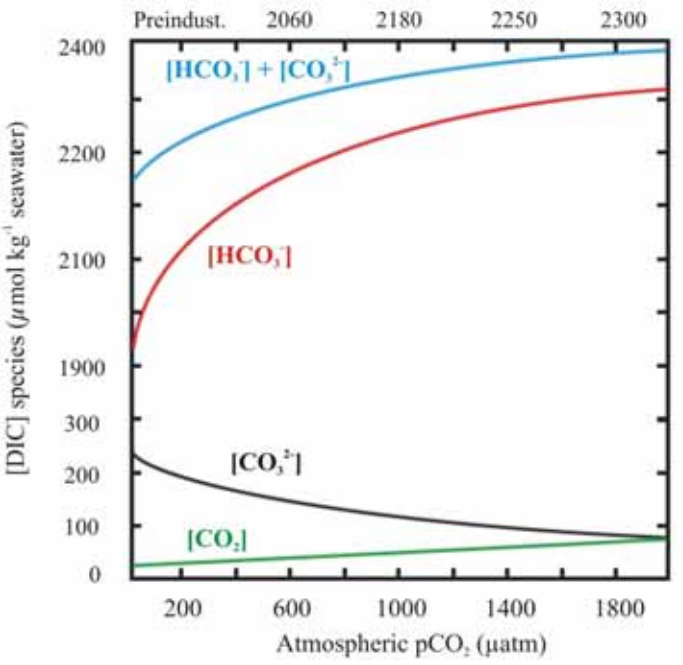

Fig. 9.1. Speciation of dissolved inorganic carbon in seawater as a function of increasing atmospheric pCO_2. $[HCO_3^-]$ and $CO_{2(aq)}$ increase with atmospheric pCO_2 as $[CO_3^{2-}]$ decreases. The decline in $[CO_3^{2-}]$ is more than offset (on a molar basis) by the rise in $[HCO_3^-]$ in terms of their contribution to total DIC. Calcification within marine organisms that utilize HCO_3^-, or a combination of CO_3^{2-} and HCO_3^-, in their calcification process may thus be enhanced under conditions of elevated atmospheric pCO_2. Calcifying organisms that utilize CO_2 directly via photosynthesis may also benefit from the rise in dissolved CO_2.

9.2. Physiological considerations

Typically, the mean pH in the cytosol, nucleoplasm, mitochondria, and plastid stroma of cells is between 7.1 and 7.8 (Raven et al. 1980; Anning et al. 1996; Venn et al. 2009), which is significantly lower than the average surrounding seawater pH (~8.1). In the calcification reservoir, elevated pH (>8.1) is thought to be regulated by voltage-gated H^+ channels, which play an important role in regulating intracellular pH (Taylor et al. 2011), thereby ensuring that carbonate ions in the calcifying fluid are kept at concentrations that promote calcification. In the metabolic compartments of calcifiers, CO_2, Ca^{2+}, HCO_3^- and CO_3^{2-} as well as oxygen (O_2), are maintained at different ratios depending on the metabolic rates and the energetic and catalytic requirements at the sites of photosynthesis, calcification, and respiration.

Photosynthesis and respiration are a sink and a source of CO_2, respectively. The biological regulation and biochemical consequences of calcification are, however, less clear. Although calcification uses CO_3^{2-} ions, unlike HCO_3^- ions and CO_2, which can cross cell membranes, there is no evidence of CO_3^{2-} transport across membranes. Therefore, it is assumed that HCO_3^- and/or CO_2 are imported into the calcification reservoir and, once inside, elevated pH with respect to the cytosol/external medium ensures conversion of part of the imported HCO_3^- or CO_2 into CO_3^{2-} ions (Allemand et al. 2004) (Fig. 9.2). This conversion requires efficient proton pumps to extrude H^+, thereby preventing acidification of the calcification fluid and the resulting decrease in calcification rates and/or increase in shell dissolution ($CaCO_3 + H^+ \rightarrow Ca^{2+} + HCO_3^-$). The supply of Ca^{2+}, whose concentration in seawater is two orders of magnitude that of CO_3^{2-}, can be controlled by Ca^{2+} stimulated V-ATPases (Araki and Gonzalez 1998). In corals, a Ca^{2+}/H^+ exchanger by which two H^+ are removed and one Ca^{2+} ion is transported into the calcification reservoir appears to serve as both a supply of Ca^{2+} ions and a homeostatic mechanism in the calicoblast (Cohen et al. 2009).

A recent study revealed that in two coccolithophore species, *Emiliania huxleyi* and *Coccolithus pelagicus*, intracellular $CaCO_3$ precipitation utilizing HCO_3^- generates protons that are rapidly extruded through the membrane *via* membrane voltage-gated H^+ in order to prevent acidification and maintain pH homeostasis (Taylor et al. 2011). The protons generated by the conversion of HCO_3^- to CO_3^{2-} were thought to increase the CO_2 availability for ribulose-1,5-bisphosphate carboxylase oxygenase (RuBisCO), particularly for the coccolithophore species *E. huxleyi*, where photosynthesis is not saturated at the ambient CO_2 levels in seawater (Paasche 1964). However, the physiological feedbacks between calcification and photosynthesis are still unclear. The coupling between photosynthesis and calcification has been proposed in coccolithophores (Buitenhuis et al. 1999), calcareous algae (Ries et al. 2010), and corals (Gattuso et al. 1999), whilst others have found that photosynthesis and calcification are decoupled in coccolithophores (Buitenhuis et al. 2001), and corals (Gattuso et al. 2000), and in some cases calcification continues in the dark, when calcification is downregulated (Trimborn et al. 2007; Leonardos et al. 2009). Furthermore, in experiments using media without Ca^{2+} to prevent calcification, no detectable effect on organic carbon production suggests that photosynthesis can be decoupled from calcification (Hertfort et al. 2002; Trimborn et al. 2007; Leonardos et al. 2009).

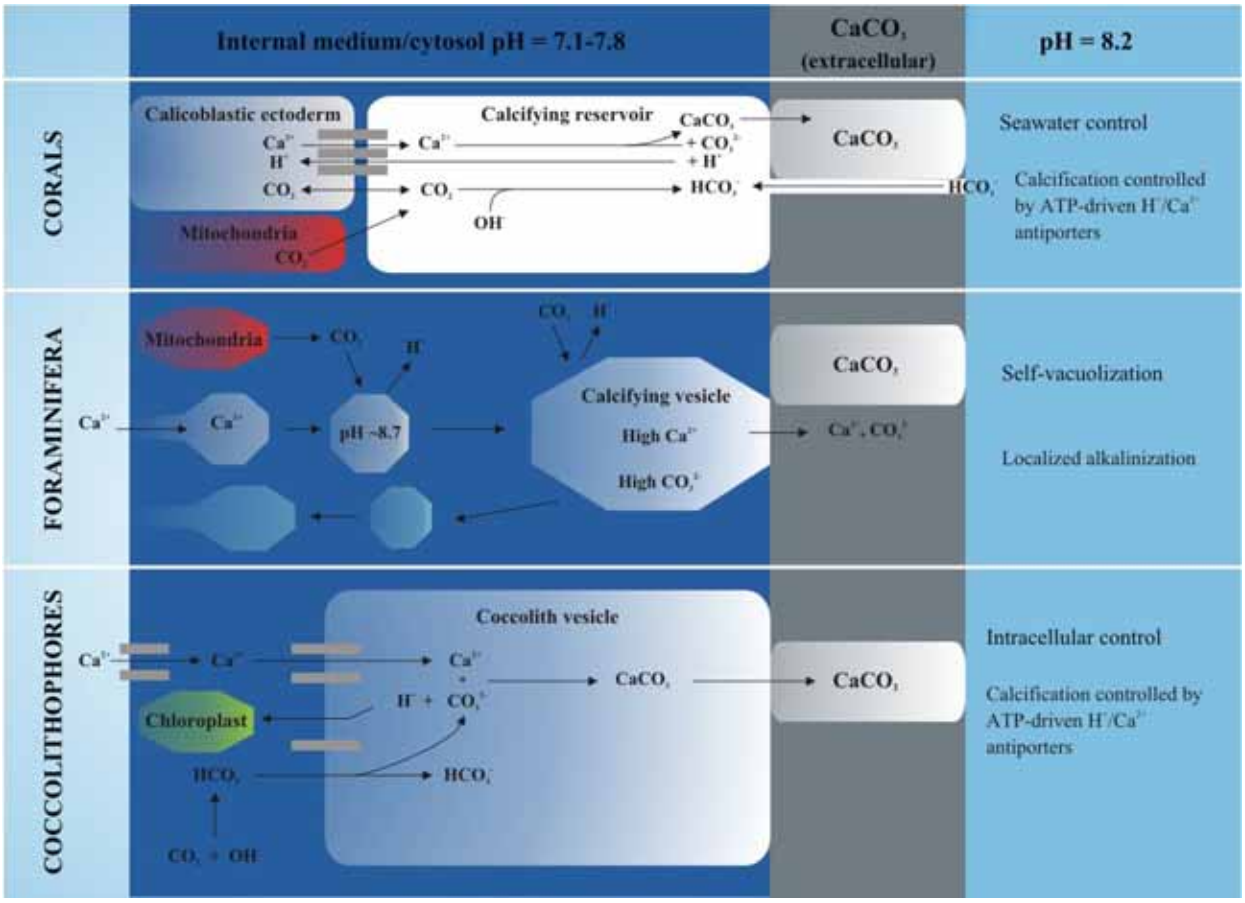

Fig. 9.2. Models describing possible calcification mechanisms in organisms that calcify extracellularly (corals, foraminifera) and intracellularly (coccolithophores). Most calcifying organisms maintain a region of calcification that is isolated from ambient seawater. The rate of calcification is likely dependent upon the organisms' ability to maintain an elevated $CaCO_3$ saturation state ($[Ca^{2+}]$, $[CO_3^{2-}]$) by exchanging Ca^{2+} and H^+ ions via a network of Ca^{2+}-ATPases and ion pumps (Allemand et al. 2004; Taylor et al. 2011). The pH of the calcifying fluid of tropical scleractinian corals (De Beer et al. 2000; Bown 2005) and some benthic foraminifera (Bentov et al. 2009) is thought to be 9.0-9.5 and ~8.7, respectively. In contrast, the pH of the organisms' cytosolic fluid is thought to be 7.2-7.5 (Venn et al. 2009).

Compartmentalization of calcification (e.g., intracellular biomineralization), and the formation of external organic layers can act as a form of protection of the biomineral from degradation and may explain the apparent resilience of some calcifiers to changes in the carbonate chemistry of seawater over the geological time scales described below. In coccolithophores, $CaCO_3$ crystals are produced intracellularly, organized into coccolith structures, coated by an organic film of polysaccharides and finally extruded across the plasma membrane. This layer is thought to protect the crystal from dissolution (Young et al. 2003), similar to the epicuticle in crustacea and echinoids, periostracum in mollusks, ectoderm in corals, and utricles in calcifying algae (Ries et al. 2009). These protective organic coverings (De Jong et al. 1976; Rodolfo-Metalpa et al. 2011), along with efficient proton pumping, and the ability to utilize CO_2 directly via

photosynthesis are amongst the most important factors controlling the calcification response of marine organisms to CO_2-induced ocean acidification (Ries et al. 2009).

9.3. Mechanisms of calcification in marine organisms

Different calcifiers possess various catalytic mechanisms and cellular calcification compartments to maintain a supply of Ca^{2+} and inorganic carbon during the process of $CaCO_3$ formation. In corals, for example, the calcifying reservoir is in indirect contact with seawater, and the extent of calcification appears to be critically dependent upon the ability of the organism to maintain elevated Ca^{2+} and pH via Ca^{2+}-ATPases and/or H^+ pumps, respectively (Cohen et al. 2009) (Fig. 9.2, 9.3). The extent to which some corals control inorganic carbon fluxes is exemplified in the species *Stylophora pistillata*, in which metabolic DIC is the source of 70-75% of the total carbon incorporated into the coral's skeleton (only 25-30 % originates from the external seawater) (Furla et al. 2000). The ability of some corals to calcify in the absence of photosynthesis (which elevates pH of the calcifying fluid via the removal of CO_2) suggests that they may exert strong physiological control (independent of photosynthesis) over the carbonate chemistry of their calcifying fluid (Ries 2010; Rodolfo-Metalpa et al. 2010; Trotter et al. 2011).

In some foraminiferal groups (including benthic), vacuolization of external seawater has been proposed as one mechanism forming the calcification reservoir with high Ca^{2+} concentrations (10.5 mmol kg^{-1} compared with <1 μmol kg^{-1} in the organism's cytosol) (Bentov et al. 2009). Active proton pumps control the pH in these vacuoles and DIC enters the vacuole by diffusion of $CO_{2(aq)}$ from the low-pH cytosol (pH~7.2-7.5) into the alkaline vacuole (pH~8.7), maintaining elevated concentrations of CO_3^{2-}. These vacuoles, enriched in [Ca^{2+}] and [CO_3^{2-}], fuse with the cell membrane and supply ions for calcification. Coccolithophore intracellular calcification, on the other hand, is completely isolated from the external seawater (Fig. 9.2). In the absence of a known trans-membrane CO_3^{2-} ion transporter, one way for corals to increase the concentration of CO_3^{2-} at the site of calcification is to import HCO_3^- or CO_2 into the calcification reservoir, and then convert the resulting HCO_3^- into CO_3^{2-} by extruding protons, pursuant to the carbonate equilibria:

$CO_2 + H_2O \rightarrow H_2CO_3$

$H_2CO_3 \rightarrow H^+ + HCO_3^-$

$HCO_3^- \rightarrow H^+ + CO_3^{2-}$

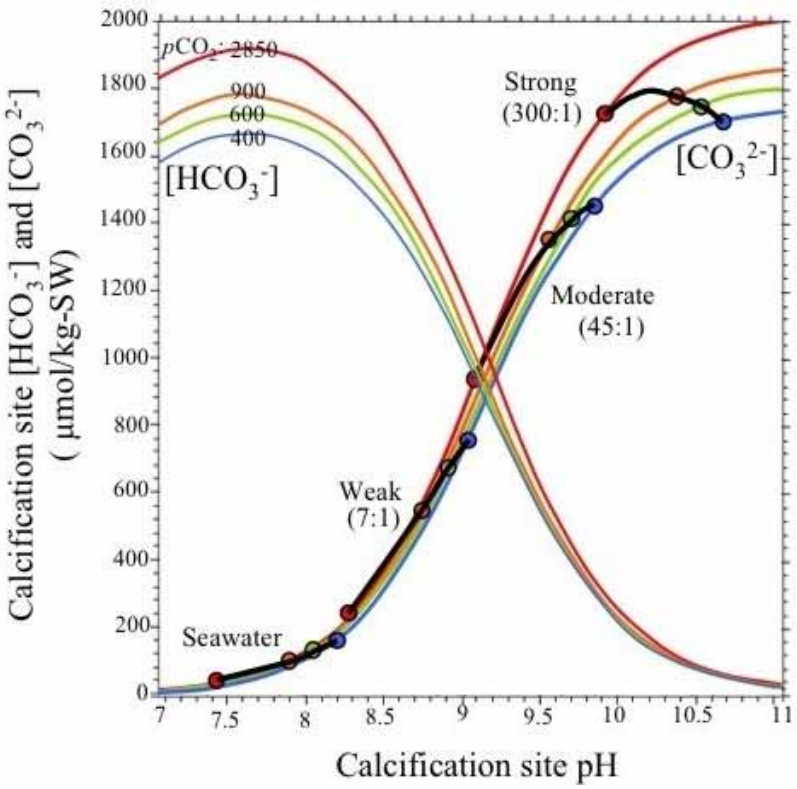

Fig. 9.3. Putative proton-pumping mechanism by which some marine calcifiers indirectly utilize HCO_3^- in the calcification process. The negative impact of ocean acidification on the calcification site [CO_3^{2-}] should be most severe for marine calcifiers with weak control over calcification site pH—e.g., those least able to convert HCO_3^- to CO_3^{2-} via proton-pumping. This simple model of indirect bicarbonate utilization via proton pumping is able to generate the full range of calcification responses observed in ocean acidification experiments (Fabry et al. 2008; Iglesias-Rodriguez et al. 2008a; Doney et al. 2009; Ries et al. 2009). Recent pH microelectrode measurements of the calcifying fluid of the temperate coral *Astrangia poculata* reveal that they maintain a fixed external:internal [H^+] ratio of approximately 85:1 (between strong and moderate), regardless of external seawater pH. External:internal [H^+] ratios are shown in parentheses.

Even in the absence of direct ion transport, CO_2 should diffuse into the coral's calcifying reservoir as the organism respires. This has been proposed as a mechanism for elevating levels of dissolved inorganic carbon in the calcification fluid (Erez et al. 2011). The negative impact of "bicarbonated oceans" on [CO_3^{2-}] at the calcification site should be most severe for marine calcifiers with weak control over calcification site pH—e.g., those least able to convert HCO_3^- to CO_3^{2-} via proton-extrusion (Ries 2011) (Fig. 9.3).

Experiments investigating the effect of decreased CO_3^{2-} and increased HCO_3^- and/or CO_2 on organism physiology have shown a variety of responses. Although many organisms exhibit a relatively linear decline in calcification under conditions of elevated pCO_2, rates of calcification in some organisms appear to be unaffected, vary in a non-uniform way, or increase in response to moderate elevations in

pCO_2 (Riebesell et al. 2000; Zondervan et al. 2002; Orr et al. 2005; Langer et al. 2006; Iglesias-Rodriguez et al. 2008b; Wood et al. 2008; Clark et al. 2009; Doney 2009; Hendriks et al. 2009; Shi et al. 2009; Ries et al. 2009, 2010; Cohen et al. 2010; Comeau et al. 2010; Hofmann et al. 2010; Rodolfo-Metalpa et al. 2010).This variable pattern has been observed for some species of coccolithophores, echinoids, crustaceans, calcareous green and coralline red algae, molluscs, and corals, suggesting that bicarbonate, in addition to carbonate, may be an important source of carbon for calcification within these taxa. This inference is bolstered by other experiments showing that calcification is enhanced by addition of HCO_3^- to seawater (Marubini and Thake 1999; Jury et al. 2010).

9.4. What controls the variability in calcification? Case study: coccolithophores.

The concentration of HCO_3^- is more than an order of magnitude greater than that of CO_3^2 and, unlike CO_3^{2-}, HCO_3^- can cross the plasma membrane of cells. It is therefore reasonable to expect that HCO_3^- import into the calcification reservoir would confer an evolutionary advantage to $CaCO_3$-producing organisms. In coccolithophores, there is strong evidence suggesting that HCO_3^- is the inorganic carbon species that crosses the cell membrane to be subsequently converted into CO_3^{2-} within the calcification reservoir to produce $CaCO_3$ (Sikes et al. 1980; Buitenhuis et al. 1999; Herfort et al. 2002; Paasche 2002). Here, we present a reanalysis of a number of datasets to compare studies on marine coccolithophore species in which the carbonate chemistry was manipulated through acid/base addition, *via* the bubbling of CO_2-air gas mixtures or through HCO_3^- addition. Unlike most ocean acidification studies, which express calcium carbonate production as a function of only CO_3^{2-} or CO_2, we re-assess calcification data by also considering HCO_3^- concentrations employed in studies using several strains of *E. huxleyi* and one strain of *Gephyrocapsa oceanica*. We used *G. oceanica* because it is closely genetically related to *E. huxleyi* (Fujiwara et al. 2001) and these species diverged only ca. 290,000 years ago (Verbeek 1990; Raffi et al. 2006), making *E. huxleyi* the youngest coccolithophore species. However there are groupings within *E. huxleyi* based on fine scale genetic differences (Medlin et al. 1996; Iglesias-Rodriguez et al. 2006) and morphological characteristics, confirmed by genetic identity.

Despite their inter- and intraspecific genetic and physiological variability in coccolithophores, our approach reveals some agreement between studies on *E. huxleyi* that used experimental methodologies that generated different ratios of alkalinity, bicarbonate, and carbonate ions (Fig. 9.1). Our analysis reveals that calcification rates are best correlated with HCO_3^- for *E. huxleyi* and with CO_3^{2-} for *G. oceanica* (Figure 4). Thus, CO_2 and CO_3^{2-} appear not to be the primary variables regulating cellular calcification within *E. huxleyi* between seawater pH 7.5 and 8.5, which encompasses the range of values predicted for the next 500 years (Doney 2009). Despite the extremely close phylogenetic relationship between these coccolithophore species, it is possible that the disparity in their responses to CO_2-induced ocean acidification arises from the studied strains of *E. huxleyi* having a more efficient mechanism for removing protons from their calcifying medium than the *G. oceanica* strain, thereby enabling more efficient conversion of HCO_3^- to CO_3^{2-} for calcification (Fig. 9.4). A recent study by Beaufort et al (2011) revealed that differentially calcified species and morphotypes are distributed in the ocean according to carbonate chemistry, suggesting some taxonomic specificity in the coccolithophore response to "bicarbonated oceans". These findings have implications for the analysis of the geological record, as well as for latitudinal adaptation to changing CO_2.

9.5. What have we learned from the past?

Throughout their evolutionary history, coccolithophores are one of the best preserved calcifying groups. They exhibit high diversity and abundance over a wide range of pCO_2, temperature, and Mg/Ca regimes (Bown et al. 2004), suggesting that they are an ecophysiologically versatile group. Over these geologic timescales, coccolithophores have demonstrated an ability to adapt to long-term (e.g., >100,000 years) changing seawater chemistry. However, even though atmospheric CO_2 levels and carbonate chemistry changes do not appear to be a dominant control on long-term coccolithophore abundance and diversity, it is worth noting that their initial appearance in the fossil record may have been linked to a long-term decline in atmospheric pCO_2 and a decrease in seawater Mg/Ca in the early Mesozoic (Erba 2006). Molecular data suggest that calcifying haptophytes (Calcihaptophyceae) originated around the Permian/Triassic (P/T) boundary, ca. 250 million years ago (Falkowski et al. 2004) and identification of coccoliths in late Triassic strata suggests that these algae evolved coccolithogenesis soon after their genetic differentiation (Bown et al. 2004). The surface water conditions of the early Mesozoic might have favoured the largely low-Mg calcitic mineralogy of coccolithophores

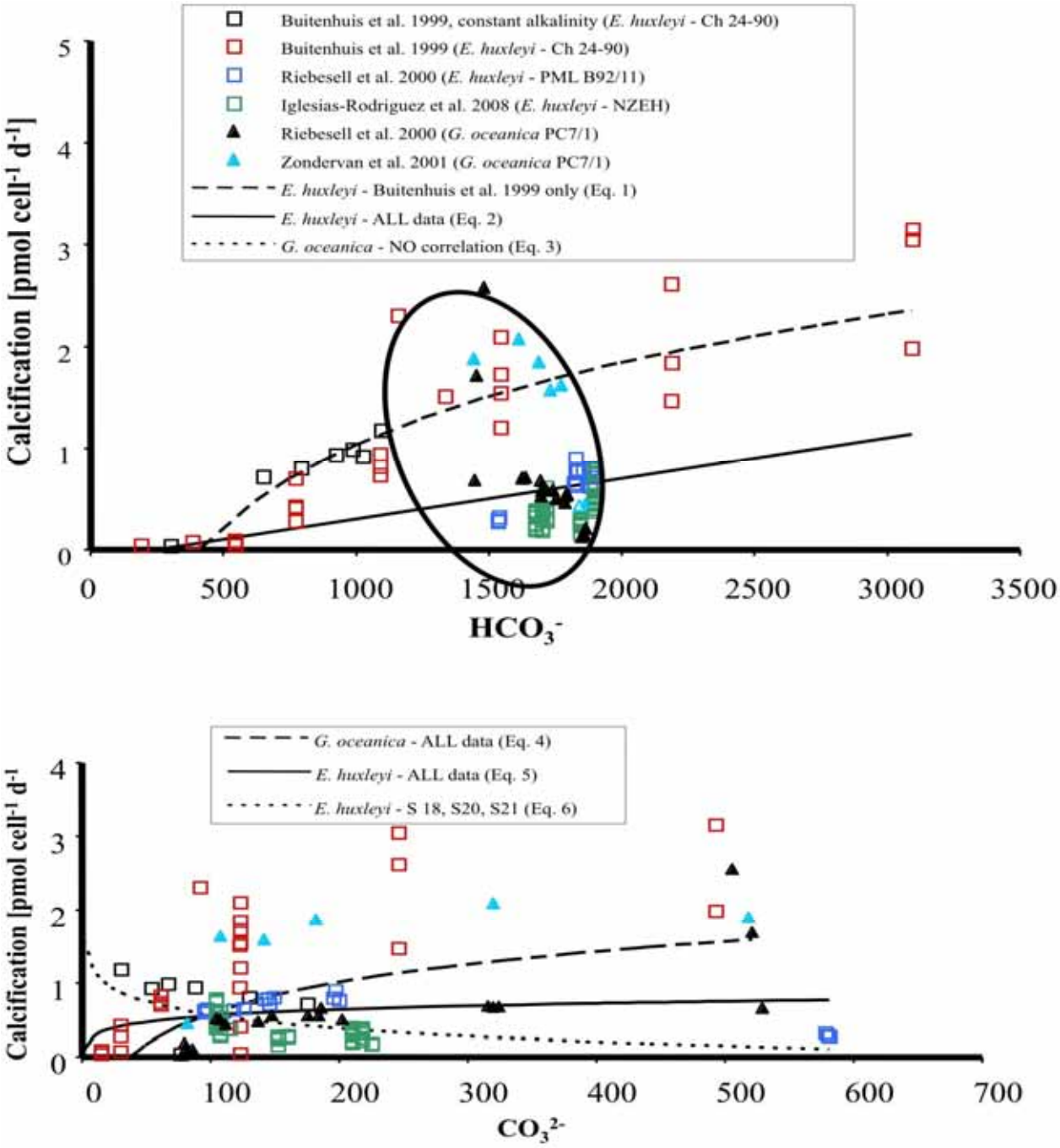

Fig. 9.4. Coccolithophorid calcification as a function of $[CO_3^{2-}]$ and $[HCO_3^-]$. Calcification in *E. huxleyi* varies primarily as a function of $[HCO_3^-]$ (*see* Eq. 1 below), and is anticorrelated with $[CO_3^{2-}]$ in the Buitenhuis et al. (1999) constant alkalinity data, and in Riebesell et al. (2000), and Iglesias-Rodriguez et al. (2008a) data (*see* Eq. 6 below). The correlation between calcification and $[CO_3^{2-}]$ in the Buitenhuis et al. (1999) data is due to correlation between $[HCO_3^-]$ and $[CO_3^{2-}]$ at fixed pCO_2, which gives the widest range of $[CO_3^{2-}]$. The Buitenhuis et al. (1999) data including constant alkalinity data for *E. huxleyi* were fit to the equation: calcification = 6.4 pmol cell^{-1} d^{-1} * (HCO_3^- - 506 µmol L^{-1})/(HCO_3^- - 506 + 2750 µmol L^{-1}). The Riebesell et al. (2000) *G. oceanica* data were fit with the regressions: calcification = 0.72 pmol cell^{-1} d^{-1} * (CO_3^{2-} - 68 µmol L^{-1})/(CO_3^{2-} - 68 + 20 µmol L-1). Both regressions are standard saturation curves following Michaelis-Menten kinetics.

Eq. (1): $\underline{y = 1.17 \text{ Ln } (x) - 7.06}$ ($r^2 = 0.78$. $F_{1,29} = 10.56$, $P < 0.01$), Eq. (2): $\underline{y = 4x10^{-4} (x) - 0.11}$ ($r^2 = 0.24$. $F_{1,123} = 6.47$, $P < 0.01$), Eq. (3): no correlation, Eq. (4): $\underline{y = 0.61 \text{ Ln } (x) - 2.24}$ ($r^2 = 0.34$. $F_{1,22} = 3.56$, $P < 0.01$), Eq. (5): $\underline{y = 0.12 \text{ Ln } (x) - 0.01}$ ($r^2 = 0.02$. $F_{1,109} = 1.58$, $P = 0.11$), Eq. (6): $\underline{y = -0.26 \text{ Ln } (x) + 1.75}$ ($r^2 = -0.13$. $F_{1,85} = 3.75$, $P < 0.01$).

(Ridgwell 2005; Erba 2006) characteristically more resilient to dissolution than high-Mg calcite. However, although the overall pattern of diversity and apparent adaptability might suggest resilience to changes in ocean pH and Ca^{2+} levels, the timescales of change in environmental conditions and carbonate chemistry is key in considering their susceptibility to abrupt carbon cycle perturbations, such as that occurring today. On million year timescales, coccolithophores can clearly adapt. Yet we need to understand how they might respond to abrupt changes in surface water chemistry on the millennial or shorter timescales, during which time ocean chemistry is not buffered and pH and saturation state are both reduced. Currently, to constrain biotic sensitivity to surface water carbonate chemistry changes on millenial time scales is difficult (Gibbs et al. 2011) and, even for the most extreme of the Cenozoic global warming events, the Paleocene-Eocene Thermal Maximum (PETM) (Zachos et al. 2008), it is unclear whether there were actually significant surface water chemistry changes accompanying warming (Gibbs et al. 2010). We have only begun to independently constrain changes in pH, saturation state and DIC for the interval before modeled estimates (Ridgwell and Schmidt 2010). Thus, the minor biotic responses in taxonomic composition and calcification recorded for surface water calcifiers across the PETM may be commensurate with modeled chemical changes (Ridgwell and Schmidt 2010). Equally, however, the lack of an obvious calcification response suggests that the calcifiers were less sensitive than we might expect, or, we have yet to measure a parameter for biomineralization exhibiting sensitivity to the apparently minimal changes in carbonate chemistry changes across the PETM (Gibbs et al. 2010). Note that we do have examples in the fossil record of more extreme and rapid intervals of environmental change with accompanying dramatic biotic disruptions that includes calcifiers, for instance, the mass extinction at the Cretaceous/Tertiary boundary (Bown 2005). However, these events are notoriously difficult to interpret, not least because of the difficulty of teasing apart the effects of ocean acidification from other coeval environmental perturbations (e.g., light limitation, anoxia, sulphide poisoning, rapid cooling/warming). We thus have yet to identify a geological interval, for which both rates of change in ocean carbonate chemistry are unambiguously analogous to what is projected for the coming centuries and where we can realistically isolate the effects of changes in carbonate chemistry from changes in other environmental parameters.

9.6. Challenges and priorities for future research

To better understand how CO_2-driven changes in inorganic carbon chemistry impact calcification rates, changes in bicarbonate ions must be monitored as well as pH, CO_3^{2-} and CO_2. This is key to improve our knowledge of how organisms respond to changes in the speciation of dissolved inorganic carbon. This approach circumvents the problem of comparing results from different experimental pH manipulations (acid/base addition *vs.* bubbling the medium with air containing different CO_2 partial pressures), which results in comparable CO_2 levels but different HCO_3^- and CO_3^{2-} levels (Gattuso et al. 2010). Determining the form(s) of carbon that organisms use to calcify will aid in interpreting the variability in responses amongst organisms and in predicting which organisms may adapt to bicarbonated oceans. The exploitation of molecular technologies could assist our efforts to understand the basis for bicarbonate uptake and subsequent biomineralization, maintenance of homeostasis, processes that physically protect the biomineral, and polysaccharides and proteins that induce $CaCO_3$ nucleation and crystal growth (De Jong et al. 1976; Marsh et al. 1992). Our understanding should improve with the future publication of genomes from calcifying species and with concerted efforts to identify novel genes involved in inorganic carbon acquisition and calcification. *In situ* investigations of organisms living in areas that are already experiencing exposure to seasonally high CO_2 (e.g., upwelling events, polar seas, estuaries) will guide our choice of model organisms and should aid in predicting how ocean acidification will impact marine calcifiers in the immediate future.

10.

Effect of nutrients availability on *Emiliania huxleyi* (NZEH) physiology in different CO_2 scenarios

Abstract

Laboratory studies have so far separately considered the impact of high CO_2 seawater and macronutrient limitation on coccolithophore physiology. Nevertheless, in order to establish the effect of ocean acidification under different nutrient regimes, such as those observed in the field, the combined effect of nutrient variation/limitation and carbonate chemistry should be considered. Here we investigate the physiological performance of *Emiliania huxleyi* (strain NZEH) in a bivariate experiment. Organisms were exposed to three CO_2 levels (255, 527 and 1200 µatm) under three nutrient conditions [nutrient replete (R), phosphate limited (-P) and nitrate limited (-N)]. We focused on calcite and organic carbon production and on nitrate and phosphate utilization by analyzing the activity of alkaline phosphatase (APase) and nitrate reductase (NRase). With increasing CO_2, particulate inorganic (PIC) and organic carbon (POC) production under R conditions showed opposing trends than those found in other strains, but a similar pattern under nutrient limitation. The PIC:POC decreased with increasing CO_2 in -P and -N cultures but not in R cultures. Coccolith length increased with CO_2 under all nutrient conditions and was 5% larger under -P compared to -N and R conditions. Coccosphere volume in -P cultures 113 % higher than in R and -N conditions but its response to CO_2 depended on the nutrient condition. In all conditions, an increase in CO_2 caused a 20 % decrease in growth rate. Maximum APase activity was found under a CO_2 of ~ 527 µatm (pH 7.90) in -P cultures. NRase

expression increased with CO_2 under R conditions. Our results suggest that *Emiliania huxleyi*'s competitive ability for nutrient uptake might be altered in future high-CO_2 oceans. The variability observed in physiological parameters highlights the importance of multiparameter studies for a correct understanding of the ecological and biochemical roles of coccolithophores.

This chapter is based on:

Rouco-Molina, M., Branson, O., **Lebrato, M.** and Iglesias-Rodriguez, M. D. in review. The effect of nitrate and phosphate availability on *Emiliania huxleyi* physiology in different CO_2 scenarios. In: *Journal of Experimental Marine Biology and Ecology*.

Acknowledgements: We thank the financial support given to MR-M by the Spanish Ministry of Science and Education through the FPU PhD program. We thank Edward Smith, John Gittins, Sonya Dyhrman, Marilda Rigobello-Masini, and Chris Daniels for technical and laboratorial assistance. This research was funded by the "European Project on Ocean Acidification" (EPOCA) under grant agreement n° 211384 (to ML and MDI-R). This work was also funded in part by The European Research Council (ERC grant 2010-ADG-267931 to Harry Elderfield).

10.1. Introduction

Since the beginning of the industrial revolution, atmospheric CO_2 has increased at the fastest rate experienced by the Earth in the last 65 million years (Zachos et al. 2001). Consequently, the increase of CO_2 dissolution in seawater alters the balance of inorganic carbon species in the ocean, leading to a decrease in pH, which is predicted to intensify over the next century (Raven et al. 2005). Phytoplankton populations depend on the physicochemical properties of seawater, primarily light, temperature and macronutrient availability (e.g. carbon, nitrate and phosphate) (Mullin 2001). Variations in these factors drive population and community structure and consequently the efficiency of the biological carbon pump (Boyd et al. 2008). Coccolithophores play a major role in calcium carbonate ($CaCO_3$) cycling by producing between 0.6 and 1.6 Pg C yr^{-1} (Balch et al. 2007) and exporting between 0.4 and 0.6 Pg C yr^{-1} (Sarmiento et al. 2002; Honjo et al. 2008) in the open ocean (Gehlen et al. 2007). *Emiliania huxleyi* is the most abundant bloom-forming coccolithophore species widely distributed worldwide (Tyrrel and Merico 2004) and its physiological response to environmental change has been widely studied. *Emiliania huxleyi*'s calcification process is affected by variations in carbon chemistry (Riebesell et al. 2000; Iglesias-Rodriguez et al. 2008a; Langer et al. 2009b). However, it is also known that the response varies if other environmental parameters like nutrient availability, temperature or light are changed simultaneously (Sciandra et al. 2003; Feng et al. 2008; de Bodt et al. 2010; Borchard et al. 2011). Intraspecific variability between *E. huxleyi* strains also explains the diversity in *E. huxleyi* responses to increasing CO_2 (Langer et al. 2009b).

Nutrient availability in the ocean varies during the year, with a typical seasonal drawdown, with nitrate, phosphate and silicate been depleted in the summer. This governs phytoplankton seasonality and succession depending on nutrient utilization efficiencies and competitive abilities (Litchman et al. 2006). *Emiliania huxleyi* normally flourishes after the demise of diatoms, when silicate and other macronutrients (e.g. nitrate and phosphate) are limiting (Litchman et al. 2006). This advantage stems from a low nutrient quota and an extremely high phosphate affinity under phosphate-limiting conditions (Riegman et al. 2000). *Emiliania huxleyi* can also take up non-nitrate nitrogen compounds (Bruhn et al. 2010), and assimilate nutrients from organic sources through the controlled expression of enzymes active in specific metabolic pathways (Dyhrman and Palenik 2003; Bruhn et al. 2010). Despite the sensitivity of *E. huxleyi* to CO_2 and the diversity of nutrient acquisition pathways, the majority of the work to date has

not considered the effect of CO_2 concentration on their capacity for nutrient assimilation (Borchard et al. 2011). One example is the effect of pH changes associated with increased CO_2 on enzymatic activity (Yamada et al. 2010), which could influence *E. huxleyi* nutrient utilization and the seasonal phytoplankton succession.

Global warming derived from an increase in greenhouse gases enhances stratification of the water column and reduces water column mixing processes that maintain the nutrient supply. The duration, timing and biogeographical regions undergoing nitrate and phosphate limitation may thus vary in future oceans (Sarmiento 1998). Considering the prevalence of nutrient limitation it is important to investigate the effect of this condition along with ocean acidification. Two previous studies have independently investigated the responses of *E. huxleyi* to high CO_2 at constant temperature under nitrogen limitation (Sciandra et al. 2003) and rising temperature under phosphorus limitation (Borchard et al. 2011) using two different *E. huxleyi* strains (TW1 PML and B92/11 respectively). The *E. huxleyi* strain NZEH (CAWPO6) (isolated in the south Pacific Ocean) is very sensitive to CO_2 changes, showing variable calcification responses under increasing CO_2 compared to other strains (Riebesell et al. 2000; Iglesias-Rodriguez et al. 2008a, b; Shi et al. 2009) under nutrient replete conditions. In this study we assess for the first time in the same experiment the combined effects of high atmospheric CO_2 and nitrate and phosphorus limitation on the *E. huxleyi* NZEH strain physiology including calcification. We also investigate for the first time the effect of CO_2 on nitrate and phosphate utilization in coccolithophores by analysing the activity of two enzymes involved in nutrient assimilation. The enzymes are "alkaline phosphatase", which is involved in the cleavage of phosphate from organic compounds under phosphate limitation, and "nitrate reductase", which catalyses the reduction of nitrate to nitrate [the first step of nitrogen assimilation in the plant cell (Solomonson and Barber 1990)]. We highlight the importance of multivariate experiments as a tool to assess possible synergistic effects of ocean acidification and other environmental parameters such as nutrient limitation on *E. huxleyi* physiology.

10.2. Materials and Methods

10.2.1. Culture conditions

Experiments were conducted in dilute batch cultures with the *E. huxleyi* strain NZEH (CAWPO6), isolated in 1992 in the South Pacific Ocean and obtained from the Plymouth Culture Collection (UK). Artificial sea-water (ASW) was prepared according to Kester et al. (1967) with different nitrogen to phosphorus concentrations to achieve nutrient-replete (R), nitrate-limited (-N) and phosphate-limited (-P) conditions (Table 10.1). Trials were conducted prior to the final incubations to ensure that cultures reached nutrient limitation (stationary phase) at the desired cell density. The three nutrient regimes were combined with three CO_2 partial pressures (255 ±3.53, 527 ±44.7 and 1205 ±99.7 µatm) corresponding to pre-industrial levels, and predictions for the middle and the end of the century respectively (Table 10.1). The medium carbonate chemistry was adjusted by additions of sodium carbonate (Na_2CO_3) and hydrochloric acid (certified 3.571 mol L^{-1} HCl, Merck) to change the relative proportion of dissolved inorganic carbon (DIC) species and restore total alkalinity (TA) respectively (Riebesell et al. 2010). The conditions mimicked changes in carbonate chemistry associated with ocean acidification (CO_2 increases while TA remains constant at ~2268 ±64,86 µmol kg^{-1}) (Table 10.1). The culture medium was filtered through sterile 0.22 µm polycarbonate filters (Milipore® Stericup™ Filter Units). All other environmental parameters remained constant: salinity = 34.00 ±0.40, temperature = 19.00 ±0.50 ºC, 12:12 h light:dark cycle, irradiance = 120.00 ±15.00 µmol quanta m^2 s^{-1} under Sylvania Standard F36W/135-T8 white fluorescent lighting (Havells Sylvania, Newhaven, United Kingdom) throughout the experiments.

10.2.2. Incubation experiments

Experiments were conducted in triplicate in 4 L Nalgene® polycarbonate bottles. After the cell inoculation at an initial concentration of 100 cells ml^{-1}, the bottles were completely filled to minimize headspace, closed and sealed with Parafilm® until harvest. A blank control bottle (containing no cells) was incubated alongside each treatment, and an additional inoculated 'test' bottle was run simultaneously to allow daily monitoring of cell density, temperature, pH and irradiance. Cell densities at the time of harvest in R cultures were 75988 ± 13159 cells ml^{-1} depending on the treatments. Cells were harvested at a low density to avoid major changes in

carbon chemistry. The -N and -P cultures were harvested two days after exponential growth stopped (assessed by daily cell counts from the test bottle) allowing cells two remain in stationary phase for two days (cell densities at the time of harvest were 71587 ± 9250 and 43288 ± 14651 cells ml^{-1} for -N and -P cultures respectively). All cultures were grown for 8-10 generations, corresponding to a maximal DIC consumption of 12%. At time 0 (pre-inoculation) and during harvesting (always conducted three hours after the beginning of the light phase), samples were collected from all experimental bottles for analysis of carbon chemistry and macronutrient concentration in the medium, particulate organic carbon (POC), inorganic carbon (PIC), nitrogen (PON) and phosphorous (POP), cell density, and scanning electron microscope (SEM) imaging. Samples were also collected for alkaline phosphatase (APase) and nitrate reductase (NRase) assays.

10.2.3. Sample analysis

10.2.3.1. Growth rate and cell volume

Growth rate was determined with a standard exponential growth equation (Reynolds 1984):

$$\mu = [\mathrm{Ln}\,(N_t) - \mathrm{Ln}\,(N_0)] / t \qquad (1)$$

where N_t and N_0 are the cell densities at the start and at the harvest day respectively, and t corresponds to the length of incubation (in days). Cell density and cell volume were determined in triplicates using a Beckman Coulter Multisizer III with a 70 μm aperture.

Table 10.1. Medium carbonate chemistry parameters at the beginning and at end of the experiment.

	Nutrient condition	**Phosphate** (µmol kg^{-1})	**Nitrate** (µmol kg^{-1})	**DIC** (µmol kg^{-})	**TA** (µmol kg^{-})	**pH_{total}**	**pCO_2** (µatm)	**$[HCO_3^-]$** (µmol kg^{-})	**$[CO_3^-]$** (µmol kg^{-})	**CO_2** (µmol kg^{-})	**ΩCal.**
Initial [a]	R	3.51	161.21	1905.80	2229.80	8.20	258.30	1674.90	222.30	8.60	5.30
End [b]		2.98 ± 0.14	149.00 ± 10.40	1807.80 ± 4.90	2141.40 ± 3.80	8.20 ± 0.00	225.50 ± 2.10	1575.10 ± 5.40	225.20 ± 0.50	7.50 ± 0.10	5.40 ± 0.00
Initial	R	4.06	154.41	2040.30	2220.60	7.90	555.60	1890.10	131.60	18.50	3.20
End		2.61 ± 0.01	147.60 ± 0.85	1937.40 ± 5.50	2113.30 ± 6.90	7.90 ± 0.00	519.10 ± 8.70	1793.20 ± 5.10	126.80 ± 2.00	17.30 ± 0.30	3.00 ± 0.00
Initial	R	3.43	156.20	2238.30	2330.30	7.70	1073.10	2117.00	85.50	35.80	2.10
End		1.66 ± 0.05	149.44 ± 0.90	2101.60 ± 13.80	2178.70 ± 11.60	7.60 ± 0.00	1080.00 ± 27.10	1990.40 ± 13.70	75.10 ± 0.90	36.00 ± 0.90	1.80 ± 0.00
Initial	-N	3.61	3.71	1891.90	2221.00	8.20	250.00	1658.40	225.20	8.30	5.40
End		2.92 ± 0.35	0.25 ± 0.11	1733.50 ± 3.70	2021.40 ± 3.40	8.20 ± 0.00	251.30 ± 4.90	1533.50 ± 5.40	191.60 ± 2.50	8.40 ± 0.20	4.60 ± 0.10
Initial	-N	3.47	3.13	2085.00	2308.10	8.00	463.50	1908.60	160.90	15.50	3.90
End		2.87 ± 0.01	0.13 ± 0.02	1917.40 ± 3.70	2111.00 ± 4.80	7.90 ± 0.00	465.30 ± 3.80	1764.90 ± 3.20	137.00 ± 1.20	15.50 ± 0.10	3.30 ± 0.00
Initial	-N	3.48	3.31	2195.10	2263.50	7.60	1229.20	2081.90	72.20	41.00	1.70
End		1.55 ± 0.00	0.08 ± 0.03	1957.60 ± 3.00	1993.70 ± 1.10	7.50 ± 0.00	1357.70 ± 24.80	1860.20 ± 3.00	52.20 ± 0.80	45.30 ± 0.80	1.30 ± 0.00
Initial	-P	0.20	158.83	1897.10	2217.20	8.20	256.30	1666.70	221.90	8.50	5.30
End		0.04± 0.00	156.65 ± 0.21	1789.90 ± 7.00	2096.50 ± 7.60	8.20 ± 0.00	242.90 ± 2.80	1573.20 ± 6.70	208.60 ± 1.60	8.10 ± 0.10	5.00 ± 0.00
Initial	-P	0.19	159.53	2169.10	2362.70	7.90	560.80	2003.80	146.60	18.70	3.50
End		0.04 ± 0.01	153.31 ± 1.48	1890.10 ± 3.00	2108.80 ± 7.70	8.00 ± 0.00	394.20 ± 14.20	1722.70 ± 5.20	154.20 ± 4.70	13.10 ± 0.50	3.70 ± 0.10
Initial	-P	0.16	152.68	2186.00	2241.00	7.60	1313.70	2075.10	67.10	43.80	1.60
End		0.03 ± 0.00	151.50 ± 0.22	2098.10 ± 3.00	2152.80 ± 3.30	7.60 ± 0.00	1252.80 ± 7.70	1991.50 ± 2.80	64.80 ± 0.40	41.80 ± 0.30	1.60 ± 0.00

[a] Average blank values at the beginning of the experiment.

[b] Average values at the end of the experiment / **N**: nutrient replete; **-N**: nitrate limited; **-P**: phosphate limited conditions.

10.2.3.2. Lith length

Lith's length was measured from scanning electron microscopy (SEM) images. For SEM sample collection, a 25 mm MF 300 filter was soaked with a drop of dilute ammonium hydroxide and a polycarbonate filter (0.22 μm pore size) was placed on top. A few drops of culture were placed on the polycarbonate filter and samples were dried on an open Petri dish (37 ºC for 24 h). A section of the top filter was cut out and sputter-coated in a Hummer VI-A gold coater and a grid of 100 images at 5000x magnification was taken at a random location on each filter using a LEO 1450 VP SEM with SmartSEM V05-1 software. Every lith in an image was measured on consecutive images along their longest axis (defined as lith length) until at least 60 of each were measured.

10.2.3.3. Particulate matter

Particulate organic carbon (POC) and nitrogen (PON) concentrations were measured using a Thermo Finnigan Flash EA1112 elemental analyzer with acetanilide standards at Plymouth Marine Laboratory (PML). Aliquots of 200 ml were filtered through two pre-combusted (400 ºC for 4 h) MF 300 filters (25 mm glass microfiber 0.70 μm pore size, Fisherbrand). Filters were frozen (-20 ºC) until the end of the experiments and fumed with sulphurous acid for 24 h in a dessicator chamber to remove inorganic carbon (Verardo et al. 1990). The filters were then dried at 60 ºC for 16 h and pelleted in pre-combusted aluminium foil (EMA; 100 x 30 mm circles; Cat. No. D3066, following Hilton et al. 1986) before analysis. For particular inorganic carbon (PIC) analysis, 200 ml of medium was filtered through 0.20 μm 47 mm diameter Nuclepore polycarbonate filters, previously rinsed twice with 5 ml dilute ammonium hydroxide solution (pH ~ 9), and washed again three times after filtering. Filters were stored in clean 50 ml Falcon tubes at -20 ºC until analysis. Sample tubes and six additional blanks were then weighed, 15 ml of 0.10 M nitric acid added and re-weighed to determine the acid volume. The filters were left for 2-3 h with regular shaking, after which 500 μl of the acid leach was removed and centrifuged (9000 rpm for 6 min). A 250 μl aliquot of the supernatant was taken to determine elemental concentrations in a Varian Vista Pro ICP-OES. The Ca^{2+} per filter and per coccolithophore (using cell density) was then calculated and extrapolated to PIC, assuming that all Ca^{2+} on the filters originated in $CaCO_3$ (Fagerbakke et al. 1994). Particulate organic phosphorus (POP) was measured using a wet-oxidation method, as described by Raimbault et al. (1999). Medium

aliquots (200 ml) were filtered through a single pre-combusted (400 ºC for 4 h) MF 300 filter (25 mm glass microfiber 0.70 μm pore size, Fisherbrand). Samples were digested with sodium tetraborate and potassium persulphate, and autoclaved before analysis in a Segmented Flow Auto Analyser (SEAL QuAAtro) at the National Oceanography Centre (Southampton, U.K.). PIC production (P_{PIC}, pmol PIC cell^{-1} d^{-1}), POC production (P_{POC}, pmol POC cell^{-1} d^{-1}), PON production (P_{PON}, pmol PON cell^{-1} d^{-1}) and POP production (P_{POP}, pmol POP cell^{-1} d^{-1}), were calculated as follows:

$$P_X = \mu * (\text{cellular content}) \quad (2)$$

where X = PIC, POC, PON or POP; cellular content = cellular inorganic carbon content (pmol PIC cell^{-1}), cellular organic carbon content (pmol POC cell^{-1}), cellular organic nitrogen content (pmol PON cell^{-1}) or cellular organic phosphorus content (pmol POP cell^{-1}); and μ= growth rate.

10.2.3.4. Medium chemistry

Medium samples (20 ml) for nutrient determination were filtered through a Millex syringe-driven 0.22 μm filter (Millipore, Billerica, MA, U.S.A) and stored at -20 ºC until analysis. Macronutrient concentrations were determined colorimetrically following Hansen and Koroleff (1999) using a Segmented Flow Auto Analyser (QuAAtro. SEAL Analytical) at the National Oceanography Centre (Southampton). Samples for carbonate chemistry were collected in 300 ml borosilicate bottles and preserved with 750 μl 3.5% $HgCl_2$ solution to prevent microbial growth during storage. These samples were later analysed to determine total alkalinity (TA) and dissolved inorganic carbon (DIC) using a Versatile Instrument for the Determination of Titration Alkalinity (VINDTA) at the National Oceanography Centre (Southampton). The carbonate system was calculated from temperature, salinity, DIC, TA and nutrients using the "CO2SYS" macro (Lewis and Wallace 1998). The equilibrium constants were from Mehrbach et al. (1973), refitted by Dickson and Millero (1987), the KSO_4 constants were from Dickson (1990), and the seawater pH scale was used.

10.2.3.5. Determination of nitrate reductase activity

Aliquots of 400 ml were centrifuged (2000 g, 4 ºC, 15 min) and the resulting pellets were snap frozen in liquid nitrogen and stored at -80 ºC. Nitrate reductase (NRase) was extracted by adding 500 µl of a solution containing 0.20 mol L^{-1} phosphate buffer (pH = 8.20), 1 mmol L^{-1} dithiothreitol (DTT) and 0.50 M methylenediaminetetra-acetic acid (EDTA) to each pellet. The resuspended material was sonicated on ice for nine 10-s bursts (30 second intervals between bursts) using a VC300 Vibracell sonicator (Sonics and Materials, USA) with a 20-kHz frecuency, 50 % duty cycle and an output of 3 (90 W). The final extract was centrifuged again (750 g, 4 ºC, 5 min) and the supernatant was used for the enzyme activity determination. NRase assays were developed according to Rigobello-Masini et al. (2006). Tests were carried out in triplicate in 1 ml at 19 ºC. The reaction mixture contained 100 µl of crude extract, 10 mmol L^{-1} KNO_3 and 2 mmol L^{-1} $MgSO_4$ and was initiated by the addition of reduced nicotinamide adenine dinucleotide (NADH) substrate to a final concentration of 0.40 mmol L^{-1}. The nitrate reductase reaction was stopped after 15 min with 250 µl of absolute ethanol at 0 ºC and with 50 mmol L^{-1} $ZnSO_4$. Activity was estimated based on the final nitrate concentration, indicated by the formation of a red AZO product after the addition of 100 µl (0.10 % weight in volume, w/v) sulphanilamide and 100 µl (0.10 % w/v) n-1-naphtyl ethylenediamine dihydrochloride (Nicholas and Nanson 1997). After these additions, the reaction mixture was centrifuged again (21000 g, 5 min) and the supernatant taken for colorimetric analysis at 543 nm. Absorbance values were converted to nitrate concentration using a calibration curve. Enzymatic activities were expressed in enzymatic units per total protein, where one unit of the enzyme activity (UEA) catalyzes the conversion of 1 µmol of nitrate to nitrite. Total protein determinations were performed with a commercial kit (Thermo Scientific Pierce® BCA Protein Assay Kit).

Table 10.2. Experimental sample properties of *Emiliania huxleyi* strain CAWPO6 (NZEH) at high CO_2 in combination with nutrient availability. Numbers in brackets refer to standard deviation (n = 3 for µ, PON, POP, PIC and POP; n > 60 for volume and coccolith length).

Nutrient condition	Initial CO_2 (µatm)	µ (d^{-1})	PON (pmol $cell^{-1}$)	POP (pmol $cell^{-1}$)	PIC (pmol $cell^{-1}$)	POC (pmol $cell^{-1}$)	Volume (μm^{-3} $cell^{-1}$)	Coccolith length (µm)
R	258.30	1.33 ± 0.01	0.106 ± 0.00	0.010 ± 0.00	0.696 ± 0.02	0.749 ± 0.05	55.06 ± 8.17	2.974 ± 0.46
R	555.60	1.36 ± 0.03	0.101 ± 0.00	0.011 ± 0.00	0.628 ± 0.06	0.742 ± 0.06	58.68 ± 4.58	2.977 ± 0.42
R	1073.10	1.07 ± 0.02	0.189 ± 0.03	0.020 ± 0.00	1.204 ± 0.08	1.426 ± 0.23	76.82 ± 2.74	3.292 ± 0.48
-N	250.00	0.93 ± 0.00	0.055 ± 0.00	0.011 ± 0.00	1.496 ± 0.07	1.269 ± 0.10	49.64 ± 2.40	3.042 ± 0.32
-N	463.50	0.92 ± 0.00	0.057 ± 0.00	0.011 ± 0.00	1.506 ± 0.07	1.346 ± 0.02	46.22 ± 3.38	3.055 ± 0.31
-N	1229.20	0.75 ± 0.00	0.060 ± 0.00	0.014 ± 0.00	1.542 ± 0.06	1.488 ± 0.08	49.70 ± 0.33	3.224 ± 0.36
-P	256.30	1.02 ± 0.01	0.132 ± 0.01	0.004 ± 0.00	1.309 ± 0.16	1.341 ± 0.09	87.82 ± 7.04	3.084 ± 0.328
-P	560.80	0.91 ± 0.01	0.161 ± 0.01	0.004 ± 0.00	2.033 ± 0.02	2.095 ± 0.12	118.67 ± 2.03	3.228 ± 0.312)
-P	1313.70	0.80 ± 0.00	0.181 ± 0.01	0.006 ± 0.00	1.451 ± 0.08	1.989 ± 0.03	104.46 ± 1.91	3.427 ± 0.403

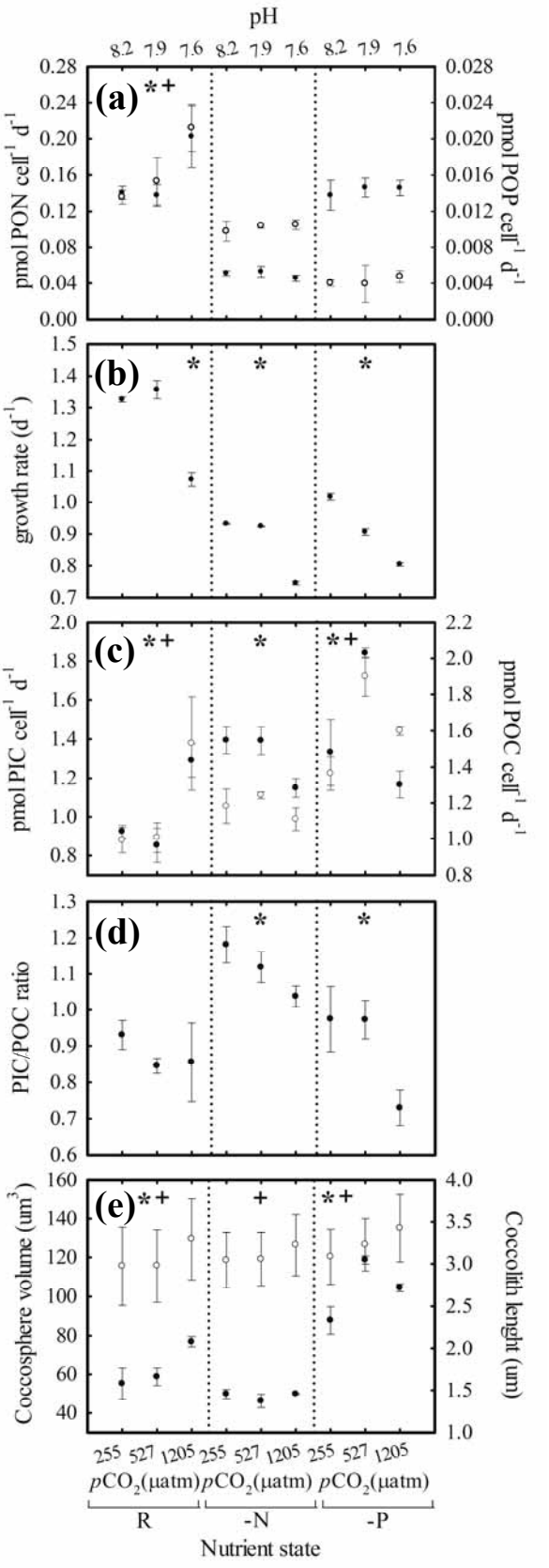

Fig. 10.1. The response of *Emiliania huxleyi* strain CAWPO6 (NZEH) to different nutrient levels under different CO_2 scenarios. (a) PON production, POP production, (b) growth rate, (c) PIC production, POC production, (d) PIC/POC, (e) coccosphere volume (μm^3) and coccolith length (μm). Closed and open circles correspond to left and right axes respectively. The symbol * and + indicate a significant difference ($p < 0.05$) within nutrient treatments on the left and right axis respectively.

10.2.3.6. Determination of alkaline phosphatase activity

Alkaline phosphatase (APase) is expressed on the cell surface of *E. huxleyi* (Dyhrman et al. 2006), allowing the activity assay to be performed on whole cells. Aliquots (40 ml) of sample were centrifuged at 2000 g and 19 ºC for 15 min and the pellets were resuspended in 2.90 ml of a solution containing 0.01 mol L^{-1} Tris buffer (pH = 9.00), 0.05 mol L^{-1} $MgCl_2$ and 0.01 mol L^{-1} $CaCl_2$. After resuspension, 100 µl of 13.50 mmol L^{-1} p-nitro-phenilphosphate (p-NPP; Sigma) substrate were added and the mixture was incubated at 19 ºC for 20 min. The reaction was stopped by the addition of 0.60 ml of 1 mol L^{-1} NaOH and samples were centrifuged again (3000 g, 19 ºC, 15 min) and the absorbance of the supernatant at 410 nm was measured. Absorbance values were transformed to p-nitrophenol (p-NP) concentration using a suitable calibration curve. One unit of enzymatic activity corresponds to 1 nmol of p-NP produced per 10^6 cells min^{-1}.

10.2.4. Statistical analysis

One way factor ANOVA were conducted using SPSS 17 (SPSS Inc., Chicago IL, USA). Linear correlation factors (r^2 value) were calculated using Sigma Plot 11.0 version (Systat Software Inc).

10.3. Results

10.3.1. Cell organic and inorganic matter production

After 8-9 generations, nitrate and phosphate in the culture media under nitrate limited (-N) and phosphate limited (-P) conditions were almost completely depleted (Table 10.1). PON and POP production under -N and -P conditions were less than half the concentration of the nutrient replete cultures (R) (Table 10.2; Fig. 10.1a). PON and POP production increased significantly with increasing CO_2 in R cultures (r^2 = 0.67 and 0.77 respectively) but did not vary under -P or -N conditions. After the culture period, net growth rates under R conditions (which were never nitrate or phosphate limited), were between 25 and 30 % higher than under -N or -P conditions respectively. In addition, under all nutrient conditions (R, -N and -P), growth rates generally decreased with rising CO_2 and a ~ 20 % decrease was observed at the highest CO_2 level (Table

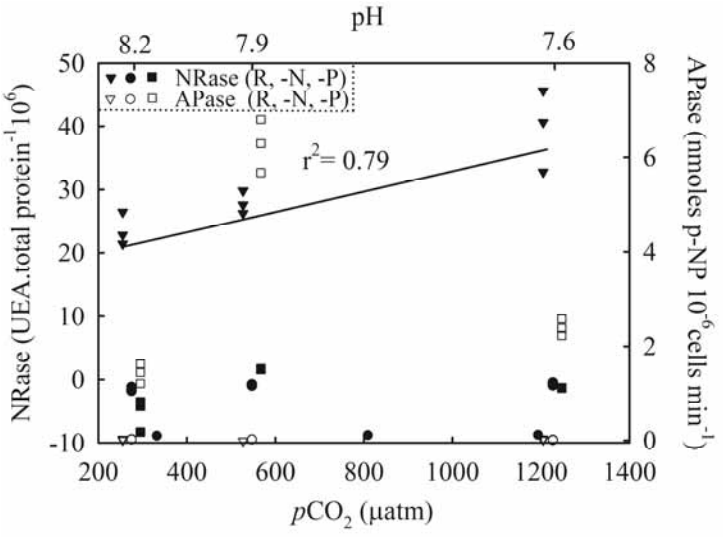

Fig. 10.2. Enzymatic response of nitrate reductase (NRase) and alkaline phosphatase (APase) to different CO_2 and nutrient scenarios in *Emiliania huxleyi* strain CAWPO6 (NZEH).

10.2; Fig. 10.1b). PIC and POC production showed different patterns depending on the combination of nutrients and CO_2 (Table 10.2; Fig. 10.1c, d). Under R conditions, PIC and POC production were ~40 % and ~50 % higher respectively at the highest CO_2 level (~1205 µatm) compared with cells grown under ~255 µatm CO_2 (Fig. 1C). PIC and POC production decreased with CO_2 under -N but the trend was non-uniform under -P conditions. At both ~255 µatm and ~527 µatm of CO_2 under -N conditions, PIC production was ~50 % higher and POC production was ~20 % higher than that observed in R cultures. Similarly, under -P conditions, PIC and POC production at both 255 µatm and 527 µatm CO_2 was also higher than under R conditions, but in this case, the highest increase (>100%) was observed at ~527 µatm. Both -N and -P cultures showed ~ 10 % lower PIC production compared with R conditions at 1250 µatm. PIC/POC did not significantly change with rising CO_2 concentrations under R conditions but a decreasing trend is present (Table 10.2; Fig.10.1e). A decreasing pattern in PIC/POC was observed in both -N and -P cultures with increasing CO_2. PIC/POC under -N conditions was on average 40% higher than under R and -P conditions.

10.3.2. Coccolith length and coccosphere volume

Coccolith length increased by ~10% over the CO_2 range considered under all the nutrient conditions (Table 10.2; Fig. 10.1f). Additionally, coccolith length under -P was significantly higher (~5%) than that observed in R and -N cultures when considering an average of all CO_2 conditions. Coccosphere volume increased by ~39% over the CO_2 range considered under R conditions. Under -N conditions, however, no differences in coccosphere volume were observed with CO_2 and coccosphere volumes were 30 and 113% lower that under R and -P conditions respectively. Coccosphere volume under -P was 87% higher than under R conditions and the highest values were observed with a CO_2 of ~527 µatm.

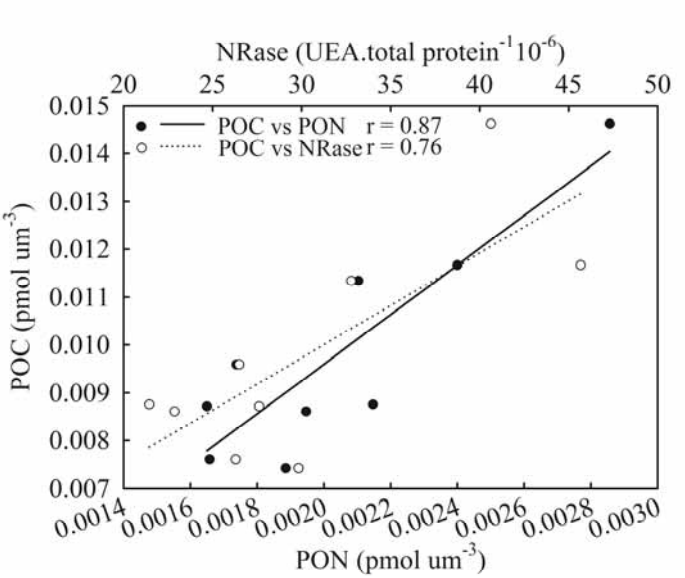

Fig. 10.3. Correlation of POC with PON and NRase under nutrient replete conditions. R-values shown in the figure.

10.3.3. Enzymatic activity

NRase was expressed under R conditions and a linear increase in its activity (r^2 = 0.79) was observed with increasing CO_2 levels (Fig. 10.2). This increase in NRase activity was accompanied by a simultaneous increase in cellular POC (Fig. 10.3). APase activity was only detected in the -P cultures and showed a maximum rate of 6.25 nmoles of p-NP 10^6 cells min^{-1} at ~527 µatm CO_2. APase activity at ~255 and ~1205 µatm CO_2 was 77 and 61% lower than at ~527 µatm CO_2. Both cellular POC and PIC showed a similar trend to APase activity with CO_2 under -P conditions (Fig. 10.4).

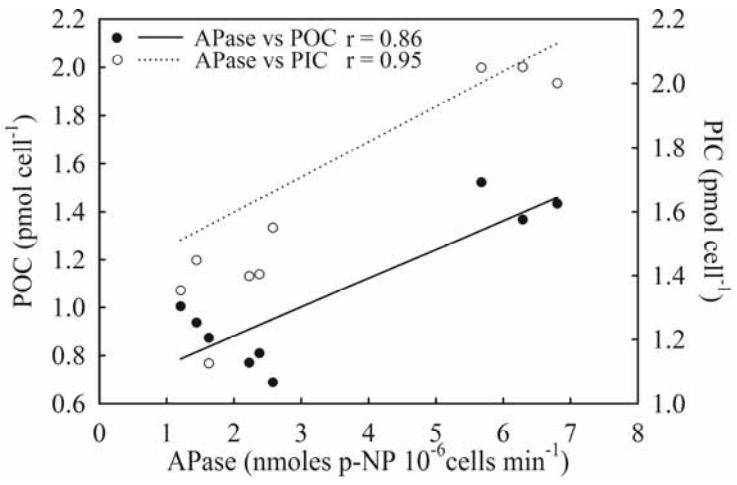

Fig. 10.4. Correlation of APase with POC and PIC under phosphorus limited conditions. R-values shown in the figure.

10.4. Discussion

10.4.1. Nutrient limitation

In this study we explored the combined effect of nitrate and phosphate availability and CO_2 concentrations on different physiological parameters in the *E. huxleyi* strain NZEH. The depletion of nitrate and phosphate in the medium, together with the decrease in PON and POP production in nitrate limited (-N) and phosphate limited (-P) cultures respectively indicates that the cultures underwent nutrient limitation. The decrease in growth rates in nutrient-limited cultures is linked to the restriction of protein synthesis under -N conditions, and to the inhibition of DNA and phospholipids synthesis under -P conditions. Both of these processes provide the necessary barrier for cell replication (Müller et al. 2008). The observed reduction in growth rate with increasing CO_2 has already

been reported in the *E. huxleyi* NZEH strain (Iglesias-Rodriguez et al. 2008a) and other strains before (Müller et al. 2010; Hoppe et al. 2011). Previous work suggests that variability in growth rates between ocean acidification studies with *E. huxleyi* might be due to differences in carbon chemistry speciation from different manipulation methods (Iglesias-Rodriguez et al. 2008b), although a comparison of some of these methods has revealed similar responses in some coccolithophore species (Shi et al. 2009; Hoppe et al. 2011). An inter-strain specific tolerance to CO_2 concentration has also explained this diversity in response (Langer et al. 2009b). Shi et al. (2009) investigated the effect of different manipulation methods on the *E. huxleyi* NZEH strain, suggesting that a decrease in growth rates could be attributed to a mechanistic effect of bubbling. Nonetheless, the decrease in growth rates in *E. huxleyi* NZEH strain in this study cannot be attributed to this, as bubbling was not the selected manipulation method. The experimental approach considered here corresponds to a close DIC manipulation (addition of HCl and Na_2CO_3 with constant TA and an increased DIC). A recent study with the same NZEH strain (Hoppe et al. 2011) did not observe changes in growth rate with CO_2 with neither TA nor DIC manipulation methods although in open DIC manipulations, values were statistically lower than in closed ones (again attributed to a mechanistic effect of bubbling). Although Hoppe et al. (2011) did not compare with the method used in this study we suggest that the reasons for the decrease in growth rates are related to causes other than the manipulation method. Cultures were not in constant suspension by steady rotation of the flasks and culture bottles were shaken twice a day. The sedimentation of the cells, however, does not seem to induce decreasing growth rate, as it was previously proposed (Hoppe et al. 2011). A similar effect would be expected in all the cultures, not just in the ones under the highest CO_2 conditions.

10.4.2. Nutrient utilization: alkaline phosphatase and nitrate reductase

This is the first study, to the best of our knowledge, investigating *E. huxleyi* alkaline phosphatase (APase) and nitrate reductase (NRase) activities under increasing CO_2. APase was only expressed in -P cultures, since phosphatases are inducible catabolic enzymes whose expression is determined by external phosphate concentration or N/P (Hoppe et al. 2003). Previous studies reported the expression of up to three different APases on the *E. huxleyi* cell surface under phosphate stressed conditions (Dyhrman and Palenik 2003). This enzyme allows phytoplankton to overcome phosphorus starvation by metabolising organic phosphorus complexes. APase was strongly affected by CO_2 partial pressure and its maximum activity was

found at a CO_2 of ~527 µatm (pH ~ 7.90). *Emiliania huxleyi* APase optimum pH has been previously investigated (Kuenzler and Perras 1965; Xu et al. 2006). These studies showed different results to our experiment. A different pH dependency was observed for APase activity from field samples showing spatial variability (Yamada et al. 2010). This indicates that optimum APase pH might vary not only between species (Kuenzler and Perras 1965) but also between strains and isolation sites (biogeography). A marked diversity in enzyme activities has also been reported for different strains of *E. huxleyi* (Xu et al 2010; Reid et al. 2011). Differences in optimum pH can also be related to the different methodologies used. The studies mentioned above investigated the effects of acidification on enzyme activity after a short incubation period at a desired pH. Considering that ocean acidification involves changes in other parameters than pH, and the possible role of organic carbon compounds in the regulation of APase activity, the study of APase activity under different CO_2s seems more appropriate to establish ecological implications. *Emiliania huxleyi*'s APase activity decreases at high CO_2 (e.g. 1200 µatm; pH 7.60), which would put *E. huxleyi* at a competitive disadvantage for phosphorus acquisition in more acidic oceans and other species might take its place as low-nutrient opportunists. Yet, the ecological implications of physiological results should be carefully considered given the high degree of genetic diversity among *E. huxleyi* strains (Iglesias-Rodriguez et al. 2006), the different responses in APase activities between them (Xu et al. 2011), as well as interactions with other levels of ecological organization.

NRase was only found in nutrient replete (R) cultures, when nitrate was present in the medium. Previous studies indicate a down regulation of proteins involved in the acquisition and assimilation of inorganic nitrogen after nitrate depletion in *E. huxleyi* (Bruhn et al. 2010). Despite the presence of nitrate in the medium, NRase was absent when cultures grew in -P conditions. Since some regulatory mechanisms involved in nitrate assimilation include phosphorylation, phosphate limitation may be impairing this process (Beardall et al. 1998). Nitrate reductase increased in the presence of higher concentrations of inorganic carbon and when nitrate and phosphate were present in the medium. A high positive correlation between POC and both NRase synthesis and nitrate incorporation (PON) was also observed (Fig. 10.3). Nitrogen and carbon metabolism are known to be tightly coupled and a decrease in photosynthetic carbon fixation limits nitrogen assimilation (Hipkin et al. 1983; Turpin 1991). A consensus about the effect of ocean acidification on NRase activity is not established and yet different studies in terrestrial plants (Fonseca et al. 1997) and phytoplankton species (Xia and

Gao 2005; Rigobello-Massini 2006) have shown a species-specific response with both increasing and decreasing trends. Different phytoplankton organisms regulate carbon and nitrogen metabolism differently. Additionally, NRase and nitrogen fixation rates depend on nutrient availability and inorganic carbon concentration in the medium (Rigobello-Masini et al. 2006). NRase is an important parameter in nitrogen cycling studies and it is an index of nitrogen incorporation rates (Berges and Harrison 1995), thus further investigation of its evolution with CO_2 is needed for a correct understanding of the cycling of nitrogen in the future oceans.

10.4.3. Calcification and organic carbon incorporation

Both cellular POC and PIC production increased at high CO_2 under nutrient replete (R) conditions (Table 10.2; Fig. 1c). This increase was accompanied by slight increases in coccosphere volume and lith size (Table 10.2; Fig. 1f). The increase in POC production at high CO_2 concentrations has been observed in previous studies before under nutrient replete and nitrate limiting (Zondervan et al. 2001, 2002; Borchard et al. 2011) and suggests that this species could be carbon limited in the present ocean. Considering the low affinity of RUBISCO for CO_2 and the low efficient carbon concentrating mechanisms (CCM) in *E. huxleyi* (Paasche 2002), any increase in available CO_2 would increase the speed of carbon fixation, and thereby cellular POC production (Barcelo e Ramos et al. 2010). Increased cellular PIC production has been observed in *E. huxleyi* NZEH strain before using different methods to manipulate carbon chemistry than the used in this study (Iglesias-Rodriguez et al. 2008a, b; Shi et al. 2009). The wide variation in calcification responses to increasing CO_2 levels between *E. huxleyi* studies has been linked to inter-strain physiological differences (Langer et al. 2009b) derived from high inter-clonal genotype variation within the *E. huxleyi* morpho-species (Iglesias-Rodriguez et al. 2006). The increase on *E. huxleyi* calcification with high CO_2 reported by Iglesias-Rodriguez et al. (2008a) has been recently associated to the use of a morphotype- R strain (NZEH), a highly calcified *E. huxleyi* morphotype with a possible genetic modification that enables it to calcify heavily in relative acidic waters (Beaufort et al. 2011). Although differences in methods for CO_2 manipulation were also proposed to be the reason for responses between studies, Schulz et al. (2009) showed that DIC and TA manipulation yield similar changes in all parameters of the carbonate system allowing direct comparison of values obtained by using different manipulation approaches. Similarly, a recent study with the NZEH strain (Hoppe et al. 2011) found a similar decrease in PIC production with increasing CO_2 when using three different manipulation

methods. This response, however, is opposite to the findings from this study. As previously discussed for growth rate, differences in PIC production between 255 and 1200 µatm CO_2 in this study are too significant to be explained solely bythe manipulation method. Discrepancies between studies using the same strain have also been found with strains others than NZEH (Langer et al. 2009b; Hoppe et al. 2011). As Hoppe et al. (2011) proposed, variability in studies with the same strain could be due to differences on the effect of temperature (Borchard et al. 2011) or light intensities (Zondervan et al. 2002). Experiments by Iglesias-Rodriguez et al. (2008a), Shi et al. (2009) and those conducted in this study used temperatures between 19 and 20ºC, almost 5ºC higher than those used in Hoppe et al. (2011). Light irradiance in this study was the lowest in all experiments using this strain but still higher than those used for physiological studies with *E. huxleyi* (Taylor et al. 2011), and still yielding the same trends in PIC production as in Iglesias-Rodriguez et al. (2008a) and Shi et al. (2009). In any case, as observed in Zondervan et al. (2002), lower light irradiances than those used in Hoppe et al. (2011) should lead to lower PIC production rather than the increase observed here and other studies using the NZEH strain. Identical experimental conditions should be used to allow direct comparison between studies of the same strain. It would also be possible that different studies are dealing with genotypically and phenotypically different strains after years of culturing under different laboratory conditions. The environmental variability to which organisms are subjected ultimately determines organism's plasticity to environmental variations. Considering the short generation time of *E. huxleyi* a few years of stock maintenance under different culture conditions (e.g. low light intensities or temperature) could lead to evolutionary divergence and the creation of new physiological traits, resulting in a new strain.

The ocean is a dynamic system and species responses differ depending on the combination of environmental changes. Due to our experimental design a comparison of PIC and POC production between R and -P or -N cultures is difficult. As Langer et al. (2012) propose the growth rate in -N or -P batch cultures is not constant, as it could be assessed by using chemostats or semi-continuous cultures where cells undergo the same level of nutrient limitation over the entire length of the experiment. In -N or -P batch cultures, cells undergo a transition from an exponential growth phase to a stationary phase, where cells are no longer dividing. As PIC and POC production is calculated using growth rate and cell quotas the increased production observed in -P and -N cultures relative to R conditions can be affected by the method to calculate production (Langer et al. 2012). Comparison of PIC and POC production between R

and either -N or -P conditions can thus only be achieved when values under nutrient limited conditions are lower or the same than under R conditions (Langer et al. 2012), as it is the case at a CO_2 of ~1200 µatm. In this case, cellular PIC and POC production was lower under both -N and -P conditions compared to R cultures. The increased PIC and POC production in -N or -P observed here could be a real increase or just an artefact from the protocol used as an increase in PIC and POC production had not been observed under -N or -P conditions (Paasche 1998; Riegman et al. 2000). Although a direct comparison between nutrient treatments cannot be done, trends within each independent nutrient condition can still be discussed as cultures were treated identically (e.g. kept at stationary phase for two days). Cellular PIC and POC production under nutrient limited conditions presented an opposite trend with CO_2 to that observed under R conditions. A decrease in cellular PIC and POC production with increasing CO_2 has been observed for other *E. huxleyi strains* under nitrogen and phosphorus limitation before (Sciandra et al. 2003; Borchard et al. 2011). In the case of -P cultures a high correlation was found between both PIC and POC production and APase activity (Fig. 4) what indicates the role of this enzyme in carbon metabolism and calcification. The role of carbon compounds in alkaline phosphatase regulation activity has also been proposed before (Siuda and Güde 1994) as well as the importance of ATP supply in carbon acquisition. (Beardall et al. 1998). ATP-ases have been associated with the coccolith vesicle, playing a role during removal of protons produced during dehydration of bicarbonate in the coccolith vesicle (Corstjens and Gonzalez 2004). Phosphorus demand and ATP-ases synthesis might be not satisfied at a CO_2 of 1200 µatm due to the low APase activity affecting the process of Ca^{+2} transport into the coccolith vesicle.

While coccolith length is correlated with CO_2, coccosphere volume was more dependent on nutrient conditions. Phosphate-limited cultures had larger cells and slightly larger coccoliths than -N and R cultures (Table 10.2; Fig. 1f). This has been previously observed (Paasche 1998) but a different trend than in R and -N cultures was observed with CO_2. Coccosphere volume increased with CO_2 under R conditions but a 11% decrease in coccosphere volume was observed with high CO_2 in -P cultures, similar to previous studies with the PML-B92/11 strain (Borchard et al. 2011). Nitrogen-depleted (-N) cells were smaller than R cells in this study (Fig. 1f) in accordance with previous work (Riegman et al. 2000; Muller et al. 2008). Coccosphere volume, however, did not decrease with CO_2 under -N conditions, in disagreement with Sciandra et al. (2003), which could be related to the different experimental approaches used. Sciandra et al (2003) experiments were performed in a chemostat, where cells where exposed to

nitrogen limitation for a longer period (~15 days) compared to 2 days in this study. In addition, volume differences between high and low CO_2 conditions in Sciandra et al. (2003) were observed 4 days after changing CO_2 conditions. This approach is different to the one used in this study where nitrogen limitation and CO_2 conditions were altered at the same time and cells were nitrogen limited for a shorter period.

The comparable variation of PIC and POC production under R conditions resulted in a constant PIC/POC as it has been previously reported with the NZEH strain (Iglesias-Rodriguez et al. 2008a). To date, no studies in ocean acidification have shown an increase in PIC/POC ratios (Ridgwell 2009). PIC/POC decreased with CO_2 under nutrient limited conditions in accordance with studies with other *E. huxleyi* strains under nitrogen (Sciandra et al. 2003) and phosphorus (Borchard et al. 2011) limitation. This finding is relevant considering the extent of oligotrophic oceanic waters, and predicting sinking speed at high CO_2 (Biermann and Engel 2010) and thus understanding how mineral ballast (Armstrong et al. 2002) could affect POC export in the future ocean The data presented here suggests that a P- and N-limited bloom in a high CO_2 ocean would have a reduced PIC/POC ratio (Table 10.2; Fig. 1e). This would reduce the gross CO_2 production of the bloom, but could also reduce the net CO_2 export to the deep ocean associated with aggregate ballasting effects of the coccoliths (Biermann and Engel 2010).

Results from this study show that despite the NZEH strain presenting different cellular PIC production patterns to other *E. huxleyi* strains with increasing CO_2 under nutrient replete conditions, PIC production trends become similar when cells undergo nutrient limitation (Table 10.2; Fig. 1c), suggesting that calcification is tightly dependent on nutrient availability. Similarly, studies using the strain PML B92/11 showed different POC production in response to ocean acidification depending on phosphorus availability (Borchard et al. 2011). Ocean acidification is not an isolated climate-related phenomenon in the oceans and there are concomitant changes in other physico-chemical properties, including temperature, mixing and macronutrient availability. It is widely accepted that the physiology of phytoplankton, including *E. huxleyi*, will change in high CO_2 ocean but it is necessary to investigate the effect of more than a single environmental parameter in order to predict and understand the direction of future changes with a greater degree of certainty. Multivariate studies also reveal the synergistic effects of environmental perturbations on important biogeochemical processes like calcification production, which will in turn determine the ecological role of *E. huxleyi* in future oceans.

11.

The effect of artificial upwelling and *in-situ* ocean acidification on coccolithophore physiology

Abstract

The rising atmospheric carbon dioxide (CO_2) concentration increases dissolved CO_2 and lowers carbonate ions (CO_3^{2-}) in the ocean (ocean acidification - OA). The effects of CO_2 have been assessed in many ways in the laboratory, but very few studies have studied them in the field. Current field approaches use the high CO_2 levels around volcanic vents to then incubate organisms in those waters or assess natural community changes. Here, we present a further field method using the natural gradient of increasing CO_2 with depth. Water was recovered in the north Atlantic Ocean using a CTD from ~ 5000 m to the chlorophyll maximum in the euphotic zone (four levels: 10-30 m, 500 m, 1000 m, and 4800 m). Then, after surface equilibration at constant temperature in sealed flasks, we incubated three strains of the cosmopolitan coccolithophore species *Emiliania huxleyi*. Medium carbonate chemistry measurements from CTD water, and then at the beginning and end of the experiment confirmed that we maintained a constant CO_2 gradient from ~ 300 to 620 µatm at constant alkalinity (~ 2320-2360 µmol kg^{-1}) and temperature (~ 15.60-15.70 °C). Nutrients were replete at all depths except in the euphotic zone, where there was N and P limitation since the experiment took place after the spring bloom. We found a small fertilization effect from the deep waters on the growth rate and PIC/POC ratio, but not on the C/N ratio, and all responses were strain-specific. Coccoliths geochemistry revealed an increase of the calcite Sr/Ca ratio with increasing depth and CO_2,

following growth rate, but also a CO_2-specific effect affecting elemental incorporation. The calcite Mg/Ca could not be adequately measured owing to a organic-Mg cleaning issues already known for *E. huxleyi*. This new approach and results suggest that this can be a robust field method after adequate optimization to test OA and fertilization of the upper ocean with deep water (e.g. artificial upwelling and geo-engineering).

This chapter is based on:

Iglesias-Rodriguez, M. D., Jones, B. M. J., Blanco-Ameijeiras, S., **Lebrato, M.** and Huete-Ortega, M. in preparation. The effect of artificial upwelling and in-situ ocean acidification on coccolithophore physiology. To be submitted: *Progress in Oceanography*.

Acknowledgements: This work was supported by the "European Project on Ocean Acidification" (EPOCA) (FP7/2007-2013 under grant agreement n° 211384) for MDI-R and the PhD of ML. We thank Richard Lampitt for giving access to this to the cruise and all the crew technical support onboard.

11.1. Introduction

The rising atmospheric carbon dioxide (CO_2) concentration following anthropogenic fossil fuel emissions increases dissolved CO_2 and lowers pH and carbonate ions (CO_3^{2-}) in the ocean, in a process termed ocean acidification (Caldeira and Wickett 2003; Doney et al. 2009). In order to better understand this issue, the scientific community has conducted more than 180 experiments during the past 15 years in controlled conditions in the laboratory, indoor and field mesocosms, and in the ocean (Nisumaa et al. 2010). Many of these studies tackle physiological, morphological, biogeochemical, and community responses in primary producers, namely dinoflagellates, diatoms and coccolithophores. This major focus on phytoplankton is due to the important role they play in particulate matter production in the euphotic zone (Behrenfeld and Falkowski 1997; Behrenfeld et al. 2005) and export to depth (Gehlen et al. 2007) as well as their importance in macronutrient cycling. Specifically, particulate organic carbon (POC) production and calcification (PIC production) have been a focus of study in coccolithophores to better understand balances in the marine carbon cycle (Buitenhuis et al. 1999; Riebesell et al. 2000; Zondervan et al. 2001, 2002; Iglesias-Rodriguez et al. 2008a; Langer et al. 2009b; Borchard et al. 2011; Langer et al. 2012). While these studies find contrasting and at the same time contradicting responses, especially on calcification and the PIC/POC ratio, a common feature is that the seawater carbonate chemistry was manipulated using different methodologies to achieve the desired CO_2 levels but not always the HCO_3^- levels (Riebesell et al. 2010).

Only a few studies have used natural CO_2 changes in the ocean to study ocean acidification, namely, the CO_2 flux from volcanic vents acidifying seawater in coastal areas of the Tyrrhenian Sea, Italy (Hall-Spencer et al. 2008). pH declined from modern (~ 8.1) to low levels (~ 7.4). Species-specific as well as whole community analyses indicated that in situ CO_2 conditions could benefit some species, while displacing others (*see* also Porzio et al. 2011). A transplantation experiment moving bryozoans from normal to low pH levels (8.1-7.43) showed that the organisms maintained net calcification but that during periods of high temperature, calcification could stop (Rodolfo-Metalpa et al. 2010). Another study on epiphytic coralline algae cover and mass calcification on sea grass meadows, showed a large decrease in both parameters with decreasing pH (Martin et al. 2009). A new method to study ocean acidification in the field (and also upwelling effects on marine biota), was first tested in 2009 on echinoid larvae, during a research cruise in the north Atlantic Ocean (Chapter 12) (*see* chapter 12). The

method used the natural gradient of increasing CO_2 at relative constant alkalinity (TA) with depth, induced among other factors by organic matter respiration (Feely et al. 2004) and increasing CO_2 solubility with decreasing temperature at depth (Weiss 1974). Using a CTD cast, water was retrieved from different depths (250 to 4700 m), and adult sea urchins were spawn in a temperature controlled room. Sea urchin larvae were grown for 5 days at 9 ºC with a natural CO_2 gradient from 350 to 570 µatm after temperature equilibration. Fertilization decreased by ~ 20 %, calcification was between 50 and 60 % below control surface water values, and morphology was not significantly affected. Results were similar to other published studies where medium carbonate chemistry was manipulated (e.g. Clark et al. 2009).

In this study, we developed further the method using the natural gradient of increasing CO_2 with depth, testing it on three strains of the cosmopolitan coccolithophore species *Emiliania huxleyi*. Experiments were conducted in temperature controlled incubation tanks with water from the chlorophyll maximum (Chla max) down to 4800 m following daily light cycles in the north Atlantic Ocean. We studied physiological (growth rate), biogeochemical (particulate matter quota/production), morphological (coccolith size - not shown in this chapter), and geochemical (coccoliths elemental composition - Mg/Ca, Sr/Ca, P/Ca, Fe/Ca) responses to the natural carbonate chemistry gradient. We discuss the value and the implications of the method in field situations to test both ocean acidification and simulated upwelling. Our results are similar to other laboratory incubations where the carbonate chemistry was manipulated. We also describe for the first time the response of elemental ratios in coccoliths using a CO_2 gradient. The new method represents a robust field tool now available to study open ocean acidification processes in a wide range of marine taxa.

11.2. Supplementary information: methods

11.2.1. Field incubations

The experiment (*see* next section) took place between May 26th and June 5th 2010 aboard RRS *James Clark Ross* in the region of the Porcupine Abyssal Plain (PAP) (~ 49.99 N° and 16.39 °W, ~ 4900 m). Five monoclonal cultures of *Emiliania huxleyi* strains originated from phytoplankton collections were maintained at 14 °C and at 200 µmol quanta m^{-2} s^{-1} in a light-controlled incubator onboard *James Clark Ross* using nutrient-replete natural seawater. NZEH

(also known as "PLY M219" and "CAWPO6") was isolated in New Zealand; RCC1212 (AC477) was isolated in the South Atlantic; CCMP88E (CCMP378) was isolated in the Gulf of Maine; CCMP1A1 (CCMP372) was isolated in the Sargasso Sea; and AC472 (TQ26) was isolated in the Tasman Sea (Table 11.1). Three of these (NZEH, CCMP88E and CCMP1A1) were obtained from Plymouth Culture Collection of the Marine Biological Association of the UK (http://www.mba.ac.uk/culture-collection/), RCC1212 was obtained from the Roscoff Culture Collection (http://www.sb-roscoff.fr/Phyto/RCC/), and AC472 from Algobank (http://www.unicaen.fr/algobank/accueil/). The strains NZEH, CCMP88E, and RCC1212 were used in two incubations with water from four depth levels from 10 to 4800 m (slightly different between incubation 1 and 2). We studied physiological [growth rate (μ)], and biogeochemical parameters [inorganic and organic carbon quota/production (PIC and POC), organic nitrogen quota/production (PON), and inorganic to organic ratios (PIC/POC and POC/PON)] under the natural CO_2 gradient present in the water column. All five strains were incubated in Chla max depth water (38 m) from incubation 2 to study strain-specific coccoliths geochemistry (elemental ratios, e.g. Mg/Ca, Sr/Ca, P/Ca, and Fe/Ca) and compare to published laboratory results of the same species (*see* Table 11.1). All strains were subcultured at low cell numbers (< 5000 cells ml^{-1}) in natural seawater (to minimize stress) until the incubations were conducted under the natural CO_2 gradient.

11.2.2. Field incubations: experimental set-up and CTD casts

Two 0.80 m^3 transparent plastic incubation tanks (plexiglass) were placed on deck (stern, port side) inside stainless steel frames with a rectangular bottom (*see* Fig. 11.1). The incubators were placed half-way between the ship running water intake pipe (from 5 m depth) and the port side. The metal frames with the incubators were tightly secured to the deck with metal rings and ropes attached to both the incubator frame and the deck. Before introducing the incubation tanks (and cover lid) in the frame, they were carefully covered with a photoselective blue filter that maintains photosynthetic active radiation (PAR) to ~ 10% of the surface values (Table 11.1). This avoids photoinhibition, mimicking natural light levels encountered by cells in the euphotic zone during the course of a day. To maintain a constant temperature in both incubations (~ 15.60-15.80 °C), we used the natural seawater flow from the 5 m depth running water intake pipe (*see* Fig. 11.1). We drilled holes on the plastic tank walls and we adjusted plumbing metal screws with o-rings (rubber) to prevent leaking. The intake hose (5 m depth ship water) was

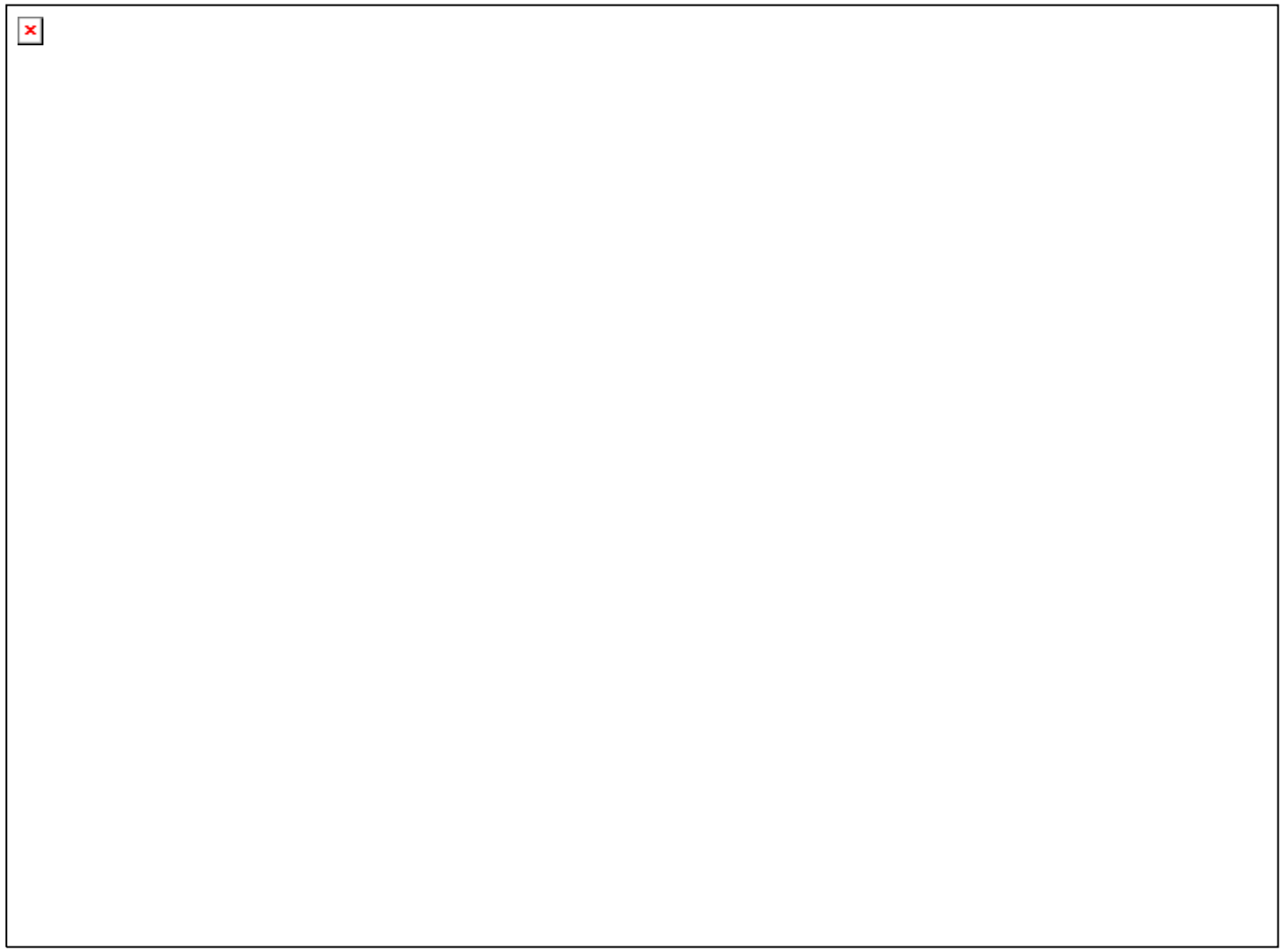

Fig. 11.1. Shipboard incubation system on the vessel deck. Images show photoselective filters, connexions, and how the seawater flows in and out of the system to maintain a constant temperature at a fixed experimental station.

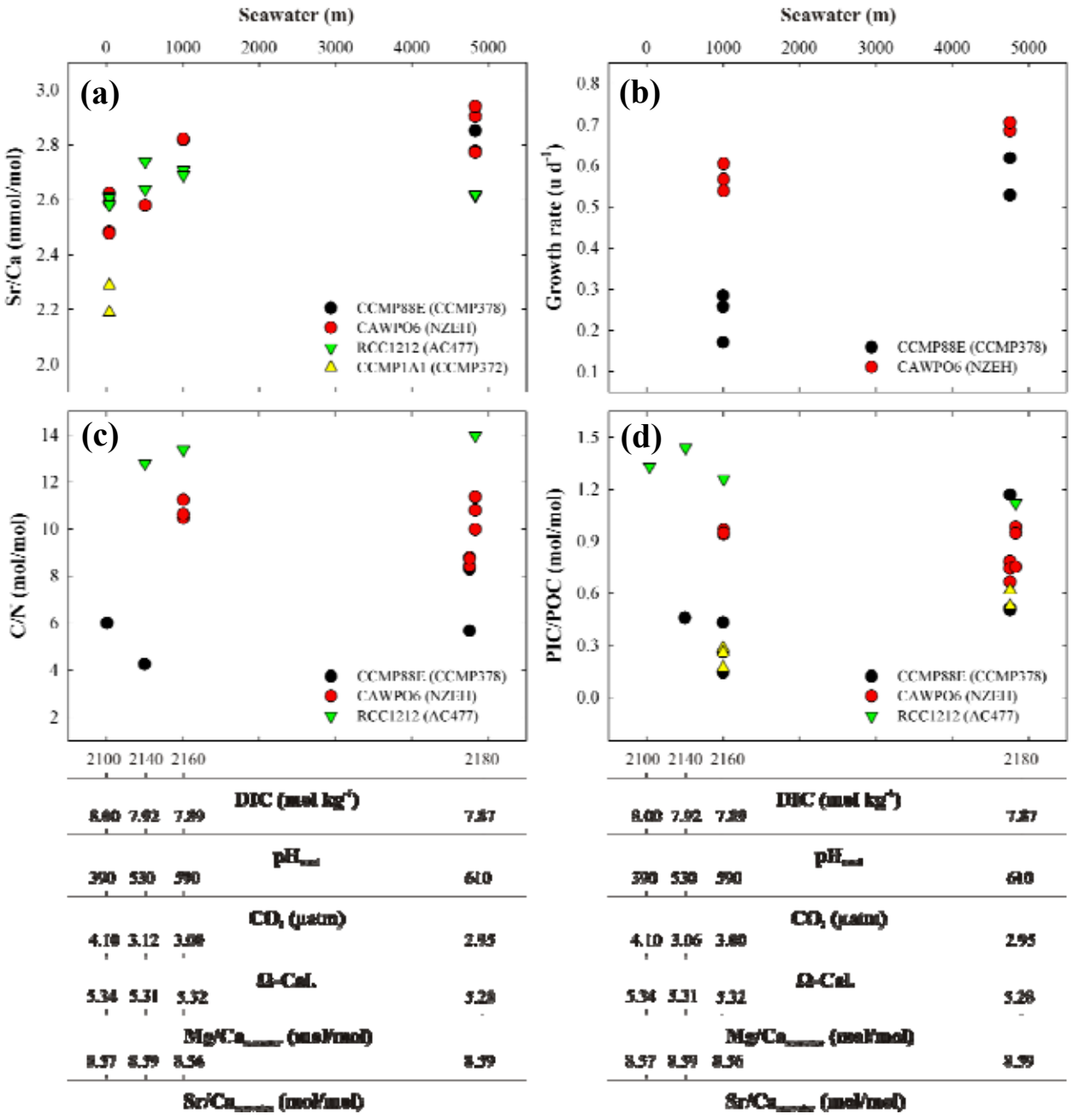

Fig. 11.2. The response of *Emiliania huxleyi* strains to the seawater conditions from different depths and thus a natural carbonate chemistry gradient. (a) Calcite Sr/Ca, (b) growth rate, (c) C/N, and (d) PIC/POC. All data from incubation 1 and 2 and the incubators are included. Bottom axes show experimental medium carbonate chemistry and seawater composition in the incubations, not in situ (no pressure effect).

Table 11.1. Strain details and experimental conditions in all incubations (shipboard on deck and in a temperature controlled incubator).

Strain	CAWPO6 (NZEH)	RCC1212 (AC477)	CCMP88E (CCMP378)	CCMP1A1 (CCMP372)	AC472 (TQ26)
Incubation type	Shipboard/Incubator	Shipboard/Incubator	Shipboard/Incubator	Incubator	Incubator
Origin	New Zealand	South Atlantic	Gulf of Maine	Sargasso Sea	Tasman Sea
Latitude	46.58 °S	34.28 °S	43.00 °N	32 N°	48.18 °S
Longitude	168.05 °E	17.18 °E	68.00 °W	62 °W	169.50 °E
Experimental conditions (shipboard and incubator)					
Temperature (°C) - shipboard [a]	15.78 ± 0.47	15.63 ± 0.47	15.71 ± 0.00	-	-
PAR (µmol quanta m^{-2} s^{-1}) - shipboard [b]	0 - 2000	0 - 2000	0 - 2000	-	-
Temperature (°C) - incubator [c]	14.00 ± 0.00	14.00 ± 0.00	14.00 ± 0.00	14.00 ± 0.00	14.00 ± 0.00
PAR (µmol quanta m^{-2} s^{-1}) - incubator [c]	200	200	200	200	200
Salinity - ALL	35.43 ± 0.28	35.40 ± 0.30	35.40 ± 0.00	35.40 ± 0.00	35.40 ± 0.00

[a] Incubation on a temperature-controlled system using the seawater continuous flow from the subsurface taken by the vessel at 5 m (*see* Fig. 11.1). The temperature was maintained constant during day and night time.
[b] Photosynthetic active radiation varied from 0 to 2000 depending on the time of the day as measured by the vessel sensor. The incubation tanks (*see* Fig. 11.1) were covered with a photoselective blue filter that reduced PAR to ~ 10% of the surface values.
[c] Temperature in the incubator was maintained constant at 14 °C (*see* Table 11.4) and PAR = 200 µmol quanta m^{-2} s^{-1}.

Table 11.2. Oceanographic and experimental data from the shipboard incubation 1 with *Emiliania huxleyi* [strain CAWPO6 (NZEH) and CCMP88E (CCMP378)].

Oceanographic parameters	**Depths (CTD cast)**			
	10 m	**502 m**	**1002 m**	**4757 m**
Temperature (°C)	15.81	11.58	10.25	2.52
Salinity	35.81	35.63	35.85	34.89
Oxygen (ml L^{-1})	5.56	6.08	6.25	7.54
Nitrate (µM)	0.85	9.25	16.35	21.50
Phosphate (µM)	0.09	0.53	1.07	1.64

Medium chemistry and sample data

E. huxleyi CCMP88E (CCMP378) - Incubation 1

	t*0*	t*n*	t*0*	t*n*	t*0*	t*n*	t*0*	t*n*
Nitrate (µM)	1.40	0.85	10.10	8.20	17.55	16.80	20.95	20.15
Phosphate (µM)	0.09	0.08	0.55	0.31	0.97	0.94	1.37	1.26
TA (µmol kg^{-1})	2362.40 ± 0.00	2360.59 ± 0.40	2347.40 ± 0.00	2346.39 ± 0.26	2375.10 ± 0.00	2369.96 ± 2.08	2348.70 ± 0.00	2340.79 ± 2.70
DIC (µmol kg^{-1})	2092.40 ± 0.00	2093.42 ± 1.80	2135.30 ± 0.00	2131.12 ± 7.54	2188.90 ± 0.00	2187.23 ± 1.71	2187.80 ± 0.00	2169.24 ± 17.73
pH_{total}	8.11 ± 0.00	8.11 ± 0.00	8.00 ± 0.00	8.01 ± 0.01	7.94 ± 0.00	7.94 ± 0.00	7.89 ± 0.00	7.92 ± 0.04
pCO_2 (µatm)	345.20 ± 0.00	349.65 ± 3.74	461.30 ± 0.00	453.04 ± 18.08	549.60 ± 0.00	558.72 ± 1.63	614.40 ± 0.00	574.38 ± 56.71
HCO_3^- (µmol kg^{-1})	1888.10 ± 0.00	1890.85 ± 3.07	1963.90 ± 0.00	1958.03 ± 11.42	2029.80 ± 0.00	2029.99 ± 1.51	2041.90 ± 0.00	2018.48 ± 25.69
CO_3^{2-} (µmol kg^{-1})	192.00 ± 0.00	190.07 ± 1.41	154.90 ± 0.00	156.87 ± 4.53	139.50 ± 0.00	137.27 ± 0.43	123.80 ± 0.00	130.12 ± 10.07
CO_2 (µmol kg^{-1})	12.30 ± 0.00	12.50 ± 0.13	16.50 ± 0.00	16.21 ± 0.65	19.60 ± 0.00	19.97 ± 0.06	22.10 ± 0.00	20.64 ± 2.04
Ω-Cal.	4.55 ± 0.00	4.51 ± 0.03	3.68 ± 0.00	3.72 ± 0.11	3.31 ± 0.00	3.25 ± 0.01	2.95 ± 0.00	3.10 ± 0.24
$Mg/Ca_{seawater}$ (mol/mol)	5.34 ± 0.01	-	5.31 ± 0.00	-	5.32 ± 0.01	-	5.28 ± 0.03	-
$Sr/Ca_{seawater}$ (mmol/mol)	8.57 ± 0.03	-	8.59 ± 0.01	-	8.56 ± 0.04	-	8.59 ± 0.01	-
Cell density (cells ml^{-1})	2159		2159		2159		2159	
Growth rate (µ)	-		-		0.23 ± 0.05		0.44 ± 0.23	
PIC quota (pmol C $cell^{-1}$)	0.10 ± 0.09		0.39 ± 0.09		0.25 ± 0.03		0.31 ± 0.02	
PIC prod. (pmol C $cell^{-1}$ d^{-1})	-		-		0.06 ± 0.02		0.14 ± 0.08	
POC quota (pmol C $cell^{-1}$)	0.76 ± 0.08		1.05 ± 0.52		1.13 ± 0.66		0.49 ± 0.18	
POC prod. (pmol C $cell^{-1}$ d^{-1})	-		-		0.27 ± 0.18		0.20 ± 0.12	

PIC/POC (mol/mol)	0.15 ± 0.13	0.46 ± 0.29	0.27 ± 0.14	0.72 ± 0.38
PON quota ((pmol N cell^{-1})	0.12 ± 0.00	0.24 ± 0.06	0.03 ± 0.01	0.07 ± 0.03
PON prod. ((pmol N cell^{-1} d^{-1})	-	-	0.01 ± 0.00	0.02 ± 0.01
C/N (mol/mol)	6.00 ± 0.34	4.25 ± 1.48	-	7.42 ± 1.51
Mg/Ca$_{calcite}$ (mmol/mol)	234.24 ± 0.00	329.79 ± 0.00	387.19 ± 0.00	43.46 ± 0.00
Sr/Ca$_{calcite}$ (mmol/mol)	-	-	-	2.85 ± 0.00
P/Ca$_{calcite}$ (mmol/mol)	261.49 ± 0.00	113.38 ± 0.00	12.72 ± 0.00	1.91 ± 0.00
Fe/Ca$_{calcite}$ (mmol/mol)	152.58 ± 0.00	264.95 ± 0.00	13.40 ± 0.00	4.90 ± 0.00

E. huxleyi CAWPO6 (NZEH) - Incubation 1

	t*0*	t*n*	t*0*	t*n*	t*0*	t*n*	t*0*	t*n*
Nitrate (µM)	1.05	0.80	10.75	8.20	18.05	16.80	20.95	19.40
Phosphate (µM)	0.09	0.08	0.55	0.54	0.94	0.88	1.37	1.13
TA (µmol kg^{-1})								
DIC (µmol kg^{-1})								
pH$_{total}$								
*p*CO$_2$ (µatm)	NOT ANALYZED (BUT SIMILAR TO CCMP88E)							
HCO$_3^-$ (µmol kg^{-1})								
CO$_3^{2-}$ (µmol kg^{-1})								
CO$_2$ (µmol kg^{-1})								
Ω-Cal.								
Mg/Ca$_{seawater}$ (mol/mol)	5.34 ± 0.01	-	5.31 ± 0.00	-	5.32 ± 0.01	-	5.28 ± 0.03	-
Sr/Ca$_{seawater}$ (mmol/mol)	8.57 ± 0.03	-	8.59 ± 0.01	-	8.56 ± 0.04	-	8.59 ± 0.01	-

Cell density (cells ml^{-1})	3787	3787	3787	3787
Growth rate (µ)	-	-	-	0.69 ± 0.01
PIC quota (pmol C cell^{-1})	1.51 ± 0.26	2.87 ± 1.79	1.75 ± 0.17	0.69 ± 0.13
PIC prod. (pmol C cell^{-1} d^{-1})	-	-	-	0.48 ± 0.08
POC quota (pmol C cell^{-1})	0.49 ± 0.12	2.23 ± 1.16	1.13 ± 0.57	0.94 ± 0.11
POC prod. (pmol C cell^{-1} d^{-1})	-	-	-	0.65 ± 0.07
PIC/POC (mol/mol)	3.17 ± 1.00	1.28 ± 0.32	1.74 ± 0.57	0.73 ± 0.06
PON quota ((pmol N cell^{-1})	0.10 ± 0.00	0.31 ± 0.12	0.24 ± 0.06	0.10 ± 0.01

PON prod. ((pmol N $cell^{-1}$ d^{-1})	-	-	-	0.07 ± 0.00
C/N (mol/mol)	4.58 ± 1.05	6.95 ± 0.90	4.55 ± 0.98	8.64 ± 0.20
$Mg/Ca_{calcite}$ (mmol/mol)	-	-	-	-
$Sr/Ca_{calcite}$ (mmol/mol)	-	-	-	-
$P/Ca_{calcite}$ (mmol/mol)	-	-	-	-
$Fe/Ca_{calcite}$ (mmol/mol)	-	-	-	-

Table 11.3. Oceanographic and experimental data from the shipboard incubation 2 with *Emiliania huxleyi* [strain CAWPO6 (NZEH) and RCC1212 (AC477)].

Oceanographic parameters	**Depths (CTD cast)**			
	38 m	**508 m**	**1010 m**	**4831 m**
Temperature (°C)	12.80	11.42	8.89	2.57
Salinity	35.66	35.58	35.46	34.90
Oxygen (ml L^{-1})	5.97	5.56	6.45	7.53
Nitrate (µM)	5.35	10.50	18.70	20.80
Phosphate (µM)	0.32	0.35	1.03	1.38

Medium chemistry and sample data

E. huxleyi CAWPO6 (NZEH) - Incubation 2

	t*0*	t*n*	t*0*	t*n*	t*0*	t*n*	t*0*	t*n*
Nitrate (µM)	4.90	4.80	12.25	8.55	14.25	12.55	20.90	20.50
Phosphate (µM)	0.27	0.22	0.60	0.46	0.94	0.64	1.55	1.20
TA (µmol kg^{-1})	2340.50 ± 0.00	2324.10 ± 13.16	2341.80 ± 0.00	2332.20 ± 17.22	2342.70 ± 0.00	2293.20 ± 4.87	-	2323.20 ± 1.45
DIC (µmol kg^{-1})	2137.70 ± 0.00	2109.20 ± 17.99	2165.70 ± 0.00	2153.20 ± 0.12	2178.00 ± 0.00	2129.30 ± 5.07	-	2160.60 ± 5.20
pH_{total}	7.97 ± 0.00	8.00 ± 0.06	7.92 ± 0.00	7.93 ± 0.03	7.88 ± 0.00	7.89 ± 0.01	-	7.88 ± 0.01
pCO_2 (µatm)	484.09 ± 0.00	448.39 ± 69.79	550.54 ± 0.00	545.94 ± 53.29	623.35 ± 0.00	584.38 ± 16.76	-	609.89 ± 7.51
HCO_3^- (µmol kg^{-1})	1971.19 ± 0.00	1936.89 ± 34.11	2012.93 ± 0.00	1999.17 ± 8.70	2029.88 ± 0.00	1984.11 ± 4.91	-	2014.54 ± 7.56
CO_3^{2-} (µmol kg^{-1})	149.19 ± 0.00	156.20 ± 18.78	132.73 ± 0.00	134.28 ± 10.63	126.31 ± 0.00	124.26 ± 0.13	-	124.53 ± 2.96
CO_2 (µmol kg^{-1})	17.28 ± 0.00	16.09 ± 2.39	20.04 ± 0.00	19.70 ± 1.79	21.81 ± 0.00	20.93 ± 0.23	-	21.55 ± 0.52
Ω-Cal.	3.54 ± 0.00	3.70 ± 0.44	3.15 ± 0.00	3.18 ± 0.25	3.00 ± 0.00	2.95 ± 0.01	-	2.97 ± 0.07
$Mg/Ca_{seawater}$ (mol/mol)	5.34 ± 0.01	-	5.31 ± 0.00	-	5.32 ± 0.01	-	5.28 ± 0.03	-
$Sr/Ca_{seawater}$ (mmol/mol)	8.57 ± 0.03	-	8.59 ± 0.01	-	8.56 ± 0.04	-	8.59 ± 0.01	-
Cell density (cells ml^{-1})	5000		5000		5000		5000	
Growth rate (µ)	-		-		0.57 ± 0.03		0.30 ± 0.01	
PIC quota (pmol C $cell^{-1}$)	2.27 ± 0.93		-		0.84 ± 0.03		1.36 ± 0.03	
PIC prod. (pmol C $cell^{-1}$ d^{-1})	-		-		0.47 ± 0.01		0.41 ± 0.02	
POC quota (pmol C $cell^{-1}$)	2.08 ± 0.75		-		0.87 ± 0.02		1.53 ± 0.21	
POC prod. (pmol C $cell^{-1}$ d^{-1})	-		-		0.50 ± 0.02		0.46 ± 0.07	

PIC/POC (mol/mol)	1.09 ± 0.11	1.75 ± 0.43	0.95 ± 0.01	0.89 ± 0.12
PON quota ((pmol N cell^{-1})	0.10 ± 0.04	0.14 ± 0.00	0.08 ± 0.00	0.14 ± 0.02
PON prod. ((pmol N cell^{-1} d^{-1})	-	-	0.04 ± 0.00	0.04 ± 0.00
C/N (mol/mol)	20.21 ± 6.08	19.08 ± 0.55	10.77 ± 0.41	10.71 ± 0.69
Mg/Ca$_{calcite}$ (mmol/mol)	16.03 ± 6.20	49.25 ± 0.00	3.11 ± 0.41	2.38 ± 0.94
Sr/Ca$_{calcite}$ (mmol/mol)	2.60 ± 0.02	2.57 ± 0.00	2.82 ± 0.01	2.84 ± 0.08
P/Ca$_{calcite}$ (mmol/mol)	1.27 ± 0.00	2.07 ± 0.00	1.53 ± 0.14	1.24 ± 0.47
Fe/Ca$_{calcite}$ (mmol/mol)	2.50 ± 1.68	4.02 ± 0.00	0.41 ± 0.03	0.62 ± 0.22

E. huxleyi RCC1212 (AC477) - Incubation 2

	t*0*	t*n*	t*0*	t*n*	t*0*	t*n*	t*0*	t*n*
Nitrate (µM)	4.95	4.90	9.33	8.55	17.50	14.25	20.90	19.95
Phosphate (µM)	0.27	0.19	0.46	0.38	1.05	0.94	1.55	1.33
TA (µmol kg^{-1})	2343.74 ± 0.00	2317.00 ± 2.41	2284.08 ± 0.00	2326.38 ± 8.06	2339.27 ± 0.00	2320.10 ± 4.83	2359.77 ± 0.00	2334.86 ± 2.50
DIC (µmol kg^{-1})	2090.72 ± 0.00	2080.53 ± 0.96	2110.35 ± 0.00	2102.43 ± 2.33	2164.78 ± 0.00	2149.47 ± 3.00	2187.00 ± 0.00	2170.89 ± 2.17
pH$_{total}$	8.07 ± 0.00	8.04 ± 0.01	7.94 ± 0.00	8.02 ± 0.02	7.91 ± 0.00	7.91 ± 0.01	7.91 ± 0.00	7.90 ± 0.01
*p*CO$_2$ (µatm)	375.72 ± 0.00	398.47 ± 6.88	511.17 ± 0.00	420.08 ± 22.43	574.66 ± 0.00	568.52 ± 9.27	580.90 ± 0.00	595.25 ± 2.75
HCO$_3^-$ (µmol kg^{-1})	1896.73 ± 0.00	1896.96 ± 2.08	1961.90 ± 0.00	1925.64 ± 8.22	2012.58 ± 0.00	2000.30 ± 2.45	2035.05 ± 0.00	2024.15 ± 3.66
CO$_3^{2-}$ (µmol kg^{-1})	180.70 ± 0.00	169.43 ± 1.70	129.19 ± 0.00	161.64 ± 6.67	131.80 ± 0.00	128.68 ± 1.61	131.19 ± 0.00	125.32 ± 2.23
CO$_2$ (µmol kg^{-1})	13.282 ± 0.00	14.14 ± 0.19	19.25 ± 0.00	15.15 ± 0.77	20.40 ± 0.00	20.49 ± 0.28	20.75 ± 0.00	21.42 ± 0.45
Ω-Cal.	4.29 ± 0.00	4.02 ± 0.04	3.06 ± 0.00	3.83 ± 0.15	3.13 ± 0.00	3.05 ± 0.03	3.13 ± 0.00	2.99 ± 0.05
Mg/Ca$_{seawater}$ (mol/mol)	5.34 ± 0.01	-	5.31 ± 0.00	-	5.32 ± 0.01	-	5.28 ± 0.03	-
Sr/Ca$_{seawater}$ (mmol/mol)	8.57 ± 0.03	-	8.59 ± 0.01	-	8.56 ± 0.04	-	8.59 ± 0.01	-

Cell density (cells ml^{-1})	4000	4000	4000	4000
Growth rate (µ)	-	-	-	-
PIC quota (pmol C cell^{-1})	3.02 ± 0.64	1.73 ± 0.29	2.50 ± 0.51	2.70 ± 0.45
PIC prod. (pmol C cell^{-1} d^{-1})	-	-	-	-
POC quota (pmol C cell^{-1})	2.34 ± 0.86	1.24 ± 0.21	2.00 ± 0.48	2.39 ± 0.16
POC prod. (pmol C cell^{-1} d^{-1})	-	-	-	-
PIC/POC (mol/mol)	1.33 ± 0.22	1.44 ± 0.49	1.26 ± 0.09	1.12 ± 0.11
PON quota ((pmol N cell^{-1})	0.14 ± 0.04	0.09 ± 0.01	0.14 ± 0.02	0.17 ± 0.01

PON prod. ((pmol N $cell^{-1}$ d^{-1})	-	-	-	-
C/N (mol/mol)	16.42 ± 0.47	12.78 ± 1.14	13.37 ± 0.76	13.96 ± 0.27
$Mg/Ca_{calcite}$ (mmol/mol)	111.92 ± 6.28	210.75 ± 90.79	71.56 ± 10.17	101.77 ± 6.67
$Sr/Ca_{calcite}$ (mmol/mol)	2.61 ± 0.00	2.63 ± 0.00	2.69 ± 0.01	2.61 ± 0.00
$P/Ca_{calcite}$ (mmol/mol)	2.01 ± 0.07	4.67 ± 1.12	2.16 ± 0.22	2.21 ± 0.00
$Fe/Ca_{calcite}$ (mmol/mol)	10.64 ± 0.07	19.18 ± 7.86	5.43 ± 1.06	8.53 ± 0.02

Table 11.4. Experimental data (at harvesting time = 72 h) from incubations with the 5 strains (*see* Table 11.1) with water from 38 m (CTD cast) at constant temperature (14 °C) in an incubator with PAR = 200 µmol quanta m^{-2} s^{-1}.

Strain	CAWPO6 (NZEH)	RCC1212 (AC477)	CCMP88E (CCMP378)	CCMP1A1 (CCMP372)	AC472 (TQ26)
Nitrate (µM)			4.90		
Phosphate (µM)			0.27		
TA (µmol kg^{-1})			2340.50		
DIC (µmol kg^{-1})			2137.70		
pH_{total}			7.97		
pCO_2 (µatm)			484.09		
HCO_3^- (µmol kg^{-1})			1971.19		
CO_3^{2-} (µmol kg^{-1})			149.19		
CO_2 (µmol kg^{-1})			17.28		
Ω-Cal.			3.54		
$Mg/Ca_{seawater}$ (mol/mol)			5.34		
$Sr/Ca_{seawater}$ (mmol/mol)			8.57		
$Mg/Ca_{calcite}$ (mmol/mol)	1.68 ± 0.30	8.47 ± 0.65	106.26 ± 28.87	341.37 ± 0.00	145.50 ± 0.00
$Sr/Ca_{calcite}$ (mmol/mol)	2.48 ± 0.00	2.58 ± 0.00	2.61 ± 0.00	2.23 ± 0.06	2.80 ± 0.00
$P/Ca_{calcite}$ (mmol/mol)	0.93 ± 0.19	1.41 ± 0.57	2.41 ± 0.62	3.72 ± 0.00	2.83 ± 0.00
$Fe/Ca_{calcite}$ (mmol/mol)	0.45 ± 0.14	1.44 ± 1.05	2.86 ± 0.68	8.25 ± 0.00	2.19 ± 0.00

connected to one side ("water in"), filling up the first tank, which was at the same time connected by pipe to the second tank ("water out to next incubator") (Fig. 11.1). When this one was filled up, a hole was drilled on the lower wall and a hose was adjusted for the water to overflow. By adjusting the 5 m depth water flow pressure, we had a continuous flowing water system at 15.71 ± 0.46 ^{o}C temperature per day or between incubation 1 and 2 (*see* Table 11.1 for individual strains) calculated from the 5 m depth water sensors installed in the ship. This system was left running from day 1 (26th May 2010) until the end of the cruise.

In order to collect water from four depths with contrasting carbonate chemistry, a conductivity-temperature-depth (CTD) rosette was calibrated in a deployment at 250 m and NISKIN bottles were fired to make sure everything was working for a complete deployment. The CTD was then deployed again on May 27th 2010 in 4758 m depth (incubation 1) and on May 31st 2010 in 4833 m depth (incubation 2).

11.2.3. Sampling strategy and coccolithophore incubations

For incubation 1, three Niskin bottles per depth were triggered at 10, 502, 1002, and 4757 m (Table 11.2) and at 38, 508, 1010, and 4831 m for incubation 2 (Table 11.2). The shallowest depth was based on the position of the chlorophyll maximum at the time of the CTD cast, while the rest were standard depths used to obtain a natural CO_2 gradient once onboard (first described in Chapter 12). Water for the incubations was filtered through Spectrum nylon mesh of 300 µm (9 cm diameter) to retain zooplankton and big particles and quickly transferred to 10 L carboys, taken to the wet-laboratory and gently filtered through a sterile 0.22 µm Polycap 36 AS disposable filter (Whatman Inc., US). Water was subsequently placed in 2.5 L Thermo Scientific Nalgene® polycarbonate bottles (Thermo Fisher Scientific Inc., US), which were completely filled (overflow) to minimize headspace, immediately closed, sealed with Parafilm® (Bemis Flexible Packaging, US) to avoid gas exchange and placed in the incubator system on deck to equilibrate with the running water temperature (15.63-15.78 °C) (Table 11.1). Salinity was between 34.90-35.90 depending on depth and incubation.

Each depth incubation was carried out in triplicate and an extra flask (a blank without cells) was used as a control. Once temperature equilibrated in the 0.80 m^3 tanks and the 2.5 L flasks (~ 1 h), coccolithophore cells from cultures at 14 °C and PAR = 200 µmol quanta m^{-2} s^{-1} were

inoculated at the following initial concentrations at all depths: 2159 cells ml^{-1} (CCMP883 - incubation 1), 3787 cells ml^{-1} (CAWPO6 - incubation 1), 5000 cells ml^{-1} (CAWPO6 - incubation 2), and 4000 cells ml^{-1} (RCC1212 - incubation 2) (Table 11.2, 3). We always started inoculation on the deepest water treatments (4757 and 4831 m) in both incubations to minimize gas exchange and thus maintain the natural CO_2 gradient between incubation flasks. Immediately afterwards, these were tightly closed and sealed again with Parafilm. The inoculation procedure was conducted as quickly as possible to minimize gas exchange, which could also alter the CO_2 gradient [although this takes a few hours when using deep water as previously observed in other shipboard incubations (see Chapter 12)]. Incubation flasks containing cells were placed inside the main incubators on deck (with the running water from 5 m depth flowing) and lids were secured until harvest. Incubations were carried out for 72 h (t*n*). This minimized total alkalinity (TA) and dissolved inorganic carbon (DIC) consumption, which at t*n* was always within 10 % of t*0* depending on the strain used (*see* Table 11.2, 11.3 and results section).

Using seawater from incubation 2, all five strains (Table 11.1, 11.4) were incubated in 0.5 L Nalgene® polycarbonate flasks, using chlorophyll maximum depth water (38 m) at 14°C, in a light-controlled (PAR = 200 µmol quanta m^{-2} s^{-1}) incubator onboard. Cells, were inoculated at 5000 cells ml^{-1} for all strains. Here, the sampling procedure at t*0* and t*n* was identical as in incubation 2 (*see* below). Sampling took place after incubation 2 was finished (*see* below).

11.2.4. Sample analysis: summary

Seawater samples were collected in triplicate at t*0* for the following parameters [beyond the continuous readings of the CTD: temperature, salinity, oxygen, and chlorophyll *a*]:

- Oxygen: Measured on incubation flasks after temperature equilibration in the tanks with an Oxygen Optode/Temperature sensor (AANDERAA 4330/4330F).

- Macronutrients (nitrate and phosphate): Samples directly collected from the Niskin bottles (to analyze the CTD cast) and from the incubation flasks (to analyze t*0*).

- Carbonate chemistry: TA and DIC samples directly collected from the Niskin bottles (to analyze the CTD cast) before and after filtration to compare results (data not shown in

this chapter). Samples also collected from the incubation flasks after temperature equilibration in the tanks (to analyze t*0*).

- Seawater elemental composition: Samples directly collected from the NISKIN bottles both to analyze CTD cast and t*0* for incubation flasks.

- Cell density: Samples taken in cellulose nitrate membrane filters and in polycarbonate filters for scanning electron microscopy (SEM) (*see* below).

Seawater samples were collected in triplicate at t*n* for the following parameters:

- Oxygen: Measured on incubation flasks just after opening them to assess biological consumption.

- Macronutrients (nitrate and phosphate): Samples collected from the incubation flasks to assess biological consumption.

- Carbonate chemistry: TA and DIC samples collected from the incubation flasks just after opening them to minimize gas exchange and to assess biological consumption.

- Cell density: Samples taken in cellulose nitrate membrane filters and in polycarbonate filters for scanning electron microscopy (SEM) (*see* below).

- POC, PON, and PIC: Samples taken on filters after the other variables were sampled (*see* below).

- Coccoliths elemental composition: Samples of coccolith material taken on filters and converted to pellets with all the remaining culture material in the flasks (*see* below).

11.2.4.1. Medium chemistry

Samples were taken for macronutrients [nitrate (NO_3^-) and phosphate (PO_4^{2-})] by filtration of 15-20 ml water through a Millex syringe-driven 0.22 μm filter (Millipore, USA) and stored at -20

ºC until required for analysis. Nitrate and phosphate concentrations were determined colorimetrically following Hansen and Koroleff (1999) using a Hitachi U-2000 spectrophotometer (Scientific-Instruments, Germany) at the Helmholtz Centre for Ocean Research Kiel (GEOMAR) (Germany). Samples for carbonate chemistry (TA and DIC) were collected in 300 ml borosilicate flasks directly from the Niskin bottle. Samples were collected in triplicates before filtration (directly from the Niskin), and after filtration. Samples were pre-filtered through a 300 μm mesh for zooplankton and large particles, and then through a 0.22 μm polycarbonate capsule. Before and after filtration samples were used to assess TA variability owing to the filtration procedure (but only filtered samples were used to work out experimental conditions). All samples were preserved with 750 μl 3.5% $HgCl_2$ solution to prevent microbial growth during storage at room temperature. Samples were analysed for TA and DIC using a Versatile Instrument for the Determination of Titration Alkalinity (VINDTA) at the National Oceanography Centre (Southampton, UK). Certified reference materials (CR) to calibrate and establish correction factors for VINDTA measurements were obtained from Dr. Andrew Dickson at the Marine Physics Laboratory of the Scripps Institute of Oceanography, University of California San Diego, USA. VINDTA-derived values for TA and DIC were corrected for various parameters including titration acid density, nutrient concentration of the sample, temperature, salinity and CRM values using a MatLab R2010b (The MathWorks, Inc. UK) script obtained from Mrs Sue Hartman at the National Oceanography Centre, Southampton, UK. Carbonate chemistry parameters were calculated from *in-situ* (incubations) temperature, salinity, DIC, TA and nutrients using the "CO2SYS" macro (Lewis and Wallace 1998). The equilibrium constants were from Mehrbach et al. (1973), refitted by Dickson and Millero (1987), the KSO_4 constants were from Dickson (1990), and the total pH scale was used.

11.2.4.2. Medium elemental composition

The concentrations of calcium (Ca^{2+}) and magnesium (Mg^{2+}) ions in water samples from all depths were measured to rule out seawater effects on calcification and elemental composition. Seawater composition was determined in triplicate by inductively coupled plasma optical emission spectrometry (ICP-OES) using a Perkin Elmer optima 4300DV at the National Oceanography Centre (Southampton, UK). The bottles for the samples were acid cleaned with nitric acid (HNO_3). Samples were diluted in 0.3M HCl and calibrated against multi-element standard solutions that bracketed the concentration ranges in the sample solutions. Standards

were prepared gravimetrically using certified and traceable VWR Aristar single-element standard solutions, Romil UpA nitric acid and Milli-Q water. A standard seawater solution (IAPSO) and Certified Reference Materials (CRM) were analyzed for cross-reference.

11.2.4.3. Growth rate and cell density

Since problems were encountered with preserved samples for flow cytometry and Coulter counting, cell counts for each incubation were made using scanning electron microscopy (SEM) analysis of filtered cultures on cellulose nitrate filters. In brief, 200 ml of cells from each incubation were gently filtered onto a 25 mm cellulose nitrate filter and dried overnight at 37 ºC. Samples were subsequently stored in airtight containers containing silica gel to prevent degradation. Scanning electron microscopy (SEM) analysis and cell counting was carried out at the National Oceanography Centre (UK) following the methods outlined by Charalampopoulou et al. (2011).

Growth rate was determined with a standard exponential growth equation (Reynolds 1984):

$$\mu = [\mathrm{Ln}\,(N_t) - \mathrm{Ln}\,(N_0)] / t \quad (1)$$

where N_t and N_0 are the cell densities at the start and at the harvest day respectively, and t corresponds to the length of incubation (in days).

11.2.4.4. Particulate matter

In order to assess cellular particulate organic carbon and nitrogen (POC and PON) content, aliquots of 200 ml of each sample were filtered through pre-combusted (400 ºC for 6 h) GF/F filters (25 mm glass microfiber 0.70 μm pore size, Whatman). Filters were frozen (-20 ºC) until required for analysis. Upon thawing, samples were fumed with H_2SO_3 for 48 h in a dessicator chamber to remove inorganic carbon (Verardo et al. 1990). The filters were subsequently dried at 60 ºC for 48 h and pelleted in pre-combusted aluminium foil (EMA 100 x 30 mm circles, following Hilton et al. 1986). POC and PON concentrations were analysed at Plymouth Marine Laboratory (UK) using a Thermo Finnigan Flash EA1112 elemental analyzer with acetanilide standards.

In order to assess cellular calcification content and rates (PIC analysis), 200 ml of medium were filtered through 0.20 μm 47 mm diameter Nuclepore polycarbonate filters, which had been twice rinsed with 5 ml of a dilute ammonium hydroxide solution (pH ~ 9.5). After filtration, samples were washed three times with this solution to prevent any $CaCO_3$ dissolution and samples were then stored at -20 ºC. Prior to analysis, filtered $CaCO_3$ was dissolved in ~ 20 ml 0.1 M HNO_3 and [Ca^{2+}] was subsequently determined at the University of Cambridge (UK) using a Varian Vista Pro inductively coupled plasma emission spectrophotometer (ICP-OES; Agilent, Stockport, UK). Instrument calibration followed procedures used for the determination of Mg/Ca in foraminiferal calcite (de Villiers et al. 2002). [Na^{+}] was measured as a proxy for residual seawater Ca^{2+}. Filters rinsed with the control medium were also analyzed and confirmed that seawater contribution to measured [Ca^{2+}] was negligible. Ca^{2+} content per filter and coccolithophore (using cell density) was then calculated and extrapolated to PIC, assuming that all Ca^{2+} on the filters was derived from $CaCO_3$ (Fagerbakke et al. 1994).

Particulate matter production (POC, PON and PIC) were calculated as follows:

$$\text{Production}_X = \mu * (\text{cellular content}) \quad (2)$$

where X = POC, PON or PIC, cellular content = cellular organic/inorganic content, and μ= growth rate.

11.2.4.5. Coccolith elemental composition

When all other samples were taken, between 800 ml and 1.5 L of each incubation flask were immediately filtered through 47 mm diameter Nuclepore polycarbonate filters (pore size 0.22 μm), without previous treatment. When the filtration slowed owing to excess calcite being retained in the filter, we changed the polycarbonate filter, using between 3 and 5 depending on sampling volume and cell density. All filters were stored in clean 50 ml Falcon tubes at -20 ºC until further treatment. In the laboratory back at the National Oceanography Centre (Southampton, UK), samples were thawed at room temperature for 2-3 h. The majority of the particulate material sedimented to the bottom of the 50 ml falcon tube during thawing and it was resuspended by gentle agitation of the filter using acid cleaned teflon tweezers. The

polycarbonate filters were carefully removed with teflon tweezers®, leaving only seawater and coccolithophores. The material was concentrated into cellular pellets (one pellet per replicate bottle) by centrifugation with a relative centrifuge force (RCF) of 1970 g for 20 minutes at 4 ºC with a Hettich ROTANTA 460RS Centrifuge (Hettich Lab Technology, Germany). After discarding the supernatant, the coccolithophore pellets were frozen at -80 ºC, dried in the oven for 24 h ad 60 °C, and kept at room temperature until further treatment.

In the laboratory, at the Department of Geology, University of Oviedo (Spain), we cleaned the pellets following the Blanco-Ameijeiras et al. (in press) optimized protocol to measure coccolithophore elemental ratios. In brief, we removed as much organic material as possible with a 1 ml pipette, and then centrifuged 3 times the remaining calcite with 2 ml of alkaline deionized water (DI), which pH_{total} was adjusted between 9 and 10 with NH_4OH to avoid carbonate dissolution. These pellets were then treated with a reductive solution [0.750 ml of 4.76 % (v/v) Hydroxylamine-hydrochloride $NH_2OH{\cdot}HCl$ + 3 8% (v/v) NH_4OH] for 24 h at 22 °C. The pellets were sonicated with the reductive solution for 20 minutes before the 24 h incubation. After the incubation, pellets were rinsed and centrifuged 4 times with 2 ml of DI water. They were then treated with an oxidative solution [2 ml of 0.33 % (v/v) H_2O_2 + 0.98 % (v/v) NaOH] for 10 minutes in the sonicator and another 10 minutes in a warm bath at 100 °C. Then, they were rinsed 2 times with 1 ml of DI water. The complete oxidation step was repeated 3 times. The final pellets were transferred to clean microfuge tubes (15 ml), dissolved in 250 µL of ultra-pure 2 % HNO_3 and diluted in 750 µl of DI water. Elemental analysis was performed in an ICP-AES, using the Thermo *i*CAP 6300 Series ICP Spectrometer (installed in the Department of Geology, University of Oviedo, Spain). To improve precision by minimizing matrix effects, all samples were diluted to similar Ca concentrations for final analysis of trace metal/Ca ratios. To this end, an aliquot of 50 µl of dissolved material was analyzed for Ca concentrations. Based on the measured Ca, the other samples were diluted to a common Ca level, seeking the highest possible Ca concentration within the range of standard calibration solutions (15, 50, 100 ppm Ca). For trace element ratios, we measured in both radial and axial mode: P (177 nm axial), Fe (259 nm radial), Ca (315 nm radial) and Sr (407 nm radial). Calibrations were performed with multi-element standards offline using the intensity ratio method of de Villiers et al. (2002).

11.3. Results and Discussion

11.3.1. A natural gradient of seawater carbonate chemistry

Total alkalinity in this study remained almost constant between 2293.20 and 2375.10 at any depth (Takahashi et al. 1979) and incubation (1 and 2) in t*0* samples. Changes < 1 % were observed between filtered and non-filtered samples. Small variations at t*n* (72 h) below 3 % were observed owing to coccolithophores calcification. Dissolved inorganic carbon and pCO_2 increased, while pH_{total} and Ω-Cal. decreased with depth in all samples and incubations at t*0* (*see* Table 11.2, 11.3; Fig. 11.2): DIC = 2090.72-2137.40 μmol kg^{-1} (euphotic zone) to 2187.00-2187.80 μmol kg^{-1} (> 4700 m), pCO_2 = 345.20-484.09 μatm (euphotic zone) to 580.90-614.40 μatm (> 4700 m), pH_{total} = 7.97-8.11 (euphotic zone) to 7.89-7.91 (> 4700 m), and Ω-Cal. = 3.54-4.55 (euphotic zone) to 2.95-3.13 (> 4700 m). At t*n*, variations below 10 % were observed for all parameters, owing to calcification (*see* Table 11.2, 11.3). Nutrients were always replete at any depth and incubation (but in the euphotic zone) both at t*0* and t*n*: $[NO_3^-]$ = 0.85-4.95 μM (euphotic zone) to 19.40-21.50 μM (> 4700 m), and $[PO_4^{2-}]$ = 0.08-0.19 μM (euphotic zone) to 1.13-1.64 μM (> 4700 m). The seawater elemental composition remain almost constant with depth (t*0* values): Mg/Ca = 5.34 mol/mol (euphotic zone) to 5.28 mol/mol (> 4700 m), and Sr/Ca = 8.57 mmol/mol (euphotic zone) to 8.59 mmol/mol (> 4700 m).

The carbonate chemistry gradient in the water column was calculated from TA and DIC samples omitting the pressure effect (t*0* samples), since incubations were conducted at atmospheric pressure and samples were taken at the surface, and after the temperature equilibrated with culture conditions (15.71 ± 0.46 °C), for ~ 1 h. Thus, the gradient used in this experiment does not exactly mimic the one in the ocean (Feely et al. 2004) at *in situ* temperature (from 15.80 to 2.50 °C) and pressure, but rather its properties when water reaches the surface, like in an upwelling event. The carbonate chemistry of these waters from different depths mimics an upwelling event and can be used as in the field to test one natural form of ocean acidification, (Riebesell et al. 2010). This approach was first used in Chapter 12 in the same station to test the natural CO_2 gradient on the physiology and development of echinoid larvae. They used as equilibration temperature 9 °C thus their carbonate chemistry is slightly different from that of this study. Our study confirms the validity of this approach to achieve a consistent carbonate chemistry gradient in the field. The higher DIC (thus CO_2) values with depth (after depressurizing the water and equilibrating at surface temperature) are a consequence of larger

DIC/TA ratios in the mesopelagic (200-1000 m) and deep waters (1000-5000 m). This is caused by cumulative enrichment of DIC at almost constant TA, induced by the respiration of the particulate matter (organic and inorganic) sinking from the euphotic and mesopelagic zones (Honjo et al. 2008), and the higher solubility of CO_2 with decreasing temperature (Weiss 1974).

Our approach highlights the usefulness of induced upwelling events to test the effect of ocean acidification with its carbonate system and natural properties. This includes nutrient limitation in the euphotic zone (therefore used as a control) and different regimes encountered at each depth layer on a seasonal basis [(proximate limiting nutrient concept (Tyrrell 1999)]. Nutrient limitation exists in the euphotic zone after the spring bloom (days to weeks) while replete conditions are present deeper in the water column (*see* Table 11.2, 11.3). The winter mixed layer in the north Atlantic ranges from 20 to 600 m (Marshall et al. 1993), which then stabilizes during spring/summer owing to stratification (pycnoclines already developing in March), allowing the natural phytoplankton to bloom. It must be noted that this cruise and the incubation took place at the end of May and beginning of June, thus we cannot rule out that the annual spring bloom just took place, depleting the nutrients in the euphotic zone. Lampitt et al. (2001) study in the same area and station revealed that the spring bloom normally starts around mid-March (based on monthly average chlorophyll concentrations from SeaWIFS), lasting until August, with chlorophyll peaks from May to June. This coincides with our study dates. In addition to our incubations, we sampled the natural phytoplankton population, which was dominated by diatoms, from the Niskin bottles at 10 m during incubation 1. Diatoms dominate the early summer deposition of particulate matter in the area (Lampitt 1985; Lampitt et al. 2001) and elsewhere (Takahashi et al. 2000), thus they were expected in the water. Surprisingly, we found few cells in the euphotic zone while inspecting in the microscope. Furthermore, the diatom cells did not grow in a trial incubation we carried out parallel to incubation 1 with the coccolithophores (with water from all depth levels). The evidence present here indicates that our study probably took place after a large bloom event, which explains the low nutrient levels in the euphotic zone during the study period. Coccolithophores have low nutrient quota (Litchman et al. 2007) and are therefore adapted to this conditions. It is thus essential to consider the nutrient condition in the natural CO_2 gradient approach (especially with euphotic zone water) because morphological (coccoliths size and morphology) and biogeochemical (particulate matter production) parameters can be controlled by individual nutrient limitation (Paasche 1998; Fritz

1999; Sciandra et al. 2003; Benner 2008; Müller et al. 2008; Kaffes et al. 2010; Borchard et al. 2011) or by co-limitation (Langer et al. 2012; *see* chapter 10).

The seawater elemental ratios (Mg/Ca and Sr/Ca) varied slighty with depth from 5.34 to 5.28 mol/mol and 8.57 to 8.59 mmol/mol respectively (following the Marcett principle of constant proportions (Marcett 1918; Millero et al. 2008)], so we can exclude any water composition effects on the calcite (Ries 2010). This contrasts with findings in other ocean basins, e.g. Pacific Ocean, where the top 1000 m are depleted in Ca^{2+} 1 % and Sr^{2+} 1-3 % relative to deep waters (Brewer et al. 1975; de Villiers 1999). This can be attributed to biological consumption of the elements, and quick dissolution at depth below the lysocline (element-specific).
Our field approach cannot reproduce upwelling events comparable to areas where the magnitude of organic matter production and respiration (thus DIC/CO_2 increase and oxygen depletion) is much higher than the north Atlantic Ocean. This includes true upwelling zones such as Peru (Humboldt current), west Africa (Benguela current, Cape Blanc), or the Arabian Sea. Our maximum DIC values remain below 2190 µmol kg^{-1} in the deepest seawater collected (> 4700 m), which coincides with the first 100-200 m of e.g. the Peru upwelling DIC (Paulmier et al. 2011). Values below the first 100 m rise to 2350 µmol kg^{-1} at 1000 m, and to 2450 µmol kg^{-1} at 3000 m, thus purely using north Atlantic deep waters, we cannot replicate these gradients. However, our approach remains acceptable to test natural upwelling and *in situ* ocean acidification in upwelling regions where there is no oxygen minimum zone or in areas of seasonal upwelling. This can include continental margins and the open ocean [e.g. Alboran Sea (Perkins et al. 1990; Sarhan et al. 2000), Mediterranean Sea (Bakun and Agostini 2001), equatorial Atlantic (Rhein et al. 2010)].

11.3.2. *Emiliania huxleyi* response to a natural carbonate chemistry gradient: results summary and other applications

The strains responded positively to increasing depth (higher CO_2), with increasing growth rate from 1000 to 5000 m water (500 to 600 µatm CO_2) (Fig. 11.2b). However, a sample problem from the other two depths did not allow to assess the response to lower field CO_2 conditions. Yet, we assume that the growth rate was smaller because the calcite Sr/Ca decreased at 500 and 10 m, which is known to follow growth rate (Stoll et al. 2002). The calcite Sr/Ca increased with depth and higher CO_2 from 2.20 to 2.80 mmol/mol (depending on strain) which has been

obserbed in controlled laboratory incubations (Müller et al. in preparation - *see* Chapter 8). There was also a strain-specific response that has been reported before for *E. huxleyi* (Blanco-Ameijeiras et al. in preparation - *see* Chapter 8). The increase in Sr/Ca likely followed growth rate, which in this case depended on CO_2 and not on temperature (maintained constant). The net CO_2 effect on Sr/Ca is difficult to understand, but it could be that an increasing calcification rate within the CO_2 concentrations tested here, reduces the cells elemental discrimination power, thus incorporating more Sr^{2+} in the calcite. This could not be assessed for the calcite Mg/Ca, since the carbonate was not well cleaned despite the robust protocol used (Blanco-Ameijeiras et al. in press). Mg/Ca data were above 1 mmol/mol with contamination proxies P/Ca and Fe/Ca varying from 1 to 20 mmol/mol, which means that the organic-Mg was not completely removed (Table 11.2, 11.3, 11.4). This problem with *E. huxleyi* has already been reported (Blanco-Ameijeiras et al. in press - *see* Chapter 8) as a consequence of high POC levels compared to PIC, that avoid an effective cleaning. Species with less POC such as *Gephyrocapsa oceanica* should be favoured to measure calcite elemental ratios (*see* Chapter 8).

The C/N ratio remained constant with increasing depth and CO_2, with variability according to strain. The PIC/POC increased slightly in some cases while it was constant in others (Iglesias-Rodriguez et al. 2008a; Shi et al. 2009), similar to the findings of Langer et al. (2009) for a variety of *E. huxleyi* strains. The nutrient depletion issue in the euphotic zone (Table 11.2, 11.3) complicates the interpretation because low N and P alone increase and decrease the PIC/POC respectively compared to replete conditions (in this study found at 500, 1000, and 5000 m) (*see* Chapter 10). With the data available we can predict that there is a small fertilization effect from the deep waters induced by the higher nutrients and higher CO_2 (below 700 µatm) concentrations. This information is important e.g. to consider geo-engineering approaches to sequester CO_2 where water is proposed to be upwelled from depth (Lovelock and Rapley 2007; Karl and Letelier 2008). While current simulations use depths down to 1000 m (Oschlies et al. 2010), industrial applications have a maximum effective operations depth of 50-200 m (www.atmocean.com). At least in the north Atlantic Ocean, upwelling from the eupthotic zone does not really fertilize coccolithophores, when compared with deeper water with higher CO_2 (Fig. 11.2). However, moving to deeper water artificial upwelling can bring other large scale problems (*see* Oschlies et al. 2010).

In conclusion, our field approach can be used to test ocean acidification following a natural CO_2 gradient and also to derive data to assess deep water fertilization effects. We think that the set-up

needs to be optimized for the right question in order to get the correct data. However, small problems associated with the experimental set up, time frame and coccolithophores responses difficulty interpretations in the current study. This should not avoid the use of this method in new studies to understand the CO_2 fertilization effect in the field.

12.

Susceptibility of echinoid larvae to artificially upwelled deep ocean waters

Abstract

A variety of marine calcifying organisms are exposed to natural carbonate chemistry gradients (deep ocean water, upwelling systems, CO_2 vents) during their life cycle. The carbonate compensation depth (CCD), below which calcium carbonate dissolves, is progressively shoaling owing to the increasing oceanic uptake of CO_2 resulting from anthropogenic emissions termed ocean acidification (OA). Little is known on how exposure to deep ocean waters affects meroplankton life cycle stages, morphology, elemental composition, and physiology. This is relevant to calcifying organisms such as echinoderms, inhabiting shelf areas exposed to abrupt ambient carbonate chemistry changes, driven for example by episodic upwelling. These events bring waters to the surface near undersaturation with respect to calcite and aragonite, which can be used to study natural CO_2 ranges. Using larvae of the subtidal sea urchin species *Psammechinus miliaris*, we conducted incubations for 5 days in the North Atlantic Ocean with seawater artificially upwelled from 4700, 4600, 4000, 2000 and 250 m to test the effect of the ambient carbonate chemistry on larval physiology. Our approach represents an alternative to artificial manipulations in laboratory incubations to assess the effect of different carbonate chemistries from deep waters in surface incubations. We show that a pCO_2 increase of ~ 200 µatm from 250 to 4700 m resulted in a decline in fertilization success (20 %) and in the calcium carbonate content (> 50 %) of the larvae but had no apparent effect on larval morphology and

organic matter content. The reduced fertilization success and decline in calcification suggest that there may be metabolic trade-offs in *P. miliaris* to adjust to changing carbon chemistry conditions in the context of ocean acidification.

This chapter is based on:

Suarez-Bosche, N., **Lebrato, M.,** Tyler, P. A. and Iglesias-Rodriguez, M. D. in review. Susceptibility of echinoid larvae to artificially upwelled deep ocean waters. In: *ESA Ecosphere*.

Acknowledgements: We thank Richard Lampitt and Colin Day, the crew and scientists of RRS *James Cook* cruise 034, for the opportunity to conduct incubations during the research expedition. We thank Darryl Green for ICP-OES analyses of seawater, Mark Stinchcombe for nutrient analysis and Robert Head for particulate carbon analysis. Dana Greely advised on use of WOCE data for the Atlantic Ocean. This work was supported by the "European Project on Ocean Acidification" (EPOCA) for M. Lebrato's PhD. The National Council of Science and Technology of Mexico (CONACyT) funded this work as part of N. Suarez-Bosche' PhD.

12.1. Introduction

In the marine environment, organisms with alternating pelagic and benthic life stages populate different layers of the water column during their life history, therefore encountering variable ambient carbonate chemistry conditions. For example, numerous echinoderms have a meroplanktonic life stage, entering pelagic waters until they settle at the seabed, where they undergo metamorphosis and develop into adult stages. Echinoderms have a wide distribution, from shallow waters on the shelf to the deep-sea in all oceans and at all latitudes. Echinoids are one of the five classes of echinoderms, which play a key role in maintaining the balance and energy flow in marine ecosystems (e.g. grazing, burrowing, calcifying) (McClintock 1994; Turon et al. 1995). Additionally, they export carbon, in some cases exceeding 1000 gr m^{-2} yr^{-1} in the form of Mg-calcite, mainly as calcium and magnesium carbonate ($CaCO_3$ and $MgCO_3$), contributing to the global carbonate export (> 0.1 Pg C yr^{-1}) (Lebrato et al. 2010). These organisms inhabit waters that are increasing in carbon dioxide (CO_2) concentration at a rate that is already measurable (Sabine et al. 2004), following anthropogenic carbon emissions. The accelerated increase of CO_2 in seawater is termed "ocean acidification" (OA) (Caldeira and Wickett 2005), resulting in an increased concentration of hydrogen (H^+) and bicarbonate ions (HCO_3^-), and a decrease in pH and carbonate ions (CO_3^{2-}). This is important because CO_3^{2-} largely controls the saturation state of calcite ($\Omega_{Cal.} = [CO_3^{2-}][Ca^{2+}]/K_{sp}$) (< 1= undersaturation; > 1= supersaturated) where K_{sp} is the solubility constant for the $CaCO_3$ biomineral (Mucci 1983). The calcite compensation depth (CCD), below which the $\Omega_{Cal.} < 1$ and the rate of production of $CaCO_3$ is exceeded by its rate of dissolution, is critical to organisms such as echinoderms that form $CaCO_3$ skeletons during their life cycle (Feely et al. 2004, 2008).

Several processes affect the magnitude of $\Omega_{Cal.}$ in the water column. Firstly, the CCD has moved closer to the surface and nearer to the coast owing to anthropogenic emissions and the increasing oceanic uptake of CO_2 (Feely et al. 2004, 2008). Recent research on echinoderms suggests that deep-sea populations (in the Southern Ocean) are already at the boundaries of the CCD undersaturated waters at 3000 m, and organisms below those depths have weakly calcified skeletons (Sewell and Hofmann 2011). Secondly, the shoaling of the CCD can be a result of natural upwelling events whereby deep high CO_2 and low $\Omega_{Cal.}$ waters surface in seasonal processes associated with major coastal currents such as the Canary Current (off northwest Africa), the Benguela Current (off Namibia), the Humboldt Current (off Peru and Chile), the

Somali Current (off Somalia) and the California Current (off California and Oregon) (Mann and Lazier 1991; Feely et al. 2008; Paulmier et al. 2011).

Echinoderms may be susceptible to variation in the seawater carbonate chemistry, including changes in CO_2 and $\Omega_{Cal.}$, which they encounter during their life history from larvae (pelagic) to adult stages (benthic). These changes have been assessed in laboratory enclosures where controlled environmental conditions allow the exploration of individual responses (e.g. morphological, developmental, and biochemical) to discrete climate relevant parameters (e.g. CO_2, temperature conditions). However, at present little is known about the responses of echinoderms to natural gradients of carbonate chemistry in the context of OA. One field approach is the use of geophysical features (e.g. volcanic CO_2 vents); natural venting sites that occur at the seabed as a consequence of volcanic activity, which emits CO_2 (> 90 %), among other gases. These sites provide natural gradients of CO_2 in benthic communities (Hall-Spencer et al. 2008; Cigliano et al. 2010). Here, we provide a natural OA study alternative, by testing on echinoids the effect of the increasing carbonate chemistry gradient with depth, using artificially upwelled waters from 5000 m to the surface. The incubations were conducted in the North Atlantic Ocean, where we investigated the effects the natural carbonate chemistry gradient on the physiology and skeleton biochemistry of larvae of *Psammechinus miliaris*. We chose *P. miliaris* because it uses high Mg-calcite to build their skeleton both as adults and juveniles (Raven et al. 2005). This polymorph of calcium carbonate is 30 times more soluble than aragonite (Politi et. al. 2004) and therefore more susceptible to dissolution under abrupt CO_2 changes (Morse et al. 2006). They live in intertidal rock pools in the Atlantic from the Scandinavia to the Azores, including the North Sea and the Baltic Sea, with a vertical distribution of < 100 m (Campbell 1977). Additionally, *P. miliaris* inhabits inshore and shelf zones exposed to riverine inputs and coastal upwelling systems such as the observed in the Baltic Sea (Myrberg et al. 2010) and the Portuguese shelf (dos Santos et al. 2008). This experimental approach provides a snapshot of the effect of short term-exposure to changes in ambient seawater chemistry conditions. These results are important in assessing the physiological plasticity of sea urchins in the context of OA in a natural setting.

12.2. Materials and Methods

12.2.1. Study site

The incubations were conducted in May 2009 aboard RRS *James Cook* in the Porcupine Abyssal Plain (PAP) (4840 m water depth). A conductivity-temperature-depth (CTD) rosette at 49 01.559 °N/015 10.226 °W was used to retrieve water from different depths (250, 2000, 4000, 4600 and 4710 m) representing different ambient carbonate chemistries (Table 12.1).

12.2.2. Experimental conditions

Adult individuals from the echinoid species *Psammechinus miliaris* were hand-collected in the intertidal at Torbay, UK (50 °N/3.33 °W) and maintained in aerated seawater aboard RRS *James Cook* until the experiment. The specimens were in healthy, and stress was minimized by using the same intertidal seawater, temperature and salinity that the organisms had in their natural habitat until the experiments were conducted. All experiments were done at 9 ±1 ^{o}C in a temperature-controlled room. This was the average sea surface temperature of the water at the time when *P. miliaris* was collected, which coincided with the spawn season. Spawning was already seen at the sampling site during collection of sea urchins (72 h before the experiment).

12.2.3. Fertilization success

The sea urchins were spawn by intracoelomic injection of 1 ml of 0.5 M KCl just before the CTD water was recovered. In the fertilization experiment, the gametes from 4 males and 2 females were taken and the quality of each gamete was checked with a microscope. Sperm motility and the eggs appearance/shape were checked. The eggs were placed in filter-sterilized seawater (0.22 µm filters, Millipore® Steriup™, Sigma-Aldrich) and sperm was collected dry. The total numbers of eggs used was counted from a 20 ml suspension determined through counts of 100 µl aliquots. The eggs were split into 20 beakers containing 200 ml of experimental water at a density of ~ 3-4 eggs ml^{-1} with water from different depths. Fertilization was performed by inoculating 1 µl of the combined sperm from all males. Sperm were activated directly in the vessels containing eggs that had been pre-acclimated to each experimental condition (water from different depths) for ~ 20 min. Sperm were counted using a haemocytometer and a final

Table 12.1. Carbonate chemistry, oceanographic experimental conditions and seawater elemental composition. Water sampled obtained with a CTD and Niskin bottles. The CO_2 concentrations correspond to the different depths for the Porcupine Abyssal Plain (PAP) site. SD indicates the standard deviation of triplicate measurements.

Depth (m)	250	2000	4000	4600	4710
Oceanographic parameters					
Temperature (°C)	11.67	3.44	2.53	2.54	2.55
Salinity	35.60 ± 0.00	34.91± 0.00	34.91± 0.00	34.91± 0.00	34.92 ± 0.00
Oxygen (ml l^{-1})	6.07	7.37	7.54	7.54	7.54
Nitrate (µmol l^{-1})	9.36 ± 0.37	17.94 ± 0.24	22.61 ± 0.30	22.95 ± 0.27	22.425 ± 0.37
Phosphate (µmol l^{-1})	0.54 ± 0.01	1.15 ± 0.01	1.49 ± 0.00	1.50 ± 0.02	1.48 ± 0.04
Silicate (µmol l^{-1})	3.62 ± 0.14	13.59 ± 0.25	43.11 ± 1.71	43.28 ± 1.36	43.11 ± 1.53
$[Ca^{2+}]_{seawater}$ (µg g^{-1})	32.32 ± 0.16	31.59 ± 0.07	31.27 ± 0.31	31.45 ± 0.15	31.73 ± 0.23
$[Mg^{2+}]_{seawater}$ (µg g^{-1})	10.07 ± 0.04	9.87 ± 0.05	9.80 ± 0.10	9.87 ± 0.03	9.96 ± 0.08
$Mg/Ca_{seawater}$ (mol/mol)	5.14 ± 0.00	5.15 ± 0.01	5.17 ± 0.00	5.17 ± 0.01	5.17 ± 0.01
Water carbon chemistry					
TA (µmol kg^{-1})					
Control	2331.80 ± 2.77	2294.19 ± 4.78	2327.95 ± 4.72	2330.56 ± 1.00	2330.68 ± 4.51
D1	2313.71 ± 2.18	2300.02 ± 1.91	2345.08 ± 7.80	2343.72 ± 3.02	2340.93 ± 5.35
D5	2312.11 ± 3.14	2278.06 ± 0.55	2323.82 ± 2.49	2360.68 ± 7.10	2328.28 ± 1.01
DIC (µmol kg^{-1})					
Control	2129.32 ± 4.40	2167.98 ± 8.26	2187.63 ± 2.69	2205.95 ± 4.12	2204.27 ± 2.29
D1	2139.03 ± 4.20	2150.25 ± 1.21	2207.29 ± 3.62	2203.02 ± 9.41	2197.63 ± 2.34
D5	2142.61 ± 4.22	2155.44 ± 3.00	2201.30 ± 2.43	2202.77 ± 8.19	2203.24 ± 8.49
pCO_2 (µatm)					
Control	357.50 ± 9.74	560.31 ± 24.77	520.49 ± 9.50	573.24 ± 19.63	566.45 ± 9.16
D1	412.53 ± 6.61	509.33 ± 13.31	534.73 ± 9.37	585.35 ± 10.70	555.13 ± 19.08
D5	425.36 ± 7.15	557.48 ± 10.04	579.42 ± 18.70	523.55 ± 27.85	571.04 ± 9.46
CO_2 (µmol kg^{-1})					
Control	16.10 ± 1.92	25.33 ± 4.74	23.53 ± 3.59	25.92 ± 0.89	25.61 ± 1.00
D1	18.58 ± 0.30	21.51 ± 2.86	24.18 ± 3.23	23.91 ± 4.44	23.27 ± 3.23
D5	19.15 ± 0.32	25.20 ± 0.45	26.20 ± 0.85	21.37 ± 2.16	25.82 ± 1.65
HCO_3^- (µmol kg^{-1})					
Control	1967.62 ± 15.6	2042.57 ± 8.15	2055.92 ± 6.98	2080.72 ± 6.08	2078.34 ± 4.63
D1	1992.19 ± 5.21	2037.05 ± 6.80	2075.91 ± 7.78	2070.16 ± 5.62	2064.14 ± 9.03
D5	1998.29 ± 5.07	2032.80 ± 3.91	2077.20 ± 4.34	2062.37 ± 1.47	2077.83 ± 8.10
CO_3^{2-} (µmol kg^{-1})					
Control	145.59 ± 5.39	100.08 ± 7.83	108.17 ± 4.05	100.63 ± 2.84	100.32 ± 3.56
D1	128.27 ± 1.40	113.29 ± 11.77	107.21 ± 4.52	108.96 ± 9.70	101.58 ± 2.97
D5	125.17 ± 1.58	97.44 ± 1.37	97.91 ± 2.75	113.39 ± 9.14	99.60 ± 5.25
Ω_{Cal}					
Control	3.46 ± 0.17	2.39 ± 0.23	2.58 ± 0.33	2.37 ± 0.07	2.39 ± 0.08
D1	3.04 ± 0.03	2.70 ± 0.28	2.56 ± 0.35	2.60 ± 0.27	2.63 ± 0.16
D5	2.97 ± 0.04	2.32 ± 0.03	2.33 ± 0.07	2.70 ± 0.22	2.37 ± 0.13
Ω_{Arg}					
Control	2.20 ± 0.13	1.51 ± 0.17	1.64 ± 0.21	1.50 ± 0.04	1.52 ± 0.05
D1	1.94 ± 0.02	1.71 ± 0.09	1.62 ± 0.12	1.65 ± 0.10	1.67 ± 0.13
D5	1.89 ± 0.02	1.47 ± 0.02	1.48 ± 0.04	1.80 ± 0.18	1.51 ± 0.08
pH_{total}					
Control	8.10 ± 0.05	7.92 ± 0.08	7.95 ± 0.06	7.91 ± 0.01	7.91 ± 0.02
D1	8.03 ± 0.01	7.98 ± 0.05	7.94 ± 0.06	7.95 ± 0.08	7.95 ± 0.06
D5	8.02 ± 0.01	7.91 ± 0.01	7.89 ± 0.01	7.94 ± 0.04	7.89 ± 0.03

concentration of 10^3 ml^{-1} was achieved, which typically yields high fertilization success and development. After 3 h, fertilization success was determined by counting eggs that had a fertilization envelope or showed cleavage at the 2 to 4 cell stage. Fertilization counts were taken from 4 replicates in each treatment (~ 60 eggs were taken from the suspension).

12.2.4. Larval development and morphology

To monitor the embryonic and larval morphology, an independent source of gametes were fertilized and placed in triplicate 2.5 L vessels at densities of 3-4 eggs per ml, for each experimental condition (15 sealed containers to minimize atmospheric CO_2 exchange). The gastrula stage (~ 24 h after fertilization) and four-armed pluteus larvae stage (5 days after fertilization) were sampled to assess developmental changes among treatments. Larvae were not fed during the incubations due to the short period of the experiments and to minimise changes in the carbonate chemistry due to photosynthetic activity of algae. Oxygen (mean = 352.1 ± 5.4 µM) and temperature (mean = 8.9 ±0.15 ^oC) were recorded daily with an Oxygen Optode/Temperature sensor (AANDERAA 3830) in each of the experimental vessels. We performed morphological analyses on larval postoral arm length (POA) and body length (BL) in specimens incubated in waters from each depth that were fixed in 4 % paraformaldehyde (EM GRADE, Science Services), and cleaned 3 times through filtered sea water. The larvae were mounted on a microscope slide and photographed for analysis. The larval characters were measured using the software Image J (available at http://rsb.info.nih.gov/ij; developed by Wayne Rasband, National Institutes of Health, Bethesda, MD).

12.2.5. Particulate carbon analyses and calcification

Total particulate carbon (TPC) and particulate organic carbon (POC) were analyzed in triplicate using 50 larvae from each experiment from larvae incubated for 5 days. Larvae were isolated and washed 3 times in phosphate buffered saline (PBS) buffer to rinse off seawater. The larvae were introduced into pre-combusted silver capsules (Elemental Microanalysis, UK) and stored at -20 ^oC for further analysis. For POC analysis, inorganic carbon was removed by acidification using a concentrated HCl solution under vacuum for 96 h. The capsules for both POC and TPC were dried at 60 ^oC for 48 h, and analyzed at Plymouth Marine Laboratory (UK) on a Thermo Finnegan flash EA1112 elemental analyzer using acetanilide as the calibration standard.

Particulate inorganic carbon (PIC) was calculated by subtracting the POC from the TPC values (Riebesell et al. 2000). The larvae were individually sampled by hand which reduces uncertainties in the measurement of carbon per larvae, since we used an exact number of larvae to ascertain precisely the bulk carbon averaged per 50 larvae. This is the first time these analyses are provided per larva.

12.2.6. Ambient seawater carbonate chemistry

Water sample aliquots for in situ dissolved inorganic carbon (DIC) and total alkalinity (TA) were collected directly from the CTD Niskin bottles 15 min before starting the experiment (immediately upon recovery of the CTD, to minimize gas exchange). The second and third sampling were 24 and 120 h after the start of the experiment to assess the changes in carbonate chemistry of the seawater during the development of the sea urchin larvae. At the start of the experiment, samples were taken at each experimental depth (in triplicate) and stored in sealed borosilicate glass bottles. An aliquot of $HgCl_2$ (0.4 mM) was added to the samples to prevent microbial growth. A Versatile INstrument for the Determination of Titration Alkalinity (VINDTA) at the National Oceanography Centre (Southampton, UK) was used to measure TA and DIC. The carbonate system [aragonite and calcite saturation ($\Omega_{Arg.}$ and $\Omega_{Cal.}$), seawater pH_{total}, partial pressure of CO_2 (pCO_2), CO_2, HCO_3^-, CO_3^{2-} concentration] was calculated from measurements of TA, DIC, temperature, salinity, and nutrients using CO2 System Calculation Program (Lewis and Wallace 1998) [using the constants of Dickson and Millero (Dickson and Millero 1987); KSO_4 Dickson; pH: total scale; cited in Lewis and Wallace 1998] and corrected for density in Matlab R2009a (The MathWorks, Inc. 2009). The experimental temperature and pressure effects on the water carbonate chemistry were taken into account in the measurements of DIC and TA at the start and end of the experiment. Additionally we provide the in situ values using the in situ temperature and pressure.

12.2.7. Scanning electron microscopy of larval skeletal rods

Larval tissue (incubated for 5 days) was removed in a mild solution of hyperchlorite diluted with a solution of distilled water saturated with sodium tetraborate (which acts as a buffer) and filtered to remove any particles in suspension. Samples (skeletal rods) were washed three times

with distilled water, mounted in SEM stubs and gold coated. Images were obtained with a Leo 1450VP scanning electron microscope.

12.2.8. Natural seawater elemental composition

The concentrations of calcium (Ca^{2+}) and magnesium (Mg^{2+}) ions in water samples from all depths were measured to rule out seawater effects on calcification (Table 12.1; Fig. 12.1d). Elemental seawater composition was determined in triplicate by inductively coupled plasma optical emission spectrometry (ICP-OES) using a Perkin Elmer optima 4300DV at the National Oceanography Centre (Southampton, UK). The bottles for the samples were acid cleaned with nitric acid (HNO_3) to avoid contamination. Samples were diluted in 0.3M HCl and calibrated against multi-element standard solutions that bracketed the concentration ranges in the sample solutions. Standards were prepared gravimetrically using certified and traceable VWR Aristar single-element standard solutions, Romil UpA nitric acid and Milli-Q water. A standard seawater solution (IAPSO) and Certified Reference Materials (CRM) were analyzed for cross-reference.

12.2.9. Statistical analyses

Data analyses were performed in Minitab 15 (Minitab 15® Statistical Software for Windows®, 2007, Coventry, UK) and Statistica 9 (StatSoft, Inc. Oklahoma, USA) software. The experimental data were analyzed with one-way ANOVA (water source as a fixed factor) with four replicates for the fertilization experiment (20 in total) and triplicates for the larval growth (15 containers in total) for every experimental condition to increase accuracy. The morphology data were normally distributed and a One-Sample Kolmogorov-Smirnov test ($P > 0.150$) was used to ensure that the distribution was homogeneous. Fertilization success, morphometric data and particulate carbon (POC and PIC) were analyzed with a one-way ANOVA. The parametric Tukey test for multiple comparisons was used for post hoc analyses.

12.3. Results

12.3.1. Natural seawater carbonate chemistry

At the PAP site, as in most open ocean sites, there is a gradient of increasing CO_2, bicarbonate ions (HCO_3^-) and dissolved inorganic carbon (DIC), and a decreasing pH, carbonate ions (CO_3^{2-}) and $\Omega_{Cal.}$ with depth, while total alkalinity (TA) remains constant (Takahashi et al. 1979) (Table 12.1). The measured carbonate chemistry (corrected for pressure and in situ temperature effect at depth) agreed well with the WOCE A16 transect line data in the region 40 °N-50 °N (Feely et al. 2004). Experimental incubations were conducted at 9 °C and surface pressure (1 atm) using water from 250 to 4710 m which remained with a carbonate chemistry gradient although the values varied once they equilibrated at the surface (*see* Table 12.1). Control incubations were aimed at comparing the carbonate chemistry of seawater with that of incubations containing sea urchin larvae to determine the extent to which the organism physiology controls inorganic carbon chemistry. An increase in CO_2 (0.5-15.9 %), HCO_3^- ions (0.4-1.5 %) and a decrease in CO_3^{2-} ions (0.7-14 %), $\Omega_{Cal.}$ (0.8-14.1 %) and $\Omega_{Arg.}$ (0.6-16.6 %) were observed on day 5 in the incubations containing larvae, compared to the control incubation. Results showed that at the end of the incubations (day 5) the DIC and HCO_3^- increased by 3.4 and 3.8 % respectively from 250 m to 4710 m. The CO_3^{2-} and $\Omega_{Cal.}$ decreased by 20.4 and 20.2 % respectively from 250 m to 4710 m.

12.3.2. Fertilization and larval development

The average number of fertilized eggs (monitored 2 h post-fertilization) was significantly different across treatments ($F_{4, 59} = 14.34$ $P < 0.001$), from 250 m to 4710 m (Fig. 12.1a). There was a 20 % difference between fertilization success in the deepest seawater samples (4000 m, 4600 m and 4710 m) (68 %) compared to the shallowest water at 250 m (85 %). However, our results showed that development and tissue morphology of *P. miliaris* larvae was not affected by deep water incubations (elevated HCO_3^-, and decreased CO_3^{2-} ions and $\Omega_{Cal.}$ with depth). Larvae incubated with water from different depths developed four-armed pluteus stage during the experiment. No effect of the deep water on larval tissue development (POA; $F_{4, 45} = 1.75$, $P = 0.157$ and BL; $F_{4, 45} = 1.15$, $P = 0.347$) was observed across treatments after 5 days (Table 12.1; Fig. 12.1b) but results were especially variable in incubations with water from below 4000 m.

12.3.3. Particulate carbon and calcification

The incubations allowed investigation of the effect of changes in ambient carbon chemistry on calcification in early stages of *P. miliaris* larvae. We used particulate inorganic carbon (PIC) as an indicator of calcium carbonate content per larvae. The PIC of larvae incubated with water from 250 m ($\Omega_{Cal.}$ = 3.46) was twice the PIC of larvae incubated at 4000 m ($\Omega_{Cal.}$ = 2.37) and was significantly different ($F_{4,\ 13}$ = 201.26 P < 0.01). The same trend was observed for the individual larvae PIC/POC ratio (Fig. 12.2a). A decline in calcification was observed in all incubations except in those with water from 250 m. Scanning electron microscopy (SEM) examinations revealed a decrease in size of the larval skeletal rods (Fig.12.3) with decreasing $\Omega_{Cal.}$, although there was no evidence of corrosion. Additionally, our results showed a decrease in seawater CO_3^{2-}/HCO_3^{2-} ratio after 5 days incubation. The CO_3^{2-}/HCO_3^{2-} ratio, compared to the control seawater, was 15 % lower in water from 250 m, 8 % in incubations with water from 2000 m and in incubations with water below 4000 m it decreased by 0.6-3 % (Fig. 12.2b). We measured the particulate organic carbon (POC) content per larva as a proxy to assess changes in larval tissue biochemistry. The POC results were not significantly different across treatments ($F_{4,\ 13}$ = 1.04 P > 0.05; Fig. 12.1c).

12.3.4. Natural seawater elemental composition

Seawater samples were taken for analysis of major ions (Ca^{2+} and Mg^{2+}) to determine the extent to which changes in seawater elements from different depths could affect the organism physiology (Table 12.1; Fig. 12.1d). There were no significant differences in the concentration of [Ca^{2+}] and [Mg^{2+}] with depth (P > 0.01). The [Ca^{2+}] and [Mg^{2+}] remained almost constant with a slight decrease with depth, from 10.5 µg/g (250 m) to 10.3 µg/g (4710 m), and 33.9 to 33.1 µg/g from 250 m to 4710 m respectively. The concentrations slightly decreased the $Mg/Ca_{seawater}$.

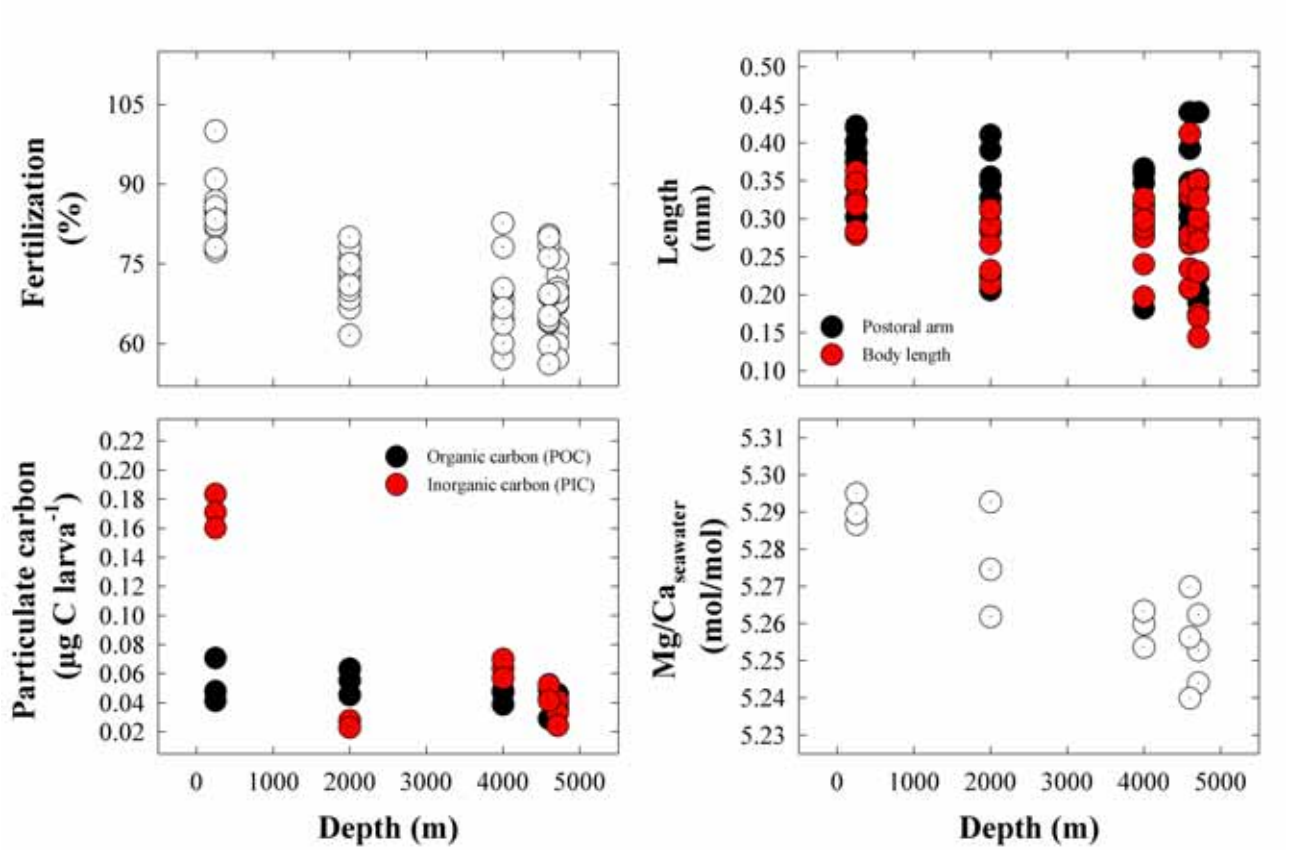

Fig. 12.1. Effects on fertilization success, larval morphology (Postoral Arm and Body Length), particulate carbon [PIC (calcification) and POC (organic carbon) in triplicates per larva at day 5 of development], and $Mg/Ca_{seawater}$. X-axis is in all cases the incubation seawater depth used at surface conditions.

12.4. Discussion

This study investigated the effect of a natural carbonate chemistry gradient using an alternative approach to others previously used (e.g. Hall-Spencer et al. 2008), in the fertilization success and larval development of the sea urchin *Psammechinus miliaris*. We established a ~ 200 µatm gradient from 4710 to 250 m at surface pressure and constant temperature, which can be used to study short-term OA effects on marine organisms in the field. The decrease in seawater pH_{total}, CO_3^{2-} ions and $\Omega_{Cal.}$ (Table 12.1) with depth resulted in a 20 % decline in fertilization success. Our results are in agreement with previous laboratory studies that supports the notion that low pH in seawater affects sperm motility and speed (Havenhand et al. 2008) and that low intracellular pH of the oocytes may prevent a successful fertilization (Grainger et al. 1979). However, recent studies indicate that acidification does not affect fertilization success in the sea urchin species *Heliocidaris erythrogramma* (Byrne et al. 2010). This suggests that the susceptibility of fertilization to ocean acidification may be species-specific.

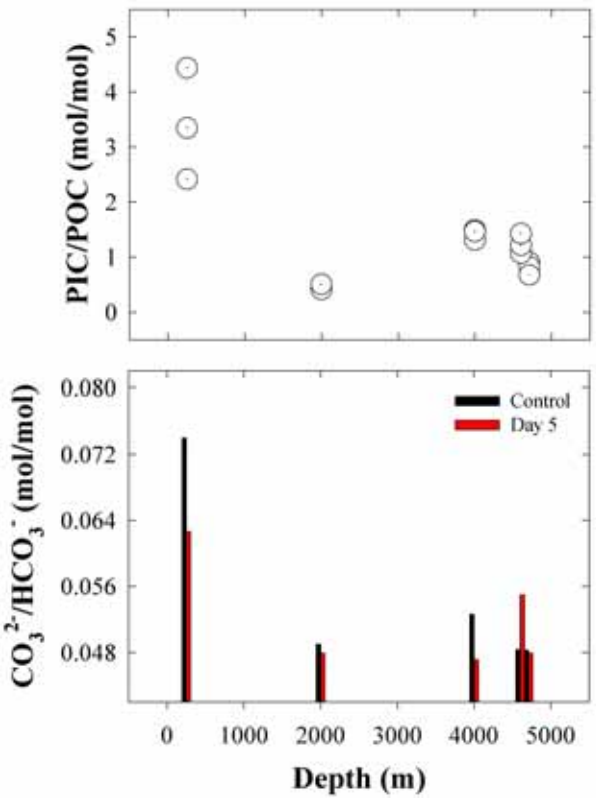

Fig. 12.2. PIC/POC values per larva. Carbonate/bicarbonate ratio in the medium from day 0 (control) to day 5.

Larval growth (body parameters) was not affected in the short-term exposure by high CO_2 (Fig. 12.1). This is supported by the notion that larval and juvenile stages of organisms are more resilient to environmental changes than adults given the varied hydrographic conditions and chemistry they experience when transported in the water column (Howell et al. 2002). During larval stages, sea urchins (e.g. *P. miliaris*) encounter large variations in carbonate chemistry conditions such as sporadic exposure to deep CO_2 rich water associated with coastal upwelling events (dos Santos et al. 2008; Feely et al. 2008), riverine inputs in coastal areas, and the changing chemistry of the water layers where they develop until metamorphosis. There was no difference in larval tissue growth or developmental stage during the experiment suggesting a phenotypic plasticity to short-term high CO_2 exposures in *P. miliaris* larvae. This contrasts with laboratory incubations, where often larvae/juveniles are seen as the most susceptible to ocean acidification (Kurihara and Shirayama 2004; Dupont et al. 2008), whereas the effect of OA may be species- and developmental stage-specific (Kroeker et al. 2010). The ambient carbonate chemistry gradient presented here indicates that shallow water echinoids have the potential to acclimate to a distinct gradient of carbon chemistry during early development at the cost of reducing calcification to maintain other vital functions such as tissue production and organic carbon balance (*see* below). Larvae grow much faster than juveniles and adults (Lorens 1981), therefore they have a quicker and tighter control on calcite incorporation. Then, they may be able to regulate calcification at later stages to reach appropiate calcite levels when exposed to high CO_2 during early stages. The question remain as if a prolonged exposure to high CO_2 during ontogenesis will irremediably reduce Mg-calcite contents in juvenile and adult organisms as well as trigger physiological consequences in adults. This tolerance has been reported during larval development in Antarctic echinoids (Clark et al. 2009). Echinoids can tolerate a certain CO_2 range by having evolved in a habitat where pH changes can exceed up to 0.1 units on a daily basis (Menendez et al. 2001),

and 0.4 units in months (Wootton et al. 2008). Additionally, meroplanktonic larvae may purposely influence their horizontal transport by sinking or swimming between overlying water masses (Sameoto et al. 2010) seeking for the most favourable gradient in carbonate chemistry.

Particulate organic carbon (POC) in the larval body remained almost constant over all depths tested, which is consistent with the lack of change in larval size. The growth of long arms (tissue) is needed to increased efficiency of food collection by the larvae (Strathmann 2007). However, larval calcification (PIC) decreased in all deep (thus high CO_2) treatments compared to the 250 m incubation. This suggests that the larvae divert energy towards growing soft tissue rather than producing long calcite skeletal rods. A decrease in calcification resulting in weaker skeletal rods has been suggested to increase potential larval mortality (Staver and Strathmann 2002) provided that the skeletal rods play important roles in larval feeding, motility and settling. However, the larvae may compensate this calcite loss by allocating energy to other vital functions. The decrease in calcification may also be a consequence of selective dissolution of Mg phases (incorporated as $MgCO_3$, thus contributing to the total PIC), which occur in the skeletal rods of sea urchins (Weber 1969; Hermans et al. 2010). This is caused by the greater susceptibility to dissolution of high-Mg calcite, compared to that of calcite alone (Morse et al. 2006). Yet, it is not clear whether and to what extent $MgCO_3$ is incorporated in early larval stages, and therefore if dissolution is an important process affecting skeletal rods formation during the first 5 days of development. In order to rule out a seawater composition control, which drives calcification in many organisms (Stanley et al. 2005; Ries 2010), we measured the $Mg/Ca_{seawater}$. Under all the experimental conditions tested, $[Ca^{2+}]$ and $[Mg^{2+}]$ remained almost constant with a

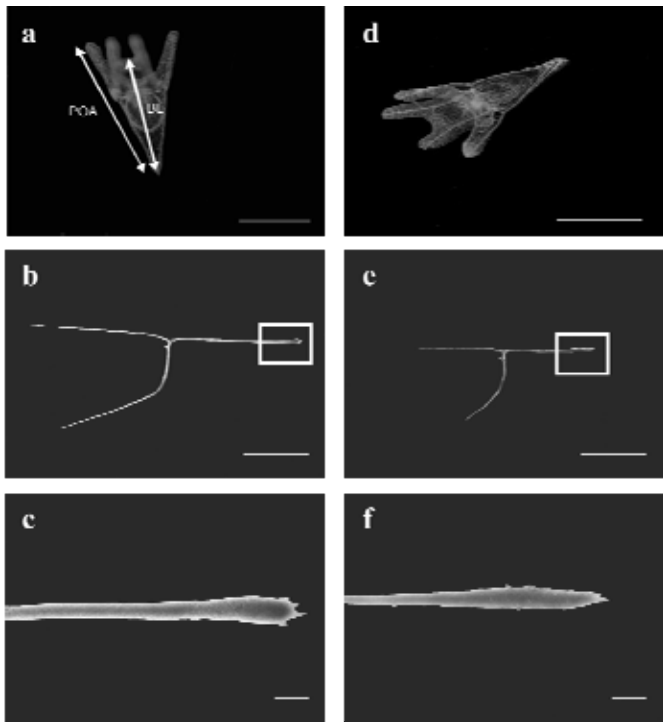

Fig. 12.3. Morphometrics and skeletal rods of *Psammechinus miliaris* larvae. The whole skeletal rods of an incubated 5 day pluteus larvae using the shallowest water 250 m (a, b, c) and the deepest 4710 m (d, e, f), scale bar represents 100 µm. Both images have superimposed white rectangles that indicate magnified areas from the tip of the rod (c and f respectively), scale bar refers to 10 µm.

slight decrease with depth, yielding an average $Mg/Ca_{seawater}$ of 5.27 mol/mol. This is on the upper limit of the Ries (2010) dataset for a variety of calcifying species. Therefore an effect of $Mg/Ca_{seawater}$ on development and calcification can be eliminated. Echinoids may have evolved the ability to cope with natural seawater carbonate chemistry changes by maintaining vital functions at the cost of calcification. However, the implications of a reduction in fertilization success could potentially decrease the abundance of these organisms with possible cascading effects throughout ecosystems. A decline in calcification may suggest metabolic trades-offs to adjust to changing carbon chemistry conditions to survive and develop to adult stages.

13.

Ontogenesis Mg-calcite in echinoids reveals adaptation traits to climate change

Abstract

Calcification in echinoids starts early after fertilization by forming an endoskeleton made of Mg-calcite. Echinoids belong to the meroplankton during early life stages, and then settle as adults at the seabed during metamorphosis. Thus, they encounter a broad range of seawater chemistries during development, which are especially relevant in the context of their high Mg-calcite skeletons and rising CO_2 levels (ocean acidification - OA). Here, we assessed for the first time the Mg-calcite composition of larvae (38 days), juveniles (1 year), and adults (2-3 years) of the same species and population in the north Atlantic Ocean to understand modern ocean geochemical ontogenesis and susceptibility to dissolution. We also studied the larvae Mg-calcite mineralogy response to high CO_2 and temperature. Echinoid larvae increased their skeleton $MgCO_3$ % and showed a parabola in $SrCO_3$ % with rising temperature, but displayed mixed responses in $MgCO_3$ % and a decrease in $SrCO_3$ % with rising CO_2. Consequently, the skeleton Mg/Ca and Sr/Ca increased with temperature and high CO_2, and decreased at modern CO_2 concentrations. During ontogenesis at modern CO_2 conditions, larvae bear at 38 days lower skeleton $MgCO_3$ % levels than the juveniles and adults (4.9, 6 and 7.8 % respectively), which makes them less susceptible to dissolution, which may represent a biological advantage in the context of OA. Conversely, skeleton $CaCO_3$ and $SrCO_3$ %s increased continuously to adult stages, inducing a large Mg/Ca and Sr/Ca decrease (from 0.86 to 0.11 mol/mol and 2.72 to 1.96

mmol/mol respectively). This evidence suggests that echinoids can actively control their Mg-calcite composition to adapt to ambient conditions, and their high degree of mineralogical plasticity may confer them an advantage to rising CO_2 conditions. These data also suggest that adult stages are more susceptible than larvae to dissolution in the context of OA, at least from a mineralogical perspective. If this can translate into higher survival rates owing to a decreasing susceptibility to dissolution at larval stages will be fundamental for the fate of echinoid population in a high CO_2 world.

This chapter is based on:

Suarez-Bosche, N., **Lebrato, M** (shared 1st authorship with S-B. N)., and Ries, J. B. in preparation. Ontogenesis Mg-calcite in echinoids reveals adaptation traits to climate change. To be submitted: *PLoS* ONE.

Acknowledgements: This work was supported by the "European Project on Ocean Acidification" (EPOCA) for M. Lebrato's PhD. The National Council of Science and Technology of Mexico (CONACyT) funded this work as part of N. Suarez-Bosche' PhD.

13.1. Introduction

The Echinodermata is a benthic calcifying taxa that has colonized ecosystems from the shallow shelf to the deep sea (Howell et al. 2002). They are divided into five classes (Asteroidea, Echinoidea, Ophiuroidea, Holothuroidea, and Crinoidea) that radiated in the early Palaeozoic (Durham 1971; Ubaghs 1975). Echinoderms belong to the meroplankton during early life stages, and then settle at the seabed during metamorphosis. Calcification starts early after oocytes fertilization, and echinoids form an endoskeleton made of Mg-calcite (Okazaki et al. 1981; Wilt and Benson 1988). The echinoids endoskeleton develops intracellularly after the gastrula stage mediated by mesenchyme primary and secondary cells. The endoskeleton is composed by spicules deposited on the blastocoel, which then elongate in a species-specific manner. Yet, there is a poor understanding of the Mg-calcite regulation and content in echinoids skeleton in larval stages. Conversely, the adult exoskeleton is well studied, being formed by a more complex biomineral matrix made of $CaCO_3$ [70-90 % (Vinogradov 1953)], $MgCO_3$ [2-25 % (Weber 1969)], with minor incorporation of $SrCO_3$ [< 1 % (Roux et al. 1995)]. The biomineral is a metastable carbonate, predominantly made of high-Mg calcite (> 4 % $MgCO_3$), although some species bear low-Mg calcite (< 4 % $MgCO_3$) (Weber 1973; Morse et al. 2006). The geochemical evolution of the echinoids exoskeleton has been attributed to proximate control factors (PCFs), namely the seawater $Mg/Ca_{seawater}$ ratio, which controls biomineralization in geological time scales (Dickson 2002). At present, the $Mg/Ca_{seawater}$ varies from ~ 4.50 mol/mol in estuaries (Zang et al. 2003), to ~ 5.20 in the open ocean (Fabricand et al. 1967), to 5.40-5.90 mol/mol in shelves (Blanco-Ameijeiras et al. in press), driving the echinoids $Mg/Ca_{calcite}$ with increasing $Mg/Ca_{seawater}$ in the ~ 4 to 6 mol/mol range (Ries 2010). Other PCFs controlling the Mg-calcite content include temperature (reviewed by Kroh and Nebelsick 2010) and salinity (Borremans et al. 2009). Ambient carbonate chemistry (namely CO_2) also governs Mg-calcite in other taxa (molluscs), with correlations to μ following food availability (Lorrain et al. 2005).

A recent concern following anthropogenic emissions of greenhouse gases is that the ocean will become enriched in CO_2, while carbonate ions (CO_3^{2-}) and the calcite saturation state (Ω) will decrease, termed ocean acidification (OA) (Caldeira and Wickett 2003). This triggered questions on the fate of echinoderms carbonate, namely Mg-calcites (Lebrato et al. 2010), and populations (Sewell and Hofmann 2011), and particularly on early development and juvenile stages (Dupont et al. 2010). There is a consensus around a negative effect of high CO_2 on the physiology

(Dupont et al. 2008, 2010), fertilization (Havenhand et al.. 2008), growth and reproduction (Sewell and Hofmann 2011), but contradictory responses in terms of calcification (Wood et al. 2008; Clark et al. 2009; Ries 2009, 2011). In particular, the response to high CO_2 and increasing temperature is poorly understood. Asteroids seem to increase the μ, probably as a compensatory mechanism (Gooding et al. 2009), while no effect is found on fertilization in echinoids (Byrne et al. 2010). For echinoids, rising CO_2 levels might come at a cost of increasing skeleton dissolution, driven by the increasing solubility of Mg-calcite with a certain mol % $MgCO_3$ (Morse et al. 2006). Despite the threat of OA to Mg-calcites, there is still a poor understanding of basic controls on skeletal elemental content ($MgCO_3$, $SrCO_3$, $Mg/Ca_{calcite}$ and $Sr/Ca_{calcite}$ ratios). Detailed knowledge is essential to assess if echinoids will be among the first responders to OA, and which life stages are most sensitive to OA in terms of skeletal Mg-calcite. Basic $MgCO_3$ data obtained during ontogenesis can help to understand changes on the saturation state with respect to Mg phases (ΩMg) (Andersson et al. 2008), and how susceptibility to dissolution could vary during the life cycle. The calculation of ΩMg depends on the stoichiometric solubility of natural Mg-calcites from the mol % $MgCO_3$, and the major ion activities (Ca^{2+}, Mg^{2+}, CO_3^{2-}), which vary at different temperatures (Millero and Pierrot 1998). Different equations predict this relationship (Morse et al. 2006), but other factors apart from the $MgCO_3$ govern solubility. This makes calculations of ΩMg only temptative.

In this study, we assessed for the first time, the Mg-calcite elemental composition in the echinoid *Psammechinus miliaris* [$CaCO_3$ %, $MgCO_3$ %, and $SrCO_3$ %, inorganic carbon (PIC) % dry weight (dw), $Mg/Ca_{calcite}$ and $Sr/Ca_{calcite}$ measured via ICP-MS], in a range of CO_2 and temperature levels, using in situ seawater. We also assessed ontogenetic geochemistry (using larvae - 38 days, post metamorphosis juveniles, and full grown adults) using only present carbonate chemistry treatments in combination with wild samples from the same population (larvae were the offspring of the adults collected). Using the mol % $MgCO_3$ in the Mg-calcite and the calculated [CO_3^{2-}] we worked out ΩMg in all CO_2 and temperature treatments. This is the first time that Mg-calcite is tracked during ontogenesis in a carbonate-producing marine organism, which helps to understand susceptibilities to OA during an organism life-cycle.

13.2. Material and Methods

13.2.1. Adult samples

Psammechinus miliaris adults/juveniles were collected near Rhosneigr, Wales (53°13'41" N; 4°31'16" W) in July 2009. We also collected *Paracentrotus lividus* adults in Cape Vidio, Spain (43°34'09" N; 6°14'09" W) in December 2007 to compare Mg-calcite adult samples from echinoids inhabiting a similar latitude and habitat in the Atlantic Ocean. Adults and juveniles were manually cleaned of debris and then rinsed three times with Milli-Q water (except a few adults used for reproduction maintained in flow-through aquaria at 14 ±1 °C). They were subsequently frozen at -20 °C in ziploc plastic bags for 24 h. Samples were then freeze dried continuously for 48 h inside their bags (Harris 1954), and then disintegrated to a homogeneous powder with a rotating metal blade. Samples were stored at room temperature until analysis.

13.2.2. CO_2 and temperature experiment

Adult *P. miliaris* (n_{males} = 3, $n_{females}$ = 3) were spawn by an inter-coelomic injection of 0.5 mol l^{-1} KCl (Strathmann 1987). The eggs of three females were spawned into beakers containing filtered seawater (FSW 0.20 µm), and the sperm of three males was collected dry and kept at 4 °C. The eggs shape/quality and the sperm motility were microscopically checked before starting the experiments. The total number of eggs was measured from a 20 ml suspension calculated through counts of 100 µl aliquots. The fertilization experiment was performed separately in replicate beakers (60 ml) containing experimental water and kept at the correct temperature (15, 18 and 20 °C) at densities of 3-4 eggs ml^{-1}. Prior to fertilization, the eggs were placed in the rearing beakers for 20 min and the amount of sperm required to achieve a sperm to egg ratio of 1000/1 was added . The sperm was briefly activated in the experimental seawater in the beakers containing the eggs. After 2 h the eggs that presented a fertilization membrane and cleavage were counted to determine fertilization success. For the experiment, two different initial CO_2 levels (~ 200 and 1000 µatm) were used at three different temperature conditions (15, 18, and 20 °C). Four replicates were used for each temperature/CO_2 combination and this set of experiments was run twice to increase accuracy of results. The embryos were reared in separate microcosms adjusted for the experimental temperature and CO_2. In all combinations, 5 L flasks

(in triplicates) per treatment were used. All microcosms were equilibrated for 36 h until the desired CO_2 and corresponding temperature were achieved.

Larvae were fed on the marine microalgae *Isochrysis galbana* and *Rhodomonas* sp. at a concentration of 6000 and 3000 cells ml^{-1} respectively. *P. miliaris* larvae were grown in natural seawater from their habitat, thus mimicking intertidal $Mg/Ca_{seawater}$ in situ (~ 5.60-5.90 mol/mol) to avoid assumptions of open ocean values (~ 5.10-5.20 mol/mol) biasing the Mg-calcite measurements. Flasks were bubbled with the desirable air/CO_2 mixtures to mimic predicted future atmospheric conditions following OA standard procedures (Riebesell et al. 2010) (Table 13.1). Dissolved oxygen (DO) levels were maintained constant by the simultaneous bubbling of air in all experimental flasks to avoid increasing the CO_2 as a consequence of low oxygen in solution (Melzner et al. 2009). The 5 L flasks were placed in 60 L tanks in a temperature-controlled room at 15 °C. Water was then warmed and maintained constant at the required temperatures [control + 3 °C (18 °C) and control + 5 °C (20 °C)] using aquarium heaters (Table 13.1). Aquarium propellers were used to homogenize the water temperature.

13.2.3. Larval pellets

Psammechinus miliaris samples for elemental analyses of larvae were obtained from pellets by filtering 1 L of the culture water (density ~ 2 larvae ml^{-1}), transferred to eppendorf tubes and kept at 4 ^{o}C to avoid degradation. The pellets were rinsed three times with seawater, centrifuged to remove any remaining seawater and weighted to obtain wet and dry weights (Table 13.2). The pellets were kept at -80 ^{o}C for 24 h and then freeze dried for 48 h.

Table 13.1. Medium chemistry used in incubations of *Psammechinus miliaris* larvae at three temperatures and two CO_2 conditions (i = day 0, and f = day 38) All data were measured in triplicates.

	15 °C		**18 °C**		**20 °C**	
	Control	**High CO_2**	**Control**	**High CO_2**	**Control**	**High CO_2**
Temp. (ºC)	15.4 ± 0.31	15.6 ± 0.42	17.8 ± 0.77	17.6 ± 0.27	20.1 ± 0.62	20.8 ± 0.75
Salinity	36	36	36	36	36	36
NO_3^- (µmol l^{-1})	0.27± 0.03	0.20 ± 0.06	1.06 ± 0.48	0.15 ± 0.06	0.19 ± 0.07	0.44 ± 0.01
PO_3^{4-} (µmol l^{-1})	0.10 ± 0.01	0.05 ± 0.01	0.08 ± 0.04	0.07 ± 0.03	0.05 ± 0.01	0.06 ± 0.02
TA (µmol kg^{-1}) $_{(i)}$	2341.66 ± 39.39	2321.66 ± 2.37	2327.82 ± 4.39	2323.69 ± 6.18	2309.66 ± 12.05	2309.79 ± 13.55
TA (µmol kg^{-1}) $_{(f)}$	2288.85 ± 41.34	2278.44 ± 6.75	2263.72 ± 11.44	2283.27 ± 7.13	2263.30 ± 2.39	2277.87 ± 12.73
DIC (µmol kg^{-1}) $_{(i)}$	1953.62 ± 60.27	2233.49 ± 23.09	1938.18 ± 23.50	2204.47 ± 1.32	1912.79 ± 56.16	2214.82 ± 7.71
DIC (µmol kg^{-1}) $_{(f)}$	2133.66 ± 39.07	2236.03 ± 19.62	2132.49 ± 22.25	2240.75 ± 15.37	2083.83 ± 8.58	2242.44 ± 16.62
$pH_{total\ (i)}$	8.31 ± 0.04	7.71 ± 0.07	8.28 ± 0.04	7.76 ± 0.02	8.26 ± 0.07	7.66 ± 0.02
$pH_{total\ (f)}$	7.89 ± 0.01	7.57 ± 0.07	7.80 ± 0.08	7.55 ± 0.03	7.88 ± 0.02	7.49 ± 0.01
pCO_2 (µatm) $_{(i)}$	193.39 ± 26.91	984.21 ± 173.34	208.64 ± 21.34	861.46 ± 37.30	220.83 ± 45.26	1099.46 ± 36.64
pCO_2 (µatm) $_{(f)}$	608.83 ± 17.41	1367.23 ± 231.60	765.84 ± 159.81	1458.25 ± 102.90	620.63 ± 33.61	1660.14 ± 59.41
CO_2 (µmol kg^{-1}) $_{(i)}$	7.09 ± 0.99	36.09 ± 6.36	7.13 ± 0.73	29.44 ± 1.27	7.07 ± 1.45	35.22 ± 1.17
CO_2 (µmol kg^{-1}) $_{(f)}$	22.33 ± 0.64	50.14 ± 8.49	26.32 ± 5.49	50.11 ± 3.54	19.88 ± 1.08	53.47 ± 1.91
HCO_3^-(µmol kg^{-1}) $_{(i)}$	1680.44 ± 72.77	2113.83 ± 28.27	1663.57 ± 38.09	2074.59 ± 3.91	1633.56 ± 84.87	2091.45 ± 5.56
HCO_3^-(µmol kg^{-1}) $_{(f)}$	1993.15 ± 36.41	2124.94 ± 21.19	2000.92 ± 34.03	2129.34 ± 15.25	1930.78 ± 12.72	2129.70 ± 15.94
CO_3^{2-}(µmol kg^{-1}) $_{(i)}$	266.09 ± 15.24	83.57 ± 11.53	267.49 ± 15.50	100.43 ± 4.06	272.15 ± 30.47	88.15 ± 3.34
CO_3^{2-}(µmol kg^{-1}) $_{(f)}$	118.19 ± 3.44	60.95 ± 10.16	105.26 ± 17.65	61.31 ± 3.43	133.17 ± 5.33	59.27 ± 1.23
Ω-Cal. $_{(i)}$	6.30 ± 0.36	1.98 ± 0.27	6.34 ± 0.37	2.38 ± 0.10	6.46 ± 0.72	2.09 ± 0.08
Ω-Cal. $_{(f)}$	2.80 ± 0.08	1.44 ± 0.24	2.51 ± 0.42	1.46 ± 0.08	3.16 ± 0.13	1.42 ± 0.03
Ω-Arg. $_{(i)}$	4.05 ± 0.23	1.27 ± 0.18	4.10 ± 0.24	1.54 ± 0.06	4.21 ± 0.47	1.36 ± 0.05
Ω-Arg. $_{(f)}$	1.80 ± 0.05	0.93 ± 0.15	1.62 ± 0.27	0.95 ± 0.05	2.06 ± 0.08	0.92 ± 0.02
ΩCal. $_{(i)}$ - manual	7.95	2.49	8.00	3.00	7.67	2.48
ΩCal. $_{(f)}$ - manual	3.53	1.82	3.14	1.83	3.75	1.67
ΩMg. $_{(i)}$ - manual	5.81	1.82	5.75	2.17	5.57	1.79
ΩMg. $_{(f)}$ - manual	2.58	1.33	2.26	1.32	2.72	1.20

Table 13.2. Dry (dw) and wet weight (wt) and the dw/wt percentage conversion ratio from the pellets of *Psammechinus miliaris* larvae in the temperature and CO_2 experiment and the juveniles/adults collected in the field. Also included are the data from adult *Paracentrotus lividus*.

1) Temperature + CO_2 experiment (*Psammechinus miliaris* larvae)					
CO_2 scenario	Temperature (°C)	*n* [a]	Wet weight (mg)	Dry weight (mg)	dw/wt %
Control	20	2	98.85 ± 7.42	5.45 ± 0.21	5.52 ± 0.20
Control	18	2	73.70 ± 28.14	4.45 ± 1.20	6.17 ± 0.72
Control	15	2	94.55 ± 57.62	5.55 ± 2.75	6.11 ± 0.81
High CO_2	20	2	74.35 ± 19.72	4.50 ± 0.00	6.27 ± 1.66
High CO_2	18	2	69.60 ± 13.01	4.50 ± 0.00	6.58 ± 1.23
High CO_2	15	2	91.45 ± 17.89	5.05 ± 0.77	5.54 ± 0.23
2) Ontogenesis at constant temperature and high CO_2 conditions					
Species - Stage	Temperature (°C)	*n* [b]	Wet weight (g)	Dry weight (g)	dw/wt %
P. miliaris - Larvae	15-20	4	84.12 mg ± 14.74	5.00 mg ± 0.77	6.14 ± 0.04
P. miliaris - Juvenile	13-19	5	12.95 ± 1.44	4.77 ± 0.79	36.83 ± 2.60
P. miliaris - Adult	13-19	9	32.26 ± 8.73	11.78 ± 1.92	37.27 ± 5.24
P. lividus - Adult	16.50	14	28.92 ± 12.45	11.52 ± 4.34	40.61 ± 3.21

[a] *n* number of pellets concentrated to measure via ICP-MS. Each pellet had an estimated number of larvae according to density per ml and it was normalized to 1000 larvae per pellet.
[b] *n* number of individuals used to measure the whole body. For *Psammechinus miliaris* larvae refer to note "a".

13.2.4. ICP-MS measurements: larval pellets and seawater

Pellet elemental composition was obtained with a Perkin Elmer Sciex ELAN 9000 inductively coupled plasma mass spectrometer (ICP-MS) at the University of North Carolina-Chapell Hill (US). Samples were lightly ground in a mortar and pestle for 10-15 s. A 0.50 gr sample of the pulverized echinoderm material was digested for 2 h in Aqua Regia at 90 °C in a microprocessor controlled digestion block. Duplicate samples were run every 15 samples, in-house controls were run every 33 samples, and digested certified standards (for instrument calibration) and blanks were run every 68 samples. Seawater samples near the area where adult *P. miliaris* specimens were collected, were measured (elemental analysis) in an ICP-AES, using the Thermo *i*CAP 6300 Series ICP Spectrometer (installed in the Department of Geology, University of Oviedo, Spain). $Mg/Ca_{seawater}$ and $Sr/Ca_{seawater}$ were determined separately by the

method of addition of standards in culture medium samples (0.22 µm filtered) diluted to 1/200 and 1/10, respectively.

13.2.5. Medium chemistry and environmental conditions

We used three temperatures measured with a thermometer [15°C (15.40 ± 0.31 °C), 18 °C (17.80 ± 0.77 °C), and 20 °C (20.10 ± 0.62 °C)] and two CO_2 conditions (~ 200 µatm and ~1000 µatm) (*see* Table 13.1 for details). Temperature and salinity remained constant during the experiment, thus geochemical changes induced by these variables can be ruled out (Borremans et al. 2009; Hermans et al. 2010). Total alkalinity (TA) and total carbon (TC) were sampled in 250 ml borosilicate bottles, fixed with 1 ml of HCl_2 (0.40 mM), and then measured in the Versatile INstrument for the Determination of Titration Alkalinity (VINDTA). Carbonate chemistry parameters were calculated from temperature, salinity, TA, TC, and nutrients using the "CO2SYS" macro (Lewis and Wallace 1998). The equilibrium constants were from Mehrbach et al. (1973), refitted by Dickson and Millero (1987), the KSO_4 constants were from Dickson (1990), and the total pH scale was used (Table 13.1). TA was constant in all temperatures and CO_2 concentrations and only dropped by ~100 units from the start to the end of the experiment (calcification during 38 days). In all treatments, the final conditions of TC and CO_2 increased from the initial values as the organisms increased calcification as they developed (Table 13.1).

The *P. miliaris* adult and juvenile field samples were collected from water with a temperature of 13 °C (measured with thermometer), and the *P. lividus* adults at 16.50 °C [year average from a buoy (www.puertogijon.es)]. The temperatures for all the field juvenile and adult specimens were within the annual range (thus we can exclude a thermal effect on the ontogenesis changes explored). Seemingly, the natural field temperature range includes the conditions used in the larval incubations (15-18 °C). We did not have information on the seawater carbonate chemistry in the field (and the annual oscillation), thus we used in situ seawater in the controls to mimic real conditions and compare larvae and juveniles/adults. Working with larvae, juveniles, and adults from the same population and exactly the same location (and using the same water), we ensured that the genetic pool and the associated Mg-calcite variability observed during ontogenesis was unique to this species and population.

13.2.6. Saturation state (Ω) calculations

For the Mg-calcite measured in all samples (larvae, juveniles, and adults) we calculated the seawater saturation state with respect to the mol % $MgCO_3$ (ΩMg). The rest of the input conditions, including $[CO_3^{2-}]$, were measured from seawater assuming equilibrium between the atmosphere and the seawater in the incubations. Saturation states were calculated based on the biogenic "cleaned" solubility curve (taken from Morse et al. 2006) using total ion activity coefficients defined for the experimental temperatures used (Millero and Pierrot 1998). The general expression for the calculation of seawater saturation state with respect to a certain mol % $MgCO_3$ was:

$$\Omega Mg = \{Mg^{2+}\}^{x} \{Ca^{2+}\}^{(1-x)} \{CO_3^{2-}\}/IAP_x \quad (1)$$

where x is the mol % $MgCO_3$ measured in echinoid larvae, juveniles, and adults (Table 13.3, 13.4). {} represents ion activities, which are calculated from observed ion concentrations multiplied by total ion activity coefficients (Table 13.3). IAP is the Ion Activity Product, which is the product of the concentrations at a metastable equilibrium (true equilibrium is never achieved with respect to Mg-calcite), obtained from stoichiometric saturation (Thorstenson and Plummer 1977). To compare with pure calcite, we also calculated ΩCal. using the same formulae:

$$\Omega Cal. = \{Ca^{2+}\} \{CO_3^{2-}\}/IAP \quad (2)$$

the IAP for Mg phases is obtained from the equation of Morse et al. (2006) on biogenic calcites: -log IAP = 8.35 - (8.90 + 10^{-3}) * mol % $MgCO_3$. Note that other relationships can be used to obtain representative IAPs, and thus the value of ΩMg will change using different mol % $MgCO_3$ values (*see* Morse et al. 2006). The calcite IAP was established at 3.311 * 10^{-9} (Table 13.3), which explains the slight deviations from the ΩCal. computed with the "CO2SYS" software (Table 13.1). The ion activities of Mg^{2+}, Ca^{2+}, and CO_3^{2-} were calculated from total activity coefficients [$\gamma_T(i)$] and total concentration ($[i]_T$) in seawater from the salinities measured during incubations. The $\gamma_T(i)$ varies with temperature and thus we used the values from the model of Millero and Pierrot (1998) at 15 °C and 20 °C. This coincides with our experimental temperatures [for $\gamma_T(i)$ at 18 °C we assigned the values from 15 °C]. The $[i]_T$ input values for

CO_3^{2-} were calculated from measured TA and TC (*see* Table 13.1, 13.2). Since we did not have in situ field [CO_3^{2-}] data (juveniles and adults), we used the values of $\gamma_T(i)$ at 15 °C (*see* below) to make ΩMg comparable between larvae and juveniles/adults. Eventually, we assessed ΩMg in two cases (Table 13.3):

(1) ΩMg of *P. miliaris* larvae (38 days) at three temperatures and two CO_2 conditions using calculated [CO_3^{2-}] from TA and TC (CO2SYS), and the measured mol % $MgCO_3$ at each condition (Table 13.4) (ΩMg results included in Tables 13.1, 13.3).

(2) ΩMg during ontogenesis based on the mol % $MgCO_3$ measured (38 days larvae, juveniles, and adults). We used a single temperature (15 °C) and two calculated [CO_3^{2-}] conditions to compare dissolution susceptibility based on ΩMg and mol % $MgCO_3$. As input data, we used calculated values at 15 °C (low CO_2: TA = 2350 µmol kg^{-1}, CO_2 = 300 µatm, CO_3^{2-} = 199.47 µmol kg^{-1}; high CO_2: TA = 2350 µmol kg^{-1}, CO_2 = 1500 µatm, CO_3^{2-} = 56.57 µmol kg^{-1}) (Table 13.3). As input mol % $MgCO_3$ we used larval data averaged between 15 and 20 °C (incubations), and the juveniles and adults field measurements from a similar temperature range (13-19 °C).

13.2.7. Data analyses

Mg-calcite data in the CO_2 and temperature experiment were statistically analyzed in Statistica 8 (StatSoft, Inc. US). Data were normally distributed, and then analyzed using a General Linear Model (GLM) testing for individual factor effects and a matrix interaction. We then used the Tukey HSD test to compare all possible pairs of means and find further interaction differences. All graphs were plotted in SigmaPlot 10.0 (Systat Software, Inc. US).

13.3. Results

13.3.1. *Psammechinus miliaris* Mg-calcite response to CO_2 and temperature

The $CaCO_3$ content tripled from ~ 3.5 % at 15 °C to ~ 10.5 % at 18 and 20 °C in low CO_2 conditions, but it remained almost constant at high CO_2 between 3.5 and 5.5 % (Fig. 13.1a). High CO_2 did not change the content at 15 °C, but halved it at 18 and 20 °C. The difference was

significant for CO_2 ($P < 0.01$) and temperature ($P < 0.01$), but not for the interaction ($P > 0.05$). The Tukey HSD test revealed only significant differences ($P < 0.05$) between 15 °C - low CO_2, and 18 °C - low CO_2, and also between 15 °C - high CO_2, and 18 °C - low CO_2. The $MgCO_3$ content almost doubled from ~ 3.5 % at 15 °C to ~ 6.5 % at 18 °C and ~ 5 % at 20 °C in low CO_2 conditions, and it also increased at high CO_2 from ~ 3 % at 15 °C, to ~ 5.5 % at 18 °C, and to ~ 6 % at 20 °C (Fig. 13.1b). High CO_2 did not change the content at 15 °C, but it slightly decreased it at 18 °C and increased it at 20 °C. The difference was not significant for CO_2 ($P > 0.05$), temperature ($P > 0.05$), or the interaction ($P > 0.05$). The Tukey HSD test revealed no significant differences. The $SrCO_3$ content first increased from ~ 0.040 % at 15 °C to ~ 0.048 % at 18 °C and then decreased to ~ 0.039 % at 20 °C in low CO_2 conditions, and it behaved similar at high CO_2, increasing from ~ 0.035 % at 15 °C to ~ 0.046 % at 18 °C, and then decreasing to ~ 0.033 % at 20 °C (Fig. 13.1b). High CO_2 slightly decreased the content at all temperatures. The difference was not significant for CO_2 ($P > 0.05$), temperature ($P > 0.05$), or the interaction ($P > 0.05$). The Tukey HSD test revealed no significant differences. The total inorganic carbon (PIC_{total}) content first tripled from ~ 0.9 % at 15 °C to ~ 2.3 % at 18 °C and then decreased to ~ 1.9 % at 20 °C in low CO_2 conditions, and it behaved slightly different at high CO_2, increasing from ~ 0.9 % at 15 and 18 °C to ~ 1.7 % at 20 °C (Fig. 13.1d). High CO_2 did not change the content at 15 °C, but decreased it by a factor of three at 18 and it remained almost constant at 20 °C. The difference was significant for CO_2 ($P < 0.01$) and temperature ($P < 0.01$), but not for the interaction ($P > 0.05$). The Tukey HSD test revealed only significant differences ($P < 0.05$) between 15 °C - low CO_2, and 18 °C - low CO_2, and also between 15 °C - high CO_2, and 18 °C - low CO_2. The $Mg/Ca_{calcite}$ ratio decreased from ~ 1.2 mol/mol at 15 °C to ~ 0.75 mol/mol at 18 °C and to ~ 0.7 mol/mol at 20 °C in low CO_2 conditions, but conversely, it increased at high CO_2 from ~ 1.1 mol/mol at 15 °C, to ~ 1.2 mol/mol at 18 °C, and to ~ 1.4 mol/mol at 20 °C (Fig. 13.1e). High CO_2 did not change the content at 15 °C, but it increased it at 18 °C and doubled it at 20 °C. The difference was not significant for CO_2 ($P > 0.05$), temperature ($P > 0.05$), or the interaction ($P > 0.05$). The Tukey HSD test revealed no significant differences. The $Sr/Ca_{calcite}$ ratio decreased from ~ 3 mmol/mol at 15 °C to ~ 2.5 mmol/mol at 18 °C and then increased to ~ 2.7 mmol/mol at 20 °C in low CO_2 conditions, but it increased at high CO_2 from ~ 2.9 mmol/mol at 15 °C, to ~ 3 mmol/mol at 18 °C, and to ~ 3.1 mmol/mol at 20 °C (Fig. 13.1f). High CO_2 did not change the content at 15 °C, but it increased it at 18 °C and 20 °C. The difference was not significant for CO_2 ($P > 0.05$), temperature ($P > 0.05$), or the interaction ($P > 0.05$). The Tukey HSD test revealed no significant differences.

Table 13.3. Raw seawater chemistry used to calculate ΩCal. and ΩMg for the different input conditions in the experiment and field conditions (only for *Psammechinus miliaris*).

Total activity coefficient = $\gamma_T(i)$ [a]			**Total conc. (T) = $[i]_T$**		**Seawater conc. (g kg^{-1})**		
Temperature (°C) [b]			$[Ca^{2+}]$	0.0103	0.416		
Ion *i*	15	20	$[Mg^{2+}]$	0.0532	1.295		
Ca^{2+}	0.203	0.200	$[CO_3^{2-}]$	*see* input data [c]			
Mg^{2+}	0.211	0.207					
CO_3^{2-}	0.047	0.045					
Ion Activity Product (IAP) [d]							
-log IAP		IAP	Mg-calcite -log IAP		Mg-calcite IAP		
Calcite	8.480	3.311 * 10^{-9}	-log IAP = 8.35 - (8.90 * 10^{-3}) * mol % $MgCO_3$		from equation [e]		
Input data							
Stage	Ion activity (a_i) = $\gamma_T(i)$ * $[i]_T$			$[i]_T$ CO_3^{2-} (µmol kg^{-1})	Temperature (°C)	ΩCal. [f]	ΩMg [g]
	CO_3^{2-}	Ca^{2+}	Mg^{2+}				
Larvae 38 days (3 temperatures + 2 CO_2 conditions)							
Initial conditions							
Larvae (high CO_2)	3.967 * 10^{-6}	2.075 * 10^{-3}	1.110 * 10^{-2}	88.15	20.10	2.48	1.79
Larvae (control)	1.224 * 10^{-5}	2.075 * 10^{-3}	1.110 * 10^{-2}	272.15	20.10	7.67	5.57
Larvae (high CO_2)	4.720 * 10^{-6}	2.107 * 10^{-3}	1.124 * 10^{-2}	100.43	17.80	3.00	2.17
Larvae (control)	1.257 * 10^{-5}	2.107 * 10^{-3}	1.124 * 10^{-2}	267.49	17.80	8.00	5.75
Larvae (high CO_2)	3.928 * 10^{-6}	2.107 * 10^{-3}	1.124 * 10^{-2}	83.57	15.40	2.49	1.82
Larvae (control)	1.250 * 10^{-5}	2.107 * 10^{-3}	1.124 * 10^{-2}	266.09	15.40	7.95	5.81
Final conditions							
Larvae (high CO_2)	2.667 * 10^{-6}	2.075 * 10^{-3}	1.110 * 10^{-2}	59.27	20.10	1.67	1.20
Larvae (control)	5.993 * 10^{-6}	2.075 * 10^{-3}	1.110 * 10^{-2}	133.17	20.10	3.75	2.72
Larvae (high CO_2)	2.882 * 10^{-6}	2.107 * 10^{-3}	1.124 * 10^{-2}	61.31	17.80	1.83	1.32
Larvae (control)	4.947 * 10^{-6}	2.107 * 10^{-3}	1.124 * 10^{-2}	105.26	17.80	3.14	2.26
Larvae (high CO_2)	2.865 * 10^{-6}	2.107 * 10^{-3}	1.124 * 10^{-2}	60.95	15.40	1.82	1.33
Larvae (control)	5.555 * 10^{-6}	2.107 * 10^{-3}	1.124 * 10^{-2}	118.19	15.40	3.53	2.58
Ontogenesis (1 temperature and 2 CO_2 conditions) [h]							
Larvae (high CO_2)	2.658 * 10^{-6}	2.107 * 10^{-3}	1.124 * 10^{-2}	56.57	15.40	1.69	1.22
Larvae (control)	9.375 * 10^{-6}	2.107 * 10^{-3}	1.124 * 10^{-2}	199.47	15.40	5.96	4.32
Juveniles (high CO_2)	2.658 * 10^{-6}	2.107 * 10^{-3}	1.124 * 10^{-2}	56.57	15.40	1.69	1.22
Juveniles (control)	9.375 * 10^{-6}	2.107 * 10^{-3}	1.124 * 10^{-2}	199.47	15.40	5.96	4.30
Adults (high CO_2)	2.658 * 10^{-6}	2.107 * 10^{-3}	1.124 * 10^{-2}	56.57	15.40	1.69	1.21
Adults (control)	9.375 * 10^{-6}	2.107 * 10^{-3}	1.124 * 10^{-2}	199.47	15.40	5.96	4.27

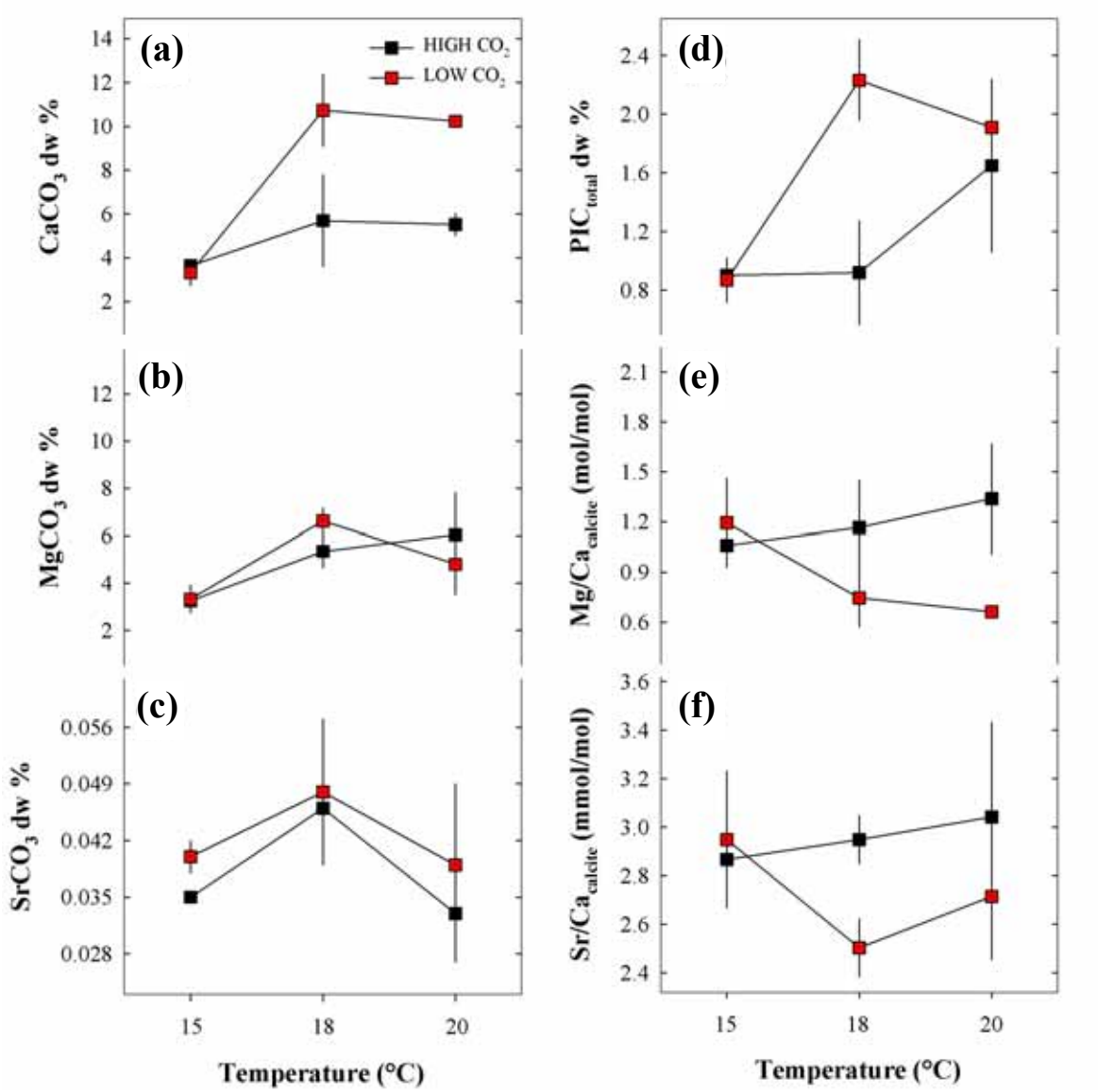

Fig. 13.1. Elemental composition of the skeleton in 38 days *Psammechinus miliaris* larvae incubated at three temperatures and two CO_2 conditions: (a) $CaCO_3$ %, (b) $MgCO_3$ %, (c) $SrCO_3$ %, (d) total PIC dry weight % (dw), (e) Mg/Ca (mol/mol) and (f) Sr/Ca (mmol/mol). At each experimental condition, measurements were done in duplicate from pellets normalized to 1000 larvae.

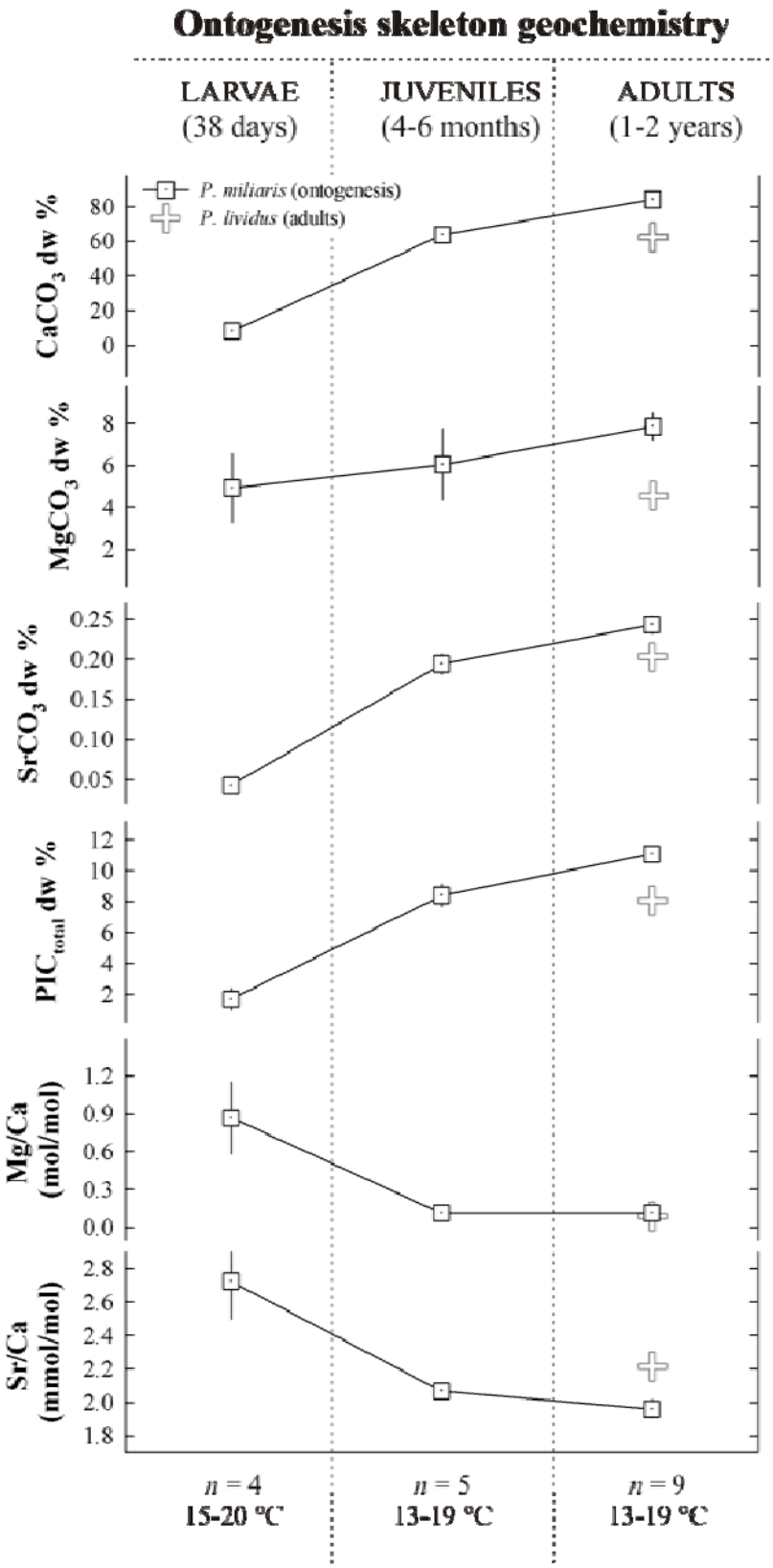

Fig. 13.2. Ontogeny changes in *Psammechinus miliaris* skeleton Mg-calcite [$CaCO_3$ %, $MgCO_3$ %, $SrCO_3$ %, total PIC dry weight % (dw), Mg/Ca (mol/mol), and Sr/Ca (mmol/mol)] cultured and collected at similar temperatures (*see* Table 13.4). Note that larvae were reared in laboratory conditions with seawater taken from the same population where juveniles an adults were collected. Thus, the geochemical changes can be attributed to the life history of this species at temperate latitudes. Skeleton elemental composition data of adult *Paracentrotus lividus* are also included for comparison.

13.3.2. Mg-calcite composition during ontogenesis in the modern ocean

The *Psammechinus miliaris* $CaCO_3$ content dramatically increased by almost a factor of eight from 38-day larvae (~ 8 %) to juveniles (~ 64 %), and then by a factor of almost 11 to adults (~ 84 %) (Fig. 13.2; Table 13.4). Conversely, the $MgCO_3$ content did not change much from larvae (~ 5 %) to juveniles (~ 6 %), but it was larger in adults (~ 8 %). The $SrCO_3$ behaved in a similar way to $CaCO_3$, increasing by almost a factor of five from larvae (~ 0.05 %) to juveniles (~ 0.2 %), and then by a factor of almost six to adults (~ 0.25 %). The PIC_{total} reflected the $CaCO_3$ influence, which dominates the inorganic carbon content, increasing by a factor of five from larvae (~ 1.8 %) to juveniles (~ 8.5 %), and then by a factor of almost seven to adults (~ 11 %). The $Mg/Ca_{calcite}$ ratio reflected the dramatic $CaCO_3$ increase and relative constant $MgCO_3$ content during ontogenesis. It decreased by almost a factor of 8 from larvae (~ 0.9 mol/mol) to juveniles (~ 0.1) and adults (~ 0.1). The $Sr/Ca_{calcite}$ ratio decreased in a moderate way from larvae (~ 2.7 mmol/mol) to juveniles (~ 2 mmol/mol) and adults (~ 1.9 mmol/mol). The ΩMg decreased during ontogenesis both at present and at high CO_2 conditions following the smaller $[CO_3^{2-}]$ and increasing mol % $MgCO_3$ (Fig. 13.3) ΩMg decreased from larvae ($\Omega Mg_{control}$ = 4.332, $\Omega Mg_{highCO2}$ = 1.228) to juveniles ($\Omega Mg_{control}$ = 4.305, $\Omega Mg_{highCO2}$ = 1.223) and to adults ($\Omega Mg_{control}$ = 4.278, $\Omega Mg_{highCO2}$ = 1.212).

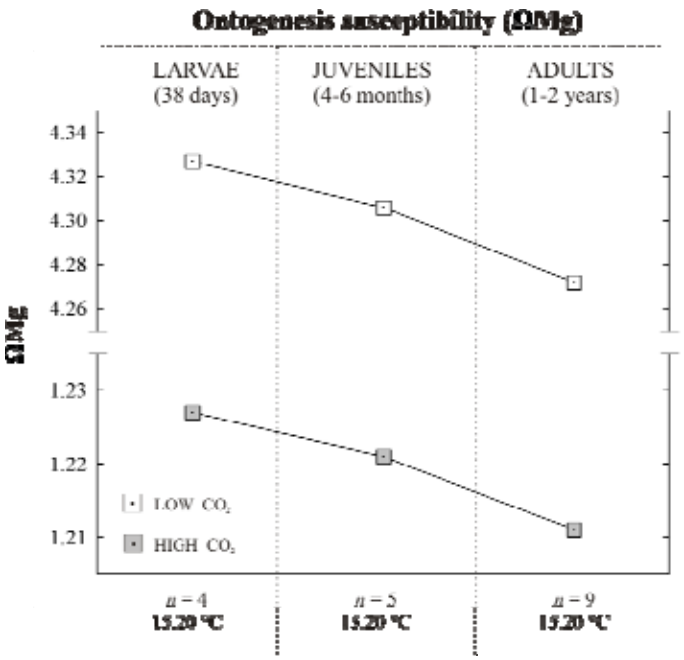

Fig. 13.3. Saturation state with respect to the measured mol % $MgCO_3$ (ΩMg) in *Psammechinus miliaris* during ontogeny For the calculations, the same temperature (15.40 °C) was used (representing the field habitat), and two CO_2 conditions were chosen. See Table 13.3 for the ΩMg calculation details.

13.4. Discussion

13.4.1 Echinoid Mg-calcite in the future ocean

Temperature alone explains major changes in the skeleton carbonate percentages ($CaCO_3$, $MgCO_3$, and $SrCO_3$), on the total inorganic carbon percentage (PIC_{total}), and on the ratios studied (except $Mg/Ca_{calcite}$, where there is a large CO_2-dependent trend). There is a general skeletal carbonate

increase with increasing temperature in modern ocean and high CO_2 conditions (except for $SrCO_3$ %, where there is an increase up to 18 °C and then a decrease to 20 °C). The $Mg/Ca_{calcite}$ and $Sr/Ca_{calcite}$ ratios were positively correlated to high CO_2, which suggests that the larvae compensate for the acidic conditions by dissolving biological $CaCO_3$ structures (chemically buffering intra and extracellular fluids). As a consequence, the $CaCO_3$ and $SrCO_3$ percentages of inner fluids would be lower at higher CO_2 conditions. The CO_2 effect can be observed in the $CaCO_3$ % at high CO_2 levels, where the temperature slightly increased the $CaCO_3$ % from ~ 4 (15 °C) to ~ 6 (18 and 20 °C), while it increased to ~ 11 (18 and 20 °C) in present conditions. The $MgCO_3$ and $SrCO_3$ percentages also decreased slightly with CO_2, which may indicate selective dissolution (even if ΩMg remained always between 5.81 and 1.20), but still the largest decrease is on the $CaCO_3$ content. The $Mg/Ca_{calcite}$ results at high CO_2 contrast with the finding of Ries (2011) where adult sea urchin spines and tests remain constant or slightly decrease (thus dissolving). We find this pattern only at 15 °C, while at 18 and 20 °C there is a large $Mg/Ca_{calcite}$ increase driven by $CaCO_3$ content. Our results agree with Ries (2011) in the way that echinoid larvae will not adapt to OA by producing less soluble form of Mg-calcite, but they will even increase $Mg/Ca_{calcite}$ ratios by maintaining Mg^{2+} levels. The $Mg/Ca_{calcite}$ and $Sr/Ca_{calcite}$ ratios were highly dependent on $[Ca^{2+}]$, the latter explaining the majority of the variation. This contrasts with previous results (Borremans et al. 2009; Hermans et al. 2010), where it was postulated that Mg^{2+} incorporation was regulating ratios variability in asteroid and echinoid juveniles. Here, we show that Mg^{2+} and Sr^{2+} remain relatively constant following temperature and CO_2 changes, while the variability is driven by Ca^{2+}. This, is in accordance with the values of PIC_{total} content, which demonstrate that the larvae grew bigger skeletal structures at high temperatures (18 to 20 ^{o}C). An increase in temperature will enhance supersaturation in seawater (*see* ΩMg change from 1.82 at 15 °C to 2.17 at 18 °C under similar CO_3^{2-} concentration) (Table 13.1) and thus the precipitation of $CaCO_3$, the main source for calcification in echinoderms (Weber 1969; Emlet 1982). Higher temperatures increase the metabolism and the ion transport (Borremans et al. 2009), therefore increasing the calcification rate in the echinoderm skeleton. Our results indicate that environmental factors can modulate echinoids Mg-calcite content during ontogenesis, when compared later with adults (*see* below).

Table 13.4. Complete dataset of the elemental composition of *Psammechinus miliaris* larvae (pellets) in the temperature and CO_2 experiment and the juveniles/adults from the field. Also included are the data from adult *Paracentrotus lividus*.

1) Temperature + CO_2 experiment (*P. miliaris* LARVAE)

CO_2 scenario	Temp. (°C)	*n* [a]	$CaCO_3$ % dw	$MgCO_3$ % dw	$SrCO_3$ % dw	Mg/Ca (mol/mol)	Sr/Ca (mmol/mol)	PIC_{total} % [b]	PIC_{CaCO3} %	PIC_{MgCO3} %	PIC_{SrCO3} % [c]
LOW	20	2	10.23 ± 0.00	4.80 ± 1.29	0.039 ± 0.010	0.662 ± 0.000	2.715 ± 0.365	1.91 ± 0.185	1.22 ± 0.000	0.685 ± 0.184	0.0032
LOW	18	2	10.72 ± 1.64	6.62 ± 0.54	0.048 ± 0.009	0.745 ± 0.174	2.503 ± 0.225	2.23 ± 0.27	1.28 ± 0.19	0.943 ± 0.077	0.0040
LOW	15	2	3.33 ± 0.59	3.33 ± 0.59	0.040 ± 0.002	1.194 ± 0.265	2.95 ± 0.389	0.87 ± 0.15	0.40 ± 0.07	0.475 ± 0.085	0.0033
HIGH	20	2	5.52 ± 0.50	6.03 ± 1.77	0.033 ± 0.006	1.338 ± 0.332	3.042 ± 0.790	1.65 ± 0.59	0.66 ± 0.06	0.860 ± 0.537	0.0027
HIGH	18	2	5.69 ± 2.10	5.35 ± 0.70	0.046 ± 0.007	1.165 ± 0.283	2.949 ± 0.159	0.92 ± 0.35	0.68 ± 0.25	0.762 ± 0.100	0.0038
HIGH	15	2	3.64 ± 0.27	3.26 ± 0.36	0.035 ± 0.000	1.060 ± 0.039	2.868 ± 0.001	0.90 ± 0.08	0.43 ± 0.03	0.464 ± 0.051	0.0029

2) Ontogenesis at present temperature and CO_2 conditions

Species - Stage	Temp. (°C)	*n* [d]	$CaCO_3$ % dw	$MgCO_3$ % dw	$SrCO_3$ % dw	Mg/Ca (mol/mol)	Sr/Ca (mmol/mol)	PIC_{total} % [b]	PIC_{CaCO3} %	PIC_{MgCO3} %	PIC_{SrCO3} % [c]
P. miliaris - Larvae	15/18/20	4	8.09 ± 4.13	4.92 ± 1.64	0.043 ± 0.004	0.867 ± 0.286	2.724 ± 0.225	1.67 ± 0.70	0.97 ± 0.49	0.70 ± 0.23	0.0035
P. miliaris - Juvenile	13-19	5	63.76 ± 4.37	6.05 ± 1.71	0.194 ± 0.012	0.112 ± 0.025	2.067 ± 0.025	8.40 ± 0.72	7.65 ± 0.52	0.72 ± 0.20	0.0233
P. miliaris - Adult	13-19	9	84.24 ± 3.45	7.86 ± 0.67	0.243 ± 0.011	0.110 ± 0.009	1.961 ± 0.054	11.08 ± 0.43	10.11 ± 0.41	0.94 ± 0.08	0.0293
P. lividus - Adult	16.50	14	62.36 ± 6.60	4.55 ± 0.50	0.203 ± 0.019	0.087 ± 0.014	2.214 ± 0.108	8.05 ± 0.78	7.48 ± 0.79	0.54 ± 0.06	0.0244

[a] *n* number of pellets concentrated to measure via ICP-MS. Each pellet had an estimated number of larvae according to density per ml and it was normalized to 1000 larvae per pellet.

[b] Total PIC = Σ $PIC\%_{total}$ = $PIC\%_{CaCO3}$ + $PIC\%_{MgCO3}$ + PIC_{SrCO3}, where inorganic carbon (as PIC) is calculated from the molecular weight proportion to the carbonate fraction: $PIC\%_{CaCO3} = CaCO_3/C = 8.333$; $PIC\%_{MgCO3} = MgCO_3/C = 7.017$, $PIC\%_{SrCO3} = SrCO_3/C = 12.267$.

[c] Standard deviation too small, so not presented here.

[d] *n* number of individuals used to measure the skeleton. For *Psammechinus miliaris* larvae refer to note "a".

They also show that it is the $CaCO_3$ and no the $MgCO_3$ content, the carbonate decreasing at high CO_2, thus driving the $Mg/Ca_{calcite}$ ratio. If this is induced by physiological regulation at the calcification site or by carbonate dissolution remains unknown, but it allows larva to maintain semi-constant $MgCO_3$ levels. Maintaining a high threshold Mg^{2+} content (even at high CO_2) increases echinoids carbonate hardness (Ma et al. 2008) and can serve to stabilize calcite during ontogenesis by causing a distortion in atomic structures, if behaving in a similar way to amorphous $CaCO_3$ (*see* Raz et al. 2000; Loste et al. 2003; Politi et al. 2010). We conclude that this tight control on $MgCO_3$ and $Mg/Ca_{calcite}$ may be an inherited trait that serves as an adaptation to OA at least in the short term.

13.4.2 Ontogenesis Mg-calcite geochemistry

After metamorphosis, juvenile and adult echinoids grow their tests by two processes: plate addition and plate enlargement or accretion. Most Palaeozoic echinoids conform to a simple conveyor belt model of growth, in which plates remain unspecialized and undifferentiated as they move from aboral to oral surface during ontogeny. We show that similar $MgCO_3$ contents are found in larvae (~ 5 %), juveniles (~ 6 %), and adults (~ 8 %), indicating that they may be established prior to metamorphosis (Fig. 13.2). Conversely, the deposition of $CaCO_3$ and $SrCO_3$ progressively continues to adult stages (incrementing by a factor of 11 and 6 respectively) (*see* Fig. 13.2), creating and thickening the plates in a conveyor belt [(from the apical disc to the mouth on the lower surface (Smith 2005)]. There is a major uptake of $CaCO_3$ immediately after metamorphosis (Smith 2005). Modern echinoderms are able to modify $CaCO_3$ uptake while skeletal growth proceeds under different environmental conditions. We explain this skeletal Mg^{2+} control as an evolutionary trait, where the first adult Mg-calcite elements are initiated within the rudiment in an earlier stage in ontogeny (Fig. 13.2). The overall juvenile and adult configuration of plates and spines takes shape during the first weeks and months following metamophosis (Gordon 1929). Maintaining high Mg^{2+} levels in skeletal Mg-calcite in the modern ocean and at high CO_2 conditions (*see* Fig. 13.1), confers organisms a way to stabilize the carbonate and also allows further morphological possibilities (Meldrum and Hyde 2001; Herfort et al. 2004; Politi et al. 2010). Therefore, it may be possible that echinoid larva favour a high $MgCO_3$ content early during ontogenesis to facilitate further skeletal development. The smaller $Mg/Ca_{calcite}$ and $Sr/Ca_{calcite}$ ratios observed in juveniles and adults are explained by an increased precipitation of $CaCO_3$ and not of $MgCO_3$. It was previously stated that these ratios

changed by an increase Mg^{2+} and Sr^{2+} incorporation under salinity and temperature gradients (Borremans et al. 2009; Hermans et al. 2010), while our data indicate that the Mg^{2+} control is tight, and it is the Ca^{2+} which regulates changes in the ratios.

The larva could main a threshold Mg^{2+} content slightly smaller than juveniles and adults to guarantee a reduced susceptibility to dissolution before metamorphosis (Fig. 13.3). This means that in high CO_2 conditions, adult echinoids will be the first responders (during ontogeny), while earlier stages (larvae and juveniles) will be more tolerant from the Mg-calcite perspective (Fig. 13.3). This will confer them a biological advantage to survive to metamorphosis and juveniles stages before being able to spawn again and withstand an episodic or permanent CO_2 rise. Contemporary research points to larval stages as the most susceptible to high CO_2 conditions (Dupont et al. 2010; Sewell and Hofmann 2011). Conversely, from a geochemical point of view, *P. miliaris* demonstrates that the larvae are capable to adapt to changes in ambient seawater carbonate chemistry by regulating their Mg-calcite contents. This geochemical plasticity seems to cease after metamorphosis, where a greater susceptibility to changes in CO_2 levels develops with a higher dissolution potential. The long-term survival of echinoid populations in the context of OA will be largely driven by the plasticity they show during larval stages and tight controls on Mg-calcite

14.

Revisiting the modern echinoderms global carbonate budget

Abstract

Biogenic carbonate production occurs in pelagic and benthic ecosystems, where the carbon produced is then exported to the seabed, where it accumulates or dissolves. Yet, benthic compartments have been widely ignored in their contribution to the global carbonate cycle, despite their importance in Mg-calcite production. This becomes especially relevant in the context of rising CO_2 levels (ocean acidification - OA), since Mg-calcites are assumed to be the first responders owing to a higher solubility than pure calcite. Here, we re-assessed the global Mg-calcite budget of a benthic group, the echinoderms, by conducting elemental analysis at the species level using inductively coupled plasma mass spectrometry (ICP-), to provide the first separate estimates of benthic $CaCO_3$, $MgCO_3$, and $SrCO_3$ production. We also measured via ICP- all other rare elements in echinoderm carbonates to provide an overview. To this end, we collected juvenile and adult echinoderms in the poles, tropics, and temperate latitudes in every ocean using a variety of field sampling techniques ranging from scuba diving to remote operated vehicles. When combining results with a literature dataset, we found global parabolic patterns in $MgCO_3$ and calcite Mg/Ca distribution (with a lot of scatter but maxima in tropics, minima in poles), with a wide variability in skeleton $SrCO_3$ concentrations. We attributed this not only to variability in temperature, physiology, and medium carbonate chemistry regimes, but also to transient mineralogical changes during ontogenesis and a small-scale seawater composition

variability (seawater Mg/Ca). The ample field variability in calcite Mg/Ca and Sr/Ca makes echinoderms a challenging phylum to use in paleoceanography reconstructions (e.g. temperature), and confounding results can appear if using field samples. The global contribution based on the three carbonates remained as follows: total inorganic carbon ($total_{PIC}$) = 0.853-0.113 g C yr^{-1}, PIC_{CaCO3} = 0.759-0.100 g C yr^{-1}, PIC_{MgCO3} = 0.105-0.014 g C yr-^{1}, and PIC_{SrCO3} = 0.0015-2.22 x 10-^{11} g C yr^{-1}. These estimations are above previous shelf and slope calculations and closer to pelagic calcites (coccolithophores and foraminifera). The echinoderms global production attributed to $MgCO_3$ indicated that ~ 12 % of the global carbonate budget originated in high Mg-calcite, which in the majority of the cases was > 6-8 mol % $MgCO_3$. We suggest that while at present Mg-calcite echinoderm populations and carbonate remains may not start dissolving, they could do so in the near future, starting at high latitudes. We suggest that the OA effect will progressively decrease the $MgCO_3$ levels in benthic Mg-calcites, and that echinoderm population may migrate to upper saturation thresholds to avoid major dissolution potential.

This chapter is based on:

Lebrato, M., Ries, J. B., McClintock, J. B., Egilsdottir, H., Lamare, M., Oschlies, A., Dupont, S. and Iglesias-Rodriguez, M. D. in preparation. Revisiting the modern echinoderms global carbonate budget. To be submitted: *ESA Ecology*.

Lebrato, M., McClintock, J. B., Amsler, M. and Ries, J. B. in preparation. Trace and elemental geochemistry in echinoderms Mg-calcite. To be submitted: *Geochemistry, Geophysics, Geosystems*.

Acknowledgements: This work was supported by the "European Project on Ocean Acidification" (EPOCA) for M. Lebrato's PhD.

14.1. General introduction

The production, export and dissolution of calcium carbonate ($CaCO_3$) is a fundamental process to many forms of marine life, representing a globally important process in regulating the Earth's carbon cycle. Biogenic carbonate production takes place in the euphotic zone (Schiebel 2002; Balch et al. 2007) and at shelf and slope depths (0-2000 m) in benthic ecosystems (Gollety et al. 2008; Lebrato et al. 2010; Hauck et al. 2012). The material eventually sediments out or it is deposited in situ, either dissolving above the lysocline (Feely et al. 2004; Berelson et al. 2007) or forming carbonate-rich sediment deposits representing a large $CaCO_3$ reservoir (Milliman and Droxler 1995; Iglesias-Rodriguez et al. 2002; Hauck et al. 2012). The Echinodermata are a carbonate-producing marine phylum that radiated in the early Palaeozoic (520 Ma) [the earliest deposits dating back to the early Cambrian (Durham 1971; Ubaghs 1975)]. Their common ancestors trace back to the Precambrian during the middle-late Neoproterozoic (550-750 Ma). Echinoderms increased in diversity during the middle Cambrian (Sprinkle 1973), and survived the Permian-Triassic extinction (250 Ma). This left five extant classes (Asteroidea, Echinoidea, Ophiuroidea, Holothuroidea, and Crinoidea) found today across large bathymetric gradients (Sokolova 1972; Gage and Tyler 1991; Ellis and Rogers 2000; Howell et al. 2002). Echinoderm remains in the fossil record are commonly found in sedimentary beds (Kroh and Nebelsick 2010), and modern deposits (Quaternary) exist in sediment cores and from subtidal to abyssal sediments (Lebrato et al. 2010).

Echinoderms have a calcite endoskeleton laid down by the mesoderm (Wilt and Benson 1988). The echinoderm body calcite is eventually "released" after death (reviewed by Rees and Dare 1993 and Lebrato et al. 2010), and it is either dissolved in situ as in molluscs (Rude and Aller 1991; Verling et al. 2005; Waldbusser et al. 2011) or deposited and incorporated into the sediments (Moran 1992; Brunskill et al. 2002). Echinoderms carbonate production differs from pelagic production owing to a higher incorporation of magnesium (Mg^{2+}) and strontium (Sr^{2+}) in the calcite lattice of the skeleton (Pilkey and Hower 1960; Weber et al. 1969; Roux et al. 1995; McClintock et al. 2011). All echinoderms (except holothurians) have a skeleton composed of high Mg-calcite (2 to < 25 mol % $MgCO_3$) (Weber 1969). The $MgCO_3$ content and the Mg/Ca were though to correlate well with temperature (*see* review by Vinogradov 1953; Chave 1954), but a recent review by Kroh and Nebelsick (2010) concluded that there is too much variability among classes, species, skeletal parts and latitude (induced by seasonal temperature changes,

carbon chemistries and salinity) to consider Mg as a palaeothermometry proxy. But, on a species-specific case and under controlled conditions it may be possible to derive a correlation (*see* Borremans et al. 2009; Hermans et al. 2010). Despite this variability, the echinoderm Mg/Ca from the fossil record has been successfully used to monitor ancient seawater composition (Dickson 2002, 2004; Ries 2004) mimicking other geochemical reconstructions (Horita et al. 2002). The Mg/Ca has been used in laboratory cultured foraminifera to re-construct past temperatures (*see* Barker et al. 2005 and references therein), while on echinoderms few data exist (*see* Borremans et al. 2009). A similar conclusion was reached by Kroh and Nebelsick (2010) for the use of Sr/Ca on palaeothermometry, although the sporadic studies measuring $SrCO_3$ and Sr/Ca in echinoderms are inconclusive (Pilkey and Hower 1960; Roux et al. 1995). Recently, Borremans et al. (2009) studied the Sr/Ca in starfish, correlating it with salinity, which implies an additional source of error in paleoreconstructions. Conversely, no correlation was found in the Sr/Ca in juvenile echinoid plates with a plateau relationship at different temperature and salinities (Hermans et al. 2010). The non-linearity found in the geochemical responses implies that Sr incorporation into the different echinoderm classes needs further study to provide a through assessment of its potential applications.

14.2. Partitioning of the global carbonate budget

The role of echinoderm derived carbonate in biogeochemical cycles from the Palaeozoic to the modern ocean has been widely ignored, with a major focus on pelagic processes (Balch et al. 2007; Gehlen et al. 2007). Research at the organism level has mainly targeted the pelagic contribution from coccolithophores (Findlay et a. 2011), which only trace back to the middle Mesozoic during the upper Triassic (250 Ma) (Wilkinson 1979; Bown et al. 2004). The contribution of benthic organisms to large-scale processes has only been recently assessed (Lebrato et al. 2010; Hauck et al. 2012). Using field data (density), $CaCO_3$ weight percentages from whole bodies [estimated from Particulate Inorganic Carbon (PIC)] and a model accounting for growth and mortality, Lebrato et al. (2010) concluded that the global echinoderms $CaCO_3$ standing stock was ~ 2.11 Pg $CaCO_3$ (0.25 Pg C as PIC), which translated into a production rate of 0.102 Pg C yr^{-1}. The contribution was below pelagic calcite production (0.4-1.8 Pg C yr-1), but echinoderms carbonate is directly delivered at the seabed, thus dissolution (if any) starts in situ and not in the water column while sinking (Berelson et al. 2007). The role of Mg-calcite during this dissolution may dictate the ultimate fate of the material (Andersson et al. 2008). The

echinoderms dataset used in Lebrato et al. (2010) did not distinguish between the carbonate source (by using directly PIC % data), thus it was not partitioned according to Ca^{2+}, Mg^{2+}, and Sr^{2+} (Lebrato et al. 2010; McClintock et al. 2011). A separation of the main carbonates is important to assess modern ocean susceptibilities to dissolution induced by the saturation state with respect to a Mg phase (ΩMg) (Morse et al. 2006; Andersson et al. 2008) and also to divide the calculation of the budget. Preferential dissolution to high Mg-calcite could also be used to assess changes in total alkalinity and the signal emitted from the shelves. Additionally, different echinoderm skeletal party vary in complexity and Mg content (Weber 1969; Henrich and Wefer 1986), and potentially on the Sr composition, governing the elemental fluxes from this taxa.

A recent concern following anthropogenic emissions of greenhouse gases is that the ocean will become enriched in CO_2, while carbonate ions (CO_3^{2-}) and thus the calcite saturation state (Ω) will decrease, termed ocean acidification (OA) (Caldeira and Wickett 2003). For high Mg-calcite organisms like echinoderms, rising CO_2 levels might come at a cost of increasing skeleton dissolution, driven by the increasing solubility of Mg-calcite with a certain mol % $MgCO_3$ (Morse et al. 2006) Echinoderms tend to inhabit environments such as the deep sea, the shelf intertidal/subtidal, and the high latitudes, where carbonate chemistry conditions are naturally more corrosive to carbonates than in low latitudes or the open ocean (Feely et al. 2004; Orr et al. 2005; Borges et al. 2006). Therefore, any major rise in CO_2 could increase living skeletal material solubility or induce large Mg-calcite sediments dissolution, buffering anthropogenic CO_2, although this remains speculative (Andersson and Mackenzie 2012). Empirical work suggests that ambient carbonate chemistry (namely CO_2) drives $MgCO_3$ variability in benthic organisms following a physiological species-specific fingerprint and environmental control (Mackenzie et al. 1983; Ries 2011). For example, the $MgCO_3$ content of coralline algae correlates negatively to increasing CO_2, while no major response occurs in echinoids (Ries 2011). Despite the threat of OA to Mg-calcites, there is still a poor understanding of basic controls on Mg^{2+} skeletal content that then is exported and contributes towards the global carbonate budget. Detailed knowledge on $MgCO_3$ is essential to assess if benthic organisms will be the first responders to OA, to which extent dissolution of metastable Mg-calcite might affect life cycles, and if large bathymetric migrations induced by shallowing of saturation horizons (Sewell and Hofmann 2011) could pose a threat to modern echinoderm populations and start dissolving echinoderm-rich deposits in shelves and slopes.

In this paper we re-assess the global echinoderms inorganic carbon (PIC) and elemental ($CaCO_3$, $MgCO_3$, and $SrCO_3$) budget by including polar (sub-Arctic and Antarctic), temperate and tropical specimens to study the latitudinal budget partitioning and provide new global figures based on the three carbonates. We present the largest and most comprehensive echinoderms Mg-calcite dataset measured via inductively coupled plasma spectrometer (ICP-) from whole bodies and separation from arms, spines and plates, and we combine them with published data to explore the elemental chemistry. For the first time we present a complete dataset on $SrCO_3$ in echinoderms, also calculating a global contribution from this carbonate. We assess the ontogenic differences (from juveniles to adults) in the carbonate content and elemental ratios. This helps to understand biases that can be introduced if the whole population size range is not included in global budget calculations. For all carbonates and elemental ratios, we provide global latitudinal trends that help to identify the most sensitive regions e.g. to potential Mg-calcite dissolution induced by OA. This work highlights the major advances made on the assessment of benthic budgets especially in polar latitudes (after McClintock et al. 2011), which are believed to be the most sensitive to global change (Sewell and Hofmann 2011). The data will also allow to assess Mg-calcite susceptibility to dissolution in benthic communities and in echinoderm sediment remains from continental margins in present and the future oceans.

14.3. Materials and methods

14.3.1. Biogenic material used

Echinoderm samples were collected between 2008 and 2011 from 2 to > 1000 m in the Atlantic, Pacific, Arctic, and Southern Ocean, from the five classes. Juveniles and adults were collected to represent the whole population that contributes to benthic carbon export. This budget excludes larval stages, which contribution is assumed minor. Individuals were measured and weighted (data in Lebrato et al. 2010 and McClintock et al. 2011), and divided as whole body, arms (plates) (some Antarctic species), calcareous rings (in some holothuroids), spines, and plates for geochemical analysis [$n_{\text{Asteroidea}}$ = 108 (9 families, 23 species), $n_{\text{Echinoidea}}$ = 94 (8 families, 12 species), $n_{\text{Ophiuroidea}}$ = 24 (4 families, 5 species), $n_{\text{Holothuroidea}}$ = 7 (3 families, 3 species), $n_{\text{Crinoidea}}$ = 3 (1 family, 1 species)] (Table 14.1; Fig. 14.1). Organisms were collected using a variety of methods including scuba diving, bottom trawling, and Remote Operated Vehicles during cruises and surveys (Table 14.1). We also collected literature data to include in

our analyses [adults: $n_{\text{Asteroidea}}$ = 23 species (8 families), $n_{\text{Echinoidea}}$ = 18 species (11 families), $n_{\text{Ophiuroidea}}$ = 18 species (8 families), $n_{\text{Crinoidea}}$ = 19 species (14 families), juveniles: $n_{\text{Asteroidea}}$ = 1 species (1 family), $n_{\text{Echinoidea}}$ = 1 species (1 family)] (Table 14.1; Table 14.5). Samples were distributed geographically from sub-Arctic regions to Antarctica with the exception of the Indian Ocean, while literature samples were available from all oceans except the south Atlantic (Fig. 14.1). The majority of samples (> 70%) originated in temperate and polar latitudes. All organisms were healthy and were collected using all necessary permits to remove marine organisms within the research area causing minimum impact. All samples were frozen at either -20 or -80 °C after collection and placed in ziplock bags.

2.2. Samples preparation and elemental analyses

All samples except sub-Arctic and Antarctic ones (Table 14.1) were stored and initially treated at the Helmholtz Centre for Ocean Research Kiel (GEOMAR, Germany) until sent for analysis at the University of North Carolina-Chapell Hill. Whole body samples for budget re-assessment were freeze-dried inside the ziplock bags for 48 h and then reduced to fine powder

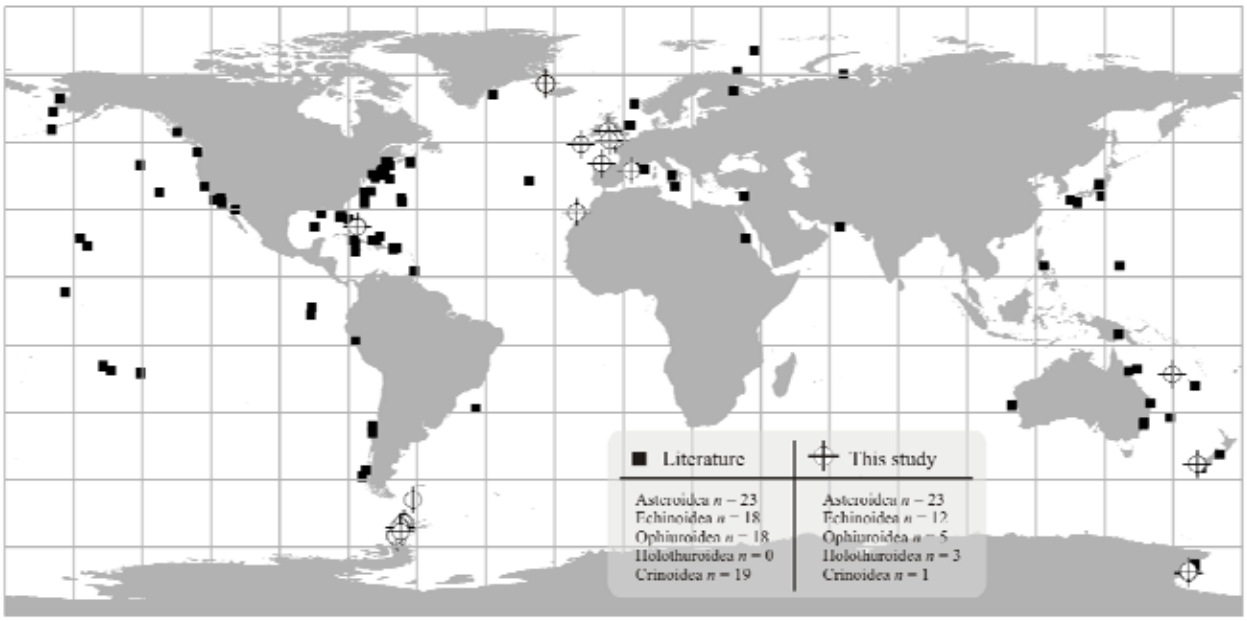

Fig. 14.1. Global distribution of the samples used for carbonate analyses of whole body (all components), spines, and plates, as well as the selected literature data (Vinogradov 1953; Weber 1969).

with a rotating metal blade (inorganic and organic material included). Some echinoids (depending on sample availability) were divided into spines and plates (only inorganic material

included) (*see* Table 14.1, 14.2). Spines were removed from the test with a razor blade, and the test pieces cut with scissors. Measurements were obtained with a Perkin Elmer Sciex ELAN 9000 inductively coupled plasma mass spectrometer (ICP-MS). Samples were lightly ground in a mortar and pestle for 10-15 s. A 0.50 gr sample of the pulverized echinoderm material was digested for 2 h in Aqua Regia at 90 °C in a microprocessor controlled digestion block. Duplicate samples were run every 15 samples, in-house controls were run every 33 samples, and digested certified standards (for instrument calibration) and blanks were run every 68 samples.

Sub-Arctic samples (Table 14.1) were analyzed at the Institute of Earth Sciences, University of Iceland. Samples were thawed and immediately cleaned with distilled water and dried at room temperature for ~ 10 days. Asteroids and ophiuroids were dried as whole organisms, but organic matter (soft tissue) was removed from echinoids, leaving only calcified material for the analysis (body parts; spines and plates). Samples were powderised and small sub-samples (1-10 mg) were placed in 20 ml acid-washed polyethylene vials. Samples were not weighted, thus only molar ratios are reported for these species (Table 14.2). 1 ml of 65% ultra pure nitric acid was added to the samples to dissolve them, and then 4 ml of Milli-Q water was added to the solution. Owing to the presence of organic material, samples were filtered through a Whatman 42 filter. The analysis took place on a Spectro CIROS inductively coupled plasma optical emission spectroscope (ICP-OES). The analytical concentration range was linear over several orders of magnitude, starting in the ppb range for most elements. Standard solutions were made from NIST-traceable calibration solutions (Spex Industries Inc.). The standards used in 0.5 % nitric acid were 30 ppm (Ca and Mg), 2 ppm (Sr) and 10 ppm (Cl, Na, K, S and P). The non-carbonate elements (Na, K, S, P and Cl), were monitored to estimate the contamination level. The low Cl and Na concentrations (below 1 ppm), indicated an efficient cleaning.

Antarctic samples (Table 14.1) were analyzed by Actlabs in Ancaster, Ontario (Canada) (www.actlabs.com). Samples treatment and methods followed those given in McClintock et al. (2011). In brief, frozen samples were thawed and dissected. For asteroids and ophiuroids, arms (thus arm plates, which are comparable to other plate data in this study) were cut and organic material was manually removed, except in two asteroids (*Kampylaster incurvatus* and *Granaster nutrix*) that were used as whole body (Table 14.1). These “whole body” results are not comparable to other specimens (Table 14.1) because the organic material was removed by soaking on sodium hypochlorite (NaClO) (Fisher). For holothurids, the calcareous ring was

extracted, and echinoids were divided into spines and plates. All samples were soaked in 10 % NaClO for a few days to remove organic matter. The remaining inorganic material was vacuumed onto filter paper rinsed with Milli-Q water for several minutes. Filters were subsequently dried at 50 °C for 48 h. Dried material was reduced to powder in a mortar. The analysis took place on a PerkinElmer inductively coupled plasma atomic emission spectroscope (ICP-AES) for Ca, Mg, and Sr. The powdered material was divided in 90-500 mg splits and dissolved in nitric (HNO_3) and hydrochloric acid (HClO) in a molar ratio of 1/3 for 2 h at 95 °C. Samples were diluted with Milli-Q water. USGS standards were analyzed every 13 samples. Analytical accuracy was within 0.01 % of the value of the standards. Using the known weights of the samples, results were reported as percentages of the dry weight in grams or moles and subsequently used to calculate molar ratios (Mg/Ca and Sr/Ca) (Table 14.2).

14.3.3. Global budget re-assessment

We combined the measurements from the three carbonates (*see* Table 14.2; Fig. 14.2) with the same field biomass dataset and algorithm used in Lebrato et al. (2010). In summary, field density data were collected at 523 stations, and using correlations of size *vs.* dry weight from all the species collected (*see* Table 2 in Lebrato et al. 2010 for equations, and Fig. 14.3 here) we translated these data into dry biomass per unit area. Note that for the new species added (sub-Arctic, tropical, and Antarctic, Table 14.1) we used a general size *vs.* dry weight correlation for the corresponding class (*see* Table 2 in Lebrato et al. 2010). Therefore, these new samples complement the re-assessment of the budget by giving a more accurate conversion factor (percentage) for each carbonate. All biomass data were normalized per square meter. Subsequently, the global budget was partitioned using the product of the dry biomass and the average carbonate percentage ($CaCO_3$, $MgCO_3$, $SrCO_3$) measured for each species (Table 14.2). When field biomass data were not available as a species, we used a general conversion figure representing an average from all the species within a class (Table 14.3). The total PIC per organism was calculated as the sum of the three carbonates:

$$Total_{PIC}\,\% = \Sigma\, PIC_{total}\,\% = PIC_{CaCO3}\,\% + PIC_{MgCO3}\,\% + PIC_{SrCO3}\,\% \quad (1)$$

where PIC is calculated from the mass proportion to the carbonate fraction measured: PIC_{CaCO3} % = $CaCO_3$/C = 8.333; PIC_{MgCO3} % = $MgCO_3$/C = 7.017, PIC_{SrCO3} % = $SrCO_3$/C = 12.267.

The new samples from polar and tropical latitudes allowed to constraint latitudinal differences with measured PIC percentages, instead of extrapolating from other samples. Final production estimates (per year) used growth and size distribution data from Smith (1972) to estimate the turnover rate caused by mortality (1.0 yr^{-1} for echinoids, 0.2 yr^{-1} for ophiuroids, and 0.3 yr^{-1} for the rest) (*see* Ebert 2001 for species-specific mortality values and complex growth-size-mortality equations). Eventually, we used data on the average depth range and area occupied by shelves (0-200 m, $10*10^{12}$ m^2), slopes (200-2000 m, $32*10^{12}$ m^2) and the abyss (>2000 m, $290*10^{12}$ m^2) to extrapolate globally (Anikouche and Sternberg 1973; Gage and Tyler 1991; Milliman 1993; Iglesias-Rodriguez et al. 2002). In the calculation of the global figures of total PIC and the three carbonates, two different methods were used. In the first one, total PIC per year was the sum of the production in the shelf, slope and abyssal depth ranges, which are calculated with three different production rates (Table 4). In the second one, total PIC per year is the global average production rate multiplied by the area (Table 4). These calculations give a range for the production budget, instead of providing a single figure. They also do not distinguish between large bathymetric gradients for entire classes, which can be a realistic assumption for large populations, specially in the abyss (Howell et al. 2002).

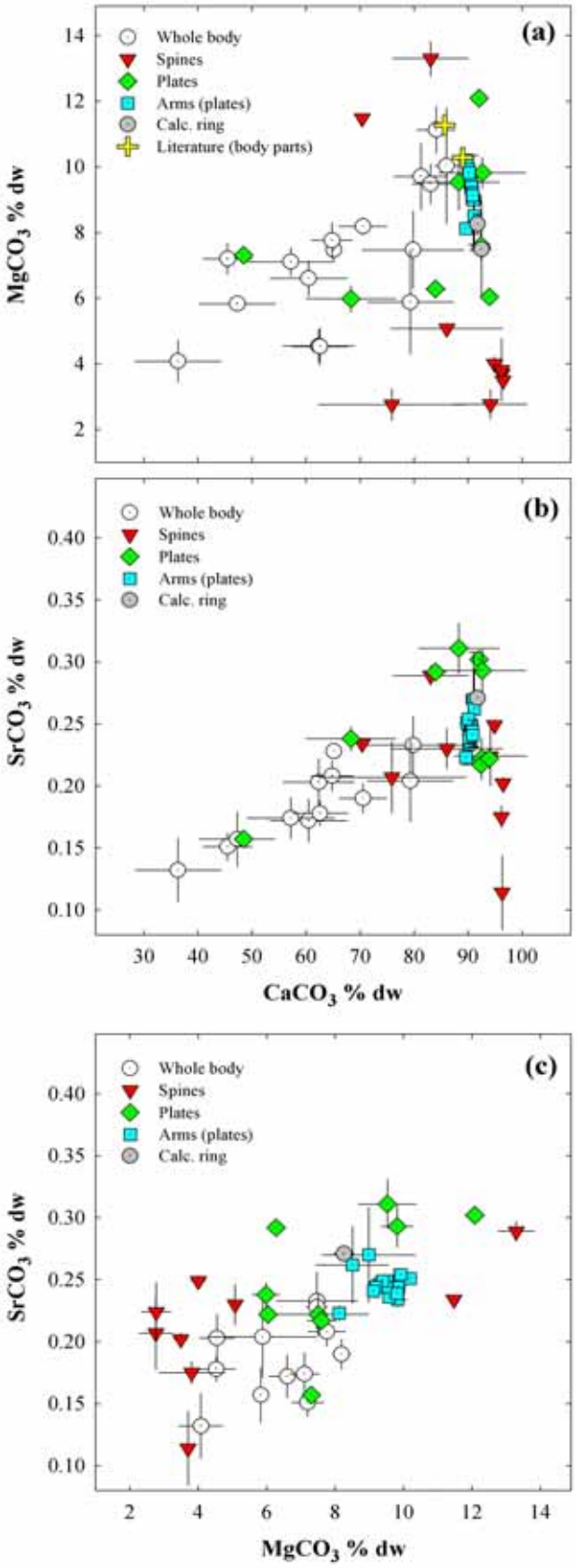

Fig. 14.2. Correlation between $MgCO_3$ % (a) and $SrCO_3$% (b) vs. $CaCO_3$ % and $SrCO_3$ vs. $MgCO_3$ for all samples. Bidirectional error bars (standard deviation) from *n* measurements are included.

14.4. Results

14.4.1. Elemental composition: echinoderms carbonate

The incorporation of Mg^{2+} did not follow that of Ca^{2+} in echinoderm whole bodies, plates, and especially spines (Fig. 14.2a), irrespectively of class and species, but it was more predictable in Sr (Fig. 14.2b). The correlation between $MgCO_3$ and $CaCO_3$ dry weight percentages was statistically significant ($F_{1,45}$ = 33.368, P < 0.01. r^2 = 0.43), and followed an exponential curve (excluding spines):

$$y = 3.373 * e^{0.011\,x} \qquad (2)$$

Many of the samples deviated from an ideal 1:1 and the exponential relationship, especially along the x- and y-axes ($CaCO_3$ and $MgCO_3$), as $MgCO_3$ was not incorporated in the same proportion. The deviation from a 1:1 line reached a maximum in spines (+40-50 %), and a minimum in whole bodies (+5-30 %). The largest differences were found in samples in $CaCO_3$ above 70 % dry weight (dw). The deviation from the exponential relationship was mainly noticeable in spines (40-80 %), and plates (10-20 %), while for whole bodies

it remained relatively stable (< 10 % except in two cases).

The correlation between $SrCO_3$ and $CaCO_3$ dry weight percentage was statistically significant ($F_{1,38} = 84.696$, $P < 0.01$. $r^2 = 0.68$), and also followed an exponential curve (excluding spines):

$$y = 0.097 * e^{0.0105\,x} \quad (3)$$

All the samples deviated from a 1:1 line between 5 and 20 % in both x- and y-axes, but were well constraint by the exponential relationship. Up to 70 % $CaCO_3$ dw, the correlation was consistent with the predictor equation, but above this level there were deviations especially in whole bodies (5-10 %), and spines (5-20 %) on the x-axis ($CaCO_3$).

The correlation between $SrCO_3$ and $MgCO_3$ dry weight percentage was statistically significant ($F_{1,42} = 30.840$, $P < 0.01$. $r^2 = 0.43$), and followed a linear curve:

$$y = 0.0106\,x + 0.145 \quad (4)$$

Samples were scattered around a 1:1 line in all cases, with deviations depending on taxonomy and skeletal part. Up to 10 % $MgCO_3$ dw, the correlation was consistent with the predictor equation, and above this level there were small deviations for spines and plates (< 10 %).

14.4.1.1 $CaCO_3$ % dry weight

Overall, higher $CaCO_3$ percentages were found in spines than in plates, and whole bodies (Fig. 14.2). The Antarctic species *Sterechinus neumayeri* had the highest $CaCO_3$ percentage in spines (96.50 ±0.20 %), followed by other Antarctic species (96.30 ±0.14 % and 96.18 ±0.96 % in *Amphineustes similis* and *Ctenocidaris perrieri* respectively). The temperate species *Pseudechinus huttoni* followed the Antarctic species (94.91 ±0.00 %). The lowest $CaCO_3$ percentage in echinoid spines was found in the temperate species *Paracentrotus lividus* (75.91 ±13.65 %), and the lowest overall in the tropical ophiuroid *Ophiura longicauda* (70.42 ±0.00 %). In plates, the highest $CaCO_3$ percentages corresponded to Antarctic species (93.96 ±0.25 %, 92.49 ±1.47 %, and 92.39 ±0.42 % in *S. neumayeri*, *A. similis*, and *C. perrieri* respectively) followed again by *P. huttoni* (92.64 ±8.03 %) (Table 14.2). Antarctic asteroids and ophiuroids

plates remained all between 89.63 ±0.11 % (*Diplopteraster verrucosus*), and 91.14 ±0.96 % (*Perknaster aurorae*). The lowest $CaCO_3$ percentage in echinoid plates was in the temperate species *P. lividus* (68.34 ±8.32 %), and the lowest overall in *Ophiura longicauda* (48.44 ±0.00 %). Holothuroidea calcareous ring values were similar to plates from the other classes (*Molpadia musculus* = 91.74 ±0.30 %, *Pseudostichopus spiculiferus* = 92.51 ±0.00 %).

The lowest overall $CaCO_3$ percentage values were found in whole bodies (Table 14.2). Echinoids had the largest $CaCO_3$ percentages (maximum: the tropical species *Cidaris blakei* = 79.32 ±7.99 %, minimum: *P. lividus* = 62.36 ±6.60 %, followed by *S. neumayeri* = 62.59 ±5.14 %). They were followed by ophiuroids (the temperate species *Ophiosium lymani* = 70.54 ±4.43 %), crinoids (the temperate species *Antedon mediterranea* = 64.84 ±3.82 %), asteroids (maximum: the temperate species *Asterina gibbosa* = 60.48 ±7.16 %, minimum: temperate species *Asterias rubens* = 36.27 ±7.91 %; the Antarctic species *Odontaster validus* = 47.28 ±7.02 had similar percentages to temperate species), and holothurians (temperate species *Holothuria forskali* = 2.60 ±1.04 %) (Table 14.2).

The correlation between whole body $CaCO_3$ % dw and the dry weight (size estimation) was statistically significant ($F_{1,65}$ = 22.42, $P < 0.01$. r^2 = 0.33), and the best fit was a polynomial equation (Fig. 14.3a):

$$y = 64.69 + 0.74\,x - 0.061\,x^2 \quad (4)$$

In small individuals of the same class (low dw), $CaCO_3$ percentages were relatively constant (50-85%), while in the largest individuals, percentages decreased between 10 and 30 % (Figure 3a). The decrease was most visible in asteroids.

Table 14.1. Samples used for carbonate analyses of body (all components), spines, and plates (and published data). Ordered by class and latitude.

Class	Family / Species	*n* [a]	Depth (m)	Lat. / Long.	Location	Collection method	Bio-material [b]
				THIS STUDY			
Asteroidea	Asteriidae / *Asterias rubens*	5	30	65.81 / -18.09	Eyjafjordur, Iceland (N Atlantic)	Trawling	Whole body
Asteroidea	Asteriidae / *Asterias rubens*	6	20	65.08 / -22.67	Breidafjordur, Iceland (N Atlantic)	Trawling	Whole body
Asteroidea	Asteriidae / *Asterias rubens*	10	10	64.04 / -22.06	Straumsvik, Iceland (N Atlantic)	Scuba diving	Whole body
Asteroidea	Solasteridae / *Solaster endeca*	4	10	64.04 / -22.06	Straumsvik, Iceland (N Atlantic)	Scuba diving	Whole body
Asteroidea	Asteriidae / *Asterias rubens*	8	2	53.24 / -4.46	Swansea (NE Atlantic)	Manual	Whole body
Asteroidea	Asterinidae / *Asterina gibbosa*	6	2	50.63 / -2.39	English Channel (NE Atlantic)	Manual	Whole body
Asteroidea	Zoroasteridae / *Zoroaster fulgens*	4	1140	49.28 / -12.36	Porcupine Sea Bight (NE Atlantic)	Semi-otter trawl	Whole body
Asteroidea	Asteriidae / *Marthasterias glacialis*	7	3	43.58 / -6.24	Cape Vidio (Cantabric Sea)	Manual	Whole body
Asteroidea	Ladidiasteridae / *Labidiaster annulatus*	9	160-170	-61.21 / -56.01	Elephant Island (Southern Ocean)	Trawling	Arm (plates)
Asteroidea	Astropectinidae / *Macroptychaster accrescens*	3	140-215	-63.53 / -62.75	Low Island (Southern Ocean)	Trawling	Arm (plates)
Asteroidea	Solasteridae / *Paralophaster godfroyi*	1	140-215	-63.53 / -62.75	Low Island (Southern Ocean)	Trawling	Arm (plates)
Asteroidea	Solasteridae / *Paralophaster* sp.	3	140-215	-63.53 / -62.75	Low Island (Southern Ocean)	Trawling	Arm (plates)
Asteroidea	Ganeriidae / *Perknaster* sp.	2	140-215	-63.53 / -62.75	Low Island (Southern Ocean)	Trawling	Arm (plates)
Asteroidea	Odontasteridae / *Acodontaster hodgsoni*	3	150-170	-64.15 / -62.74	Dallmann Bay (Southern Ocean)	Trawling	Arm (plates)
Asteroidea	Asterinidae / *Kampylaster incurvatus*	4	150-170	-64.15 / -62.74	Dallmann Bay (Southern Ocean)	Trawling	Whole body
Asteroidea	Odontasteridae / *Odontaster penicillatus*	1	150-170	-64.15 / -62.74	Dallmann Bay (Southern Ocean)	Trawling	Arm (plates)
Asteroidea	Poraniidae / *Porania antarctica*	3	150-170	-64.15 / -62.74	Dallmann Bay (Southern Ocean)	Trawling	Arm (plates)
Asteroidea	Asteriidae / *Diplasterias brandti*	3	5-40	-64.77 / -64.05	Arthur Harbor (Southern Ocean)	Scuba diving	Arm (plates)
Asteroidea	Asteriidae / *Granaster nutrix*	5	5-40	-64.77 / -64.05	Arthur Harbor (Southern Ocean)	Scuba diving	Whole body
Asteroidea	Asteriidae / *Neosmilaster georgianus*	3	5-40	-64.77 / -64.05	Arthur Harbor (Southern Ocean)	Scuba diving	Arm (plates)
Asteroidea	Odontasteridae / *Odontaster meridionalis*	3	5-40	-64.77 / -64.04	SE Boneparte Pt. (Southern Ocean)	Scuba diving	Arm (plates)
Asteroidea	Ganeriidae / *Perknaster aurorae*	3	5-40	-64.78 / -63.99	Stepping Stones (Southern Ocean)	Scuba diving	Arm (plates)

Asteroidea	Odontasteridae / *Acodontaster conspicuus*	1	5-40	-65.07 / -63.97	Lemaire Channel (Southern Ocean)	Scuba diving	Arm (plates)
Asteroidea	Ganeriidae / *Perknaster fuscus antracticus*	1	5-40	-65.07 / -63.97	Lemaire Channel (Southern Ocean)	Scuba diving	Arm (plates)
Asteroidea	Echinasteridae / *Henricia sp.*	2	145-175	-65.67 / -67.40	Renaud Island (Southern Ocean)	Trawling	Arm (plates)
Asteroidea	Pterasteridae / *Diplopteraster verrucosus*	2	850-950	-66.29 / - 66.60	Banana Trench (Southern Ocean)	Trawling	Arm (plates)
Asteroidea	Odontasteridae / *Odontaster validus*	6	18	-77.63 / 146.41	Antarctica (Southern Ocean)	ROV	Whole body
Echinoidea	Strongylocentrotidae / *Strongylocentrotus droebachiensis*	5	30	65.81 / -18.09	Eyjafjordur, Iceland (N Atlantic)	Trawling	Body parts
Echinoidea	Strongylocentrotidae / *Strongylocentrotus droebachiensis*	5	20	65.08 / -22.67	Breidafjordur, Iceland (N Atlantic)	Trawling	Body parts
Echinoidea	Echinidae / *Echinus esculentus*	3	20	65.08 / -22.67	Breidafjordur, Iceland (N Atlantic)	Trawling	Body parts
Echinoidea	Echinidae / *Echinus esculentus*	5	10	64.04 / -22.06	Straumsvik, Iceland (N Atlantic)	Scuba diving	Body parts
Echinoidea	Strongylocentrotidae / *Strongylocentrotus droebachiensis*	5	10	64.04 / -22.06	Straumsvik, Iceland (N Atlantic)	Scuba diving	Body parts
Echinoidea	Parechinidae / *Psammechinus miliaris*	14	1	50.35 / -4.13	English Channel (NE Atlantic)	Manual	Whole body
Echinoidea	Parechinidae / *Paracentrotus lividus*	14	2	43.58 / -6.24	Cape Vidio (Cantabric Sea)	Manual	Whole body
Echinoidea	Parechinidae / *Paracentrotus lividus*	3	1	29.13 / -13.60	Lanzarote (E Atlantic)	Manual	Spines, plates
Echinoidea	Toxopneustidae / *Tripneustes ventricosus*	2	6	25.12 / -77.29	Paradise Island (W Atlantic)	Manual	Whole body
Echinoidea	Cidaridae / *Cidaris blakei*	2	595	24.83 / -77.50	South West Reef (W Atlantic)	Submersible	Whole body
Echinoidea	Diadematidae / *Diadema setosum*	3	0.5	-18.85 / 159.75	Aitukai Island (SW Pacific)	Manual	Spines, plates
Echinoidea	Echinometridae / *Evechinus chloroticus*	6	5	-45.30 / 166.97	Doubtful Sound (SW Pacific)	Scube diving	Spines, plates
Echinoidea	Temnopleuridae / *Pseudechinus huttoni*	5	8	-45.41 / 167.10	Doubtful Sound (SW Pacific)	Scuba diving	Spines, plates
Echinoidea	*Inc. sed.* [c] / *Amphineustes similis*	4	670-700	-64.75 / -65.47	Renaud Island (Southern Ocean)	Trawling	Spines, plates
Echinoidea	Cidaridae / *Ctenocidaris perrieri*	3	670-700	-64.75 / -65.47	Hugo Island (Southern Ocean)	Trawling	Spines, plates
Echinoidea	Echinidae / *Sterechinus neumayeri*	6	5-40	-65.07 / -63.97	Lemaire Channel (Southern Ocean)	Scuba diving	Spines, plates
Echinoidea	Echinidae / *Sterechinus neumayeri*	9	15	-77.06 / 164.42	Antarctica (Southern Ocean)	Scuba diving	Whole body
Holothuroidea	Holothuriidae / *Holothuria forskali*	3	3	43.58 / -6.24	Cape Vidio (Cantabric Sea)	Manual	Whole body
Holothuroidea	Molpadiidae / *Molpadia musculus*	3	670-700	-64.75 / -65.47	Hugo Island (Southern Ocean)	Trawling	Calcareous ring
Holothuroidea	Synallactidae / *Pseudostichopus spiculiferus*	1	850-950	-66.29 / - 66.60	Banana Trench (Southern Ocean)	Trawling	Calcareous ring
Ophiuroidea	Ophiactidae / *Ophiopholis aculeata*	11	10	64.04 / -22.06	Straumsvik, Iceland (N Atlantic)	Scuba diving	Whole body

Ophiuroidea	Ophiolepididae / *Ophiosium lynami*	6	1140	49.20 / -12.30	Porcupine Sea Bight (NE Atlantic)	Semi-otter trawl	Whole body
Ophiuroidea	Ophiuridae / *Ophiura longicauda*	3	1	29.12 / -13.56	Lanzarote (E Atlantic)	Manual	Spines, plates
Ophiuroidea	Ophiuridae / *Ophionotus victoriae*	3	5-40	-64.77 / -64.05	Arthur Harbor (Southern Ocean)	Scuba diving	Arm (plates)
Ophiuroidea	Ophiacanthidae / *Ophiosparte gigas*	1	5-40	-64.77 / -64.05	Arthur Harbor (Southern Ocean)	Scuba diving	Arm (plates)
Crinoidea	Antedonidae / *Antedon mediterranea*	3	63	41.43 / 2.32	Catalan Sea (Mediterranean Sea)	Benthic trawl	Whole body
				LITERATURE - adults [d]			
Asteroidea	see Table A1	23	n/a [e]	*see* Appendix A	*see* Appendix A	n/a	Body parts
Echinoidea	see Table A1	18	n/a	*see* Appendix A	*see* Appendix A	n/a	Body parts
Ophiuroidea	see Table A1	18	n/a	*see* Appendix A	*see* Appendix A	n/a	Body parts
Crinoidea	see Table A1	21	n/a	*see* Appendix A	*see* Appendix A	n/a	Body parts
				LITERATURE - juveniles [d]			
Asteroidea	Asteriidae / *Asterias rubens*	52 [f]	Intertidal	*see* Appendix A	*see* Appendix A	Manual	Plates
Echinoidea	Parechinidae / *Paracentrotus lividus*	76 [f]	Subtidal	*see* Appendix A	*see* Appendix A	Scuba diving	Plates

[a] *n* number of samples collected from different size classes during field surveys and selected from the literature.

[b] This indicates the targeted material for subsequent carbonate ICP-MES analyses. In come cases the whole body with organic matter was not available, thus we used spines, plates, and tests. In the case of starfish arms (Antarctic data), they are representative of the entire body (only as inorganic carbon, thus not comparable to "whole body" data, which include organic material).

[c] *Inc. sed.* is in latin *Incertae sedis* and it is used in taxonomy in cases where a species has not been classified correctly yet.

[d] Samples were selected from the literature to complement the latitudinal trends (body parts). Full description of species and locations in Table 14.5.

[e] n/a indicates not available and/or not applicable.

[f] *See* table A2 for number of samples incubated at each temperature in the laboratory.

Table 14.2. Samples carbonate percentages and elemental ratios and the published values used. Data ordered by class and latitude.

Class	Species	Bio-material	*n* [a]	$CaCO_3$% dw [b]	$MgCO_3$% dw	$SrCO_3$% dw	Mg/Ca (mol/mol)	Sr/Ca (mmol/mol)	PIC% (ICP) [c]	PIC% (Coul.) [d]	PIC% (CaCO3)	PIC% (MgCO3)	PIC% (SrCO3)
						THIS STUDY							
Asteroidea	*A. rubens*	Whole body	5	n/a [e]	n/a	n/a	0.128 ± 0.009	2.885 ± 0.028	n/a	n/a	n/a	n/a	n/a
Asteroidea	*A. rubens*	Whole body	6	n/a	n/a	n/a	0.125 ± 0.004	2.799 ± 0.063	n/a	n/a	n/a	n/a	n/a
Asteroidea	*A. rubens*	Whole body	10	n/a	n/a	n/a	0.131 ± 0.013	2.793 ± 0.058	n/a	n/a	n/a	n/a	n/a
Asteroidea	*S. endeca*	Whole body	4	n/a	n/a	n/a	0.153 ± 0.002	2.791 ± 0.036	n/a	n/a	n/a	n/a	n/a
Asteroidea	*A. rubens*	Whole body	8	36.27 ± 7.91	4.08 ± 0.64	0.132 ± 0.026	0.136 ± 0.020	2.490 ± 0.102	4.94	5.85	4.35	0.582	0.0108
Asteroidea	*A. gibbosa*	Whole body	6	60.48 ± 7.16	6.60 ± 0.53	0.172 ± 0.017	0.130 ± 0.010	1.938 ± 0.109	8.21	7.35	7.26	0.941	0.0141
Asteroidea	*Z. fulgens*	Whole body	4	57.18 ± 8.08	7.11 ± 0.43	0.174 ± 0.017	0.148 ± 0.013	2.080 ± 0.091	7.89	8.96	6.86	1.013	0.0142
Asteroidea	*M. glacialis*	Whole body	7	45.48 ± 4.52	7.20 ± 0.47	0.151 ± 0.011	0.188 ± 0.011	2.263 ± 0.150	6.49	6.49	5.45	1.026	0.0123
Asteroidea	*L. annulatus*	Arm (plates)	9	90.12 ± 0.05	9.87 ± 0.05	0.249 ± 0.003	0.127 ± 0.001	2.761 ± 0.029	n/a	n/a	n/a	n/a	n/a
Asteroidea	*M. accrescens*	Arm (plates)	3	90.17 ± 0.27	9.83 ± 0.27	0.234 ± 0.006	0.129 ± 0.004	2.597 ± 0.074	n/a	n/a	n/a	n/a	n/a
Asteroidea	*P. godfroyi*	Arm (plates)	1	90.41 ± 0.00	9.59 ± 0.00	0.236 ± 0.000	0.126 ± 0.000	2.609 ± 0.000	n/a	n/a	n/a	n/a	n/a
Asteroidea	*Paralophaster* sp.	Arm (plates)	3	90.72 ± 0.10	9.28 ± 0.10	0.246 ± 0.007	0.121 ± 0.001	2.712 ± 0.077	n/a	n/a	n/a	n/a	n/a
Asteroidea	*Perknaster* sp.	Arm (plates)	2	91.01 ± 1.36	8.99 ± 1.36	0.270 ± 0.038	0.117 ± 0.019	2.959 ± 0.375	n/a	n/a	n/a	n/a	n/a
Asteroidea	*A. hodgsoni*	Arm (plates)	3	90.15 ± 0.03	9.85 ± 0.03	0.244 ± 0.007	0.130 ± 0.000	2.698 ± 0.252	n/a	n/a	n/a	n/a	n/a
Asteroidea	*K. incurvatus*	Whole body	4	90.72 ± 1.27	9.28 ± 1.27	0.259 ± 0.025	0.122 ± 0.018	2.859 ± 0.252	n/a	n/a	n/a	n/a	n/a
Asteroidea	*O. penicillatus*	Arm (plates)	1	90.09 ± 0.00	9.91 ± 0.00	0.254 ± 0.000	0.131 ± 0.000	2.824 ± 0.000	n/a	n/a	n/a	n/a	n/a
Asteroidea	*P. antarctica*	Arm (plates)	3	89.80 ± 0.12	10.20 ± 0.12	0.251 ± 0.005	0.135 ± 0.002	2.796 ± 0.053	n/a	n/a	n/a	n/a	n/a
Asteroidea	*D. brandti*	Arm (plates)	3	90.48 ± 0.25	9.52 ± 0.25	0.249 ± 0.001	0.125 ± 0.004	2.750 ± 0.018	n/a	n/a	n/a	n/a	n/a
Asteroidea	*G. nutrix*	Whole body	5	91.71 ± 0.86	8.29 ± 0.86	0.286 ± 0.020	0.107 ± 0.012	3.115 ± 0.189	n/a	n/a	n/a	n/a	n/a
Asteroidea	*N. georgianus*	Arm (plates)	3	90.63 ± 0.09	9.37 ± 0.09	0.245 ± 0.001	0.123 ± 0.001	2.708 ± 0.013	n/a	n/a	n/a	n/a	n/a
Asteroidea	*O. meridionalis*	Arm (plates)	3	90.50 ± 0.06	9.50 ± 0.06	0.244 ± 0.003	0.125 ± 0.001	2.693 ± 0.027	n/a	n/a	n/a	n/a	n/a
Asteroidea	*P. aurorae*	Arm (plates)	3	91.14 ± 0.96	8.51 ± 1.05	0.262 ± 0.031	0.115 ± 0.014	2.876 ± 0.309	n/a	n/a	n/a	n/a	n/a

Asteroidea	*A. conspicuus*	Arm (plates)	1	90.61 ± 0.00	9.39 ± 0.00	0.249 ± 0.000	0.123 ± 0.000	2.752 ± 0.000	n/a	n/a	n/a	n/a	n/a
Asteroidea	*P. fuscus antarcticus*	Arm (plates)	1	90.08 ± 0.00	9.92 ± 0.00	0.254 ± 0.000	0.131 ± 0.000	2.825 ± 0.000	n/a	n/a	n/a	n/a	n/a
Asteroidea	*Henricia* sp.	Arm (plates)	2	90.18 ± 0.12	9.82 ± 0.12	0.239 ± 0.005	0.129 ± 0.002	2.653 ± 0.056	n/a	n/a	n/a	n/a	n/a
Asteroidea	*D. verrucosus*	Arm (plates)	2	89.63 ± 0.11	8.12 ± 0.01	0.223 ± 0.006	0.137 ± 0.002	n/a	n/a	n/a	n/a	n/a	n/a
Asteroidea	*O. validus*	Whole body	3	47.28 ± 7.02	5.83 ± 0.14	0.157 ± 0.022	0.148 ± 0.020	2.259 ± 0.027	6.51	n/a	5.67	0.830	0.0128
Echinoidea	*S. droebachiensis*	Body parts [f]	5	n/a	n/a	n/a	0.062 ± 0.004	2.381 ± 0.090	n/a	n/a	n/a	n/a	n/a
Echinoidea	*S. droebachiensis*	Body parts [f]	5	n/a	n/a	n/a	0.066 ± 0.006	2.357 ± 0.127	n/a	n/a	n/a	n/a	n/a
Echinoidea	*E. esculentus*	Body parts [f]	3	n/a	n/a	n/a	0.077 ± 0.002	2.627 ± 0.005	n/a	n/a	n/a	n/a	n/a
Echinoidea	*E. esculentus*	Body parts [f]	5	n/a	n/a	n/a	0.076 ± 0.003	2.569 ± 0.074	n/a	n/a	n/a	n/a	n/a
Echinoidea	*S. droebachiensis*	Body parts [f]	5	n/a	n/a	n/a	0.061 ± 0.005	2.315 ± 0.148	n/a	n/a	n/a	n/a	n/a
Echinoidea	*P. miliaris*	Whole body	14	79.85 ± 9.39	7.47 ± 1.18	0.233 ± 0.023	0.111 ± 0.013	1.984 ± 0.067	10.66	9.69	9.58	1.066	0.0190
Echinoidea	*P. lividus*	Whole body	14	62.36 ± 6.60	4.55 ± 0.50	0.203 ± 0.019	0.087 ± 0.014	2.215 ± 0.108	8.15	8.95	7.48	0.650	0.0166
Echinoidea	*P. lividus*	Spines	3	75.91 ± 13.65	2.76 ± 0.48	0.207 ± 0.029	0.044 ± 0.014	1.860 ± 0.089	9.52	n/a	9.11	0.394	0.0169
Echinoidea	*P. lividus*	Plates	3	68.34 ± 8.32	5.98 ± 0.40	0.238 ± 0.010	0.105 ± 0.014	2.373 ± 0.195	9.07	n/a	8.20	0.853	0.0194
Echinoidea	*T. ventricosus*	Whole body	2	65.17 ± 0.00	7.49 ± 0.31	0.228 ± 0.006	0.136 ± 0.005	2.375 ± 0.062	8.90	7.61	7.82	1.065	0.0186
Echinoidea	*C. blakei*	Whole body	2	79.32 ± 7.99	5.88 ± 1.59	0.204 ± 0.033	0.087 ± 0.019	1.745 ± 0.162	10.37	10.42	9.52	0.839	0.0167
Echinoidea	*D. setosum*	Spines	3	83.07 ± 6.99	13.30 ± 0.53	0.289 ± 0.008	0.191 ± 0.022	2.327 ± 0.197	11.89	n/a	9.96	1.896	0.0236
Echinoidea	*D. setosum*	Plates	3	92.06 ± 0.381	12.09 ± 0.29	0.302 ± 0.001	0.155 ± 0.003	2.223 ± 0.023	12.79	n/a	11.04	1.723	0.0247
Echinoidea	*E. chloroticus*	Spines	3	86.07 ± 10.33	5.08 ± 0.16	0.230 ± 0.016	0.071 ± 0.010	1.823 ± 0.112	11.07	n/a	10.32	0.725	0.0188
Echinoidea	*E. chloroticus*	Plates	3	88.31 ± 7.49	9.53 ± 0.84	0.311 ± 0.020	0.128 ± 0.003	2.390 ± 0.140	11.98	n/a	10.59	1.359	0.0254
Echinoidea	*P. huttoni*	Spines	2	94.91 ± 0.00	4.00 ± 0.22	0.249 ± 0.004	0.047 ± 0.003	1.680 ± 0.057	11.98	n/a	11.39	0.571	0.0203
Echinoidea	*P. huttoni*	Plates	3	92.64 ± 8.03	5.57 ± 0.46	0.293 ± 0.017	0.126 ± 0.016	2.143 ± 0.067	11.93	n/a	11.11	0.795	0.0239
Echinoidea	*A. similis*	Spines	2	96.30 ± 0.14	3.70 ± 0.14	0.114 ± 0.060	0.046 ± 0.002	1.185 ± 0.623	n/a	n/a	n/a	n/a	n/a
Echinoidea	*A. similis*	Plates	4	92.49 ± 1.47	7.51 ± 1.47	0.222 ± 0.017	0.097 ± 0.021	2.405 ± 0.187	n/a	n/a	n/a	n/a	n/a
Echinoidea	*C. perrieri*	Spines	3	96.18 ± 0.96	3.81 ± 0.96	0.175 ± 0.009	0.047 ± 0.012	1.823 ± 0.100	n/a	n/a	n/a	n/a	n/a
Echinoidea	*C. perrieri*	Plates	3	92.39 ± 0.42	7.61 ± 0.42	0.217 ± 0.005	0.098 ± 0.006	2.346 ± 0.046	n/a	n/a	n/a	n/a	n/a

Echinoidea	*S. neumayeri*	Spines	3	96.50 ± 0.20	3.49 ± 0.20	0.202 ± 0.005	0.043 ± 0.003	2.095 ± 0.057	n/a	n/a	n/a	n/a	n/a
Echinoidea	*S. neumayeri*	Plates	6	93.96 ± 0.25	6.04 ± 0.25	0.222 ± 0.008	0.076 ± 0.003	2.507 ± 0.166	n/a	n/a	n/a	n/a	n/a
Echinoidea	*S. neumayeri*	Whole body	3	62.59 ± 5.14	4.53 ± 0.56	0.178 ± 0.010	0.085 ± 0.008	1.930 ± 0.057	8.17	n/a	7.51	0.646	0.0145
Echinoidea	*S. neumayeri*	Spines	3	94.14 ± 6.70	2.77 ± 0.44	0.224 ± 0.024	0.034 ± 0.003	1.607 ± 0.067	11.71	n/a	11.29	0.395	0.0183
Echinoidea	*S. neumayeri*	Plates	3	83.99 ± 1.87	6.28 ± 0.28	0.292 ± 0.002	0.088 ± 0.003	2.357 ± 0.035	11.00	n/a	10.07	0.896	0.0239
Holothuroidea	*H. forskali*	Whole body	3	2.60 ± 1.04	n/a	n/a	n/a	n/a	n/a	0.41	0.31	n/a	n/a
Holothuroidea	*M. musculus*	Calcareous ring	3	91.74 ± 0.30	8.26 ± 0.30	0.271 ± 0.005	0.107 ± 0.004	2.951 ± 0.000	n/a	n/a	n/a	n/a	n/a
Holothuroidea	*P. spiculiferus*	Calcareous ring	1	92.51 ± 0.00	7.49 ± 0.00	0.561 ± 0.000	0.096 ± 0.000	6.065 ± 0.000	n/a	n/a	n/a	n/a	n/a
Ophiuroidea	*O. aculeata*	Whole body	11	n/a	n/a	n/a	0.140 ± 0.003	2.775 ± 0.049	n/a	n/a	n/a	n/a	n/a
Ophiuroidea	*O. lynami*	Whole body	6	70.54 ± 4.43	8.19 ± 0.26	0.190 ± 0.012	0.138 ± 0.006	1.833 ± 0.060	9.65	9.35	8.46	1.168	0.0155
Ophiuroidea	*O. longicauda*	Spines	1	70.42 ± 0.00	11.48 ± 0.00	0.234 ± 0.000	0.193 ± 0.000	3.326 ± 0.000	10.10	n/a	8.45	1.636	0.0191
Ophiuroidea	*O. victoriae*	Arm (plates)	3	90.80 ± 0.17	9.20 ± 0.17	0.244 ± 0.009	0.120 ± 0.002	2.685 ± 0.100	n/a	n/a	n/a	n/a	n/a
Ophiuroidea	*O. gigas*	Arm (plates)	1	90.87 ± 0.00	9.13 ± 0.00	0.241 ± 0.000	0.115 ± 0.000	2.651 ± 0.000	n/a	n/a	n/a	n/a	n/a
Ophiuroidea	*O. longicauda*	Plates	1	48.44 ± 0.00	7.31 ± 0.00	0.157 ± 0.000	0.179 ± 0.000	2.250 ± 0.000	6.87	n/a	5.81	1.043	0.0128
Crinoidea	*A. mediterranea*	Whole body	3	64.84 ± 3.82	7.76 ± 0.54	0.208 ± 0.012	0.142 ± 0.017	2.190 ± 0.274	8.90	8.74	7.78	1.107	0.0170
						LITERATURE - adults							
Asteroidea	*see* Appendix A	Body parts [f]	23	85.67 ± 3.96	11.27 ± 2.41	n/a	0.149 ± 0.030	n/a	11.89	n/a	10.28	1.606	n/a
Echinoidea	*see* Appendix A	Body parts [f]	18	89.04 ± 3.63	10.29 ± 3.27	n/a	0.114 ± 0.031	n/a	12.15	n/a	10.68	1.466	n/a
Ophiuroidea	*see* Appendix A	Body parts [f]	18	87.33 ± 3.54	11.31 ± 3.13	n/a	0.142 ± 0.040	n/a	12.09	n/a	10.48	1.611	n/a
Crinoidea	*see* Appendix A	Body parts [f]	21	87.27 ± 1.98	11.21 ± 2.07	n/a	0.149 ± 0.125	n/a	12.07	n/a	10.47	1.597	n/a
						LITERATURE - juveniles							
Asteroidea	*A. rubens* - 1 [g]	Plates	34	n/a	n/a	n/a	0.094 ± 0.005	2.380 ± 0.075	n/a	n/a	n/a	n/a	n/a
Asteroidea	*A. rubens* - 2	Plates	18	n/a	n/a	n/a	0.100 ± 0.006	2.273 ± 0.062	n/a	n/a	n/a	n/a	n/a
Echinoidea	*P. lividus* - 1 [h]	Plates	6	n/a	n/a	n/a	0.091 ± 0.005	2.833 ± 0.051	n/a	n/a	n/a	n/a	n/a
Echinoidea	*P. lividus* - 2	Plates	8	n/a	n/a	n/a	0.093 ± 0.003	2.937 ± 0.074	n/a	n/a	n/a	n/a	n/a
Echinoidea	*P. lividus* - 3	Plates	8	n/a	n/a	n/a	0.108 ± 0.007	3.150 ± 0.092	n/a	n/a	n/a	n/a	n/a

Echinoidea	*P. lividus* - 4	Plates	9	n/a	n/a	n/a	0.113 ± 0.007	2.966 ± 0.111	n/a	n/a	n/a	n/a	n/a
Echinoidea	*P. lividus* - 5	Plates	11	n/a	n/a	n/a	0.118 ± 0.012	3.145 ± 0.163	n/a	n/a	n/a	n/a	n/a
Echinoidea	*P. lividus* - 6	Plates	8	n/a	n/a	n/a	0.109 ± 0.006	3.012 ± 0.195	n/a	n/a	n/a	n/a	n/a
Echinoidea	*P. lividus* - 7	Plates	13	n/a	n/a	n/a	0.118 ± 0.005	2.923 ± 0.148	n/a	n/a	n/a	n/a	n/a
Echinoidea	*P. lividus* - 8	Plates	13	n/a	n/a	n/a	0.118 ± 0.010	2.946 ± 0.161	n/a	n/a	n/a	n/a	n/a

[a] *n* number of samples selected to measure via ICP. In the literature it represents the number of samples used.

[b] "dw" stand for dry weight and it is used in the table, text, and figures.

[c] Total $PIC_{ICP\text{-}MES}$ % is calculated as: $PIC_{ICP\text{-}MES}$ % = Σ $total_{PIC}$ % = PIC_{CaCO3} % + PIC_{MgCO3} % + PIC_{SrCO3} %, where inorganic carbon (PIC) is calculated from the molecular weight proportion to the carbonate fraction: PIC_{CaCO3} % = $CaCO_3$/C = 8.333; PIC_{MgCO3} % = $MgCO_3$/C = 7.017, PIC_{SrCO3} % = $SrCO_3$/C = 12.267 (all data presented in this table).

[d] Total $PIC\%_{(Coul.)}$ for comparison as used in the budget calculation of Lebrato et al. (2010) using Coulometer analyses of a number of the samples re-assessed in this study.

[e] n/a indicates that data are not available and/or not applicable.

[f] Body parts are a mixture of all the inorganic material (tests, spines, plates).

[g] The number after the species represent the treatment in the experiment: 1=11 °C, 2=18 °C.

[h] The number after the species represent the treatment in the experiment: 1=13.23 °C, 2=13.50 °C, 3=18.48 °C, 4=18.82 °C, 5=20.66 °C, 6=20.83 °C, 7=24.18 °C, 8=24.30 °C.

Table 14.3. Echinoderm budget re-assessment data (mean conversion factor).

Class	Species	Bio-material	*n* [a]	$CaCO_3$% dw[b]	$MgCO_3$% dw	$SrCO_3$% dw	PIC% $_{(ICP)}$[c]	PIC% (Coul.)[d]	PIC% (CaCO3)	PIC% (MgCO3)	PIC% (SrCO3)
Asteroidea (rest lats.)	This study	Whole body	25	49.85	6.25	0.158	6.88	7.16	5.98	0.891	0.0129
Asteroidea (Antarctic)	This study	Whole body	3	47.28	5.83	0.157	6.51	7.16	5.67	0.832	0.0128
Echinoidea (Temperate)	This study	Whole body	28	71.10	6.01	0.218	9.40	9.32	8.53	0.858	0.0178
Echinoidea (Tropical)	This study	Whole body	4	72.25	6.68	0.217	9.64	9.01	8.67	0.952	0.0177
Echinoidea (Antarctic)	This study	Whole body	3	62.59	4.53	0.178	8.17	9.32	7.51	0.646	0.0145
Ophiuroidea (all lats.)	This study	Whole body	6	70.54	8.19	0.190	9.65	9.35	8.46	1.168	0.0155
Holothuroidea (all lats.)	This study	Whole body	3	2.60	n/a	n/a	0.31	0.41	0.31	n/a	n/a
Crinoidea (all lats.)	This study	Whole body	3	64.84	7.76	0.208	8.90	8.74	7.78	1.107	0.0170

Table 14.4. Echinoderms global carbonate production based on the three carbonates.

Mean values	$Total_{PIC}$ (g C m^2 yr^{-1})	PIC_{CaCO3} [a] (g C m^2 yr^{-1})	PIC_{MgCO3} [a] (g C m^2 yr^{-1})	PIC_{SrCO3} [a] (g C m^2 yr^{-1})
GLOBAL (n = 523) [b]	2.57	2.28	0.31	0.004
(min. – max.)	1.78 x 10^{-8} – 157.90	1.55 x 10^{-8} – 138.51	2.21 x 10^{-9} – 19.09	3.39 x 10^{-11} – 0.25
Total (Pg C yr^{-1}) - sum [c]	**0.113** [e]	**0.100**	**0.014**	**2.22 x 10^{-4}**
Total (mol C yr^{-1}) - sum [c]	**9.41 * 10^{12}** [e]	**8.33 * 10^{12}**	**1.16 * 10^{12}**	**1.85 * 10^{10}**
Total (Pg C yr^{-1}) - single [d]	**0.853**	**0.759**	**0.105**	**0.0015**
Total (mol C yr^{-1}) - single [d]	**7.10 * 10^{13}**	**6.32 * 10^{13}**	**8.75 * 10^{12}**	**1.25 * 10^{11}**
SHELF (0-200 m) (n = 164)	6.86	6.07	0.80	0.01
(min. – max.)	9.05 x 10^{-8} – 157.90	7.87 x 10^{-8} – 138.51	1.17 x 10^{-8} – 19.09	1.69 x 10^{-10} – 0.25
Total (Pg C yr^{-1})	**0.068**	**0.060**	**0.0079**	**1.20 x 10^{-4}**
SLOPE (200-2000 m) (n = 180)	0.45	0.42	0.06	0.001
(min. – max.)	1.78 x 10^{-8} – 33.37	1.55 x 10^{-8} – 29.08	2.21 x 10^{-9} – 4.25	3.39 x 10^{-11} – 0.06
Total (Pg C yr^{-1})	**0.0145**	**0.013**	**0.0022**	**3.33 x10^{-5}**
ABYSSAL (> 2000 m) (n = 78)	0.10	0.09	0.01	0.0002
(min. – max.)	1.79 x 10^{-7} – 3.46	1.02 x 10^{-6} – 3.01	1.02 x 10^{-7} – 0.44	2.13 x 10^{-11} – 0.006
Total (Pg C yr^{-1})	**0.030**	**0.026**	**0.0044**	**6.40 x10^{-5}**

[a] Carbon production calculated using the molecular weight proportion to the carbonate fraction: PIC_{CaCO3} % = $CaCO_3$/C = 8.333; PIC_{MgCO3} % = $MgCO_3$/C = 7.017, PIC_{SrCO3} % = $SrCO_3$/C = 12.267.
[b] This is a global mean including shelf, slope, and abyssal data.
[c] This global estimate is the sum of the shelf, slope and abyssal calculations with their corresponding production rate.
[d] This global estimate uses a single global conversion factor as the average of n = 523 for $Total_{PIC}$ and each of the three carbonates.
[e] The previous estimation from Lebrato et al. (2010) using a Coulometer was 0.102 Pg C yr^{-1}.

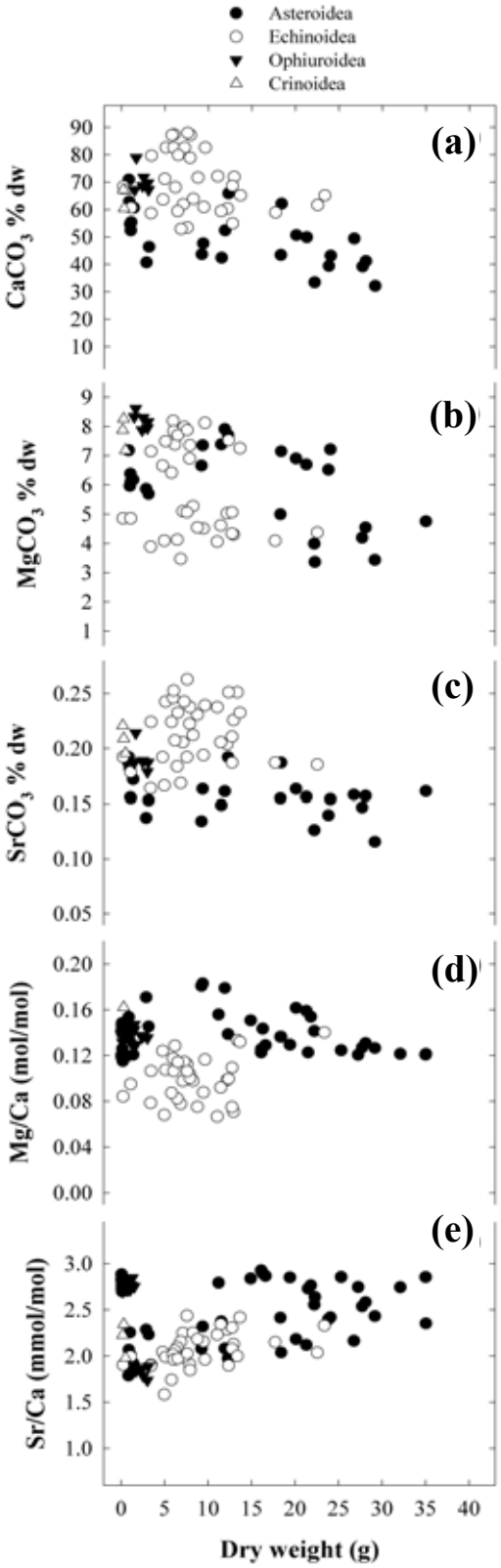

Fig. 14.3. Correlations between whole body $CaCO_3$ (a), $MgCO_3$ (b), $SrCO_3$ (c) as well as Mg/Ca (d) and Sr/Ca (e) with dry weight (size estimation).. Note that in the case of Mg/Ca and Sr/Ca, sub-Arctic (Iceland) data are also included from Asteroidea and Ophiuroidea (whole body only).

14.4.1.2 $MgCO_3$ % dry weight

Overall, large $MgCO_3$ percentages were found in the spines of some species, but not in all compared with plates (Table 14.2; Fig. 14.2;). The tropical species *Diadema setosum* had the highest spines $MgCO_3$ percentage (13.30 ±0.53 %), followed by the ophiuroid *O. longicauda* (11.48 ±0.00 %). *S. neumayeri* had the lowest $MgCO_3$ percentage (2.77 ±0.44 %) (Table 14.2). In plates, *D. setosum* had the highest $MgCO_3$ percentage (12.09 ±0.29 %), while the lowest was for *P. huttoni* (5.57 ±0.46 %). The ophiuroid *O. longicauda* had 7.31 ±0.00 %. All Antarctic echinoid species had similar $MgCO_3$ percentages (between 6.04 ±0.25 % and 7.61 ±0.42 %) to other temperate species (Table 14.2). Antarctic asteroids and ophiuroids plates remained all between 8.12 ±0.01 % (*D. verrucosus*), and 10.20 ±0.12 % (*Porania antarctica*). Holothuroidea calcareous rings values were similar to plates from the other classes (*Molpadia musculus* = 8.26 ±0.30 %, *Pseudostichopus spiculiferus* = 7.49 ±0.00 %).

$MgCO_3$ measurements in whole bodies were similar to plates (Table 14.2). Ophiuroids had the highest $MgCO_3$ percentage (*O. lymani* = 8.19 ±0.26 %), followed by crinoids (*A. mediterranea* = 7.76 ±0.54 %). Then, echinoids (maximum: the tropical species *Tripneutes ventricosus* = 7.49 ±0.31 %, minimum: *S. neumayeri* = 4.53 ±0.56 %), and asteroids (maximum: the temperate species *Marthasterias glacialis* = 7.20 ±0.47 %, minimum: *A. rubens* = 4.08 ±0.64 %; the

Antarctic species *O. validus* = 5.83 ±0.14 % had similar values to temperate species) (Table 14.2).

The correlation between whole body $MgCO_3$ % dw and the dry weight (size estimation) was statistically significant ($F_{1,66} = 13.36$, $P < 0.01$. $r^2 = 0.16$), and the best fit was a linear equation (Fig. 14.3b):

$$y = 6.93 - 0.076\,x \qquad (5)$$

$MgCO_3$ percentages were relatively constant, and only decreased with increasing organism weight especially in asteroids and echinoids.

16.4.1.3 $SrCO_3$ % dry weight

Overall higher $SrCO_3$ percentages were found in plates than in spines and the whole body (Fig. 14.2; Table 14.2). In echinoids, the temperate species *Evechinus chloroticus* had the highest plates $SrCO_3$ percentage (0.311 ±0.020 %), while the lowest was in the Antarctic *C. perrieri* (0.217 ±0.005 %). Antarctic species had smaller $SrCO_3$ percentage than the rest (between 0.217 ±0.005 % and 0.292 ±0.002 %). The ophiuroid *O. longicauda* had the lowest $SrCO_3$ percentage overall (0.157 ±0.000 %) (Table 14.2). Holothuroidea calcareous ring values were similar to plates from the other classes (*Molpadia musculus* = 0.271 ±0.005 %, *Pseudostichopus spiculiferus* = 0.561 ±0.000 %). In spines, the highest $SrCO_3$ percentage corresponded to *D. setosum* (0.289 ±0.008 %), and the lowest to *A. similis* (0.114 ±0.060 %), while Antarctic species remained slightly below temperate and tropical (between 0.114 ±0.060 % and 0.224 ±0.024 %). *O. longicauda* had also a similar spines $SrCO_3$ percentage to some echinoid spines (0.234 ±0.000) (Table 14.2). Antarctic asteroids and ophiuroids plates remained all between 0.223 ±0.006 % (*D. verrucosus*), and 0.286 ±0.020 % (*G. nutrix*).

$SrCO_3$ data in whole bodies were overall lower than plates and spines (Table 14.2). Echinoids had the highest $SrCO_3$ percentage (maximum: *P. miliaris* = 0.233 ±0.023 %, minimum: *S. neumayeri* = 0.178 ±0.010 %), followed by crinoids (*A. mediterranea* = 0.208 ±0.012 %), ophiuroids (*O. lymani* = 0.190 ±0.012 %), and asteroids (maximum: the temperate species *Zoroaster fulgens* = 0.174 ±0.017 %, minimum: *A. rubens* = 0.132 ±0.026 %; the Antarctic species *O. validus* = 0.022 ±0.140 had similar percentages to temperate species) (Table 14.2).

The correlation between whole body $SrCO_3$ % dw and the dry weight (size estimation) was statistically significant ($F_{1,67}$ = 9.33, P < 0.01. r^2 = 0.24), and the best fit was a polynomial equation (Figure 3b):

$$y = 0.18 + 2.83*10^{-3}\, x - 1.51*10^{-4}\, x^2 \quad (6)$$

In general, $SrCO_3$ percentages were relatively constant (< 40 % change), with a decreasing trend induced by the lower $SrCO_3$ percentages in asteroids in comparison to echinoids.

14.4.1.4 Carbonate Mg/Ca

Overall, higher Mg/Ca were encountered in whole bodies than in spines (except in *D. setosum* and *O. longicauda*) and plates (Table 14.2). Asteroids had the highest whole body Mg/Ca (maximum: *M. glacialis* = 0.188 ±0.011 mol/mol, minimum: the sub-Arctic species *A. rubens* = 0.125 ±0.004 mol/mol). Antarctic species had a higher Mg/Ca (*O. validus* = 0.148 ±0.020 mol/mol) than the sub-Arctic species *A. rubens* (0.128-0.131 mol/mol), but below others such *Solaster endeca* (0.153 ±0.002 mol/mol). Crinoids (*A. mediterranea* = 0.142 ±0.017 mol/mol), and ophiuroids followed (the sub-Arctic species *Ophiopholis aculeata* = 0.140 ±0.003 mol/mol, and *O. lymani* = 0.138 ±0.006 mol/mol). The lowest whole body Mg/Ca values were found in echinoids (maximum: *T. ventricosus* = 0.188 ±0.011 mol/mol, minimum: *S. neumayeri* = 0.085 ±0.008 mol/mol) (Table 14.2). In plates, the highest Mg/Ca was in the ophiuroid *O. longicuda* (0.179 ±0.000 mol/mol), followed by echinoids (maximum: *D. setosum* = 0.155 ±0.003 mol/mol, minimum: *S. neumayeri* = 0.043 ±0.003 mol/mol) (Table 14.2). Antarctic asteroids and ophiuroids plates remained all between 0.107 ±0.0.12 mol/mol (*G. nutrix*), and 0.137 ±0.002 mol/mol (*D. verrucosus*). Holothuroidea calcareous ring values were similar to whole bodies and plates from the other classes (*Molpadia musculus* = 0.107 ±0.004 mol/mol *Pseudostichopus spiculiferus* = 0.096 ±0.000 mol/mol).

In spines, the highest Mg/Ca was found in *O. longicauda* too (0.193 ±0.000 mol/mol), and in the echinoid *D. setosum* (0.191 ±0.022 mol/mol). The lowest Mg/Ca was found in *S. neumayeri* (0.034 ±0.003 mol/mol) (Table 14.2). In body parts (tests, spines, and plates) from sub-Arctic species, averaged values of all inorganic material remained between 0.062 and 0.077 mol/mol, thus below values of temperate species plates and similar to spines. However, the lowest Mg/Ca

(*Strongylocentrotus droebachiensis* = 0.061 ±0.005 mol/mol), was still above *S. neumayeri* spines (0.034 ±0.003 mol/mol), and similar to plates (0.088 ±0.003 mol/mol) (Table 14.2).

The correlation between whole body Mg/Ca and dry weight (size estimation) was statistically significant ($F_{1,93} = 6.87$, $P < 0.05$. $r^2 = 0.07$), and the best fit was a linear equation (Fig. 14.3b):

$$y = 0.11 + 3.12*10^{-4}\, x \quad (7)$$

The Mg/Ca remained constant with increasing organism weight.

14.4.1.5 Carbonate Sr/Ca

There was a large variability in the Sr/Ca depending on species and class (Table 14.2). Overall, a higher Sr/Ca was found in asteroid plates and whole bodies than in the rest (except in the ophiuroid *O. longicauda*). In asteroids, the largest Sr/Ca was found in plates of Antarctic species (maximum: *Perknaster* sp. = 2.959 ±0.375 mmol/mol, minimum: *Macroptychaster accrescens* = 2.597 ±0.074 mmol/mol), similar to sub-Arctic species. This was followed by ophiuroids (maximum: *Ophionotus victoriae* = 2.685 ±0.100 mmol/mol, minimum: *O. longicauda* = 2.250 ±0.000 mmol/mol) and echinoids (maximum: *S. neumayeri* = 2.507 ±0.166 mmol/mol, minimum: *P. huttoni* = 2.143 ±0.067 mmol/mol) (Table 14.2). Holothuroidea calcareous ring values were high, similar to whole bodies and plates from the other classes [(*Molpadia musculus* = 2.951 ±0.000 %, *Pseudostichopus spiculiferus* = 6.065 ±0.000 % (this is consequence of a high $SrCO_3$, and could be an analytical outlayer)].

For whole bodies, the highest vales were found in sub-Arctic species (*A. rubens* = 2.885 ±0.028 mmol/mol), while the lowest was in temperate species (*A. gibbosa* = 1.938 ±0.109 mmol/mol). Ophiuroids followed (*O. aculeata* = 2.775 ±0.049 mmol/mol, and *O. lymani* = 1.833 ±0.060 mmol/mol), and then echinoids (maximum: *T. ventricosus* = 2.375 ±0.062 mmol/mol, minimum: *C. blakei* = 1.745 ±0.162 mmol/mol), and crinoids (*A. mediterranea* = 2.190 ±0.274 mmol/mol) (Table 14.2). In spines, the highest Sr/Ca was in *O. longicauda* (3.326 ±0.000 mmol/mol), which was the highest value in the dataset, followed by echinoids (maximum: *D. setosum* = 2.390 ±0.140 mmol/mol, minimum: *A. similis* = 1.185 ±0.623 mmol/mol; lowest value in the dataset) (Table 14.2). In body parts (tests, spines, and plates combined) from sub-Arctic species,

averaged Sr/Ca values of all inorganic material remained between 2.315 and 2.627 mmol/mol in all cases. Thus, similar to values of temperate species plates, and above spines (also true in comparison with *S. neumayeri*) (Table 14.2).

The correlation between whole body Sr/Ca and the dry weight (size estimation) was statistically significant ($F_{1,93} = 4.87$, $P < 0.05$. $r^2 = 0.38$), and the best fit was a linear equation (Fig. 14.3b):

$$y = 1.95 + 0.016\,x \qquad (8)$$

The Sr/Ca increased with increasing organism weight, and the largest difference was found in asteroids (> 50 % change)

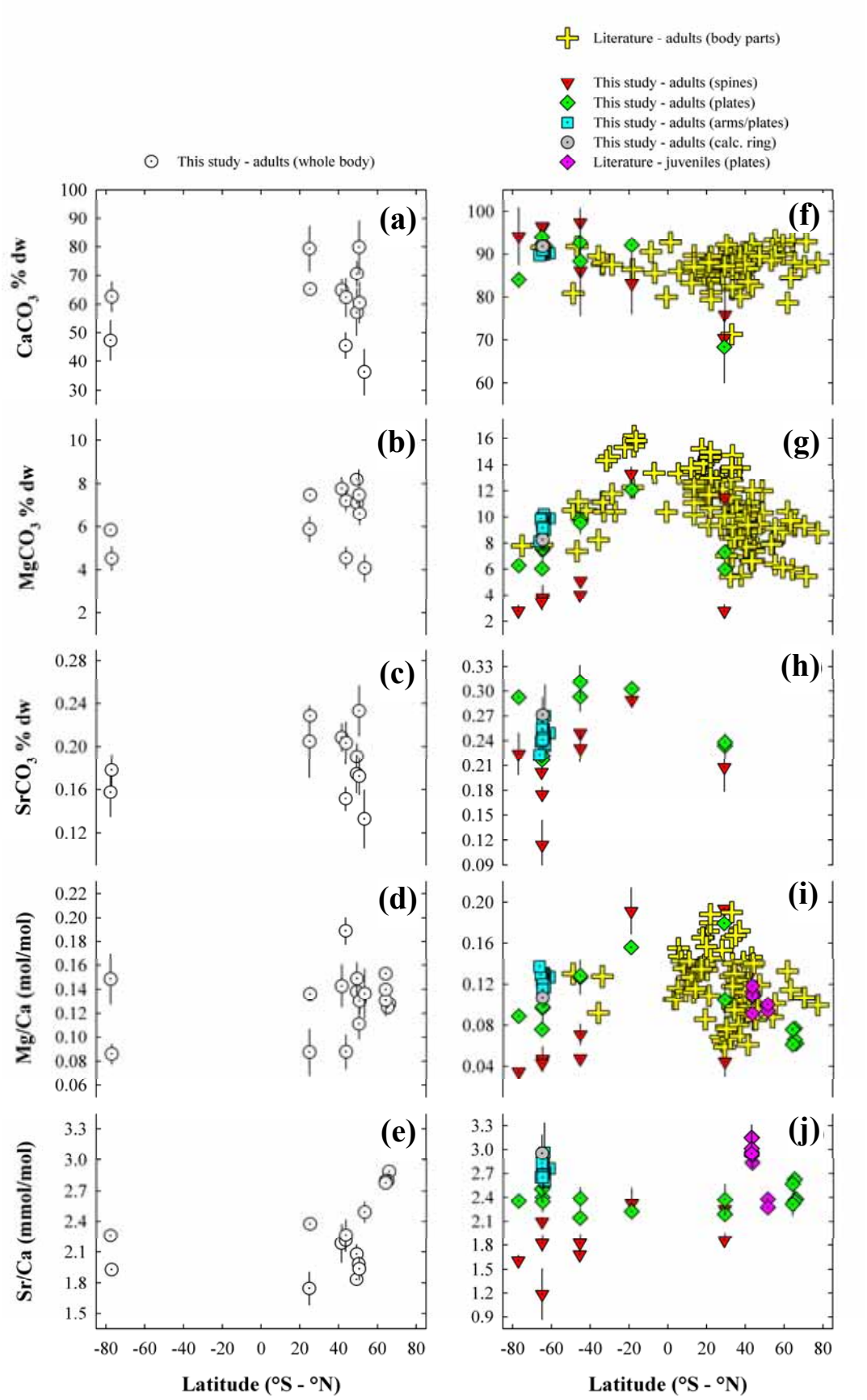

Fig. 14.4. Latitudinal patterns of echinoderm carbonate from the whole body, including test, spines, plates, and also for spines and plates (published data included): (a) - (f) $CaCO_3$ %, (b) - (g) $MgCO_3$ %, (c) - (h) $SrCO_3$ %, (d) - (i) Mg/Ca, and (e) - (j) Sr/Ca. Only data from the left side panel (whole body) were used in the re-assessment of the budget. Unidirectional error bars (standard deviation) from *n* measurements (*see* Table 14.2) are included.

14.4.1.6. $Total_{PIC}$ % dry weight (all carbonates)

The $total_{PIC}$ percentage results per species differed from the PIC_{CaCO3} % (which dominates the carbonate), because the inorganic carbon acquired as $MgCO_3$ does not linearly increase with increasing $CaCO_3$ in all cases (*see* Fig. 14.2a). There was a large variability depending on the body part and the species and class (Table 2). The highest $total_{PIC}$ percentages were measured in echinoid plates [maximum: *D. setosum* = 12.79 % (likely overestimated by the machine because it cannot be above 12.00), minimum: *P. lividus* = 9.07 %]. The ophiuroid *O. longicauda* had a lower $total_{PIC}$ percentage (6.87 %) (Table 14.2). In spines, the highest $total_{PIC}$ percentage corresponded to echinoids (maximum: *P. huttoni* = 11.98 %, minimum: *P. lividus* = 9.52 %), while the ophiuroid *O. longicauda* had a similar value to them (10.10 %) (Table 2). Measurements in whole bodies were always smaller than in plates and spines (Table 2). Overall, echinoids had the highest $total_{PIC}$ percentage (maximum: *P. miliaris* = 10.66 %, minimum: *P. lividus* = 8.15 %), followed by ophiuroids (*O. lymani* = 9.65), crinoids (*A. mediterranea* = 8.90 %), and asteroids (maximum: *A. gibbosa* = 8.21 %, minimum: *A. rubens* = 4.94 %) (Table 14.2). Holothurians had very small $total_{PIC}$ percentages completely derived from the $CaCO_3$ fraction (2.60 %). Antarctic organisms (*S. neumayeri* and *O. validus*) had similar percentages to some temperate species in the same class (Table 14.2).

14.4.2. Global patterns in echinoderms carbonate

14.4.2.1 Whole body and budget re-assessment

Echinoderms whole body carbonate percentages and ratios changed as a function of species (Table 14.2), but also latitude (Fig. 14.4). $CaCO_3$ percentages increased from sub-Polar to temperate and tropical latitudes in the northern hemisphere (<50 % change), but there was not a clear pattern in the tropics (few samples available). Antarctic samples were similar to some temperate ones ($CaCO_3$ = 45-65 %), but well below tropical (Fig. 14.4a). $MgCO_3$ percentages showed a similar pattern to $CaCO_3$, reaching a maximum in temperate latitudes (> 7 %), with no further increase in the tropics. Antarctic individuals remained below 6 % (Fig. 14.4b). $SrCO_3$ percentages were also similar to $CaCO_3$ and $MgCO_3$, and remained below 0.30 % at any latitude, and were on average highest in the tropics (0.20-0.24 %). In Antarctic samples they remained below 0.20 % (Fig. 14.4c). The Mg/Ca was relatively constant across latitude in the

northern hemisphere, with a slight decrease from sub-Polar to temperate latitudes (from ~ 0.16 to ~ 0.13 mol/mol). Antarctic organisms were in some cases similar to temperate ones (~ 0.15 mol/mol), or the lowest in the dataset (~ 0.09 mol/mol) (Fig. 14.4d). The Sr/Ca decreased with latitude in the northern hemisphere to the tropics, from ~ 3 mmol/mol to < 1.80 mmol/mol. Sub-Polar individuals had the highest Sr/Ca (~ 3 mmol/mol), while Antarctic organisms were similar to some temperate ones (~ 1.90-2.30 mmol/mol).

These latitudinal trends translated into different conversion percentages from the dry weight (size function), which were then applied to the different classes and species (Table 14.3). If the field biomass data were from a species measured, the corresponding carbonate percentage was used (Table 14.2), otherwise a general percentage was applied (Table 14.3). For all carbonates and PIC percentages ($CaCO_3$, $MgCO_3$, $SrCO_3$), and for the $total_{PIC}$ percentage (Table 14.3), the following latitudinal divisions (as mean values) were applied: Antarctic and the rest of latitudes (Asteroidea), Antarctic, temperate and tropical (Echinoids), and all latitudes (Ophiuroidea, Holothuroidea, Crinoidea). The conversion percentages used here were slightly different from those in Lebrato et al. (2010) measured with a Coulometer (Johnson et al. 1998). The grand average difference between the $total_{PIC\text{-}ICP\text{-}MES}$ and $total_{PIC\text{-}Coul.}$ was ~ 1.20 %, and it was divided 50:50 as positive or negative (depending on the ICP-MES or the Coulometer value being higher or lower), in the 8 major latitudinal divisions used (Table 14.3): Asteroidea (rest lats. = -2.80 %, Antarctic = -6.5 %), Echinoidea (temperate = +0.80 %, tropical = +6.30 %, Antarctic = -11.50 %), Holothuroidea (all lats. = -1 %), Ophiuroidea (all lats. = +3 %), and Crinoidea (all lats. = +1.60 %).

14.4.2.2 Other carbonate components

The latitudinal pattern in echinoderm body parts (mainly tests), spines, and plates was different from whole bodies (Figure 4), and clear trends were observed. $CaCO_3$ percentages remained roughly constant from the Arctic to the Antarctic (including published results), with no peak in the tropical regions (Fig. 14.4f). The response of $MgCO_3$ percentages followed a parabola, with a maximum from 20 °N to 20 °S between 14 and 16 %. The lowest values in the Arctic were between 6 and 10% (published), and in Antarctica they were between 2 (spines) and 10 % (body parts). Values in temperate latitudes remained between 6 and 13 % depending on the hemisphere (Fig. 14.4g). $SrCO_3$ percentages responded in a similar way to $MgCO_3$, with an increase towards

the tropics in plates (> 0.30 %) and spines (> 0.27 %), and lower values towards the poles (< 0.25 %) (Figure 4h). The Mg/Ca trend was similar to the $MgCO_3$ percentage, with a maximum in the tropics (0.16-0.20 mol/mol), and a large decrease towards the Artic (0.05-0.11 mol/mol) and Antarctic (0.03-0.12 mol/mol) latitudes (Figure 4i). The Sr/Ca trend was relatively constant with no tropical maximum, between 2.10 and 2.70 mmol/mol. The lowest ratio was found in Antarctic waters (~ 1.20 mmol/mol). The highest values were found in published juvenile plates (> 2.80 mmol/mol) at temperate latitudes (Fig. 14.4j).

14.4.3. Partitioning of the global echinoderms budget

The mean global echinoderms production as inorganic carbon ($total_{PIC}$) was 2.57 g C m^2 yr^{-1} [maximum = 157.90 g C m^2 yr^{-1} (ophiuroids), minimum = 1.78 * 10^{-8} g C m^2 yr^{-1} (crinoids)] (Table 4). Using shelf (0.068 Pg C yr^{-1}), slope (0.0145 Pg C yr^{-1}), and abyssal (0.030 Pg C yr^{-1}) annual production values and corresponding areas ("sum"), the total contribution was 0.113 Pg C yr^{-1} or 9.41 *10^{12} mol C yr^{-1} (Pg = Gt = 10^{12} g C), and using a single global production value ("single") it was 0.853 Pg C yr^{-1} or 7.10 *10^{13} mol C yr^{-1} (Table 4). This was partitioned among the three carbonates as follows: Global PIC_{CaCO3} production = 2.28 g C m^2 yr^{-1} (maximum = 138.51 g C m^2 yr^{-1}, minimum = 1.55 * 10^{-8} g C m^2 yr^{-1}), and total contribution = 0.100 Pg C yr^{-1} (sum) or 8.33 *10^{12} mol C yr^{-1}, 0.759 Pg C yr^{-1} or 6.32 *10^{13} mol C yr^{-1} (single). Global PIC_{MgCO3} production = 0.31 g C m^2 yr^{-1} (maximum = 19.09 g C m^2 yr^{-1}, minimum = 2.21 * 10^{-9} g C m^2 yr^{-1}), and total contribution = 0.014 Pg C yr^{-1} or 1.16 *10^{12} mol C yr^{-1} (sum), 0.105 Pg C yr^{-1} or 8.75 *10^{12} mol C yr^{-1} (single). Global PIC_{SrCO3} production = 0.004 g C m^2 yr^{-1} (maximum = 0.25 g C m^2 yr^{-1}, minimum = 3.39 * 10^{-11} g C m^2 yr^{-1}), and total contribution = 2.22 * 10^{-4} Pg C yr^{-1} or 1.85 *10^{10} mol C yr^{-1} (sum), 0.0015 Pg C yr^{-1} or 1.25 *10^{11} mol C yr^{-1} (single).

14.5. Discussion

14.5.1. Vital and ambient controls on Mg-calcite

Field and empirical evidence suggests that salinity and temperature (Borremans et al. 2009; Hermans et al. 2010), ambient and high CO_2 concentrations (Ries 2011), seasonality (Lorrain et al. 2005), food availability and growth rate (Weber, 1969, 1973) and bathymetry (Roux et al. 1995) drive changes in echinoderms Mg-calcite elemental composition. When combining all the

above factors and adding a species-specific/genetic component (Vinogradov 1953; *see* Table 14.2), a likely ontogenic variability (Sumich and McCauley 1972; *see* Fig. 14.3), and different between skeletal parts (Weber 1969; *see* Table 14.2), it is reasonable to assume that the latitudinal Mg-calcite trend has not been resolved yet. Furthermore, the complications in obtaining complete and reliable field meta-data associated with all factors at collection site (and time) prevents a major synergistic understanding of Mg-calcites in echinoderms (Sumich and McCauley 1972). Here, we present for the first time a detailed echinoderms $SrCO_3$ content in Mg-calcite dataset (Table 14.2), which inherits the same issues as Mg^{2+} to explain large scale variability and applications for paleo studies. Sr^{2+} content in biogenic calcites follows Mg^{2+} (*see* Fig. 14.2; Carpenter and Lohmann 1992) but then other factors mainly linked to physiology and discrimination at calcification site govern its content in echinoderms (*see* discussions of Hermans et al. 2010). After analyzing our dataset, we point out two new major issues beyond temperature and latitudinal controls on Mg-calcite composition (which have already been widely discussed) (Chave 1954; Dodd 1967; Weber 1973; Dickson 2004; *see* McClintock et al. 2011 for re-analysis): (1) size class control (ontogenic), and (2) small-scale seawater composition variability.

On the ontogenesis side, we observe that the calcite Mg/Ca remains stable with increasing size (juvenile to adults) but this is mainly driven by a parallel decrease in $CaCO_3$ and $MgCO_3$ content (also seen by Borremans et al. 2009 in starfish and originally proposed by Sumich and McCauley 1972 on echinoids) (Fig. 14.3). Conversely, calcite Sr/Ca increased with size induced by an almost constant $SrCO_3$ trend and a decreasing $CaCO_3$ content. This is contrary to Borremans et al. (2009) findings, although we compared different age classes and we observed general trends within and across classes using field conditions. In brief, younger developmental stages grow much faster than adults, thus Mg^{2+} and Sr^{2+} should be incorporated faster as smaller crystals are built, which does not necessarily mean that the percentage per dry mass should increase. The Mg^{2+} content has been negatively correlated to the Brody-Bertalanffy growth constant (*see* Ebert 2001, 2007), where the echinoderm growth rate decreases as the size reaches a maximum (aging) (*see* Dodd 1967; Weber 1969). Therefore, fast growth should eventually lead to less $MgCO_3$ in their bodies as we observe among all classes (Fig. 14.3). It can also be that less Mg^{2+} is incorporated into newly-formed plates as the organism ages, or that Mg^{2+} is replaced by Ca^{2+} after initial deposition. This is the most likely explanation for the overall echinoderm decrease in $MgCO_3$ % dw with size and thus age in our samples (Fig. 14.3), with a

small temperature effect as proposed by Sumich and McCauley (1972). This issue could potentially explain differences among species measured at similar latitudes if there is not a distinction between size classes and developmental stage (not available from Chave 1954, Weber 1969, 1973). This ontogenic geochemistry needs to be assessed from larval stages to juveniles to understand the full life cycle and determinate life-stage susceptibility to OA based on the skeleton mineralogy. Furthermore, if this ontogenesis change is not considered in sediment samples used for pale reconstructions, large errors can be introduced.

We find robust $MgCO_3$ and $SrCO_3$ % dw latitudinal trends following a parabola from the Arctic to the Antarctic (minimum: 2-4 % and 0.12-0.16 % respectively) and maximum (14-16 % and 0.30-0.33 % respectively) at the tropics (Fig. 14.4) for whole bodies and also for body parts (spines and plates). Conversely, $CaCO_3$ % dw remains relatively constant. The whole overall trend is likely explained by temperature and saturation state regimes as previously discussed in the literature. However, we propose another source of variability, following small-scale seawater composition changes that induce skeletal parts content variability within the same latitude or across latitudes. Many of the samples used originate in coastal areas, where salinity changes can modify seawater composition (*see* Ingram et al. 1998). The absorption route of echinoderms skeletal Ca^{2+} is seawater (Lewis et al. 1990) and for Mg^{2+} and Sr^{2+} should be the same (Hermans et al. 2010), although Sr^{2+} is highly dependant on the crystal growth rate. In the field, the surface seawater Sr/Ca remains constant between a salinity of 10 and 35, although across large latitudinal gradients in the Atlantic and Pacific Ocean and with depth, Sr/Ca changes from 1 to 3 % (largest variability at high latitudes near upwelling areas) (de Villiers 1999). This probably follows differences in biological consumption and dissolution (Bernstein et al. 1992; de Villiers 1999; Martin et al. 2010). It remains unknown how this small variability translates to benthic waters and then to the $SrCO_3$ content of biogenic calcites. Conversely, the seawater Mg/Ca increases with increasing salinity in estuaries (Ingram et al. 1998) from 2.99 mol/mol at salinity 2.80 to 5.15 mol/mol at salinity 30. While in other estuaries and coastal regions it goes from 4.58 mol/mol at salinity 15.60 to 5.18 mol/mol at salinity 24 (Zang et al. 2003). Further evidence from surface shelf waters in the Atlantic Ocean indicates that seawater Mg/Ca decreases from shelf to offshore regions under the same salinity range (35) from 5.90 to 5.13 mol/mol (Blanco-Ameijeiras et al. in press) driving calcifying algae Mg/Ca calcite ratios. Therefore, the assumption that benthic ecosystems calcification takes place in a seawater Mg/Ca around 5.13 mol/mol is misleading, as this value is extrapolated solely from surface open waters

and vertical profiles (e.g. Fabricand et al. 1967). Calcite mineralogy can change significantly with varying ambient seawater Mg/Ca (*see* Choudens-Sanchez and Gonzalez 2009), which is reflected in benthic organisms skeletal mineralogy (Ries 2009). If this variability translates to the seabed, and we assume present ocean Mg/Ca values including estuaries, shelves and the open ocean to vary from 4 to 6 mol/mol we can expect the echinoderm Mg-calcite to reflect this pattern. Small-scale seawater composition changes could then be considered as another mineralogical source of variability in the modern ocean. Therefore, it becomes clear that disentangling the modern seawater effect (Ries 2010) from temperature (Chave 1954), ambient carbonate chemistry (Morse and Mackenzie 1990; Ries 2011), physiology (Weber 1969; Ebert 2001) and the species-specific responses mediated by a genetic control (Raup 1966) may prove challenging. This should be carefully considered when making appropiate choices to constraint paleo reconstruction estimates based on echinoderm high Mg-calcite during the Holocene.

14.5.2. Echinoderms Mg-calcite in the future ocean: from species to global budgets

The OA effects on echinoderms are expected to occur in a species- or class-specific manner at the organisms level, scaling up to population and community levels. Echinoderms with low motility abilities (e.g. burrowers) will likely inhabit permanently undersaturated waters, while others may have the alternative to move to shallower horizons (during larval dispersal and search of an optimum substrate). At first, they are likely to withstand high CO_2 conditions by modulating Mg-calcite contents and diverting energy to other vital functions. In Ries (2011) experiments, echinoderms seemed to adapt well to high CO_2 with little variations in mineralogy, but this may just reflect a broad tolerance around a certain CO_2 range. They could face more difficulties to calcify once this CO_2 range starts to broaden seasonally induced by OA. However, they could alternatively adopt surviving strategies such as settling outside the undersaturated horizons. Sewell and Hofmann (2011) suggested that settling outside these ranges could reduce pressure on calcification, inducing positive growth. Yet, this will largely depend on food availability and environmental/substratum conditions resembling those that are optimum for the species. Now, going back to larvae and juvenile stages, field evidence suggests that post-juvenile settlement outside the adult range results in large mortality rates (Howell et al. 2002). In some cases, this is explained by threshold thermal tolerances (Young et al. 1998). We suggest that echinoderms will respond in a species-specific manner to OA following mineralogy (as

proposed by Sewell and Hofmann 2011) (Table 14.2) among others factors, by changing first settlement behaviour out of undersaturated horizons, but that there may carry-over effects on the adult stages by induced early mortality. We also suggest that echinoderm Mg-calcite composition may vary during early ontogenesis (Sumich and McCauley 1972) as observed in foraminifera (Sadekov et al. 2005; Dueñas-Bohorquez et al. 2011), to adapt to transient ambient carbonate chemistry changes (Fig. 14.3). From juvenile to adult stages we observed an overall decrease in both $CaCO_3$ and $MgCO_3$ contents (Fig. 14.3), which can be related to a decrease in the growth rate with age (Ebert 2001; York 2011), but also to more constant conditions in the optimum adult bathymetric range in comparison with larvae and juveniles. These developmental stages, naturally encounter larger carbonate chemistry ranges thus they may need to change composition quick to maximize adaptation potential. This can be attributed to a higher dissolution susceptibility if settling outside the adult range, which bounces back to the hypothesis of induced mortality if CO_2 keeps rising and juveniles have to settle in shallower horizons. Sewell and Hofmann (2011) also propose that only echinoids living above saturation horizons for their mineral content, could produce calcified young's. This could be overcome by transient allocation of energy to reproduction, while diverting it from other functions, thus reducing the adult Mg-calcite content by decreasing growth rate and skeletal crystal growth (Ebert 2007), and then recovering the original $MgCO_3$ levels after the reproduction period. Seasonal changes in the Mg-calcite composition could also reflect the reproduction period per se. Furthermore, calcified larvae and juveniles are probably more flexible and resilient to ambient carbonate chemistry changes as they inhabit a wide variety of water layers from fertilization to settlement (Clark et al. 2009). Thus, we may expect a parabolic relationship of Mg-calcite during ontogenesis, from low levels at the start [(there is also echinoid evidence from juveniles stages (McClintock et al 2011)] to high levels at adult stages, and then a further decrease as organisms become old (Fig. 14.3). Certainly, a tight control on the Mg-calcite content during the life cycle controlling dissolution (buffer) and net Mg^{2+} incorporation could help echinoderms to maintain adequate calcification levels. Another intriguing hypothesis is that if echinoderms reduce Mg-calcite content following OA and colonize shallower habitats, skeletons may become weaker facilitating the action of crushing predators or increasing disease vulnerability (Raven et al. 2005). Certainly, Antarctic echinoderms, which have the lowest Mg-calcite content (also below Arctic species) (McClintock et al. 2011; *see* Table 14.2) could also bear naturally a lower $MgCO_3$ dw % in the skeleton following the absence of evolutionary pressure from the missing crushing predators in Antarctica. Adult echinoderms probably

modulate the Mg^{2+} content (and also Sr^{2+}) on a seasonal basis independently of age, following major trends of temperature, ambient carbonate chemistry but also growth rate following food availability (e.g. very seasonal in polar areas and the deep sea). This has already been observed in molluscs (Lorrain et al. 2005; Vander Putten et al. 2000), bryozoans (Barnes et al. 2007; Smith et al. 2007), and coralline algae with changes from 1 to 2 % mol $MgCO_3$ from spring to summer (Haas et al. 1935). A seasonal signal could further explain disparity in field results from the same species collected at different times of the year in the same latitude. This seasonal elemental composition variability likely affects within a tight range any study intending to reconstruct e.g. temperature or other parameters from echinoderm calcite.

Overall, Antarctic echinoderms have similar $CaCO_3$ %s as the rest, but a much lower $MgCO_3$ content than tropical species (McClintock et al. 2011; Table 14.2; Fig. 14.4). They have however a similar percentage as temperate and Arctic species, specially in whole bodies and plates (Fig. 14.4). Thus, their Mg-calcite sediment contribution is expect to be lowest in the poles, followed by temperate and tropical latitudes. However, it is not clear if the overall contribution will be lower in the poles because populations at low latitudes attain very high densities (Gutt 1988; Moya et al. 2003), thus while Mg-calcite qualitative contribution can be small, quantitatively it can be compensated. In Antarctica, the sediment calcite content varies with depth, with maxima at the main shelf and shelf break resulting from different accumulation processes (Hauck et al. 2012). Low Mg-calcite dominates sediments, which for the echinoderm component can be attributed both to a lower $MgCO_3$ (McClintock et al. 2011) production per se and sediment dissolution leaving eventually a low percentage. In Antarctic, echinoderms explain at least half of the benthic calcite standing stocks, thus it is expected that their high Mg-calcite particles are among the first responders to OA. Shallowing of saturation horizons may cause slow dissolution of echinoderm remains that comprise between 5 and 30 % of sediment particles in some cases (Kroh and Nebelsick 2010). However, local dissolution can be driven by organic matter remineralization at the seabed increasing the dissolved inorganic carbon and thus CO_2. In reality, dissolution will be governed by several factors creating patchiness depending on the intensity, and the $MgCO_3$ % deposited. Carbonates distribution and accumulation is normally patchy on its own, being driven by current transport, dissolution, and overlying productivity regimes (Hillenbrand et al. 2003; Hauck et al. 2012). Since most upper ocean waters are supersaturated with respect to calcite, aragonite, and the majority of metastable Mg-calcite forms [except in upwelling regions (*see* Feely et al. 2008; Paulmier et al. 2011) and estuaries

(Feely et al. 2010)], major dissolution can only take place below the lysocline (Berger 1968; Chen et al. 1988). Global calcite dissolution is estimated around 3.33 *10^{13} mol C yr^{-1} below 2000 m and 8.33 * 10^{13} mol C yr^{-1} between 100 and 1500 m (Berelson et al. 2007), with a total sink (dissolution + burial in sediments) around 1.25 * 10^{14} mol C yr^{-1} (Catubig et al. 1998). Calcite dissolution in shelves alone is similar to the open ocean at around 1.60-3.10 * 10^{13} mol yr^{-1} (Chen 2002). Our inorganic carbon echinoderms production estimates range from 9.41 * 10^{12} to 7.10 * 10^{13} mol C yr^{-1}, which could explain a large proportion of the above figures at least in the shelves (Table 14.4). Our new echinoderm calculations are above previous shelves and slopes estimates between 2 * 10^{12} and 1 * 10^{13} mol C yr^{-1} and even coral reefs (9 * 10^{12} mol C yr^{-1}) (Iglesias-Rodriguez et al. 2002). They are however within the range of pelagic estimates (including fish and foraminifera), ranging from 3 * 10^{12} to 1.50 * 10^{14} mol C yr^{-1} (Schiebel 2002; Moore et al. 2004; Balch et al. 2007; Wilson et al. 2009), although the solubility of e.g. fish carbonates is much higher (Woosley et al. 2012). Echinoderms inorganic carbon production attributed to Mg-calcite from 3 to 15 mol % $MgCO_3$ (in this study), ranges from 1.16 * 10^{12} to 8.75 * 10^{12} mol C yr^{-1} (Table 14.4). This means that ~ 12 % of the global echinoderms carbonate budget originates in high Mg-calcite, which in the majority of the cases is > 6-8 mol % $MgCO_3$ (*see* Table 14.2 for raw data). Echinoderms biomass concentrates in shelves and slopes from 0 to 2000 m globally (Table 14.4) with peaks down to 800-1000 m at all latitudes (Lebrato et al. 2010). However, large populations exist below 1000 m (Howell et al. 2002), and also from 3000 to 6500 m (Sokolova 1972, 1994). These species may be somehow adapted to undersaturated conditions and their remains may undergo complete dissolution once dead and deposited at the seabed, since deep waters are certainly undersaturated with respect to any echinoderm mol % $MgCO_3$ (Table 14.2). Yet, it remains to be measured the skeletal mineralogy in deep sea populations. In the deep sea, the maintenance of optimum calcification conditions may be linked to food input as are their distribution and adaptation traits (Sokolova 1972). A reduction of labile resources availability following organic detritus export linked to climate change or major regime shifts (Smith et al. 2008), will be the main factor altering deep echinoderm calcification as water masses are already close or undersaturated (Feely et al. 2004). In some cases, it has been observed that the skeletal mol % $MgCO_3$ per se nearly halves from 10 to 1000 m in the same species explained as a temperature dependence (Clarke and Wheeler 1922; Roux et al. 1995), while it increases in others (Sumich and McCauley 1972). This contradiction may be explained from different size classes involved, which $MgCO_3$ content decreases with age, irrespectively of temperature and depth (Fig. 14.3). Therefore, while at present, Mg-calcite

deposits may not start dissolving except in deep areas, they could do so in the near future, especially in polar latitudes (Andersson et al. 2008). Particularly, shelf and slope Mg-calcite dissolution of echinoderm and other macrozoobenthic remains (Hauck et al. 2012) should play the most important role in buffering seawater alkalinity (Chen 2002), as the saturation horizons shallow and the Mg-calcite deposits get in contact with undersaturated waters. However, Andersson et al. (2003) showed in a modelling effort that even if 40 % of the ocean reservoir of high Mg-calcite (> 15 mol % $MgCO_3$) would dissolve, there will be no significant buffering effect in surface waters. Dissolution will be largest in benthic ecosystems, with a gradual decrease in benthic $MgCO_3$ content, impoverishing the sediment surface (Taylor et al. 2008). Echinoderms bear up to 14-16 % $MgCO_3$ dw in tropical regions [but it can go up to 20-22 % dw (*see* compilation by Vinogradov 1953) and 40 % dw in the teeth (Märkel et al. 1971)] and between 2 and 12 % $MgCO_3$ dw in polar and temperate regions (in this study), thus many species are near the threshold to start dissolution (Sewell and Hofmann 2011). If macrozoobenthic remains dissolution can somehow buffer the water column will depend on water masses exchange and if the metastable carbonate dissolution is large enough to act on a short time scale. Other carbonates such as $SrCO_3$ correlate positively with $MgCO_3$ content in biogenic calcites (Carpenter and Lohmann 1992), which was also observed in our echinoderms dataset (Fig. 14.2, 14.4). Therefore, as the $MgCO_3$ content decreases owing to dissolution, we can expect $SrCO_3$ to follow, decreasing both carbonates contribution to inorganic carbon export. $SrCO_3$ contribution to the global echinoderms budget remain below 1 % ($1.85 * 10^{10}$ to $1.25 * 10^{11}$ mol C yr^{-1}) (Table 14.4), thus the reduction in this carbonate to the inorganic carbon contribution will be negligible.

Other factors beyond the chemical composition of Mg-calcite driving possible dissolution include echinoderm particle size once death and deposited (Keir 1980), microstructures and skeletal framework (Walter and Morse 1984), organic coatings resistance to decomposition and individual crystal size correlating negatively with mol % $MgCO_3$ (Henrich and Wefer 1986), and mechanical breakdown (Metzler et al. 1982). Mechanical disintegration is especially relevant, varying from highly dynamic shelf systems where particle abrasion should be high (producing smaller echinoderm particles with a larger surface area in contact with water) (e.g. Brunskill et al. 2002), to tranquil deep sea settings, where whole echinoderm remains have been observed (Lebrato et al. 2010). Natural corrosion of echinoderm particles was described by Henrich and Wefer (1986) from 400 to 3600 m during 52 days in the Southern Ocean.

Dissolution started very slowly on internal parts in a step-wise manner until all internal cements were depleted. Internal dissolution can be attributed to organic matter decomposition governing large CO_2 micro gradients, further corroding the skeleton. External dissolution evidence appeared towards the end of the experiment with highly visible irregular corrosion marks. This evidence suggests a slow but continuous (likely subjected to carbonate chemistry annual cyclicities) dissolution of echinoderm high Mg-calcite deposits if saturation horizons move progressively to shallower horizons. This will lead towards a lo Mg-calcite sedimentary composition and increasing bioerosion rates (Smith and Lawton 2010). Different classes and species remains may dissolve at different paces, also induced by differences in permeability (Binyon 1980) and ambient carbonate chemistry, as observed in molluscs (Powell et al. 2011; Waldbusser et al. 2011), and the same applies to skeletal parts. For example, echinoid spines are directly exposed to seawater, making them apparently the most susceptible to dissolution, but conversely they bear a much lower mol % $MgCO_3$ than plates and bodies (except in some cases) (Table 14.2; Fig. 14.2, 14.4). This means that the echinoderm body plan per se may delay dissolution once deposited at the seabed. However, these other factors besides mineralogy affecting dissolution should be considered when assessing results from living echinoderms. This should serve to avoid making major statements based purely on mol % $MgCO_3$ or calcite/aragonite saturation state without making a separation of the material mechanical and structural properties (Henrich and Wefer 1986) of the different echinoderm classes and species (Kroh and Nebelsick 2010).

14.6. Appendix A

14.6.1. A1

Table 14.5. Raw data from all species used in this study (from the literature). Data ordered by class and latitude.

Class	Family	Species	Lat.	Long.	Location
Asteroidea	Asteriidae	*Asterias linckii*	65.81	39.73	White Sea (Arctic Ocean)
Asteroidea	Asteriidae	*Sclerasterias tanneri*	61.68	3.31	Norwegian Sea
Asteroidea	Ctenodiscidae	*Ctenodiscus crispatus*	46.9	-59.1	Newfoundland (Atlantic Ocean)
Asteroidea	Asteriidae	*Asterias vulgaris*	44.79	-66.92	Eastport Maine (Atlantic Ocean)
Asteroidea	Asteriidae	*Asterias acervata borealis*	43.58	-65.17	Nova Scotia (Atlantic Ocean)
Asteroidea	Asteriidae	*Asterina pectinifera*	43.2	141.05	Japan Sea (Pacific Ocean)
Asteroidea	Asteriidae	*Asterias forbesi*	41.42	-70.8	Vineyard Sound (Atlantic Ocean)
Asteroidea	Odontasteridae	*Odontaster hispidus*	41.3	-70.8	Marthas Vineyard (Atlantic Ocean)
Asteroidea	Astropectinidae	*Plutonaster agassizii*	41.3	-70.8	Marthas Vineyard (Atlantic Ocean)
Asteroidea	Benthopectinidae	*Pontaster tenuispinus*	41.3	-70.8	Marthas Vineyard (Atlantic Ocean)
Asteroidea	Asteriidae	*Leptasterias compta*	40.28	-69.85	Cape Cod (Atlantic Ocean)
Asteroidea	Benthopectinidae	*Benthopecten spinosus*	39.25	-68.13	Cape Cod (Atlantic Ocean)
Asteroidea	Asteriidae	*Urasterias linckii*	35.71	-73.5	Cape Hatteras (Atlantic Ocean)
Asteroidea	Asteriidae	*Asterias tanneri*	35.71	-73.5	Cape Hatteras (Atlantic Ocean)
Asteroidea	Asteriidae	*Asterina miniata*	35.2	-121.3	California (Pacific Ocean)
Asteroidea	Asteriidae	*Marthasterias glacialis*	35.2	-121.3	California (Pacific Ocean)
Asteroidea	Astropectinidae	*Astropecten americanus*	26.9	-82.8	West Florida (Atlantic Ocean)
Asteroidea	Asteriidae	*Asterina minuta*	18.04	-67.96	British West Indies (Atlantic Ocean)
Asteroidea	Ophidiasteridae	*Linckia guildingii*	18.04	-67.96	British West Indies (Atlantic Ocean)
Asteroidea	Ophidiasteridae	*Linckia laevigata*	18.04	-67.96	British West Indies (Atlantic Ocean)
Asteroidea	Acanthasteridae	*Acanthaster planci*	5.86	-162.08	Palmyra Island (Pacific Ocean)
Asteroidea	Ctenodiscidae	*Ctenodiscus procurator*	-35.7	-72.8	Chile (Pacific Ocean)
Asteroidea	Ctenodiscidae	*Ctenodiscus australis*	-43.6	-74	Patagonia (Pacific Ocean)
Echinoidea	Strongylocentrotidae	*Strongylocentrotus droebachiensis*	74	49	Barents Sea
Echinoidea	Strongylocentrotidae	*Strongylocentrotus droebachiensis*	64	-38	Greenland Sea
Echinoidea	Echinarachniidae	*Echinarachnius parma*	59.2	-165.8	Bering Sea (Arctic Ocean)
Echinoidea	Echinarachniidae	*Echinarachnius parma*	41.3	-71.3	New England

Echinoidea	Arbaciidae	*Arbacia lixula*	40.76	14.35	Bay of Naples (Mediterranean Sea)
Echinoidea	Echinidae	*Echinus esculentus*	38	-1.02	Mediterranean Sea
Echinoidea	Echinidae	*Echinus affinis*	35.71	-73.5	Cape Hatteras (Atlantic Ocean)
Echinoidea	Toxopneustidae	*Lytechinus anamesus*	35.2	-121.3	California (Pacific Ocean)
Echinoidea	Clipeasteridae	*Clypeaster testudinarius*	33.4	134.6	South Japan Sea (Pacific Ocean)
Echinoidea	Strongylocentrotidae	*Strongylocentrotus fragilis*	29	-115	South California (Pacific Ocean)
Echinoidea	Cidaridae	*Prionocidaris baculosa*	28.02	34.97	Red Sea
Echinoidea	Cidaridae	*Tetrocidaris affinis*	26.9	-82.8	Florida (Atlantic Ocean)
Echinoidea	Echinometridae	*Echinometra lucunter*	18.04	-67.96	British West Indies (Atlantic Ocean)
Echinoidea	Clypeasteroidea	*Echinodiscus sexiesperforatus*	18.04	-67.96	British West Indies (Atlantic Ocean)
Echinoidea	Mellitidae	*Encope californica*	-1	-91.01	Galapagos (Pacific Ocean)
Echinoidea	Arbaciidae	*Tetrapygus niger*	-9.4	-78.5	Peru (Pacific Ocean)
Echinoidea	Echinometridae	*Heterocentrotus mammillatus*	-27.64	-144.33	Tuamotu (Pacific Ocean)
Echinoidea	Toxopneustidae	*Lytechinus albus*	-43.6	-74	Patagonia (Pacific Ocean)
Ophiuroidea	Gorgonocephalidae	*Gorgonocephalus arcticus*	68.2	39.2	Kola Peninsula (Barents Sea)
Ophiuroidea	Gorgonocephalidae	*Gorgonocephalus caryi*	61.3	-166.3	Bering Sea (Arctic Ocean)
Ophiuroidea	Ophiactidae	*Ophiopholis aculeata japonica*	53.91	-166.5	Unalaska (Arctic Ocean)
Ophiuroidea	Gorgonocephalidae	*Gorgonocephalus arcticus*	41.5	-70.3	Cape Cod (Atlantic Ocean)
Ophiuroidea	Ophiurinae	*Ophioglypha sarsii*	39.54	-72.35	New England slope (Atlantic Ocean)
Ophiuroidea	Gorgonocephalidae	*Gorgonocephalus eucnemis*	38.3	139	Japan Sea (Pacific Ocean)
Ophiuroidea	Ophionereididae	*Ophionereis eurybrachiplax*	38.3	139	Japan Sea (Pacific Ocean)
Ophiuroidea	Ophiurinae	*Ophioglypha lütkeni*	35.2	-121.3	California (Pacific Ocean)
Ophiuroidea	Ophiacanthidae	*Ophiocamax fasciculata*	21.4	-76.7	Caribbean Sea
Ophiuroidea	Ophiotrichidae	*Ophiothrix angulata*	21.4	-76.7	Cuba (Caribbean Sea)
Ophiuroidea	Ophiocomidae	*Ophiocoma erinaceus*	20.1	-155.3	Hawaii (Pacific Ocean)
Ophiuroidea	Ophiodermatidae	*Ophioderma cinerum*	18.5	-66.6	Puerto Rico (Caribbean Sea)
Ophiuroidea	Ophiocomidae	*Ophiocoma aethiops*	18.04	-67.96	Gulf of California (Pacific Ocean)
Ophiuroidea	Ophiomyxidae	*Ophiomixa flaccida*	18.04	-67.96	British West Indies (Atlantic Ocean)
Ophiuroidea	Ophiomyxidae	*Ophiomixa flaccida*	18.04	-67.96	British West Indies (Atlantic Ocean)
Ophiuroidea	Ophiocomidae	*Ophiocoma pumila*	18.04	-67.96	British West Indies (Atlantic Ocean)
Ophiuroidea	Ophiolepididae	*Ophiomusium lymani*	-1	-91.01	Galapagos (Pacific Ocean)
Ophiuroidea	Ophiurinae	*Ophioglypha lymani*	-35.7	-72.8	Chile (Pacific Ocean)
Crinoidea	Hyocrinidae	*Ptilocrinus pinnatus*	53.1	-130	British Columbia (Pacific Ocean)
Crinoidea	Antedonidae	*Florometra asperrima*	47.1	-124.2	Washington (Pacific ocean)
Crinoidea	Bourgueticrinidae	*Bythocrinus robustus*	42.3	-70.77	Massachussets (Atlantic Ocean)
Crinoidea	Antedonidae	*Hathrometra dentata*	41.3	-70.8	Marthas Vineyard (Atlantic Ocean)
Crinoidea	Antedonidae	*Heliometra glacialis*	40.3	139.3	North Japan Sea (Pacific Ocean)
Crinoidea	Zenometridae	*Psathyrometra fragilis*	35.07	139.7	Japan Sea (Pacific Ocean)
Crinoidea	Pentametrocrinidae	*Pentametrocrinus japonicus*	34.9	138.5	Japan Sea (Pacific Ocean)

Crinoidea	Charitometridae	*Crinometra concinna*	28.05	-96.02	Gulf of Mexico (Atlantic Ocean)
Crinoidea	Isocrinidae	*Isocrinus decorus*	21.4	-76.7	Cuba (Caribbean Sea)
Crinoidea	Isocrinidae	*Isocrinus decorus*	21.4	-76.7	Cuba (Caribbean Sea)
Crinoidea	Isselicrinidae	*Endoxocrinus parra*	21.4	-76.7	Cuba (Caribbean Sea)
Crinoidea	Isselicrinidae	*Endoxocrinus parra*	21.4	-76.7	Cuba (Caribbean Sea)
Crinoidea	Tropiometridae	*Tropiometra picta*	21.4	-76.7	Cuba (Caribbean Sea)
Crinoidea	Comasteridae	*Capillaster multiradiata*	7.85	116.9	Philippines (Pacific Ocean)
Crinoidea	Mariametridae	*Pachylometra patula*	7.85	116.9	Philippines (Pacific Ocean)
Crinoidea	Zygometridae	*Catoptometra ophiura*	7.85	116.9	Philippines (Pacific Ocean)
Crinoidea	Isocrinidae	*Hypalocrinus naresianus*	7.85	116.9	Philippines (Pacific Ocean)
Crinoidea	Himerometridae	*Craspedometra anceps*	7.85	116.9	Philippines (Pacific Ocean)
Crinoidea	Tropiometridae	*Tropiometra carinata*	-22.98	-43.2	Río de Janeiro (Atlantic Ocean)
		Literature - Juveniles (plates) (Borremans et al. 2009; Hermans et al. 2010)			
Asteroidea	Asteriidae	*Asterias rubens* (*n* = 34)	51.35	-3.23	Knokke (North Sea)
Asteroidea	Asteriidae	*Asterias rubens* (*n* = 18)	51.35	-3.23	Knokke (North Sea)
Echinoidea	Parechinidae	*Paracentrotus lividus* (*n* = 6)	43.27	5.34	Endoume (Mediterranean Sea)
Echinoidea	Parechinidae	*Paracentrotus lividus* (*n* = 8)	43.27	5.34	Endoume (Mediterranean Sea)
Echinoidea	Parechinidae	*Paracentrotus lividus* (*n* = 8)	43.27	5.34	Endoume (Mediterranean Sea)
Echinoidea	Parechinidae	*Paracentrotus lividus* (*n* = 9)	43.27	5.34	Endoume (Mediterranean Sea)
Echinoidea	Parechinidae	*Paracentrotus lividus* (*n* = 11)	43.27	5.34	Endoume (Mediterranean Sea)
Echinoidea	Parechinidae	*Paracentrotus lividus* (*n* = 8)	43.27	5.34	Endoume (Mediterranean Sea)
Echinoidea	Parechinidae	*Paracentrotus lividus* (*n* = 13)	43.27	5.34	Endoume (Mediterranean Sea)
Echinoidea	Parechinidae	*Paracentrotus lividus* (*n* = 13)	43.27	5.34	Endoume (Mediterranean Sea)

14.7. Addendum: Trace and rare elemental geochemistry in echinodems Mg-calcite

14.7.1. Justification for an "addendum"

Hereafter, I develop a brief contribution to Chapter 14 (*Revisiting the modern echinoderms global carbonate budget*) from results obtained while measuring $CaCO_3$, $MgCO_3$, and $SrCO_3$ with an inductively coupled plasma mass spectrometer (ICP-MS). In brief, the ICP-MS analytical output provides a large set of other trace and rare elements besides Ca^{2+}, Mg^{2+}, and Sr^{2+} that we used to provide a complete database for echinoderms and also to search latitudinal trends that may for example help in desinging experiments to develop paleoproxies.

14.7.2 . Brief summary

All biogenic samples were the same described in Section 14.3 and the material was identically treated as for the measurements of the carbonates. The following elements and ratios normallized to [Ca^{2+}] were available (Table 14.6): Li, Be, Mg, Al, P, S, K, Sc, Ti, V, Cr, Mn, Fe, Co, Ni, Cu, Zn, Ga, Ge, As, Se, Rb, Sr, Y, Zr, Mo, Ag, Cd, Sn, Sb, Te, Ba, La, Ce, Nd, Dy, W, Re, Au, Hg, Tl, Pb, Bi, and U. Units of concentrationa and ratios were changed to appropiate decimals depending on element concentration, from parts-per-thousand (ppt) to parts-per-million (ppm), and from milimol (mmol) to nanomol (nmol). For interpretation, we divided results as "whole body", "spines", and "plates+calcareous ring" (Table 14.7, 8, 9), and the last two were combined in graphs (Fig. 14.5, 6, 7, 8, 9, 10) per class. We also studied the elements trend with latitude (Fig. 14.9,10).

In whole body, asteroids and echinoids showed a large variability of in element concentration depending on the species, while the variability in the other classes was much smaller (Fig. 14.5). Total element concentration was dominated by Ca, followed by Mg, K, Sr, Fe, Ba, Zn, and B in all classes. In spines+plates+ring, variability was smaller overall, and total element concentration was similar as for whole body (Fig. 14.6). Whole body ratios per element were relatively constant for all classes except for asteroids, while the contrary was true in spines+plates+ring but for echinoids (. 14.7, 8). Whole body latitudinal trends increased linearly with increasing latitude in Li/Ca, Mg/Ca (temperature), K/Ca, Sc/Ca, Zn/Ca, Ge/Ca, Rb/Ca, Sr/Ca (temperature/growth rate), Ba/Ca, Ce/Ca, and Nd/Ca (water masses signature), while in the rest they remained flat or there were not enough

data (Fig. 14.9, 10). Spines+plates+ring increasing ratio trend with latitude were observed in Li/Ca, B/Ca, Sc/Ca, Ge/Ca, Rb/Ca, Dy/Ca, and Re/Ca, while decreasing in Mg/Ca, As/Ca, Se/Ca, Sr/Ca, and remained flat or or there not enough data in the rest (Fig. 14.10). Variability in whole body makes these samples difficult to use to correlate seawater properties with the element, although the latitudinal trends for certian elements indicate that as for the widely known Mg and Sr, there may be other elements (especially Li, B, Ba, or Nd) that could be potentially used as proxies for some water property. Some of these elements reflect the different temperature, salinity, carbonate chemistry and physiological regulation exerted by organisms. The problem with using whole bodies is that all different body parts are mixed in the analysis and in sediment remains only smaller parts are conserved. Therefore, the use of spines and plates becomes more relevant. The latitude analysis of the components reveals some potentially interesting trends especially in the case if Li/Ca, B/Ca, Se/Ca, Re/Ca, and Dy/Ca, although it remains unclear which property correlates with them or if they depend on physiological regulation. Future laboratory experiments in echinoderms Mg-calcite should measure routinely all these elements along with Ca, Mg, and Sr to look for additional robust trends that may be indicators of temperature, salinity, or carbonate chemistry since the present use of echinoderms elemental ratios is only optimized for seawater composition (e.g. Dickson 2002). This dataset can also be used as a baseline to assess trace and heavy elements (e.g. As, Pb, U, Cu, Cd) that could be used as monitoring variables for contamination in seawater using echinoderms as indicators. The latest use we propose is for industrial applications, where e.g. an echinoderm-based fertilizer for agricultural use can be developed as we now have a complete chemistry description of echinoderms carbonate. Using an optimization procedure and composition it can be developed for e.g. estabilize and neutralize the pH of agricultural soils and provide some key marine salts and constituents for plants growth.

Table 14.6. List of elements measured, atomic weights, units (of concentration and ratios), and ICP detection limits for each element.

Symbol	Element	Atomic weight	Units	Detection limit
Ca		40.08	ppt	0.01
Li	Lithium	6.94	ppm (wt)	0.10
Li/Ca			mmol/mol	
Be	Beryllium	9.01	ppm (wt)	0.5
Be/Ca			mmol/mol	
B	Boron	10.81	ppm (wt)	10
B/Ca			mmol/mol	
Mg	Magnesium	24.31	ppt (wt)	0.01
Mg/Ca			mmol/mol	
Al	Aluminum	26.98	ppm (wt)	0.01
Al/Ca			µmol/mol	
P	Phosphorus	30.97	ppm (wt)	0.001
P/Ca			µmol/mol	
S	Sulfur	32.06	ppm (wt)	0.01
S/Ca			µmol/mol	
K	Potassium	39.10	ppm (wt)	0.01
K/Ca			mmol/mol	
Sc	Scandium	44.96	ppm (wt)	1
Sc/Ca			µmol/mol	
Ti	Titanium	47.88	ppm (wt)	0.01
Ti/Ca			µmol/mol	
V	Vanadium	50.94	ppm (wt)	1
V/Ca			mmol/mol	
Cr	Chromium	52.00	ppm (wt)	1
Cr/Ca			mmol/mol	
Mn	Manganese	54.94	ppm (wt)	5
Mn/Ca			mmol/mol	
Fe	Iron	55.85	ppm (wt)	0.01
Fe/Ca			mmol/mol	
Co	Cobalt	58.93	ppm (wt)	1
Co/Ca			µmol/mol	
Ni	Nicklel	58.69	ppm (wt)	1
Ni/Ca			mmol/mol	
Cu	Copper	63.55	ppm (wt)	1
Cu/Ca			mmol/mol	
Zn	Zinc	65.39	ppm (wt)	2
Zn/Ca			mmol/mol	
Ga	Gallium	69.72	ppm (wt)	10
Ga/Ca			µmol/mol	
Ge	Germanium	72.59	ppm (wt)	0.10
Ge/Ca			µmol/mol	
As	Arsenic	74.92	ppm (wt)	2
As/Ca			µmol/mol	
Se	Selenium	78.96	ppm (wt)	0.10
Se/Ca			µmol/mol	
Rb	Rubidium	85.47	ppm (wt)	0.10
Rb/Ca			µmol/mol	

Sr Sr/Ca	Strontium	87.62	ppm (wt) mmol/mol	1
Y Y/Ca	Yttrium	88.91	ppm (wt) µmol/mol	1
Zr Zr/Ca	Zirconium	91.22	ppm (wt) µmol/mol	1
Mo Mo/Ca	Molybdenum	95.94	ppm (wt) µmol/mol	1
Ag Ag/Ca	Silver	107.90	ppm (wt) µmol/mol	0.2
Cd Cd/Ca	Cadmium	112.40	ppm (wt) µmol/mol	0.5
Sn Sn/Ca	Tin	118.70	ppm (wt) µmol/mol	0.05
Sb Sb/Ca	Antimony	121.80	ppm (wt) µmol/mol	2
Te Te/Ca	Tellurium	127.60	ppm (wt) µmol/mol	1
Ba Ba/Ca	Barium	137.30	ppm (wt) mmol/mol	10
La La/Ca	Lanthanum	138.90	ppm (wt) µmol/mol	10
Ce Ce/Ca	Cerium	140.10	ppm (wt) µmol/mol	0.01
Nd Nd/Ca	Neodymium	144.20	ppm (wt) µmol/mol	0.02
Dy Dy/Ca	Dysprosium	162.50	ppm (wt) µmol/mol	0.00
W W/Ca	Tungsten	183.85	ppm (wt) µmol/mol	10
Re Re/Ca	Rhenium	186.20	ppm (wt) nmol/mol	0.00
Au Au/Ca	Gold	197.00	ppm (wt) nmol/mol	0.50
Hg Hg/Ca	Mercury	200.59	ppm (wt) µmol/mol	1
Tl Tl/Ca	Thallium	204.38	ppm (wt) µmol/mol	2
Pb Pb/Ca	Lead	207.20	ppm (wt) µmol/mol	2
Bi Bi/Ca	Bismuth	208.98	ppm (wt) µmol/mol	2
U U/Ca	Uranium	238.02	ppm (wt) µmol/mol	10

Table 14.7. Whole body Mg-calcite trace and rare elemental geochemistry results classified using latitude and class.

WHOLE BODY																															
	TEMPERATE				ANTARCTIC				TEMPERATE				TROPICAL				ANTARCTIC				TEMPERATE				TEMPERATE				TEMPERATE			
	Asteroidea								Echinoidea												Ophiuroidea				Holothuroidea				Crinoidea			
Symbol	**max.**	**min.**	**avg**	**SD**	**max.**	**min.**	**avg**	**SD**	**max.**	**min.**	**avg**	**SD**	**max.**	**min.**	**avg**	**SD**	**max.**	**min.**	**avg**	**SD**	**max.**	**min.**	**avg**	**SD**	**max.**	**min.**	**avg**	**SD**	**max.**	**min.**	**avg**	**SD**
Ca	284	87	190	47	293	163	244	47	359	212	285	48	349	261	295	38	274	235	251	21	316	269	283	18	14	6	10	4	269	242	260	15
Li	3.50	1.80	2.36	0.50	3.50	2.70	3.10	0.40	7.20	1.90	4.20	1.78	3.40	1.90	2.78	0.54	3.90	3.40	3.70	0.26	4.10	3.30	3.58	0.27	1.90	1.20	1.67	0.40	5.70	4.30	5.07	0.71
Li/Ca	0.12	0.05	0.07	0.01	0.10	0.09	0.09	0.00	0.12	0.05	0.08	0.02	0.08	0.04	0.06	0.01	0.09	0.08	0.09	0.00	0.08	0.07	0.07	0.00	1.17	0.77	0.98	0.20	0.14	0.09	0.11	0.02
Be					0.50	0.50	0.50	0.00																								
Be/Ca					0.01	0.01	0.01	0.00																								
B	98.00	32.00	51.92	19.07	71.00	46.00	55.58	7.15	84.00	30.00	48.43	15.10	117.00	54.00	82.00	24.99	90.00	58.00	71.00	16.82	54.00	46.00	50.83	3.25	66.00	39.00	55.33	14.36	83.00	73.00	78.67	5.13
B/Ca	1.79	0.67	1.01	0.26	1.46	0.58	0.89	0.27	0.91	0.46	0.62	0.10	1.66	0.63	1.06	0.41	1.37	0.88	1.06	0.28	0.73	0.59	0.67	0.05	24.51	17.23	20.64	3.66	1.23	1.01	1.13	0.11
Mg	23	10	17	4	26	16	23	4	28	10	17	5	22	12	19	4	14	11	13	2	25	23	24	1	13	10	12	2	24	21	22	2
Mg/Ca	207	120	153	28	194	129	156	21	133	67	99	18	140	68	107	30	95	79	86	8	147	129	138	6	2850	1312	2035	773	162	127	143	18
Al					0.04	0.01	0.02	0.01																								
Al/Ca					0.28	0.05	0.11	0.08																								
P					0.02	0.01	0.01	0.00																								
P/Ca					0.07	0.04	0.05	0.01																								
S					0.52	0.42	0.48	0.04																								
S/Ca					2.58	2.10	2.31	0.19																								
K	6800	2200	4308	1307	8800	200	2142	3520	3300	1100	2489	547	5800	900	2960	2346	5600	4800	5267	416	3000	2300	2617	271	12500	8600	10733	1976	4300	3400	3800	458
K/Ca	80.12	8.54	25.75	14.44	55.34	0.70	11.66	20.21	13.70	4.28	9.19	2.44	22.78	3.24	11.06	9.68	23.62	17.96	21.71	3.25	11.18	8.11	9.52	1.11	1494.16	801.28	1146.50	346.45	16.39	13.00	15.02	1.78
Sc	0.90	0.10	0.35	0.19	1.00	0.50	0.91	0.18	0.70	0.10	0.43	0.21	0.50	0.20	0.32	0.13	0.50	0.30	0.40	0.10	0.40	0.30	0.35	0.05	0.90	0.20	0.53	0.35	0.90	0.30	0.60	0.30
Sc/Ca	3.30	0.34	1.71	0.89	4.25	2.40	3.35	0.55	2.10	0.31	1.33	0.57	1.28	0.68	0.95	0.30	1.83	1.14	1.42	0.36	1.33	0.85	1.11	0.20	56.50	30.22	42.17	13.30	2.98	1.00	2.06	1.00
Ti																																
Ti/Ca																																
V	13.00	1.00	7.00	2.83	13.00	1.00	3.50	4.25	14.00	1.00	6.96	3.89	15.00	5.00	8.80	4.49	9.00	4.00	6.00	2.65	8.00	4.00	6.00	1.41	9.00	3.00	7.00	3.46	16.00	6.00	12.00	5.29
V/Ca	0.07	0.00	0.03	0.02	0.05	0.00	0.01	0.02	0.04	0.00	0.02	0.01	0.03	0.02	0.02	0.01	0.03	0.01	0.02	0.01	0.02	0.01	0.02	0.00	0.63	0.40	0.51	0.12	0.05	0.02	0.04	0.02
Cr	29.20	3.80	10.60	7.22	18.10	1.00	5.26	6.06	14.00	3.80	8.96	2.52	14.40	5.70	10.24	3.77	8.60	7.80	8.13	0.42	20.20	6.10	12.15	5.41	17.60	5.60	10.97	6.10	16.70	4.00	11.07	6.47
Cr/Ca	0.12	0.01	0.04	0.03	0.07	0.00	0.02	0.03	0.03	0.01	0.02	0.01	0.03	0.02	0.03	0.01	0.03	0.02	0.03	0.00	0.05	0.02	0.03	0.02	0.96	0.67	0.78	0.15	0.05	0.01	0.03	0.02
Mn	40.00	3.00	11.25	9.66	19.00	5.00	9.92	5.65	141.00	3.00	50.96	49.22	17.00	2.00	9.00	7.28	6.00	5.00	5.67	0.58	25.00	5.00	13.17	7.22	6.00	1.00	4.00	2.65	80.00	24.00	52.33	28.01
Mn/Ca	0.12	0.01	0.04	0.03	0.07	0.01	0.03	0.02	0.29	0.01	0.12	0.11	0.04	0.01	0.02	0.02	0.02	0.01	0.02	0.00	0.06	0.01	0.03	0.02	0.39	0.12	0.26	0.13	0.24	0.07	0.15	0.09
Fe	700	200	429	123	600	100	258	219	1600	400	889	370	800	400	640	182	500	500	500	0	900	600	683	117	200	100	167	58	1800	800	1367	513
Fe/Ca	2.46	1.11	1.63	0.33	2.31	0.24	0.89	0.87	3.29	1.24	2.18	0.61	1.80	1.10	1.54	0.30	1.53	1.31	1.44	0.11	2.25	1.54	1.74	0.28	12.81	10.11	11.70	1.41	5.34	2.14	3.83	1.60
Co	2.40	0.20	0.50	0.49	1.00	0.30	0.83	0.30	0.80	0.20	0.46	0.17	0.50	0.30	0.40	0.10	0.40	0.30	0.37	0.06	0.60	0.40	0.48	0.08	0.20	0.10	0.17	0.06	0.80	0.40	0.60	0.20
Co/Ca	8.16	0.96	1.75	1.62	3.24	1.10	2.28	0.74	1.60	0.64	1.08	0.26	1.07	0.78	0.91	0.13	1.12	0.87	0.99	0.13	1.42	0.98	1.16	0.17	12.15	9.58	11.08	1.34	2.25	1.02	1.59	0.62
Ni	24.20	3.50	8.76	4.90	8.10	1.00	3.90	2.64	13.00	5.70	9.45	1.99	13.10	7.30	10.00	2.14	8.50	7.00	7.70	0.75	12.70	8.30	10.38	1.58	3.00	0.50	2.03	1.34	9.60	7.70	8.83	1.00
Ni/Ca	0.08	0.02	0.03	0.01	0.03	0.00	0.01	0.01	0.03	0.02	0.02	0.00	0.03	0.02	0.02	0.00	0.02	0.02	0.02	0.00	0.03	0.02	0.03	0.00	0.16	0.06	0.12	0.05	0.03	0.02	0.02	0.00
Cu	493	2	65	121	45	1	10	15	4	1	2	1	34	2	13	13	8	2	6	3	52	17	35	12	2	2	2	0	10	4	6	3
Cu/Ca	1.23	0.00	0.19	0.31	0.13	0.00	0.03	0.05	0.01	0.00	0.00	0.00	0.07	0.00	0.03	0.02	0.02	0.01	0.01	0.01	0.10	0.04	0.08	0.02	0.17	0.08	0.12	0.05	0.02	0.01	0.02	0.01
Zn	235	19	106	71	98	12	37	34	36	7	18	8	59	8	27	20	315	298	307	9	156	101	118	20	36	22	30	7	173	98	146	41

Zn/Ca	1.06	0.04	0.39	0.30	0.37	0.03	0.11	0.12	0.07	0.02	0.04	0.02	0.10	0.02	0.05	0.03	0.80	0.67	0.75	0.08	0.33	0.20	0.26	0.05	2.28	1.57	1.87	0.36	0.42	0.22	0.35	0.11
Ga	1.81	0.02	0.54	0.52	10.00	0.57	7.77	4.04	1.70	0.02	0.88	0.53	1.08	0.18	0.52	0.37	0.88	0.42	0.66	0.23	0.67	0.10	0.44	0.24	1.67	0.26	0.80	0.76	1.70	0.32	1.08	0.70
Ga/Ca	5.04	0.04	1.77	1.62	27.37	1.76	17.61	9.11	2.73	0.04	1.72	0.91	1.78	0.40	0.96	0.59	2.08	1.03	1.50	0.53	1.34	0.18	0.92	0.50	67.61	13.35	42.25	27.30	4.04	0.69	2.44	1.68
Ge	3.20	0.70	1.42	0.60	2.80	1.80	2.23	0.51	1.60	0.40	1.12	0.32	1.40	0.70	0.92	0.29	2.20	1.10	1.57	0.57	1.60	1.00	1.15	0.23	4.00	0.90	2.33	1.56	3.20	0.90	2.10	1.15
Ge/Ca	7.83	1.55	4.39	1.98	7.11	5.34	6.51	1.01	2.81	0.76	2.17	0.47	2.21	1.48	1.70	0.31	5.00	2.58	3.47	1.33	3.08	1.75	2.25	0.46	155.53	84.23	114.43	36.88	6.57	1.85	4.48	2.40
As	30.00	9.80	17.17	5.52	18.10	2.00	5.53	6.53	9.90	3.30	6.13	1.45	24.90	11.70	16.48	5.04	14.20	10.00	11.87	2.14	21.60	10.00	14.95	4.33	62.50	33.60	47.67	14.47	36.60	22.30	28.73	7.26
As/Ca	112.53	18.46	51.70	21.37	58.75	3.65	14.65	19.64	18.88	5.33	11.85	3.39	38.17	21.96	29.56	5.88	31.26	22.26	25.43	5.06	40.26	19.17	28.34	8.16	3046.61	2240.19	2547.14	436.32	72.79	44.51	59.22	14.17
Se	2.20	0.70	1.56	0.44	3.40	2.80	3.10	0.30	1.00	0.40	0.66	0.17	1.20	0.60	0.82	0.24	1.60	1.20	1.43	0.21	2.70	1.70	2.22	0.39	6.70	2.50	4.40	2.13	4.30	2.50	3.23	0.95
Se/Ca	12.25	1.97	4.55	2.25	8.72	7.88	8.35	0.43	1.92	0.61	1.20	0.33	1.75	1.07	1.41	0.33	3.34	2.22	2.94	0.62	4.80	3.21	4.00	0.74	239.50	181.29	211.96	29.23	8.11	5.24	6.28	1.59
Rb	2.30	0.70	1.56	0.47	2.50	2.40	2.43	0.06	1.30	0.50	0.86	0.27	1.20	0.40	0.78	0.36	1.70	1.60	1.67	0.06	1.10	0.80	0.93	0.14	3.80	2.40	3.30	0.78	2.50	1.30	2.03	0.64
Rb/Ca	11.86	1.42	4.16	2.08	7.19	5.14	6.13	1.03	2.56	0.65	1.50	0.63	2.16	0.66	1.29	0.72	3.39	2.74	3.14	0.35	1.88	1.34	1.55	0.24	190.75	125.49	157.05	32.68	4.84	2.27	3.71	1.31
Sr	1140	502	910	151	1780	815	1454	343	1560	1000	1295	155	1380	987	1271	160	1140	972	1057	84	1270	1060	1132	71	110	64	91	24	1310	1160	1237	75
Sr/Ca	2.64	1.79	2.24	0.24	3.18	2.23	2.71	0.32	2.44	1.85	2.10	0.15	2.42	1.58	2.00	0.36	2.00	1.89	1.93	0.06	1.89	1.74	1.83	0.06	4.92	3.54	4.18	0.70	2.34	1.98	2.18	0.19
Y	0.39	0.01	0.10	0.12	1.00	0.09	0.78	0.40	0.08	0.01	0.04	0.02	0.18	0.04	0.11	0.06	0.15	0.08	0.11	0.04	0.20	0.13	0.16	0.03	0.24	0.11	0.18	0.07	0.45	0.17	0.31	0.14
Y/Ca	1.55	0.02	0.31	0.41	2.15	0.22	1.38	0.71	0.11	0.02	0.06	0.02	0.23	0.07	0.17	0.07	0.25	0.15	0.19	0.05	0.31	0.20	0.26	0.04	8.40	7.62	8.02	0.39	0.84	0.29	0.54	0.28
Zr	2.80	0.80	1.84	0.50	1.70	1.00	1.16	0.29	4.40	1.80	3.16	0.71	3.50	2.50	3.04	0.48	2.60	2.20	2.37	0.21	2.90	2.40	2.63	0.18	0.10	0.10	0.10	0.00	2.50	2.10	2.23	0.23
Zr/Ca	5.33	3.75	4.25	0.42	4.04	1.50	2.24	0.99	6.19	3.51	4.88	0.75	4.82	4.21	4.52	0.27	4.30	3.98	4.15	0.16	4.41	3.67	4.10	0.29	7.45	3.09	4.82	2.31	4.54	3.43	3.80	0.64
Mo	0.60	0.04	0.25	0.14	1.18	0.19	0.88	0.32	0.33	0.14	0.23	0.05	0.50	0.19	0.32	0.15	0.23	0.08	0.15	0.08	0.43	0.13	0.25	0.11	6.65	1.88	3.59	2.66	0.51	0.23	0.36	0.14
Mo/Ca	1.15	0.08	0.57	0.30	2.65	0.44	1.52	0.61	0.54	0.19	0.35	0.08	0.80	0.26	0.47	0.26	0.35	0.14	0.24	0.11	0.63	0.20	0.37	0.16	195.64	83.18	137.31	56.35	0.79	0.36	0.58	0.22
Ag	1.03	0.00	0.25	0.29	9.30	0.20	1.33	2.60	0.16	0.02	0.07	0.03	0.04	0.00	0.02	0.02	0.03	0.00	0.01	0.02	0.92	0.10	0.25	0.33	0.04	0.00	0.02	0.02	0.12	0.05	0.08	0.03
Ag/Ca	2.42	0.00	0.49	0.63	12.38	0.25	2.08	3.58	0.21	0.02	0.09	0.05	0.05	0.00	0.02	0.02	0.05	0.00	0.02	0.03	1.19	0.14	0.33	0.42	1.64	0.05	0.95	0.81	0.16	0.07	0.12	0.04
Cd	5.72	0.29	1.45	1.36	65.60	2.30	20.01	20.00	0.19	0.07	0.13	0.03	1.33	0.10	0.48	0.51	1.02	0.58	0.77	0.22	6.20	1.48	3.14	1.75	0.16	0.05	0.12	0.06	0.22	0.08	0.16	0.07
Cd/Ca	10.20	0.79	2.59	2.24	143.51	2.83	35.32	42.01	0.32	0.10	0.17	0.07	1.36	0.14	0.54	0.51	1.50	0.75	1.11	0.37	8.22	1.67	4.05	2.41	4.46	3.02	3.83	0.74	0.29	0.12	0.22	0.09
Sn	33.00	0.05	4.06	8.19	1.67	0.54	0.98	0.60	0.25	0.05	0.08	0.05	2.50	0.11	0.96	0.99	0.66	0.08	0.37	0.29	3.26	1.10	2.17	0.72	0.05	0.05	0.05	0.00	0.26	0.05	0.16	0.11
Sn/Ca	44.22	0.08	6.22	11.39	2.57	1.34	1.96	0.87	0.33	0.05	0.10	0.07	2.65	0.14	1.03	1.02	0.81	0.11	0.49	0.35	3.48	1.33	2.57	0.74	2.86	1.19	1.85	0.89	0.33	0.06	0.21	0.14
Sb	1.20	0.02	0.15	0.29	2.00	0.02	1.51	0.90	0.03	0.02	0.02	0.00	0.05	0.02	0.04	0.01	0.02	0.02	0.02	0.00	0.05	0.03	0.04	0.01	0.02	0.02	0.02	0.00	0.10	0.04	0.06	0.03
Sb/Ca	1.39	0.03	0.21	0.36	3.13	0.03	1.93	1.19	0.03	0.02	0.03	0.00	0.05	0.02	0.04	0.01	0.03	0.02	0.03	0.00	0.05	0.04	0.05	0.01	1.12	0.46	0.72	0.35	0.14	0.05	0.08	0.05
Te	0.65	0.21	0.42	0.11	3.00	0.41	1.04	0.66	0.93	0.38	0.71	0.18	0.73	0.51	0.62	0.10	0.54	0.42	0.49	0.06	0.65	0.48	0.56	0.06	0.42	0.11	0.21	0.18	0.74	0.49	0.65	0.14
Te/Ca	1.20	0.39	0.72	0.20	4.32	0.71	1.36	0.96	1.12	0.46	0.79	0.17	0.71	0.61	0.66	0.04	0.65	0.56	0.61	0.04	0.76	0.54	0.62	0.08	9.29	3.08	6.08	3.11	0.93	0.57	0.79	0.19
Ba	138.00	37.60	65.84	26.77	111.00	48.00	83.57	20.02	36.70	12.20	21.23	6.02	51.70	26.50	38.08	10.95	81.30	51.00	68.67	15.76	64.80	36.10	44.60	10.30	156.00	37.50	100.17	59.54	118.00	27.80	73.17	45.10
Ba/Ca	0.17	0.06	0.10	0.04	0.20	0.07	0.10	0.04	0.04	0.01	0.02	0.01	0.05	0.03	0.04	0.01	0.10	0.06	0.08	0.02	0.07	0.04	0.05	0.01	3.21	1.86	2.62	0.69	0.13	0.03	0.08	0.05
La					10.00	10.00	10.00	0.00																								
La/Ca					13.74	9.85	11.23	1.71																								
Ce	15.60	4.80	8.88	2.72	14.30	11.50	12.87	1.40	3.83	1.44	2.44	0.66	9.04	3.02	5.64	2.92	8.20	4.60	6.45	1.80	8.74	6.13	7.23	1.01	17.10	5.00	11.40	6.08	11.40	3.48	7.65	3.98
Ce/Ca	18.45	8.42	13.60	3.18	22.47	17.69	19.61	2.52	4.28	1.20	2.55	0.91	8.53	3.31	5.35	2.44	9.65	5.60	7.36	2.08	8.71	5.55	7.35	1.16	344.51	242.44	298.67	51.82	12.12	3.71	8.46	4.31
Nd	0.09	0.02	0.04	0.02	0.25	0.10	0.17	0.08	0.06	0.02	0.03	0.01	0.11	0.02	0.07	0.04	0.05	0.04	0.04	0.01	0.12	0.07	0.09	0.02	0.22	0.07	0.15	0.08	0.58	0.17	0.38	0.21
Nd/Ca	0.26	0.02	0.07	0.06	0.37	0.17	0.25	0.11	0.05	0.02	0.03	0.01	0.09	0.02	0.06	0.03	0.06	0.04	0.05	0.01	0.12	0.07	0.09	0.02	5.46	3.13	3.96	1.30	0.67	0.18	0.41	0.25
Dy	0.04	0.00	0.01	0.01	0.02	0.01	0.01	0.00	0.01	0.00	0.01	0.00	0.02	0.00	0.02	0.01	0.02	0.01	0.01	0.01	0.02	0.01	0.02	0.00	0.04	0.01	0.03	0.02	0.09	0.03	0.06	0.03
Dy/Ca	0.09	0.00	0.02	0.02	0.02	0.01	0.02	0.00	0.01	0.00	0.00	0.00	0.02	0.00	0.01	0.01	0.02	0.01	0.01	0.01	0.02	0.01	0.01	0.00	0.90	0.54	0.72	0.18	0.09	0.03	0.06	0.03
W					10.00	10.00	10.00	0.00																								
W/Ca					10.38	7.44	8.48	1.29																								
Re	0.01	0.00	0.00	0.00	0.00	0.00	0.00	0.00	0.00	0.00	0.00	0.00	0.00	0.00	0.00	0.00	0.00	0.00	0.00	0.00	0.00	0.00	0.00	0.00	0.00	0.00	0.00	0.00	0.01	0.00	0.00	0.00
Re/Ca	9.90	0.82	3.23	2.36	3.96	1.16	2.36	1.44	2.01	0.61	1.02	0.46	1.51	0.62	0.89	0.36	2.66	0.92	1.71	0.88	1.60	0.68	1.02	0.41	76.88	45.48	65.11	17.11	4.45	0.80	2.28	1.92
Au	0.00	0.00	0.00	0.00	0.00	0.00	0.00	0.00	0.01	0.00	0.00	0.00	0.00	0.00	0.00	0.00	0.00	0.00	0.00	0.00	0.00	0.00	0.00	0.00	0.00	0.00	0.00	0.00	0.00	0.00	0.00	0.00

Au/Ca	4.01	0.36	1.03	1.01	0.62	0.46	0.55	0.08	6.33	0.28	0.68	1.15	0.86	0.29	0.54	0.25	0.43	0.37	0.41	0.03	2.33	0.71	1.59	0.65	17.24	7.16	11.16	5.35	0.91	0.38	0.57	0.30
Hg																																
Hg/Ca																																
Tl																																
Tl/Ca					1.87	1.34	1.53	0.23																								
Pb	11.50	0.60	2.94	2.69	2.00	0.89	1.75	0.46	3.37	0.20	1.19	1.00	2.60	0.12	1.15	1.13	0.56	0.34	0.43	0.12	1.47	0.94	1.25	0.17	0.83	0.20	0.62	0.36	6.15	3.12	4.76	1.53
Pb/Ca	8.83	0.58	3.18	2.64	1.84	0.93	1.38	0.30	1.91	0.16	0.74	0.56	1.58	0.09	0.69	0.65	0.40	0.27	0.33	0.06	0.91	0.65	0.85	0.10	14.16	6.56	10.68	3.84	4.42	2.25	3.56	1.15
Bi					2.00	2.00	2.00	0.00																								
Bi/Ca					1.83	1.31	1.49	0.23																								
U	1.30	0.20	0.52	0.37	10.00	0.50	7.64	4.27	0.30	0.10	0.14	0.07	0.30	0.10	0.20	0.07	0.20	0.10	0.17	0.06	0.40	0.30	0.38	0.04	0.20	0.10	0.13	0.06	0.40	0.30	0.37	0.06
U/Ca	2.32	0.15	0.55	0.53	8.02	0.45	5.04	2.86	0.21	0.05	0.08	0.04	0.19	0.06	0.12	0.05	0.14	0.07	0.11	0.04	0.25	0.19	0.23	0.02	3.01	1.19	2.35	1.01	0.28	0.19	0.24	0.05

Table 14.8. Spines Mg-calcite trace and rare elemental geochemistry results classified using latitude and class.

	SPINES															
	TROPICAL				TEMPERATE				ANTARCTIC				TEMPERATE			
	Echinoidea				Echinoidea				Echinoidea				Ophiuroidea			
Symbol	**max.**	**min.**	**avg**	**SD**	**max.**	**min.**	**avg**	**SD**	**max.**	**min.**	**avg**	**SD**	**max.**	**min.**	**avg**	**SD**
Ca	365	252	318	42	406	307	368	43	408	99	262	85	282	282	282	0
Li	4.70	2.90	3.98	0.64	7.20	5.60	6.24	0.67	8.70	7.30	7.77	0.81	2.90	2.90	2.90	0.00
Li/Ca	0.08	0.06	0.07	0.01	0.11	0.09	0.10	0.01	0.12	0.12	0.12	0.00	0.06	0.06	0.06	0.00
Be									0.50	0.50	0.50	0.00				
Be/Ca									0.02	0.01	0.01	0.00				
B	61.00	34.00	46.50	9.93	56.00	42.00	49.00	5.92	73.00	25.00	44.27	12.51	73.00	73.00	73.00	0.00
B/Ca	0.72	0.38	0.55	0.14	0.64	0.38	0.50	0.09	1.54	0.40	0.69	0.32	0.96	0.96	0.96	0.00
Mg	39	7	23	17	15	11	13	2	12	4	8	2	33	33	33	0
Mg/Ca	205	36	118	82	82	45	62	15	85	31	55	16	194	194	194	0
Al									0.13	0.01	0.04	0.04				
Al/Ca									1.96	0.06	0.38	0.65				
P									0.02	0.00	0.01	0.00				
P/Ca									0.22	0.02	0.06	0.07				
S									0.51	0.15	0.38	0.12				
S/Ca									2.85	1.74	2.14	0.45				
K	700	300	467	186	200	200	200	0	300	100	191	70	2700	2700	2700	0
K/Ca	2.44	0.84	1.55	0.74	0.67	0.50	0.56	0.07	3.12	0.43	0.89	0.76	9.81	9.81	9.81	0.00
Sc	1.00	0.10	0.48	0.43	0.90	0.70	0.80	0.07	1.10	0.90	1.00	0.04	0.70	0.70	0.70	0.00
Sc/Ca	2.82	0.25	1.33	1.18	2.37	1.54	1.97	0.36	9.04	2.22	3.88	1.84	2.21	2.21	2.21	0.00
Ti									0.01	0.01	0.01	0.00				
Ti/Ca									0.08	0.03	0.04	0.02				
V	17.00	1.00	8.83	8.23	16.00	6.00	12.40	4.16	20.00	1.00	5.36	6.96	13.00	13.00	13.00	0.00
V/Ca	0.04	0.00	0.02	0.02	0.04	0.01	0.03	0.01	0.04	0.00	0.01	0.01	0.04	0.04	0.04	0.00
Cr	12.90	1.50	6.58	5.41	10.20	8.30	9.50	0.71	46.00	1.00	7.35	13.24	12.80	12.80	12.80	0.00
Cr/Ca	0.03	0.00	0.02	0.01	0.03	0.02	0.02	0.00	0.09	0.00	0.02	0.02	0.03	0.03	0.03	0.00
Mn	5.00	1.00	2.50	1.76	4.00	1.00	1.60	1.34	19.00	1.00	8.09	5.75	16.00	16.00	16.00	0.00
Mn/Ca	0.01	0.00	0.01	0.00	0.01	0.00	0.00	0.00	0.14	0.00	0.03	0.04	0.04	0.04	0.04	0.00
Fe	1300	400	900	443	1400	1300	1380	45	2500	100	882	839	600	600	600	0
Fe/Ca	2.95	1.14	2.00	0.91	3.04	2.47	2.72	0.27	13.83	0.30	2.86	3.92	1.53	1.53	1.53	0.00
Co	0.60	0.20	0.43	0.19	0.50	0.50	0.50	0.00	1.00	0.50	0.90	0.20	0.40	0.40	0.40	0.00
Co/Ca	1.29	0.54	0.91	0.36	1.11	0.84	0.94	0.12	6.90	0.94	2.78	1.60	0.96	0.96	0.96	0.00
Ni	12.60	6.40	9.88	2.15	13.10	11.10	12.30	0.90	15.00	1.00	5.85	5.35	7.70	7.70	7.70	0.00
Ni/Ca	0.02	0.02	0.02	0.00	0.02	0.02	0.02	0.00	0.04	0.00	0.02	0.01	0.02	0.02	0.02	0.00
Cu	1	0	1	0	1	0	0	0	6	0	3	2	3	3	3	0
Cu/Ca	0.00	0.00	0.00	0.00	0.00	0.00	0.00	0.00	0.02	0.00	0.01	0.01	0.01	0.01	0.01	0.00
Zn	7	1	3	2	8	3	5	2	68	15	42	16	16	16	16	0
Zn/Ca	0.01	0.00	0.01	0.00	0.01	0.00	0.01	0.00	0.19	0.04	0.11	0.05	0.03	0.03	0.03	0.00
Ga	2.73	0.02	1.13	1.23	2.23	1.57	1.96	0.24	10.00	2.03	7.87	3.64	1.45	1.45	1.45	0.00
Ga/Ca	4.97	0.04	1.98	2.21	4.18	2.22	3.13	0.71	58.30	3.23	21.77	15.51	2.96	2.96	2.96	0.00
Ge	2.00	0.10	1.05	0.81	1.60	1.40	1.52	0.08	2.10	1.70	1.90	0.20	2.80	2.80	2.80	0.00
Ge/Ca	3.49	0.22	1.78	1.38	2.70	1.90	2.31	0.34	2.90	2.60	2.78	0.16	5.48	5.48	5.48	0.00
As	9.70	4.60	6.05	2.01	7.40	4.00	5.46	1.49	8.20	2.00	3.59	2.73	66.50	66.50	66.50	0.00
As/Ca	16.37	6.82	10.23	3.30	10.60	5.38	8.05	2.35	11.53	4.44	6.92	3.29	126.15	126.15	126.15	0.00
Se	0.70	0.50	0.58	0.10	0.80	0.20	0.56	0.25	0.80	0.40	0.60	0.20	1.40	1.40	1.40	0.00
Se/Ca	1.21	0.70	0.94	0.20	1.16	0.30	0.78	0.36	1.12	0.50	0.82	0.31	2.52	2.52	2.52	0.00
Rb	0.30	0.20	0.23	0.05	0.10	0.10	0.10	0.00	0.20	0.10	0.13	0.06	1.10	1.10	1.10	0.00
Rb/Ca	0.56	0.26	0.36	0.13	0.15	0.12	0.13	0.02	0.23	0.13	0.16	0.06	1.83	1.83	1.83	0.00
Sr	1770	1080	1475	288	1500	1310	1414	92	1500	425	1097	271	1390	1390	1390	0
Sr/Ca	2.46	1.80	2.12	0.29	1.95	1.64	1.77	0.11	2.35	1.56	1.97	0.29	2.25	2.25	2.25	0.00
Y	0.04	0.02	0.03	0.01	0.05	0.01	0.03	0.02	1.00	0.02	0.73	0.45	0.08	0.08	0.08	0.00
Y/Ca	0.06	0.02	0.04	0.01	0.07	0.01	0.04	0.03	4.57	0.02	1.64	1.30	0.13	0.13	0.13	0.00
Zr	4.60	2.60	3.82	0.87	5.80	4.70	5.18	0.42	5.90	1.00	2.21	2.08	2.70	2.70	2.70	0.00
Zr/Ca	6.26	4.26	5.24	0.84	6.73	5.63	6.22	0.42	6.45	0.00	3.15	2.28	4.21	4.21	4.21	0.00
Mo	0.20	0.04	0.11	0.06	0.10	0.06	0.08	0.02	1.00	0.06	0.75	0.43	0.33	0.33	0.33	0.00
Mo/Ca	0.28	0.05	0.14	0.09	0.14	0.06	0.10	0.03	4.24	0.07	1.54	1.18	0.49	0.49	0.49	0.00
Ag	0.01	0.00	0.00	0.00	0.00	0.00	0.00	0.00	0.20	0.00	0.15	0.09	0.17	0.17	0.17	0.00
Ag/Ca	0.01	0.00	0.01	0.00	0.00	0.00	0.00	0.00	0.75	0.00	0.27	0.22	0.23	0.23	0.23	0.00
Cd	0.23	0.13	0.18	0.04	0.28	0.04	0.14	0.11	1.10	0.23	0.57	0.27	0.12	0.12	0.12	0.00
Cd/Ca	0.33	0.13	0.20	0.07	0.33	0.04	0.15	0.12	2.17	0.23	0.94	0.63	0.15	0.15	0.15	0.00
Sn	0.05	0.05	0.05	0.00	0.20	0.05	0.10	0.06	0.05	0.05	0.05	0.00	0.05	0.05	0.05	0.00

Sn/Ca	0.07	0.05	0.05	0.01	0.22	0.04	0.10	0.07	0.05	0.04	0.04	0.00	0.06	0.06	0.06	0.00
Sb	0.13	0.02	0.04	0.04	0.03	0.02	0.02	0.00	2.00	0.02	1.46	0.92	0.02	0.02	0.02	0.00
Sb/Ca	0.12	0.02	0.04	0.04	0.03	0.02	0.02	0.00	6.67	0.02	2.39	1.91	0.02	0.02	0.02	0.00
Te	1.26	0.37	0.82	0.44	1.01	0.83	0.95	0.07	2.00	0.85	1.07	0.31	0.84	0.84	0.84	0.00
Te/Ca	1.25	0.40	0.80	0.40	0.94	0.72	0.81	0.08	3.19	0.74	1.47	0.79	0.94	0.94	0.94	0.00
Ba	46.60	8.20	31.85	14.82	27.70	19.50	23.50	2.95	37.00	16.00	24.89	8.61	114.00	114.00	114.00	0.00
Ba/Ca	0.04	0.01	0.03	0.01	0.02	0.01	0.02	0.00	0.05	0.02	0.03	0.01	0.12	0.12	0.12	0.00
La									10.00	10.00	10.00	0.00				
La/Ca									29.27	11.97	14.40	6.02				
Ce	6.10	0.84	3.71	1.94	2.90	2.12	2.57	0.31	3.82	2.75	3.32	0.54	16.20	16.20	16.20	0.00
Ce/Ca	5.52	0.67	3.37	1.70	2.60	1.52	2.03	0.40	2.69	2.18	2.51	0.29	16.43	16.43	16.43	0.00
Nd	0.02	0.02	0.02	0.00	0.03	0.02	0.02	0.00	0.02	0.02	0.02	0.00	0.05	0.05	0.05	0.00
Nd/Ca	0.02	0.02	0.02	0.00	0.03	0.01	0.02	0.01	0.02	0.01	0.01	0.00	0.05	0.05	0.05	0.00
Dy	0.01	0.00	0.00	0.00	0.01	0.00	0.00	0.00	0.01	0.01	0.01	0.00	0.01	0.01	0.01	0.00
Dy/Ca	0.01	0.00	0.00	0.00	0.01	0.00	0.00	0.00	0.00	0.00	0.00	0.00	0.01	0.01	0.01	0.00
W									10.00	10.00	10.00	0.00				
W/Ca									22.11	9.05	10.88	4.55				
Re	0.00	0.00	0.00	0.00	0.00	0.00	0.00	0.00	0.00	0.00	0.00	0.00	0.01	0.01	0.01	0.00
Re/Ca	1.36	0.59	0.80	0.29	1.91	0.53	1.43	0.53	1.78	1.06	1.34	0.39	4.58	4.58	4.58	0.00
Au	0.00	0.00	0.00	0.00	0.00	0.00	0.00	0.00	0.00	0.00	0.00	0.00	0.00	0.00	0.00	0.00
Au/Ca	0.73	0.28	0.38	0.17	0.33	0.25	0.28	0.03	1.40	0.28	0.67	0.63	0.36	0.36	0.36	0.00
Hg									1.00	1.00	1.00	0.00				
Hg/Ca									2.03	0.83	1.00	0.42				
Tl									2.00	2.00	2.00	0.00				
Tl/Ca									3.98	1.63	1.96	0.82				
Pb	0.42	0.04	0.22	0.15	5.30	0.08	1.87	2.43	2.00	0.05	1.57	0.79	0.41	0.41	0.41	0.00
Pb/Ca	0.26	0.02	0.14	0.09	3.03	0.04	1.01	1.35	3.92	0.03	1.47	1.05	0.28	0.28	0.28	0.00
Bi									2.00	2.00	2.00	0.00	0.00			
Bi/Ca									3.89	1.59	1.91	0.80	0.00			
U	0.20	0.10	0.12	0.04	0.10	0.10	0.10	0.00	10.00	0.10	7.30	4.62	0.40	0.40	0.40	0.00
U/Ca	0.13	0.05	0.06	0.03	0.05	0.04	0.05	0.01	17.08	0.04	6.12	4.88	0.24	0.24	0.24	0.00

Table 14.9. Plates and calcareous ring Mg-calcite trace and rare elemental geochemistry results classified using latitude and class.

	PLATES + CALCAREOUS RING																											
	ANTARCTIC				TROPICAL				TEMPERATE				ANTARCTIC				TROPICAL				ANTARCTIC				ANTARCTIC			
	Asteroidea				Echinoidea				Echinoidea				Echinoidea				Ophiuroidea				Ophiuroidea				Holothuroidea			
Symbol	**max.**	**min.**	**avg**	**SD**	**max.**	**min.**	**avg**	**SD**	**max.**	**min.**	**avg**	**SD**	**max.**	**min.**	**avg**	**SD**	**max.**	**min.**	**avg**	**SD**	**max.**	**min.**	**avg**	**SD**	**max.**	**min.**	**avg**	**SD**
Ca	316	204	225	26	370	238	321	56	405	321	362	29	344	202	244	46	194	194	194	#¡DIV/0!	225	216	221	4	646	286	379	178
Li					5.30	3.40	4.05	0.72	7.70	5.80	6.80	0.74	6.80	6.10	6.47	0.35	2.00	2.00	2.00	0.00								
Li/Ca					0.08	0.06	0.07	0.01	0.13	0.10	0.11	0.01	0.11	0.11	0.11	0.00	0.06	0.06	0.06	0.00								
Be	0.50	0.50	0.50	0.00	0.00	0.00	0.00	0.00	0.00	0.00	0.00	0.00	0.50	0.50	0.50	0.00	0.00	0.00	#¡DIV/0!	#¡DIV/0!	0.50	0.50	0.50	0.00	0.50	0.50	0.50	0.00
Be/Ca	0.01	0.01	0.01	0.00									0.01	0.01	0.01	0.00					0.01	0.01	0.01	0.00				
B	60.00	34.00	44.03	5.93	65.00	38.00	51.17	9.91	89.00	58.00	75.17	11.86	83.00	32.00	49.88	16.90	50.00	50.00	50.00	0.00	39.00	35.00	37.50	1.91	63.00	30.00	42.25	14.36
B/Ca	1.01	0.55	0.73	0.12	0.86	0.38	0.62	0.21	0.90	0.64	0.77	0.10	0.97	0.52	0.75	0.16	0.96	0.96	0.96	0.00	0.65	0.59	0.63	0.03	0.49	0.36	0.43	0.06
Mg	26	21	23	1	36	16	26	10	29	25	28	2	19	14	16	2	21	21	21	0	23	21	22	1	52	25	33	13
Mg/Ca	189	133	172	14	160	89	130	29	142	109	128	11	145	85	111	17	179	179	179	0	170	163	167	3	155	133	145	9
Al	0.14	0.01	0.04	0.04									0.01	0.01	0.01	0.00					0.01	0.01	0.01	0.00	0.03	0.01	0.02	0.01
Al/Ca	0.98	0.05	0.26	0.25									0.07	0.06	0.07	0.00					0.07	0.07	0.07	0.00	0.07	0.05	0.06	0.01
P	0.03	0.01	0.02	0.00									0.01	0.00	0.00	0.00					0.01	0.01	0.01	0.00	0.02	0.01	0.01	0.01
P/Ca	0.17	0.06	0.10	0.03									0.04	0.01	0.03	0.01					0.05	0.04	0.05	0.01	0.05	0.04	0.04	0.01
S	0.52	0.42	0.46	0.02									0.48	0.37	0.44	0.04					0.44	0.42	0.43	0.01	0.96	0.46	0.59	0.25
S/Ca	2.74	2.06	2.56	0.16									2.72	2.10	2.46	0.21					2.48	2.40	2.44	0.03	2.01	1.86	1.97	0.07
K	300	200	235	48	2700	200	1150	1037	1100	300	433	327	400	100	219	98	4000	4000	4000	0	200	200	200	0	500	200	275	150
K/Ca	1.47	0.92	1.08	0.20	11.63	0.56	4.31	4.43	3.31	0.76	1.25	1.01	1.25	0.45	0.89	0.24	21.14	21.14	21.14	0.00	0.95	0.91	0.93	0.02	0.79	0.70	0.73	0.04
Sc	1.00	1.00	1.00	0.00	0.80	0.10	0.48	0.32	0.90	0.70	0.78	0.08	1.60	1.00	1.07	0.17	0.90	0.90	0.90	0.00	1.00	1.00	1.00	0.00	1.00	1.00	1.00	0.00
Sc/Ca	4.37	2.82	4.01	0.38	1.94	0.29	1.27	0.70	2.35	1.54	1.95	0.32	4.41	2.92	3.94	0.33	4.14	4.14	4.14	0.00	4.13	3.96	4.04	0.07	3.12	1.38	2.66	0.85
Ti	0.01	0.01	0.01	0.00									0.01	0.01	0.01	0.00					0.01	0.01	0.01	0.00	0.01	0.01	0.01	0.00
Ti/Ca	0.04	0.03	0.04	0.00									0.04	0.04	0.04	0.00					0.04	0.04	0.04	0.00	0.03	0.01	0.02	0.01
V	6.00	1.00	2.00	1.33	17.00	1.00	6.67	6.28	11.00	5.00	8.83	2.32	29.00	1.00	5.56	9.92	10.00	10.00	10.00	0.00	1.00	1.00	1.00	0.00	4.00	1.00	1.75	1.50
V/Ca	0.02	0.00	0.01	0.00	0.04	0.00	0.01	0.01	0.02	0.01	0.02	0.01	0.07	0.00	0.01	0.02	0.04	0.04	0.04	0.00	0.00	0.00	0.00	0.00	0.00	0.00	0.00	0.00
Cr	15.00	1.00	3.73	3.36	11.00	2.00	6.53	3.78	11.00	8.70	9.48	0.83	53.50	1.00	6.13	13.46	15.40	15.40	15.40	0.00	1.00	1.00	1.00	0.00	55.00	1.00	14.75	26.84
Cr/Ca	0.05	0.00	0.01	0.01	0.02	0.01	0.01	0.01	0.02	0.02	0.02	0.00	0.12	0.00	0.02	0.03	0.06	0.06	0.06	0.00	0.00	0.00	0.00	0.00	0.07	0.00	0.02	0.03
Mn	45.00	5.00	12.14	9.32	4.00	1.00	2.67	1.03	101.00	2.00	25.33	38.45	31.00	5.00	11.38	8.40	14.00	14.00	14.00	0.00	5.00	5.00	5.00	0.00	295.00	113.00	197.50	75.55
Mn/Ca	0.15	0.01	0.04	0.03	0.01	0.00	0.01	0.00	0.18	0.00	0.05	0.07	0.10	0.02	0.03	0.02	0.05	0.05	0.05	0.00	0.02	0.02	0.02	0.00	0.75	0.13	0.46	0.26
Fe	2300	100	508	592	1300	400	867	441	1400	1200	1300	89	1600	100	356	553	400	400	400	0	100	100	100	0	700	100	350	265
Fe/Ca	7.79	0.25	1.63	1.92	2.53	1.18	1.84	0.68	2.79	2.46	2.58	0.13	3.42	0.31	0.85	1.14	1.48	1.48	1.48	0.00	0.33	0.32	0.33	0.01	1.00	0.24	0.63	0.33
Co	1.00	1.00	1.00	0.00	0.60	0.30	0.47	0.15	0.60	0.50	0.57	0.05	1.00	0.50	0.91	0.19	0.30	0.30	0.30	0.00	1.00	1.00	1.00	0.00	1.00	1.00	1.00	0.00
Co/Ca	3.33	2.15	3.06	0.29	1.14	0.67	0.98	0.22	1.13	1.00	1.06	0.05	3.37	0.99	2.69	0.81	1.05	1.05	1.05	0.00	3.15	3.02	3.09	0.05	2.38	1.05	2.03	0.65
Ni	15.00	1.00	3.32	3.33	12.60	7.50	9.92	2.44	13.90	10.90	12.47	1.14	13.20	1.00	3.26	4.42	7.00	7.00	7.00	0.00	2.00	1.00	1.25	0.50	35.00	1.00	9.75	16.84
Ni/Ca	0.05	0.00	0.01	0.01	0.02	0.02	0.02	0.00	0.03	0.02	0.02	0.00	0.03	0.00	0.01	0.01	0.02	0.02	0.02	0.00	0.01	0.00	0.00	0.00	0.04	0.00	0.01	0.02
Cu	16	1	4	4	1	0	1	0	1	0	1	0	7	0	4	2	8	8	8	0	3	1	2	1	55	6	19	24
Cu/Ca	0.05	0.00	0.01	0.01	0.00	0.00	0.00	0.00	0.00	0.00	0.00	0.00	0.02	0.00	0.01	0.01	0.02	0.02	0.02	0.00	0.01	0.00	0.00	0.00	0.05	0.01	0.03	0.02
Zn	91	11	40	22	7	3	5	2	6	3	4	1	61	4	33	19	39	39	39	0	23	20	21	2	411	9	110	201

Zn/Ca	0.26	0.03	0.11	0.06	0.02	0.00	0.01	0.00	0.01	0.00	0.01	0.00	0.16	0.01	0.09	0.05	0.12	0.12	0.12	0.00	0.06	0.05	0.06	0.00	0.39	0.02	0.11	0.18
Ga	10.00	10.00	10.00	0.00	1.78	0.02	0.91	0.86	2.28	1.60	1.88	0.27	10.00	2.47	8.72	2.77	1.84	1.84	1.84	0.00	10.00	10.00	10.00	0.00	10.00	10.00	10.00	0.00
Ga/Ca	28.18	18.19	25.88	2.42	2.79	0.04	1.47	1.30	3.84	2.27	3.01	0.62	28.46	4.23	22.01	8.30	5.45	5.45	5.45	0.00	26.61	25.55	26.08	0.46	20.10	8.90	17.13	5.49
Ge					1.60	0.20	1.05	0.60	1.80	1.40	1.57	0.16	2.90	1.90	2.53	0.55	3.60	3.60	3.60	0.00								
Ge/Ca					2.41	0.36	1.74	0.79	2.92	2.04	2.41	0.41	4.87	3.12	4.16	0.92	10.25	10.25	10.25	0.00								
As	6.00	2.00	2.19	0.81	11.00	5.60	8.47	1.99	7.80	3.40	5.77	1.78	9.20	2.00	3.12	2.44	122.00	122.00	122.00	0.00	2.00	2.00	2.00	0.00	2.00	2.00	2.00	0.00
As/Ca	12.56	3.73	5.20	1.56	22.25	9.85	14.74	5.53	12.67	5.05	8.54	2.72	14.96	4.63	6.39	3.36	336.42	336.42	336.42	0.00	4.95	4.76	4.85	0.09	3.74	1.66	3.19	1.02
Se					1.20	0.40	0.65	0.29	0.60	0.40	0.52	0.10	0.50	0.20	0.37	0.15	1.50	1.50	1.50	0.00								
Se/Ca					2.56	0.55	1.13	0.75	0.95	0.53	0.73	0.15	0.74	0.30	0.55	0.22	3.92	3.92	3.92	0.00								
Rb					1.00	0.10	0.45	0.37	0.30	0.10	0.15	0.08	0.30	0.20	0.27	0.06	1.60	1.60	1.60	0.00								
Rb/Ca					1.97	0.13	0.76	0.74	0.41	0.12	0.20	0.12	0.43	0.28	0.37	0.08	3.87	3.87	3.87	0.00								
Sr	1820	1350	1494	110	1810	1340	1605	214	1960	1660	1793	117	1750	1170	1421	178	932	932	932	0	1490	1390	1443	43	3330	1580	2038	862
Sr/Ca	3.20	2.63	3.06	0.13	2.58	2.18	2.30	0.15	2.49	2.10	2.27	0.16	2.98	2.33	2.69	0.19	2.20	2.20	2.20	0.00	3.03	2.94	2.99	0.04	2.62	2.36	2.49	0.11
Y	1.00	1.00	1.00	0.00	0.06	0.02	0.03	0.02	0.02	0.01	0.01	0.01	1.00	0.02	0.82	0.39	0.10	0.10	0.10	0.00	1.00	1.00	1.00	0.00	1.00	1.00	1.00	0.00
Y/Ca	2.21	1.43	2.03	0.19	0.11	0.02	0.05	0.03	0.03	0.01	0.02	0.01	2.23	0.03	1.65	0.81	0.23	0.23	0.23	0.00	2.09	2.00	2.04	0.04	1.58	0.70	1.34	0.43
Zr	1.00	1.00	1.00	0.00	5.00	2.80	3.90	1.01	5.20	4.60	4.92	0.26	5.10	1.00	1.74	1.60	1.70	1.70	1.70	0.00	1.00	1.00	1.00	0.00	1.00	1.00	1.00	0.00
Zr/Ca	2.15	1.39	1.98	0.18	5.95	4.48	5.28	0.57	6.43	5.55	5.98	0.36	6.67	1.90	2.82	1.82	3.85	3.85	3.85	0.00	2.03	1.95	1.99	0.04	1.54	0.68	1.31	0.42
Mo	2.00	1.00	1.03	0.16	0.24	0.08	0.15	0.07	0.08	0.05	0.07	0.01	1.00	0.01	0.83	0.37	1.04	1.04	1.04	0.00	1.00	1.00	1.00	0.00	1.00	1.00	1.00	0.00
Mo/Ca	2.64	1.46	1.92	0.19	0.42	0.09	0.21	0.13	0.10	0.06	0.08	0.02	2.07	0.01	1.55	0.71	2.24	2.24	2.24	0.00	1.93	1.86	1.90	0.03	1.46	0.65	1.24	0.40
Ag	3.20	0.20	0.36	0.63	0.04	0.00	0.01	0.02	0.03	0.00	0.01	0.01	0.20	0.00	0.16	0.08	0.65	0.65	0.65	0.00	0.20	0.20	0.20	0.00	0.20	0.20	0.20	0.00
Ag/Ca	5.48	0.24	0.62	1.10	0.06	0.00	0.02	0.02	0.03	0.00	0.01	0.01	0.37	0.00	0.27	0.13	1.25	1.25	1.25	0.00	0.34	0.33	0.34	0.01	0.26	0.12	0.22	0.07
Cd	252.00	2.40	42.97	53.44	0.90	0.11	0.42	0.35	0.22	0.04	0.11	0.07	1.50	0.44	0.78	0.33	4.41	4.41	4.41	0.00	1.50	1.10	1.30	0.18	2.40	0.50	0.98	0.95
Cd/Ca	416.01	4.02	68.64	87.71	1.35	0.11	0.53	0.52	0.21	0.04	0.11	0.07	2.43	0.48	1.21	0.61	8.11	8.11	8.11	0.00	2.48	1.79	2.10	0.31	1.32	0.61	0.79	0.35
Sn					0.05	0.05	0.05	0.00	0.05	0.05	0.05	0.00	0.05	0.05	0.05	0.00	0.05	0.05	0.05	0.00								
Sn/Ca					0.07	0.05	0.05	0.01	0.05	0.04	0.05	0.00	0.05	0.05	0.05	0.00	0.09	0.09	0.09	0.00								
Sb	2.00	2.00	2.00	0.00	0.05	0.02	0.03	0.01	0.11	0.02	0.04	0.03	2.00	0.02	1.63	0.80	0.02	0.02	0.02	0.00	2.00	2.00	2.00	0.00	2.00	2.00	2.00	0.00
Sb/Ca	3.23	2.08	2.96	0.28	0.04	0.02	0.03	0.01	0.11	0.02	0.04	0.04	3.26	0.02	2.41	1.19	0.03	0.03	0.03	0.00	3.05	2.93	2.99	0.05	2.30	1.02	1.96	0.63
Te	2.00	1.00	1.16	0.37	1.28	0.44	0.83	0.41	1.50	1.07	1.20	0.16	1.35	1.00	1.05	0.12	0.62	0.62	0.62	0.00	1.00	1.00	1.00	0.00	1.00	1.00	1.00	0.00
Te/Ca	2.96	0.99	1.64	0.55	1.09	0.45	0.78	0.27	1.31	0.92	1.04	0.14	1.55	1.10	1.37	0.11	1.00	1.00	1.00	0.00	1.45	1.40	1.42	0.03	1.10	0.49	0.94	0.30
Ba	98.00	27.00	54.32	18.18	41.50	30.50	36.63	4.09	39.90	26.30	30.90	5.02	68.20	20.00	30.46	16.16	104.00	104.00	104.00	0.00	56.00	37.00	44.25	8.54	207.00	92.00	123.75	55.57
Ba/Ca	0.11	0.04	0.07	0.02	0.05	0.03	0.03	0.01	0.03	0.02	0.03	0.01	0.06	0.03	0.03	0.01	0.16	0.16	0.16	0.00	0.08	0.05	0.06	0.01	0.10	0.09	0.10	0.00
La	10.00	10.00	10.00	0.00									10.00	10.00	10.00	0.00	10.00	10.00	10.00	0.00	10.00	10.00	10.00	0.00	10.00	10.00	10.00	0.00
La/Ca	14.14	9.13	12.99	1.21									14.28	12.49	12.97	0.50	14.87	14.87	14.87	0.00	13.36	12.82	13.09	0.23	10.09	4.47	8.60	2.76
Ce					4.74	3.16	3.77	0.65	4.27	2.60	3.50	0.56	7.38	4.91	6.53	1.40	14.20	14.20	14.20	0.00								
Ce/Ca					5.70	2.55	3.53	1.28	3.58	2.03	2.79	0.56	6.42	4.18	5.55	1.20	20.94	20.94	20.94	0.00								
Nd					0.03	0.02	0.02	0.00	0.05	0.02	0.03	0.01	0.02	0.02	0.02	0.00	0.03	0.03	0.03	0.00								
Nd/Ca					0.03	0.02	0.02	0.01	0.04	0.01	0.02	0.01	0.02	0.02	0.02	0.00	0.04	0.04	0.04	0.00								
Dy					0.01	0.00	0.00	0.00	0.01	0.00	0.00	0.00	0.01	0.01	0.01	0.00	0.01	0.01	0.01	0.00								
Dy/Ca					0.01	0.00	0.00	0.00	0.00	0.00	0.00	0.00	0.00	0.00	0.00	0.00	0.01	0.01	0.01	0.00								
W	10.00	10.00	10.00	0.00									10.00	10.00	10.00	0.00					10.00	10.00	10.00	0.00	10.00	10.00	10.00	0.00
W/Ca	10.69	6.90	9.81	0.92									10.79	9.44	9.80	0.37					10.09	9.69	9.89	0.17	7.62	3.37	6.50	2.08
Re					0.00	0.00	0.00	0.00	0.00	0.00	0.00	0.00	0.00	0.00	0.00	0.00	0.00	0.00	0.00	0.00								
Re/Ca					1.81	0.58	1.06	0.50	2.39	0.53	1.31	0.60	1.96	1.88	1.92	0.04	4.44	4.44	4.44	0.00								
Au					0.01	0.00	0.00	0.00	0.00	0.00	0.00	0.00	0.00	0.00	0.00	0.00	0.00	0.00	0.00	0.00								

Au/Ca					6.89	0.39	2.84	2.49	0.32	0.25	0.28	0.02	2.72	0.30	1.30	1.27	0.52	0.52	0.52	0.00								
Hg	1.00	1.00	1.00	0.00									1.00	1.00	1.00	0.00					1.00	1.00	1.00	0.00	1.00	1.00	1.00	0.00
Hg/Ca	0.98	0.63	0.90	0.08									0.99	0.86	0.90	0.03					0.93	0.89	0.91	0.02	0.70	0.31	0.60	0.19
Tl	2.00	2.00	2.00	0.00									2.00	2.00	2.00	0.00					2.00	2.00	2.00	0.00	8.00	2.00	3.50	3.00
Tl/Ca	1.92	1.24	1.77	0.17									1.94	1.70	1.76	0.07					1.82	1.74	1.78	0.03	2.43	1.33	1.62	0.54
Pb	2.00	2.00	2.00	0.00	0.24	0.10	0.15	0.05	3.27	0.07	0.88	1.30	2.00	0.11	1.66	0.74	0.55	0.55	0.55	0.00	2.00	2.00	2.00	0.00	2.00	2.00	2.00	0.00
Pb/Ca	1.90	1.22	1.74	0.16	0.13	0.06	0.09	0.02	1.76	0.03	0.47	0.70	1.92	0.06	1.43	0.67	0.55	0.55	0.55	0.00	1.79	1.72	1.75	0.03	1.35	0.60	1.15	0.37
Bi	2.00	2.00	2.00	0.00									2.00	2.00	2.00	0.00					2.00	2.00	2.00	0.00	2.00	2.00	2.00	0.00
Bi/Ca													1.90	1.66	1.72	0.07					1.78	1.70	1.74	0.03	1.34	0.59	1.14	0.37
U	10.00	10.00	10.00	0.00	1.10	0.10	0.27	0.41	0.10	0.10	0.10	0.00	10.00	0.10	8.14	3.99	0.30	0.30	0.30	0.00	10.00	10.00	10.00	0.00	19.00	10.00	12.25	4.50
U/Ca	8.25	5.33	7.58	0.71	0.61	0.05	0.15	0.23	0.05	0.04	0.05	0.00	8.34	0.05	6.16	3.04	0.26	0.26	0.26	0.00	7.80	7.48	7.64	0.13	5.89	4.95	5.60	0.44

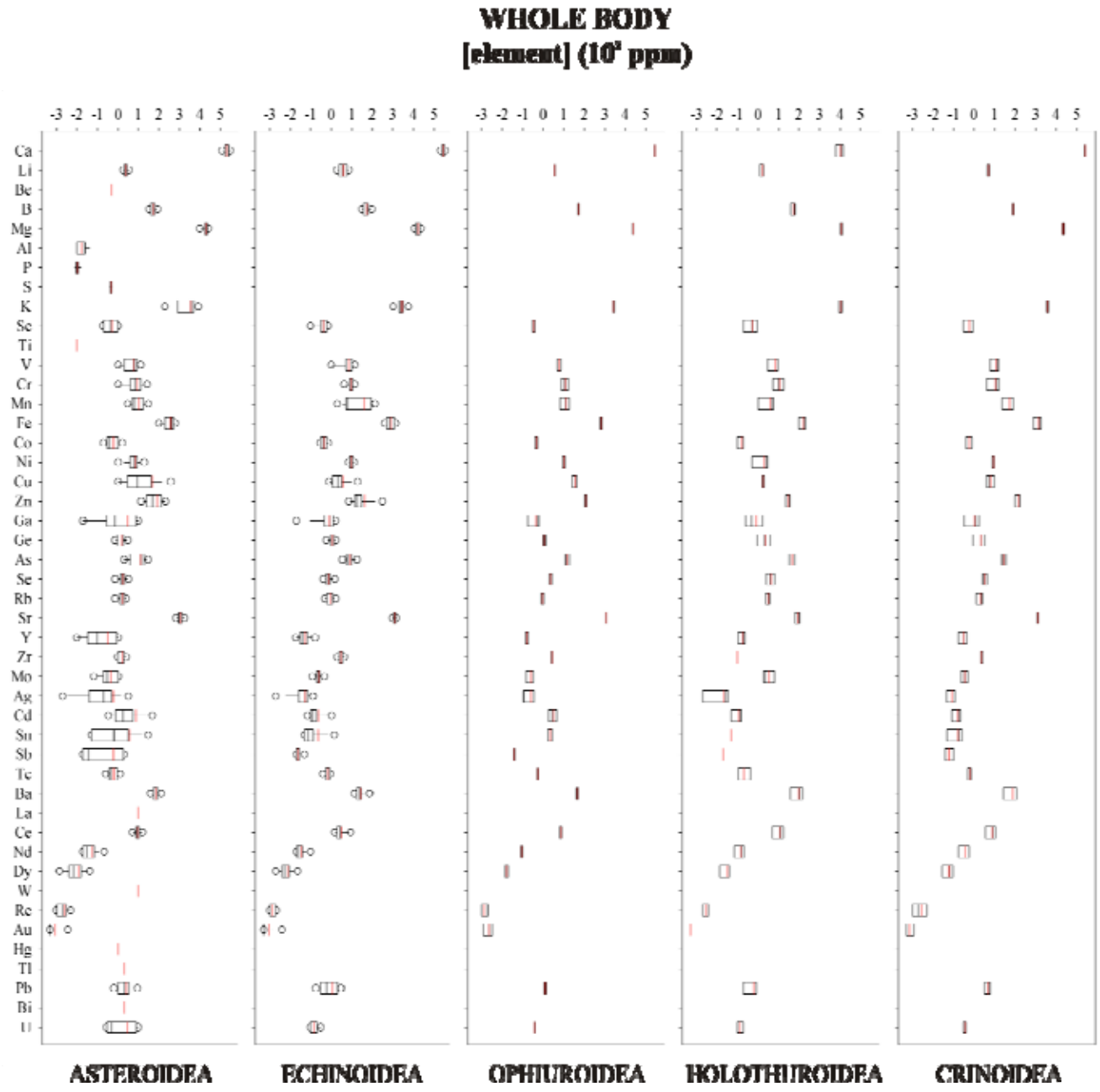

Fig. 14.5. Individual element concentration in whole bodies. Data reported in ppm (10^x, where the x-axis values are the exponent).

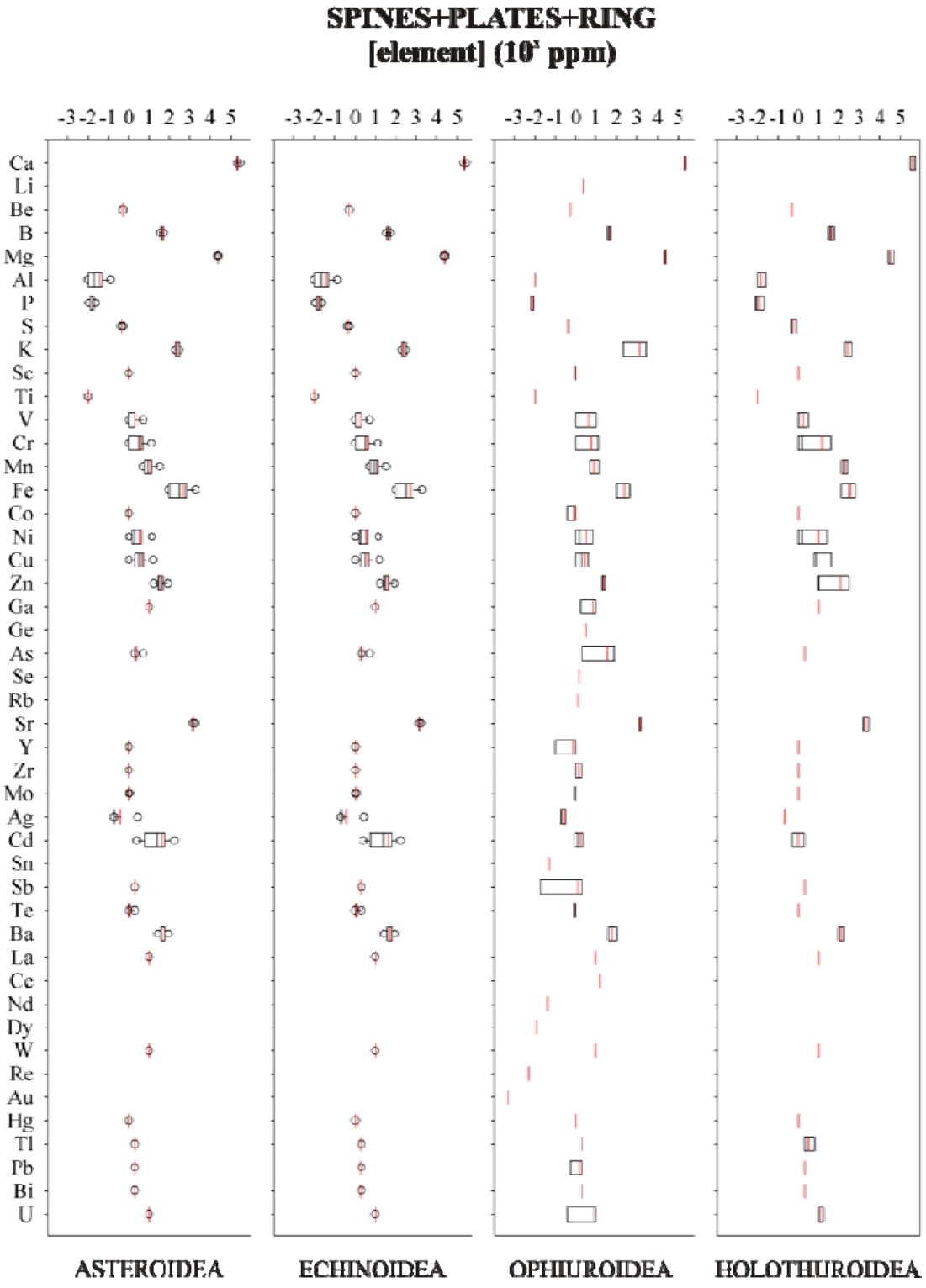

Fig. 14.6. Individual element concentration in spines, plates, and calcareous ring (holothurians only). Data reported in ppm (10^x, where the x-axis values are the exponent).

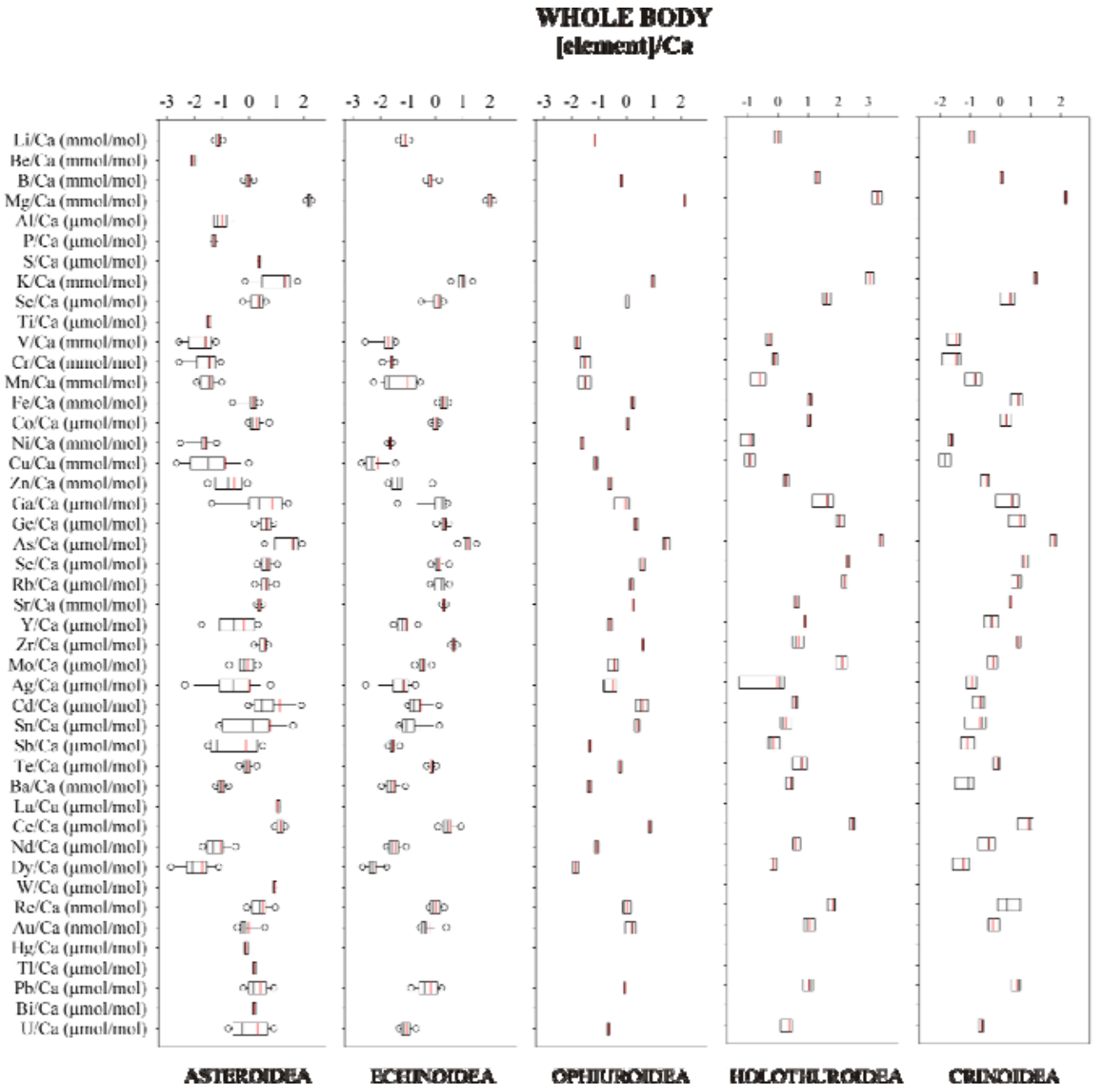

Fig. 14.7. Individual elemental ratios (normalized to Ca^{2+}) in whole bodies. Data reported in xmol/mol, where x is mili (m), micro (µ), or nano (n), depending on elemental concentration.

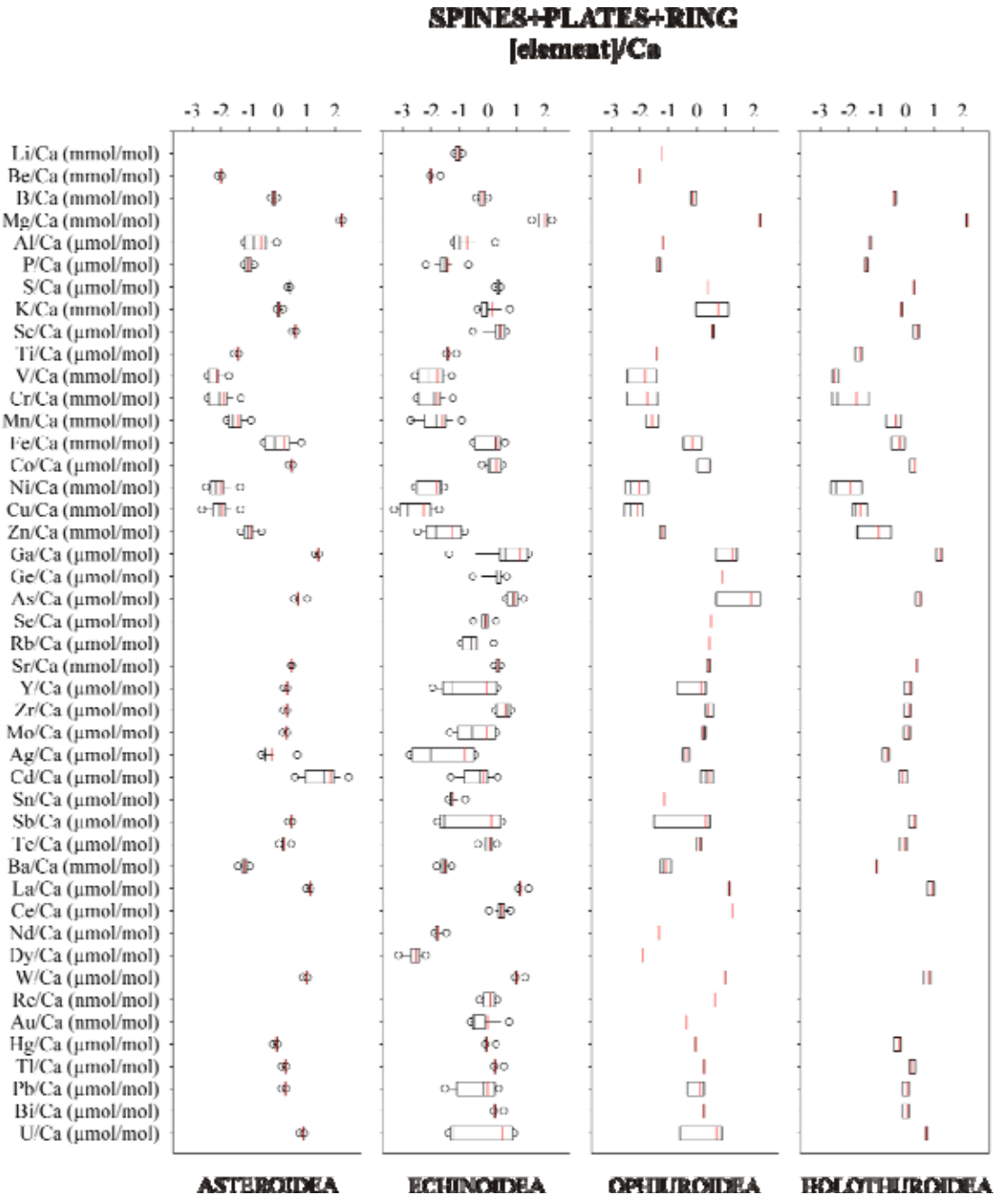

Fig. 14.8. Individual elemental ratios (normalized to Ca^{2+}) in spines, plates, and calcareous ring (holothurians only). Data reported in xmol/mol, where x is mili (m), micro (µ), or nano (n), depending on elemental concentration.

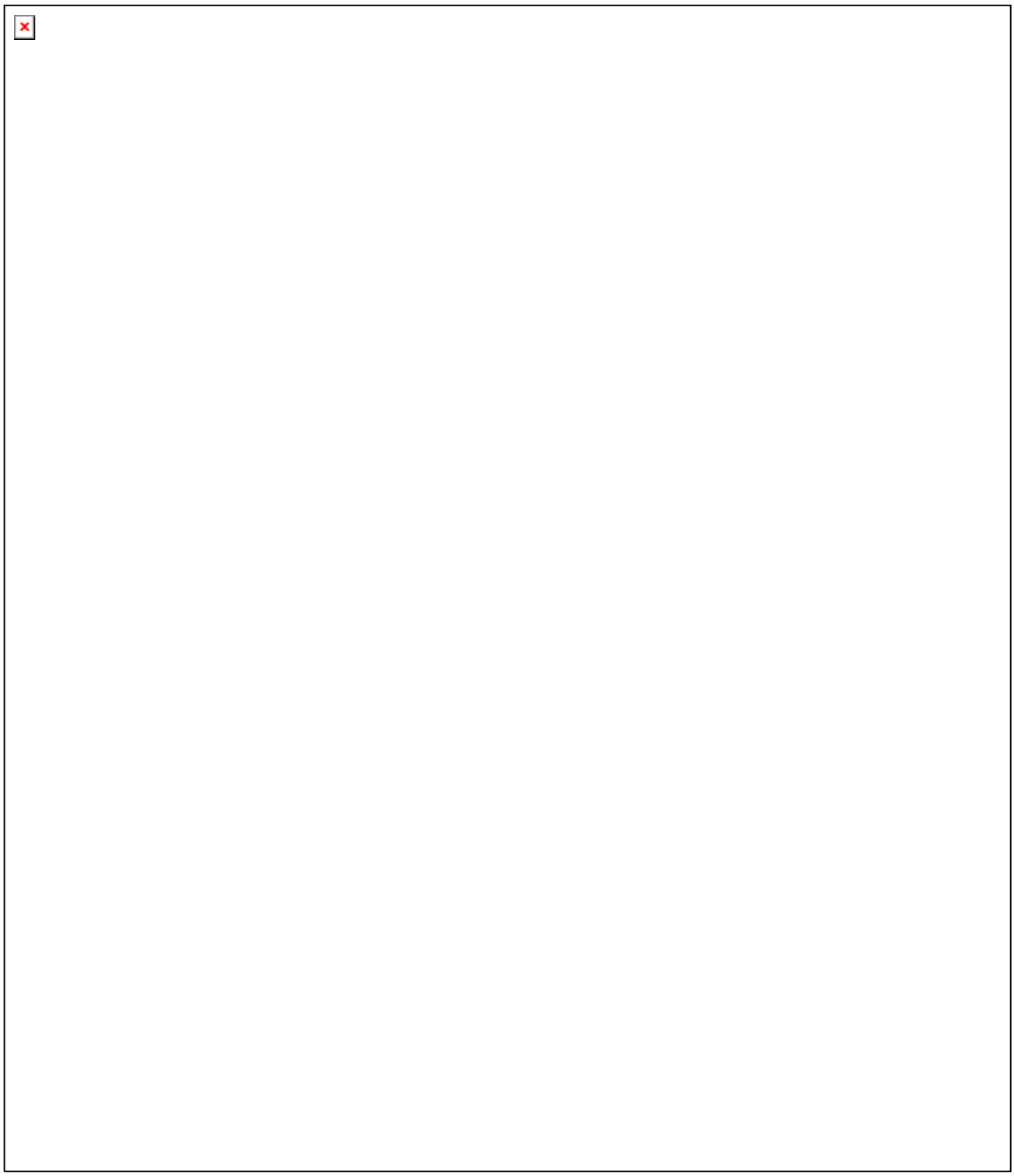

Fig. 14.9. Individual elemental ratios in whole bodies *vs.* latitude. Data reported in xmol/mol, where x is mili (m), micro (μ), or nano (n), depending on elemental concentration.

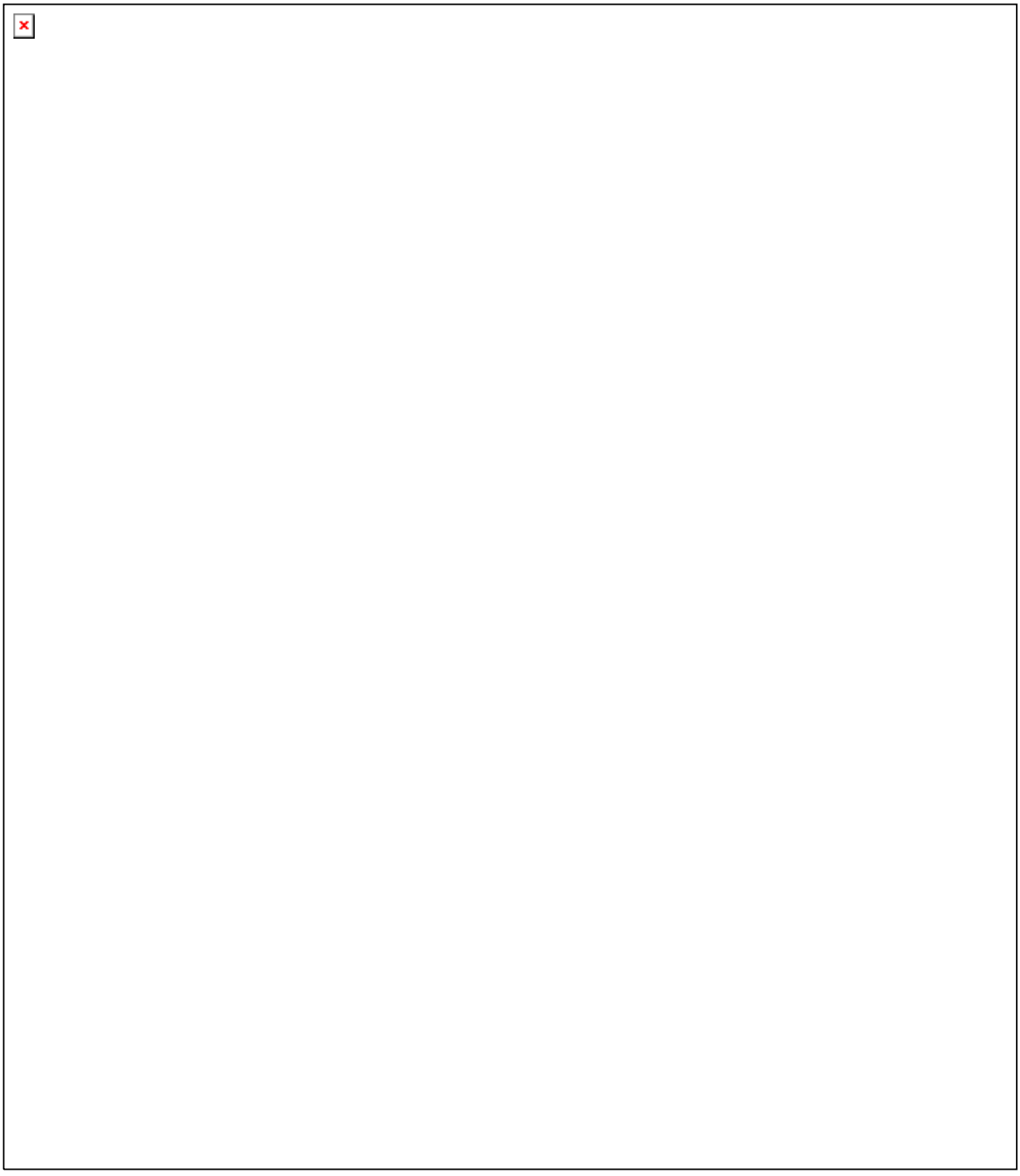

Fig. 14.10. Individual elemental ratios in spines, plates, and calcareous ring (holothurians only) *vs.* latitude. Data reported in xmol/mol, where x is mili (m), micro (μ), or nano (n), depending on elemental concentration.

15.

Seawater saturation state of Mg-calcite reveals imminent ocean acidification risks to marine ecosystems

Abstract

Biogenic calcite, aragonite, and also metastable Mg-calcite (low: < 4 % $MgCO_3$, high: > 4% $MgCO_3$) are secreted by marine organisms in their skeletons. Mg-calcite dominates benthic ecosystems and the sediments, therefore its production and dissolution are relevant in the context of ocean acidification (OA), since Mg-calcite with a certain mol % $MgCO_3$ becomes more soluble than calcite and aragonite alone. The dissolution of carbonates is governed by the seawater saturation state with respect to the skeletal mineral phase (calcite and aragonite) (ΩCal./Arag.), which also changes as a function of the mol % $MgCO_3$ (ΩMg). However, ΩMg estimations are not currently used in empirical and modelling work using species-specific mol % $MgCO_3$ owing to the uncertainties in the calculations. Here, we put together a global dataset of measured (via inductively coupled plasma mass spectrometry, ICP-), skeleton mol % $MgCO_3$ benthic (20 classes) and pelagic (1 class) taxa from 0 to 1200 m in combination with field temperature, salinity and carbonate chemistry. We recovered in situ ambient data combining the GLODAP dataset with the samples meta-data (latitude, longitude, and depth) using a "NEAR 3D" analysis to identify the nearest field

values (temperature, salinity and CO_3^{2-}) to the samples. We then calculated the species-specific ΩMg using the "biogenic cleaned" and "biogenic minimally prepared" curves, using a new set of corrections for in situ pressure, temperature and salinity. Eventually we re-calculated all trends decreasing the modern ocean in situ CO_3^{2-} concentration by 20 and 50 % to simulate future OA scenarios and provide a preliminary species-specific risk assessment. Our results indicate that keystone shelf and slope species in a wide variety of ecosystems are near or already co-habit with transient skeletal mineral undersaturation (ΩMg < 1). ΩMg undersaturation will become permanent in the future in many ecosystems, following the rising CO_2 and decreasing CO_3^{2-} concentrations starting from the poles. Therefore, experimental and modelling ecosystem-based conclusions based on ΩCal. and ΩArag. ignoring the Mg-calcite effect, are likely to derive into misleading conclusions to truly understand the magnitude of OA in the ocean.

This chapter is based on:

Lebrato, M., Andersson, A. J., Ries, J. B., McClintock, J. B., Oschlies, A. and Iglesias-Rodriguez, M. D. in preparation. Seawater saturation state of carbonates in benthic organisms in a high CO_2 world. To be submitted: *PLoS ONE*.

Acknowledgements: We thank Bianca Willie for advise on geostatistical methods and computer help. This work was supported by the "European Project on Ocean Acidification" (EPOCA) for M. Lebrato's PhD.

15.1. Introduction

Marine calcification is a fundamental biological process for pelagic and benthic organisms to construct skeletons and guarantee survival in the ocean. Upon death, the calcite skeletal remains (e.g. tests, exoskeletons, coccoliths) sink in the water column (potentially dissolving) and/or are subsequently deposited directly at the seabed (Hauck et al. 2012), where they undergo early diagenetic alterations involving dissolution, reprecipitation and recrystallization (Morse and Mackenzie 1990; Brunskill et al. 2002; Berelson et al. 2007). Biogenic calcite, aragonite, and also metastable Mg-calcite (low: < 4 % $MgCO_3$, high: > 4% $MgCO_3$) are secreted by organisms, and the Mg^{2+} skeleton content is controlled by several biotic and environmental factors including temperature, salinity, light, carbonate chemistry, food supply/growth rate, and ambient seawater composition (Chave 1954; Weber 1973; Mackenzie and Morse 1983; Ries 2009). The rate of Mg-calcite dissolution is in turn governed by two main factors:

(1) Thermodynamic: The solubility of the skeletal mineral phase and the seawater saturation state with respect to this phase. This is governed by the ambient carbonate chemistry, temperature and salinity as well as the skeletal mol % $MgCO_3$.

(2) Kinetic: Processes such as Mg-calcite microarchitecture (Walter and Morse 1984), dissolved inhibitors (phosphate and Mg^{2+}), and diffusional limitations (Lowenstam 1954; Walter and Morse, 1984; 1985).

Mg-calcite is widely present in the marine environment (Morse et al. 2006), thus its dissolution potential becomes increasingly important in the context of rising CO_2 levels (decreasing CO_3^{2-} concentration), which is termed ocean acidification (OA) (Caldeira and Wickett 2003). The OA effects on marine organisms drive physiological, morphological, and biogeochemical changes that may change ecosystem functioning in the future (Doney et al. 2009). The few studies targetting organisms Mg-calcite mineralogy response to high CO_2, suggest a variable response (Ries 2011), which in some cases could increase skeletal susceptibility to dissolution. There are concerns that some benthic ecosystems may already live at a "limiting" seawater saturation state threshold, especially at high latitudes and at depth (Andersson et al. 2008; Sewell and Hofmann 2011) and

some may have started to undergo dissolution. The dissolution process of pure calcite is governed by the seawater saturation state with respect to the skeletal mineral phase (calcite and aragonite) (Ω). It depends on the calcium (Ca^{2+}) and the carbonate ion (CO_3^{2-}) concentrations, the temperature, salinity, pressure, and the stoichiometric solubility product (*K*sp) (*see* next section for detailed calculations and assumptions):

$$\Omega Cal./\ \Omega Arag. = [Ca^{2+}] * [CO_3^{2-}] / Ksp_{Cal./Arag.}$$

Dissolution is assumed to start below a nominal value of 1. This equation is currently used by experimentalists and modellers to define Ω levels, which are used as a "monitoring variable" to study thresholds in the field and predict when and where OA will impact marine ecosystems (Feely et al. 2004; Steinacher et al. 2009; Yamamoto-Kawai et al. 2009; Frölicher and Joos 2010). Seeminlgy, the nominal value of 1 is assumed to be a "natural" tipping point (e.g. McNeil and Matear 2008), which could induce irreversible changes in marine communities. These large-scale studies ignore in the calculations the fact that in modern marine ecosystems (except pelagic coccolithophores), the carbonates are dominated high Mg-calcite (Chave 1954). This changes the saturation state (ΩMg) with respect to a certain mol % $MgCO_3$ (Andersson et al. 2008), assuming a true carbonate chemistry equilibrium is established between the atmosphere and water (Morse et al. 2006). Therefore, general discussions on saturation states at a regional and global scale lack a species-specific component based on Mg-calcite measurements, which is a reasonable way to understand ecosystem changes driven by OA. Temptative ΩMg calculations depend on the Ca^{2+}, Mg^{2+}, and CO_3^{2-} concentrations, the mol % $MgCO_3$ of the biogenic calcite, the in situ temperature, salinity and pressure, and the ion activity product (IAP) for a certain mol % $MgCO_3$ (*see* next section for detailed calculations and assumptions):

$$\Omega Mg = \{Mg^{2+}\}^{x} * \{Ca^{2+}\}^{(1-x)} * \{CO_3^{2-}\} / IAP_x$$

where *x* is the mol % $MgCO_3$ measured in the organism, and the IAP_x is empirically calculated from the the mol % $MgCO_3$ using the "biogenic clean" and "biogenic minimally prepared curves" (Mackenzie et al. 1983; Bischoff et al.1987, 1993; and Morse and Mackenzie 1990).

In this paper we put together a global dataset of empirically determined skeleton mol % $MgCO_3$ in benthic and pelagic taxa in combination with field temperature, salinity and carbonate chemistry. We then used it to calculate species-specific ΩMg. Input field data were recovered combining the GLODAP dataset (Key et al. 2004) with the samples meta-data (latitude, longitude, and depth) using a "NEAR 3D" analysis (ESRI 2011) to identify the nearest field values (temperature, salinity and CO_3^{2-}) to our samples. We then calculated the species-specific ΩMg using the "biogenic cleaned" and "biogenic minimally prepared" curves (IAP *vs.* mol % $MgCO_3$), using a new set of corrections for in situ pressure, temperature and salinity assuming the same behaviour as calcite. We provide global trends of ΩMg for each organism and class, correlations with mol % $MgCO_3$, and a comparison with ΩCal. and ΩArag. Our calculations suggest that experimental and modelling ecosystem-based discussions based on ΩCal. and ΩArag. alone ignoring the Mg-calcite effect, are likely to derive into misleading conclusions to truly understand the magnitude of OA in the ocean.

15.2. Materials and methods

15.2.1. Field datasets and analytics

The skeleton measurements from field organisms used were derived from new samples (only for Echinodermata), and from the literature in the other cases (*see* Table 15.1, 15.3, 15.4 for details). Echinoderm samples were collected between 2008 and 2011 from 2 to 1200 m in the Atlantic, Pacific, Arctic, and Southern Ocean, from the five classes. Juveniles and adults were collected to represent the whole population. Individuals were measured and weighted (original methods in Lebrato et al. 2010 and McClintock et al. 2011), and divided as whole body, arms (plates) (some Antarctic species), calcareous rings (in some holothuroids), spines, and plates for geochemical

Table 15.1. Details of taxa used, skeleton mineralogy, and biogeography.

Organisms				Field data			Mg-calcite - Analytics [a]				In situ conditions - NEAR 3D analysis [b]				
Taxa	Class	Species	*n*	Depth (m)	Lat.	Long.	$CaCO_3$ % dw	$MgCO_3$ % dw	Mg/Ca (mol/mol)	Sal.	Temp. (°C)	Temp. (°K)	CO_3^{2-} (µmol kg^{-1}) [c] present	CO_3^{2-} (µmol kg^{-1}) [c] < 20 %	CO_3^{2-} (µmol kg^{-1}) [c] < 50 %
Echinodermata	Asteroidea	*Asterias rubens*	8	2	53.24	-4.46	36.270	4.080	0.134	35.47	19.45	292.60	193.40	154.72	96.70
Echinodermata	Asteroidea	*Asterina gibossa*	6	2	50.63	-2.39	60.480	6.600	0.130	35.44	15.95	289.10	193.47	154.78	96.74
Echinodermata	Asteroidea	*Zoroaster fulgens*	4	1140	49.28	-12.36	57.180	7.110	0.148	35.46	10.06	283.21	133.46	106.77	66.73
Echinodermata	Asteroidea	*Marthasterias glacialis*	7	3	43.58	-6.24	45.480	7.200	0.188	35.11	19.10	292.25	189.76	151.81	94.88
Echinodermata	Asteroidea	*Labidiaster annulatus*	9	175	-61.21	-56.01	90.120	9.870	0.130	34.03	1.54	274.69	97.85	78.28	48.93
Echinodermata	Asteroidea	*Macroptychaster accrescens*	3	180	-63.53	-62.75	90.170	9.830	0.129	34.03	1.54	274.69	97.85	78.28	48.93
Echinodermata	Asteroidea	*Paralophaster godfroyi*	1	180	-63.53	-62.75	90.410	9.590	0.126	34.03	1.54	274.69	97.85	78.28	48.93
Echinodermata	Asteroidea	*Paralophaster sp.*	3	180	-63.53	-62.75	90.720	9.280	0.121	34.03	1.54	274.69	97.85	78.28	48.93
Echinodermata	Asteroidea	*Perknaster sp.*	2	180	-63.53	-62.75	91.010	8.990	0.117	34.03	1.54	274.69	97.85	78.28	48.93
Echinodermata	Asteroidea	*Acodontaster hodgsoni*	3	160	-64.15	-62.74	90.150	9.850	0.130	34.03	1.54	274.69	97.85	78.28	48.93
Echinodermata	Asteroidea	*Kampylaster incurvatus*	4	160	-64.15	-62.74	90.720	9.280	0.121	34.03	1.54	274.69	97.85	78.28	48.93
Echinodermata	Asteroidea	*Odontaster penicillatus*	1	160	-64.15	-62.74	90.090	9.910	0.131	34.03	1.54	274.69	97.85	78.28	48.93
Echinodermata	Asteroidea	*Porania antarctica*	3	160	-64.15	-62.74	89.800	10.200	0.135	34.03	1.54	274.69	97.85	78.28	48.93
Echinodermata	Asteroidea	*Diplasterias brandti*	3	30	-64.77	-64.05	90.480	9.520	0.125	34.03	1.54	274.69	97.85	78.28	48.93
Echinodermata	Asteroidea	*Granaster nutrix*	5	30	-64.77	-64.05	91.710	8.290	0.107	34.03	1.54	274.69	97.85	78.28	48.93
Echinodermata	Asteroidea	*Neosmilaster georgianus*	3	30	-64.77	-64.05	90.630	9.370	0.123	34.03	1.54	274.69	97.85	78.28	48.93
Echinodermata	Asteroidea	*Odontaster meridionalis*	3	30	-64.77	-64.04	90.500	9.500	0.125	34.03	1.54	274.69	97.85	78.28	48.93
Echinodermata	Asteroidea	*Perknaster aurorae*	3	30	-64.78	-63.99	91.140	8.510	0.111	34.03	1.54	274.69	97.85	78.28	48.93
Echinodermata	Asteroidea	*Acodontaster conspicuus*	1	30	-65.07	-63.97	90.610	9.390	0.123	34.03	1.54	274.69	97.85	78.28	48.93
Echinodermata	Asteroidea	*Perknaster fuscus antracticus*	1	30	-65.07	-63.97	90.080	9.920	0.131	34.03	1.54	274.69	97.85	78.28	48.93
Echinodermata	Asteroidea	*Henricia sp.*	2	155	-65.67	-67.40	90.180	9.820	0.129	34.03	1.54	274.69	97.85	78.28	48.93
Echinodermata	Asteroidea	*Diplopteraster verrucosus*	2	900	-66.29	-66.60	89.630	8.120	0.108	34.03	1.54	274.69	97.85	78.28	48.93
Echinodermata	Asteroidea	*Odontaster validus*	6	18	-77.63	-146.41	47.280	5.830	0.146	34.20	1.28	274.43	91.83	73.46	45.91
Echinodermata	Crinoidea	*Antedon mediterranea*	3	63	41.43	2.32	64.840	7.760	0.142	35.32	9.64	282.79	138.10	110.48	69.05
Echinodermata	Echinoidea	*Psammechinus miliaris*	14	1	50.35	-4.13	79.850	7.470	0.111	35.11	19.10	292.25	189.76	151.81	94.88
Echinodermata	Echinoidea	*Paracentrotus lividus*	14	2	43.58	-6.24	62.360	4.550	0.087	36.97	20.57	293.72	225.18	180.14	112.59
Echinodermata	Echinoidea	*Paracentrotus lividus*	3	1	29.13	-13.60	75.910	2.760	0.043	36.86	20.16	293.31	232.94	186.35	116.47
Echinodermata	Echinoidea	*Paracentrotus lividus*	3	1	29.13	-13.60	68.340	5.980	0.104	36.17	25.83	298.98	251.71	201.37	125.86
Echinodermata	Echinoidea	*Tripneustes ventricosus*	2	6	25.12	-77.29	65.170	7.490	0.136	36.10	14.83	287.98	222.09	177.67	111.04
Echinodermata	Echinoidea	*Cidaris blakei*	2	595	24.83	-77.50	79.320	5.880	0.088	35.71	22.56	295.71	238.74	190.99	119.37
Echinodermata	Echinoidea	*Diadema setosum*	3	0.5	-18.85	159.75	83.070	13.300	0.190	35.71	22.56	295.71	238.74	190.99	119.37

Echinodermata	Echinoidea	*Diadema setosum*	3	0.5	-18.85	159.75	92.060	12.090	0.156	34.15	7.34	280.49	130.46	104.37	65.23
Echinodermata	Echinoidea	*Evechinus chloroticus*	3	5	-45.30	166.97	86.070	5.080	0.070	34.15	7.34	280.49	130.46	104.37	65.23
Echinodermata	Echinoidea	*Evechinus chloroticus*	3	5	-45.30	166.97	88.310	9.530	0.128	34.15	7.34	280.49	130.46	104.37	65.23
Echinodermata	Echinoidea	*Pseudechinus huttoni*	2	8	-45.41	167.10	94.910	4.000	0.050	34.15	7.34	280.49	130.46	104.37	65.23
Echinodermata	Echinoidea	*Pseudechinus huttoni*	3	8	-45.41	167.10	92.640	5.570	0.071	33.87	1.01	274.16	111.82	89.46	55.91
Echinodermata	Echinoidea	*Amphineustes similis*	2	685	-64.75	-65.47	96.300	3.700	0.046	33.87	1.01	274.16	111.82	89.46	55.91
Echinodermata	Echinoidea	*Amphineustes similis*	4	685	-64.75	-65.47	92.490	7.510	0.096	33.87	1.01	274.16	111.82	89.46	55.91
Echinodermata	Echinoidea	*Ctenocidaris perrieri*	3	685	-64.75	-65.47	96.180	3.810	0.047	33.87	1.01	274.16	111.82	89.46	55.91
Echinodermata	Echinoidea	*Ctenocidaris perrieri*	3	685	-64.75	-65.47	92.390	7.610	0.098	34.34	1.32	274.47	102.46	81.97	51.23
Echinodermata	Echinoidea	*Sterechinus neumayeri*	3	30	-65.07	-63.97	96.500	3.490	0.043	33.87	3.01	276.16	121.82	97.46	60.91
Echinodermata	Echinoidea	*Sterechinus neumayeri*	6	30	-65.07	-63.97	93.960	6.040	0.076	33.92	3.99	277.14	119.53	95.62	59.76
Echinodermata	Echinoidea	*Sterechinus neumayeri*	3	30	-65.07	-63.97	94.140	2.770	0.035	33.87	3.01	276.16	121.82	97.46	60.91
Echinodermata	Echinoidea	*Sterechinus neumayeri*	3	30	-65.07	-63.97	83.990	6.280	0.089	33.87	3.01	276.16	121.82	97.46	60.91
Echinodermata	Echinoidea	*Sterechinus neumayeri*	3	15	-77.06	164.42	62.590	4.530	0.086	33.87	3.01	276.16	121.82	97.46	60.91
Echinodermata	Holothuroidea	*Molpadia musculus*	3	685	-64.75	-65.47	91.740	8.260	0.107	33.84	2.95	276.10	111.76	89.41	55.88
Echinodermata	Holothuroidea	*Pseudostichopus spiculiferus*	1	900	-66.29	-66.60	92.510	7.490	0.096	35.46	10.06	283.21	133.46	106.77	66.73
Echinodermata	Ophiuroidea	*Ophiosium lynami*	6	1140	49.20	-12.30	70.540	8.190	0.138	36.86	20.16	293.31	232.04	185.63	116.02
Echinodermata	Ophiuroidea	*Ophiura longicauda*	1	1	29.12	-13.56	70.400	11.480	0.194	33.87	2.90	276.05	123.26	98.60	61.63
Echinodermata	Ophiuroidea	*Ophiura longicauda*	1	1	29.12	-13.56	48.440	7.310	0.179	33.87	2.90	276.05	123.26	98.60	61.63
Echinodermata	Ophiuroidea	*Ophionotus victoriae*	3	30	-64.77	-64.05	90.800	9.200	0.120	36.86	20.16	293.31	232.04	185.63	116.02
Echinodermata	Ophiuroidea	*Ophiosparte gigas*	1	30	-64.77	-64.05	90.870	9.130	0.119	37.98	17.54	290.69	246.65	197.32	123.32
Echinodermata	Asteroidea	*Asterias linckii*	1	20	65.81	39.73	88.010	9.460	0.128	34.52	17.58	290.73	198.69	158.95	99.34
Echinodermata	Asteroidea	*Orthasterias tanneri*	1	30	61.68	3.31	86.410	10.690	0.147	35.09	8.07	281.22	179.42	143.54	89.71
Echinodermata	Asteroidea	*Ctenodiscus crispatus*	1	80	46.90	-59.10	88.480	8.780	0.118	33.13	-0.87	272.28	88.68	70.94	44.34
Echinodermata	Asteroidea	*Asterias vulgaris*	1	10	44.79	-66.92	91.060	7.790	0.102	33.83	9.25	282.40	231.81	185.45	115.90
Echinodermata	Asteroidea	*Asterias acervata borealis*	1	40	43.58	-65.17	86.390	9.600	0.132	35.09	8.07	281.22	179.42	143.54	89.71
Echinodermata	Asteroidea	*Asterina pectinifera*	1	10	43.20	141.05	82.510	12.050	0.173	35.72	13.61	286.76	186.56	149.25	93.28
Echinodermata	Asteroidea	*Asterias forbesi*	1	10	41.42	-70.80	88.190	8.240	0.111	35.20	11.27	284.42	174.45	139.56	87.23
Echinodermata	Asteroidea	*Odontaster hispidus*	1	40	41.30	-70.80	87.160	10.580	0.144	33.09	17.60	290.75	163.99	131.19	81.99
Echinodermata	Asteroidea	*Plutonaster agassizii*	1	10	41.30	-70.80	89.180	9.090	0.121	32.71	21.39	294.54	173.17	138.53	86.58
Echinodermata	Asteroidea	*Pontaster tenuispinus*	1	40	41.30	-70.80	89.340	8.860	0.118	34.52	17.58	290.73	198.69	158.95	99.34
Echinodermata	Asteroidea	*Astropecten andromeda*	1	10	41.30	-70.80	78.670	10.420	0.157	34.52	17.58	290.73	198.69	158.95	99.34
Echinodermata	Asteroidea	*Leptasterias compta*	1	100	40.28	-69.85	86.570	10.270	0.141	34.52	18.51	291.66	175.82	140.66	87.91
Echinodermata	Asteroidea	*Benthopecten spinosus*	1	100	39.25	-68.13	86.420	9.880	0.136	35.72	13.61	286.76	186.56	149.25	93.28
Echinodermata	Asteroidea	*Astropecten articulatus*	1	200	35.71	-73.50	85.080	13.020	0.182	35.72	13.61	286.76	186.56	149.25	93.28
Echinodermata	Asteroidea	*Urasterias linckii*	1	200	35.71	-73.50	88.250	8.910	0.120	35.72	13.61	286.76	186.56	149.25	93.28
Echinodermata	Asteroidea	*Asterias tanneri*	1	200	35.71	-73.50	87.440	10.280	0.140	35.72	13.61	286.76	186.56	149.25	93.28
Echinodermata	Asteroidea	*Asterina miniata*	1	10	35.20	-121.30	88.060	11.240	0.152	35.72	13.61	286.76	186.56	149.25	93.28
Echinodermata	Asteroidea	*Marthasterias glacialis*	1	30	35.20	-121.30	85.990	8.290	0.114	36.72	23.73	296.88	252.33	201.86	126.16
Echinodermata	Asteroidea	*Astropecten americanus*	1	10	26.90	-82.80	87.930	10.110	0.136	36.72	23.73	296.88	252.33	201.86	126.16

Echinodermata	Asteroidea	*Asterina minuta*	1	15	18.04	-67.96	86.770	12.530	0.171	33.65	17.00	290.15	177.33	141.86	88.66
Echinodermata	Asteroidea	*Linckia guildingii*	1	30	18.04	-67.96	83.420	14.310	0.204	36.63	21.94	295.09	249.23	199.39	124.62
Echinodermata	Asteroidea	*Linckia laevigata*	1	30	18.04	-67.96	85.630	9.320	0.129	37.02	21.78	294.93	230.65	184.52	115.32
Echinodermata	Asteroidea	*Acanthaster planci*	1	25	5.86	-162.08	85.990	13.330	0.184	33.93	28.88	302.03	247.41	197.93	123.70
Echinodermata	Asteroidea	*Ctenodiscus procurator*	1	30	-35.70	-72.80	87.520	11.160	0.151	34.84	27.32	300.47	251.49	201.19	125.75
Echinodermata	Asteroidea	*Ctenodiscus australis*	1	10	-43.60	-74.00	80.780	10.510	0.154	34.84	27.32	300.47	251.49	201.19	125.75
Echinodermata	Crinoidea	*Heliometra glacialis*	1	20	68.20	39.20	88.500	9.500	0.127	34.96	6.73	279.88	176.54	141.23	88.27
Echinodermata	Crinoidea	*Ptilocrinus pinnatus*	1	10	53.10	-130.00	88.480	7.910	0.106	32.33	7.14	280.29	121.11	96.89	60.56
Echinodermata	Crinoidea	*Florometra asperrima*	1	12	47.10	-124.20	89.450	9.440	0.125	33.05	13.40	286.55	157.09	125.67	78.55
Echinodermata	Crinoidea	*Bythocrinus robustus*	1	40	42.30	-70.77	87.160	10.090	0.137	32.71	21.39	294.54	173.17	138.53	86.58
Echinodermata	Crinoidea	*Hathrometra dentata*	1	30	41.30	-70.80	83.470	9.360	0.133	34.38	27.65	300.80	233.89	187.11	116.94
Echinodermata	Crinoidea	*Psathyrometra fragilis*	1	20	35.07	139.70	87.770	9.250	0.125	34.38	27.65	300.80	233.89	187.11	116.94
Echinodermata	Crinoidea	*Pentametrocrinus japonicus*	1	20	34.90	138.50	87.340	10.150	0.138	32.71	21.39	294.54	173.17	138.53	86.58
Echinodermata	Crinoidea	*Crinometra concinna*	1	40	28.05	-96.02	87.960	11.690	0.158	35.54	19.72	292.87	198.10	158.48	99.05
Echinodermata	Crinoidea	*Isocrinus decorus*	1	50	21.40	-76.70	88.200	11.690	0.157	34.13	17.12	290.27	121.66	97.33	60.83
Echinodermata	Crinoidea	*Endoxocrinus parra*	1	60	21.40	-76.70	88.130	11.620	0.157	33.58	29.38	302.53	242.51	194.01	121.25
Echinodermata	Crinoidea	*Tropiometra picta*	1	30	21.40	-76.70	87.510	11.770	0.160	33.58	29.38	302.53	242.51	194.01	121.25
Echinodermata	Crinoidea	*Promachocrinus kerguelensis*	1	20	11.17	-60.68	91.550	7.860	0.102	33.58	29.38	302.53	242.51	194.01	121.25
Echinodermata	Crinoidea	*Capillaster multiradiata*	1	30	7.85	116.90	86.320	12.690	0.175	33.58	29.38	302.53	242.51	194.01	121.25
Echinodermata	Crinoidea	*Pachylometra patula*	1	30	7.85	116.90	85.810	12.200	0.169	33.58	29.38	302.53	242.51	194.01	121.25
Echinodermata	Crinoidea	*Catoptometra ophiura*	1	30	7.85	116.90	86.460	11.680	0.160	33.58	29.38	302.53	242.51	194.01	121.25
Echinodermata	Crinoidea	*Hypalocrinus naresianus*	1	30	7.85	116.90	89.660	10.160	0.135	36.17	25.83	298.98	251.71	201.37	125.86
Echinodermata	Crinoidea	*Parametra granulata*	1	30	7.85	116.90	87.860	11.080	0.150	36.17	25.83	298.98	251.71	201.37	125.86
Echinodermata	Crinoidea	*Craspedometra anceps*	1	30	7.85	116.90	86.930	12.340	0.169	36.17	25.83	298.98	251.71	201.37	125.86
Echinodermata	Crinoidea	*Zygometra microdiscus*	1	40	-5.99	134.10	85.480	13.370	0.186	36.91	23.39	296.54	245.45	196.36	122.73
Echinodermata	Crinoidea	*Tropiometra carinata*	1	15	-22.98	-43.20	83.130	13.740	0.196	35.16	27.24	300.39	256.78	205.43	128.39
Echinodermata	Crinoidea	*Pilometra mülleri*	1	20	-33.85	151.26	87.940	11.130	0.150	33.97	29.14	302.29	240.31	192.25	120.15
Echinodermata	Echinoidea	*Strongylocentrotus droebachiensis*	1	40	64.00	-38.00	93.130	5.990	0.076	34.83	7.12	280.27	127.16	101.73	63.58
Echinodermata	Echinoidea	*Echinarachnius parma*	1	32	59.20	-165.80	92.130	6.130	0.079	32.94	8.46	281.61	141.05	112.84	70.52
Echinodermata	Echinoidea	*Arbacia pustulosa*	1	15	40.76	14.35	90.080	7.720	0.102	33.85	9.80	282.95	139.04	111.23	69.52
Echinodermata	Echinoidea	*Echinus esculentus*	1	10	38.00	-1.02	89.640	8.840	0.117	34.38	27.14	300.29	223.35	178.68	111.67
Echinodermata	Echinoidea	*Paracentrotus lividus*	1	5	37.24	13.68	89.400	8.530	0.113	34.93	29.38	302.53	243.07	194.46	121.54
Echinodermata	Echinoidea	*Echinus affinis*	1	200	35.71	-73.50	88.960	5.410	0.072	33.09	17.60	290.75	163.99	131.19	81.99
Echinodermata	Echinoidea	*Lytechinus anamesus*	1	20	35.20	-121.30	77.910	7.440	0.113	36.63	21.94	295.09	249.23	199.39	124.62
Echinodermata	Echinoidea	*Clypeaster testudinarius*	1	20	33.40	134.60	91.290	8.410	0.109	37.98	17.54	290.69	246.65	197.32	123.32
Echinodermata	Echinoidea	*Strongylocentrotus fragilis*	1	60	29.00	-115.00	88.440	6.950	0.093	33.78	12.53	285.68	144.37	115.50	72.19
Echinodermata	Echinoidea	*Prionocidaris baculosa*	1	15	28.02	34.97	89.330	10.670	0.142	32.94	8.46	281.61	141.05	112.84	70.52
Echinodermata	Echinoidea	*Tetrocidaris affinis*	1	10	26.90	-82.80	89.350	9.300	0.124	36.08	26.28	299.43	251.16	200.93	125.58
Echinodermata	Echinoidea	*Echinometra lucunter*	1	20	18.04	-67.96	83.870	11.560	0.164	37.98	17.54	290.69	246.65	197.32	123.32
Echinodermata	Echinoidea	*Mellita sexiesperforatus*	1	30	18.04	-67.96	85.020	11.910	0.166	31.96	9.77	282.92	156.89	125.51	78.45
Echinodermata	Echinoidea	*Encope californica*	1	20	-1.00	-91.01	79.940	10.380	0.154	33.58	29.38	302.53	242.51	194.01	121.25

Echinodermata	Echinoidea	*Tetrapygus niger*	1	20	-9.40	-78.50	90.520	6.270	0.082	36.19	25.42	298.57	258.80	207.04	129.40
Echinodermata	Echinoidea	*Heterocentrotus mammillatus*	1	20	-27.64	-144.33	86.420	12.260	0.168	40.40	23.37	296.52	282.07	225.66	141.04
Echinodermata	Echinoidea	*Lytechinus albus*	1	10	-43.60	-74.00	91.730	7.380	0.096	33.58	29.38	302.53	242.51	194.01	121.25
Echinodermata	Ophiuroidea	*Gorgonocephalus caryi*	1	15	61.30	-166.30	84.360	9.660	0.136	32.52	8.09	281.24	163.96	131.17	81.98
Echinodermata	Ophiuroidea	*Astrophyton sp.*	1	60	56.00	2.90	89.670	9.110	0.121	35.20	11.27	284.42	174.45	139.56	87.23
Echinodermata	Ophiuroidea	*Ophiopholis aculeata japonica*	1	10	53.91	-166.50	91.160	8.010	0.104	34.51	23.85	297.00	246.10	196.88	123.05
Echinodermata	Ophiuroidea	*Gorgonocephalus arcticus*	1	10	41.50	-70.30	86.600	9.530	0.131	32.57	9.62	282.77	143.70	114.96	71.85
Echinodermata	Ophiuroidea	*Ophioglypha sarsii*	1	100	39.54	-72.35	87.650	9.840	0.133	34.51	23.85	297.00	246.10	196.88	123.05
Echinodermata	Ophiuroidea	*Gorgonocephalus eucnemis*	1	50	38.30	139.00	88.440	8.390	0.113	35.24	10.50	283.65	167.52	134.02	83.76
Echinodermata	Ophiuroidea	*Ophionereis eurybrachiplax*	1	50	38.30	139.00	85.530	13.380	0.186	34.20	23.49	296.64	213.34	170.67	106.67
Echinodermata	Ophiuroidea	*Ophioglypha lütkeni*	1	200	35.20	-121.30	86.340	10.190	0.140	34.52	18.51	291.66	175.82	140.66	87.91
Echinodermata	Ophiuroidea	*Ophiothrix angulata*	1	200	21.40	-76.70	87.240	11.680	0.159	32.86	14.31	287.46	147.12	117.69	73.56
Echinodermata	Ophiuroidea	*Ophiocamax fasciculata*	1	100	21.40	-76.70	91.300	7.620	0.099	36.82	23.81	296.96	267.33	213.86	133.66
Echinodermata	Ophiuroidea	*Ophiocoma erinaceus*	1	20	20.10	-155.30	86.830	12.050	0.165	36.82	23.81	296.96	267.33	213.86	133.66
Echinodermata	Ophiuroidea	*Ophioderma cinerum*	1	30	18.50	-66.60	85.090	14.080	0.196	36.82	23.81	296.96	267.33	213.86	133.66
Echinodermata	Ophiuroidea	*Ophiocoma aethiops*	1	25	18.04	-67.96	92.120	7.040	0.091	36.82	23.81	296.96	267.33	213.86	133.66
Echinodermata	Ophiuroidea	*Ophiomixa flaccida*	1	120	18.04	-67.96	81.020	14.560	0.213	34.16	27.86	301.01	237.55	190.04	118.78
Echinodermata	Ophiuroidea	*Ophiocoma pumila*	1	120	18.04	-67.96	84.440	12.970	0.182	36.53	24.79	297.94	257.40	205.92	128.70
Echinodermata	Ophiuroidea	*Ophiomusium lymani*	1	200	-1.00	-91.01	92.700	6.610	0.085	33.48	6.24	279.39	166.29	133.04	83.15
Echinodermata	Ophiuroidea	*Ophioglypha lymani*	1	30	-35.70	-72.80	89.500	8.240	0.109	36.53	24.79	297.94	257.40	205.92	128.70
Coralline algae	-	*Lithothamnium sp.*	1	10	78.00	20.00	84.830	8.670	0.121	35.09	8.07	281.22	179.42	143.54	89.71
Coralline algae	-	*Lithothamnium soriferum*	1	10	75.00	20.00	80.900	9.560	0.140	34.38	3.83	276.98	164.72	131.78	82.36
Coralline algae	-	*Lithothamium glaciale*	1	10	75.00	20.00	83.100	13.190	0.188	36.66	22.27	295.42	247.54	198.03	123.77
Coralline algae	-	*Lithothamnium fornicatum*	1	10	72.00	20.00	88.610	10.090	0.135	35.09	8.07	281.22	179.42	143.54	89.71
Coralline algae	-	*Lithothamnium polymorphum*	1	10	57.00	12.00	74.220	9.100	0.146	32.92	8.45	281.60	178.18	142.54	89.09
Coralline algae	-	*Corallina squamata* - 29-Nov	1	5	50.60	-2.30	71.680	10.530	0.174	35.60	14.57	287.72	194.74	155.79	97.37
Coralline algae	-	*Corallina squamata* - 29-Jan	1	5	50.60	-2.30	72.420	9.650	0.158	35.64	14.40	287.55	192.09	153.67	96.04
Coralline algae	-	*Corallina squamata* - 26-Mar	1	5	50.60	-2.30	70.400	9.260	0.156	35.63	14.55	287.70	210.98	168.78	105.49
Coralline algae	-	*Corallina squamata* - 28-May	1	5	50.60	-2.30	71.050	8.670	0.145	31.79	13.16	286.31	172.11	137.69	86.06
Coralline algae	-	*Corallina squamata* - 01-Jul	1	5	50.60	-2.30	72.340	9.340	0.153	37.98	17.54	290.69	246.65	197.32	123.32
Coralline algae	-	*Corallina squamata* - 13-Aug	1	5	50.60	-2.30	71.290	9.790	0.163	32.86	14.31	287.46	167.12	133.69	83.56
Coralline algae	-	*Corallina squamata* - 12-Sep	1	5	50.60	-2.30	71.370	10.340	0.172	34.70	30.15	303.30	257.24	205.79	128.62
Coralline algae	-	*Corallina squamata* - 10-Oct	1	5	50.60	-2.30	72.460	10.190	0.167	34.70	30.15	303.30	258.24	206.59	129.12
Coralline algae	-	*Corallina officinalis*	1	5	49.60	-1.20	86.680	12.060	0.165	34.70	30.15	303.30	259.24	207.39	129.62
Coralline algae	-	*Lithothamnium calcareum*	1	10	48.08	-4.00	84.600	12.040	0.169	34.70	30.15	303.30	260.24	208.19	130.12
Coralline algae	-	*Lithophyllum incrustans*	1	10	48.00	-3.00	87.100	11.140	0.152	36.61	24.55	297.70	258.94	207.15	129.47
Coralline algae	-	*Phymatolithon compactum*	1	10	48.00	-55.00	87.210	10.930	0.149	36.61	24.55	297.70	258.94	207.15	129.47
Coralline algae	-	*Lithophyllum tortuosum*	1	20	44.00	9.00	77.580	9.830	0.150	34.67	28.50	301.65	259.46	207.56	129.73
Coralline algae	-	*Lithophyllum proboscideum*	1	15	37.00	-122.00	72.000	8.150	0.134	35.40	26.65	299.80	262.09	209.67	131.05
Coralline algae	-	*Goniolithon strictum - old*	1	30	25.00	-75.00	74.850	24.000	0.381	29.37	34.79	307.94	260.70	208.56	130.35

Coralline algae	-	*Goniolithon strictum - old*	1	30	25.00	-75.00	74.290	23.740	0.379	34.73	30.10	303.25	256.96	205.57	128.48
Coralline algae	-	*Goniolithon strictum - young*	1	30	25.00	-75.00	75.420	22.980	0.362	34.58	28.29	301.44	235.47	188.38	117.74
Coralline algae	-	*Lithophyllum pachydermum*	1	30	25.00	-75.00	83.060	15.430	0.221	34.23	29.17	302.32	238.10	190.48	119.05
Coralline algae	-	*Goniolithon acropectum*	1	20	18.00	-68.00	79.050	19.240	0.289	34.60	28.66	301.81	234.24	187.39	117.12
Coralline algae	-	*Amphiroa fragilissima*	1	10	18.00	-68.00	76.230	17.470	0.272	34.60	27.33	300.48	208.18	166.54	104.09
Coralline algae	-	*Lithothamnium nodosum*	1	5	0.00	-90.00	91.040	6.060	0.079	35.55	15.58	288.73	193.68	154.95	96.84
Coralline algae	-	*Lithophyllum oncodes*	1	30	-7.00	56.00	80.930	18.170	0.267	35.55	15.58	288.73	193.69	154.95	96.85
Coralline algae	-	*Goniolithon orthoblastum*	1	10	-10.00	145.00	86.220	13.660	0.188	35.55	15.58	288.73	193.69	154.95	96.85
Coralline algae	-	*Lithothamnium erubescens*	1	10	-10.00	123.00	81.590	16.960	0.247	35.55	15.58	288.73	193.69	154.95	96.85
Coralline algae	-	*Archaeolithothamium episporum*	1	10	-10.00	80.00	83.470	13.090	0.186	35.55	15.58	288.73	193.69	154.95	96.85
Coralline algae	-	*Lithothamnium kaiseri*	1	10	-15.00	-172.00	72.800	16.150	0.263	35.55	15.58	288.73	193.69	154.95	96.85
Coralline algae	-	*Porolithon craspedium*	1	10	-15.00	-172.00	75.390	16.800	0.265	35.55	15.58	288.73	193.69	154.95	96.85
Coralline algae	-	*Porolithon oncodes*	1	10	-15.00	-172.00	78.200	13.750	0.209	35.55	15.58	288.73	193.69	154.95	96.85
Foraminifera	-	*Pulvinulina menardii* - pelagic	1	20	40.56	-66.15	77.020	3.670	0.057	34.46	23.63	296.78	219.31	175.45	109.66
Foraminifera	-	*Polytrema mineaccum* - benthic	1	100	25.00	-77.00	90.110	9.330	0.123	34.23	30.01	303.16	248.76	199.01	124.38
Foraminifera	-	*Orbitolites marginatis* - benthic	1	50	24.60	-81.96	89.010	10.550	0.141	34.38	29.29	302.44	278.83	223.07	139.42
Foraminifera	-	*Amphistegina lessonii* - pelagic	1	20	16.10	-22.95	92.850	4.900	0.063	34.68	25.82	298.97	251.31	201.04	125.65
Foraminifera	-	*Sphaeroidina dehiscens* - pelagic	1	20	12.40	121.60	84.380	1.790	0.025	36.10	26.49	299.64	256.56	205.25	128.28
Foraminifera	-	*Orbitolites complanata* - benthic	1	30	-17.30	177.47	86.460	12.520	0.172	36.10	26.49	299.64	256.56	205.25	128.28
Hydrocorallia	-	*Millepora alcicornis*	1	10	24.60	-81.96	98.220	0.950	0.011	36.17	25.83	298.98	251.71	201.37	125.86
Hydrocorallia	-	*Distichopora nitida*	1	20	7.40	151.50	98.220	0.240	0.003	36.81	26.46	299.61	261.14	208.91	130.57
Hydrocorallia	-	*Millepora braziliensis*	1	30	-12.20	-36.80	96.770	1.280	0.016	33.91	29.09	302.24	249.15	199.32	124.57
Hexacorallia	-	*Madracis decactis*	1	20	32.40	-64.90	99.060	0.760	0.009	36.10	26.49	299.64	256.56	205.25	128.28
Hexacorallia	-	*Siderastrea radians*	1	20	32.40	-64.90	99.270	0.480	0.006	36.10	26.49	299.64	256.56	205.25	128.28
Hexacorallia	-	*Flabellum alabastrum*	1	10	26.00	-77.20	99.420	0.370	0.004	36.10	26.49	299.64	256.56	205.25	128.28
Hexacorallia	-	*Acropora cervicornis*	1	15	26.00	-77.20	99.490	0.450	0.005	36.10	26.49	299.64	256.56	205.25	128.28
Hexacorallia	-	*Favia fragum*	1	20	24.60	-81.96	99.200	0.390	0.005	36.10	26.49	299.64	256.56	205.25	128.28
Hexacorallia	-	*Dasmosmilia lymani*	1	10	24.60	-81.96	98.710	0.630	0.008	36.63	21.35	294.50	256.94	205.55	128.47
Hexacorallia	-	*Balanophyllia floridana*	1	10	24.54	-81.80	98.050	1.110	0.013	35.36	26.32	299.47	257.85	206.28	128.93
Hexacorallia	-	*Paracyathus defilipii*	1	10	24.54	-81.80	98.320	0.870	0.011	36.77	23.72	296.87	262.37	209.90	131.19
Hexacorallia	-	*Deltocyathus italicus*	1	20	18.50	-63.51	98.980	0.540	0.006	36.63	21.35	294.50	256.94	205.55	128.47
Hexacorallia	-	*Desmophyllum ingens*	1	15	-36.55	-73.00	99.210	0.590	0.007	33.80	9.92	273.15	141.30	113.04	70.65
Octocorallia	-	*Gorgonia sp.*	1	30	54.60	154.40	88.830	9.290	0.124	33.58	29.38	302.53	242.51	194.01	121.25
Octocorallia	-	*Alcyonium carneum*	1	50	45.18	-55.85	84.500	6.660	0.094	34.13	29.00	302.15	239.41	191.52	119.70
Octocorallia	-	*Paramuricea borealis*	1	50	45.18	-55.85	85.110	8.030	0.112	34.75	23.78	296.93	233.86	187.09	116.93
Octocorallia	-	*Alcyonium carneum*	1	50	45.18	-55.85	-	6.660		32.54	2.23	275.38	106.34	85.07	53.17
Octocorallia	-	*Pennatula aculeata*	1	50	44.45	-58.51	85.620	7.710	0.107	34.25	29.62	302.77	254.57	203.66	127.29

Octocorallia	-	*Paragorgia arborea*	1	50	44.36	-63.75	88.040	9.050	0.122	36.77	23.72	296.87	262.37	209.90	131.19
Octocorallia	-	*Paragorgia arborea*	1	50	43.00	-62.00	-	9.050		32.88	13.39	286.54	179.79	143.83	89.89
Octocorallia	-	*Corallium elatior*	1	40	42.25	130.91	86.570	11.560	0.159	33.64	8.23	281.38	159.71	127.77	79.86
Octocorallia	-	*Primnoa resedaeformis*	1	30	42.25	130.91	-	9.290		35.56	20.25	293.40	214.53	171.63	107.27
Octocorallia	-	*Primnoa reseda*	1	40	42.25	-63.25	-	6.180		35.48	23.06	296.21	240.96	192.77	120.48
Octocorallia	-	*Rhipidogorgia flabellum*	1	20	32.40	-64.90	83.380	12.640	0.180	35.48	23.06	296.21	240.96	192.77	120.48
Octocorallia	-	*Pleurocorallium johnsoni*	1	30	25.75	-20.20	93.870	6.030	0.076	35.48	23.06	296.21	240.96	192.77	120.48
Octocorallia	-	*Gorgonia acerosa*	1	50	24.60	-81.96	85.760	13.390	0.185	35.48	23.06	296.21	240.96	192.77	120.48
Octocorallia	-	*Leptogorgia pulchra*	1	80	24.60	-108.25	-	13.710		36.68	27.77	300.92	269.08	215.27	134.54
Octocorallia	-	*Xiphigorgia anceps*	1	20	24.47	-81.55	80.960	13.040	0.191	34.61	24.17	297.32	221.42	177.13	110.71
Octocorallia	-	*Muricea echinata*	1	10	22.86	-106.10	83.790	12.280	0.174	32.17	13.67	286.82	149.26	119.41	74.63
Octocorallia	-	*Leptogorgia rigida*	1	150	22.86	-109.79	-	14.130		33.09	10.98	284.13	137.16	109.73	68.58
Octocorallia	-	*Heliopora cerulea*	1	20	12.40	121.60	98.930	0.350	0.004	36.53	24.69	297.84	257.40	205.92	128.70
Octocorallia	-	*Tubipora purpurea*	1	10	1.33	103.83	84.610	12.230	0.172	34.20	23.49	296.64	213.34	170.67	106.67
Octocorallia	-	*Phyllogorgia quercifolia*	1	10	-3.83	-32.41	-	15.730		32.57	6.50	279.65	116.43	93.14	58.22
Octocorallia	-	*Ctenocella pectinata*	1	20	-10.00	142.20	-	15.650		34.38	27.65	300.80	233.89	187.11	116.94
Octocorallia	-	*Muricea humilis*	1	30	-12.20	-36.80	84.470	12.640	0.178	34.52	17.58	290.73	198.69	158.95	99.34
Octocorallia	-	*Gorgonia subfruticosa*	1	45	-18.00	-178.00	79.840	13.430	0.200	34.52	17.58	290.73	198.69	158.95	99.34
Octocorallia	-	*Plexaurella grandiflora*	1	20	-28.40	155.67	85.610	13.790	0.191	34.52	17.58	290.73	198.69	158.95	99.34
Octocorallia	-	*Eunicella papillose*	1	30	-34.21	18.35	62.050	5.720	0.109	34.13	17.12	290.27	121.66	97.33	60.83
Octocorallia	-	*Eunicella alba*	1	30	-34.22	18.48	68.700	7.050	0.122	34.17	13.17	286.32	137.43	109.95	68.72
Octocorallia	-	*Eunicella tricoronata*	1	30	-34.22	18.48	70.750	7.310	0.123	34.70	30.15	303.30	257.24	205.79	128.62
Octocorallia	-	*Lophogorgia flamea*	1	30	-34.22	18.48	75.510	7.990	0.126	35.51	14.55	287.70	128.14	102.51	64.07
Bryozoa	-	*Flustra membranacea*	1	50	59.17	-151.60	87.920	6.940	0.094	31.68	1.60	274.75	153.84	123.07	76.92
Bryozoa	-	*Cellepora incrassata*	1	50	44.69	-62.69	91.770	6.070	0.079	35.56	20.25	293.40	214.53	171.63	107.27
Bryozoa	-	*Schizoporella unicornis*	1	10	41.35	-70.79	95.970	0.630	0.008	31.68	1.60	274.75	153.84	123.07	76.92
Bryozoa	-	*Bugula turrita*	1	40	41.23	-70.07	64.510	10.190	0.188	32.67	3.72	276.87	94.96	75.97	47.48
Bryozoa	-	*Lepralia sp.*	1	20	40.80	14.20	90.820	5.020	0.066	37.99	18.54	291.69	246.65	197.32	123.32
Bryozoa	-	*Amathia spiralis*	1	20	35.22	-75.60	90.430	9.570	0.126	35.72	13.61	286.76	186.56	149.25	93.28
Bryozoa	-	*Holoporella albirostris*	1	20	24.47	-81.55	95.280	2.590	0.032	35.72	13.61	286.76	186.56	149.25	93.28
Bryozoa	-	*Bugula neritina*	1	20	24.47	-81.55	63.290	11.080	0.208	31.68	1.60	274.75	153.84	123.07	76.92
Bryozoa	-	*Microporella grisea*	1	20	-28.40	155.67	96.900	1.110	0.014	35.72	13.61	286.76	186.56	149.25	93.28
Brachiopoda	-	*Terebratulina septentrionalis*	1	30	44.87	-66.91	96.780	1.370	0.017	34.46	23.63	296.78	219.31	175.45	109.66
Brachiopoda	-	*Laqueus californicus*	1	80	24.60	-108.25	98.300	0.680	0.008	34.79	18.07	291.22	201.94	161.55	100.97
Mollusca	Amphineura	*Mopalia muscosa*	1	120	34.39	-119.70	98.370	0.450	0.005	33.58	39.38	312.53	242.51	194.01	121.25
Mollusca	Bivalvia	*Astarte borealis*	1	50	74.16	54.40	98.700	0.620	0.007	35.56	17.46	290.61	195.19	156.15	97.60
Mollusca	Bivalvia	*Tellina calcarea*	1	40	74.16	54.33	98.840	0.710	0.009	33.52	29.26	302.41	237.13	189.71	118.57
Mollusca	Bivalvia	*Pecten groenlandicus*	1	20	73.50	68.83	90.000	0.800	0.011	36.66	22.69	295.84	248.58	198.86	124.29

Mollusca	Bivalvia	*Pecten islandicus*	1	40	71.50	47.00	97.600	1.280	0.016	34.57	25.51	298.66	222.38	177.91	111.19
Mollusca	Bivalvia	*Pecten dislocatus*	1	10	26.81	-82.29	98.000	1.000	0.012	35.02	8.36	281.51	178.97	143.18	89.49
Mollusca	Bivalvia	*Pecten ventricosus*	1	10	22.86	-106.10	98.980	0.730	0.009	35.09	8.07	281.22	105.33	84.26	52.67
Mollusca	Bivalvia	*Placuna orbicularis*	1	10	16.83	120.26	99.220	0.700	0.008	32.93	5.10	278.25	105.33	84.26	52.67
Mollusca	Cephalopoda	*Nautilus pompilius*	1	100	8.53	123.03	99.500	0.160	0.002	33.80	29.76	302.91	239.93	191.94	119.97
Mollusca	Cephalopoda	*Sepia officinalis*	1	10	5.84	118.27	98.320	1.620	0.020	33.50	0.00	273.15	150.49	120.39	75.24
Mollusca	Cephalopoda	*Argonauta argo*	1	50	-35.82	175.39	93.760	6.020	0.076	33.91	10.93	284.08	131.88	105.50	65.94
Mollusca	Cirripedia	*Scalpellum regium*	1	5	52.92	-132.29	97.020	2.230	0.027	34.20	23.49	296.64	213.34	170.67	106.67
Mollusca	Cirripedia	*Balanus hameri*	1	20	41.23	-70.07	99.070	0.750	0.009	33.65	17.00	290.15	177.33	141.86	88.66
Mollusca	Cirripedia	*Balanus amphitrite*	1	5	38.92	-74.91	95.630	1.630	0.020	32.86	14.31	287.46	167.12	133.69	83.56
Mollusca	Cirripedia	*Lepas anatifera*	1	10	24.47	-81.55	97.270	2.490	0.030	32.76	10.07	283.22	133.16	106.53	66.58
Mollusca	Cirripedia	*Mitella polymerus*	1	10	22.86	-106.10	97.470	2.110	0.026	33.49	1.30	274.45	165.83	132.66	82.92
Mollusca	Gastropoda	*Neptunea despecta*	1	20	69.63	57.35	98.520	1.170	0.014	34.40	8.45	281.60	203.08	162.46	101.54
Mollusca	Gastropoda	*Natica clausa*	1	20	60.50	-46.91	98.540	0.840	0.010	34.20	23.49	296.64	213.34	170.67	106.67
Mollusca	Gastropoda	*Tachyrhynchus erosa*	1	30	52.90	158.76	97.000	1.020	0.012	34.20	23.49	296.64	213.34	170.67	106.67
Mollusca	Gastropoda	*Nassa tegula*	1	20	36.62	-121.91	99.220	0.370	0.004	36.69	23.84	296.99	251.09	200.87	125.54
Mollusca	Gastropoda	*Nassa isculpta*	1	50	32.34	-118.43	97.080	1.780	0.022	34.61	24.08	297.23	217.84	174.27	108.92
Mollusca	Scaphopoda	*Dentalium solidum*	1	30	41.23	-70.07	99.130	0.200	0.002	32.85	10.77	283.92	146.62	117.30	73.31
Crustacea	Amphipoda	*Tryphosa pinguis*	1	30	41.52	-70.67	74.640	4.840	0.077	35.20	11.27	284.42	174.45	139.56	87.23
Crustacea	Decapoda	*Crago dalli*	1	40	59.17	-151.60	54.830	10.050	0.218	33.75	4.84	277.99	64.67	51.74	32.34
Crustacea	Decapoda	*Pagurus rathbuni*	1	210	58.46	-175.22	78.030	5.800	0.088	36.69	23.84	296.99	251.09	200.87	125.54
Crustacea	Decapoda	*Homarus americanus* - small	1	30	43.84	-69.64	78.980	7.740	0.116	32.54	9.23	282.38	118.47	94.78	59.24
Crustacea	Decapoda	*Homarus americanus* - medium	1	30	43.84	-69.64	70.580	8.120	0.137	33.09	17.60	290.75	163.99	131.19	81.99
Crustacea	Decapoda	*Homarus americanus* - large	1	30	43.84	-69.64	65.140	8.770	0.160	34.77	25.68	298.83	233.55	186.84	116.77
Crustacea	Decapoda	*Homarus americanus*	1	50	41.35	-70.79	79.500	8.020	0.120	35.20	11.27	284.42	174.45	139.56	87.23
Crustacea	Decapoda	*Libinia emarginata*	1	20	41.35	-70.79	76.440	8.650	0.134	35.72	13.61	286.76	186.56	149.25	93.28
Crustacea	Decapoda	*Munida iris*	1	20	37.62	-76.26	82.640	8.710	0.125	32.17	13.67	286.82	149.26	119.41	74.63
Crustacea	Decapoda	*Pandalus platyceros*	1	50	36.62	-121.91	60.940	8.090	0.158	35.20	11.27	284.42	174.45	139.56	87.23
Crustacea	Decapoda	*Palinurus argus*	1	60	21.84	-71.33	76.870	12.580	0.194	35.20	11.27	284.42	174.45	139.56	87.23
Crustacea	Decapoda	*Grapsus grapsus*	1	60	-9.36	46.40	72.770	6.180	0.101	35.20	11.27	284.42	174.45	139.56	87.23
Crustacea	Stomatopoda	*Chloridella empusa*	1	20	24.47	-81.55	28.560	15.990	0.665	35.20	11.27	284.42	174.45	139.56	87.23

[a] Literature data were measured via X-Ray difraction (*see* original ciation in Table 15.3 for methods) and the new data via inducted coupled plasma spectroscopy (ICP) (*see* text for the different procedures).

[b] *See* text for NEAR 3D analysis procedure to recover in situ field data.

[c] Scenarios of future CO_3^{2-} taken assuming a 10, 30 and 50 % reduction in the ion concentration with the other variables remaining constant.

Table 15.2. Details of the ion activity products (IAPs) corrected for in situ salinity, temperature and pressure and the correspondent activity coefficients [$\gamma_T(i)$] used, calculated from in situ temperature.

Organisms			Field data				Ion Activity Product (IAP) (S-T-P corrected) [a]				Activity coefficients - $\gamma_T(i)$ (T-corrected) [b]		
Taxa	Class	Species	Depth (m)	Lat.	Long.	mol % $MgCO_3$	Calcite	Aragonite	Mg-calcite (cleaned) [c]	Mg-calcite (minimally prepared) [c]	CO_3^{2-}	Mg^{2+}	Ca^{2+}
Echinodermata	Asteroidea	*Asterias rubens*	2	53.24	-4.46	4.807	4.3753E-07	6.7370E-07	1.0433E-08	9.4245E-09	0.0461	0.2067	0.1996
Echinodermata	Asteroidea	*Asterina gibossa*	2	50.63	-2.39	7.740	4.3805E-07	6.8024E-07	1.1919E-08	1.5972E-08	0.0471	0.2095	0.2010
Echinodermata	Asteroidea	*Zoroaster fulgens*	1140	49.28	-12.36	8.331	4.3876E-07	6.8930E-07	1.2294E-08	1.7837E-08	0.0489	0.2143	0.2034
Echinodermata	Asteroidea	*Marthasterias glacialis*	3	43.58	-6.24	8.435	4.3207E-07	6.6622E-07	1.2163E-08	1.7895E-08	0.0462	0.2070	0.1998
Echinodermata	Asteroidea	*Labidiaster annulatus*	175	-61.21	-56.01	11.506	4.1578E-07	6.6196E-07	1.3720E-08	3.0506E-08	0.0514	0.2211	0.2068
Echinodermata	Asteroidea	*Macroptychaster accrescens*	180	-63.53	-62.75	11.460	4.1578E-07	6.6196E-07	1.3692E-08	3.0257E-08	0.0514	0.2211	0.2068
Echinodermata	Asteroidea	*Paralophaster godfroyi*	180	-63.53	-62.75	11.185	4.1578E-07	6.6196E-07	1.3524E-08	2.8801E-08	0.0514	0.2211	0.2068
Echinodermata	Asteroidea	*Paralophaster sp.*	180	-63.53	-62.75	10.830	4.1578E-07	6.6196E-07	1.3310E-08	2.7023E-08	0.0514	0.2211	0.2068
Echinodermata	Asteroidea	*Perknaster sp.*	180	-63.53	-62.75	10.497	4.1578E-07	6.6196E-07	1.3112E-08	2.5456E-08	0.0514	0.2211	0.2068
Echinodermata	Asteroidea	*Acodontaster hodgsoni*	160	-64.15	-62.74	11.483	4.1578E-07	6.6196E-07	1.3706E-08	3.0381E-08	0.0514	0.2211	0.2068
Echinodermata	Asteroidea	*Kampylaster incurvatus*	160	-64.15	-62.74	10.830	4.1578E-07	6.6196E-07	1.3310E-08	2.7022E-08	0.0514	0.2211	0.2068
Echinodermata	Asteroidea	*Odontaster penicillatus*	160	-64.15	-62.74	11.552	4.1578E-07	6.6196E-07	1.3748E-08	3.0758E-08	0.0514	0.2211	0.2068
Echinodermata	Asteroidea	*Porania antarctica*	160	-64.15	-62.74	11.883	4.1578E-07	6.6196E-07	1.3954E-08	3.2643E-08	0.0514	0.2211	0.2068
Echinodermata	Asteroidea	*Diplasterias brandti*	30	-64.77	-64.05	11.105	4.1577E-07	6.6194E-07	1.3475E-08	2.8389E-08	0.0514	0.2211	0.2068
Echinodermata	Asteroidea	*Granaster nutrix*	30	-64.77	-64.05	9.692	4.1577E-07	6.6194E-07	1.2646E-08	2.2034E-08	0.0514	0.2211	0.2068
Echinodermata	Asteroidea	*Neosmilaster georgianus*	30	-64.77	-64.05	10.933	4.1577E-07	6.6194E-07	1.3371E-08	2.7527E-08	0.0514	0.2211	0.2068
Echinodermata	Asteroidea	*Odontaster meridionalis*	30	-64.77	-64.04	11.082	4.1577E-07	6.6194E-07	1.3461E-08	2.8272E-08	0.0514	0.2211	0.2068
Echinodermata	Asteroidea	*Perknaster aurorae*	30	-64.78	-63.99	9.945	4.1577E-07	6.6194E-07	1.2791E-08	2.3057E-08	0.0514	0.2211	0.2068
Echinodermata	Asteroidea	*Acodontaster conspicuus*	30	-65.07	-63.97	10.956	4.1577E-07	6.6194E-07	1.3385E-08	2.7640E-08	0.0514	0.2211	0.2068
Echinodermata	Asteroidea	*Perknaster fuscus antracticus*	30	-65.07	-63.97	11.563	4.1577E-07	6.6194E-07	1.3755E-08	3.0820E-08	0.0514	0.2211	0.2068
Echinodermata	Asteroidea	*Henricia sp.*	155	-65.67	-67.40	11.449	4.1578E-07	6.6196E-07	1.3685E-08	3.0195E-08	0.0514	0.2211	0.2068
Echinodermata	Asteroidea	*Diplopteraster verrucosus*	900	-66.29	-66.60	9.496	4.1584E-07	6.6205E-07	1.2538E-08	2.1277E-08	0.0514	0.2211	0.2068
Echinodermata	Asteroidea	*Odontaster validus*	18	-77.63	-146.41	6.847	4.1811E-07	6.6560E-07	1.1182E-08	1.3289E-08	0.0416	0.1949	0.1937
Echinodermata	Crinoidea	*Antedon mediterranea*	63	41.43	2.32	8.747	4.3657E-07	6.8648E-07	1.2481E-08	1.9150E-08	0.0490	0.2146	0.2035
Echinodermata	Echinoidea	*Psammechinus miliaris*	1	50.35	-4.13	5.357	4.3207E-07	6.6622E-07	1.0593E-08	1.0303E-08	0.0462	0.2070	0.1998
Echinodermata	Echinoidea	*Paracentrotus lividus*	2	43.58	-6.24	3.260	4.6088E-07	7.0633E-07	1.0123E-08	7.4265E-09	0.0457	0.2058	0.1992
Echinodermata	Echinoidea	*Paracentrotus lividus*	1	29.13	-13.60	7.021	4.5936E-07	7.0483E-07	1.1955E-08	1.4545E-08	0.0459	0.2062	0.1993
Echinodermata	Echinoidea	*Paracentrotus lividus*	1	29.13	-13.60	8.770	4.4530E-07	6.7270E-07	1.2647E-08	1.9465E-08	0.0442	0.2016	0.1971
Echinodermata	Echinoidea	*Tripneustes ventricosus*	6	25.12	-77.29	6.905	4.4850E-07	6.9758E-07	1.1694E-08	1.4007E-08	0.0475	0.2104	0.2015
Echinodermata	Echinoidea	*Cidaris blakei*	595	24.83	-77.50	15.407	4.3994E-07	6.7150E-07	1.6867E-08	6.3373E-08	0.0451	0.2043	0.1984
Echinodermata	Echinoidea	*Diadema setosum*	0.5	-18.85	159.75	14.036	4.3994E-07	6.7150E-07	1.5860E-08	4.9560E-08	0.0451	0.2043	0.1984

Echinodermata	Echinoidea	*Diadema setosum*	0.5	-18.85	159.75	5.975	4.1886E-07	6.6224E-07	1.0695E-08	1.1303E-08	0.0497	0.2164	0.2045
Echinodermata	Echinoidea	*Evechinus chloroticus*	5	-45.30	166.97	11.116	4.1886E-07	6.6224E-07	1.3473E-08	2.8429E-08	0.0497	0.2164	0.2045
Echinodermata	Echinoidea	*Evechinus chloroticus*	5	-45.30	166.97	4.714	4.1886E-07	6.6224E-07	1.0107E-08	9.0157E-09	0.0497	0.2164	0.2045
Echinodermata	Echinoidea	*Pseudechinus huttoni*	8	-45.41	167.10	6.545	4.1886E-07	6.6224E-07	1.0973E-08	1.2521E-08	0.0497	0.2164	0.2045
Echinodermata	Echinoidea	*Pseudechinus huttoni*	8	-45.41	167.10	4.363	4.1338E-07	6.5863E-07	9.9178E-09	8.4392E-09	0.0516	0.2215	0.2070
Echinodermata	Echinoidea	*Amphineustes similis*	685	-64.75	-65.47	8.793	4.1338E-07	6.5863E-07	1.2100E-08	1.8681E-08	0.0516	0.2215	0.2070
Echinodermata	Echinoidea	*Amphineustes similis*	685	-64.75	-65.47	4.492	4.1338E-07	6.5863E-07	9.9753E-09	8.6364E-09	0.0516	0.2215	0.2070
Echinodermata	Echinoidea	*Ctenocidaris perrieri*	685	-64.75	-65.47	8.908	4.1338E-07	6.5863E-07	1.2163E-08	1.9072E-08	0.0516	0.2215	0.2070
Echinodermata	Echinoidea	*Ctenocidaris perrieri*	685	-64.75	-65.47	4.117	4.2007E-07	6.6855E-07	9.9280E-09	8.1730E-09	0.0515	0.2212	0.2069
Echinodermata	Echinoidea	*Sterechinus neumayeri*	30	-65.07	-63.97	7.091	4.1397E-07	6.5837E-07	1.1194E-08	1.3747E-08	0.0510	0.2199	0.2062
Echinodermata	Echinoidea	*Sterechinus neumayeri*	30	-65.07	-63.97	5.333	4.1496E-07	6.5918E-07	1.0352E-08	1.0037E-08	0.0507	0.2191	0.2058
Echinodermata	Echinoidea	*Sterechinus neumayeri*	30	-65.07	-63.97	3.272	4.1397E-07	6.5837E-07	9.4303E-09	6.9294E-09	0.0510	0.2199	0.2062
Echinodermata	Echinoidea	*Sterechinus neumayeri*	30	-65.07	-63.97	7.369	4.1397E-07	6.5837E-07	1.1335E-08	1.4451E-08	0.0510	0.2199	0.2062
Echinodermata	Echinoidea	*Sterechinus neumayeri*	15	-77.06	164.42	9.658	4.1403E-07	6.5845E-07	1.2563E-08	2.1787E-08	0.0510	0.2199	0.2062
Echinodermata	Holothuroidea	*Molpadia musculus*	685	-64.75	-65.47	8.770	4.1348E-07	6.5767E-07	1.2061E-08	1.8563E-08	0.0510	0.2199	0.2062
Echinodermata	Holothuroidea	*Pseudostichopus spiculiferus*	900	-66.29	-66.60	9.577	4.3876E-07	6.8930E-07	1.3002E-08	2.2305E-08	0.0489	0.2143	0.2034
Echinodermata	Ophiuroidea	*Ophiosium lynami*	1140	49.20	-12.30	13.343	4.5936E-07	7.0483E-07	1.5880E-08	4.5204E-08	0.0459	0.2062	0.1993
Echinodermata	Ophiuroidea	*Ophiura longicauda*	1	29.12	-13.56	10.738	4.1386E-07	6.5826E-07	1.3185E-08	2.6441E-08	0.0510	0.2200	0.2062
Echinodermata	Ophiuroidea	*Ophiura longicauda*	1	29.12	-13.56	10.658	4.1386E-07	6.5826E-07	1.3137E-08	2.6063E-08	0.0510	0.2200	0.2062
Echinodermata	Ophiuroidea	*Ophionotus victoriae*	30	-64.77	-64.05	8.562	4.5936E-07	7.0483E-07	1.2812E-08	1.9174E-08	0.0459	0.2062	0.1993
Echinodermata	Ophiuroidea	*Ophiosparte gigas*	30	-64.77	-64.05	9.081	4.7802E-07	7.3771E-07	1.3534E-08	2.1721E-08	0.0466	0.2083	0.2004
Echinodermata	Asteroidea	*Asterias linckii*	20	65.81	39.73	11.197	4.2357E-07	6.5619E-07	1.3568E-08	2.8941E-08	0.0466	0.2082	0.2004
Echinodermata	Asteroidea	*Orthasterias tanneri*	30	61.68	3.31	11.036	4.3290E-07	6.8265E-07	1.3761E-08	2.8726E-08	0.0495	0.2158	0.2042
Echinodermata	Asteroidea	*Ctenodiscus crispatus*	80	46.90	-59.10	10.256	4.0207E-07	6.4250E-07	1.2680E-08	2.3832E-08	0.0522	0.2230	0.2077
Echinodermata	Asteroidea	*Asterias vulgaris*	10	44.79	-66.92	12.237	4.1433E-07	6.5354E-07	1.4031E-08	3.4423E-08	0.0491	0.2149	0.2037
Echinodermata	Asteroidea	*Asterias acervata borealis*	40	43.58	-65.17	12.443	4.3290E-07	6.8265E-07	1.4658E-08	3.6971E-08	0.0495	0.2158	0.2042
Echinodermata	Asteroidea	*Asterina pectinifera*	10	43.20	141.05	9.116	4.4269E-07	6.9063E-07	1.2793E-08	2.0627E-08	0.0478	0.2114	0.2020
Echinodermata	Asteroidea	*Asterias forbesi*	10	41.42	-70.80	9.635	4.3476E-07	6.8183E-07	1.2932E-08	2.2357E-08	0.0485	0.2133	0.2029
Echinodermata	Asteroidea	*Odontaster hispidus*	40	41.30	-70.80	13.070	4.0194E-07	6.2437E-07	1.4203E-08	3.8974E-08	0.0466	0.2082	0.2004
Echinodermata	Asteroidea	*Plutonaster agassizii*	10	41.30	-70.80	13.991	3.9438E-07	6.0729E-07	1.4617E-08	4.5398E-08	0.0455	0.2052	0.1988
Echinodermata	Asteroidea	*Pontaster tenuispinus*	40	41.30	-70.80	11.963	4.2358E-07	6.5620E-07	1.4044E-08	3.3208E-08	0.0466	0.2082	0.2004
Echinodermata	Asteroidea	*Astropecten andromeda*	10	41.30	-70.80	11.517	4.2358E-07	6.5620E-07	1.3765E-08	3.0654E-08	0.0466	0.2082	0.2004
Echinodermata	Asteroidea	*Leptasterias compta*	100	40.28	-69.85	12.979	4.2320E-07	6.5414E-07	1.4689E-08	3.9815E-08	0.0463	0.2075	0.2000
Echinodermata	Asteroidea	*Benthopecten spinosus*	100	39.25	-68.13	12.317	4.4269E-07	6.9064E-07	1.4771E-08	3.6630E-08	0.0478	0.2114	0.2020
Echinodermata	Asteroidea	*Astropecten articulatus*	200	35.71	-73.50	10.612	4.4269E-07	6.9063E-07	1.3682E-08	2.6975E-08	0.0478	0.2114	0.2020
Echinodermata	Asteroidea	*Urasterias linckii*	200	35.71	-73.50	10.348	4.4269E-07	6.9064E-07	1.3521E-08	2.5727E-08	0.0478	0.2114	0.2020
Echinodermata	Asteroidea	*Asterias tanneri*	200	35.71	-73.50	15.090	4.4270E-07	6.9065E-07	1.6730E-08	6.0238E-08	0.0478	0.2114	0.2020
Echinodermata	Asteroidea	*Asterina miniata*	10	35.20	-121.30	12.135	4.4269E-07	6.9063E-07	1.4650E-08	3.5449E-08	0.0478	0.2114	0.2020
Echinodermata	Asteroidea	*Marthasterias glacialis*	30	35.20	-121.30	10.405	4.5545E-07	6.9199E-07	1.3831E-08	2.6522E-08	0.0448	0.2033	0.1979
Echinodermata	Asteroidea	*Astropecten americanus*	10	26.90	-82.80	11.975	4.5545E-07	6.9199E-07	1.4841E-08	3.5147E-08	0.0448	0.2033	0.1979

Echinodermata	Asteroidea	*Asterina minuta*	15	18.04	-67.96	9.692	4.1057E-07	6.3794E-07	1.2394E-08	2.1595E-08	0.0468	0.2087	0.2006
Echinodermata	Asteroidea	*Linckia guildingii*	30	18.04	-67.96	11.780	4.5488E-07	6.9475E-07	1.4694E-08	3.3900E-08	0.0453	0.2047	0.1986
Echinodermata	Asteroidea	*Linckia laevigata*	30	18.04	-67.96	14.536	4.6124E-07	7.0450E-07	1.6804E-08	5.6157E-08	0.0454	0.2049	0.1987
Echinodermata	Asteroidea	*Acanthaster planci*	25	5.86	-162.08	15.441	3.1019E-07	4.7556E-07	1.6043E-08	6.0553E-08	0.0432	0.1992	0.1958
Echinodermata	Asteroidea	*Ctenodiscus procurator*	30	-35.70	-72.80	16.547	4.2292E-07	6.3717E-07	1.7289E-08	7.5716E-08	0.0437	0.2004	0.1965
Echinodermata	Asteroidea	*Ctenodiscus australis*	10	-43.60	-74.00	10.876	4.2292E-07	6.3717E-07	1.3402E-08	2.7379E-08	0.0437	0.2004	0.1965
Echinodermata	Crinoidea	*Heliometra glacialis*	20	68.20	39.20	11.082	4.3078E-07	6.8076E-07	1.3755E-08	2.8890E-08	0.0499	0.2169	0.2047
Echinodermata	Crinoidea	*Ptilocrinus pinnatus*	10	53.10	-130.00	9.254	3.9264E-07	6.2334E-07	1.1807E-08	1.9395E-08	0.0498	0.2166	0.2045
Echinodermata	Crinoidea	*Florometra asperrima*	12	47.10	-124.20	11.013	4.0264E-07	6.3130E-07	1.2973E-08	2.6998E-08	0.0479	0.2116	0.2020
Echinodermata	Crinoidea	*Bythocrinus robustus*	40	42.30	-70.77	10.922	3.9438E-07	6.0730E-07	1.2735E-08	2.6178E-08	0.0455	0.2052	0.1988
Echinodermata	Crinoidea	*Hathrometra dentata*	30	41.30	-70.80	10.795	4.1549E-07	6.2584E-07	1.3190E-08	2.6656E-08	0.0436	0.2002	0.1963
Echinodermata	Crinoidea	*Psathyrometra fragilis*	20	35.07	139.70	11.826	4.1549E-07	6.2584E-07	1.3815E-08	3.2069E-08	0.0436	0.2002	0.1963
Echinodermata	Crinoidea	*Pentametrocrinus japonicus*	20	34.90	138.50	11.758	3.9438E-07	6.0730E-07	1.3222E-08	3.0413E-08	0.0455	0.2052	0.1988
Echinodermata	Crinoidea	*Crinometra concinna*	40	28.05	-96.02	12.945	4.3856E-07	6.7473E-07	1.5061E-08	4.0636E-08	0.0460	0.2065	0.1995
Echinodermata	Crinoidea	*Isocrinus decorus*	50	21.40	-76.70	13.582	4.1770E-07	6.4826E-07	1.4948E-08	4.3940E-08	0.0468	0.2086	0.2006
Echinodermata	Crinoidea	*Endoxocrinus parra*	60	21.40	-76.70	14.717	4.0140E-07	6.0219E-07	1.5378E-08	5.2659E-08	0.0431	0.1988	0.1956
Echinodermata	Crinoidea	*Tropiometra picta*	30	21.40	-76.70	14.161	4.0140E-07	6.0219E-07	1.4999E-08	4.7664E-08	0.0431	0.1988	0.1956
Echinodermata	Crinoidea	*Promachocrinus kerguelensis*	20	11.17	-60.68	13.571	4.0140E-07	6.0219E-07	1.4607E-08	4.2873E-08	0.0431	0.1988	0.1956
Echinodermata	Crinoidea	*Capillaster multiradiata*	30	7.85	116.90	11.838	4.0140E-07	6.0219E-07	1.3513E-08	3.1418E-08	0.0431	0.1988	0.1956
Echinodermata	Crinoidea	*Pachylometra patula*	30	7.85	116.90	12.888	4.0140E-07	6.0219E-07	1.4166E-08	3.7930E-08	0.0431	0.1988	0.1956
Echinodermata	Crinoidea	*Catoptometra ophiura*	30	7.85	116.90	14.320	4.0140E-07	6.0219E-07	1.5107E-08	4.9042E-08	0.0431	0.1988	0.1956
Echinodermata	Crinoidea	*Hypalocrinus naresianus*	30	7.85	116.90	13.582	4.4530E-07	6.7270E-07	1.5698E-08	4.6146E-08	0.0442	0.2016	0.1971
Echinodermata	Crinoidea	*Parametra granulata*	30	7.85	116.90	13.502	4.4530E-07	6.7270E-07	1.5642E-08	4.5491E-08	0.0442	0.2016	0.1971
Echinodermata	Crinoidea	*Craspedometra anceps*	30	7.85	116.90	13.673	4.4530E-07	6.7270E-07	1.5762E-08	4.6904E-08	0.0442	0.2016	0.1971
Echinodermata	Crinoidea	*Zygometra microdiscus*	40	-5.99	134.10	15.904	4.5877E-07	6.9759E-07	1.7800E-08	7.1501E-08	0.0449	0.2036	0.1980
Echinodermata	Crinoidea	*Tropiometra carinata*	15	-22.98	-43.20	9.197	4.2805E-07	6.4473E-07	1.2537E-08	2.0435E-08	0.0437	0.2005	0.1965
Echinodermata	Crinoidea	*Pilometra mülleri*	20	-33.85	151.26	15.486	4.0763E-07	6.1153E-07	1.6086E-08	6.1088E-08	0.0432	0.1990	0.1957
Echinodermata	Echinoidea	*Strongylocentrotus droebachiensis*	40	64.00	-38.00	7.033	4.2893E-07	6.7760E-07	1.1425E-08	1.3922E-08	0.0498	0.2166	0.2046
Echinodermata	Echinoidea	*Echinarachnius parma*	32	59.20	-165.80	7.195	4.0142E-07	6.3513E-07	1.0932E-08	1.3615E-08	0.0494	0.2155	0.2040
Echinodermata	Echinoidea	*Arbacia pustulosa*	15	40.76	14.35	8.643	4.1469E-07	6.5349E-07	1.1943E-08	1.8069E-08	0.0490	0.2145	0.2035
Echinodermata	Echinoidea	*Echinus esculentus*	10	38.00	-1.02	7.358	4.1581E-07	6.2737E-07	1.1305E-08	1.4390E-08	0.0438	0.2006	0.1965
Echinodermata	Echinoidea	*Paracentrotus lividus*	5	37.24	13.68	9.830	4.2253E-07	6.3219E-07	1.2801E-08	2.2722E-08	0.0431	0.1988	0.1956
Echinodermata	Echinoidea	*Echinus affinis*	200	35.71	-73.50	8.712	4.0194E-07	6.2437E-07	1.1679E-08	1.7836E-08	0.0466	0.2082	0.2004
Echinodermata	Echinoidea	*Lytechinus anamesus*	20	35.20	-121.30	6.359	4.5489E-07	6.9477E-07	1.1519E-08	1.2819E-08	0.0453	0.2047	0.1986
Echinodermata	Echinoidea	*Clypeaster testudinarius*	20	33.40	134.60	9.968	4.7802E-07	7.3770E-07	1.4084E-08	2.5466E-08	0.0466	0.2083	0.2004
Echinodermata	Echinoidea	*Strongylocentrotus fragilis*	60	29.00	-115.00	8.146	4.1343E-07	6.4838E-07	1.1635E-08	1.6465E-08	0.0481	0.2123	0.2024
Echinodermata	Echinoidea	*Prionocidaris baculosa*	15	28.02	34.97	10.325	4.0140E-07	6.3510E-07	1.2580E-08	2.3865E-08	0.0494	0.2155	0.2040
Echinodermata	Echinoidea	*Tetrocidaris affinis*	10	26.90	-82.80	10.853	4.4352E-07	6.6917E-07	1.3850E-08	2.8206E-08	0.0440	0.2013	0.1969
Echinodermata	Echinoidea	*Echinometra lucunter*	20	18.04	-67.96	9.035	4.7802E-07	7.3770E-07	1.3506E-08	2.1542E-08	0.0466	0.2083	0.2004
Echinodermata	Echinoidea	*Mellita sexiesperforatus*	30	18.04	-67.96	12.089	3.8730E-07	6.1289E-07	1.3254E-08	3.1875E-08	0.0490	0.2145	0.2035
Echinodermata	Echinoidea	*Encope californica*	20	-1.00	-91.01	13.434	4.0139E-07	6.0219E-07	1.4518E-08	4.1836E-08	0.0431	0.1988	0.1956

Echinodermata	Echinoidea	*Tetrapygus niger*	20	-9.40	-78.50	14.229	4.4598E-07	6.7456E-07	1.6176E-08	5.1876E-08	0.0443	0.2020	0.1972
Echinodermata	Echinoidea	*Heterocentrotus mammillatus*	20	-27.64	-144.33	12.420	5.1766E-07	7.8600E-07	1.6711E-08	4.2019E-08	0.0449	0.2036	0.1981
Echinodermata	Echinoidea	*Lytechinus albus*	10	-43.60	-74.00	13.832	4.0140E-07	6.0219E-07	1.4779E-08	4.4931E-08	0.0431	0.1988	0.1956
Echinodermata	Ophiuroidea	*Gorgonocephalus caryi*	15	61.30	-166.30	11.265	3.9542E-07	6.2657E-07	1.2981E-08	2.7945E-08	0.0495	0.2158	0.2042
Echinodermata	Ophiuroidea	*Astrophyton sp.*	60	56.00	2.90	11.116	4.3476E-07	6.8183E-07	1.3821E-08	2.9164E-08	0.0485	0.2133	0.2029
Echinodermata	Ophiuroidea	*Ophiopholis aculeata japonica*	10	53.91	-166.50	9.807	4.2031E-07	6.4040E-07	1.2691E-08	2.2457E-08	0.0447	0.2032	0.1979
Echinodermata	Ophiuroidea	*Gorgonocephalus arcticus*	10	41.50	-70.30	9.370	3.9610E-07	6.2605E-07	1.1926E-08	1.9896E-08	0.0490	0.2146	0.2036
Echinodermata	Ophiuroidea	*Ophioglypha sarsii*	100	39.54	-72.35	15.498	4.2031E-07	6.4040E-07	1.6386E-08	6.2319E-08	0.0447	0.2032	0.1979
Echinodermata	Ophiuroidea	*Gorgonocephalus eucnemis*	50	38.30	139.00	10.635	4.3534E-07	6.8364E-07	1.3547E-08	2.6792E-08	0.0488	0.2139	0.2032
Echinodermata	Ophiuroidea	*Ophionereis eurybrachiplax*	50	38.30	139.00	11.471	4.1583E-07	6.3458E-07	1.3568E-08	3.0031E-08	0.0449	0.2035	0.1980
Echinodermata	Ophiuroidea	*Ophioglypha lütkeni*	200	35.20	-121.30	9.635	4.2322E-07	6.5416E-07	1.2641E-08	2.1854E-08	0.0463	0.2075	0.2000
Echinodermata	Ophiuroidea	*Ophiothrix angulata*	200	21.40	-76.70	11.872	3.9965E-07	6.2571E-07	1.3407E-08	3.1315E-08	0.0476	0.2109	0.2017
Echinodermata	Ophiuroidea	*Ophiocamax fasciculata*	100	21.40	-76.70	8.250	4.5699E-07	6.9409E-07	1.2587E-08	1.8064E-08	0.0448	0.2033	0.1979
Echinodermata	Ophiuroidea	*Ophiocoma erinaceus*	20	20.10	-155.30	16.287	4.5699E-07	6.9409E-07	1.8058E-08	7.6375E-08	0.0448	0.2033	0.1979
Echinodermata	Ophiuroidea	*Ophioderma cinerum*	30	18.50	-66.60	16.828	4.5699E-07	6.9410E-07	1.8502E-08	8.4152E-08	0.0448	0.2033	0.1979
Echinodermata	Ophiuroidea	*Ophiocoma aethiops*	25	18.04	-67.96	15.034	4.5699E-07	6.9410E-07	1.7070E-08	6.0996E-08	0.0448	0.2033	0.1979
Echinodermata	Ophiuroidea	*Ophiomixa flaccida*	120	18.04	-67.96	13.991	4.1179E-07	6.2012E-07	1.5132E-08	4.6996E-08	0.0435	0.2000	0.1963
Echinodermata	Ophiuroidea	*Ophiocoma pumila*	120	18.04	-67.96	13.571	4.5182E-07	6.8445E-07	1.5853E-08	4.6531E-08	0.0445	0.2025	0.1975
Echinodermata	Ophiuroidea	*Ophiomusium lymani*	200	-1.00	-91.01	7.752	4.0909E-07	6.4861E-07	1.1389E-08	1.5286E-08	0.0500	0.2173	0.2049
Echinodermata	Ophiuroidea	*Ophioglypha lymani*	30	-35.70	-72.80	8.920	4.5181E-07	6.8444E-07	1.2865E-08	2.0204E-08	0.0445	0.2025	0.1975
Coralline algae	-	*Lithothamnium sp.*	10	78.00	20.00	10.129	4.3290E-07	6.8265E-07	1.3212E-08	2.4413E-08	0.0495	0.2158	0.2042
Coralline algae	-	*Lithothamnium soriferum*	10	75.00	20.00	11.151	4.2154E-07	6.6919E-07	1.3609E-08	2.8850E-08	0.0508	0.2192	0.2059
Coralline algae	-	*Lithothamium glaciale*	10	75.00	20.00	15.283	4.5519E-07	6.9456E-07	1.7205E-08	6.3574E-08	0.0452	0.2045	0.1985
Coralline algae	-	*Lithothamnium fornicatum*	10	72.00	20.00	11.758	4.3290E-07	6.8265E-07	1.4214E-08	3.2693E-08	0.0495	0.2158	0.2042
Coralline algae	-	*Lithothamnium polymorphum*	10	57.00	12.00	10.623	4.0116E-07	6.3475E-07	1.2745E-08	2.5166E-08	0.0494	0.2155	0.2040
Coralline algae	-	*Corallina squamata* - 29-Nov	5	50.60	-2.30	14.002	4.4067E-07	6.8624E-07	1.5869E-08	4.9360E-08	0.0475	0.2106	0.2016
Coralline algae	-	*Corallina squamata* - 29-Jan	5	50.60	-2.30	13.980	4.4143E-07	6.8761E-07	1.5874E-08	4.9228E-08	0.0476	0.2108	0.2016
Coralline algae	-	*Corallina squamata* - 26-Mar	5	50.60	-2.30	12.956	4.4120E-07	6.8705E-07	1.5154E-08	4.0951E-08	0.0475	0.2107	0.2016
Coralline algae	-	*Corallina squamata* - 28-May	5	50.60	-2.30	12.717	3.8431E-07	6.0465E-07	1.3541E-08	3.5434E-08	0.0480	0.2118	0.2021
Coralline algae	-	*Corallina squamata* - 01-Jul	5	50.60	-2.30	11.460	4.7802E-07	7.3770E-07	1.5059E-08	3.3279E-08	0.0466	0.2083	0.2004
Coralline algae	-	*Corallina squamata* - 13-Aug	5	50.60	-2.30	9.531	3.9964E-07	6.2569E-07	1.2069E-08	2.0577E-08	0.0476	0.2109	0.2017
Coralline algae	-	*Corallina squamata* - 12-Sep	5	50.60	-2.30	27.269	4.1825E-07	6.2442E-07	2.7830E-08	5.1538E-07	0.0429	0.1982	0.1953
Coralline algae	-	*Corallina squamata* - 10-Oct	5	50.60	-2.30	26.986	4.1825E-07	6.2442E-07	2.7479E-08	4.8988E-07	0.0429	0.1982	0.1953
Coralline algae	-	*Corallina officinalis*	5	49.60	-1.20	26.158	4.1825E-07	6.2442E-07	2.6475E-08	4.2225E-07	0.0429	0.1982	0.1953
Coralline algae	-	*Lithothamnium calcareum*	10	48.08	-4.00	17.805	4.1825E-07	6.2442E-07	1.8195E-08	9.4383E-08	0.0429	0.1982	0.1953
Coralline algae	-	*Lithophyllum incrustans*	10	48.00	-3.00	22.049	4.5331E-07	6.8713E-07	2.3252E-08	2.1341E-07	0.0445	0.2027	0.1976
Coralline algae	-	*Phymatolithon compactum*	10	48.00	-55.00	20.085	4.5331E-07	6.8713E-07	2.1290E-08	1.5004E-07	0.0445	0.2027	0.1976
Coralline algae	-	*Lithophyllum tortuosum*	20	44.00	9.00	18.612	4.1929E-07	6.2948E-07	1.8870E-08	1.0909E-07	0.0433	0.1995	0.1960
Coralline algae	-	*Lithophyllum proboscideum*	15	37.00	-122.00	19.338	4.3241E-07	6.5228E-07	1.9904E-08	1.2688E-07	0.0439	0.2010	0.1967
Coralline algae	-	*Goniolithon strictum - old*	30	25.00	-75.00	15.915	3.3210E-07	4.9511E-07	1.4452E-08	5.8141E-08	0.0415	0.1945	0.1935

Coralline algae	-	*Goniolithon strictum - old*	30	25.00	-75.00	15.814	4.1865E-07	6.2509E-07	1.6649E-08	6.6072E-08	0.0429	0.1982	0.1954
Coralline algae	-	*Goniolithon strictum - young*	30	25.00	-75.00	19.516	4.1801E-07	6.2811E-07	1.9607E-08	1.2802E-07	0.0434	0.1997	0.1961
Coralline algae	-	*Lithophyllum pachydermum*	30	25.00	-75.00	15.170	4.1169E-07	6.1722E-07	1.5970E-08	5.8120E-08	0.0431	0.1990	0.1957
Coralline algae	-	*Goniolithon acropectum*	20	18.00	-68.00	20.863	4.1809E-07	6.2743E-07	2.0838E-08	1.6306E-07	0.0433	0.1994	0.1959
Coralline algae	-	*Amphiroa fragilissima*	10	18.00	-68.00	7.114	4.1910E-07	6.3168E-07	1.1247E-08	1.3855E-08	0.0437	0.2004	0.1965
Coralline algae	-	*Lithothamnium nodosum*	5	0.00	-90.00	12.260	4.3988E-07	6.8353E-07	1.4649E-08	3.6049E-08	0.0472	0.2098	0.2012
Coralline algae	-	*Lithophyllum oncodes*	30	-7.00	56.00	11.254	4.3988E-07	6.8353E-07	1.4001E-08	3.0095E-08	0.0472	0.2098	0.2012
Coralline algae	-	*Goniolithon orthoblastum*	10	-10.00	145.00	10.807	4.3988E-07	6.8353E-07	1.3723E-08	2.7776E-08	0.0472	0.2098	0.2012
Coralline algae	-	*Lithothamnium erubescens*	10	-10.00	123.00	10.129	4.3988E-07	6.8353E-07	1.3312E-08	2.4597E-08	0.0472	0.2098	0.2012
Coralline algae	-	*Archaeolithothamium episporum*	10	-10.00	80.00	10.899	4.3988E-07	6.8353E-07	1.3780E-08	2.8237E-08	0.0472	0.2098	0.2012
Coralline algae	-	*Lithothamnium kaiseri*	10	-15.00	-172.00	11.414	4.3988E-07	6.8353E-07	1.4103E-08	3.0973E-08	0.0472	0.2098	0.2012
Coralline algae	-	*Porolithon craspedium*	10	-15.00	-172.00	12.043	4.3988E-07	6.8353E-07	1.4507E-08	3.4673E-08	0.0472	0.2098	0.2012
Coralline algae	-	*Porolithon oncodes*	10	-15.00	-172.00	11.872	4.3988E-07	6.8353E-07	1.4395E-08	3.3623E-08	0.0472	0.2098	0.2012
Foraminifera	-	*Pulvinulina menardii* - pelagic	20	40.56	-66.15	4.328	4.1968E-07	6.3990E-07	9.9113E-09	8.3939E-09	0.0448	0.2034	0.1979
Foraminifera	-	*Polytrema mineaccum* - benthic	100	25.00	-77.00	2.118	4.1098E-07	6.1442E-07	8.8848E-09	5.5905E-09	0.0429	0.1983	0.1954
Foraminifera	-	*Orbitolites marginatis* - benthic	50	24.60	-81.96	5.765	4.1400E-07	6.2024E-07	1.0512E-08	1.0800E-08	0.0431	0.1989	0.1957
Foraminifera	-	*Amphistegina lessonii* - pelagic	20	16.10	-22.95	14.524	4.2159E-07	6.3838E-07	1.5736E-08	5.2508E-08	0.0442	0.2016	0.1971
Foraminifera	-	*Sphaeroidina dehiscens* - pelagic	20	12.40	121.60	12.283	4.4373E-07	6.6901E-07	1.4775E-08	3.6473E-08	0.0440	0.2011	0.1968
Foraminifera	-	*Orbitolites complanata* - benthic	30	-17.30	177.47	10.887	4.4373E-07	6.6902E-07	1.3877E-08	2.8393E-08	0.0440	0.2011	0.1968
Hydrocorallia	-	*Millepora alcicornis*	10	24.60	-81.96	1.126	4.4530E-07	6.7270E-07	8.9731E-09	4.9408E-09	0.0442	0.2016	0.1971
Hydrocorallia	-	*Distichopora nitida*	20	7.40	151.50	1.516	4.5521E-07	6.8579E-07	9.2846E-09	5.3877E-09	0.0440	0.2011	0.1968
Hydrocorallia	-	*Millepora braziliensis*	30	-12.20	-36.80	0.285	4.0680E-07	6.1047E-07	8.1170E-09	3.9914E-09	0.0432	0.1990	0.1958
Hexacorallia	-	*Madracis decactis*	20	32.40	-64.90	1.315	4.4373E-07	6.6901E-07	9.0292E-09	5.0998E-09	0.0440	0.2011	0.1968
Hexacorallia	-	*Siderastrea radians*	20	32.40	-64.90	1.031	4.4373E-07	6.6901E-07	8.9149E-09	4.8466E-09	0.0440	0.2011	0.1968
Hexacorallia	-	*Flabellum alabastrum*	10	26.00	-77.20	0.463	4.4373E-07	6.6901E-07	8.6902E-09	4.3767E-09	0.0440	0.2011	0.1968
Hexacorallia	-	*Acropora cervicornis*	15	26.00	-77.20	0.747	4.4373E-07	6.6901E-07	8.8018E-09	4.6058E-09	0.0440	0.2011	0.1968
Hexacorallia	-	*Favia fragum*	20	24.60	-81.96	0.439	4.4373E-07	6.6901E-07	8.6809E-09	4.3582E-09	0.0440	0.2011	0.1968
Hexacorallia	-	*Dasmosmilia lymani*	10	24.60	-81.96	0.901	4.5519E-07	6.9636E-07	9.0197E-09	4.8185E-09	0.0455	0.2052	0.1989
Hexacorallia	-	*Balanophyllia floridana*	10	24.54	-81.80	0.640	4.3202E-07	6.5241E-07	8.5896E-09	4.4308E-09	0.0440	0.2012	0.1969
Hexacorallia	-	*Paracyathus defilipii*	10	24.54	-81.80	0.534	4.5631E-07	6.9328E-07	8.8914E-09	4.5211E-09	0.0448	0.2033	0.1979
Hexacorallia	-	*Deltocyathus italicus*	20	18.50	-63.51	0.569	4.5519E-07	6.9636E-07	8.8864E-09	4.5402E-09	0.0455	0.2052	0.1989
Hexacorallia	-	*Desmophyllum ingens*	15	-36.55	-73.00	0.700	4.1192E-07	6.5691E-07	8.3483E-09	4.3407E-09	0.0519	0.2223	0.2074
Octocorallia	-	*Gorgonia sp.*	30	54.60	154.40	0.415	4.0139E-07	6.0219E-07	8.0914E-09	4.0493E-09	0.0431	0.1988	0.1956
Octocorallia	-	*Alcyonium carneum*	50	45.18	-55.85	14.195	4.1031E-07	6.1563E-07	1.5248E-08	4.8677E-08	0.0432	0.1991	0.1958
Octocorallia	-	*Paramuricea borealis*	50	45.18	-55.85	13.434	4.2414E-07	6.4609E-07	1.5034E-08	4.3324E-08	0.0448	0.2033	0.1979
Octocorallia	-	*Alcyonium carneum*	50	45.18	-55.85	9.024	3.9478E-07	6.3015E-07	1.1786E-08	1.8770E-08	0.0512	0.2205	0.2065
Octocorallia	-	*Pennatula aculeata*	50	44.45	-58.51	15.554	4.1156E-07	6.1608E-07	1.6252E-08	6.2282E-08	0.0430	0.1986	0.1956

Octocorallia	-	*Paragorgia arborea*	50	44.36	-63.75	15.509	4.5631E-07	6.9329E-07	1.7417E-08	6.6344E-08	0.0448	0.2033	0.1979
Octocorallia	-	*Paragorgia arborea*	50	43.00	-62.00	10.841	4.0006E-07	6.2751E-07	1.2813E-08	2.6055E-08	0.0479	0.2116	0.2020
Octocorallia	-	*Corallium elatior*	40	42.25	130.91	7.810	4.1150E-07	6.5037E-07	1.1450E-08	1.5489E-08	0.0494	0.2157	0.2041
Octocorallia	-	*Primnoa resedaeformis*	30	42.25	130.91	15.960	4.3860E-07	6.7385E-07	1.7246E-08	6.9804E-08	0.0458	0.2061	0.1993
Octocorallia	-	*Primnoa reseda*	40	42.25	-63.25	6.719	4.3608E-07	6.6488E-07	1.1346E-08	1.3254E-08	0.0450	0.2038	0.1982
Octocorallia	-	*Rhipidogorgia flabellum*	20	32.40	-64.90	8.261	4.3608E-07	6.6488E-07	1.2159E-08	1.7477E-08	0.0450	0.2038	0.1982
Octocorallia	-	*Pleurocorallium johnsoni*	30	25.75	-20.20	8.562	4.3608E-07	6.6488E-07	1.2325E-08	1.8445E-08	0.0450	0.2038	0.1982
Octocorallia	-	*Gorgonia acerosa*	50	24.60	-81.96	9.347	4.3608E-07	6.6488E-07	1.2766E-08	2.1233E-08	0.0450	0.2038	0.1982
Octocorallia	-	*Leptogorgia pulchra*	80	24.60	-108.25	14.660	4.5220E-07	6.7849E-07	1.6682E-08	5.6689E-08	0.0436	0.2001	0.1963
Octocorallia	-	*Xiphigorgia anceps*	20	24.47	-81.55	14.252	4.2170E-07	6.4180E-07	1.5534E-08	4.9969E-08	0.0446	0.2030	0.1977
Octocorallia	-	*Muricea echinata*	10	22.86	-106.10	9.393	3.8968E-07	6.1189E-07	1.1779E-08	1.9713E-08	0.0478	0.2114	0.2019
Octocorallia	-	*Leptogorgia rigida*	150	22.86	-109.79	10.566	4.0344E-07	6.3544E-07	1.2746E-08	2.4976E-08	0.0486	0.2135	0.2030
Octocorallia	-	*Heliopora cerulea*	20	12.40	121.60	15.113	4.5187E-07	6.8473E-07	1.6991E-08	6.1364E-08	0.0445	0.2026	0.1975
Octocorallia	-	*Tubipora purpurea*	10	1.33	103.83	14.660	4.1583E-07	6.3457E-07	1.5657E-08	5.3206E-08	0.0449	0.2035	0.1980
Octocorallia	-	*Phyllogorgia quercifolia*	10	-3.83	-32.41	7.079	3.9595E-07	6.2881E-07	1.0780E-08	1.3218E-08	0.0500	0.2171	0.2048
Octocorallia	-	*Ctenocella pectinata*	20	-10.00	142.20	10.841	4.1549E-07	6.2584E-07	1.3217E-08	2.6876E-08	0.0436	0.2002	0.1963
Octocorallia	-	*Muricea humilis*	30	-12.20	-36.80	7.253	4.2357E-07	6.5619E-07	1.1367E-08	1.4267E-08	0.0466	0.2082	0.2004
Octocorallia	-	*Gorgonia subfruticosa*	45	-18.00	-178.00	7.810	4.2357E-07	6.5619E-07	1.1654E-08	1.5765E-08	0.0466	0.2082	0.2004
Octocorallia	-	*Plexaurella grandiflora*	20	-28.40	155.67	10.566	4.2357E-07	6.5619E-07	1.3189E-08	2.5845E-08	0.0466	0.2082	0.2004
Octocorallia	-	*Eunicella papillose*	30	-34.21	18.35	15.870	4.1771E-07	6.4826E-07	1.6565E-08	6.6239E-08	0.0468	0.2086	0.2006
Octocorallia	-	*Eunicella alba*	30	-34.22	18.48	16.344	4.1917E-07	6.5609E-07	1.6982E-08	7.2373E-08	0.0479	0.2118	0.2021
Octocorallia	-	*Eunicella tricoronata*	30	-34.22	18.48	18.052	4.1825E-07	6.2442E-07	1.8398E-08	9.8652E-08	0.0429	0.1982	0.1953
Octocorallia	-	*Lophogorgia flamea*	30	-34.22	18.48	18.142	4.3942E-07	6.8438E-07	1.9068E-08	1.0348E-07	0.0475	0.2107	0.2016
Bryozoa	-	*Flustra membranacea*	50	59.17	-151.60	0.747	3.8270E-07	6.1254E-07	7.9476E-09	4.1588E-09	0.0514	0.2210	0.2068
Bryozoa	-	*Cellepora incrassata*	50	44.69	-62.69	1.315	4.3860E-07	6.7385E-07	8.9352E-09	5.0467E-09	0.0458	0.2061	0.1993
Bryozoa	-	*Schizoporella unicornis*	10	41.35	-70.79	7.126	3.8271E-07	6.1255E-07	1.0583E-08	1.3058E-08	0.0514	0.2210	0.2068
Bryozoa	-	*Bugula turrita*	40	41.23	-70.07	8.134	3.9694E-07	6.3242E-07	1.1353E-08	1.6042E-08	0.0508	0.2193	0.2059
Bryozoa	-	*Lepralia sp.*	20	40.80	14.20	5.905	4.7804E-07	7.3592E-07	1.1731E-08	1.2282E-08	0.0463	0.2075	0.2000
Bryozoa	-	*Amathia spiralis*	20	35.22	-75.60	3.060	4.4269E-07	6.9064E-07	9.7474E-09	6.9615E-09	0.0478	0.2114	0.2020
Bryozoa	-	*Holoporella albirostris*	20	24.47	-81.55	11.162	4.4269E-07	6.9064E-07	1.4024E-08	2.9775E-08	0.0478	0.2114	0.2020
Bryozoa	-	*Bugula neritina*	20	24.47	-81.55	11.872	3.8271E-07	6.1255E-07	1.3097E-08	3.0591E-08	0.0514	0.2210	0.2068
Bryozoa	-	*Microporella grisea*	20	-28.40	155.67	12.888	4.4269E-07	6.9064E-07	1.5154E-08	4.0575E-08	0.0478	0.2114	0.2020
Brachiopoda	-	*Terebratulina septentrionalis*	30	44.87	-66.91	1.622	4.1968E-07	6.3990E-07	8.7777E-09	5.1669E-09	0.0448	0.2034	0.1979
Brachiopoda	-	*Laqueus californicus*	80	24.60	-108.25	0.806	4.2751E-07	6.6122E-07	8.5683E-09	4.5194E-09	0.0465	0.2078	0.2002
Mollusca	Amphineura	*Mopalia muscosa*	120	34.39	-119.70	0.190	3.8898E-07	5.6233E-07	7.9585E-09	3.8639E-09	0.0401	0.1908	0.1916
Mollusca	Bivalvia	*Astarte borealis*	50	74.16	54.40	7.068	4.3963E-07	6.8018E-07	1.1591E-08	1.4190E-08	0.0467	0.2083	0.2004
Mollusca	Bivalvia	*Tellina calcarea*	40	74.16	54.33	1.918	4.0066E-07	6.0142E-07	8.6440E-09	5.2942E-09	0.0431	0.1989	0.1957
Mollusca	Bivalvia	*Pecten groenlandicus*	20	73.50	68.83	1.185	4.5496E-07	6.9338E-07	9.1331E-09	5.0691E-09	0.0451	0.2041	0.1983

Mollusca	Bivalvia	*Pecten islandicus*	40	71.50	47.00	0.866	4.2019E-07	6.3697E-07	8.5004E-09	4.5195E-09	0.0442	0.2019	0.1972
Mollusca	Bivalvia	*Pecten dislocatus*	10	26.81	-82.29	1.516	4.3183E-07	6.8073E-07	8.9549E-09	5.1964E-09	0.0494	0.2156	0.2041
Mollusca	Bivalvia	*Pecten ventricosus*	10	22.86	-106.10	0.948	4.3290E-07	6.8265E-07	8.7487E-09	4.7036E-09	0.0495	0.2158	0.2042
Mollusca	Bivalvia	*Placuna orbicularis*	10	16.83	120.26	0.735	4.0095E-07	6.3740E-07	8.1947E-09	4.2812E-09	0.0504	0.2182	0.2054
Mollusca	Cephalopoda	*Nautilus pompilius*	100	8.53	123.03	0.830	4.0442E-07	6.0568E-07	8.2899E-09	4.3865E-09	0.0430	0.1985	0.1955
Mollusca	Cephalopoda	*Sepia officinalis*	10	5.84	118.27	0.842	4.0760E-07	6.5044E-07	8.3870E-09	4.4450E-09	0.0519	0.2223	0.2074
Mollusca	Cephalopoda	*Argonauta argo*	50	-35.82	175.39	0.534	4.1552E-07	6.5344E-07	8.3048E-09	4.2228E-09	0.0486	0.2136	0.2030
Mollusca	Cirripedia	*Scalpellum regium*	5	52.92	-132.29	0.237	4.1583E-07	6.3457E-07	8.1933E-09	4.0033E-09	0.0449	0.2035	0.1980
Mollusca	Cirripedia	*Balanus hameri*	20	41.23	-70.07	0.439	4.1057E-07	6.3794E-07	8.1807E-09	4.1070E-09	0.0468	0.2087	0.2006
Mollusca	Cirripedia	*Balanus amphitrite*	5	38.92	-74.91	2.106	3.9964E-07	6.2570E-07	8.6477E-09	5.4326E-09	0.0476	0.2109	0.2017
Mollusca	Cirripedia	*Lepas anatifera*	10	24.47	-81.55	1.209	3.9882E-07	6.2960E-07	8.3067E-09	4.6251E-09	0.0489	0.2142	0.2034
Mollusca	Cirripedia	*Mitella polymerus*	10	22.86	-106.10	1.386	4.0795E-07	6.5033E-07	8.5854E-09	4.8956E-09	0.0515	0.2213	0.2069
Mollusca	Gastropoda	*Neptunea despecta*	20	69.63	57.35	0.996	4.2269E-07	6.6689E-07	8.6045E-09	4.6556E-09	0.0494	0.2155	0.2040
Mollusca	Gastropoda	*Natica clausa*	20	60.50	-46.91	0.889	4.1583E-07	6.3457E-07	8.4367E-09	4.4999E-09	0.0449	0.2035	0.1980
Mollusca	Gastropoda	*Tachyrhynchus erosa*	30	52.90	158.76	1.929	4.1583E-07	6.3457E-07	8.8400E-09	5.4229E-09	0.0449	0.2035	0.1980
Mollusca	Gastropoda	*Nassa tegula*	20	36.62	-121.91	2.943	4.5486E-07	6.9090E-07	9.8837E-09	6.9481E-09	0.0447	0.2032	0.1979
Mollusca	Gastropoda	*Nassa isculpta*	50	32.34	-118.43	2.495	4.2181E-07	6.4214E-07	9.1640E-09	6.0661E-09	0.0447	0.2030	0.1978
Mollusca	Scaphopoda	*Dentalium solidum*	30	41.23	-70.07	2.637	4.0009E-07	6.3072E-07	8.8743E-09	5.9871E-09	0.0487	0.2137	0.2031
Crustacea	Amphipoda	*Tryphosa pinguis*	30	41.52	-70.67	9.381	4.3476E-07	6.8183E-07	1.2786E-08	2.1364E-08	0.0485	0.2133	0.2029
Crustacea	Decapoda	*Crago dalli*	40	59.17	-151.60	6.812	4.1271E-07	6.5517E-07	1.1007E-08	1.3020E-08	0.0504	0.2184	0.2055
Crustacea	Decapoda	*Pagurus rathbuni*	210	58.46	-175.22	14.592	4.5487E-07	6.9091E-07	1.6676E-08	5.6154E-08	0.0447	0.2032	0.1979
Crustacea	Decapoda	*Homarus americanus* - small	30	43.84	-69.64	11.712	3.9560E-07	6.2572E-07	1.3239E-08	3.0264E-08	0.0491	0.2149	0.2037
Crustacea	Decapoda	*Homarus americanus* - medium	30	43.84	-69.64	9.462	4.0194E-07	6.2437E-07	1.2079E-08	2.0403E-08	0.0466	0.2082	0.2004
Crustacea	Decapoda	*Homarus americanus* - large	30	43.84	-69.64	7.253	4.2315E-07	6.4089E-07	1.1383E-08	1.4287E-08	0.0442	0.2018	0.1971
Crustacea	Decapoda	*Homarus americanus*	50	41.35	-70.79	10.106	4.3476E-07	6.8183E-07	1.3209E-08	2.4331E-08	0.0485	0.2133	0.2029
Crustacea	Decapoda	*Libinia emarginata*	20	41.35	-70.79	10.175	4.4269E-07	6.9064E-07	1.3416E-08	2.4944E-08	0.0478	0.2114	0.2020
Crustacea	Decapoda	*Munida iris*	20	37.62	-76.26	9.058	3.8967E-07	6.1187E-07	1.1603E-08	1.8565E-08	0.0478	0.2114	0.2019
Crustacea	Decapoda	*Pandalus platyceros*	50	36.62	-121.91	9.496	4.3476E-07	6.8183E-07	1.2852E-08	2.1810E-08	0.0485	0.2133	0.2029
Crustacea	Decapoda	*Palinurus argus*	60	21.84	-71.33	10.244	4.3476E-07	6.8183E-07	1.3291E-08	2.4941E-08	0.0485	0.2133	0.2029
Crustacea	Decapoda	*Grapsus grapsus*	60	-9.36	46.40	18.433	4.3476E-07	6.8183E-07	1.9196E-08	1.0834E-07	0.0485	0.2133	0.2029
Crustacea	Stomatopoda	*Chloridella empusa*	20	24.47	-81.55	5.695	4.3476E-07	6.8183E-07	1.0835E-08	1.1028E-08	0.0485	0.2133	0.2029

[a] Corrections used from the CO2SYS Matlab script equations. For Mg-calcite, corrections applied from pure calcite. *See* text for details.

[b] Calculations.done from Millero and Pierrot (1998) using correlation equations. *See* text for details.

[c] Solubility -log IAPs taken from Mackenzie et al. (1983), Bischoff et al (1987, 1993), and Morse and Mackenzie (1990) and divided as "cleaned" and "minimally prepared" curves.

analysis [$n_{\text{Asteroidea}}$ = 108 (23 species), $n_{\text{Echinoidea}}$ = 85 (11 species), $n_{\text{Ophiuroidea}}$ = 12 (5 species), $n_{\text{Holothuroidea}}$ = 4 (2 species), $n_{\text{Crinoidea}}$ = 3 (1 species)] (Table 15.3). Organisms were collected using a variety of methods including scuba diving, bottom trawling, and Remote Operated Vehicles during cruises and surveys (Table 15.3). All organisms were healthy and were collected using all necessary permits to remove marine organisms within the research area causing minimum impact. All samples were frozen at either -20 or -80 °C after collection and placed in ziplock bags. All echinoderm samples except Antarctic ones were stored and initially treated at the Helmholtz Centre for Ocean Research Kiel (GEOMAR, Germany) until sent for analysis at the University of North Carolina-Chapell Hill. Whole body samples were freeze-dried inside the ziplock bags for 48 h and then reduced to powder with a rotating metal blade. Some echinoids were divided into spines and plates (*see* Table 15.3). Spines were removed from the test with a razor blade, and the test pieces cut with scissors. Measurements were obtained with a Perkin Elmer Sciex ELAN 9000 inductively coupled plasma mass spectrometer (ICP-MS). Samples were lightly ground in a mortar and pestle for 10-15 s. A 0.50 gr sample of the pulverized echinoderm material was digested for 2 h in Aqua Regia at 90 °C in a microprocessor controlled digestion block. Duplicate samples were run every 15 samples, in-house controls were run every 33 samples, and digested certified standards (for instrument calibration) and blanks were run every 68 samples. Antarctic samples were analyzed by Actlabs in Ancaster, Ontario (Canada) (www.actlabs.com). Samples treatment and methods followed those given in McClintock et al. (2011). In brief, frozen samples were thawed and dissected. For asteroids and ophiuroids, arms (thus arm plates) were cut and organic material was manually removed, except in two asteroids (*Kampylaster incurvatus* and *Granaster nutrix*) that were used as whole body. For holothurids, the calcareous ring was extracted, and echinoids were divided into spines and plates. All samples were soaked in 10 % NaClO for a few days to remove organic matter. The remaining inorganic material was vacuumed onto filter paper rinsed with Milli-Q water for several minutes. Filters were subsequently dried at 50 °C for 48 h. Dried material was reduced to powder in a mortar. The analysis took place on a PerkinElmer inductively coupled plasma atomic emission spectroscope (ICP-AES) for Ca, Mg, and Sr. The powdered material was divided in 90-500 mg splits and dissolved in nitric (HNO_3) and hydrochloric acid (HClO) in a molar ratio of 1/3 for 2 h at 95 °C. Samples were diluted with Milli-Q water. USGS standards were analyzed every 13 samples. Analytical accuracy was within 0.01 % of the value of the standards. For all samples, we used the sample weight to report $MgCO_3$ as percentages of the dry weight in grams or moles and subsequently used in other calculations (Table 15.1, 15.4; Fig. 15.2; Fig. 15.3a).

For other organisms (including echinoderms), we compiled literature data on skeletal parts (spines and plates) mainly measured via X-Ray difraction (*see* original references in Table 15.3 for details). Data were included in the dataset only if there was a $MgCO_3$ wt % or mol % measurement, and if latitude, longitude, and depth were given. This was the only way to link literature data to ambient seawater conditions (not reported in the original paper in many cases) using a "NEAR 3D" analysis (*see* below). The following taxa-class were used: Echinodermata-Asteroidea (25 species), Echinodermata-Echinoidea (17 species), Echinodermata-Ophiuroidea (17 species), Echinodermata-Crinoidea (21 species), Rhodophyta-Coralline algae (24 species), pelagic and Protista-Benthic Foraminifera (6 species), Anthozoa-Hydrocorallia (3 species), Anthozoa-Hexacorallia (10), Anthozoa-Octocorallia (27 species), Ectoprocta-Bryozoa (9 species), Lophophorata-Brachiopoda (2 species), Mollusca-Amphineura (1 species), Mollusca-Bivalvia (7 species), Mollusca-Cephalopoda (3 species), Mollusca-Cirripedia (5 species), Mollusca-Gastropoda (5 species), Mollusca-Scaphopoda (1 species), Crustacea-Amphipoda (1 species), Crustacea-Decapoda (11 species), and Crustacea-Stomatopoda (1 species). In the case of coralline algae, we compiled a monthly time-series dataset on mol % $MgCO_3$ (Haas et al. 1935) used to work out seasonal variability in saturation states using in situ conditions (Table 15.1, 15.3, 15.4).

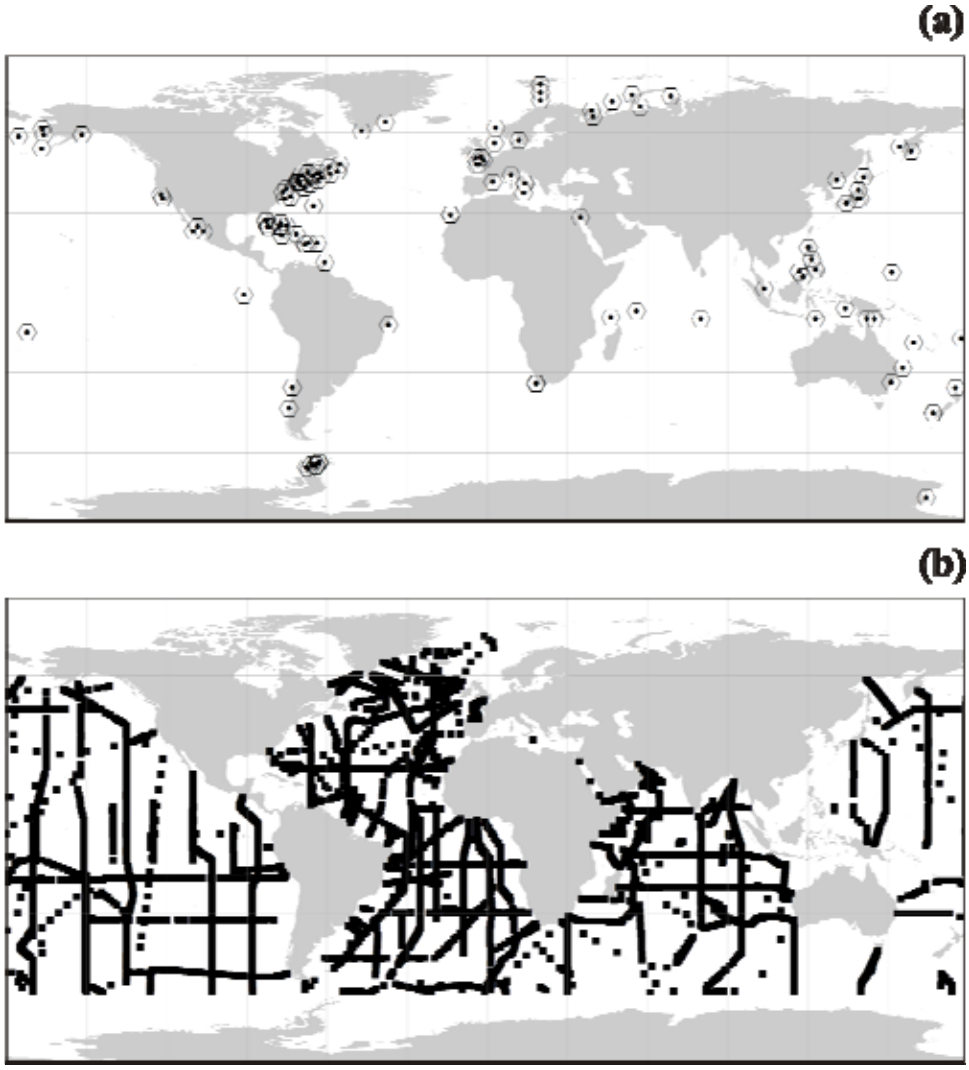

Fig. 15.1. (a) Samples global distribution (*see* Table 15.1 and 15.3 for details). (b) Ambient seawater carbonate chemistry, temperature and salinity data used to attribute values to sample location using NEAR 3D analysis (*see* text).

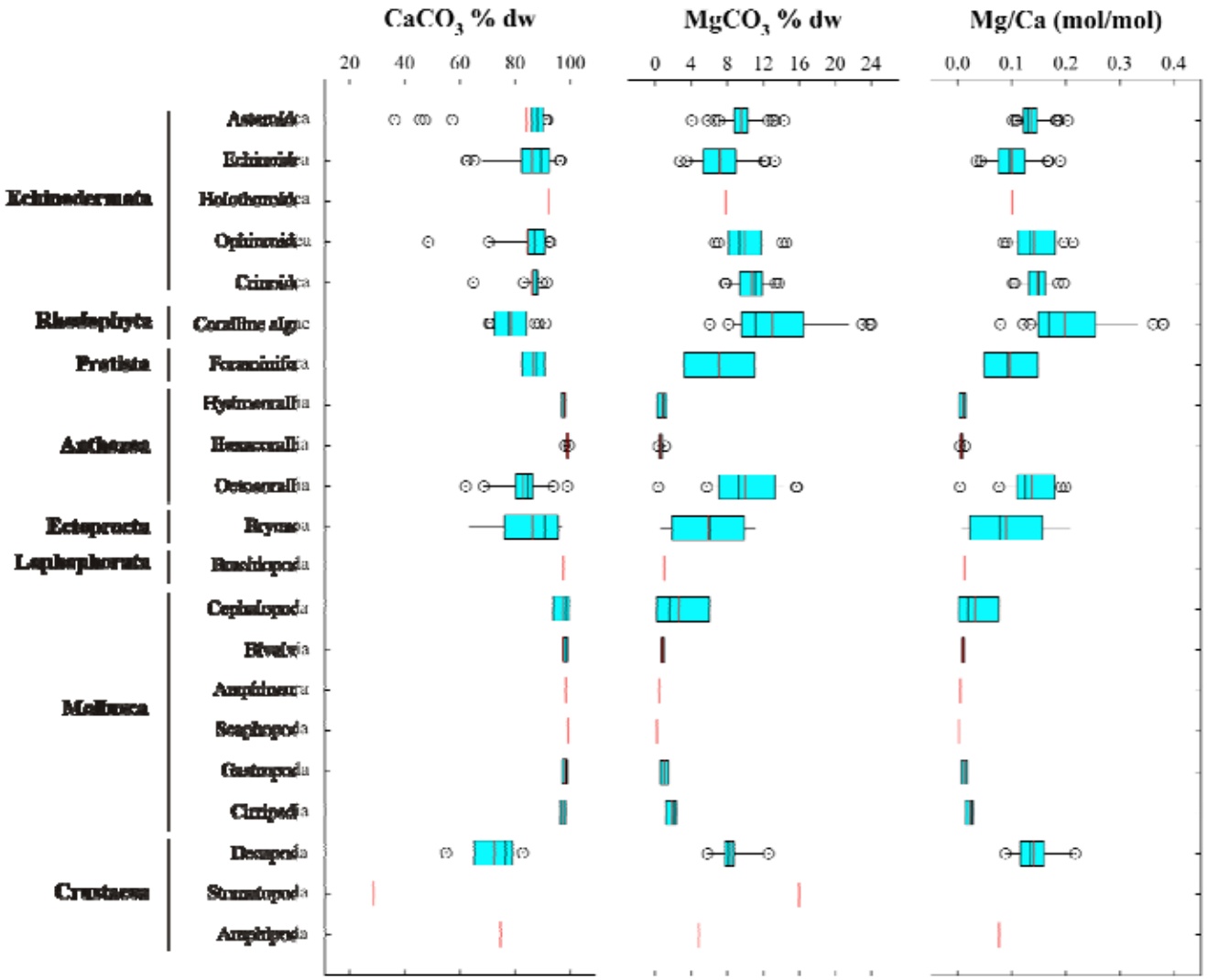

Fig. 15.2. Box plots of skeletal mineralogy ($CaCO_3$ and $MgCO_3$ % dw and Mg/Ca) of all organisms used in this study. Variability reflects different geographical origins, life stages, ambient seawater regimes and taxonomy (*see* Table 15.1 and 15.2 for details).

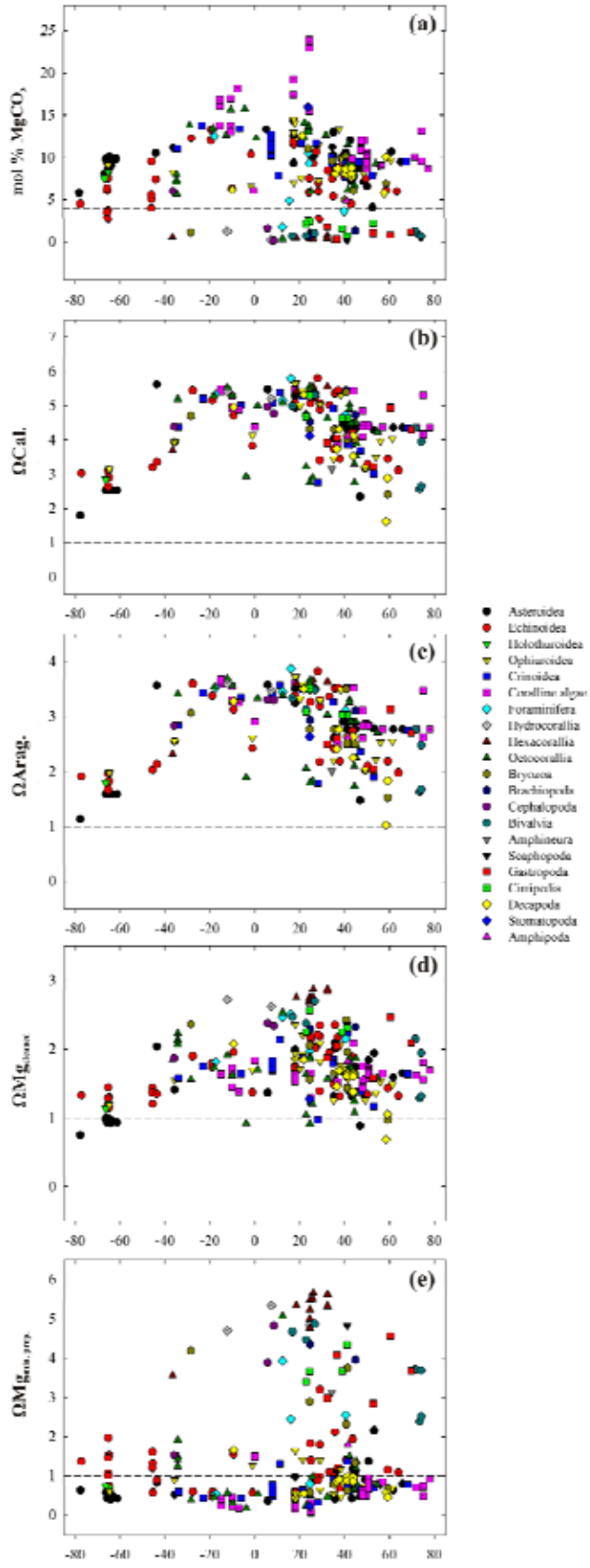

Fig. 15.3. Trends of measured organism mol % $MgCO_3$ (a), calculated ΩCal. (b), ΩArag. (c), $\Omega Mg_{cleaned}$ (d), and $\Omega Mg_{min.\ prep.}$ (e) *vs.* organism latitude at present CO_3^{2-} conditions. In (a) the dashed line shows the separation of low and high Mg-calcite organisms. In (b), (c), (d), and (e), the dashed line shows the theoretical start of dissolution of the mineral. In (b), (c), (d), and (e), the dashed line shows the theoretical start of dissolution of the mineral.

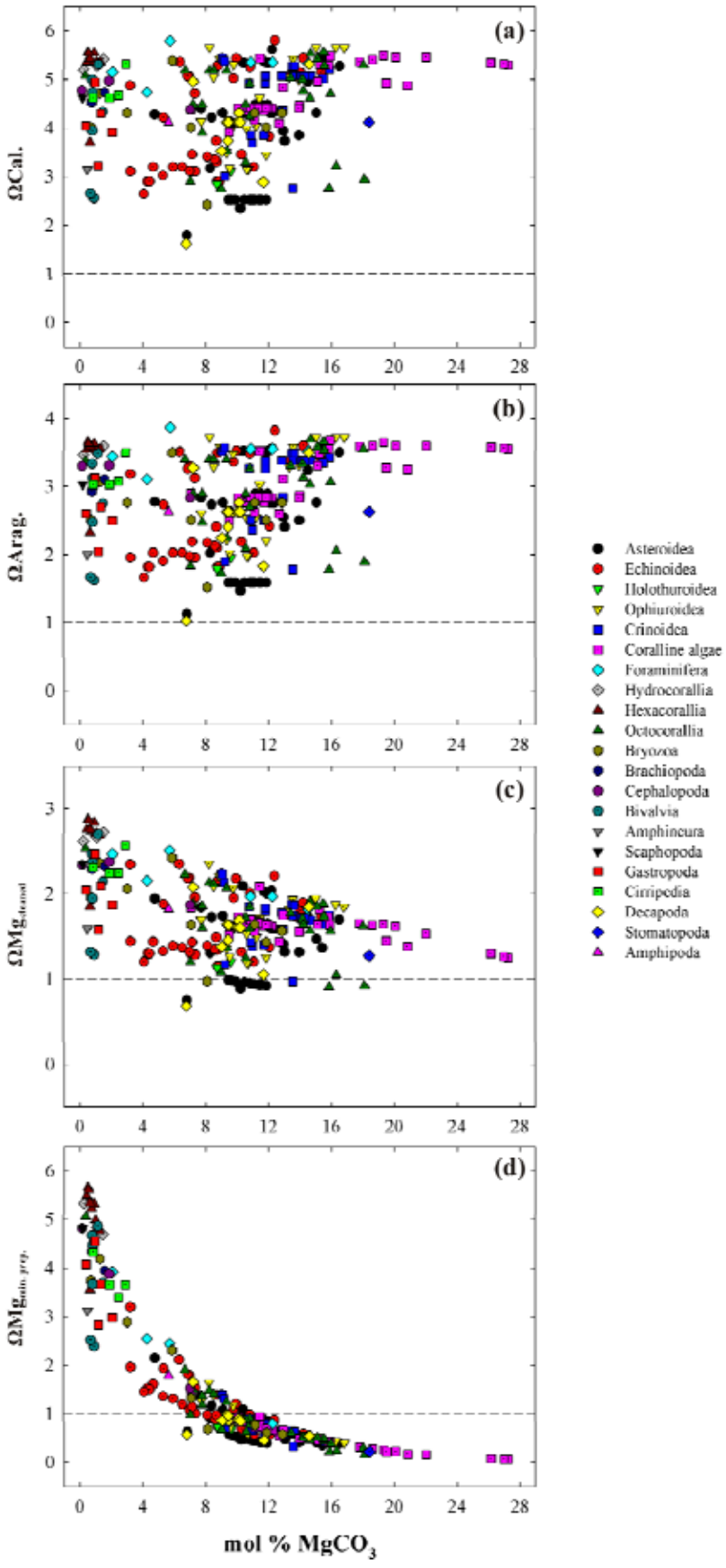

Fig. 15.4- Trends of ΩCal. (a), ΩArag. (b), $\Omega Mg_{cleaned}$ (c), and $\Omega Mg_{min.\ prep.}$ (d) *vs.* measured mol % $MgCO_3$ at present CO_3^{2-} conditions. The dashed line shows the theoretical start of dissolution of the mineral.

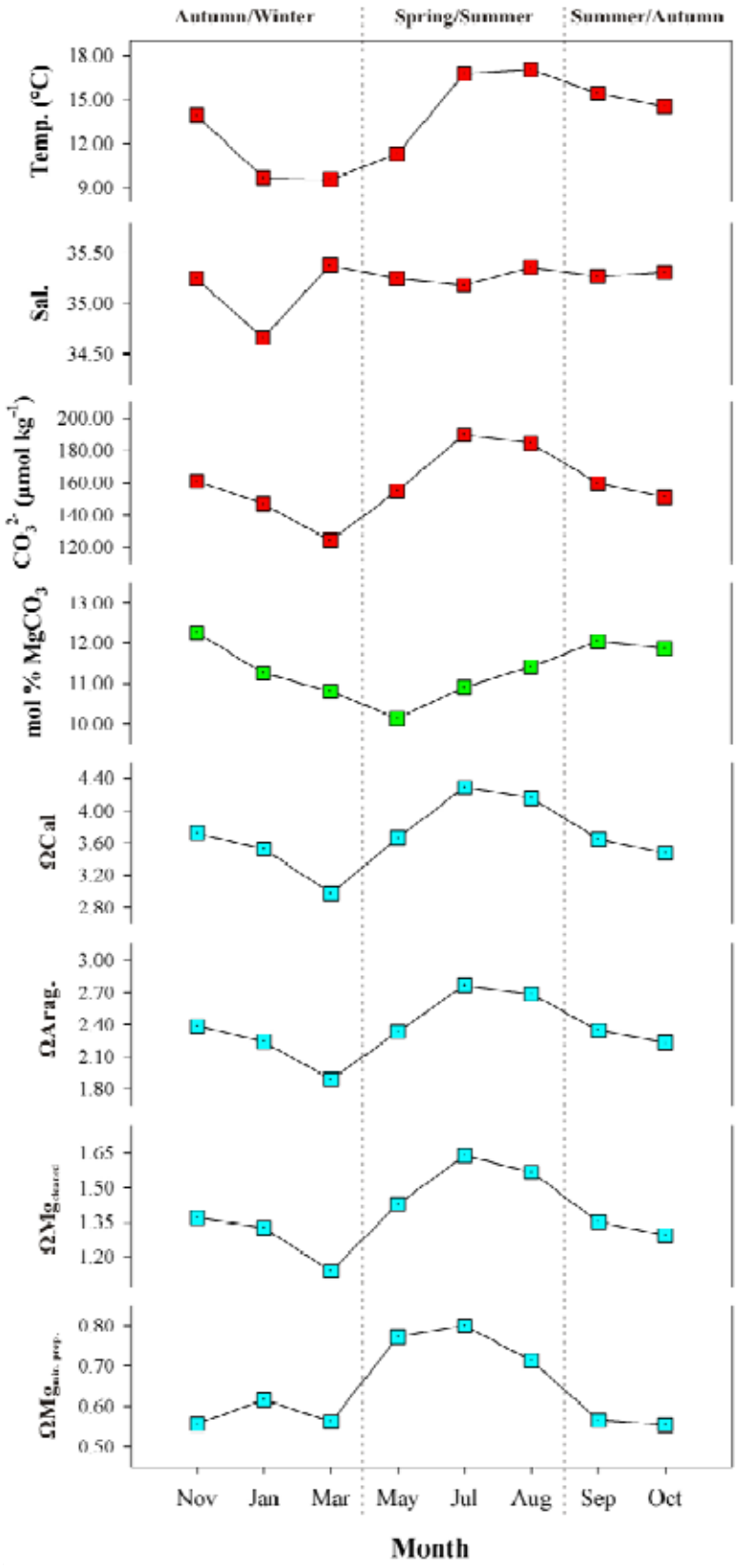

Fig. 15.5. Seasonal changes in the skeletal mol % $MgCO_3$ in the coralline algae *Corallina squamata* during 11 months at 5 m in the Dorset coast (Atlantic Ocean). Also calculated the ΩCal., ΩArag., $\Omega Mg_{cleaned}$, and $\Omega Mg_{min.\ prep.}$ over time based on the mol % $MgCO_3$ seasonal variability and the in situ seasonal ambient water variability (seawater data derived from Dumousseaud et al. 2010 dataset, and coralline algae data derived from Haas et al. 1935).

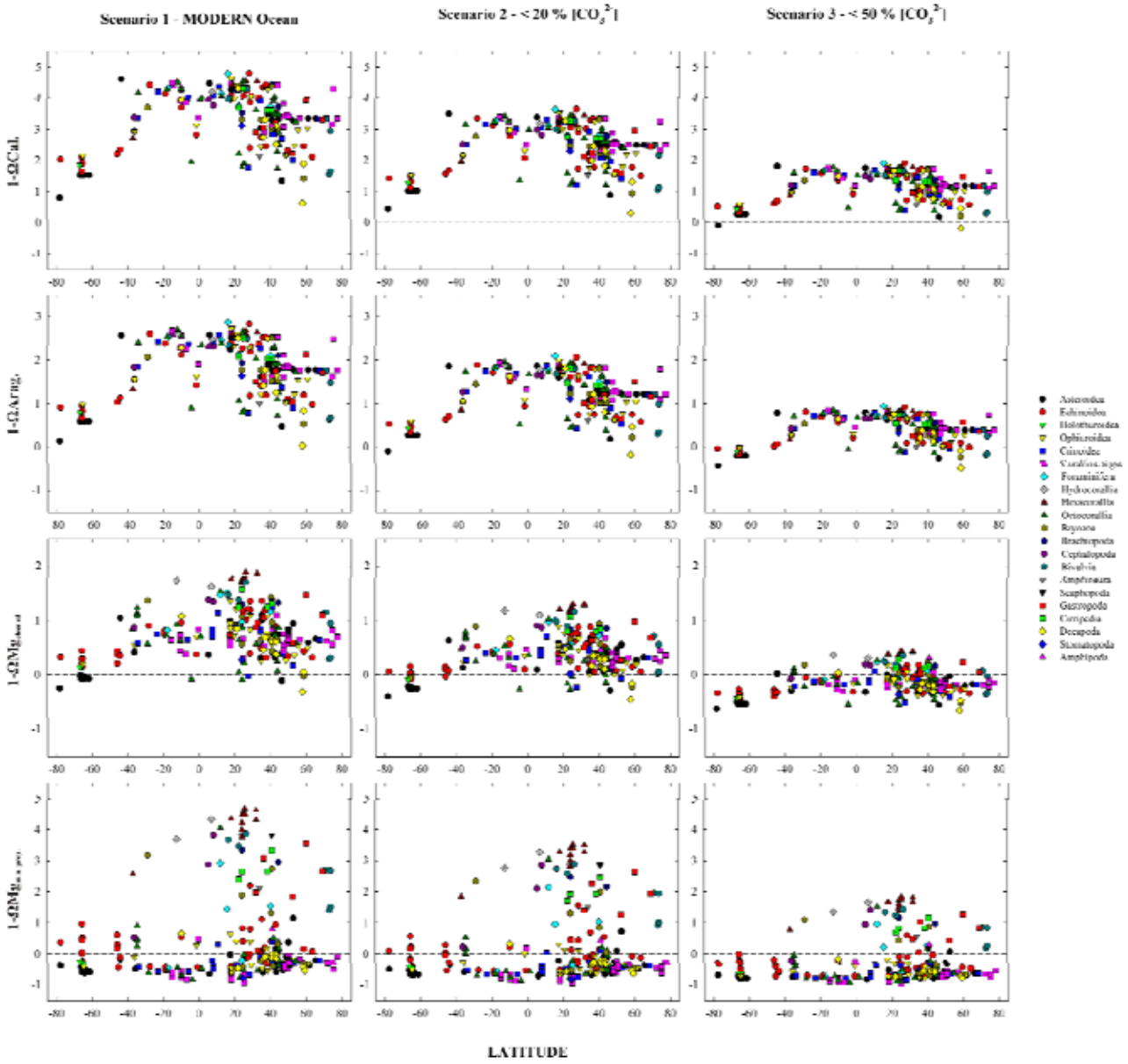

Fig. 15.6. Trends of "dissolution potential" (1 - ΩX) for calcite, aragonite, $Mg_{cleaned}$, and $Mg_{min.\ prep.}$ at present (1st column), and future conditions [reduction of CO_3^{2-} in 20 % (2nd column) and 50 % (3rd column)] *vs.* organism latitude. Positive values indicate no dissolution and negative values the start of dissolution, assuming it proceeds below ΩX = 1.

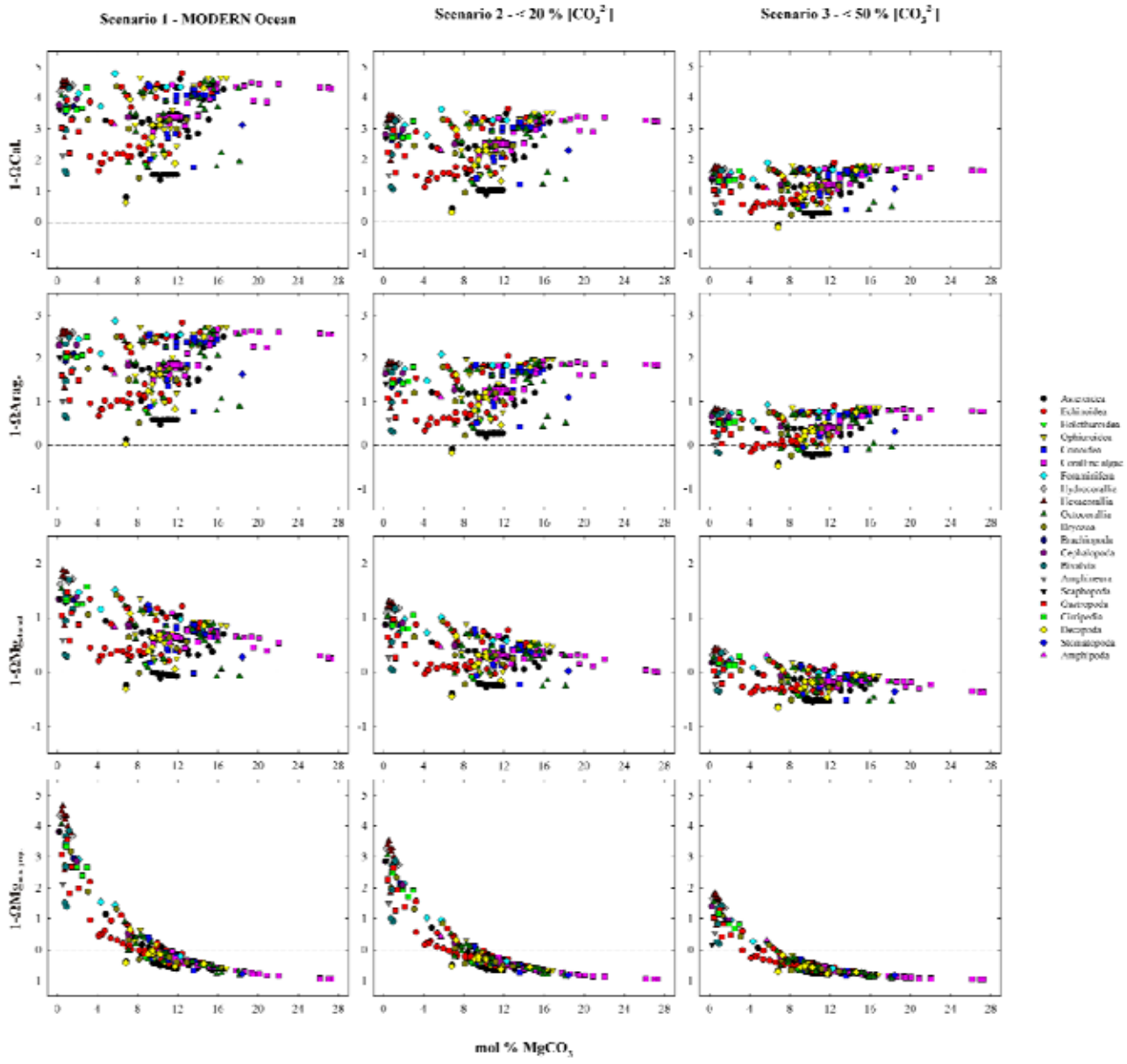

Fig. 15.7. Trends of "dissolution potential" (1 - ΩX) for calcite, aragonite, $Mg_{cleaned}$, and $Mg_{min.\ prep.}$ at present (1st column), and future conditions [reduction of CO_3^{2-} in 20 % (2nd column) and 50 % (3rd column)] *vs.* measured mol % $MgCO_3$. Positive values indicate no dissolution and negative values the start of dissolution, assuming it proceeds below ΩX = 1.

15.2.2. Organisms ambient seawater conditions: "NEAR 3D" analysis

Every organism had an original latitude, longitude and depth value attached, therefore it was possible to compile representative in situ field data on ambient temperature, salinity and carbonate chemistry (only the CO_3^{2-} concentration extracted, assuming CO_2 was equilibrated with the atmosphere) (Fig. 1a). We did this by attributing to each data point the nearest value in a 3D matrix using the GLODAP (Key et al. 2004) dataset at a global scale, and the Dumousseaud et al. (2010) dataset at a regional scale for the English Channel (Fig. 1b) (*see* those papers for the methoology in calculating the seawater carbonate chemistry system). The latter was also used to derive average monthly values for the calculation of seasonal saturation states using variation in mol % $MgCO_3$ in coralline algae (Fig. 5). On the global dataset 3D matrix, each data point for temperature, salinity and CO_3^{2-} represented the average condition for the time of the measurement. Therefore, our calculations cannot distinguish a seasonal component in the ambient variable (except for coralline algae) driving saturation states. Our calculations represent a "snapshot" in time at large scale, and the actual species-specific saturation states will vary during the year. The actual ambient seawater data attribution to the organisms geographical and depth information was done in ArcGIS 10.0 (ESRI 2011) using the 3D Analyst tool "NEAR 3D". In brief, this tool works out the distance from each input feature (organism latitude, longitude, and depth) to the nearest feature, in this case given by the carbonate chemistry (CO_3^{2-}) at a certain latitude, longitude and depth, within a certain search radius. The pre-requisite for this algorithm to work is a data frame *XYZ* (organism) *vs.* $X_iY_iZ_i$ (seawater property) geometry for both datasets to be comparable and linked data to be extractable. In simple terms, we plotted both datasets in a 2D map and coverted them to 3D, and then the algorithm determined the nearest seawater data point from our organisms using a diagonal in a 3D matrix. Eventually, we had the species-specific ambient conditions derived from the calculations above (Table 15.1; Fig. 15.8).

15.2.3. Saturation state calculations and in situ corrections

The seawater saturation state with respect to calcite and aragonite was calculated as:

$$\Omega\text{Cal./Arag.} = \{Ca^{2+}\} * \{CO_3^{2-}\} / IAP_{Cal./Arag.} \quad (1)$$

The seawater saturation state with respect to a certain mol % $MgCO_3$ was calculated as:

$$\Omega\text{Mg} = \{Mg^{2+}\}^{x} * \{Ca^{2+}\}^{(1-x)} * \{CO_3^{2-}\} / IAP_{x} \quad (2)$$

where x is the mol % $MgCO_3$ calculated from the organism measurements (*see* Table 15.1, 15.2, 15.4). {} in Eq. 1 and 2 represents ion activities (i) (*see* Table 15.2), which were calculated from the total activity coefficients of each ion [$\gamma_T(i)$] and the total seawater concentration ([i]$_T$):

$$\{i\} = \gamma_T(i) * [i]_T \quad (3)$$

The $\gamma_T(i)$ is controlled by the seawater composition (at in situ pressure and temperature) and were obtained from the Millero and Pierrot (1998) model using linear correlations. The general equations used to work out $\gamma_T(i)$ from the corresponding field temperatures (in °C) for each organism were:

$$\gamma_T(CO_3^{2-}) = -0.0003 * T_{\circ C} + 0.0519 \quad (4)$$

$$\gamma_T(Mg^{2+}) = -0.0008 * T_{\circ C} + 0.2223 \quad (5)$$

$$\gamma_T(Ca^{2+}) = -0.0004 * T_{\circ C} + 0.2074 \quad (6)$$

where $T_{\circ C}$ is the individual in situ field temperature obtained from the NEAR 3D analysis.

The field [i]$_T$ for each sample (except for CO_3^{2-}) was calculated following the Marcet's Principle of seawater constant proportions following in situ salinity for each sample:

$[CO_3^{2-}]_T$ = field input data from the NEAR 3D analysis and < 20 and < 50 % decrease for simulation of future OA scenarios.

$$[Mg^{2+}]_T = (S * 1.295/35.00) / 24.305 \quad (7)$$

$$[Ca^{2+}]_T = (S * 0.416/35.00) / 40.078 \quad (8)$$

where S is the individual in situ field salinity obtained from the NEAR 3D analysis.

IAP was the Ion Activity Product, which is the product of the ion activities at equilibrium determined at a condition originally referred to as stoichiometric saturation (Plummer and Mackenzie 1974; Morse et al. 2006). For calcite and aragonite we obtained the IAP from the Mucci (1983) equations corrected for in situ temperature ($T_{\circ K}$) and salinity (S) (Table 15.2):

$$-\log IAP_{Cal.}(T, S) = -171.9065 - (0.077993 * T_{\circ K}) + 2839.319 / T_{\circ K} + (71.595 * \log_{10}(T_{\circ K}) / \log_{10} + (-0.77712 + 0.0028426 * T_{\circ K} + 178.34 / T_{\circ K}) * \sqrt{(S)} - 0.07711 * S + 0.0041249 * \sqrt{(S)} * S \quad (9)$$

$$-\log IAP_{Arag.}(T, S) = -171.945 - (0.077993 * T_{\circ K}) + 2903.293 / T_{\circ K} + (71.595 * \log_{10}(T_{\circ K}) / \log_{10} + (-0.068393 + 0.0017276 * T_{\circ K} + 88.135 / T_{\circ K}) * \sqrt{(S)} - 0.10018 * S + 0.0059415 * \sqrt{(S)} * S \quad (10)$$

where individual temperature (T) is in kelvin (°K). IAPs were taken from the anti-log.

The individual IAPs were corrected for the pressure effect using the Ingle (1975) and Millero (1979, 1995) equations (Table 15.2):

Calcite:

$$delta VK_{Cal.} = -48.76 + 0.5304 * T_{\circ C} \quad (11)$$

$$kappa K_{Cal.} = (-11.76 + 0.3692 * T_{\circ C}) / 1000 \quad (12)$$

$$LnK_{Cal.} = (- \mathit{delta}VK_{Cal.} + 0.5 * \mathit{kappa}K_{Cal.} * P) * P / RT_{\circ K} \quad (13)$$

where $RT_{\circ K}$ is the products of the gas constant (83.145) and the kelvin temperature, while P is pressure in bars. Then, the $IAP_{Cal.}$ is the product of the T and S corrected values and the anti-ln of Eq. 13:

$$IAP_{Cal.}(T, S, P) = IAP_{Cal.}(T, S) * e^{LnKCal.} \quad (14)$$

Aragonite:

$$\mathit{delta}VK_{Arag.} = \mathit{delta}VK_{Cal.} + 2.80 \quad (15)$$

$$\mathit{kappa}K_{Arag.} = -\mathit{kappa}K_{Cal.} \quad (16)$$

$$LnK_{Arag.} = (- \mathit{delta}VK_{Arag.} + 0.5 * \mathit{kappa}K_{Arag.} * P) * P / RT_{\circ K} \quad (17)$$

where $RT_{\circ K}$ is the products of the gas constant (83.145) and the kelvin temperature, while P is pressure in bars. Then, the $IAP_{Arag.}$ is the product of the T and S corrected IAP values and the anti-ln of Eq. 17:

$$IAP_{Arag.}(T, S) = IAP_{Arag.}(T, S) * e^{LnKArag.} \quad (18)$$

For each mol % $MgCO_3$, we calculated the individual IAP_x using the biogenic "clean" and biogenic "minimally prepared" experimental solubility curves (Fig. 15.9) (Mackenzie et al. 1983; Bischoff et al.1987, 1993; and Morse and Mackenzie 1990). These two curves differ in the way the materials used during dissolution are prepared. There is not enough information on which curve represents better Mg-calcite dissolution in the marine environment, thus we provided results using both. A limitation in using these curves is that a true equilibrium is never established between Mg-calcite and the solution (Garrels and Wollast 1978), thus our calculations remain temptative. The IAP_x was calculated individually for each mol % $MgCO_3$ from a linear equation following the "cleaned" and "minimally prepared" curves (Fig. 15.9) at $T_{\circ C}$ = 25 °C and S = 35.00:

$$-\log IAP_{cleaned} = -0.0195 * \text{mol \% } MgCO_3 + 8.4817 \quad (19)$$

$$-\log IAP_{min.\ prep.} = -0.0779 * \text{mol \% } MgCO_3 + 8.8066 \quad (20)$$

IAPs were taken from the anti-log.

We developed a T, S, and P correction (Fig. 15.10) of the IAP_x for any mol % $MgCO_3$ since the "cleaned" and "minimally prepared" curves were empirically determined at $T_{°C}$ = 25 °C, S = 35.00, and P = 1 atm. In our dataset, $T_{°C}$ ranged from -0.86 to 39.38 °C, S ranged from 29.37 to 40.40 (*see* Fig. 15.8), and P ranged from 0.049 to 111.790 bars (Table 15.2). First, we corrected the IAP_x for any mol % $MgCO_3$ assuming a similar behaviour to calcite, thus using the $IAP_{Cal.}$ correlation to the field T and S data obtained from the NEAR 3D analysis (Fig. 15.10):

$$-\log IAP_{Cal.} = -0.0006 * T + 6.3825 \quad (21)$$

$$-\log IAP_{Cal.} = -0.0153 * S + 6.9016 \quad (22)$$

The $IAP_{Cal.}$ correlated negatively with T and S, but correlation was positive between them:

$$S = 0.0546 * T + 33.769 \quad (23)$$

For calculating the equations above we removed 3 outliers (T = 39.38 and 34.78 °C, S = 29.37) (compare Fig. 15.8 with 15.10), but we conserved them for the saturation state calculations. Then, we used a multiple regression model (e.g. $y = \beta_1 + \beta_2 * x_2 + \beta_3 * x_3 + u$) with T and S as predictors to work out the $IAP_{Cal.}$ equation ($P < 0.01$) for our set of field samples:

$$IAP_{Cal.} = 6.9271 - 0.01161 * S + 0.00028 * T \quad (24)$$

This equation was used to correct the original IAP_x from the mol % $MgCO_3$ in Eq. 19 and 20 for T and S. This was done by substituting the intercept of Eq. 24 (6.9271), by Eq. 19 and 20:

$$-\log IAP_{cleaned}\ (T, S) = (-0.0195 * \text{mol \% } MgCO_3 + 8.4817) - (0.01161 * S) + (0.00028 * T) \quad (25)$$

$$-\log IAP_{min.\ prep.}\ (T, S) = (-0.0779 * \text{mol \% } MgCO_3 + 8.8066) - (0.01161 * S) + (0.00028 * T) \quad (26)$$

IAPs were taken from the anti-log.

They were finally corrected for P assuming a similar behaviour to calcite by using the correction factor calculated in Eq. 13 (Table 15.2):

$$-\log IAP_{cleaned}\ (T, S, P) = -\log IAP_{cleaned}\ (T, S) * e^{\ LnKCal.} \quad (27)$$

$$-\log IAP_{min.\ prep.}\ (T, S, P) = -\log IAP_{min.\ prep.}\ (T, S) * e^{\ LnKCal.} \quad (28)$$

The corrected IAPs were taken from the anti-log, and used in the calculation of ΩMg for the two curves.

15.3. Results and discussion

15.3.1. Skeletal Mg-calcite mineralogy

The skeleton $CaCO_3$ dw % levels remained above 70 % in almost all cases, except in some echinoderms (asteroid and ophiuroid whole bodies) and crustaceans (decapoda) (Fig. 15.2). The lowest were found in crustaceans and the highest in molluscs (*see* Table 15.1, 15.9 for details). The overall trend in skeleton $MgCO_3$ dw % was much variable in comparison with the $CaCO_3$. Overall $MgCO_3$ dw % composition varied from < 0.5 to 24 dw %, with the highest values in coralline algae, followed by octocorals, echinoderms, and bryozoans (Table 15.1, 15.3; Fig. 15.2). There was a large $MgCO_3$ dw % variability within the same taxa as a consequence of different species, latitudes and ambient seawater regimes, which has been widely discussed in the literature (Chave 1954; Weber 1963). The Mg/Ca behaved in a similar way to the $MgCO_3$ dw % since the $CaCO_3$ values were relatively constant, and therefore the $MgCO_3$ caused the majority of the variations (*see* Table 15.1, 15.4; Fig. 15.2). The distribution of the mol % $MgCO_3$ with latitude followed a parabolic

relationship from pole to pole, with two maxima at 20 °S and °N, with a substantial decrease towards high latitudes, much accentuated in Antarctica (Fig. 15.3a) (McClintock et al. 2011). As a generality, this follows decreasing temperatures and lower saturation states reducing the Mg-calcite content at the species level, although there are exceptions. Those organisms with low Mg-calcite (< 4 % mol $MgCO_3$) did not really exhibit a latitudinal trend, which may provide them an advantage in the context of OA (*see* below). However, this was obvious for high Mg-calcite (> 4 % mol $MgCO_3$) organisms, which may come at their disadvantage by increasing skeleton dissolution potential. Many organisms at high latitudes above 60 °S and °N still bear high Mg-calcite skeletons from 4 to 14 % mol $MgCO_3$ (Fig. 15.3a), which may indicate they cohabit with transient undersaturation (*see* below).

15.3.2. Taxa-specific saturation state in the modern ocean and in the context of OA

Using modern ocean CO_3^{2-} values, the taxa and species-specific skeleton ΩCal./ΩArag.values remained above undersaturation (Ω = 1) for all organisms, following a parabolic relationship with latitude (Fig. 15.3b,c). A few exceptional low values (~ 2 and 1 respectively) were found at high latitudes, with predominant values from 2.5 to 4, and 1.5 to 2.5 respectively. In temperate and tropical latitudes we found the highest ΩCal./ΩArag. values from 5 to 6 and 2 to 4 respectively, with a wide variability especially in the northern hemisphere (from 3 to 6 and 2 to 4 respectively) (Fig. 15.3b, c). The $\Omega Mg_{cleaned}$ trend was similar to ΩCal./ΩArag., although much closer to undersaturation, especially at temperate and polar latitudes (Fig. 15.3d). Antarctic asteroid skeletons were undersaturated with respect to their Mg-calcite, and also some sub-arctic decapods, temperate crinoids, and tropical octocorallians (all in the 0.7-1 range). More than 90 % of the organisms were in the $\Omega Mg_{cleaned}$ 1 to 2 range, especially in the southern hemisphere, and ~ 30 % in the 1 to 1.5 range. The $\Omega Mg_{min.\ prep.}$ trend showed a wide spectrum of saturation states following a rough parabola with latitude (Fig. 15.3e). More than 50 % of all organisms were living in undersaturated conditions at any latitude (0.2-0.8), with no peak in the poles (0.5-1), and > 70 % were below $\Omega Mg_{min.\ prep.}$ = 1.5. Actually, the largest percentage of organisms in undersaturated conditions was found at temperate latitudes in the northen hemisphere. For example, all coralline algae were co-habiting with undersaturation, as well as many decapods. Echinoderms were near the undersaturation threshold or just below it, and many anthozoa (hydrocorallia, hexacorallia, and

octocorallia) and molluscs were well above it. The relationship of ΩCal./ΩArag. *vs.* the organism skeleton mol % $MgCO_3$ did not show any pattern, since the saturation state of calcite/aragonite does not depend on the Mg-calcite (Fig. 15.4a, b). The $\Omega Mg_{cleaned}$ showed a linearly decreasing trend with increasing mol % $MgCO_3$, with a large variability at any mol % $MgCO_3$ driven by the in situ temperature, salinity and CO_3^{2-} conditions (Fig. 15.4c). The analysis using the biogenic "cleaned" solubility curve revealed that those organisms with the largest mol % $MgCO_3$ were not necessarily at the lowest saturation states. The organisms closest to undersaturation or just below it, were those from low temperatures (poles) and/or living in naturally low CO_3^{2-} conditions (*see* Table 15.1). The $\Omega Mg_{min.\ prep.}$ showed a decreasing exponential trend with increasing mol % $MgCO_3$, flatting out from 8 % onwards. This coincided with the onset of undersaturated conditions, which dominated many organisms ambient seawater. The analysis using the biogenic "minimally prepared" solubility curve indicated that the skeleton mol % $MgCO_3$ (above 8 %) had a large influence on the saturation state as a consequence of a stepper slope in the predictor equation (*see* Fig. 15.9. This means that any organism with a mol % $MgCO_3$ above 7-10 % could already experience undersaturation depending on ambient sewater conditions. In a special case, we used data from Haas et al. (1935), which observed that the coralline algae *Corallina squamata* varied monthly its mol % $MgCO_3$ during 11 months at 5 m in the Dorset coast (Atlantic Ocean) (Fig. 15.5). We compiled from the NEAR 3D analysis (based on seawater data from Dumousseaud et al. 2010) the averaged temperature, salinity, and CO_3^{2-} values closest to the area to work out transient saturation states. The mol % $MgCO_3$ decreased from autumn/winter (max. in November = 12.26 %) to spring/summer (min. in May = 8.67 %), and then increased again in late summer/autumn (max. in September = 12.04 %), following CO_3^{2-} and temperature. Therefore, all saturation states (ΩCal., ΩArag., $\Omega Mg_{cleaned}$, and $\Omega Mg_{min.\ prep.}$) decreased during autumn/winter (min. in March: 2.97, 1.88, 1.13, and 0.56 respectively), increased in spring/summer (max. in July: 4.29, 2.76, 1.63, and 0.79 respectively), and decreased again in late summer/autumn (min. in October: 3.47, 2.23, 1.29, and 0.55 respectively) following the seasonal CO_3^{2-} (the strongest effect), temperature and the skeletal mol % $MgCO_3$ cycle (Fig. 15.5).

We assessed "dissolution potential" (1- ΩX) to define which organisms will likely suffer from undersaturation (negative values) and supersaturation (positive values) (Fig. 15.5, 15.6). Using $[CO_3^{2-}]$ data decreased by 20 and 50 % from modern ocean concentrations (simulating future OA)

(Fig. 15.8), we observed the same trends with latitude for all saturation states as in the modern ocean. The only difference was that the dissolution potential increased at the species level as [CO_3^{2-}] decreased (Fig. 15.8). A 20 and 50 % [CO_3^{2-}] reduction indicated that if only ΩCal./ΩArag. were calculated, it would be predicted that almost all organisms will not start dissolving their skeletons (only 1 to 10 % of the species). When $\Omega Mg_{cleaned}$ and $\Omega Mg_{min.\ prep.}$ were considered, the proportion of skeletons that may start dissolving increased radically, especially at a 50 % [CO_3^{2-}] reduction (60 to 80 % of the species). The latitude trends indicated a higher dissolution potential in the poles (Fig. 15.5), although a reduced mol % $MgCO_3$ compensated this, and in the 50 % [CO_3^{2-}] decrease, they were at almost the same dissolution potential (considering $\Omega Mg_{cleaned}$ and $\Omega Mg_{min.\ prep.}$) as temperate latitudes counterparts. Ignoring latitude, the mol % $MgCO_3$ per se will eventually govern the dissolution potential (Fig. 15.6). At present, organisms with skeleton Mg-calcite > 9-10 mol % $MgCO_3$ may experience transient dissolution, with a 20 and 50 % [CO_3^{2-}] decrease, the threshold will go down to 7-8 and 4-5 mol % $MgCO_3$ respectively (Fig. 15.6). This means that in the worse case scenario at a 50 % [CO_3^{2-}] reduction, almost all high Mg-calcite organisms (> 4 mol % $MgCO_3$) will start dissolving, but not low Mg-calcite species.

A decreasing CO_3^{2-} concentration and a lower Ω (any mineral form) favour Mg-calcite deposits of low magnesium content (Mackenzie et al. 1983). In organisms the same happens, thus those bearing skeletons with a 8 mol % $MgCO_3$ or less will be at a competitive advantage with those secreting high Mg-calcite material (Andersson et al. 2008; Fig. 15.4). It may well be that species in ecosystems evolve in the short term towards a lower skeleton mol % $MgCO_3$. In a scenario with a [CO_3^{2-}] decreased by 20 and 50 %, species secreting below 8-12 % and 4-8 % respectively may be at an advantage and they could become dominant. This situation will become advantageous for molluscs and crustaceans in detriment of echinoderms, coralline algae, foraminifera and anthozoans (Fig. 15.2). It can be observed that a "tipping point" is defined by the skeleton mol % $MgCO_3$ correlated with the ambient conditions, but that this tipping point is flexible and it migrates down with the mol % $MgCO_3$ as ΩMg (biogenic "cleaned" and "minimally prepared") decreases. Benthic ecosystems could suffer in the next decades from a profound transformation driven my the [CO_3^{2-}] decrease, changing the Mg-calcite content to low Mg-calcite. The consequences for the functioning of ecosystems as a whole would remain then unknown, although it can be predicted that organisms would either secrete more stable calcite forms, and/or migrate towards supersaturated water masses

and regions. The hot discussion topic on "tipping points" following CO_2 levels or mineral saturation states gets complicated with the concept of species-specific ΩMg with respect to the skeleton mol % $MgCO_3$. The problem is that the modern ocean envelope of CO_2 regimes in contrasting ecosystems (Hofmann et al. 2011) combined with seasonal changes in carbonate chemistry at all latitudes (Tyrrell et al. 2008; Steinacher et al. 2009; Dumousseaud et al. 2010; *see* Fig. 15.5), and the ΩMg variability at the species level (Fig. 15.3, 15.4) makes a general tipping point discussion misleading. Furthermore, OA is thought to induce a pH drop in 0.3/0.4 units by 2011 (Feely et al. 2004), but this will no occur at the same rate or with the same intensity in all parts of the ocean, thus species-specific ΩMg will even vary in the same species from different latitudes. Arguably, generalities on tipping points can be confusing because they can be considered species-, latitude- and mineralogy-specific, therefore a consensus around a certain CO_2 level is irrelevant at this point. McNeil and Matear (2008) modelling results suggested that at an atmospheric CO_2 of 450 ppm, wintertime aragonite could start to show transient undersaturation in the Southern Ocean, which can be seen as a tipping point. This only would apply to aragonite-forming organisms e.g. pteropods (Yamamoto-Kawai et al. 2009), since ΩMg for benthic communities in the poles varies from 0.7 to 1.2 depending on organism and skeleton mol % $MgCO_3$ (Fig. 15.3, 15.4). Contrary to current predictions that indicate that by 2050 and 2100 the poles will start to experience permanent aragonite undersaturation (Orr et al. 2005; McNeil and Matear 2008; Steinacher et al. 2009), benthic Mg-calcite organisms with mol % $MgCO_3$ in skeletons above 8-14 % already cohabit with these conditions (Fig. 15.3, 15.4). This is within the predictions of Andersson et al. (2008) at about 12 mol % $MgCO_3$, although they only used three (12, 15, and 18) nominal mol % $MgCO_3$ as input data. This means that a wide range of organisms bearing this skeleton mineralogy will be the first responders to OA. Modern organisms living in the poles have either evolved in these natural near-corrosive conditions and thus have physiological mechanisms to counteract dissolution, or they suffer from transient seasonal dissolution (Fig. 15.5) that they compensate by reducing their skeleton mol % $MgCO_3$ (Haas et al. 1935). There is evidence that Antarctic echinoderm larvae are more resilient to CO_2 increases (ΩMg decrease) than temperate counterparts (Clarke et al. 2009). This would confirm an adaptation to low ΩMg conditions, although it is unclear what will happen it these high Mg-calcite organisms are pushed into undersaturation with seasonal or permanent amplification of OA. It can be that Mg-calcite organisms and then sedimentary carbonates decrease in the Mg content (Andersson et al. 2008) through decreasing skeleton Mg incorporation and

dissolution respectively. But, it is not clear if this benthic dissolution could somehow buffer seawater alkalinity, delaying the CO_2 effect (Andersson et al. 2003). If Mg-calcite dissolution can buffer the water column will depend on water masses exchange and if the metastable Mg-calcite dissolution is large enough to act on a short time scale. This will in turn facilitate more atmospheric CO_2 uptake (Garrels and Mackenzie 1980).

In conclusion, if current CO_2 emission scenarios are used as biogeochemical model baselines, and then simply extrapolated to every ecosystem ignoring the specis-specific Mg-calcite issues, a large and valueable amount of detail is lost. It is also problematic to put out of context the use of "surface" ΩCal./Arag. values to understand OA, as they only represent conditions for calcifying pelagic communities (coccolithophores, pteropods, and foraminifera) in the upper ocean. Benthic ecosystem harbour different biogeochemical processes, although both are linked through water masses and particulate matter export. In benthic ecosystems, localized benthic undersaturation is induced by organic matter sinking, deposition and remineralization. This can be especially true in the benthic boundary layer in shelves, where are large dissolved inorganic carbon and alkalinity fluxes follow anaerobic respiration (Thomas et al. 2009). This is a seasonal process following pulses of organic matter mainly after the phytoplankton spring bloom (temperate latitudes) (Lampitt et al. 2001) or thawing of ice in the poles. It can also be driven by riverine freshwater inputs, which decrease Ω (all) on their own (from CO_3^{2-} changes) and brings large amounts of organic matter that then remineralizes in the shelves (Chierici and Fransson 2009). If we combine this with the species-specific ΩMg following skeleton mol % $MgCO_3$, we end up with a myriad of ambient saturation conditions especially in shelf and slopes environments that need to be fully considered in the context of OA. We need to find and use the right complexity for the right question, and this applies directly to the general use of ΩCal./Arag. in modelling efforts to differentiate pelagic and benthic ecosystems, and the correct experimental interpretation of Mg-calcite processes. We need to move urgently from a large scale understanding to an organism-level assessment using ΩMg for the specific mineralogy. Then, probably, it is plausible to return to the global perspective to put ΩMg together with seasonal changes and functioning of marine ecosystems in the context of OA.

Appendix A

Table 15.3. Details of sample collection and material used.

Taxa	Class	Species	*n*	Depth (m)	Lat.	Long.	Location	Material	Collection	Reference
Echinodermata	Asteroidea	*Asterias rubens*	8	2	53.24	-4.46	Swansea (Atlantic Ocean)	Whole body	Manual	NEW
Echinodermata	Asteroidea	*Asterina gibossa*	6	2	50.63	-2.39	English Channel (Atlantic Ocean)	Whole body	Manual	NEW
Echinodermata	Asteroidea	*Zoroaster fulgens*	4	1140	49.28	-12.36	Porcupine Sea Bight (Atlantic Ocean)	Whole body	Semi-otter trawl	NEW
Echinodermata	Asteroidea	*Marthasterias glacialis*	7	3	43.58	-6.24	Cape Vidio (Cantabric Sea)	Whole body	Manual	NEW
Echinodermata	Asteroidea	*Labidiaster annulatus*	9	175	-61.21	-56.01	Elephant Island (Southern Ocean)	Plates	Trawling	NEW
Echinodermata	Asteroidea	*Macroptychaster accrescens*	3	180	-63.53	-62.75	Low Island (Southern Ocean)	Plates	Trawling	NEW
Echinodermata	Asteroidea	*Paralophaster godfroyi*	1	180	-63.53	-62.75	Low Island (Southern Ocean)	Plates	Trawling	NEW
Echinodermata	Asteroidea	*Paralophaster sp.*	3	180	-63.53	-62.75	Low Island (Southern Ocean)	Plates	Trawling	NEW
Echinodermata	Asteroidea	*Perknaster sp.*	2	180	-63.53	-62.75	Low Island (Southern Ocean)	Plates	Trawling	NEW
Echinodermata	Asteroidea	*Acodontaster hodgsoni*	3	160	-64.15	-62.74	Dallmann Bay (Southern Ocean)	Plates	Trawling	NEW
Echinodermata	Asteroidea	*Kampylaster incurvatus*	4	160	-64.15	-62.74	Dallmann Bay (Southern Ocean)	Whole body	Trawling	NEW
Echinodermata	Asteroidea	*Odontaster penicillatus*	1	160	-64.15	-62.74	Dallmann Bay (Southern Ocean)	Plates	Trawling	NEW
Echinodermata	Asteroidea	*Porania antarctica*	3	160	-64.15	-62.74	Dallmann Bay (Southern Ocean)	Plates	Trawling	NEW
Echinodermata	Asteroidea	*Diplasterias brandti*	3	30	-64.77	-64.05	Arthur Harbor (Southern Ocean)	Plates	Scuba diving	NEW
Echinodermata	Asteroidea	*Granaster nutrix*	5	30	-64.77	-64.05	Arthur Harbor (Southern Ocean)	Whole body	Scuba diving	NEW
Echinodermata	Asteroidea	*Neosmilaster georgianus*	3	30	-64.77	-64.05	Arthur Harbor (Southern Ocean)	Plates	Scuba diving	NEW
Echinodermata	Asteroidea	*Odontaster meridionalis*	3	30	-64.77	-64.04	SE Boneparte Pt. (Southern Ocean)	Plates	Scuba diving	NEW
Echinodermata	Asteroidea	*Perknaster aurorae*	3	30	-64.78	-63.99	Stepping Stones (Southern Ocean)	Plates	Scuba diving	NEW
Echinodermata	Asteroidea	*Acodontaster conspicuus*	1	30	-65.07	-63.97	Lemaire Channel (Southern Ocean)	Plates	Scuba diving	NEW
Echinodermata	Asteroidea	*Perknaster fuscus antracticus*	1	30	-65.07	-63.97	Lemaire Channel (Southern Ocean)	Plates	Scuba diving	NEW
Echinodermata	Asteroidea	*Henricia sp.*	2	155	-65.67	-67.40	Renaud Island (Southern Ocean)	Plates	Trawling	NEW
Echinodermata	Asteroidea	*Diplopteraster verrucosus*	2	900	-66.29	-66.60	Banana Trench (Southern Ocean)	Plates	Trawling	NEW
Echinodermata	Asteroidea	*Odontaster validus*	6	18	-77.63	-146.41	Antarctica (Southern Ocean)	Whole body	ROV	NEW
Echinodermata	Crinoidea	*Antedon mediterranea*	3	63	41.43	2.32	Catalan Sea (Mediterranean Sea)	Whole body	Manual	NEW
Echinodermata	Echinoidea	*Psammechinus miliaris*	14	1	50.35	-4.13	English Channel (Atlantic Ocean)	Whole body	Manual	NEW
Echinodermata	Echinoidea	*Paracentrotus lividus*	14	2	43.58	-6.24	Cape Vidio (Cantabric Sea)	Whole body	Manual	NEW
Echinodermata	Echinoidea	*Paracentrotus lividus*	3	1	29.13	-13.60	Lanzarote (Atlantic Ocean)	Spines, Plates	Manual	NEW
Echinodermata	Echinoidea	*Paracentrotus lividus*	3	1	29.13	-13.60	Lanzarote (Atlantic Ocean)	Plates	Manual	NEW
Echinodermata	Echinoidea	*Tripneustes ventricosus*	2	6	25.12	-77.29	Paradise Island (Atlantic Ocean)	Whole body	Submersible	NEW
Echinodermata	Echinoidea	*Cidaris blakei*	2	595	24.83	-77.50	South West Reef (Atlantic Ocean)	Whole body	Manual	NEW
Echinodermata	Echinoidea	*Diadema setosum*	3	0.5	-18.85	159.75	Aitukai Island (Pacific Ocean)	Spines	Manual	NEW

Echinodermata	Echinoidea	*Diadema setosum*	3	0.5	-18.85	159.75	Aitukai Island (Pacific Ocean)	Plates	Scube diving	NEW
Echinodermata	Echinoidea	*Evechinus chloroticus*	3	5	-45.30	166.97	Doubtful Sound (Pacific Ocean)	Spines	Scube diving	NEW
Echinodermata	Echinoidea	*Evechinus chloroticus*	3	5	-45.30	166.97	Doubtful Sound (Pacific Ocean)	Plates	Scuba diving	NEW
Echinodermata	Echinoidea	*Pseudechinus huttoni*	2	8	-45.41	167.10	Doubtful Sound (Pacific Ocean)	Spines	Scuba diving	NEW
Echinodermata	Echinoidea	*Pseudechinus huttoni*	3	8	-45.41	167.10	Doubtful Sound (Pacific Ocean)	Plates	Trawling	NEW
Echinodermata	Echinoidea	*Amphineustes similis*	2	685	-64.75	-65.47	Renaud Island (Southern Ocean)	Spines	Trawling	NEW
Echinodermata	Echinoidea	*Amphineustes similis*	4	685	-64.75	-65.47	Renaud Island (Southern Ocean)	Plates	Trawling	NEW
Echinodermata	Echinoidea	*Ctenocidaris perrieri*	3	685	-64.75	-65.47	Hugo Island (Southern Ocean)	Spines	Trawling	NEW
Echinodermata	Echinoidea	*Ctenocidaris perrieri*	3	685	-64.75	-65.47	Hugo Island (Southern Ocean)	Plates	Scuba diving	NEW
Echinodermata	Echinoidea	*Sterechinus neumayeri*	3	30	-65.07	-63.97	Lemaire Channel (Southern Ocean)	Spines	Scuba diving	NEW
Echinodermata	Echinoidea	*Sterechinus neumayeri*	6	30	-65.07	-63.97	Lemaire Channel (Southern Ocean)	Plates	Scuba diving	NEW
Echinodermata	Echinoidea	*Sterechinus neumayeri*	3	30	-65.07	-63.97	Lemaire Channel (Southern Ocean)	Spines	Scuba diving	NEW
Echinodermata	Echinoidea	*Sterechinus neumayeri*	3	30	-65.07	-63.97	Lemaire Channel (Southern Ocean)	Plates	Scuba diving	NEW
Echinodermata	Echinoidea	*Sterechinus neumayeri*	3	15	-77.06	164.42	Antarctica (Southern Ocean)	Whole body	Trawling	NEW
Echinodermata	Holothuroidea	*Molpadia musculus*	3	685	-64.75	-65.47	Hugo Island (Southern Ocean)	Calcareous ring	Trawling	NEW
Echinodermata	Holothuroidea	*Pseudostichopus spiculiferus*	1	900	-66.29	-66.60	Banana Trench (Southern Ocean)	Calcareous ring	Semi-otter trawl	NEW
Echinodermata	Ophiuroidea	*Ophiosium lynami*	6	1140	49.20	-12.30	Porcupine Sea Bight (Atlantic Ocean)	Whole body	Manual	NEW
Echinodermata	Ophiuroidea	*Ophiura longicauda*	1	1	29.12	-13.56	Lanzarote (Atlantic Ocean)	Spines	Scuba diving	NEW
Echinodermata	Ophiuroidea	*Ophiura longicauda*	1	1	29.12	-13.56	Lanzarote (Atlantic Ocean)	Plates	Scuba diving	NEW
Echinodermata	Ophiuroidea	*Ophionotus victoriae*	3	30	-64.77	-64.05	Arthur Harbor (Southern Ocean)	Plates	Manual	NEW
Echinodermata	Ophiuroidea	*Ophiosparte gigas*	1	30	-64.77	-64.05	Arthur Harbor (Southern Ocean)	Plates	Benthic trawl	NEW
Echinodermata	Asteroidea	*Asterias linckii*	1	20	65.81	39.73	White Sea (Arctic Ocean)	Plates	*see* original	Clarke and Wheeler 1922
Echinodermata	Asteroidea	*Orthasterias tanneri*	1	30	61.68	3.31	Norwegian Sea (Atlantic Ocean)	Plates	*see* original	Samoilov and Terentieva 1925
Echinodermata	Asteroidea	*Ctenodiscus crispatus*	1	80	46.90	-59.10	Newfoundland (Atlantic Ocean)	Plates	*see* original	Clarke and Wheeler 1922
Echinodermata	Asteroidea	*Asterias vulgaris*	1	10	44.79	-66.92	Eastport Maine (Atlantic Ocean)	Plates	*see* original	Clarke and Wheeler 1922
Echinodermata	Asteroidea	*Asterias acervata borealis*	1	40	43.58	-65.17	Nova Scotia (Atlantic Ocean)	Plates	*see* original	Schmelck 1901
Echinodermata	Asteroidea	*Asterina pectinifera*	1	10	43.20	141.05	Japan Sea (Pacific Ocean)	Plates	*see* original	Clarke and Wheeler 1922
Echinodermata	Asteroidea	*Asterias forbesi*	1	10	41.42	-70.80	Vineyard Sound (Atlantic Ocean)	Plates	*see* original	Clarke and Wheeler 1922
Echinodermata	Asteroidea	*Odontaster hispidus*	1	40	41.30	-70.80	Marthas Vineyard (Atlantic Ocean)	Plates	*see* original	Clarke and Wheeler 1922
Echinodermata	Asteroidea	*Plutonaster agassizii*	1	10	41.30	-70.80	Marthas Vineyard (Atlantic Ocean)	Plates	*see* original	Clarke and Wheeler 1922
Echinodermata	Asteroidea	*Pontaster tenuispinus*	1	40	41.30	-70.80	Marthas Vineyard (Atlantic Ocean)	Plates	*see* original	Clarke and Wheeler 1922
Echinodermata	Asteroidea	*Astropecten andromeda*	1	10	41.30	-70.80	Marthas Vineyard (Atlantic Ocean)	Plates	*see* original	Clarke and Wheeler 1922
Echinodermata	Asteroidea	*Leptasterias compta*	1	100	40.28	-69.85	Cape Cod (Atlantic Ocean)	Plates	*see* original	Clarke and Wheeler 1922
Echinodermata	Asteroidea	*Benthopecten spinosus*	1	100	39.25	-68.13	Cape Cod (Atlantic Ocean)	Plates	*see* original	Clarke and Wheeler 1923
Echinodermata	Asteroidea	*Astropecten articulatus*	1	200	35.71	-73.50	Cape Hatteras (Atlantic Ocean)	Plates	*see* original	Clarke and Wheeler 1922
Echinodermata	Asteroidea	*Urasterias linckii*	1	200	35.71	-73.50	Cape Hatteras (Atlantic Ocean)	Plates	*see* original	Clarke and Wheeler 1922
Echinodermata	Asteroidea	*Asterias tanneri*	1	200	35.71	-73.50	Cape Hatteras (Atlantic Ocean)	Plates	*see* original	Clarke and Wheeler 1922
Echinodermata	Asteroidea	*Asterina miniata*	1	10	35.20	-121.30	California (Pacific Ocean)	Plates	*see* original	Clarke and Wheeler 1922
Echinodermata	Asteroidea	*Marthasterias glacialis*	1	30	35.20	-121.30	California (Pacific Ocean)	Plates	*see* original	Schmelck 1901

Echinodermata	Asteroidea	*Astropecten americanus*	1	10	26.90	-82.80	West Florida (Atlantic Ocean)	Plates	*see* original	Clarke and Wheeler 1922
Echinodermata	Asteroidea	*Asterina minuta*	1	15	18.04	-67.96	British West Indies (Atlantic Ocean)	Plates	*see* original	Clarke and Wheeler 1922
Echinodermata	Asteroidea	*Linckia guildingii*	1	30	18.04	-67.96	British West Indies (Atlantic Ocean)	Plates	*see* original	Clarke and Wheeler 1922
Echinodermata	Asteroidea	*Linckia laevigata*	1	30	18.04	-67.96	British West Indies (Atlantic Ocean)	Plates	*see* original	Clarke and Wheeler 1922
Echinodermata	Asteroidea	*Acanthaster planci*	1	25	5.86	-162.08	Palmyra Island (Pacific Ocean)	Plates	*see* original	Clarke and Wheeler 1922
Echinodermata	Asteroidea	*Ctenodiscus procurator*	1	30	-35.70	-72.80	Chile (Pacific Ocean)	Plates	*see* original	Clarke and Wheeler 1922
Echinodermata	Asteroidea	*Ctenodiscus australis*	1	10	-43.60	-74.00	Patagonia (Pacific Ocean)	Plates	*see* original	Clarke and Wheeler 1922
Echinodermata	Crinoidea	*Heliometra glacialis*	1	20	68.20	39.20	Kola Peninsula (Barents Sea)	Plates	*see* original	Terentieva 1932
Echinodermata	Crinoidea	*Ptilocrinus pinnatus*	1	10	53.10	-130.00	British Columbia (Pacific Ocean)	Plates	*see* original	Clarke and Wheeler 1922
Echinodermata	Crinoidea	*Florometra asperrima*	1	12	47.10	-124.20	Washington (Pacific ocean)	Plates	*see* original	Clarke and Wheeler 1922
Echinodermata	Crinoidea	*Bythocrinus robustus*	1	40	42.30	-70.77	Massachussets (Atlantic Ocean)	Plates	*see* original	Clarke and Wheeler 1922
Echinodermata	Crinoidea	*Hathrometra dentata*	1	30	41.30	-70.80	Marthas Vineyard (Atlantic Ocean)	Plates	*see* original	Clarke and Wheeler 1922
Echinodermata	Crinoidea	*Psathyrometra fragilis*	1	20	35.07	139.70	Japan Sea (Pacific Ocean)	Plates	*see* original	Clarke and Wheeler 1922
Echinodermata	Crinoidea	*Pentametrocrinus japonicus*	1	20	34.90	138.50	Japan Sea (Pacific Ocean)	Plates	*see* original	Clarke and Wheeler 1922
Echinodermata	Crinoidea	*Crinometra concinna*	1	40	28.05	-96.02	Gulf of Mexico (Atlantic Ocean)	Plates	*see* original	Clarke and Wheeler 1922
Echinodermata	Crinoidea	*Isocrinus decorus*	1	50	21.40	-76.70	Cuba (Caribbean Sea)	Plates	*see* original	Clarke and Wheeler 1922
Echinodermata	Crinoidea	*Endoxocrinus parra*	1	60	21.40	-76.70	Cuba (Caribbean Sea)	Plates	*see* original	Clarke and Wheeler 1922
Echinodermata	Crinoidea	*Tropiometra picta*	1	30	21.40	-76.70	Cuba (Caribbean Sea)	Plates	*see* original	Clarke and Wheeler 1922
Echinodermata	Crinoidea	*Promachocrinus kerguelensis*	1	20	11.17	-60.68	Tobago (Atlantic Ocean)	Plates	*see* original	Clarke and Wheeler 1922
Echinodermata	Crinoidea	*Capillaster multiradiata*	1	30	7.85	116.90	Philippines (Pacific Ocean)	Plates	*see* original	Clarke and Wheeler 1922
Echinodermata	Crinoidea	*Pachylometra patula*	1	30	7.85	116.90	Philippines (Pacific Ocean)	Plates	*see* original	Clarke and Wheeler 1922
Echinodermata	Crinoidea	*Catoptometra ophiura*	1	30	7.85	116.90	Philippines (Pacific Ocean)	Plates	*see* original	Clarke and Wheeler 1922
Echinodermata	Crinoidea	*Hypalocrinus naresianus*	1	30	7.85	116.90	Philippines (Pacific Ocean)	Plates	*see* original	Clarke and Wheeler 1922
Echinodermata	Crinoidea	*Parametra granulata*	1	30	7.85	116.90	Philippines (Pacific Ocean)	Plates	*see* original	Clarke and Wheeler 1922
Echinodermata	Crinoidea	*Craspedometra anceps*	1	30	7.85	116.90	Philippines (Pacific Ocean)	Plates	*see* original	Clarke and Wheeler 1922
Echinodermata	Crinoidea	*Zygometra microdiscus*	1	40	-5.99	134.10	New Guinea (Pacific Ocean)	Plates	*see* original	Clarke and Wheeler 1922
Echinodermata	Crinoidea	*Tropiometra carinata*	1	15	-22.98	-43.20	Rio de Janeiro (Atlantic Ocean)	Plates	*see* original	Clarke and Wheeler 1922
Echinodermata	Crinoidea	*Pilometra mülleri*	1	20	-33.85	151.26	Sydney Harbor (Pacific Ocean)	Plates	*see* original	Clarke and Wheeler 1922
Echinodermata	Echinoidea	*Strongylocentrotus droebachiensis*	1	40	64.00	-38.00	Greenland Sea (Atllantic Ocean)	Plates	*see* original	Clarke and Wheeler 1922
Echinodermata	Echinoidea	*Echinarachnius parma*	1	32	59.20	-165.80	Bering Sea (Arctic Ocean)	Plates	*see* original	Terentieva 1932
Echinodermata	Echinoidea	*Arbacia pustulosa*	1	15	40.76	14.35	Bay of Naples (Mediterranean Sea)	Plates	*see* original	Clarke and Wheeler 1922
Echinodermata	Echinoidea	*Echinus esculentus*	1	10	38.00	-1.02	Mediterranean Sea	Plates	*see* original	Clarke and Wheeler 1922
Echinodermata	Echinoidea	*Paracentrotus lividus*	1	5	37.24	13.68	Sicily (Mediterranean Sea)	Plates	*see* original	Clarke and Wheeler 1922
Echinodermata	Echinoidea	*Echinus affinis*	1	200	35.71	-73.50	Cape Hatteras (Atlantic Ocean)	Plates	*see* original	Clarke and Wheeler 1922
Echinodermata	Echinoidea	*Lytechinus anamesus*	1	20	35.20	-121.30	California (Pacific Ocean)	Plates	*see* original	Clarke and Wheeler 1922
Echinodermata	Echinoidea	*Clypeaster testudinarius*	1	20	33.40	134.60	South Japan Sea (Pacific Ocean)	Plates	*see* original	Terentieva 1932
Echinodermata	Echinoidea	*Strongylocentrotus fragilis*	1	60	29.00	-115.00	South California (Pacific Ocean)	Plates	*see* original	Clarke and Wheeler 1922
Echinodermata	Echinoidea	*Prionocidaris baculosa*	1	15	28.02	34.97	Red Sea	Plates	*see* original	Bütschli 1908
Echinodermata	Echinoidea	*Tetrocidaris affinis*	1	10	26.90	-82.80	Florida (Atlantic Ocean)	Plates	*see* original	Clarke and Wheeler 1922
Echinodermata	Echinoidea	*Echinometra lucunter*	1	20	18.04	-67.96	British West Indies (Atlantic Ocean)	Plates	*see* original	Terentieva 1932

Echinodermata	Echinoidea	*Mellita sexiesperforatus*	1	30	18.04	-67.96	British West Indies (Atlantic Ocean)	Plates	*see* original	Clarke and Wheeler 1922
Echinodermata	Echinoidea	*Encope californica*	1	20	-1.00	-91.01	Galapagos (Pacific Ocean)	Plates	*see* original	Clarke and Wheeler 1922
Echinodermata	Echinoidea	*Tetrapygus niger*	1	20	-9.40	-78.50	Peru (Pacific Ocean)	Plates	*see* original	Clarke and Wheeler 1922
Echinodermata	Echinoidea	*Heterocentrotus mammillatus*	1	20	-27.64	-144.33	Tuamotu (Pacific Ocean)	Plates	*see* original	Terentieva 1932
Echinodermata	Echinoidea	*Lytechinus albus*	1	10	-43.60	-74.00	Patagonia (Pacific Ocean)	Plates	*see* original	Clarke and Wheeler 1922
Echinodermata	Ophiuroidea	*Gorgonocephalus caryi*	1	15	61.30	-166.30	Bering Sea (Arctic Ocean)	Plates	*see* original	Clarke and Wheeler 1922
Echinodermata	Ophiuroidea	*Astrophyton sp.*	1	60	56.00	2.90	North Sea	Plates	*see* original	Clarke and Wheeler 1922
Echinodermata	Ophiuroidea	*Ophiopholis aculeata japonica*	1	10	53.91	-166.50	Unalaska (Arctic Ocean)	Plates	*see* original	Clarke and Wheeler 1922
Echinodermata	Ophiuroidea	*Gorgonocephalus arcticus*	1	10	41.50	-70.30	Cape Cod (Atlantic Ocean)	Plates	*see* original	Clarke and Wheeler 1922
Echinodermata	Ophiuroidea	*Ophioglypha sarsii*	1	100	39.54	-72.35	New England slope (Atlantic Ocean)	Plates	*see* original	Clarke and Wheeler 1922
Echinodermata	Ophiuroidea	*Gorgonocephalus eucnemis*	1	50	38.30	139.00	Japan Sea (Pacific Ocean)	Plates	*see* original	Schmelck 1901
Echinodermata	Ophiuroidea	*Ophionereis eurybrachiplax*	1	50	38.30	139.00	Japan Sea (Pacific Ocean)	Plates	*see* original	Clarke and Wheeler 1922
Echinodermata	Ophiuroidea	*Ophioglypha lütkeni*	1	200	35.20	-121.30	California (Pacific Ocean)	Plates	*see* original	Clarke and Wheeler 1922
Echinodermata	Ophiuroidea	*Ophiothrix angulata*	1	200	21.40	-76.70	Cuba (Caribbean Sea)	Plates	*see* original	Clarke and Wheeler 1922
Echinodermata	Ophiuroidea	*Ophiocamax fasciculata*	1	100	21.40	-76.70	Caribbean Sea	Plates	*see* original	Clarke and Wheeler 1922
Echinodermata	Ophiuroidea	*Ophiocoma erinaceus*	1	20	20.10	-155.30	Hawaii (Pacific Ocean)	Plates	*see* original	Clarke and Wheeler 1922
Echinodermata	Ophiuroidea	*Ophioderma cinerum*	1	30	18.50	-66.60	Puerto Rico (Caribbean Sea)	Plates	*see* original	Clarke and Wheeler 1922
Echinodermata	Ophiuroidea	*Ophiocoma aethiops*	1	25	18.04	-67.96	Gulf of California (Pacific Ocean)	Plates	*see* original	Clarke and Wheeler 1922
Echinodermata	Ophiuroidea	*Ophiomixa flaccida*	1	120	18.04	-67.96	British West Indies (Atlantic Ocean)	Plates	*see* original	Clarke and Wheeler 1922
Echinodermata	Ophiuroidea	*Ophiocoma pumila*	1	120	18.04	-67.96	British West Indies (Atlantic Ocean)	Plates	*see* original	Clarke and Wheeler 1922
Echinodermata	Ophiuroidea	*Ophiomusium lymani*	1	200	-1.00	-91.01	Galapagos (Pacific Ocean)	Plates	*see* original	Clarke and Wheeler 1922
Echinodermata	Ophiuroidea	*Ophioglypha lymani*	1	30	-35.70	-72.80	Chile (Pacific Ocean)	Plates	*see* original	Clarke and Wheeler 1922
Coralline algae	-	*Lithothamnium sp.*	1	10	78.00	20.00	Spitzbergen (Barents Sea)	Skeleton	*see* original	Högbom 1894
Coralline algae	-	*Lithothamnium soriferum*	1	10	75.00	20.00	Spitzbergen (Barents Sea)	Skeleton	*see* original	Högbom 1894
Coralline algae	-	*Lithothamium glaciale*	1	10	75.00	20.00	Spitzbergen (Barents Sea)	Skeleton	*see* original	Högbom 1894
Coralline algae	-	*Lithothamnium fornicatum*	1	10	72.00	20.00	Norwegian Sea	Skeleton	*see* original	Lemoine 1910
Coralline algae	-	*Lithothamnium polymorphum*	1	10	57.00	12.00	North Sea	Skeleton	*see* original	Högbom 1894
Coralline algae	-	*Corallina squamata* - 29-Nov	1	5	50.60	-2.30	Dorset (Atlantic Ocean)	Skeleton	*see* original	Haas et al. 1935
Coralline algae	-	*Corallina squamata* - 29-Jan	1	5	50.60	-2.30	Dorset (Atlantic Ocean)	Skeleton	*see* original	Haas et al. 1935
Coralline algae	-	*Corallina squamata* - 26-Mar	1	5	50.60	-2.30	Dorset (Atlantic Ocean)	Skeleton	*see* original	Haas et al. 1935
Coralline algae	-	*Corallina squamata* - 28-May	1	5	50.60	-2.30	Dorset (Atlantic Ocean)	Skeleton	*see* original	Haas et al. 1935
Coralline algae	-	*Corallina squamata* - 01-Jul	1	5	50.60	-2.30	Dorset (Atlantic Ocean)	Skeleton	*see* original	Haas et al. 1935
Coralline algae	-	*Corallina squamata* - 13-Aug	1	5	50.60	-2.30	Dorset (Atlantic Ocean)	Skeleton	*see* original	Haas et al. 1935
Coralline algae	-	*Corallina squamata* - 12-Sep	1	5	50.60	-2.30	Dorset (Atlantic Ocean)	Skeleton	*see* original	Haas et al. 1935
Coralline algae	-	*Corallina squamata* - 10-Oct	1	5	50.60	-2.30	Dorset (Atlantic Ocean)	Skeleton	*see* original	Haas et al. 1935
Coralline algae	-	*Corallina officinalis*	1	5	49.60	-1.20	Normandy (Atlantic Ocean)	Skeleton	*see* original	Clarke and Wheeler 1922
Coralline algae	-	*Lithothamnium calcareum*	1	10	48.08	-4.00	Atlantic Ocean	Skeleton	*see* original	Clarke and Wheeler 1922
Coralline algae	-	*Lithophyllum incrustans*	1	10	48.00	-3.00	English Channel (Atlantic Ocean)	Skeleton	*see* original	Clarke and Wheeler 1922
Coralline algae	-	*Phymatolithon compactum*	1	10	48.00	-55.00	Newfoundland (Atlantic Ocean)	Skeleton	*see* original	Clarke and Wheeler 1922

Coralline algae	-	*Lithophyllum tortuosum*	1	20	44.00	9.00	Genoa (Mediterranean Sea)	Skeleton	*see* original	Lipman and Shelley 1924
Coralline algae	-	*Lithophyllum proboscideum*	1	15	37.00	-122.00	Monterey Bay (Pacific Ocean)	Skeleton	*see* original	Lipman and Shelley 1924
Coralline algae	-	*Goniolithon strictum - old*	1	30	25.00	-75.00	Bahamas (Atlantic Ocean)	Skeleton	*see* original	Lipman and Shelley 1924
Coralline algae	-	*Goniolithon strictum - old*	1	30	25.00	-75.00	Bahamas (Atlantic Ocean)	Skeleton	*see* original	Vaughan 1918
Coralline algae	-	*Goniolithon strictum - young*	1	30	25.00	-75.00	Bahamas (Atlantic Ocean)	Skeleton	*see* original	Clarke and Wheeler 1922
Coralline algae	-	*Lithophyllum pachydermum*	1	30	25.00	-75.00	Bahamas (Atlantic Ocean)	Skeleton	*see* original	Clarke and Wheeler 1922
Coralline algae	-	*Goniolithon acropectum*	1	20	18.00	-68.00	Puerto Rico (Atlantic Ocean)	Skeleton	*see* original	Clarke and Wheeler 1922
Coralline algae	-	*Amphiroa fragilissima*	1	10	18.00	-68.00	Puerto Rico (Atlantic Ocean)	Skeleton	*see* original	Högbom 1894
Coralline algae	-	*Lithothamnium nodosum*	1	5	0.00	-90.00	Galapagos Islands (Pacific Ocean)	Skeleton	*see* original	Payen 1843
Coralline algae	-	*Lithophyllum oncodes*	1	30	-7.00	56.00	Madagascar (Indian Ocean)	Skeleton	*see* original	Lemoine 1910
Coralline algae	-	*Goniolithon orthoblastum*	1	10	-10.00	145.00	Murray Isle (Pacific Ocean)	Skeleton	*see* original	Lemoine 1910
Coralline algae	-	*Lithothamnium erubescens*	1	10	-10.00	123.00	Timor (Indian Ocean)	Skeleton	*see* original	Clarke and Wheeler 1922
Coralline algae	-	*Archaeolithothamium episporum*	1	10	-10.00	80.00	Panama (Pacific Ocean)	Skeleton	*see* original	Lemoine 1910
Coralline algae	-	*Lithothamnium kaiseri*	1	10	-15.00	-172.00	Samoa (Pacific Ocean)	Skeleton	*see* original	Lipman and Shelley 1924
Coralline algae	-	*Porolithon craspedium*	1	10	-15.00	-172.00	Rose Atoll (Pacific Ocean)	Skeleton	*see* original	Clarke and Wheeler 1922
Coralline algae	-	*Porolithon oncodes*	1	10	-15.00	-172.00	Samoa (Pacific Ocean)	Skeleton	*see* original	Clarke and Wheeler 1922
Foraminifera	-	*Pulvinulina menardii* - pelagic	1	20	40.56	-66.15	Atlantic Ocean	Shell	*see* original	Clarke and Wheeler 1922
Foraminifera	-	*Polytrema mineaccum* - benthic	1	100	25.00	-77.00	Bahamas (Atlantic Ocean)	Shell	*see* original	Clarke and Wheeler 1922
Foraminifera	-	*Orbitolites marginatis* - benthic	1	50	24.60	-81.96	Florida (Atlantic Ocean)	Shell	*see* original	Brady 1884
Foraminifera	-	*Amphistegina lessonii* - pelagic	1	20	16.10	-22.95	Cape Verde (Atlantic Ocean)	Shell	*see* original	Brady 1884
Foraminifera	-	*Sphaeroidina dehiscens* - pelagic	1	20	12.40	121.60	Philippines (Pacific Ocean)	Shell	*see* original	Clarke and Wheeler 1922
Foraminifera	-	*Orbitolites complanata* - benthic	1	30	-17.30	177.47	Fiji (Pacific Ocean)	Shell	*see* original	Clarke and Wheeler 1922
Hydrocorallia	-	*Millepora alcicornis*	1	10	24.60	-81.96	Florida (Atlantic Ocean)	Skeleton	*see* original	Clarke and Wheeler 1922
Hydrocorallia	-	*Distichopora nitida*	1	20	7.40	151.50	Micronesia (Pacific Ocean)	Skeleton	*see* original	Clarke and Wheeler 1922
Hydrocorallia	-	*Millepora braziliensis*	1	30	-12.20	-36.80	Brazil (Atlantic Ocean)	Skeleton	*see* original	Clarke and Wheeler 1922
Hexacorallia	-	*Madracis decactis*	1	20	32.40	-64.90	Bermuda (Atlantic Ocean)	Skeleton	*see* original	Clarke and Wheeler 1922
Hexacorallia	-	*Siderastrea radians*	1	20	32.40	-64.90	Bermuda (Atlantic Ocean)	Skeleton	*see* original	Clarke and Wheeler 1922
Hexacorallia	-	*Flabellum alabastrum*	1	10	26.00	-77.20	Bahamas (Atlantic Ocean)	Skeleton	*see* original	Clarke and Wheeler 1922
Hexacorallia	-	*Acropora cervicornis*	1	15	26.00	-77.20	Bahamas (Atlantic Ocean)	Skeleton	*see* original	Clarke and Wheeler 1922
Hexacorallia	-	*Favia fragum*	1	20	24.60	-81.96	Florida (Atlantic Ocean)	Skeleton	*see* original	Clarke and Wheeler 1922
Hexacorallia	-	*Dasmosmilia lymani*	1	10	24.60	-81.96	Florida (Atlantic Ocean)	Skeleton	*see* original	Clarke and Wheeler 1922
Hexacorallia	-	*Balanophyllia floridana*	1	10	24.54	-81.80	Florida (Atlantic Ocean)	Skeleton		Clarke and Wheeler 1922
Hexacorallia	-	*Paracyathus defilipii*	1	10	24.54	-81.80	Florida (Atlantic Ocean)	Skeleton	*see* original	Clarke and Wheeler 1922
Hexacorallia	-	*Deltocyathus italicus*	1	20	18.50	-63.51	-		*see* original	Clarke and Wheeler 1922
Hexacorallia	-	*Desmophyllum ingens*	1	15	-36.55	-73.00	Chile (Pacific Ocean)	Skeleton	*see* original	Clarke and Wheeler 1922
Octocorallia	-	*Gorgonia sp.*	1	30	54.60	154.40	Sea of Okhotsk (Pacific Ocean)	Skeleton	*see* original	Clarke and Wheeler 1922

Octocorallia	-	*Alcyonium carneum*	1	50	45.18	-55.85	Newfoundland (Atlantic Ocean)	Skeleton	*see* original	Clarke and Wheeler 1922
Octocorallia	-	*Paramuricea borealis*	1	50	45.18	-55.85	Grand Banks (Atlantic Ocean)	Skeleton	*see* original	Clarke and Wheeler 1922
Octocorallia	-	*Alcyonium carneum*	1	50	45.18	-55.85	Newfoundland (Atlantic Ocean)	Skeleton	*see* original	Clarke and Wheeler 1922
Octocorallia	-	*Pennatula aculeata*	1	50	44.45	-58.51	Banquereau (Atlantic Ocean)	Skeleton	*see* original	Clarke and Wheeler 1922
Octocorallia	-	*Paragorgia arborea*	1	50	44.36	-63.75	Nova Scotia (Atlantic Ocean)	Skeleton	*see* original	Phillips 1922
Octocorallia	-	*Paragorgia arborea*	1	50	43.00	-62.00	Nova Scotia (Atlantic Ocean)	Skeleton	*see* original	Vinogradov 1933
Octocorallia	-	*Corallium elatior*	1	40	42.25	130.91	Japan Sea (Pacific Ocean)	Skeleton	*see* original	Clarke and Wheeler 1922
Octocorallia	-	*Primnoa resedaeformis*	1	30	42.25	130.91	Japan Sea (Pacific Ocean)	Skeleton	*see* original	Clarke and Wheeler 1922
Octocorallia	-	*Primnoa reseda*	1	40	42.25	-63.25	Nova Scotia (Atlantic Ocean)	Skeleton	*see* original	Velimirov and Böhm 1976
Octocorallia	-	*Rhipidogorgia flabellum*	1	20	32.40	-64.90	Bermuda (Atlantic Ocean)	Skeleton	*see* original	Velimirov and Böhm 1976
Octocorallia	-	*Pleurocorallium johnsoni*	1	30	25.75	-20.20	Canary Islands (Atlantic Ocean)	Skeleton	*see* original	Velimirov and Böhm 1976
Octocorallia	-	*Gorgonia acerosa*	1	50	24.60	-81.96	Florida (Atlantic Ocean)	Skeleton	*see* original	Velimirov and Böhm 1976
Octocorallia	-	*Leptogorgia pulchra*	1	80	24.60	-108.25	California (Pacific Ocean)	Skeleton	*see* original	Clarke and Wheeler 1922
Octocorallia	-	*Xiphigorgia anceps*	1	20	24.47	-81.55	Florida (Atlantic Ocean)	Skeleton	*see* original	Clarke and Wheeler 1922
Octocorallia	-	*Muricea echinata*	1	10	22.86	-106.10	California (Pacific Ocean)	Skeleton	*see* original	Clarke and Wheeler 1922
Octocorallia	-	*Leptogorgia rigida*	1	150	22.86	-109.79	California (Pacific Ocean)	Skeleton	*see* original	Clarke and Wheeler 1922
Octocorallia	-	*Heliopora cerulea*	1	20	12.40	121.60	Philippines (Pacific Ocean)	Skeleton	*see* original	Clarke and Wheeler 1922
Octocorallia	-	*Tubipora purpurea*	1	10	1.33	103.83	Singapore (Indian Ocean)	Skeleton	*see* original	Clarke and Wheeler 1922
Octocorallia	-	*Phyllogorgia quercifolia*	1	10	-3.83	-32.41	Brazil (Atlantic Ocean)	Skeleton	*see* original	Murray and Renard 1891
Octocorallia	-	*Ctenocella pectinata*	1	20	-10.00	142.20	Torres Strait (Pacific Ocean)	Skeleton	*see* original	Vinogradov 1933
Octocorallia	-	*Muricea humilis*	1	30	-12.20	-36.80	Brazil (Atlantic Ocean)	Skeleton	*see* original	Clarke and Wheeler 1922
Octocorallia	-	*Gorgonia subfruticosa*	1	45	-18.00	-178.00	Fiji (Pacific Ocean)	Skeleton	*see* original	Clarke and Wheeler 1922
Octocorallia	-	*Plexaurella grandiflora*	1	20	-28.40	155.67	Australia (Pacific Ocean)	Skeleton	*see* original	Clarke and Wheeler 1922
Octocorallia	-	*Eunicella papillose*	1	30	-34.21	18.35	Cape Town (Atlantic Ocean)	Skeleton	*see* original	Clarke and Wheeler 1922
Octocorallia	-	*Eunicella alba*	1	30	-34.22	18.48	False Bay (Indian Ocean)	Skeleton	*see* original	Clarke and Wheeler 1922
Octocorallia	-	*Eunicella tricoronata*	1	30	-34.22	18.48	False Bay (Indian Ocean)	Skeleton	*see* original	Clarke and Wheeler 1922
Octocorallia	-	*Lophogorgia flamea*	1	30	-34.22	18.48	False Bay (Indian Ocean)	Skeleton	*see* original	Clarke and Wheeler 1922
Bryozoa	-	*Flustra membranacea*	1	50	59.17	-151.60	Alaska (Pacific Ocean)	Skeleton	*see* original	Clarke and Wheeler 1922
Bryozoa	-	*Cellepora incrassata*	1	50	44.69	-62.69	Grand Banks (Atlantic Ocean)	Skeleton	*see* original	Clarke and Wheeler 1922
Bryozoa	-	*Schizoporella unicornis*	1	10	41.35	-70.79	Vineyard Sounds (Atlantic Ocean)	Skeleton	*see* original	Clarke and Wheeler 1922
Bryozoa	-	*Bugula turrita*	1	40	41.23	-70.07	Georges Bank (Atlantic Ocean)	Skeleton	*see* original	Clarke and Wheeler 1922
Bryozoa	-	*Lepralia sp.*	1	20	40.80	14.20	Naples (Mediterranean Sea)	Skeleton	*see* original	Clarke and Wheeler 1922
Bryozoa	-	*Amathia spiralis*	1	20	35.22	-75.60	Cape Hatteras (Atlantic Ocean)	Skeleton	*see* original	Clarke and Wheeler 1922
Bryozoa	-	*Holoporella albirostris*	1	20	24.47	-81.55	Florida (Atlantic Ocean)	Skeleton	*see* original	Clarke and Wheeler 1922
Bryozoa	-	*Bugula neritina*	1	20	24.47	-81.55	Florida (Atlantic Ocean)	Skeleton	*see* original	Clarke and Wheeler 1922
Bryozoa	-	*Microporella grisea*	1	20	-28.40	155.67	Australia (Pacific Ocean)	Skeleton	*see* original	Clarke and Wheeler 1922
Brachiopoda	-	*Terebratulina septentrionalis*	1	30	44.87	-66.91	Easport (Atlantic Ocean)	Shell	*see* original	Clarke and Wheeler 1922
Brachiopoda	-	*Laqueus californicus*	1	80	24.60	-108.25	California (Pacific Ocean)	Shell	*see* original	Clarke and Wheeler 1922

Mollusca	Amphineura	*Mopalia muscosa*	1	120	34.39	-119.70	Santa Barbara (Pacific Ocean)	Shell	*see* original	Clarke and Wheeler 1922
Mollusca	Bivalvia	*Astarte borealis*	1	50	74.16	54.40	Novaia Zemlya (White Sea)	Shell	*see* original	Clarke and Wheeler 1922
Mollusca	Bivalvia	*Tellina calcarea*	1	40	74.16	54.33	Novaia Zemlya (White Sea)	Shell	*see* original	Clarke and Wheeler 1922
Mollusca	Bivalvia	*Pecten groenlandicus*	1	20	73.50	68.83	Barents Sea (Arctic Ocean)	Shell	*see* original	Clarke and Wheeler 1922
Mollusca	Bivalvia	*Pecten islandicus*	1	40	71.50	47.00	Barents Sea (Arctic Ocean)	Shell	*see* original	Clarke and Wheeler 1922
Mollusca	Bivalvia	*Pecten dislocatus*	1	10	26.81	-82.29	Charlotte Harbor (Atlantic Ocean)	Shell	*see* original	Samoilov and Terentieva 1925
Mollusca	Bivalvia	*Pecten ventricosus*	1	10	22.86	-106.10	California (Pacific Ocean)	Shell	*see* original	Samoilov and Terentieva 1925
Mollusca	Bivalvia	*Placuna orbicularis*	1	10	16.83	120.26	Philippines (Pacific Ocean)	Shell	*see* original	Samoilov and Terentieva 1925
Mollusca	Cephalopoda	*Nautilus pompilius*	1	100	8.53	123.03	Mindanao (Pacific Ocean)	Shell	*see* original	Clarke and Wheeler 1922
Mollusca	Cephalopoda	*Sepia officinalis*	1	10	5.84	118.27	Philippines (Pacific Ocean)	Shell	*see* original	Terentieva 1925
Mollusca	Cephalopoda	*Argonauta argo*	1	50	-35.82	175.39	Pacific Ocean	Shell	*see* original	Clarke and Wheeler 1922
Mollusca	Cirripedia	*Scalpellum regium*	1	5	52.92	-132.29	Queen Charlotte I (Pacific Ocean)	Shell	*see* original	Clarke and Wheeler 1922
Mollusca	Cirripedia	*Balanus hameri*	1	20	41.23	-70.07	Georges Bank (Atlantic Ocean)	Shell	*see* original	Clarke and Wheeler 1922
Mollusca	Cirripedia	*Balanus amphitrite*	1	5	38.92	-74.91	Cape May (Atlantic Ocean)	Shell	*see* original	Clarke and Wheeler 1922
Mollusca	Cirripedia	*Lepas anatifera*	1	10	24.47	-81.55	Florida (Atlantic Ocean)	Shell	*see* original	Clarke and Wheeler 1922
Mollusca	Cirripedia	*Mitella polymerus*	1	10	22.86	-106.10	California (Pacific Ocean)	Shell	*see* original	Samoilov and Terentieva 1925
Mollusca	Gastropoda	*Neptunea despecta*	1	20	69.63	57.35	Barents Sea	Shell	*see* original	Samoilov and Terentieva 1925
Mollusca	Gastropoda	*Natica clausa*	1	20	60.50	-46.91	Barents Sea	Shell	*see* original	Clarke and Wheeler 1922
Mollusca	Gastropoda	*Tachyrhynchus erosa*	1	30	52.90	158.76	Kamchatka (Pacific Ocean)	Shell	*see* original	Clarke and Wheeler 1922
Mollusca	Gastropoda	*Nassa tegula*	1	20	36.62	-121.91	Monterey Bay (Pacific Ocean)	Shell	*see* original	Clarke and Wheeler 1922
Mollusca	Gastropoda	*Nassa isculpta*	1	50	32.34	-118.43	Cortez Bank (Pacific Ocean)	Shell	*see* original	Clarke and Wheeler 1922
Mollusca	Scaphopoda	*Dentalium solidum*	1	30	41.23	-70.07	Georges Bank (Atlantic Ocean)	Shell	*see* original	Clarke and Wheeler 1922
Crustacea	Amphipoda	*Tryphosa pinguis*	1	30	41.52	-70.67	Woods Hole (Atlantic Ocean)	Carapace	*see* original	Clarke and Wheeler 1922
Crustacea	Decapoda	*Crago dalli*	1	40	59.17	-151.60	Alaska (Pacific Ocean)	Carapace	*see* original	Clarke and Wheeler 1922
Crustacea	Decapoda	*Pagurus rathbuni*	1	210	58.46	-175.22	Bering Sea (Arctic Ocean)	Carapace	*see* original	Clarke and Wheeler 1922
Crustacea	Decapoda	*Homarus americanus* - small	1	30	43.84	-69.64	Boothbay Harbor (Atlantic Ocean)	Carapace	*see* original	Clarke and Wheeler 1922
Crustacea	Decapoda	*Homarus americanus* - medium	1	30	43.84	-69.64	Boothbay Harbor (Atlantic Ocean)	Carapace	*see* original	Clarke and Wheeler 1922
Crustacea	Decapoda	*Homarus americanus* - large	1	30	43.84	-69.64	Boothbay Harbor (Atlantic Ocean)	Carapace	*see* original	Clarke and Wheeler 1922
Crustacea	Decapoda	*Homarus americanus*	1	50	41.35	-70.79	Vineyard Sounds (Atlantic Ocean)	Carapace	*see* original	Clarke and Wheeler 1922
Crustacea	Decapoda	*Libinia emarginata*	1	20	41.35	-70.79	Vineyard Sounds (Atlantic Ocean)	Carapace	*see* original	Clarke and Wheeler 1922
Crustacea	Decapoda	*Munida iris*	1	20	37.62	-76.26	Chesapeake Bay (Atlantic Ocean)	Carapace	*see* original	Clarke and Wheeler 1922
Crustacea	Decapoda	*Pandalus platyceros*	1	50	36.62	-121.91	Monterey Bay (Pacific Ocean)	Carapace	*see* original	Clarke and Wheeler 1922
Crustacea	Decapoda	*Palinurus argus*	1	60	21.84	-71.33	West Indies (Atlantic Ocean)	Carapace	*see* original	Clarke and Wheeler 1922
Crustacea	Decapoda	*Grapsus grapsus*	1	60	-9.36	46.40	Aldabra Island (Indian Ocean)	Carapace	*see* original	Clarke and Wheeler 1922
Crustacea	Stomatopoda	*Chloridella empusa*	1	20	24.47	-81.55	Florida (Atlantic Ocean)	Carapace	*see* original	Clarke and Wheeler 1922

Table 15.4. Summary of skeletal mineralogy.

Taxa	Class	Statistic	$CaCO_3$ % dw	$MgCO_3$ % dw	Mg/Ca (mol/mol)	mol % $MgCO_3$
Echinodermata	Asteroidea	avg	84.085	9.558	0.136	11.142
		SD	12.602	1.807	0.022	2.071
		max.	91.710	14.310	0.204	16.547
		min.	36.270	4.080	0.102	4.807
	Echinoidea	avg	86.150	7.226	0.101	8.449
		SD	9.157	2.786	0.039	3.213
		max.	96.500	13.300	0.190	15.407
		min.	62.360	2.760	0.035	3.260
	Ophiuroidea	avg	92.125	7.875	0.102	9.214
		SD	0.544	0.544	0.008	0.628
		max.	92.510	8.260	0.107	9.658
		min.	91.740	7.490	0.096	8.770
	Holothuroidea	avg	84.593	9.921	0.141	11.554
		SD	10.003	2.345	0.037	2.677
		max.	92.700	14.560	0.213	16.828
		min.	48.440	6.610	0.085	7.752
	Crinoidea	avg	87.331	10.961	0.149	12.747
		SD	1.946	1.646	0.024	1.878
		max.	91.550	13.740	0.196	15.904
		min.	83.130	7.860	0.102	9.197
Coiralline algae	-	avg	78.557	13.031	0.198	15.059
		SD	6.206	4.687	0.075	5.261
		max.	91.040	24.000	0.381	27.269
		min.	70.400	6.060	0.079	7.114
Foraminifera	-	avg	86.638	7.127	0.097	8.318
		SD	5.548	4.267	0.057	4.934
		max.	92.850	12.520	0.172	14.524
		min.	77.020	1.790	0.025	2.118
Hydrocorallia	-	avg	97.737	0.823	0.010	0.976
		SD	0.837	0.531	0.007	0.629
		max.	98.220	1.280	0.016	1.516
		min.	96.770	0.240	0.003	0.285
Hexacorallia	-	avg	98.971	0.619	0.007	0.734
		SD	0.474	0.234	0.003	0.277
		max.	99.490	1.110	0.013	1.315

		min.	98.050	0.370	0.004	0.439
Octocorallia	-	avg	82.845	10.021	0.137	11.651
		SD	8.400	3.677	0.049	4.218
		max.	98.930	15.730	0.200	18.142
		min.	62.050	0.350	0.004	0.415
Bryozoa	-	avg	86.321	5.911	0.090	6.912
		SD	13.042	3.909	0.072	4.543
		max.	96.900	11.080	0.208	12.888
		min.	63.290	0.630	0.008	0.747
Brachiopoda	-	avg	97.540	1.025	0.013	1.214
		SD	1.075	0.488	0.006	0.577
		max.	98.300	1.370	0.017	1.622
		min.	96.780	0.680	0.008	0.806
Mollusca	Cephalopoda	avg	97.193	2.600	0.033	3.058
		SD	3.031	3.050	0.039	3.578
		max.	99.500	6.020	0.076	7.068
		min.	93.760	0.160	0.002	0.190
	Bivalvia	avg	97.334	0.834	0.010	0.989
		SD	3.284	0.230	0.003	0.272
		max.	99.220	1.280	0.016	1.516
		min.	90.000	0.620	0.007	0.735
	Amphineura	avg	98.370	0.450	0.005	0.534
		SD	0.000	0.000	0.000	0.000
		max.	98.370	0.450	0.005	0.534
		min.	98.370	0.450	0.005	0.534
Mollusca	Scaphopoda	avg	99.130	0.200	0.002	0.237
		SD	0.000	0.000	0.000	0.000
		max.	99.130	0.200	0.002	0.237
		min.	99.130	0.200	0.002	0.237
	Gastropoda	avg	98.072	1.036	0.013	1.227
		SD	0.984	0.513	0.006	0.607
		max.	99.220	1.780	0.022	2.106
		min.	97.000	0.370	0.004	0.439
	Cirripedia	avg	97.292	1.842	0.023	2.179
		SD	1.228	0.686	0.008	0.809
		max.	99.070	2.490	0.030	2.943
		min.	95.630	0.750	0.009	0.889

Crustacea	Decapoda	avg	72.429	8.428	0.141	9.845
		SD	8.734	1.815	0.039	2.083
		max.	82.640	12.580	0.218	14.592
		min.	54.830	5.800	0.088	6.812
	Stomatopoda	avg	28.560	15.990	0.665	18.433
		SD	0.000	0.000	0.000	0.000
		max.	28.560	15.990	0.665	18.433
		min.	28.560	15.990	0.665	18.433
	Amphipoda	avg	74.640	4.840	0.077	5.695
		SD	0.000	0.000	0.000	0.000
		max.	74.640	4.840	0.077	5.695
		min.	74.640	4.840	0.077	5.695

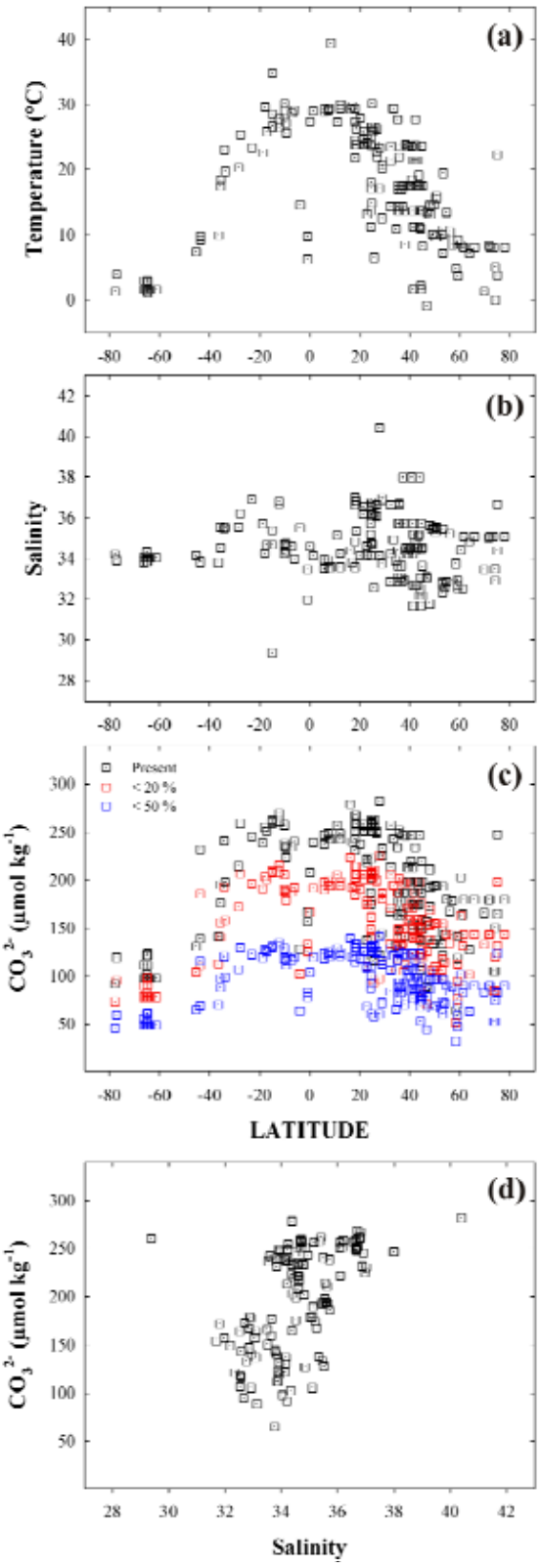

Fig. 15.8. Trends of temperature (a), salinity (b), and CO_3^{2-} at present and future scenarios (c) with latitude, and salinity *vs.* present CO_3^{2-} (d) for each organism recovered from the NEAR 3D analysis.

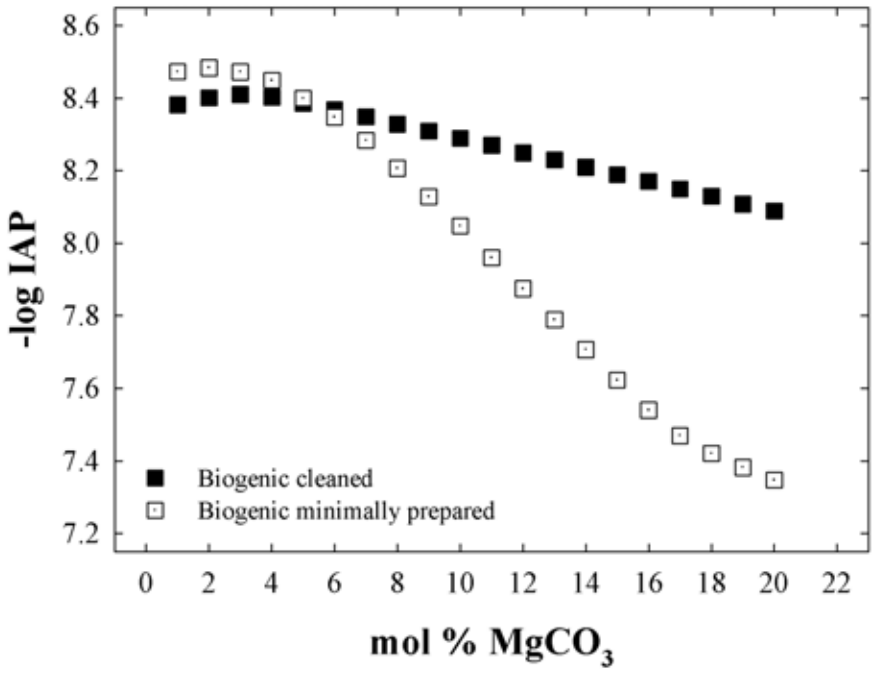

Fig. 15.9. Solubility curves of biogenic Mg-calcite *vs.* mol % $MgCO_3$ empirically obtained used in the calculation of the saturation state (*see* Fig.15.3 for the different outcomes).

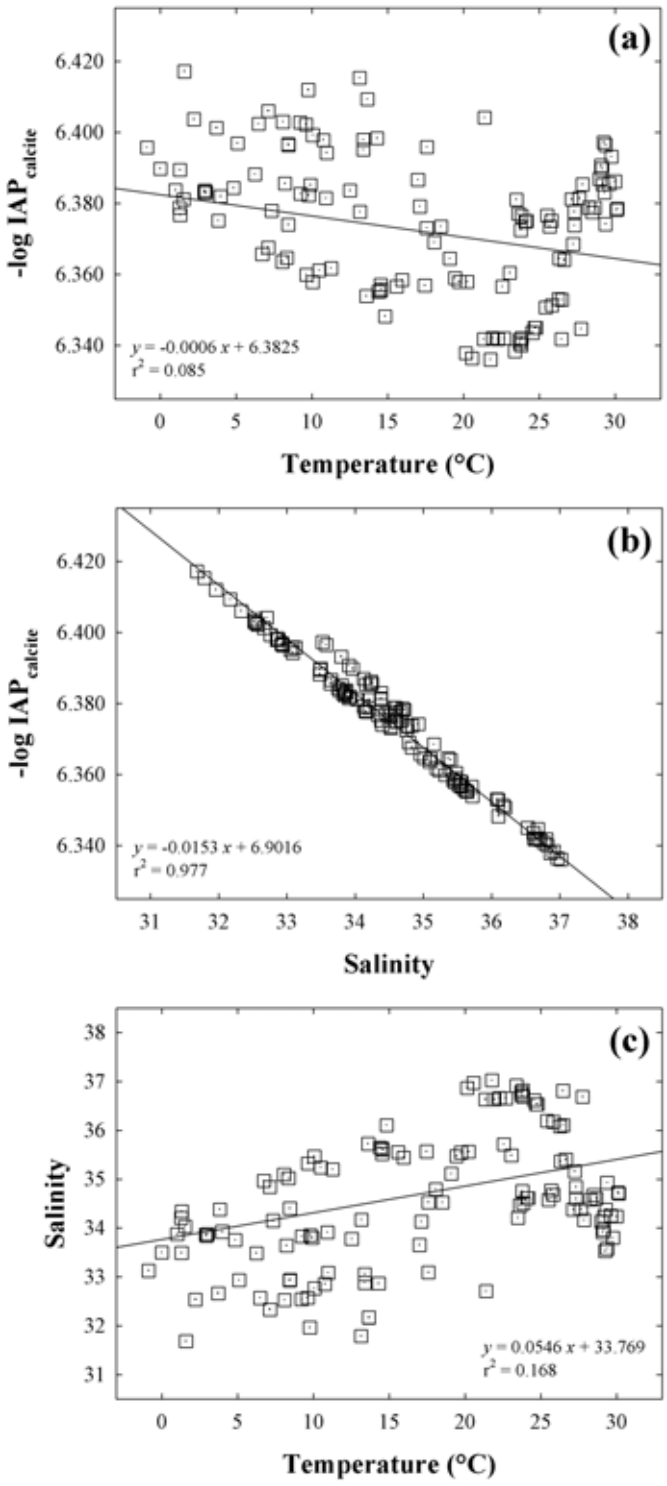

Fig. 15.10. Correction of the temperature (T) and salinity (S) effect on the Mg-calcite IAP from the calcite data. (a) -log $IAP_{Cal.}$ *vs.* T, (b) -log $IAP_{Cal.}$ *vs.* S, and (c) field samples T *vs.* S. The correlations for calcite were based on the corrected IAPs for T and S using in situ field data. The multiple regression equation to correct the Mg-calcite IAP from T and S is: -log IAP = 6.9271 - 0.01161 S + 0.00028 T. *See* text for details of calculations.

16.

European Project on Ocean Acidification: meta-analysis to guide future experiments and modeling

Abstract

Meta-analytical methods aim to compare multiple data sets from independent experiments, focusing on a particular process or parameter. Similar to traditional statistical approaches, the outcomes of a meta-analysis depend on data availability and quality. Experimental set-ups differ, e.g. because of different scientific goals and/or different measurement protocols, and a meta-analysis aims at identifying common characteristics among various experiments. Ideally, the meta-analysis can provide a coherent picture of different, sometimes contradicting, outcomes of different experiments, although this has not been the case in ocean acidification (Dupont et al. 2010; Hendriks and Duarte 2010; Kroeker et al. 2010). Because the field of ocean acidification is still in its infancy, the pre-European Project on Ocean Acidification (EPOCA) data available in 2009 for the identification of general patterns or for a detailed understanding of individual processes was still limited. At present, several robust meta-analysis papers dealing with organisms responses have been published, and although general patterns emerge, many basic questions remain unanswered (*see* chapter 9). During our work at EPOCA, we focused on experimental and modeling gaps identification. Gaps were then

tackled by providing new experimental (*see* chapters 3, 7, 8, 9, 10, 13, 14, and 15) and modeling results (*see* chapter 4) of use both in biogeochemistry and in paleoceanography. We also developed a new method to test ocean acidification in the field (*see* chapters 11, 12). Our working approach prevented an early meta-analysis of the experimental results available in 2009, which were already being analyzed by three different groups (*see* above). Here, we conducted a preliminary analysis to guide further research using EPOCA datasets available in 2009. We mainly intended to understand the use of experimental and mesocosm data in biogeochemical models (latest update in Nisumaa et al. 2010). This helped identifying which species and conditions were being used and where more experimental efforts should be re-directed to improve model results variability.

This chapter is based on:

Lebrato, M., Oschlies, A., Schartau, M., Riebesell, U. and Schulz, K. G. 2009. Mesocosm meta-analysis results to guide future experiment and modeling efforts. In: Deliverable D9.3 to the European Commission within the Seventh Framework Programme.

16.2. On the use of experimental and mesocosm data in biogeochemical models

16.2.1. Pelagic mesocosms: a representation of the upper water column

Mesocosm data with respect to ocean acidification are scarce (Table 16.1) and traditional meta-analysis routines are not really appropriate at this stage. A reasonable number of independent datasets on ocean acidification impacts have been obtained from laboratory experiments that mostly include a series of replicates. Our analysis therefore included laboratory data in our attempt to guide efforts for improving parameterizations of CO_2 effects on marine biota in biogeochemical models. We concentrated on identifying current data needs and also discussing briefly some problems that may arise when combining different datasets to constrain model parameterisations.

Enclosures that isolate a body of water are a common scientific tool used in freshwater and marine science (Petterson et al. 1939; Strickland and Terhune 1961). Mesocosms large enough to limit the effects of the enclosing walls have the advantage to maintain and monitor the development of a natural community and thus capture joint interactions of autotrophic and heterotrophic processes at a certain time and space. Ideally, pelagic mesocosms are freely drifting at appropriate locations where they include all compartments of the local pelagic ecosystem ranging e.g. from coccolithophores, diatoms, and N-fixers to gelatinous zooplankton. Yet, for logistic and technical reasons, until now, the majority of mesocosm experiments have been carried out in inshore waters (e.g. Engel et al. 2005; Kim et al. 2006) (*see* Table 16.1), representing the local community at a certain time of the year. Thus, an extrapolation to open ocean environments may be problematic if the inshore plankton community differs from a natural plankton assemblage found offshore or if the sampled inshore plankton community is driven by local benthic processes. The results of mesocosm experiments must thus be interpreted within the context of the geographic location where they were conducted (the development of a global network of specific mesocosms targeting bioprovinces would be useful here), and also in terms of the specific community they enclosed. A number of key compartments of the pelagic ecosystem have not yet been included in mesocosms investigating the effect of high CO_2 (e.g. pteropods, foraminifera, gelatinous zooplankton). Naturally, some species and higher trophic levels are excluded from the mesocosm enclosures. Thereby, some feedbacks may be absent in the mesocosm, which may lead to different responses in a high CO_2 world.

16.2.2. On the use of mesocosm and experimental data in models

Microbial populations in mesocosm experiments contribute substantially to the total biomass (e.g. Ovreas et al. 2003; Grossart et al. 2006), whereas laboratory experiments often include only a single strain of a particular organism, keeping bacteria concentrations as low as possible (axenic cultures). When assessing e.g. export ratios (PIC/POC and POC/PON) in mesocosms (Delille et al. 2005), the bulk particulate organic fraction (POC and PON) includes the entire community (above a certain size) and not only the calcifyers, which may be a focus of laboratory experiments that will then report much higher PIC/POC ratio (Ridgwell et al. 2009 and references therein). Furthermore, in laboratory and in mesocosm experiments a significant fraction of organic matter (POM) can sometimes be attributed to the accumulation of extra-cellular organic matter, which simply derives from phytoplankton exudation (or from cell lysis) and the subsequent coagulation of dissolved organic matter (DOM) (Engel et al. 2004; Schartau et al. 2007). This extracellular POM (thus POC) formation introduces a bias towards lower bulk PIC/POC ratios compared to PIC/POC ratios derived from cellular growth.

Such systematic differences between mesocosms and laboratory studies need to be considered when deriving model parameterizations for open-ocean conditions (*see* Table 16.2). Another aspect to take into account is that environmental conditions such as nutrient concentrations, carbonate chemistry, or temperature are often held constant in laboratory experiments (tightly controlled only in chemostats), but evolve over time in mesocosms (Fig. 16.1). It may thus be reasonable to develop process parameterizations first from strain-specific laboratory experiments and, in a second step, calibrate the parameter values of the process parameterisations embedded into an ecosystem model against community-specific mesocosm data. For the development of model parameterisations applicable to global simulations of future emission scenarios, a large range of environmental conditions has to be considered. In this respect, it might be useful to set up future mesocosm

Table 16.1. A selection of pelagic and benthic mesocosm studies testing the effects of pCO_2 on organisms in the EPOCA database, for which meta-data is available.

Reference	Species	Strain	Lat.[e]	Long.[e]	pCO_2 manip.	pCO_2 equil./error [f] (h / µatm)	NO_3 (µmol l^{-1})	PO_4 (µmol l^{-1})	PAR (µmol photons m^{-2} s^{-1})	Temp. [g] (°C)	Salinity [g]
PELAGIC MESOCOSMS											
Bergen 2001[a]	*E. huxleyi*	Norway	60.30°N	5.20°E	CO_2-enriched air	96 / ± 6	15.5 - 0.1	0.5 - 0.01	598 ± 213	11.5 ± 1.2	31.04 ± 0.1
Bergen 2003 [b]	*E huxleyi*	″ [d]	″	″	″	72-96 / ± 12	8.6 - 0.1	0.3	-	8.2 ± 0.5	30.06 ± 0.2
Bergen 2005 [c]	Diatoms ″	″ [d]	″	″	″	48 / ± 45	14 - 0	0.7 - 0	90-560	10.05 ± 0.8	31.1 ± 0.1
Kim et al. 2006	Diatoms Microflagellates Cryptomonads	-	34.6°N	128.5°W	N-enriched air Ambient air Air with 3% CO_2	24 / ± 200	23	0.9	-	13.5 ± 0.5	30.90 ± 0.7
BENTHIC MESOCOSMS											
Bibby et al. 2007	*Littorina littorea*	-	50.30°N	4.10°W	CO_2-bubbling	- / ± 0	-	-	-	15	35
Kuffner et al. 2008	Crustose algae	-	21.40°N	157.80°W	HCl diluted	- / ± 39	-	-	-	25.8 ± 1.4	34.90 ± 0.4

In all tables the symbol ″ indicates same as the raw immediately above.
In all tables the symbol - indicates that the data were not available or stated in that particular study.

[a] References: Engel et al. 2004; Rochelle-Newall et al. 2004; Delille et al. 2005; Engel et al. 2005; Benthien et al. 2007.

[b] References: Grossart et al. 2006; Engel et al. 2008; Lovdal et al. 2008.

[c] References: Riebesell et al. 2007; Vogt et al. 2007; Wingenter et al. 2007; Larsen et al. 2008; Schulz et al. 2008; Tanaka et al. 2008.

[d] Norwegian natural strains, which probably were more than 1 single strain.

[e] Geographic position belongs to the area where the mesocosm was installed, or otherwise it indicates the strain/species isolation/collection area.

[f] "pCO_2 equil." = system equilibration time from start of carbon chemistry manipulation, "error" = standard deviation of the CO_2 treatment (in the case of multiple treatments, the highest was always used) (if "error" = 0, no error was stated or available for calculation from the original data). Yet in any experiment pCO_2 there are likely variations owing to the way the carbon system works.

[g] Mean and standard deviation value from start to end. *See* specific papers or raw data for the trend integrated over time.

Table 16.2. A selection of meta-data used in parameterizations of the export ratio (PIC/POC) in biogeochemical models assimilating experimental, mesocosm, and field data to produce prognostic estimates of export production, atmospheric feedbacks, and other parameters in the global carbon cycle and future climate change scenarios.

MODELS TYPE I (Experiment/mesocosm assimilation data)										
Model reference	**Parameterized species**	**Strain**	**Lat.**	**Long.**	**Light cycle**	**PAR** (μmol photons m^{-2} s^{-1})	**Temp.** (°C)	**Data assimilation**	**Carbonate chemistry**	**Experiment reference**
Zondervan et al. 2001	*E. huxleyi*	PML B92/11	60.26°N	5.40°E	16:8, 24:0	150	15	Lab. experiment	HCl-NaOH	Zondervan et al. 2001
Heinze 2004	*G. oceanica*	PC7/1	38.26°N	9.78°W	16:8	150	15	〃	〃	〃
Gehlen et al. 2007	*E. huxleyi*	PML B92/11	60.26°N	5.40°E	16:8, 24:0	15, 30, 80, 150	15	Lab. experiment	HCl-NaOH	Zondervan et al. 2002
Gangsto et al. 2008	〃 Pteropods	Norway 〃	60.30°N 〃	5.20°E 〃	- 〃	598 ± 213 〃	11.5 ± 1.2 〃	Mesocosm 〃	CO_2-enriched air 〃	Bergen 2001 〃

MODELS TYPE II (Field assimilation data)	
	Derivation of parameterization
Archer et al. 2000	POC/PIC ratio estimated from sediment traps and global alkalinity values
Moore et al. 2002	PIC/POC ratio of small phytoplankton primary production estimated from field data
Ridgwell et al. 2007	PIC/POC ratio derived via a thermodynamically-based description of carbonate precipitation rate depending on Omega-Ca (Ω)
Schmittner et al. 2008	PIC/POC ratio of "non-diazotrophic detritus" production estimated from tracer-derived estimates of the rain ratio.

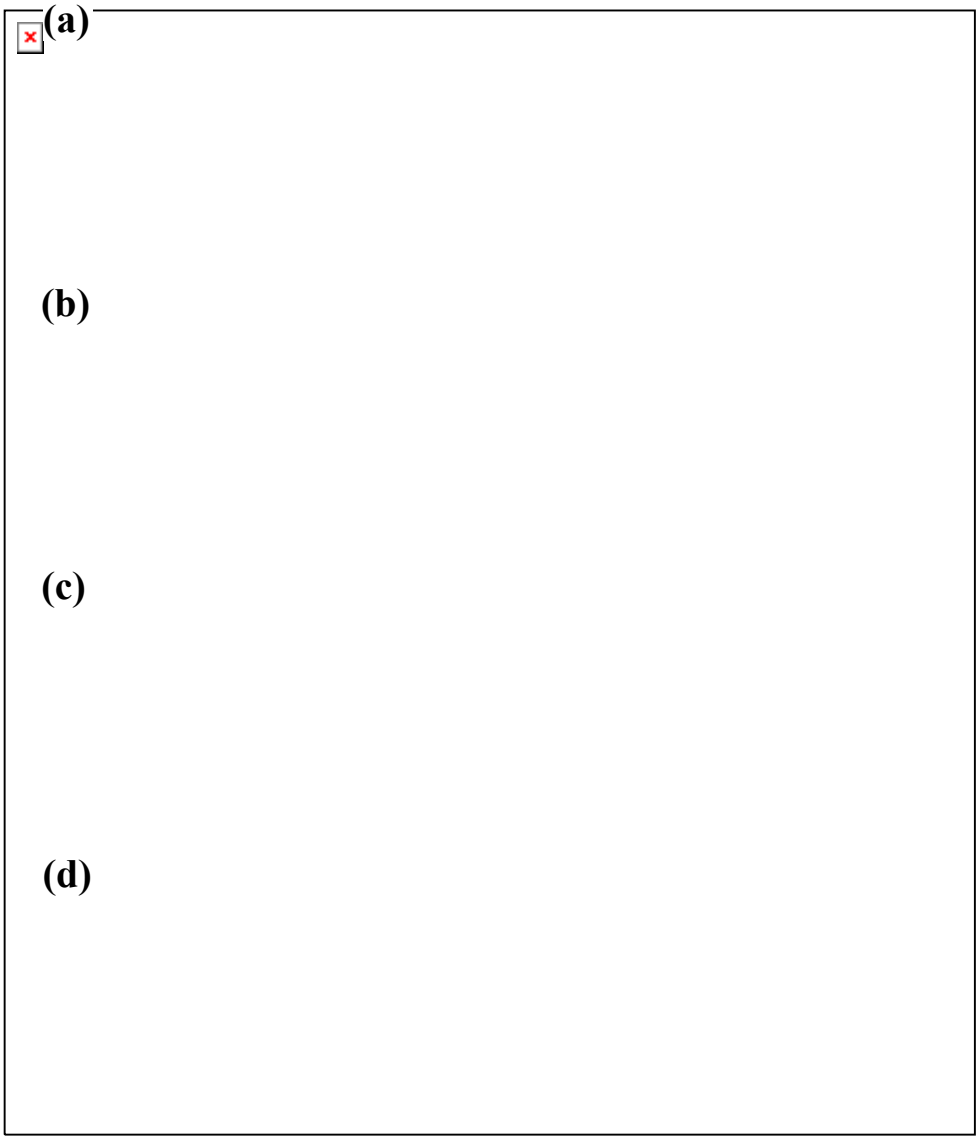

Fig. 16.1. The relationship between pCO_2, temperature, and salinity *vs.* time in mesocosms, the field, and laboratory experimental studies (including indoor mesocosms). The main panels are schematic illustrations, the small inserts show real data. "C" represents the control (present pCO_2), "T_x" is the treatment (future high pCO_2 scenario) (more treatments can be added). Error bars do not represent measured values, they only show the likely variations in the carbon system over time owing to e.g. diurnal cycles. (a) Field mesocosm where the carbon system freely drifts after the start of the experiment. Temperature and salinity drift accordingly. (b) Field mesocosm where the carbon system is controlled and maintained within limits. Temperature and salinity are also maintained. (c) A representation of field data, where the errors in the pCO_2 can be higher due to diurnal and seasonal cycles. Temperature and salinity also oscillate accordingly. (d) Laboratory experiment (including indoor mesocosms), where the carbon system, the temperature, and salinity are maintained constant within narrow limits. Note that mesocosms and field measurements normally generate a time series of relevant data, while measurements a typically taken after a fixed acclimation period in laboratory experiments.

experiments that include variations in light and temperature in addition to variations in CO_2 [(e.g indoor mesocosms (Sommer et al. 2007)]. Based upon logistic and financial constraints for setting up a series of mesocosm with replicates, this may be achieved by side experiments. For example,

subsamples from the mesocosms can be collected at specific times of the experiments to be exposed to different light and temperature conditions. This might also help us to further improve our understanding of the differences seen in sensitivity of the marine biota to variations in CO_2. The current alternative to a series of replicates of mesocosms is to apply a gradient approach, where all mesocosms are manipulated with or exposed to different CO_2 conditions. This gradient approach (Bach et al. 2011; Krug et al. 2011) may help to resolve lower and upper limits in carbon production, for example in coccolithophores, where data were scarce in the Ω-Cal. range from 0 to 2 (Fig. 16.2). In addition, the gradient approach allows to identify thresholds or tipping points as well as optimum curves for different physiological and biogeochemical parameters (Sett, S. 2010 - Master Thesis).

16.2.3. Benthic mesocosms: sediment-water column interactions

Mesocosm experiment set-ups connecting the surface waters down to the sediments were pioneered in limnological research (Lund 1972). An example used in the marine environment is the "plankton tower" developed by von Bodungen et al. (1976) in the Kiel Bight. Benthic set-ups maintaining bottom communities e.g. on soft sediments have been developed for a long time (Silverberg et al. 1995). Until now, few benthic mesocosm experiments as such have investigated the effects of ocean acidification (Table 16.1). Yet, there have been other initiatives to e.g. study coral reef communities in tanks or indoor pools, resembling benthic mesocosms (Langdon et al. 2000) and also soft-sediment communities (Widdicombe et al. 2009). Benthic mesocosms can evolve towards a very complex approach, where a link between the water column and the sediment is studied directly. Not only material derived from coccolithophores and diatoms (and other phytoplankton groups) reaches the seabed, but also other biogenic products derived e.g. from gelatinous zooplankton in the water column (carcasses, discarded housings, faecal pellets) and from the inhabitants of the seabed themselves. In between, the meroplankton (pelagic larvae of benthic species) also interact with the autotrophic community. The effects of CO_2 on all compartments are far from clear, but in the real world there will be interactions and feedbacks, with many processes being coupled, evolving parallel to synergistic/antagonistic responses to CO_2. For example, temperature drives in some cases the response over the CO_2 effect (Byrne et al. 2009; Borchard et al. 2011). As an example, a reduction in the quantity and quality of the POC flux to the ocean's interior (as a consequence of reductions in Net Primary Production) (Buesseler et al. 2007) will probably affect benthic populations by reducing

densities and altering reproductive responses (Smith et al. 2008). Moreover, those benthic compartments may also be affected on their own by ocean acidification (echinoderms: Byrne et al. 2009; Dupont et al. 2009, molluscs: Gazeau et al. 2007, coralline algae: Kuffner et al. 2008).

16.2.4. Global biogeochemical models: towards a sensitive assimilation of mesocosm and experimental data

The extrapolation of experimental findings to regional or global scales and future CO_2 emission scenarios is an important way to assess the overall impact of ocean acidifcation on marine ecosystems and their role in the global biogeochemical cycles (Schmittner et al. 2005, 2008). In general, biogeochemical models require simplified representations (parameterizations) of complex processes and may therefore not incorporate some details that are already established within the experimental community. Given this need for simplification, the central demand of the modelling community is, first of all, a specification of those biogeochemical processes and variables that show greatest sensitivity to varying CO_2 concentrations and thus pH conditions (*see* meta-analysis by Kroeker et al. 2010). So far, emphasis has been placed on the production and export of calcium carbonate and its subsequent dissolution (Orr et al. 2005; Gehlen et al. 2007; Gangsto et al. 2008). Models differ in the way they simulate calcium carbonate production (Table 16.3; Fig. 16.3). Some models aim to simulate the production of calcium carbonate by living biomass (Moore et al. 2002), others produce calcium carbonate only when detritus is formed and calcium carbonate starts to sink through the water column (Aumont and Bopp 2006; Gehlen et al. 2007; Schmittner et al. 2008). Models also differ with respect to prior assumptions made for constraining the respective parameterisations. Based on the calibration process, two groups can be identified (Table 16.3, Fig. 16.3):

(a) Type I: Calibrations based on culture experiments and mesocosm data (e.g. Gehlen et al. 2007; Gangsto et al. 2008). This approach has the advantage that responses to changes in CO_2 are predicted using datasets integrated from tightly controlled laboratory and mesocosm experiments. A disadvantage is that their model parameterizations depend on a limited amount of data that are represented by a few strains of the coccolithophorid *Emiliania huxleyi* (*see* Table 16.3; Fig. 16.4). Strain-specific responses are now a common feature (Langer et al. 2006, 2009; Beaufort et al. 2011), and may well limit the general reliability of model results if taken out of the context where data were integrated. Care has to

be taken when combining laboratory results with mesocosm data (which should be more representative of the ocean) in parameterizations, which mixes individual strain responses after a certain acclimation time with community responses over time (usually a bloom event) (Fig. 16.2). An example is the correct choice of PIC/POC export ratios. Using experimental data, relatively high values for this parameter are used [e.g. PIC/POC = 0.8, accounting for a slightly higher POC production (Gehlen et al. 2007; Gangsto et al. 2008)]. Maximum PIC/POC production estimates derived from mesocosms, approach the field estimates more closely than cell-specific data (PIC/POC ~ 0.2-0.3) (Delille et al. 2005). The low values are caused by the inclusion of other pelagic compartments such as bacteria, diatoms, and dinofallegates in the POC fraction. Conversely, laboratory-based cultures for *E. huxleyi* can be several times larger than the field PIC/POC of the entire community. Other coccolithophore species (e.g. *Calcidiscus leptoporus*) have PIC/POC ratios even twice as large as *E. huxleyi* (Fig. 16.2) (Langer et al. 2012).

A concern raised by Ridgwell et al. (2007) is whether *E. huxleyi* is an adequate representative of global calcification in the pelagic realm (Fig. 16.4), and whether other pelagic calcifiers such as foraminifera (Schiebel 2002) have to be considered as well. This again stresses the modellers' needs for a specification of the relative importance of individual calcifying groups within a natural plankton assembly. Furthermore, other coccolithophore species such as *C. leptoporus* (Broerse et al. 2000; Ziveri et al. 2000), *Cocolithus pelagicus* (Andruleit 2000; Baumann et al. 2000), and *Gephyrocapsa oceanica* (Baumann et al. 2000; Mergulhao et al. 2006) are quantitatively important in sediment trap records and in the sediments. This suggests that in many biogeographical provinces (e.g. temperate, sub-tropical and tropical) *E. huxleyi* does not dominate the carbon export. Gangsto et al. (2008) modelled a further pelagic group (pteropods), under the assumptions of "models type I" for *E. huxleyi*.

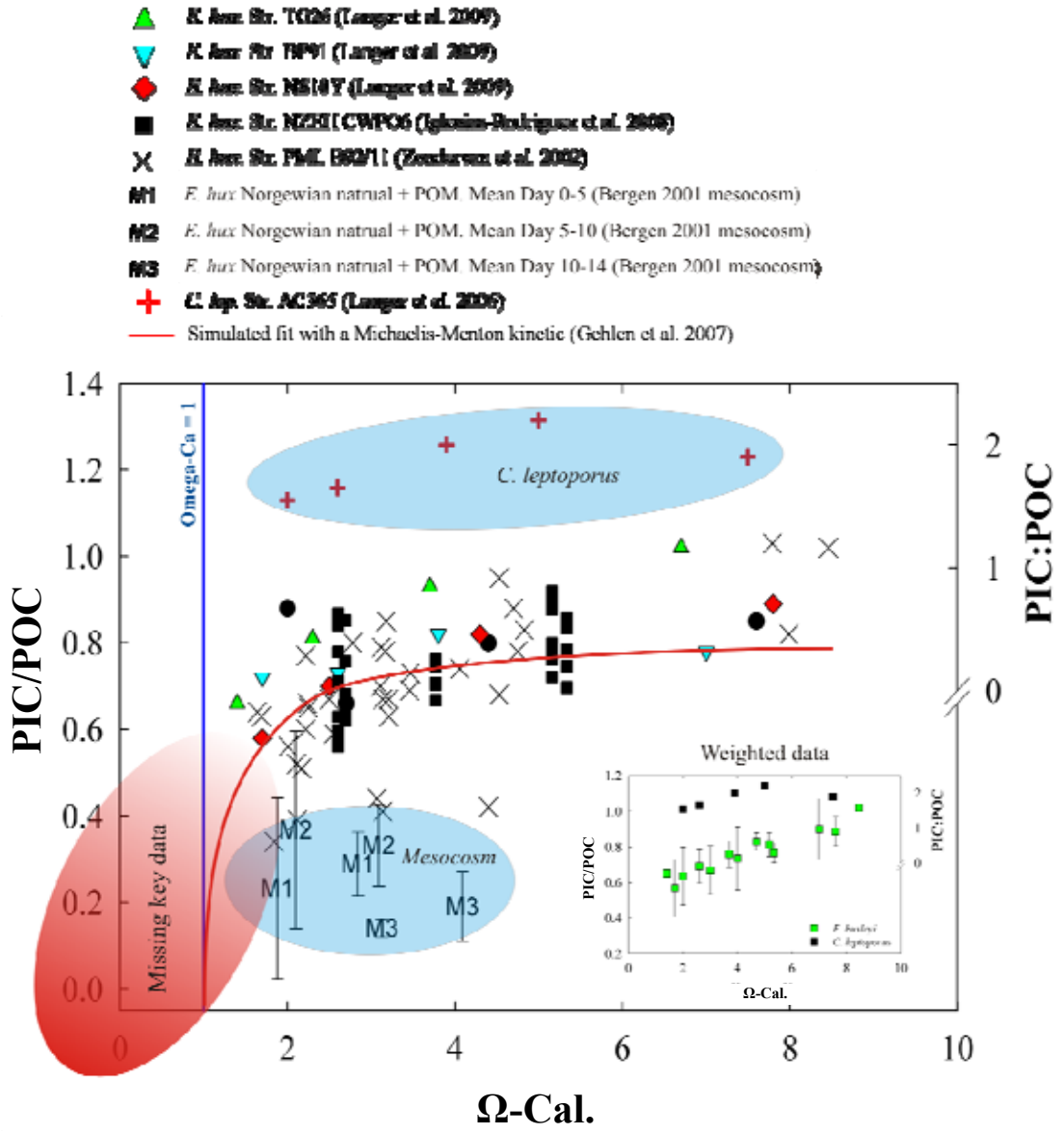

Fig. 16.2. The relationship between the PIC/POC ratio of coccolithophores and ΩCal. in laboratory experiments and mesocosms. Two species were used: *Emiliania huxleyi* (6 strains), and *Calcidiscus leptoporus* (1 strain). The main figure shows a fit to all data, while the smaller figure shows the averaged replicates. The red line is the fitted Michaelis-Menton kinetic formulation used by Gehlen et al. (2007). The scatter in the *E. huxleyi* data represents experiment runs at different light cycles and light intensity conditions. Note that the PIC/POC ratio from *C. leptoporus* is in some cases twice as high as in *E. huxleyi* for the same Ω-Cal. Seemingly, the mesocosm PIC/POC data from *E. huxleyi* and other POM material derived from autotrophs and some heterotrophs can be half than the data from experimental set-ups from different methods. This originates in a higher POC production in mesocosms (e.g. by other autotrophic and heterotrophic compartments), which is measured along with the calcifying cells. The POC measured can also be biased by the response of other phytoplankton non-calcifying species. Care is needed when combining data sets for the purpose of parameterizations in global biogeochemical models.

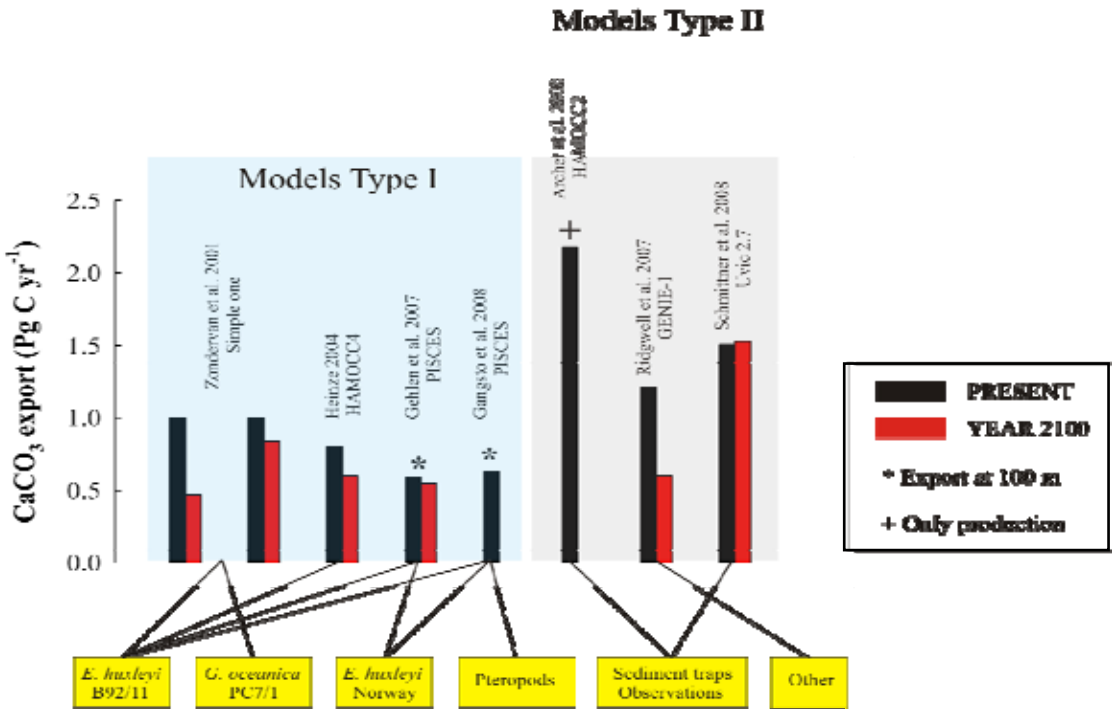

Fig. 16.3. A selection of the models included in Table 16.3 with the data integrated divided into the two groups identified. Note that the X-axis includes the data they assimilated (*see* Table 16.3)

Table 16.3. Further consideration of the models and outputs selected in Table 16.2 and Fig. 16.3.

Reference	Model	Present $CaCO_3$ export ($Pg\ C\ yr^{-1}$) a	Yr. 2100 $CaCO_3$ export ($Pg\ C\ yr^{-1}$)	$\Delta CaCO_3$ export ($Pg\ C\ yr^{-1}$)	Comments
MODELS TYPE I (EXPERIMENT/MESOCOSM ASSIMILATION DATA)					
Zondervan et al. 2001	-	1	0.47-0.84	-0.16 to -0.53	Model calibrated against a very limited amount of data, one of the very few studies explicitly admitting ill-conditioning of the results. 7 condition-specific scenarios for 2 coccolithophore species at different light cycles run separately. Output shows major differences owing to the light cycle and the species used.
Heinze 2004	HAMOCC 4	0.80 [b]	0.60	-0.20	Model calibrated against data from lab experiments (Zondervan et al. 2001) on two coccolithophore species. Not clear whether the parameterization is applied for both species or only for *E. huxleyi*, or if all light cycles data are combined or there is some kind of selection.
Gehlen et al. 2007	PISCES	0.59[c]	0.55	-0.04	Model calibrated against more data than its predecessors from a lab experiment (Zondervan et al. 2002) using different light cycles and light intensities, and against data from the Bergen (2001) mesocosm experiment (Delille et al. 2005).
Gangsto et al. 2008	″	0.63 [c], 0.32 [d]	-	-	Model calibrated by the same data as Gehlen et al. (2007), assuming that pteropods respond to carbonate chemistry (Ω-Cal.) in a way similar to that of coccolithophores.
MODELS TYPE II (FIELD ASSIMILATION DATA)					
Archer et al. 2000	HAMOCC2	2.18 [e]	-	-	$CaCO_3$ production assumed more important in the tropics. All aragonite assumed to dissolve in the upper water column.
Aumont and Bopp 2006	PISCES	-	-	-	PIC/POC ratio maximum value at 0.4 , e.g. lower than data from experimental work, but well above Sarmiento et al. (2002), Jin et al. (2006) observational data.
Ridgwell et al. 2007	GENIE-1	1.21 [b], 0.62 [d]	0.6	-0.6	Explicit assertion that *E. huxleyi* may not be an adequate global representative to include in models. Pelagic foraminiferal fluxes (Schiebel 2002) ignored in models. Assumption of no carbonate production for Ω-Cal. < 1. Explicitly stated the pure thermodynamic dependence of Ω-Cal.

Schmittner et al. 2008	UVic 2.7	1.51	1.53	+0.02	No explicit dependence of $CaCO_3$ production on carbonate chemistry. $CaCO_3$ production implicitly assumed to increase with temperature. PIC/POC mean global value of 0.097 well below lab experimental work, but consistent with field observations (Sarmiento et al. 2002; Jin et al. 2006).

[a] For comparison: 1) Observations of production values in the euphotic zone: 0.8-1.4 (Feely et al. 2004), 1.14 (Jin et al. 2006), 0.8-1.6 (Berelson et al. 2007); 2) Observations of 100 m export values: 0.6 (Sarmiento et al. 2002); 3) Observations of 2000 m export values: 0.41 (Iglesias-Rodriguez et al. 2002), 0.4 (Feely et al. 2004), 0.6 (Berelson et al. 2007).

[b] No information on the export depth for the value, so export assumed to originate in the euphotic zone.

[c] Export at 100 m depth.

[d] Export at 2000 m depth.

[e] Only a production term given.

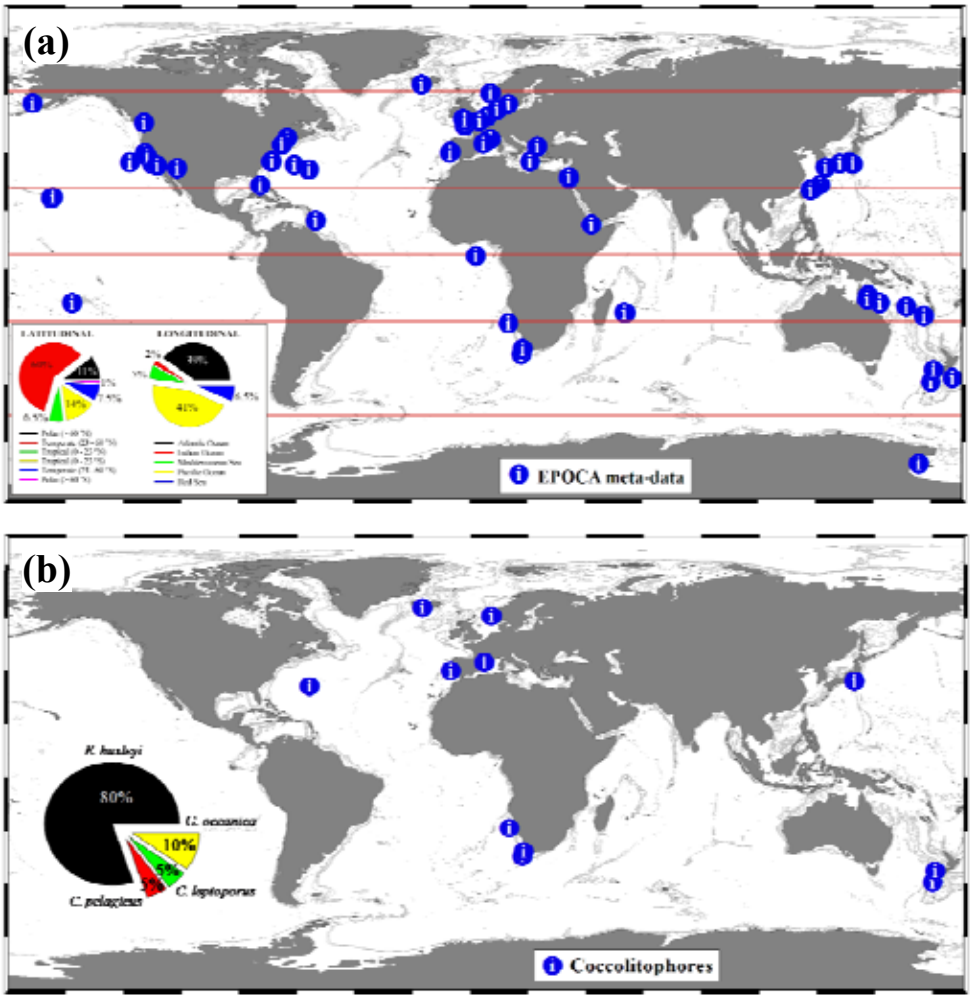

Fig. 16.4. Biogeographical distribution of the EPOCA meta-data from experimental and mesocosm work available in 2009 (*see* Nisumaa et al. 2010 for updates). (a) The complete data sets including organism-level experiments, indoor, and field mesocosms, and also field measurements and benthic and whole community experiments. The graphs show the partitioning (as percentages) according to major latitudinal and longitudinal divisions (per ocean). (b) The distribution of the coccolithophorid data within the EPOCA dataset. The graph shows the partitioning of the different species.

(b) Type II: Calibrations using biogeochemical tracer observations and sediment trap data (Sarmiento et al. 2002; Jin et al. 2006; Ridgwell et al. 2007; Schmittner et al. 2008). Here, emphasis is put on the net impact of calcification and export on biogeochemical tracer distributions (mainly alkalinity and dissolved inorganic carbon) rather than on the process of calcification itself. These models may nevertheless make additional assumptions about the mechanisms involved, e.g. by including temperature effects (Schmittner et al. 2008), or by assuming no calcification below Ω-Cal. = 1 (Ridgwell et al. 2007), which is not correct (*see* Krug et al. 2011).

Of crucial importance is the transparency of the individual model approaches. An explicit and critical description of prior model assumptions will also foster the communication between the experimental and the modelling community. As planned within the EPOCA consortium, the gradual improvement of large-scale biogeochemical models for ocean acidification is expected by means of establishing models of intermediate complexity that focus on individual processes. These process-orientated models should simulate different mesocosm or laboratory experiments and may thus provide validated parameterizations that can enter large-scale models.
The lack of laboratory or mesocosm data to constrain even relatively simple parameterisations makes it difficult to develop robust parameterizations for the production and fate of calcium carbonate in the future ocean, which will very likely be warmer and more acidic. Experiments such as field mesocosms investigating the combined effects of CO_2 and temperature on pelagic communities would help to better constrain our parameterizations. The evolution of both type I and type II models should aim towards a common framework, where the impacts of all three major pelagic calcifiers (coccolithophores, foraminifera, and pteropods) are included into one or multiple parameterizations. The addition of benthic carbonate production and dissolution, which has been ignored to date in many carbon cycle models, should also be considered.

16.2.5. Conclusions and recommendations

- Develop a global network of mesocosm experiments targeting different ecosystems and their responses to ocean acidification. EPOCA's Svalbard experiments will contribute to this (http://epocaarctic2010.wordpress.com/).

- Obtain more information on calcification in the low Ω-Cal. range between 0 and 2 (e.g. Krug et al. 2011) to adequate model formulations to reality.

- Obtain and use more data on calcifying species other than coccolithophores, especially benthic compartments, and incorporate them in models.

- Obtain information on joint effects of warming and acidification to improve parameterisations applicable to future ocean conditions (e.g. Sett 2010 - Master Thesis ; Borchard et al. 2011).

- Ensure that model descriptions are complete and transparent in terms of underlying assumptions used in the various parameterisations and their calibration.

- Investigate possible impacts of acidification-related changes in benthic processes on the water column.

17.

Conclusions and outlook

The goal of this thesis was to bring together various organic and inorganic biological pump processes in the context of global change an ocean acidification (OA) to either gain fundamental knowledge about them or extend their applications. I undertook different approaches starting with meta-analysis of data and ideas (Chapter 16) to find out gaps and specific processes and aspects that needed either basic data (empirically determined or acquired in the field) or a modeling approach. I also obtained data to then develop the specific parameterization for the model. This working approach facilitates immediate transfer of data and knowledge across different disciplines in a short time period. The outcomes of this work flow allow to move quickly across disciplines that need urgent attention, without leaving important details aside.

The processes studied around organic carbon cycling, shed new light on basic questions around the origin of gelatinous carbon fluxes, the remineralization dynamics, the sinking rate, or the biomass distribution at the seabed. The new findings question the lack of a temperature-based formulation in other particle-based models for organic matter, which could result in model export flux under and over estimations. The reconciliation of sediment trap fluxes with models has not worked so far, and the optimization of a temperature component should be prioritized. On the inorganic carbon side, the development of a new geochemical protocol to clean organic-Mg in coccolithophores opens a novel research line to use calcite Mg/Ca as a palaeoproxy or to understand how Mg^{2+} incorporation varies with rising temperature and CO_2. The seawater Mg/Ca changes from coastal to the offshore explaining coccolith calcite Mg/Ca values, suggest

that we may need to re-assess the current paradigm of seawater constant proportions (Marcet Principle), or at least re-calibrate it for the modern ocean.

The ontogenesis geochemistry in echinoids sheds light on transient changes in skeleton mineralogy from larvae to adults. The early incorporation of high Mg-calcite during ontogeny probably stabilizes calcite and is a trait favouring adaptation to the environment. However, the higher Mg^{2+} percentage in adults means that from a skeleton mineralogy perspective they are more susceptible to OA. The further assessment of echinoderms Mg-calcite leads to a new figure of the echinoderms global carbon export contribution based on $CaCO_3$, $MgCO_3$, and $SrCO_3$, challenging present perceptions of the relative important of pelagic *vs.* benthic sources. Using data on the mol % $MgCO_3$ of benthic organisms I developed new calculations of the species-specific saturation state of Mg-calcite (ΩMg) to compare with ΩCal. and ΩArag. Many ecosystem live near or may cohabit with OA already, and that they either do well in these conditions or there is an imminent risk for migration towards upper water masses, where conditions are more favourable. I propose that the use of ΩMg should be adopted by experimentalists and modellers to express their results, as the current interpretations can be misleading. We also need improved empirical data on the Mg-calcite solubility and its true relationship to a temperature gradient.

The results presented here intended to close slightly the gap between experimentalists and modellers working in the carbon cycle by providing a flow process of data-to-parameterization and process descriptions. Yet, only time will tell if the results and suggestions are really taken into the scientific community. Working half way between experiments and models proves challenging since one cannot really assess which side should weight more. However, it proves extremely efficient and I truly believe this contribution should lead to further research advances in the marine sciences field.

Authors contribution

- Chapter 2 is a paper published at *Hydrobiologia* (publicly available: http://www.springerlink.com/content/ q742673688110u8h/).

> **Lebrato, M.,** Pitt, K. A., Sweetman, A. K., Jones, D. O. B., Cartes, J. E. ,Oschlies, A., Condon, R. H., Molinero, J. C., Adler, L., Gaillard, C., Lloris, D. and Billett, D. S. M. 2012. Jelly-falls historic and recent observations: a synthesis to drive future research directions. In: *Hydrobiologia* DOI: 10.1007/s10750-012-1046-8.

Lebrato had the original idea of the review paper, and then compiled the data, analyzed them, and wrote the manuscript at GEOMAR. Pitt proposed the theoretical model and provided a first diagram and ideas to develop it. The rest of the authors either provided valuable text comments or actual data.

- Chapter 3 is a paper finished pending submission to *Geophysical Research Letters*.

> **Lebrato, M.,** de Jesus Mendes, P., Steinberg, D. K., Cartes, J. E., Jones, B. M., Birsa, L., Benavides, R. and Oschlies, A. in preparation. Jelly biomass sinking speed reveals a fast carbon export mechanism. To be submitted: *Geophysical Research Letters*.

Lebrato had the original idea of conducting this new experiment, and then contacted all co-authors to provide samples and technical support. The laboratory experiments were conducted by Lebrato and de Jesus Mendes at the Oceanlab facilities in Jacobs University (Bremen). Steinberg conducted the field experiments in a research cruise in Antarctica and then sent the samples to Lebrato. Benavides provided technical support at GEOMAR to analyze the biochemistry of the samples (analyses condcuted by Kerstin Nachtigall). de Jesus Mendes carried out the video analyses in Bremen. Lebrato analysed the final datasets. The rest of the authors provided valuable text comments or actually sent the samples to Lebrato at GEOMAR.

- Chapter 4 is a paper published at *Limnology and Oceanography* (publicly available: http://www.aslo.org/lo/toc/vol_56/issue_5/1917.pdf).

> **Lebrato, M.,** Pahlow, M., Oschlies, A., Pitt, K. W., Jones, D. O. B., Molinero, J-C. and Condon, R. H. 2011. Depth attenuation of organic matter export associated with jelly-falls. In: *Limnology and Oceanography* 56: 1917-1928.

Lebrato had the original idea of developing a new parameterization of the gelatinous biomass export ratio and compiled all data at GEOMAR. Then, he invited Pahlow to assist in the actual equation development and calculations. Once the parameterizations were finished, the rest of the authors were invited to provide discussion inputs. All data was analyzed by Lebrato, and checked by Pahlow. Oschlies also checked the calculations and the actual application to global models and parameterizations.

- Chapter 5 is a paper finished pending submission to *PLoS ONE*.

> **Lebrato, M.,** Molinero, J-C., Cartes, J., Lloris, D., Beni-Casadella, L. and Melin, F. in preparation. Jelly biomass export follows regime shifts in a continental shelf. To be submitted: *PLoS ONE*.

Cartes first contacted Lebrato to ask if there would be an interest on the non-commercial species trawling dataset (Pyrosome depositions) maintained in Barcelona (Spain). After Lebrato realized the importance of the data, he took over and coordinated the data acquisition. Trawling data were provided by Lloris in Barcelona, and satellite data by Melin at the EU Commission JRC (France). The bathymetric data and maps were put together by Beni-Casadella in Barcelona. Molinero conducted all time-series analysis with Lebrato at GEOMAR and then both put a final version of the manuscript text. The other authors also contributed to the discussion.

- Chapter 6 is a paper published at *ESA Ecology* (publicly available: http://www.esajournals.org/doi/abs/10.1890/11-0302.1).

> Lucas, C. H., Pitt, K. A., Purcell, J. E., **Lebrato, M.** and Condon, R. H. 2011. What's in a jellyfish? Proximate and elemental composition and biometric relationships for use in biogeochemical studies. In: *ESA Ecology* 92: 1704-1704. *ESA Ecological Archives* E092-144.

Lucas put together the dataset and conducted the analyses. Lebrato contributed with a large dataset and also provided French publications analysis. Lebrato also contributed to the discussions along with the other authors.

- Chapter 7 is a paper published at *Geochimica et Cosmochimica Acta* (publicly available: http://www.sciencedirect.com/science/article/pii/S0016703712002487?v=s5). The last part of the chapter comes from a proposal sent to the German DFG.

> Blanco-Ameijeiras, S., **Lebrato, M** (shared 1st authorship with S.B.A)., Stoll, H. M., Iglesias-Rodriguez, M. D., Mendez-Vicente, A., Sett, S., Müller, M. N., Oschlies, A. and Schulz, K. G. in press. Removal of organic magnesium in coccolithophore carbonates. *Geochimica et Cosmochimica Acta*.

Lebrato had the original idea, and then designed, managed, and coordinated the project from start to end at GEOMAR, and supervised Blanco-Ameijeiras during her Master thesis (Southampton, UK) and 6 months work at GEOMAR (DAAD scholarship). Müller provided valuable help and expertise in all phases of the project both at GEOMAR and UTAS (Tasmania). Blanco-Ameijeiras conducted the experimental work with *Emiliania huxleyi* and *Calcidiscus leptoporus* at the laboratory facilities of Iglesias-Rodriguez in Southampton, while Sett and Lebrato provided the *Gephyrocapsa oceanica* samples at GEOMAR under the supervision of Schluz. Blanco-Ameijeiras and Lebrato measured via ICP all samples at Stoll laboratory in Oviedo (Spain), and she provided valuable assistance and expertise. Blanco-Ameijeiras and Lebrato wrote all text, while the rest of authors contributed to the discussions.

- Chapter 8 are three papers in preparation (*see* in brackets after them, for proposed submission journal) and some samples (measured by us) also come from a published paper by Krug et al. 2011 (http://www.biogeosciences.net/8/771/2011/bg-8-771-2011.pdf) and two PhD theses (Müller - Müller, M. N. 2009. Calcification in coccolithophores: Effects of environmental conditions and palaeoproxy calibrations. Doctoral thesis, University of Kiel, p 154.and Wiebe - Wiebe, P. 2008. Response of coccolithophores to ocean acidification and ocean warming. Master thesis, University of Kiel, p 50.).

> Blanco-Ameijeiras, S., **Lebrato, M** (shared 1st authorship with S.B.A)., Stoll, H. M., Iglesias-Rodriguez, M. D., Mendez-Vicente, A. and Oschlies, A. in preparation. Coccolithophores carbonate ratios within the concept of species. To be submitted: *ESA Ecology*.
>
> Müller, N. M., **Lebrato, M** (shared 1st authorship with M. N. M)., Blanco-Ameijeiras, S., Stoll, H. M., Mendez-Vicente, A. Sett, S., Schulz, K. G. and Oschlies, A. in preparation. Coccolithophores carbonate ratios in a high CO_2 world. To be submitted: *Nature Geosciences*.
>
> Blanco-Ameijeiras, S., **Lebrato, M** (shared 1st authorship with S. B. A)., Stoll, H. M., Mendez-Vicente, A. Schulz, K. G. and Oschlies, A. in preparation. Coccolithophores Sr/Ca and Mg/Ca temperature proxy optimization and development. To be submitted: *Geochemistry Geophysics Geosystems*.

Lebrato had the original idea, and then designed, managed, and coordinated the project from start to end at GEOMAR, and supervised Blanco-Ameijeiras during her Master thesis in Southampton and 6 months work at GEOMAR (DAAD Scholarship). Müller provided valuable help and expertise in all phases of the project and he provided data from his own PhD thesis at GEOMAR, Wiebe PhD thesis and Krug et al. (2011) experiments at GEOMAR to measure again samples for elemental composition at Stoll laboratory in Oviedo (Spain). Blanco-Ameijeiras conducted the experimental work with *Emiliania huxleyi* and *Calcidiscus leptoporus* at the laboratory facilities of Iglesias-Rodriguez in Southampton, while Sett and Lebrato provided the *Gephyrocapsa oceanica* samples (high CO_2) at GEOMAR under the supervision of Schluz. Blanco-Ameijeiras conducted the temperature calibration experiment under the supervision of Lebrato and Schulz at GEOMAR. Blanco-Ameijeiras and Lebrato measured via ICP all samples at Stoll laboratory in Oviedo, and she provided valuable assistance and expertise. Blanco and Lebrato jointly wrote all summary text for these manuscripts.

- Chapter 9 is a paper that has been in review at *Nature Climate Change*, but that has recently been rejected, thus it is pending modifications for re-submission.

> Iglesias-Rodriguez, M. D., **Lebrato, M.,** Buitenhuis, E., Ries, J., Gibbs, S. J., Schofield, O. M. and Lampitt, R. S. in preparation. The future of marine calcification. To be re-submitted: *Nature Climate Change*.

Iglesias-Rodriguez had the original idea and she put together the paper structure and then split tasks. Lebrato contributed with figures and data analyses and then major discussions. Lebrato also wrote parts of the manuscript.

- Chapter 10 is a paper in review at the *Journal of Experimental Marine Biology and Ecology* that has received a first round of feedback by reviewers and it is now been modified for re-submission. It is accepted with suitable revision. It was also included in Rouco-Molina's PhD thesis (Rouco Molina, M. 2011. Genetic mechanisms and adaptive strategies of primary producers (microalgae and cyanobacteria) under a global change scenario. Veterinary Faculty. Complutense University of Madrid. Doctoral Thesis, p. 332.).

> Rouco-Molina, M., Branson, O., **Lebrato, M.** and Iglesias-Rodriguez, M. D. in review. The effect of nitrate and phosphate availability on *Emiliania huxleyi* physiology in different CO_2 scenarios. In: *Journal of Experimental Marine Biology and Ecology.*

Iglesias-Rodriguez had the original idea, and then Rouco-Molina conducted all experimental work under her supervision in Southampton (UK). However, since artificial seawater was used, Lebrato provided the calculations (after technical help from Schulz, *see* Chapter 8) and supervised Rouco-Molina for the whole experiment from GEOMAR. Lebrato contributed considerably with large manuscript sections, and also in the response to reviewers.

- Chapter 11 is a paper in preparation, pending submission to *Progress in Oceanography*, where the editor has already expressed interest.

> Iglesias-Rodriguez, M. D., Jones, B. M. J., Blanco-Ameijeiras, S., **Lebrato, M.** and Huete-Ortega, M. in preparation. The effect of artificial upwelling and in-situ ocean acidification on coccolithophore physiology. To be submitted: *Progress in Oceanography*.

The original idea of the paper comes from Iglesias-Rodriguez after the results using the same approach in 2009 (*see* Chapter 12) with echinoid larvae. Lebrato was invited to the research cruise and conducted the shipboard offshore experiments along with the others. Jones and Blanco-Ameijeiras took care of sample analytics, while Lebrato took care of geochemistry aspects and incubations set-up management. Lebrato and Blanco-Ameijeiras analyzed samples for elemental composition via ICP at Stoll laboratory in Oviedo (Spain). The version provided here was fully written by Lebrato with methodological corrections by Jones. This version is currently iterated with the other authors for a final version.

- Chapter 12 is a paper in review at *ESA Ecosphere* that is still pending the first review round. It was also included in Suarez-Bosche's PhD thesis (Suarez-Bosche, N. 2011. Acclimation and phenotypic plasticity of echinoderm larvae in a changing ocean. University of Southampton, Faculty of Engineering Science and Mathematics, School of Ocean and Earth Science, Doctoral Thesis, p. 229.).

> Suarez-Bosche, N., **Lebrato, M.,** Tyler, P. A. and Iglesias-Rodriguez, M. D. in review. Susceptibility of echinoid larvae to artificially upwelled deep ocean waters. In: *ESA Ecosphere*.

Suarez-Bosche and Iglesias-Rodriguez had the original idea to conduct this experiment onboard a research cruise. Lebrato was later invited to provide comments and feedback on coordination, logistics, approach and analyses. Suarez-Bosche provided a first manuscript version, where Lebrato later wrote substantial parts of the text.

- Chapter 13 is a paper finished pending submission to *PLoS ONE*. It was also included in Suarez-Bosche's PhD thesis (Suarez-Bosche, N. 2011. Acclimation and phenotypic plasticity of echinodern larvae in a changing ocean. University of Southampton, Faculty of Engineering Science and Mathematics, School of Ocean and Earth Science, Doctoral Thesis, p. 229.).

> Suarez-Bosche, N., **Lebrato, M** (shared 1st authorship with S-B. N)., and Ries, J. B. in preparation. Ontogenesis Mg-calcite in echinoids reveals adaptation traits to climate change. To be submitted: *PLoS* ONE.

Lebrato had the original idea, and suggested Suarez-Bosche to sample larval pellets from her CO_2 and temperature experiments to assess mineralogy and then combine results with Lebrato echinoderm juvenile and adult samples. Ries conducted all ICP measurements in North Carolina (US). Lebrato wrote the whole paper version included here. Suarez-Bosche is using this version to provide a final manuscript for official journal submission.

- Chapter 14 are two papers, one finished pending submission to *ESA Ecology*, and the second one still under preparation to likely submitt to *Geochemistry, Geophysics, Geosystems*.

> **Lebrato, M.,** Ries, J. B., McClintock, J. B., Egilsdottir, H., Lamare, M., Oschlies, A., Dupont, S. and Iglesias-Rodriguez, M. D. in preparation. Revisiting the modern echinoderms global carbonate budget. To be submitted: *ESA Ecology*.

> **Lebrato, M.,** McClintock, J. B., Amsler, M. and Ries, J. B. in preparation. Trace and elemental geochemistry in echinoderms Mg-calcite. To be submitted: *Geochemistry, Geophysics, Geosystems*.

Lebrato had the original idea, thus he coordinated and acquired all samples, except Arctic and Antarctic ones, which were kindly collected and measured by Egilsdottir (Iceland) and McClintock (Alabama, US) respectively. All other analyses were conducted by Ries via ICP in North Carolina (US). Lebrato wrote the full paper presented here. The other authors provided comments.

- Chapter 15 is a paper finished pending submission to *PLoS ONE*.

> **Lebrato, M.,** Andersson, A. J., Ries, J. B., McClintock, J. B., Oschlies, A. and Iglesias-Rodriguez, M. D. in preparation. Seawater saturation state of Mg-calcite reveals imminent ocean acidification risks to marine ecosystems. To be submitted: *PLoS ONE*.

Lebrato had the original idea and then developed it with Andersson and Ries. Lebrato compiled all data and samples, and then Ries analyzed them via ICP in North Carolina (US). Andersson provided feedback and expertise to re-direct the work and he provided data to calculate $MgCO_3$ solubility at Scripps Institution of Oceanography (US). Lebrato conducted geostatistical work (NEAR 3D) at the Integrated School of Ocean Sciences (ISOS) in Kiel with the assistance of Bianca Willie (CAU). Lebrato wrote the whole manuscript presented here, which is pending Andersson feedback to provide a final version.

- Chapter 16 is a deliverable finished and submitted to the EU project office (EPOCA), and only available upon request at the EPOCA office (http://www.epoca-project.eu/).

> **Lebrato, M.,** Oschlies, A., Schartau, M., Riebesell, U. and Schulz, K. G. 2009. Mesocosm meta-analysis results to guide future experiment and modeling efforts. In: Deliverable D9.3 to the European Commission within the Seventh Framework Programme.

Lebrato put the dataset together and then produced the figures and tables. The rest of the authors provided feedback to change the deliverable, and a final version was amended by Oschlies before submission.

___ *Prof. Dr. Andreas Oschlies as thesis supervisor of Mr. Mario Lebrato confirms that this is a cumulative dissertation, consisting of separate chapters for the different types of publications and the way the work was published. Since publications have multiple authors, I confirm that the candidate has conducted the above mentioned tasks in each chapter/publication*___

Kiel, _____ 2012

Bibliography

Abello, P., Carbonell, A. and Torres, P. 2002. Biogeography of epibenthic crustaceans on the shelf and upper slope off the Iberian Peninsula Mediterranean coasts: implications for the establishment of natural management areas. Scientia Marina 66: 183-198.

Acuña, J. L. 2001. Pelagic Tunicates: Why Gelatinous? American Naturalist 158: 100-107.

Alamaru, A., Bronstein, O., Dishon, G. and Loya, Y. 2009. Opportunistic feeding by the fungiid coral *Fungia scruposa* on the moon jellyfish *Aurelia aurita*. Coral Reefs 28: 865.

Alldredge, A. L. and Gotschalk, C. C. 1989. Direct observation of the mass flocculation of diatom blooms: characteristic settling velocities and for of diatom aggregates. Deep-Sea Research 36: 159-171.

Alldredge, A. L. and Silver, M. W. 1988. Characteristics, dynamics and significance of marine snow. Progress in Oceanography 20: 41-82.

Allemand, D., Ferrier-Pages, C., Furla, P., Houlbreque, F., Puverel, S., Reynaud, S., Tambutte, E., Tambutte, S. and Zoccola, D. 2004. Biomineralization in reef-building corals: from molecular mechanisms to environmental control. General Palaeontology (Palaeobiochemistry) 3: 453-467.

Anand, P., Elderfield, H. and Conte, M. H. 2003. Calibration of Mg/Ca thermometry in planktonic foraminiferal from a sediment trap series. Paleoceanography 18: 1050, DOI:10.1029/2002PA000846

Anderson, T. R. and Pondaven, P. 2003. Non-Redfield carbon and nitrogen cycling in the Sargasso sea: pelagic imbalances and export flux. Deep-Sea Research 50: 573-591.

Andersen, V. and Sardou, J. 1994. *Pyrosoma atlanticum* (Tunicata, Thaliacea): diel migration and vertical distribution as a function of colony size. Journal of Plankton Research 16: 337-349.

Andersen, V., Sardou, J and Nival, P. 1992. The diel migrations and vertical distributions of zooplankton and micronekton in the Northwestern Mediterranean Sea. 2. Siphonophores, hydromedusae and pyrosomids. Journal of Plankton Research 14: 1155-1169.

Andersson, A. J. and Mackenzie, F. T. 2012. Revisiting four scientific debates in ocean acidification research. Biogeosciences 9: 893-905.

Andersson, A. J., Mackenzie, F. T. and Bates, N. R. 2008. Life on the margin: implications of ocean acidification on Mg-calcite, high latitude and cold-water marine calcifiers. Marine Ecology Progress Series 373: 265-273.

Andersson, A. J., Mackenzie, F. T. and Ver, L. M. 2003. Solution of shallow-water carbonates: an insignificant buffer against rising atmospheric CO_2. Geology 31: 513-516.

Andruleit, H. A., von Rad, U., Brans, A. and Ittekkot, V. 2000. Coccolithophore fluxes from sediment traps in the northeastern Arabian Sea off Pakistan. Marine Micropaleontology 38: 285-308.

Anikouche, W. A. and Sternberg, R. W. 1973. The world ocean. An introduction to oceanography. Prentice-Hall, Englewood Cliffs, New Jersey.

Anning, T., Nimer, N. A., Merrett, M. J. and Brownlee, C. 1998. Costs and benefits of calcification in coccolithophorids. Journal of Marine Systems 9: 45-56.

Anonymous. 1998. Campagne internationale de chalutage démersal en Méditerranée (MEDITS): manuel des protocoles. Biologia Marina Mediterranea 5: 515-572.

Apstein, C. 1910. Hat ein Organismus in der Tiefe Gelebt, in der er gefischt ist? Internationale Revue der gesamten Hydrobiologie und Hydrographie 3: 17-33.

Arai, M, N. 2005. Predation on pelagic coelenterates: a review. Journal of the Marine Biological Association of the United Kingdom 85: 523-536.

Araki, Y. and González, E. L. 1998. V- and P-type Ca^{21}-stimulated ATPases in a calcifying strain of *Pleurochrysis* sp. (Haptophyceae). Journal of Phycology 34: 79-88.

Archer, D., Winguth, A., Lea, D. and Mahowald, N. 2000. What caused the glacial/interglacial atmospheric pCO_2 cycles? Review of Geophysics 38: 159-189.

Armstrong, R. A., Lee, C., Hedges, J. I., Honjo, S. and Wakeham, S. G. 2002. A new, mechanistic model for organic carbon fluxes in the ocean: based on the quantitative association of POC with ballast minerals. Deep Sea Research II 49: 219-236.

Asper, V. A. and Smith, W. O. Jr. 2003. The distribution of particulate organic carbon and its dynamics in the southern Ross Sea. In DiTullio, G. R. and Dunbar, R. B (eds.), Biogeochemistry of the Ross Sea, Washington DC, American Geophysical Union.

Atkinson, A., Siegel, V., Pakhomov, E. and Rothery, P. 2004. Long-term decline in krill stock and increase in salps within the Southern Ocean. Nature 432: 100-103.

Aumont, O. and Bopp, L. 2006. Globalizing results from ocean *in situ* iron fertilization studies. Global Biogeochemical Cycles 20.

Bach, L. T., Schulz, K. G. and Riebesell, U. 2011. Distinguishing between the effects of ocean acidification and ocean carbonation in the coccolithophore *Emiliania huxleyi*. Limnology and Oceanography 55: 2040-2050.

Behrenfeld, M. J. and Falkowski, P. G. 1997. A consumer's guide to phytoplankton primary productivity models. Limnology and Oceanography 42: 1479-1491.

Bailey, D. M., King, N. J. and Priede, I. G. 2007. Cameras and carcasses: historical and current methods for using artificial food falls to study deep-water animals. Marine Ecology Progress Series 350: 179-191.

Bakun, A. and Agostini, V. N. 2001. Seasonal patterns of wind-induced upwelling/downwelling in the Mediterranean Sea. Scientia Marina 65: 243-257.

Balch, W., Drapeau, D., Bowler, B. and Booth, E. 2007. Prediction of pelagic calcification rates using satellite measurements. Deep Sea Research II 54: 478-495.

Baldock, J. A., Masiello, C. A., Gelinas, Y. and Hedges, J. I. 2004. Cycling and composition of organic matter in terrestrial and marine ecosystems. Marine Chemistry 92: 39-64.

Barcelos e Ramos, J., Müller, M. N. and Riebesell, U. 2010. Short-term response of the coccolithophore *Emiliania huxleyi* to abrupt changes in seawater carbon dioxide concentrations. Biogeosciences 7: 177-186.

Barker S., Cacho I., Benway H. and Tachikawa K. 2005. Planktonic foraminiferal Mg/Ca as a proxy for past oceanic temperatures: a methodological overview and data compilation for the Last Glacial Maximum. Quaternary Science Reviews 24: 821-834.

Barker S., Greaves M. and Elderfield H. 2003. A study of cleaning procedures used for foraminiferal Mg/Ca paleothermometry. Geochemistry Geophysics Geosystems 4: 8407.

Bastian, T., Stokes, D., Kelleher, J. E., Hays, G. C., Davenport, J. and Doyle, T. K. 2011. Fisheries bycatch data provide insights into the distribution of the mauve stinger (*Pelagia noctiluca*) around Ireland. ICES Journal of Marine Science 68: 436-443.

Baumann, K. H., Andruleit, H. and Samtleben, C. 2000. Coccolithophores in the Nordic Seas: comparison of living communities with surface sediment assemblages. Deep Sea Research 47: 1743-1772.

Beaufort, L., Probert, I., de Garidel-Thoron, T., Bendif, E. M., Ruiz-Pino, D., Metzl, N., Goyet, C., Buchet, N., Coupel, P., Grelaud, M., Rost, B., Rickaby, R. E. M., and de Vargas, C. 2011. Sensitivity of coccolithophores to carbonate chemistry and ocean acidification. Nature 476: 80-83.

Beaulieu, S. E. 2002. Accumulation and fate of phytodetritus on the sea floor. Oceanography and Marine Biology Annual Review 40: 171-232.

Beardall, J., A. Johnston, and J. Raven. 1998. Environmental regulation of CO_2-concentrating mechanisms in microalgae. Canadian Journal of Botany 76: 1010–1017.

Behrenfeld, M. J., Boss, E., Siegel, D. A. and Shea, D. M. 2005. Carbon-based ocean productivity and phytoplankton physiology from space. Global Biogeochemical Cycles 19: GB1006.

Behrenfeld, M. J. and Falkowski, P. G. 1997. Photosynthetic rates derived from satellite-based chlorophyll concentration. Limnology and Oceanography 42: 1-20.

Benner, I. and Passow, U. 2010. Utilization of organic nutrients by coccolithophores. Marine Ecology Progress Series 404: 21-29.

Benthien, A., Zondervan, I., Engel, A., Hefter, J., Terbrüggen A. and Riebesell, U. 2007. Carbon isotopic fractionation during a mesocosm bloom experiment dominated by *Emiliania huxleyi*: effects of CO_2 concentration and primary production. Geochimica et Cosmochimica Acta 71: 1528-1541.

Bentov, S., Brownlee, C. and Erez, J. 2009. The role of seawater endocytosis in the biomineralization process in calcareous foraminifera. PNAS 106: 21500-21504.

Berelson W. M., Balch W. M., Najjar R., Feely R. A, Sabine C. and Lee K. 2007. Relating estimates of $CaCO_3$ production, export, and dissolution in the water column to measurements of $CaCO_3$ rain into sediment traps and dissolution on the sea floor: a revised global carbonate budget. Global Biogeochemical Cycles 21: GB1024.

Berelson, W. M. 2002. Particle settling rates increase with depth in the ocean. Deep Sea Research II 49: 237-251.

Berger, W. H. 1968. Planktonic foraminifera: selective solution and paleoclimatic interpretation. Deep Sea Research 15: 31-43.

Berges, J. A. and Harrison, P. J. 1995. Nitrate reductase activity quantitatively predicts the rate of nitrate incorporation under steady state light limitation: a revised assay and characterization of the enzyme in three species of marine phytoplankton. Limnology and Oceanography 40: 82-93.

Bernstein, R. E., Byrne, R. H., Betzer, P. R. and Greco, A. M. 1992. Morphologies and transformations of celestite in seawater: the role of acantharians in the strontium and barium geochemistry. Geochimica et Cosmochimica Acta 56: 3273-3279.

Bernstein, R. E., Betzer, P. R., Feely, R. A., Byrne, R. H., Lamb, M. F. and Michaels, A. F. 1987. Acantharian fluxes and strontium to chlorinity ratios in the north Pacific Ocean. Science 237: 1490-94.

Bertrand, J. A., Gil de Sola, L., Papaconstantinou, C., Relini, G. and Souplet, A. 2002. The general specifications of the Medits surveys. In Abello, P., Bertrand, J. A., Gil de Sola, L., Papaconstantinou, C., Relini, G. and Souplet, A. (eds.), Mediterranean Marine Demersal Resources, The MEDITS International Trawl Survey (1994-1999). Scientia Marina 66: 9-17.

Bertrand, J. A. and Relini, G. (eds.), 2000. Demersal resources in the Mediterranean. Proceedings of the symposium held in Pisa, 18-21 March 1998. Actes de Colloques. Ifremer, Plouzané 26: 238.

Bian, N. and Martin, P. A. 2010. Investigating the fidelity of Mg/Ca and other elemental data from reductively cleaned planktonic foraminifera. Paleoceanography 25: PA2215.

Bibby, R., Cleall-Harding, P., Rundle, S., Widdicombe, S. and Spicer, J. 2007. Ocean acidification disrupts induced defenses in the intertidal gastropod *Littorina littorea*. Biology Letters 3: 699-701.

Biermann, A. and Engel, A. 2010. Effect of CO_2 on the properties and sinking velocity of aggregates of the coccolithophore *Emiliania huxleyi*. Biogeosciences 7: 1017-1029.

Billett, D. S. M., Bett, B. J., Jacobs, C. L., Rouse, I. P. and Wigham, B. D. 2006. Mass deposition of jellyfish in the deep Arabian Sea. Limnology and Oceanography 51: 2077-2083.

Billett, D. S.M., Lampitt, R. S., Rice, A. L. and Mantoura, R. F. C. 1983. Seasonal sedimentation of phytoplankton to the deep-sea benthos. Nature 302: 520-522.

Binyon, J. 1976. The permeability of the asteroid body wall to water and potassium ions. Journal of the Marine Biological Association of the UK 56: 639-647.

Bischoff, J. L., Fitzpatrick, J. A. and Rosenbauer, R. J. 1993. The solubility and stabilization of ikaite ($CaCO_3$ $6H_2O$) from 0° to 25 °C: Environmental and paleoclimatic implications for thinolite tufa. Journal of Geology 101: 21-33..

Bischoff, W. D., Mackenzie, F. T. and Bishop, F. C. 1987. Stabilities of synthetic Mg-calcites in aqueous solution: comparison with biogenic materials. Geochimica et Cosmochimica Acta 51: 1413-1423..

Blanco-Ameijeiras, S. 2010. Intraspecific variability in the biogeochemistry of Emiliania huxleyi: carbon production and elemental ratios of coccoliths. Master thesis, University of Southampton and University of Basque Country.

Blanco-Ameijeiras, S., Lebrato, M., Stoll, H. M., Iglesias-Rodriguez, M. D., Mendez-Vicente, A., Sett, S., Müller, M. N., Oschlies, A. and Schulz, K. G. 2012. Removal of organic magnesium in coccolithophore carbonates. Geochimica et Cosmochimica Acta DOI http://dx.doi.org/10.1016/j.gca.2012.04.043

Borchard, C., Borges, A. V., Handel, N. and Engel, A. 2011. Biogeochemical response of *Emiliania huxleyi* (PML B92/11) to elevated CO_2 and temperature under phosphorous limitation: A chemostat study. Journal of Experimental Marine Biology and Ecology 410: 61-71.

Borges, A. V., Schiettecatte, L-S., Abril, G., Delille, B. and Gazeau, F. 2006. Carbon dioxide in European coastal waters. Estuarine, Coastal and Shelf Science 70: 375-387.

Borremans, C., Hermans, J., Baillon, S., André, L. and Dubois, P. 2009. Salinity effects on the Mg/Ca and Sr/Ca in starfish skeletons and the echinoderm relevance for paleoenvironmental reconstructions. Geology 37: 351-354

Boucher, J., Ibanez, F. and Prieur, L. 1987. Daily and seasonal variations in the spatial distribution of zooplankton populations in relation to the physical structure in the Ligurian front, Journal of Marine Research 45: 133-173..

Bown, P. R. 2005. Calcareous nannoplankton evolution: a tale of two oceans. Micropaleontology 51: 299-308.

Bown P. R., Lees J. A. and Young J. R. 2004. Calcareous nannoplankton evolution and diversity through time. In Thierstein, H. and Young, J. R (eds.), Coccolithophores: From Molecular Processes to Global Impact. Springer Verlag Berlin Heidelberg, Germany. pp. 481-508.

Boyd, P. W., Doney, S. C., Strzepek, R., Dusenberry, J., Lindsay, K. and Fung, I. 2008. Climate-mediated changes to mixed-layer properties in the Southern Ocean: assessing the phytoplankton response. Biogeosciences 5: 847–864.

Boye, M. and van der Berg C. G. 2000. Iron availability and the release of iron-complexing ligands by *Emiliania huxleyi*. Marine Chemistry 70: 277-287.

Boyle, E. A. 1983. Manganese carbonate overgrowths on foraminifera tests. Geochimica et Cosmochimica Acta 47: 1815-1819.

Boyle, E. A. 1981. Cadmium, Zinc, Copper, and Barium in foraminifera tests. Earth and Planetary Science Letters 53: 11-35.

Brewer, P. G., Wong, G. T. F., Bacon, M. P. and Spencer, D. W. 1975. An oceanic calcium problem? Earth and Planetary Science Letters 26: 81-87

Brodeur, R. D., Decker, M. B., Ciannelli, L., Purcell, J. E., Bond, N. A., Stabeno, P. J., Acuna, E. and Hunt, G. L. Jr. 2008. Rise and fall of jellyfish in the eastern Bering Sea in relation to climate regime shifts. Progress in Oceanography 77: 103-111.

Broerse, A. T. C., Ziveri, P., Hinte, v. J. E., and Honjo, S. 2000. Coccolithophore export production, seasonal species composition and coccolith $CaCO_3$ fluxes in the NE Atlantic (34 °N, 21 °W and 48 °N, 21 °W). Deep Sea Research 47: 1877-1905.

Bruhn, A., LaRoche, J. and Richardson, K. 2010. *Emiliania huxleyi* (Prymnesiophyceae): Nitrogen-metabolism genes and their expression in response to external nitrogen sources. Journal of Phycology 14: 266-277.

Bruland, K. W. and Silver, M. W. 1981. Sinking rates of fecal pellets from gelatinous zooplankton (Salps, Pteropods, Doliolids). Marine Biology 63: 295-300.

Brunskill, G. B., Zagorskis, I. and Pfitzner, J. 2002. Carbon burial rates in sediments and a carbon mass balance of the Herbert River region of the Great Barrier Reef continental shelf, North Queensland. Estuarine and Coastal Shelf Science 54: 677-700.

McDonnell, A. M. P and Buesseler, K. O. 2010. Variability in the average sinking velocity of marine particles. Limnology and Oceanography 55: 2085-2096.

Buesseler, K. O. and Boyd, P. W.. 2009. Shedding light on processes that control particle export and flux attenuation in the twilight zone of the open ocean. Limnology and Oceanography 54: 1210-1232.

Buesseler, K. O., Lamborg, C. H., Boyd, P. W., Lam, P. J., Trull, T. W., Bidigare, R. R., Bishop, J. K. B., Casciotti, K. L., Dehairs, F., Elskens, M., Honda, M., Karl, D. M., Siegel, D. A., Silver, M. A., Steinberg, D. K., Valdes, J., Van Mooy, B. and Wilson, S. 2007. Revisiting carbon flux through the ocean's twilight zone. Science 316: 567-570.

Buesseler, K. O., Bacon, M. P., Cochran, K. and Livingston, H. D. 1992. Carbon and nitrogen export during the JGOFS North Atlantic Bloom Experiment estimated from ^{234}Th,^{238}U disequilibria. Deep Sea Research I 39: 1115-1137.

Buitenhuis, E. T., Pangerc, T., Franklin, D., Le Quéré, C. and Malin, G. 2008. Growth rates of six coccolithophorid strains as a function of temperature. Limnology and Oceanography 53: 1181-1185.

Buitenhuis, E. T., van der Wal, P. and de Baar, H. J. W. 2001. Blooms of *Emiliania huxleyi* are sinks of atmospheric carbon dioxide: a field and mesocosm study derived simulation. Global Biogeochemical Cycles 15: 577-587.

Buitenhuis, E. T., de Baar, H. J. W. and Veldhuis, M. J. W. 1999. Photosynthesis and calcification by *Emiliania huxleyi* (Prymnesiophyceae) as a function of inorganic carbon species. Journal of Phycology 35: 949-959.

Burd, A. B., Hansell,D. A., Steinberg, D. K., Anderson, T. R., Arıstegui, J., Baltar, F., Beaupre, S. R., Buesseler, K. O., DeHairs, F., Jackson, G. A., Kadko, D., Koppelmann, R., Lampitt, R. S., Nagata, T., Reinthaler, T., Robinson, C., Robison, B. H., Tamburini, C. and Tanaka, T. 2010. Assessing the apparent imbalance between geochemical and biochemical indicators of meso- and bathypelagic biological activity, What the @$#! is wrong with present calculations and carbon budgets? Deep Sea Research 57: 1557-1571.

Byrne, M., Soars, N., Selvakumaraswamy, P., Dworjanyn, S. A. and Davis, A. R. 2010. Sea urchin fertilization in a warm, acidified and high pCO_2 ocean across a range of sperm densities. Marine Environmental Research 69: 234-239

Byrne, M., Ho, M., Selvakumaraswamy, P., Nguyen, H. D., Dworjanyn, S. A. and Davis, A. R. 2009. Temperature, but not pH, compromises sea urchin fertilization and early development under near-future climate change scenarios. Proceedings of the Royal Society B-Biological Sciences doi:10.1098/rspb.2008.1935

Cacchione, D. A., Rowe, G. T. and Malahoff, A. 1978. Submersible investigation of outer Hudson submarine canyon. In Stanley, D. J. and Kelling, G. (eds.), Sedimentation in canyons, fans and trenches. Stroudsburg Pennsylvania, Dowden, Hutchinson and Ross: 42-50.

Caldeira, K. and Wickett, M. E. 2005. Ocean model predictions of chemistry changes from carbon dioxide emissions to the atmosphere and ocean. Journal of Geophysical Research 110: C09S04.

Caldeira, K. and Wickett, M. E. 2003. Anthropogenic carbon and ocean pH. Nature 425: 365-365.

Campbell, A. C. 1977. The Hamlyn Guide to the seashore and shallow seas of Britain and Europe. Hamlyn Publishing Group, London, pp. 320.

Cargo, D. G. 1976. Some effects of tropical storm Agnes on the sea nettle population in the Chesapeake Bay. In Davis, J. and Laird, B. (eds.), The Effects of Tropical Storm Agnes on the Chesapeake Bay Estuarine System. Chesapeake Bay Consortium 54: 417-424.

Caron, D. A., Madin, L. P. and Cole, J. J. 1989. Composition and degradation of salp fecal pellets: implications for vertical flux in oceanic environments. Journal of Marine Research 47: 829-850.

Caron, D. A., Davis, P. G. Madin, L. P. and Sieburth, J. M. 1986. Enrichment of microbial populations in macroaggregates (marine snow) from surface waters of the North Atlantic. Journal of Marine Research 44: 543-565.

Carpenter, S. J. and Lohmann, K. 1992, Sr/Mg ratios of modern marine calcite: Empirical indicators of ocean chemistry and precipitation rate: Geochimica et Cosmochimica Acta 56: 1837-1849

Carrasson, M. and Cartes, J. E. 2002. Trophic relationships in a Mediterranean deep-sea fish community partition of food resources, dietary overlap and connections within the benthic boundary layer. Marine Ecology Progress Series 241: 41-55.

Cartes, J. E., Fanelli, E., Papiol, V. and Maynou, F. 2010. Trophic relationships at interannual spatial and temporal scales of macro and megafauna around a submarine canyon off the Catalonian coast (western Mediterranean). Journal of Sea Research 63: 180-190.

Cartes, J. E., Papiol, V., Palanques, A., Guillen, J. and Demestre, M. 2007. Dynamics of suprabenthos off the Ebro Delta (Catalan Sea, western Mediterranean), spatial and temporal patterns and relationships with environmental factors. Estuarine Coastal and Shelf Science 75: 501-515.

Cartes, J. E. 1993a. Diets of deep-water pandalid shrimps on the Western Mediterranean slope. Marine Ecology Progress Series 96: 49-61.

Cartes, J. E. 1993b. Diets of two deep-sea decapods *Nematocarcinus exilis* (Caridea: Nematocarcinidac) and *Munida tenuimana* (Anomura: Galatheidae) on the Western Mediterranean slope. Ophelia 37: 213-229.

Catubig, N. R., Archer, D. E., Francois, R., deMenocal, P., Howard, W. and Yu, E-F. 1998. Global deep-sea burial rate of calcium carbonate during the Last Glacial Maximum, Paleoceanography 13: 298-310.

Charalampopoulou, A., Poulton, A. J., Tyrrell, T. and Lucas, M. 2011. Irradiance and pH affect coccolithophore community composition on a transect between the North Sea and the Arctic Ocean. Marine Ecology Progress Series 431: 25-43.

Chave, K. E. 1954, Aspects of the biogeochemistry of magnesium: 1. Calcareous marine organisms. Journal of Geology 62: 266-283..

Chen, C-T. A. 2002. Shelf-vs. dissolution-generated alkalinity above the chemical lysocline. Deep-Sea Research II 49: 5365-5375.

Chen, C. T. A., Feely, R. A. and Gendron, J. F. 1988. Lysocline, calcium carbonate compensation depth, and calcareous sediments in the North Pacific. Pacific Science 42: 237-252.

Chereskin, B. M., Wong, Y.-S. and Castelfranco, P. A. 1982. *In vitro* synthesis of the chlorophyll isocyclic ring: Transformation of magnesium-protoporphyrin IX and magnesium-protoporphyrin IX monomethyl ester into magnesium-2,4-divinyl pheoporphyrin a_5. Plant Physiology 70: 987-993.

Chierici, M. and Fransson, A. 2009. Calcium carbonate saturation in the surface water of the Arctic Ocean. Undersaturation in freshwater influenced shelves: Biogeosciences 6: 2421-2432.

Choudens-Sanchez, V. and Gonzalez, L. A. 2009. Calcite and aragonite precipitation under controlled instantaneous supersaturation: elucidating the role of $CaCO_3$ saturation state and Mg/Ca ratio on calcium carbonate polymorphism. Journal of Sedimentary Research 79: 363-376.

Chu, S. P. 1946. The utilization of organic phosphorus by phytoplankton. Journal of the Marine Biological Association of the UK 26: 258 295.

Cigliano, M., Gambi, M. C., Rodolfo-Metalpa, R., Patti, F. P., Hall-Spencer, J. M. 010. Effects of ocean acidification on invertebrate settlement at volcanic CO_2 vents. Marine Biology 157: 2489-2502,.

Clarke, A., Holmes, L. J. and Gore, D. J. 1992. Proximate and composition of gelatinous zooplankton from the Southern Ocean. Journal of Experimental Marine Biology and Ecology 155: 55-68.
Clark, D., Lamare, M. and Barker, M. 2009. Response of sea urchin pluteus larvae (Echinodermata: Echinoidea) to reduced seawater pH: a comparison among a tropical, temperate, and a polar species. Marine Biology 156: 1125-1137.

Claustre, H., Bishop, J., Boss, E., Bernard, S., Berthon, J-F., Coatanoan, C., Johnson, K., Lotiker, A., Ulloa, O., Perry, M. J., D'Ortenzio, F., D'andon, O. H. F. and Uitz, J. 2010. Bio-optical profiling floats as new observational tools for biogeochemical and ecosystem studies: potential synergies with ocean colour remote sensing. OceanObs'09, Venice, Italy, September 21-25.

Coble, P. G., del Castillo, C. E. and Avril, B. 1998. Distribution and optical properties of CDOM in the Arabian Sea during the 1995 Southwest Monsoon. Deep Sea Research II 45: 2195-2223.

Cohen, A. L., McCorkle, D. C. and de Putron, S. 2010. Why corals are about ocean acidification: the role of nutrition. Ocean Sciences Meeting, February 22-26, Portland, Oregon, USA.

Cohen, A. L. and Holcomb, M. C. 2009. Why corals care about ocean acidification: uncovering the mechanism. Oceanography 22: 118-127.

Collier, R. and Edmond, J. 1984. The trace element geochemistry of marine biogenic particulate matter. Progress in Oceanography 13: 113-199.

Comeau, S., Jeffree, R., Teyssie, J. L. and Gattuso, J. P. 2010. Response of the Arctic Pteropod *Limacina helicina* to Projected Future Environmental Conditions. PLoS ONE 5: 7.

Company, J. B., Puig, P., Sardà, F., Palanques, A., Latasa, M. and Scharek, R..2008. Climate influence on deep-sea populations. PLoS ONE 3: e1431.

Condon, R. H., Graham, W. M., Duarte, C. M., Pitt, K. A., Lucas, C. H., Haddock S. H. D., Sutherland, K. R., Robinson, K. L., Dawson, M. N., Decker, M. B., Mill, C. E., Purcell, J. E., Malej, A., Mianzan, H., Uye, S-I., Gelcich, S. and Madin, L. P. 2012. Questioning the rise of gelatinous zooplankton in the world's oceans. BioScience 62: 160-169.

Condon, R. H., Steinberg, D. K., del Giorgio, P. A., Bouvier, T. C., Bronk, D. A., Graham, W. A. and Ducklow, H. W. 2011. Jellyfish blooms result in a major microbial respiratory sink of carbon in marine systems. Proceedings of the National Academy of Sciences 108: 10225-10230.

Condon, R. H., Steinberg, D. K. and Bronk, D. A. 2010. Production of dissolved organic matter and inorganic nutrients by gelatinous zooplankton in the York River estuary, Chesapeake Bay. Journal of Plankton Research 32: 153-170.

Condon, R. H. and Steinberg, D. K. 2008. Development, biological regulation, and fate of ctenophore blooms in the York River estuary, Chesapeake Bay. Marine Ecology Progress Series 369: 153-168.

Conte, M. H., Dickey, T. H., Weber, J. C., Johnson, R. J. and Knap, A. H. 2003. Transient physical forcing of pulsed export of bioreactive material to the deep Sargasso Sea. Deep Sea Research I 50: 1157-1187.

Corstjens, P. A. L. M, and Gonzalez, E. L. 2004. Effects of nitrogen and phosphorus availability on the expression of the coccolith-vesicle v-ATPase (subunit) of Pleurochrysis (Haptophyta). Journal of Phycology 40:82-87 .

Cosson, N., Sibuet, M. and Galeron, J. 1997. Community structure and spatial heterogeneity of the deep-sea macrofauna at three contrasting stations in the tropical northeast Atlantic. Deep Sea Research I 44: 247-269.

Cowper, T. R. 1960. Occurrence of *Pyrosoma* on the continental Slope. Nature 187: 878-879.
Cox, P. M., Bets, R. A., Jones, C. D., Spall, S. A. and Totterdell, I. J. 2000. Acceleration of global warming due to carbon-cycle feedbacks in a coupled climate model. Nature 408: 184-187.

Culkin, F. and Cox, R. A. 1966. Sodium, potassium, magnesium, calcium, and strontium in sea water. Deep-Sea Research 13: 789-804.

D'Alimonte, D. and Zibordi, G. 2003. Phytoplankton determination in an optically complex coastal region using a multilayer perceptron neural network. IEEE Transaction on Geoscience and Remote Sensing 41: 2861-2868.

D'Alimonte, D., Mélin, F., Zibordi, G., Berthon, J-F. 2003. Use of the novelty detection technique to identify the range of applicability of the empirical ocean color algorithms. IEEE Transaction on Geoscience and Remote Sensing 41: 2833-2843.

Danovaro, R., Dinet, A., Duineveld, G. and Tselepides, A. 1999. Benthic response to particulate fluxes in different trophic environments : a comparison between the Gulf of Lions-Catalan Sea (western-Mediterranean) and the Cretan Sea (eastern-Mediterranean). Progress in Oceanography 44: 287-312.

Daskalov, G. M., Grishin, A. N., Rodionov, S. and Mihneva, V. 2007. Trophic cascades triggered by overfishing reveal possible mechanisms of ecosystem regime shifts. PNAS 104: 10518-10523.

Davenport, J. and Balazs, G. H. 1991. "Fiery Pyrosomas": Are Pyrosomas an important items in the diet of leatherback turtles? British Herpetological Society Bulletin 37: 33-38.

De Beer, D., Kühl, M., Stambler, N. and Vaki, L. 2000. A microsensor study of light enhanced Ca^{2+} uptake and photosynthesis in the reef-building hermatypic coral *Favia* sp. Marine Ecology Progress Series 194:75-85.

De Bodt, C., N. Van Oostende, J. Harlay, K. Sabbe, and L. Chou. 2010. Individual and interacting effects of pCO_2 and temperature on *Emiliania huxleyi* calcification: study of the calcite production, the coccolith morphology and the coccosphere size. Biogeosciences 7: 1401-1412.

De Jong, E. W., Bosch, L. and Westbroek, P. 1976. Isolation and characterization of a Ca^{2+}-binding polysaccharide associated with coccoliths of *Emiliania huxleyi* (Lohmann) Kamptner. European Journal of Biochemistry 70: 611-621.

De La Rocha, C. L., Nowald, N. and Passow, U. 2008. Interactions between diatom aggregates. minerals, particulate organic carbon, and dissolved organic matter: Further implications for the ballast hypothesis. Global Biogeochemical Cycles 22: GB4005.

de Vargas, C., Saez, A. G., Medlin, L. K and Thierstein, H. R. 2004. Super-species in the calcareous plankton. In Thierstein, H. and Young, J. R. (eds.), Coccolithophores: From Molecular Processes to Global Impact. Springer Verlag Berlin Heidelberg, Germany. pp. 271-299.

de Villiers, S., Greaves, M. and Elderfield, H. 2002. An intensity ratio calibration method for the accurate determination of Mg/Ca and Sr/Ca of marine carbonates by ICP-AES. Geochemistry Geophysics Geosystems 3.

de Villiers, S. 1999. Seawater strontium and Sr/Ca variability in the Atlantic and Pacific oceans. Earth and Planetary Science Letters 171: 623-634.

Deibel, D. and Paffemhöfer, G-A. 2009. Predictability of patches of neritic salps and doliolids (Tunicata, Thaliacea). Journal of Plankton Research 31: 1571-1579.

Delille, B., Harlay, J., Zondervan, I., Jacquet, S., Chou, L., Wollast, R., Bellerby, R. G. J.,Frankignoulle, M., Borges, A. V., Riebesell, U. and Gattuso, J. P. 2005. Response of primary production and calcification to changes of pCO_2 during experimental blooms of the coccolithophorid *Emiliania huxleyi*. Global Biogeochemical Cycles 19.

Delgado, M. 1990. Phytoplankton distribution along the Spanish coast of the Alboran Sea. Scientia Marina 54: 169-178.

Delille B., Harlay J., Zondervan I., Jacquet S., Chou L., Wollast R., Bellerby R.G.J., Frankignoulle M., Borges A.V., Riebesell U. and Gattuso J-P. 2005. Response of primary production and calcification to changes of pCO_2 during experimental blooms of the coccolithophorid *Emiliania huxleyi*. Global Biogeochemical Cycles 19: GB2023.

Demicco, R. V., Lowenstein, T. K., Hardie, L. A. and Spencer, R. J. 2005. Model of seawater composition for the Phanerozoic. Geology 33: 877-880.

Dickson, J. A. D. 2004. Echinoderm skeletal preservation: Calcite:aragonite seas and the Mg/Ca ratio of Phanerozoic oceans. Journal of Sedimentary Research 74: 355-365.

Dickson, J. A. D., Afghan, J. D. and Anderson, G. C. 2003. Reference materials for oceanic CO_2 analysis: a method for the certification of total alkalinity. Marine Chemistry 80: 185-197.

Dickson, J. A. D. 2002. Fossil echinoderms as monitor of the Mg/Ca ratio of Phanerozoic oceans. Science 298: 1222-1224.

Dickson, A. 1990. Thermodynamics of the dissociation of boric acid in synthetic seawater from 273.15 to 18.15 K. Deep Sea Research 37: 755-766.

Dickson, A., and F. Millero. 1987. A comparison of the equilibrium constants for the dissociation of carbonic acid in seawater media. Deep Sea Research 34: 1733-1743.

Dodd, J. R. 1967. Magnesium and strontium in calcareous skeletons: A review. Journal Palaeontology 41: 1313-1329.

Doney, S. 2009. The consequences of human-driven ocean acidification for marine life. Biology Reports 1: 36.

Doney, S. C., Balch, W. M., Fabry, V. J. and Feely, R. A. 2009. Ocean acidification a critical emerging problem for the ocean sciences. Oceanography 22: 16-25

Dong, Z., Dongyan, J., John, K., 2010. Jellyfish blooms in China: dominant species, causes and consequences. Marine Pollution Bulletin 60: 954-963.

dos Santos, A., Santons, A. M., Conway, D. V. P. 2007. Horizontal and vertical distribution of cirripede cyprid larvae in the Portuguese coastal upwelling ecosystem: implications for offshore transport. Marine Ecology Progress Series 359: 171-183.

Doyle, T. K., Houghton, D. R., McDevitt, R., Davenport, J. and Hays, G. C. 2007. The energy density of jellyfish: estimates from bomb-calorimetry and proximate-composition. Journal of Experimental Marine Biology and Ecology 343: 239-252.

Drazen, J. C., Popp, B. N., Choy, C. A., Clemente, T., de Forest, L. and Smith, K. L. 2008. Bypassing the abyssal benthic food web: macrourid diet in the eastern North Pacific inferred from stomach content and stable isotopes analyses. Limnology and Oceanography 53: 2644-2654.

Drits, A. V., Arashkevich, E. G., Semenova, T. N. 1992. Pyrosoma atlanticum (Tunicata, Thaliacea): grazing impact on phytoplankton standing stock and role in organic carbon flux. Journal Plankton Research 14: 799-809.

Dueñas-Bohórquez, A., Raitzsch, M., de Nooijer, L. J. and Reichart, G-J. 2011. Independent impacts of calcium and carbonate ion concentration on Mg and Sr incorporation in cultured benthic foraminifera. Marine Micropaleontology 81: 122-130.

Duggins, D. O. 1981. Sea urchins and kelp, the effects of short term changes in urchin diet. Limnology and Oceanography 26: 391-394.

Dumousseaud, C., Achterberg, E. P., Tyrrell, T., Charalampopoulou, A., Schuster, U., Hartman, M. and Hydes, D. J. 2010. Contrasting effects of temperature and winter mixing on the seasonal and inter-annual variability of the carbonate system in the Northeast Atlantic Ocean. Biogeosciences 7: 1481-1492.

Dupont, S., Ortega-Martinez, O. and Thorndyke, M. 2010. Impact of near-future ocean acidification on echinoderms. Ecotoxicology 19: 449-462.

Dupont, S. and Thorndyke, M. C. 2009. Impact of CO_2-driven ocean acidification on invertebrates early life-history. What we know, what we need to know and what we can do. Biogeosciences 6: 3109-3131.

Dupont, S., Havenhand, J., Thorndyke, W., Peck, L. and Thorndyke, M. 2008. Near-future level of CO_2-driven ocean acidification radically affects larval survival and development in the brittlestar *Ophiothrix fragilis*. Marine Ecology-Progress Series 373: 285-294.

Durham, J. W. 1971. The fossil record and the origin of the Deuterostomata. Proceedings National American Paleontological Convention 2: 1104-1132.

Dyhrman, S. T., Haley, S. T., Birkeland, S. R., Wurch, L. L., Cipriano, M. J. and McArthur, A. J. 2006. Long Serial Analysis of Gene Expression for Gene Discovery and Transcriptome Profiling in the Widespread Marine Coccolithophore *Emiliania huxleyi*. Applied and Environmental Microbiology 72: 252-260.

Dyhrman, S. T. and Palenik, B. 2003. Characterization of ectoenzyme activity and phosphate-regulated proteins in the coccolithophore *Emiliania huxleyi*. Journal of Plankton Research 25: 1215-1225.

Ebert, T.A. 2007. Growth and survival of post settlement sea urchins. In: Lawrence, J. M. (ed.), Edible Sea Urchins: Biology and Ecology, 2nd edition. Elsevier, Oxford, pp. 95-134.

Ebert, T. A. 2001. Growth and survival of post-settlement sea urchins. In Lawrence, J. M. (ed.), Sea Urchins: Biology and Ecology Edible Developments in Aquaculture and Fisheries Science pp. 79-102.

Edmond, J. M. 1970. High precision determination of titration alkalinity and total carbon dioxide content of sea water by potentiometric titration. Deep-Sea Research 17: 737-750.

Eggins, S., De Deckker, P. and Marschall, J. 2003. Mg/Ca variation in planktonic foraminifera tests: implications for reconstructing palaeo-seawater temperature and habitat migration. Earth and Planetary Science Letters 212: 291-306.

Ellis, J. R. and Rogers, S. I. 2000. The distribution, relative abundance and diversity of echinoderms in the eastern English Channel, Bristol Channel and Irish Sea. Journal of the Marine Biological Association of the UK 80: 127-138.

Emlet, R. B. 1982. Echinoderm calcite: Mechanical analysis from larval spines. Biological Bulletin 163: 264-275.

Engel, A., Schulz, K. G., Riebesell, U., Bellerby, R., Delille, B. and Schartau, M. 2008. Effects of CO_2 on particle size distribution and phytoplankton abundance during a mesocosm bloom experiment (PeECE II). Biogeosciences 5: 509-521.

Engel, A., Zondervan, I., Aerts, K., Beaufort, L., Benthien, A., Chou, L., Delille, B., Gattuso, J-P., Harlay, J, Heemann, C., Hoffmann, L., Jacquet, S., Nejstgaard, J., Pizay, M. D., Rochelle-Newall, E., Schneider, U., Terbrueggen, A. and Riebesell, U. 2005. Testing the direct effect of CO_2 concentration on a bloom of the coccolithophorid *Emiliania huxleyi* in mesocosm experiments. Limnology and Oceanography 50: 493-507.

Engel, A., Thoms, S., Riebesell, U. Rochelle-Newall, E. and Zondervan, I. 2004. Polysaccharide aggregation as a potential sink or marine dissolved organic carbon. Nature 428: 929-932.

Erba, E. 2006. The first 150 million years history of calcareous nannoplankton: Biosphere-geosphere interactions. Palaeogeography Palaeoclimatology Palaeoecology 232: 237-250.

Erez, J., Reynaud, S., Silverman, J., Schneider, K. and Allemand, D. 2011. Coral Calcification Under Ocean Acidification and Global Change. In Dubinksy, Z. and Stambler, N. (eds.), Coral Reefs: An Ecosystem in Transition. Springer Science, New York. pp. 151-176.

ESRI 2011. ArcGIS Desktop: Release 10. Redlands, CA: Environmental Systems Research Institute

Estrada, M., Varela, R., Salat, J., Cruzado, A., and Arias, E. 1999. Spatio-temporal variability of the winter phytoplankton distribution across the Catalan and North Balearic fronts (NW Mediterranean), Journal of Plankton Research 21: 1-20.

Estrada, M., Varela, R., Salat, J., Cruzado, A., and Arias, E. 1999. Spatio-temporal variability of the winter phytoplankton distribution across the Catalan and North Balearic fronts (NW Mediterranean). Journal of Plankton Research 21: 1-20.

Fabricand, B. P., Imbimbo, E. S. and Brey, M. E. 1967. Atomic absorption analyses for Ca, Li, K, Rb, and Sr at two Atlantic Ocean stations. Deep-Sea Research 14: 185-189.

Fabry, V. J., Seibel, B. A, Feely, R. A. and Orr, J. C. 2008. Impacts of ocean acidification on marine fauna and ecosystem processes. ICES Journal of Marine Science 65: 414-432.

Fagerbakke, K., Heldal, M., Norland, S., Heimdal, B. and Btvik, H. 1994. Chemical composition and size of coccoliths from enclosure experiments and a Norwegian fjord. Sarsia 79: 349-355.

Falkowski, P. G., Schofield, O., Katz, M. E., van de Schootbrugge, B. and Knoll, A. H. 2004. Why is the land green and the ocean red? In Thierstein, H. and Young, J. R. (eds.), Coccolithophores: From Molecular Processes to Global Impact. Elsevier. pp. 429-453.

Fanelli, E., Cartes, J. E. and Papiol, V. 2011. Food web structure of deep-sea macrozooplankton and micronekton off the Catalan slope: Insight from stable isotopes. Journal of Marine Systems 87: 79-89.

Fanelli, E. and Cartes, J. E. 2008. Spatio-temporal variability in the diet of two pandalid shrimps in the western Mediterranean evidenced from gut contents and stable isotope analysis: influence on the reproductive cycle. Marine Ecology Progress Series 355: 219-233.

Fasham, M. J. R., Ducklow, H. W. and McKelvie, D. S. 1990. A nitrogen-based model of plankton dynamics in the oceanic mixed layer. Journal of Marine Research 48: 591-639.

Feely, R. A., Simone, R. A., Newton, J., Sabine, C. L. Warner, M., Devol, A., Krembs, C. and Maloy, C. 2010. The combined effects of ocean acidification, mixing, and respiration on pH and carbonate saturation in an urbanized estuary. Estuarine, Coastal and Shelf Science 88: 442-449.

Feely, R. A., Sabine, C. L, Hernandez-Ayon, J. M., Ianson, D. and Hales, B. 2008. Evidence for upwelling of corrosive "acidified" water onto the continental shelf. Science 320: 1490-1492

Feely R. A., Sabine C. L., Lee K., Berelson W., Kleypas J., Fabry V.J. and Millero F. J. 2004. Impact of Anthropogenic CO_2 on the $CaCO_3$ System in the Oceans. Science 305: 362-366.

Feng, Y., Warner, M. E., Zhang, Y., Sun, Y., Fu, F-X., Rose, J. M., Hutchins, D. A. 2008. Interactive effects of increased pCO2, temperature and irradiance on the marine coccolithophore *Emiliania huxleyi* (Prymnesiophyceae). European Journal of Phycology 43:87-98.

Fernandez de Puelles, M. L. and Molinero, J-C. in review. Increasing variance in zooplankton uncover hydroclimate changes over the period 1994-2003 in the Balearic Sea, Western Mediterranean. Journal of Plankton Research.

Findlay, H. S., Calosi, P. and Crawfurd, K. 2011. Determinants of the PIC:POC response in the coccolithophore *Emiliania huxleyi* under future ocean acidification scenarios. Limnology and Oceanography 56: 1168-1178.

Fiorentini, L., Dremière, P-Y., Leonori, I., Sala, A. and Palumbo, V. 1999. Efficiency of the bottom trawl used for the Mediterranean international trawl survey (MEDITS). Aquatic Living Resources 12: 187-205.

Fiorini, S., Middelburg, J. J. and Gattuso, J-P. 2011. Testing the effects of elevated pCO_2 on coccolithophores (Prymnesiophyceae): comparison between haploid and diploid life stages. Journal of Phycology 47: 1229-1463.

Fischer, G. and Karakas, G. 2009. Sinking rates and ballast composition of particles in the Atlantic Ocean: implications for the organic carbon fluxes to the deep ocean. Biogeosciences 6: 85-102.

Fonseca, F., Bowsher, C. and Stulen, I. 1997. Impact of elevated atmospheric carbon dioxide on nitrate reductase transcription and activity in leaves and roots of *Plantago major*. Physiologia Plantarum 100: 940-948.

Fortier, L., Le Fèvre, J. and Legendre, L. 1994. Export of biogenic carbon to fish and to the deep ocean: the role of large planktonic microphages. Journal of Plankton Research 16: 809-839.

Fowler, S. W. and Knauer, G. A. 1986. Role of large particles in the transport of elements and organic compounds through the oceanic water column. Progress in Oceanography 16: 147-194.

Franco, M. A., Soetaert, K., Costa, M. J., Vincx, M. and Vanaverbeke, J. 2008. Uptake of phytodetritus by meiobenthos using ^{13}C labelled diatoms and Phaeocystis in two contrasting sediments from the North Sea. Journal of Experimental Marine Biology and Ecology 362: 1-8.

Francois, R., Honjo, S., Krishfield, R. and Manganini, S. 2002. Factors controlling the flux of organic carbon to the bathypelagic zone of the ocean. Global Biogeochemical Cycles 16: 1887.

Franqueville, C. 1971. Macroplancton profond (invertebrates) de la M6diterran6e nord-occidentale. Tethys 3: 11-56.

Fritz, J. J. 1999. Carbon fixation and coccolith detachment in the coccolithophore *Emiliania huxleyi* in nitrate-limited cyclostats. Marine Biology 133: 509-518.

Frölicher, T. L. and Joos, F. 2010. Reversible and irreversible impacts of greenhouse gas emissions in multi-century projections with the NCAR global coupled carbon cycle-climate model. Climate Dynamics 35: 1439-1459.

Frost, J. R., Jacoby, C. A., Frazer, T. K. and Zimmerman, A. R. 2012. Pulse perturbations from bacterial decomposition of *Chrysaora quinquecirrha* (Scyphozoa: Pelagiidae). Hydrobiologia DOI: 10.1007/s10750-012-1042-z.

Frost, P. C., Stelzer, R. S., Lamberti, G. A. and Elser, J. J. 2002. Ecological stoichiometry of trophic interactions in the benthos: Understanding the role of C:N:P ratios in littoral and lotic habitats. Journal of the North American Benthological Society 21: 515-528.

Fujii, M. F., Murashige, S., Ohnishi, Y., Yuzawa, A., Miyasaka, H., Suzuki, Y. and Komiyama, H. 2002. Decomposition of phytoplankton in seawater. Part I: Kinetic analysis of the effect of organic matter concentration. J. Oceanogr. 58: 433-438.

Fujiwara, H. and Shigei, M. 1990. Correlation of embryonic temperature sensitivity of sea urchins with spawning season. Journal of Experimental Marine Biology and Ecology 136: 123-139.

Furla, P. Galgani, I. Durand, I. and Allemand, D. 2000. Sources and mechanisms of inorganic carbon transport for coral calcification and photosynthesis. Journal of Experimental Biology 203: 3445.

Gage, J. D. and Tyler, P. A. 1991. Deep-sea Biology: A Natural History of Organisms at the Deep-sea Floor, Cambridge University Press.

Gaillard, C., Goy, J., Bernier, P., Bourseau, J. P., Gall, J. C., Barale, G., Buffetaut, E. and Wenz, S. 2006. New jellyfish taxa from the Upper Jurassic lithographic limestone of Cerin (France): taphonomy and ecology. Palaeontology 49: 1287-1302.

Galil, B. S. and Goren, M. 1994. The deep sea Levantine fauna- new records and rare occurrences. Senckenb. Marit 25: 41-52.

Gangsto, R., Gehlen, M., Schneider, B., Bopp, L., Aumont, O. and Joos, F. 2008. Modeling the marine aragonite cycle: changes under rising carbon dioxide and its role in shallow water $CaCO_3$ dissolution. Biogeosciences 5: 1057-1072.

Gao, Y., Smith, G. J. and Alberte, R. S. 1993. Nitrate Reductase from the Marine Diatom *Skeletonema costatum*. Plant Physiology 103: 1437-1445.

Garrels, R. M. and Wollast, R. 1978. Discussion of Equilibrium criteria for two-component solids reacting with fixed composition in an aqueous phase - example: the magnesian calcites, by D. C. Thorstenson and L. N. Plummer. American Journal of Science 278: 1469-1474.

Garrels, R. M. and Mackenzie, F. T. 1972. A quantitative model for the sedimentary rock cycle, Marine Chemistry 1: 27-41.

Gattuso, J.-P., Gao, K., Lee, K., Rost, B. and Schulz, K. G. 2010. Approaches and tools to manipulate the carbonate chemistry. In Riebesell U., Fabry V. J., Hansson L. and Gattuso J-P. (eds.), EPOCA Guide to best practices in ocean acidification research and data reporting EUR 24328 EN, European Commission, Belgium. pp. 41-52.

Gattuso, J.-P., Allemand, D. and Frankignoulle, M. 1999. Photosynthesis and calcification at cellular, organismal and community levels in coral reefs: a review on interactions and control by carbonate chemistry. American Zoologist 39: 160-183.

Gatz, A. J., Kennedy, V. S. and Mihursky, J. A. 1973. Effects of temperature on activity and mortality of the scyphozoan medusa *Chrysaora quinquecirrha*. Chesapeake Science 14: 171-180.

Gazeau, F., Quiblier, C., Jansen, J. M., Gattuso, J-P., Middelburg, J. J. and Heip, C. H. R. 2007. Impact of elevated CO_2 on shellfish calcification. Geophysical Research Letters 34.

Gehlen, M., Gangstø, R., Schneider, B., Bopp, L., Aumont, O. and Ethe, C. 2007. The fate of pelagic $CaCO_3$ production in a high CO_2 ocean: a model study. Biogeosciences 4: 505-519.

Gibbs, S. J., Robinson, S. A., Bown, P. R., Jones, T. D. and Henderiks, J. 2011. Comment on "Calcareous nannoplankton response to surface-water acidification around Oceanic Anoxic Event 1a." Science 332: 175.

Gibbs, S. J., Stoll, H. M., Bown, P. R. and Bralower, T. J. 2010. Ocean acidification and surface water carbonate production across the Paleocene–Eocene thermal maximum. Earth and Planetary Science Letters 295: 583-592.

Gili, J.-M., Rossi, S., Pages, F., Orejas, C., Teixido, N., Lopez-Gonzalez, P. J. and Arntz, W. E. 2006. A new trophic link between the pelagic and benthic systems on the Antarctic shelf. Marine Ecology Progress Series 322: 43-49.

Godeaux, J. 1976. *Pyrosoma atlanticum*, Peron 1804 (*P. giganteum*), Lesueur, 1804 - *P. elegans*, Lesueur, 1804). Tunicata, Thaliacea, Pyrosomidae - Rapport Communication 23: 71-72.

Golden Software. 2002. Surfer: A powerful contouring, gridding, and surface mapping package for scientists and engineers, version 8. 01. Golden Software. (http://www.goldensoftware.com/).

Goldman, S. F. and Sedberry, G. R. 2010. Feeding habits of some demersal fish on the Charleston Bump off the southeastern United States. ICES Journal of Marine Science 68: 390-398.

Gollety, C., Gentil, F. and Davoult, D. 2008. Secondary production, calcification and CO_2 fluxes in the cirripedes *Chthamalus montagui* and *Elminius modestus*. Oecologia 44: 1146–1153.

Gonzalez, H. E., Ortiz, V. C., and Sobarzo, M. 2000. The role of faecal material in the particulate organic carbon flux in the Northern Humboldt Curent, Chile (230 S), before and during the 1997-1998 El Niño. Journal of Plankton Research 22: 499-529.

Gooday, A. J., Bett, B. J., Escobar, E., Ingole, B., Levin, L. A., Neira, C., Raman, A. V. and Sellanes, J. 2010. Habitat heterogeneity and its influence on benthic biodiversity in oxygen minimum zones. Marine Ecology 31: 125-147.

Gooday, A. J. and Turley, C. M. 1990. Responses by benthic organisms to inputs of organic material to the ocean floor: A review. Philosophical Transactions of the Royal Society London. 331: 119-138.

Gooding, R., Harley, C. and Tang, E. 2009. Elevated water temperature and carbon dioxide concentration increase the growth of a keystone echinoderm. Proceedings of the National Academy of Sciences 106: 9316-9321.

Gordon, M. R. and Seymour, J. E. 2008. Quantifying movement of the tropical Australian cubozoan *Chironex fleckeri* using acoustic telemetry. Hydrobiologia 616: 87-97.

Gordon, I. 1929. Skeletal development in *Arbacia*, *Echinarachnius* and *Leptasterias*. Philosophical Transactions of the Royal Society of London B 217: 289-334.

Gorsky, G., Fisher, N. S. and Fowler, S. W. 1984. Biogenic debris from the pelagic tunicate, *Oikopleura dioica*, and its role in the vertical transport of a transuranium element. Estuarine, Coastal and Shelf Science 18: 13-23.

Grainger, J. L., Winker, M. M., Shen, S. S. and Steinhardt, R. A. 1979. Intracellular pH controls protein synthesis rate in the sea urchin egg and early embryo. Developmental Biology 68: 396-406.

Granata, T. C., Estrada, M., Zika, U. and Merry, C. 2004: Evidence for enhanced primary production resulting from relative vorticity induced upwelling in the Catalan Current, 2004. Scientia Marina 68: 113-119.

Grassle, J. F. and Grassle, J. P. 1994. Notes from the abyss, the effects of a patchy supply of organic material and larvae on soft-sediment benthic communities. In Giller, P. S., Hildrew, A. G. and Raffaelli, D. G. (eds.), Aquatic Ecology, Scale, Pattern and Process, 34th Symposium of the British Ecological Society, Blackwell Scientific Publications, Oxford. pp. 499-515.

Grassle, J. F. and Morse-Porteus, L. S. 1987. Macrofaunal colonization of disturbed deep-sea environments and the structure of deep-sea benthic communities. Deep Sea Research I 34: 1911-1950.

Gregg, W., Ginoux, P., Schopf, P. and Casey, N. 2003. Phytoplankton and iron, validation of a global three-dimensional ocean biogeochemical model. Deep-Sea Research II 50: 3143-3169.

Griffin, D. J. G. and Yaldwyn, J. C. 1970. Giant colonies of pelagic tunicate (*Pyrosoma spinosum*) from SE Australia and New Zealand. Nature 226: 464.

Grossart, H. P., Allgaier, M., Passow, U. and Riebesell, U. 2006. Testing the effect of CO_2 concentration on the dynamics of marine heterotrophic bacterioplankton. Limnology and Oceanography 51: 1-11.

Guilderson, T. P., Fairbanks, R. G. and Rubenstone, J. L. 1994. Tropical temperature variations since 20,000 years ago: modulating interhemispheric climate change. Science 263: 663-665.

Guillard, R. R. L. 1975. Culture of phytoplankton for feeding marine invertebrates. In Smith, W. L. and Chaney, M. H. (eds.), Culture of Marine Invertebrate Animals. Plenum Press, New York. pp. 29-60.

Guillard, R. R. L. and Ryther, J. H. 1962. Studies of marine planktonic diatoms: 1. *Cyclotella nana* (Hustedt) and *Detonula confervacea* (Cleve Gran). Canadian Journal of Microbiology 8: 229-239.

Gussone, N., Hönisch, B., Heuser, A., Eisenhauer, A., Spindler, M. and Hemleben, C. 2009. A critical evaluation of calcium isotope ratios in tests of planktonic foraminifers. Geochimica et Cosmochimica Acta 73: 7241-7255.

Gutt, J. 1988. Zur Verbreitung und Ökologie der Seegurken (Holothuroidea, Echinodermata) im Weddellmeer (Antarktis). Berichte zur Polarforschung 41: 1-87.

Haas, P., Hill, G. and Karstens, W. K. H. 1935. The metabolism of calcareous algae. II. The seasonal variation in certain metabolic products of *Corallina squamata* Ellis. Annales Botanici 49: 609-19.

Haddock, S. H. D. 2004. A golden age of gelata: past and future research on planktonic ctenophores and cnidarians. Hydrobiologia 530/531: 549-556.

Hall-Spencer, J. M., Rodolfo-Metalpa, R., Martin, S., Ransome, E., Fine, M., Turner, S. M., Rowley, S. J., Tedesco, D. and Buia, M. C. 2008. Volcanic carbon dioxide vents show ecosystem effects of ocean acidification. Nature 454: 96-99.

Hansen, K. and Koroleff, F. 1999. Determination of nutrients. In Grasshoff, K., Kremlingand, K. and Ehrhardt, M. (eds.), Methods of Seawater Analysis. Wiley. pp.159-228.

Hansson, L. J. and Norrman, B. 1995. Release of dissolved organic carbon (DOC) by the scyphozoan jellyfish *Aurelia aurita* and its potential influence on the production of planktic bacteria. Marine Biology 121: 527-532.

Harbison, G. R., McAlister, V. L. and Gilmer, R. W. 1986. The response of the salp, *Pegea confoederata,* to high levels of particulate material: starvation in the midst of plenty. Limnology and Oceanography 31: 371-382.

Hardie, L. A. 1996. Secular variation in seawater chemistry: An explanation for the coupled secular variation in the mineralogies of marine limestones and potash evaporites over the past 600 m.y. Geology 24: 279-283.

Hare, C. E., Leblanc, K., Ditullio, G. R., Kudela, R. M., Zhang, Y., Lee, P. A., Riseman, S. and Hutchins, D. A. 2007. Consequences of increased temperature and CO_2 for phytoplankton community structure in the Bering Sea. Marine Ecology Progress Series 352: 9-16.

Harris, R. J. C. 1954. Biological applications of freezing and drying. Academic Press. New York.

Hauck, J., Gerdes, D., Hillenbrand, C-D., Hoppema, M., Kuhn, G., Nehrke, G., Völker, C. and Wolf-Gladrow, D. A. 2012. Distribution and mineralogy of carbonate sediments on Antarctic shelves. Journal of Marine Systems 90: 77-87.

Havenhand, J. N., Butler, F. R., Thorndyke, M. C. and Williamson, J. E. 2008. Near-future levels of ocean acidification reduce fertilization success in a sea urchin. Current Biology 18: 651-652.

Hays, G. C., Doyle, T. K., Houghton, J. D. R., Lilley, M. K. S., Metcalfe, J. D. and Righton, D. 2008. Diving behaviour of jellyfish equipped with electronic tags. Journal of Plankton Research 30: 325-331.

Heinze, C. 2004. Simulating oceanic $CaCO_3$ export production in the greenhouse. Geophysical Research Letters 31.

Hendricks, I. E. and Duarte, C. M. 2010. Ocean acidification: Separating evidence from judgement - a reply to Dupont et al. Estuarine Coastal and Shelf Science 89: 186-90.

Hendriks, I., Duarte, C. and Álvarez, M. 2009. Vulnerability of marine biodiversity to ocean acidification: A meta-analysis. Estuarine, Coastal and Shelf Science 86: 157-164.

Henrich, R. and Wefer, G. 1986. Dissolution of biogenic carbonates: effects of skeletal structure. Marine Geology 71: 341-362.

Henriksen, K., Stipp, S. L. S., Young, J. and Marsh, M. E. 2004. Biological control on calcite crystallization: AFM investigation of coccolith polysaccharide function. American Mineralogist 89: 1586-1596.

Herfort, L., Loste, E., Meldrum, F. and Thake, B. 2004. Structural and physiological effects of calcium and magnesium in *Emiliania huxleyi* (Lohmann) Hay and Mohler. Journal of Structural Biology 148: 307-314.

Herfort, L., Thake, B. and Roberts, J. 2002. Acquisition and use of bicarbonate by *Emiliania huxleyi*. New Phytologist 156: 427-436.

Hermans, J., Borremans, C., Willenz, P., Andre, L. and Dubois, P. 2010. Temperature, salinity and growth rate dependences of Mg/Ca and Sr/Ca ratios of the skeleton of the sea urchin *Paracentrotus lividus* (Lamarck): an experimental approach. Marine Biology 157: 1293-1300.

Hillenbrand, C. D., Grobe, H., Diekmann, B., Kuhn, G. and Fütterer, D. K. 2003. Distribution of clay minerals and proxies for productivity in surface sediments of the Bellingshausen and Amundsen seas (West Antarctica) - relation to modern environmental conditions. Marine Geology 193: 253-271.

Hilton, J., Lishman, J. P., Mackness, S. and Heaney, S. I. 1986. An automated method for the analysis of particulate carbon and nitrogen in natural waters. Hydrobiologia 141: 269-271.

Hipkin, C. R., Thomas, R. J. and Syrett, P. J. 1983. Effects of nitrogen deficiency on nitrate reductase, nitrate assimilation and photosynthesis in unicellular marine algae. Marine Biology 77: 101-105.

Hirst, A. G. and Lucas, C. H. 1998. Salinity influences body mass quantification in the scyphomedusa *Aurelia aurita*: important implications for body mass determination in gelatinous zooplankton. Marine Ecology Progress Series 165: 259-269.

Ho, T-Y., Quigg, A., Finkel, Z. V., Milligan, A. J., Wyman, K., Falkowski, P. G. and Morel, F. M. M. 2003. The elemental composition of some marine phytoplankton. Journal of Phycology 39: 1145-1159.

Hofmann, G.E., Barrry, J.P., Edmunds, P.J., Gates, R.D., Hutchins, D.A., Klinger, T., Sewell, M.A., 2010. The effect of ocean acidification on calcifying organisms in marine ecosystems: an organism to ecosystem perspective. Annu. Rev. Ecol. Evol. Syst. 41, 127-147.

Honjo, S., Manganini, S. J., Krishfield, R. A. and Francois, R. 2008. Particulate organic carbon fluxes to the ocean interior and factors controlling the biological pump: a synthesis of global sediment trap programs since 1983. Progress in Oceanography 76: 217-285.

Honjo, S., Dymond, J., Prell, W. and Ittekkot, V. 1999. Monsoon-controlled export fluxes to the interior of the Arabian Sea. Deep Sea Research II 46: 1859-1902.

Honjo, S. 1976. Coccoliths: production, transportation and sedimentation. Marine Micropaleontology 1: 65-79.

Hoppe, C. J. M., Langer, G. and Rost, B. 2011. *Emiliania huxleyi* shows identical responses to elevated pCO_2 in TA and DIC manipulations. Journal of Experimental Marine Biology and Ecology 406: 54-62.

Hoppe, C. J. M., Langer, G., Rokitta, S. D., Wolf-Gladrow, D. A. and Rost, B. 2010. On CO_2 perturbation experiments: over-determination of carbonate chemistry reveals inconsistencies. Biogeosciences Discussions 7: 1707-1726.

Hoppe, H.G. 2003. Phosphatase activity in the sea. Hydrobiologia 493: 187-200.

Horita, J., Zimmerman, H. and Holland, H. D. 2002. The chemical evolution of seawater during the Phanerozoic: Implications from the record of marine evaporites. Geochimica et Cosmochimica Acta 66.

Houghton, J. D. R., Doyle, T. K., Davenport, J., Lilley, M. K. S., Wilson, R. P. and Hays, G. C. 2007. Stranding events provide indirect insights into the seasonality and persistence of jellyfish medusae (Cnidaria: Scyphozoa). Hydrobiologia 589: 1-13.

Howell, K. L., Billett, D. S. M. and Tyler, P. A. 2002. Depth-related distribution and abundance of seastars (Echinodermata: Asteroidea) in the Porcupine Seabight and Porcupine Abyssal Plain, N.E. Atlantic. Deep-Sea Research I 49: 1901-1920.

Hurd, C. L., Hepburn, C. D., Currie, K. I., Raven, J. A. and Hunter, K. A. 2009 Testing the effects of ocean acidification on algal metabolism: considerations for experimental design. Journal of Phycology 45: 1030-1051.

Hurley, D. E. and McKnight, D. G. 1959. Occurrence of *Pyrosoma* on the sea-floor 160 metres deep. Nature 183: 554-555.

Huwer, B., Storr-Paulsen, M., Riisgård, H. U. and Haslob, H. 2008. Abundance, horizontal and vertical distribution of the invasive ctenophore *Mnemiopsis leidyi* in the central Baltic Sea, November 2007. Aquatic Invasions 3: 113-124.

Iglesias-Rodriguez M. D., Halloran P. R., Rickaby R. E. M, Hall I. R., Colmenero-Hidalgo E., Gittins J. R., Green D. R. H., Tyrrell T., Gibbs S. J., von Dassow P., Rehm E., Armbrust E. V. and Boessenkool K. P. 2008. Phytoplankton Calcification in a High-CO_2 World. Science 320: 336-340.

Iglesias-Rodriguez, M. D., Buitenhuis, E. T., Raven, J. A., Schofield, O., Poulton, A. J., Gibbs, S., Halloran, P. R. and de Baar, H. J. W. 2008b. Response to Comment on "Phytoplankton Calcification in a High-CO2 World". Science 322: 1466.

Iglesias-Rodriguez, M. D., Schofield, O., Batley, J. and Medlin, L. K. 2006. Intraspecific genetic diversity in the marine coccolithophore *Emiliania huxleyi* (prymnesiophyceae): the use of microsatellite analysis in marine phytoplankton population studies. Journal of Phycology 42: 526-536.

Iglesias-Rodriguez, M. D., R. Armstrong, R. A. Feely, R. Hood, J. Kleypas, J. D. Milliman, C. Sabine, and J. Sarmiento. 2002. Progress made in the study of ocean's calcium carbonate budget. EOS Transactions, American Geophysical Union 83: 374-375.

Iguchi, N., Ishikawa, R., Sato, O., Onishi, T. and Maeda, T. 2006. Decomposition rate of the giant jellyfish *Nemopilema nomurai* in Sado Island. FRA, Japan Sea National Fisheries Research Institute report. http://jsnfri.fra.affrc.go.jp/Kurage/kurage_hp18/Sado_bunkai.pdf

Ingle, S. E. 1975. Solubility of calcite in the ocean. Marine Chemistry 3: 310-319.

Ingram, B. L., De Deckker, P., Chivas, A. R., Conrad, M. E. and Byrne, A. R. 1998. Stableisotopes, Sr/Ca, and Mg/Ca in biogenic carbonates from Petaluma Marsh, Northern California, USA. Geochimica et Cosmochimica Acta 62 19/20: 3229-3237.

IOC, IHO, and BODC. 2003. Centenary Edition of the GEBCO Digital Atlas, published on CD-ROM on behalf of the Intergovernmental Oceanographic Commission and the International Hydrographic Organization as part of the General Bathymetric Chart of the Oceans. British Oceanographic Data Centre. Liverpool, United Kingdom.

Jackson, J. B. C. 2008. Ecological extinction and evolution in the brave new ocean. Proceedings of the National Academy of Sciences 105: 11458-11465.

Jackson, G. A., Maffione, R., Costello, D. K., Alldredge, A. L, Logan, B. E. and Dam, H. G. 1997. Particle size spectra between 1 mm and 1 cm at Monterey Bay determined using multiple instruments. Deep-Sea Research I 44: 1739-1767.

Jahnke, R. A. 1996. The global ocean flux of particulate organic carbon, areal distribution and magnitude. Global Biogeochemical Cycles 10: 71-88.

Jiang, S., Dickey, T. D., Steinberg, D. K. and Madin, L. P. 2007. Temporal variability of zooplankton biomass from ADCP backscatter time series data at the Bermuda Testbed Mooring site. Deep Sea Research I 54: 608-636.

Jin, X., Gruber, N., Dunne, J. P., Sarmiento, J. L. and Armstrong, R. A. 2006. Diagnosing the contribution of phytoplankton functional groups to the production and export of particulate organic carbon, $CaCO_3$, and opal from global nutrient and alkalinity distributions. Global Biogeochemical Cycles 20.

Johns, B., Marsaleix, P., Estournel, C. and Vehil, R. 1992. On the wind-driven coastal upwelling in the Gulf of Lions. Journal of Marine Systems 3: 309-320.

Johnson, K. M., Dickson, A. G., Eischeid, G., Goyet, C., Guenther, P., Key, R. M., Millero, F. J., Purkerson, D., Sabine, C. L., Schottle, R. G., Wallace, D. W. R., Wilke, R. J. and Winn, C.D. 1998. Coulometric total carbon dioxide analysis for marine studies: assessment of the quality of total inorganic carbon measurements made during the US Indian Ocean CO2 Survey 1994-1996. Marine Chemistry. 63: 21-37.

Jones, D. O. B. 2009. Using existing industrial remotely operated vehicles for deep-sea science. Zoologica Scripta 38: 41-47.

Jones, D. O. B., Roterman, C. N. and Gates, A. R. 2010. Shell Gro SERPENT final report. Southampton, UK, National Oceanography Centre Southampton. (National Oceanography Centre Southampton Research and Consultancy Report: 79).

Jumars, P. A. 1976. Deep-sea species diversity. Does it have a characteristic scale? Journal of Marine Research 34: 217-246.

Jury, C., Whitehead, R. F. and Szmant, A. 2010. Effects of variations in carbonate chemistry on the calcification rates of *Madracis auretenra* (= *Madracis mirabilis* sensu Wells, 1973): bicarbonate concentrations best predict calcification rates. Global Change Biology 16: 1632-1644.

Kaffes, A., Thoms, S., Trimborn, S., Rost, B., Langer, G., Richter, K.-U., Köhler, A., Norici, A. and Giordano, M. 2010. Carbon and nitrogen fluxes in the marine coccolithophore Emiliania huxleyi grown under different nitrate concentrations. Journal of Experimental Marine Biology and Ecology 393: 1-8.

Karl, D. M. and Letelier, R. M. 2008. Nitrogen fixation-enhanced carbon sequestration in low nitrate, low chlorophyll seascapes. Marine Ecology Progress Series 364: 257-268.

Karpen, V., Viergutz, T. and Thomsen, L. 2007. Baltic Observatory for Oceanographic Monitoring. Sea Technology, July 2007, 18-20.

Katija, K. and Dabiri, J. O. 2009. A viscosity-enhanced mechanism for biogenic ocean mixing. Nature 460: 624-626.

Kaufmann, R. S. and Smith, K. L. 1997. Activity patterns of mobile epibenthic megafauna at an abyssal site in the eastern North Pacific: results from a 17-month time-lapse photographic study. Deep Sea Research I 44: 559-579.

Kayano, K. and Shiraiwa, Y. 2009. Physiological regulation of coccolith polysaccharide production by phosphate availability in the coccolithophorid *Emiliania huxleyi*. Plant and Cell Physiology 50: 1522-1531.

Keir, R. S. The dissolution kinetics of biogenic carbonates in seawater. Geochimica et Cosmochimica Acta 44: 241-252.

Kemp, W. M., Smith, E: M. Marvin-DiPasquale, M. and Boynton, W. R. 1997. Organic carbon balance and net ecosystem metabolism in Chesapeake Bay. Marine Ecology Progress Series 150: 229-248.

Kester, D., Duedall, I., Connors, D. and Pytkowicz, R. 1967. Preparation of artificial seawater. Limnology and Oceanography 12: 176-179.

Key, R. M., Kozyr, A., Sabine, C. L., Lee, K., Wanninkhof, R., Bullister, J., Feely, R. A., Millero, F., Mordy, C. and Peng, T. H. 2004. A global ocean carbon climatology, results from GLODAP. Global Biogeochemical Cycles 18.

Kim, J. M., Lee, K., Shin, K., Kang, J. H., Jang, P. G. and Jang, M. C. 2006. The effect of seawater CO_2 concentration on growth of a natural phytoplankton assemblage in a controlled mesocosm experiment. Limnology and Oceanography 51: 1629-1636.

Knappertsbusch, M.and Brummer, G-J. A. 1995. A sediment trap investigation of sinking coccolithophorids in the North Atlantic. Deep Sea Research I 42: 1083-1109.

Kogovšek, T., Bogunović, B. and Malej, A. 2010. Recurrence of bloom-forming scyphomedusae: wavelet analysis of a 200-year time-series. Hydrobiologia 645: 81-96.

Komar, P. D. 1980. Settling velocities or circular cylinders at low Reynolds numbers: Journal of Geology 88: 327-336.

Kovalev, A. V. and Piontkovski, S. A. 1998. Interannual changes in the biomass of the Black Sea gelatinous zooplankton. Journal of Plankton Research 20: 1377-1385.

Kriest, I., and Oschlies, A. 2008. On the treatment of particulate organic matter sinking in large-scale models of marine biogeochemical cycles. Biogeosciences 5: 55.72.

Kriest, I. and Evans, G. 1999. Representing phytoplankton aggregates in biogeochemical models, Deep-Sea Research I 46: 1841-1859.

Kroeker, K. J., Kordas, R. L., Crim, R. N. and Singh, G. G. 2010. Meta-analysis reveals negative yet variable effects of ocean acidification on marine organisms. Ecology Letters 13: 1419.1434.

Kroh, A. and Nebelsick, J. H. 2010. Echinoderms and Oligo-Miocene carbonate systems: potential applications in sedimentology and environmental reconstruction. International Association of Sedimentologist Special Publication 42: 201-228.

Krug, S. A., Schulz, K. G. and Riebesell, U. 2011. Effects of changes in carbonate chemistry speciation on *Coccolithus braarudii*: a discussion of coccolithophorid sensitivities, Biogeosciences 8: 771-777.

Kuenen, P. H. 1950. Marine geology. John Wiley.

Kuenzler, E. J. and Perras, J. P. 1965. Phosphatases of marine algae. Biological Bulletin 128: 271-284.

Kuffner I. B., Andersson A. J., Jokiel P. L., Rodgers K. S. and Mackenzie F. T. 2007. Decreased abundance of crustose coralline algae due to ocean acidification. Nature Geoscience 1: 114-117.

Kurihara, H. and Shirayama, Y. 2004. Effects of increased atmospheric CO_2 on sea urchin early development. Marine Ecology Progress Series 274: 161-169.

Kuss, J. and Kremling, K. 1999. Spatial variability of particle associated trace elements in near-surface waters of the North Atlantic (30 degrees N/60 degrees W to 60 degrees N/2 degrees W), derived by large-volume sampling. Marine Chemistry 68: 71-86.

Lampitt, R. S., Boorman, B., Brown, L., Lucas, M., Salter, I., Sanders, R., Saw, K., Seeyave, S., Thomalla, S. J. and Turnewitsch, R. 2008. Particle export from the euphotic zone: Estimates using a novel drifting sediment trap, ^{234}Th and new production. Deep-Sea Research I 55: 1484-1500.

Lampitt, R. S., Bett, B. J., Kiriakoulakis, K., Popova, E. E., Ragueneau, O., Vangriesheim, A. and Wolff, G. A. 2001. Material supply to the deep-seafloor in the Northeast Atlantic. Progress in Oceanography 50: 27-63.

Lampitt, R. S. 1985. Evidence for the seasonal deposition of detritus to the deep-sea floor and its subsequent resuspension. Deep-Sea Research 32: 885-897.

Langdon, C., Takahashi, T., Sweeney, C., Chipman, D., Goddard, J., Marubini, F., Aceves, H., Barnett, H. and Atkinson, M. J. 2000. Effect of calcium carbonate saturation state on the calcification rate of an experimental coral reef. Global Biogeochemical Cycles 14: 639-654

Langer, G., Oetjen, K. and Brenneis, T. 2012. Calcification of Calcidiscus leptoporus under nitrogen and phosphorus limitation. Journal of Experimental Marine Biology and Ecology 413: 131-137.

Langer, G., Nehrke, G., Thoms, S. and Stoll, H. 2009a. Barium partitioning in coccoliths of *Emiliania huxleyi*. Geochimica et Cosmochimica Acta 73: 2899-2906.

Langer, G., Nehrke, G., Probert, I., Ly J. and Ziveri, P. 2009b. Strain-specific responses of *Emiliania huxleyi* to changing seawater carbonate chemistry. Biogeosciences 6: 2637-2646.

Langer, G., Gussone, N., Nehrke, G., Riebesell, U., Eisenhauer, A., Kuhnert, H., Rost, B., Trimborn, S. and Thoms, S. 2006a. occolith strontium to calcium ratios in *Emiliania huxleyi*: The dependence on seawater strontium and calcium concentrations. Limnology and Oceanography 51: 310-320.

Langer, G., Geisen, M., Baumann, K.- H., Kläs, J., Riebesell, U., Thoms, S. and Young, J. R. 2006b. Species-specific responses of calcifying algae to changing seawater carbonate chemistry. Geochemistry Geophysics Geosystems 7: Q09006.

Larsen, J. B., Larsen, A., Thyrhaug, R., Bratbak, G. and Sandaa, R. A. 2008. Response of marine viral populations to a nutrient induced phytoplankton bloom at different pCO_2 levels. Biogeosciences 5: 523-533.

Larson, R. J. 1986. Water content, organic content, and carbon and nitrogen composition of medusae from the northeast Pacific. Journal of Experimental Marine Biology and Ecology 99: 107-120.

Laws, E. A. 2004. Export flux and stability as regulators of community composition in pelagic marine biological communities: implications for regime shifts. Progress in Oceanography 60: 343-354.

Laws, E., Falkowski, P. G., Smith, W., Ducklow, H. and McCarthy, J. 2000. Temperature effects on export production in the open ocean. Global Biogeochemical Cycles 14: 1231-1246.

Lebrato, M., Pitt, K. A., Sweetman, A. K., Jones, D. O. B., Cartes, J. E., Oschlies, A., Condon, R. H., Molinero, J-C., Adler, L., Gaillard, C., Lloris, D. and Billett, D. S. M. 2012. Jelly-falls historic and recent observations: a review to drive future research directions. Hydrobiologia DOI: 10.1007/s10750-012-1046-8.

Lebrato, M., Pahlow, M., Oschlies, A., Pitt, K. A., Jones, D. O. B., Molinero, J-C. and Condon, R. H. 2011. Depth attenuation of organic matter export associated with jelly-falls. Limnology and Oceanography 56: 1917-1928.

Lebrato, M., Iglesias-Rodriguez, M. D., Feely, R. A., Greeley, D., Jones, D. O. B, Suarez-Bosche, N. E., Lampitt, R. S., Cartes, J. A., Green, D. and Alker, B. 2010. Global contribution of echinoderms to the marine carbon cycle: a re-assessment of the oceanic $CaCO_3$ budget and the benthic compartments. Ecological Monographs 80: 441-467

Lebrato, M. and Jones, D. O. B. 2009. Mass deposition event of *Pyrosoma atlanticum* carcasses off Ivory Coast (West Africa). Limnology and Oceanography 54: 1197-1209.

Lee, B-G. and Fisher, N. 1993. Release rate of trace elements and protein from decomposing debris. 1. Phytoplankton debris. Journal of Marine Research 51: 391-421.

Lefèvre, D., Minas, H. J., Minas, M., Robinson, C., Williams, P. J. L. and Woodward, E. M. S. 1997. Review of gross community production, primary production, net community production and dark respiration in the Gulf of Lions. Deep-Sea Research 44: 801-832.

Legong, L., Tutone, A. F., Drummond, R. S. M., Gardner, R. C. and Luan, S. 2001. A novel family of magnesian transport genes in Arabidopsis. The Plant Cell 13: 2761-2775.

Leonardos, N., Read, B., Thake, B. and Young, J. R. 2009. No mechanistic dependence of photosynthesis on calcification in the coccolithophorid *Emiliania huxleyi* (Haptophyta). Journal of Phycology 45: 1046-1051.

Leroy, J. 1926. Necessite du magnesium pour la croissance de la souris. Comptes Rendus des Seances de la Society Biologique 94: 431-433.

Levin, L. A., Etter, R. J., Rex, M. A., Gooday, A. J., Smith, C. R., Pineda, J., Stuart, C. T., Hessler, R. R. and Pawson, D. 2001. Environmental influences on regional deep-sea species diversity. Annual Review of Ecology, Evolution, and Systematics 32: 51-93.

Lewis, C. A., Ebert, T. A. and Boren, M. E. 1990. Allocation of ^{45}calcium to body components of starved and fed purple sea urchins (*Strongylocentrorus purpuratus*). Marine Biology 105: 213-222.

Lewis, E. and Wallace, D. W. R. 1998. Program Developed for CO_2 System Calculations. ORNL/CDIAC- 105. Carbon Dioxide Information Analysis Centre.

Licandro, P., Conway, D. V. P., Daly Yahia, M. N., Fernandez de Puelles, M. L, Gasparini, S., Hecq, J. H., Tranter, P. and Kirby, R. R. 2010. A blooming jellyfish in the northeast Atlantic and Mediterranean. Biology Letters 6: 688-691.

Litchman, E., Klausmeier, C. A., Schofield, O. M. and Falkowski, P. G. 2007. The role of functional traits and trade-offs in structuring phytoplankton communities: scaling from cellular to ecosystem level. Ecology letters 10: 1170-1181.

Litchman, E., Klausmeier, C. A., Miller, J. R., Schofield, O. M. and Falkowski, P. G. 2006. Multi-nutrient, multi-group model of present and future oceanic phytoplankton communities. Biogeosciences 3: 585-606.

Loeb, V., Siegel, V., Holm-Hansen, O., Hewitt, R., Fraser, W., Trivelpiece, W. and Trivelpiece, S, 1997. Effects of sea-ice extent and krill or salp dominance on the Antarctic food web. Nature 387: 897-900.

Lombard, F. and Kiorbe, T. P. 2010. Marine snow originating from appendicularian houses: Age-dependent settling characteristics. Deep Sea Research I 57: 1304-1313.

Lombard, F., Legendre, L., Picheral, M., Sciandra, A. and Gorsky, G. 2010. Prediction of ecological niches and carbon export by appendicularians using a new multispecies ecophysiological model. Marine Ecology Progress Series 398: 109-125.

Lorens, R. B. 1981. Sr, Cd, Mn and Co distribution coefficients in calcite as a function of calcite precipitation rate. Geochimica et Cosmochimica Acta 45: 553-561.

Lorrain, A., Gillikin, D., Paulet, Y.M., Chavaud, L., Lemercier, A., Navez, J. and Andre, L. 2005. Strong kinetic effects on Sr/Ca ratios in the calcitic bivalve *Pecten maximus*. Geology 33: 965-968.

Loste, E., Wilson, R. M., Seshadri, R., and Meldrum, F. C. 2003, The role of magnesium in stabilizing amorphous calcium carbonate and controlling calcite morphologies. Journal of Crystal Growth 254: 206-218.

Lovdal, T., Eichner, C., Grossart, H. P., Carbonnel, V., Chou, L., Martin-Jezequel, V. and Thingstad, T. F. 2008. Competition for inorganic and organic forms of nitrogen and phosphorus between phytoplankton and bacteria during an *Emiliania huxleyi* spring bloom. Biogeosciences 5: 371-383.

Lovelock, J. F. and Rapley, C. G. 2007. Ocean pipes could help the Earth to cure itself. Nature 449: 403.

Lowenstam, H. A. 1954. Factors affecting the aragonite:calcite ratios in carbonate-secreting marine organisms. Journal of Geology 62: 284-322.

Lucas, C. H., Pitt, K. A., Purcell, J. E., Lebrato, M. and Condon, R. H. 2011. What's in a jellyfish? Proximate and elemental composition and biometric relationships for use in biogeochemical studies. Ecology 92: 1704.

Lucas, C. H. 2001. Reproduction and life history strategies of the common jellyfish, A. aurita, in relation to its ambient environment. Hydrobiologia 451: 229-246.

Lund, J. W. G. 1972. Preliminary observations on the use of large experimental tubes in lakes.Verhandlungen - Internationale Vereinigung fuer Theoretische und Angewandte Limnologie 18: 71-77.

Lusk, J. E., Williams, R. J. P. and Kennedy, E. P. 1968. Magnesium and the Growth of *Escherichia coli*. The Journal of Biological Chemistry 243: 2618-2624.

Lutz, M., Dunbar, R. and Caldeira, K. 2002. Regional variability in the vertical flux of particulate organic carbon in the ocean interior. Global Biogeochemical Cycles 16: 1037-1055.

Lynam, C. P., Attrill, M. J. and Skogen, M. D. 2010. Climatic and oceanic influences on the abundance of gelatinous zooplankton in the North Sea. Journal of the Marine Biological Association of the UK 90: 1153-1159.

Lynam, C. P., Gibbons, M. J., Axelsen, B. E., Sparks, C. A. J., Coetzee, J., Heywood, B. G. and Brierley, A. S. 2006. Jellyfish overtake fish in a heavily fished ecosystem. Current Biology 16: 492-493.

Ma, X., Chang, P. R., Yu, J. and Wang, N. 2008. Preparation and properties of biodegradable poly(propylene carbonate)/thermoplastic dried starch composites. Carbohydrate Polymers 71: 229-234.

Mackenzie, F. T., Bischoff, W. D., Bishop, F. C., Loijens, M., Schoonmaker, R. and Wollast, R. 1983. Magnesian calcites: Low temperature occurrence, solubility, and solid solution behavior. Carbonates: Mineralogy and Chemistry, Reviews in Mineralogy 11: 97-144.

Madin, L. P. 1982. Production, composition and sedimentation of salp fecal pellets in oceanic waters. Marine Biology 67: 39-45.

Madin, L. P. 1991. Distribution and taxonomy of zooplankton in the Alboran Sea and adjacent western Mediterranean. A literature survey and field guide. Report for Harbor Branch Oceanographic Institution and Naval Oceanographic and Atmospheric Research Laboratory. W.H.O.I. Technical Report 91-26. 148. pp.

Madin, L. P. and Deibel, D. 1998. Feeding and energetics of thaliacea. In Bone, Q. (ed.), The Biology of Pelagic Tunicates. Oxford University Press, Oxford. pp. 81-103.

Madin, L. P., Kremer, P., Wiebe, P. H., Purcell, J. E., Horgan, E. H. and Nemazie, D. A. 2006. Periodic swarms of the salp Salpa aspera in the slope water off the NE United States: biovolume, vertical migration, grazing, and vertical flux. Deep Sea Research I 53: 804-819.

Mann, K. H. and Lazier, J. R. 1991. Dynamics of marine ecosystems. Biological-physical interactions in the oceans. Blackwell, Oxford.

Marcet, A. 1918. On the Specific Gravity, and Temperature of Sea Waters, in Different Parts of the Ocean, and in Particular Seas; With Some Account of Their Saline Contents. Philosophical Transactions of the Royal Society of London 109: 161-208.

Marchant, M., Hebbeln, D. and Wefer, G. 1999. High resolution planktic foraminiferal record of the last 13:300 years from the upwelling area off Chile. Marine Geology 61: 115-128.

Märkel, K., Kubanek, F. and Willgallis, A. 1971. Polykristalliner Calcit bei Seeigeln (Echinodermata, Echinoidea). Zeitschrift Zellforschung 11: 355-377.

Marshall, J. C., Nurser, A. J. G. and Williams, R. G. 1993. Inferring the subduction rate and period over the North Atlantic. American Meteorological Society 23: 1315-1329.

Martin, J. and Miquel, J-C. 2010. High downward flux of mucilaginous aggregates in the Ligurian Sea during summer 2002. Similarities with the mucilage phenomenon in the Adriatic Sea. Marine Ecology 31: 393-406.

Martin, S. and Gattuso, J-P. 2009. Response of Mediterranean coralline algae to ocean acidification and elevated temperature. Global Change Biology 15: 2089-2100.

Martin, P. A. and Lea, D. W. 2002. A simple evaluation of cleaning procedures on fossil benthic foraminiferal Mg/Ca. Geochemistry Geophysics Geosystems 10: doi:10.1029/2001GC000280

Martin, J. H., Knauer, G. A., Karl, D. M. and Broenkow, W. W. 1987. VERTEX: Carbon cycling in the northeast Pacific. Deep-Sea Research I 34: 267-285.

Martin, J. H., Bruland, K. W. and Broenkow, W. W. 1976. Cadmium transport in the California Current. In Windom, H. and Duce, R. (eds.), Marine pollutant transfer. Heath, Lexington, MA. pp. 159-184.

Martin, J-L. M. and Knauer, G. A. 1973. The elemental composition of plankton. Geochimica et Cosmochimica Acta 37: 1639-1653.

Marubini, F. and Thake, B. 1999. Bicarbonate addition promotes coral growth. Limnology and Oceanography 44: 716-720.

McClain, C. R., Rex, M. A. and Jabbour, R. 2005. Deconstructing bathymetric body size patterns in deep-sea gastropods. Marine Ecology Progress Series 297: 181-187.

McClintock, J. B., Amsler, M. O., Angus, R. A., Challener, R. C., Schram, J. B., Amsler, C. D., Mah, C. L., Cuce, J. and Barker, B. J. 2011. The Mg-calcite composition of Antarctic echinoderms: Important implications for predicting the impacts of ocean acidification. The Journal of Geology 119: 457-466.

McClintock, J. B. 1994. Trophic biology of antarctic shallow-water echinoderms. Marine Ecology Progress Series 111: 191-202.

McDonnell, A. M. P. and Buesseler, K. O. 2010. Variability in the average sinking velocity of marine particles. Limnology and Oceanography 55: 2085-2096.

McNeil, B. I. and Matear, R. J. 2008. Southern Ocean acidification: A tipping point at 450-ppm atmospheric CO_2. PNAS 105: 18860-18864.

Mehrbach, C., Culberson, C., Hawley, J. and Pytkowicz, R. 1973. Measurement of the apparent dissociation constants of carbonic acid in seawater at atmospheric pressure. Limnology and Oceanography 18: 897-907.

Meldrum, F. C. and Hyde, S. 2001. Morphological influence of magnesium and organic additives on the precipitation of calcite. Journal of Crystal Growth 231: 544-558.

Mélin, F., Vantrepotte, V., Clerici, M., D'Alimonte, D., Zibordi, G., Berthon, J.-F. and Canuti, E. 2011. Multi-sensor satellite time series of optical properties and chlorophyll-a concentration in the Adriatic Sea. Progress in Oceanography 91: 229-244.

Melzner, F., Gutowska, M. A., Langenbuch, M., Dupont, S., Lucassen, M., Thorndyke, M. C., Bleich, M. and Pörtner, H. O. 2009. Physiological basis for high CO_2 tolerance in marine ectothermic animals: pre-adaptation through lifestyle and ontogeny? Biogeosciences 6: 2313-2331.

Menendez, M., Martinez, M. and Comin, F. A. 2001. A comparative study of the effect of pH and inorganic carbon resources on the photosynthesis of three floating macroalgae species of a Mediterranean coastal lagoon. Journal of Experimental Marine Biology and Ecology 256: 123-136.

Merckelbach, L. M. and Ridderinkhof, H. 2006. Estimating suspended sediment concentration from ADCP backscatterance at a site with strong tidal currents. Ocean Dynamics 56: 153-168.

Mergulhao, L. P., Mohan, R., Murty, V. S. N., Guptha, M. V. S. and Sinha, D. K. 2006. Coccolithophore from the central Arabian Sea: sediment trap results. Journal of Earth System Sciences 115: 415-428.

Metzler, C. V., Wenkam, C. R. and Berger, W. R. 1982. Dissolution of foraminifera in the eastern equatorial Pacific: an in situ experiment. Journal of Foraminiferal Research 12: 362-368.

Middelburg, J. J., Barranguet, C., Boschker, H. T. S., Herman, P. M. J., Moens, T. and Heip, C. H. R. 2000. The fate of intertidal microphytobenthos carbon: an in situ ^{13}C-labeling study. Limnology Oceanography 45: 1224-1234.

Millero, F. J., Feistel, R., Wright, D. G. and McDougall, T. J. 2008. The composition of standard seawater and the definition of the reference-composition salinity scale. Deep Sea Research I 55: 50-72.

Millero, F. J. and Pierrot, D. 1998. A chemical equilibrium model for natural waters. Aquatic Geochemistry 4: 153-198.

Millero, F. J. 1995. The thermodynamics of the carbonic acid system in the ocean. Geochimica et Cosmochimica Acta 59: 661-667.

Millero, F. J. 1979. The thermodynamics of the carbonate system in seawater at atmospheric pressure. Geochimica et Cosmochimica Acta 43: 1651-1661.

Milliman, J. D. and Droxler, A. W. 1996. Neritic and pelagic carbonate sedimentation in the marine environment: Ignorance is not bliss. Geologische Rundschau 85: 496-504.

Milliman, J. D. 1993. Production and accumulation of calcium carbonate in the ocean: budget of a nonsteady state. Global Biogeochemical Cycles 7: 927-957.

Millot, C. and Wald, L. 1981. Upwelling in the Gulf of Lions. In Francis, F. A. (ed.), Coastal Upwelling, American Geophysical Union, Washington, DC. pp. 529.

Mills, C. E. 2001. Jellyfish blooms: are populations increasing globally in response to changing ocean conditions? Hydrobiologia 451: 55-68.

Mills, C. E. 1993. Natural mortality in NE Pacific coastal hydromedusae: grazing predation, wound healing and senescence. Bulletin of Marine Science 53: 194-203.

Mills, C. E. 1981. Diversity of swimming behaviours in hydromedusae as related to feeding and utilization of space. Marine Biology 64: 185-189.

Miyake, H., Lindsay, D. L., Kitamura, M. and Nishida, S. 2005. Occurrence of the scyphomedusa *Parumbrosa polylobata* Kishinouye, 1910 in Suruga Bay, Japan. Journal of Plankton Biology and Ecology 52: 58-66.

Miyake, H., Lindsay, D. L., Hunt, J. C. and Hamatsu, T. 2002. Scyphomedusa *Aurelia limbata* (Brandt, 1838) found in deep waters off Kushiro, Hokkaido, Northern Japan. Journal of Plankton Biology and Ecology 49: 44-46.

Molinero, J-C., Hidalgo, M. Coll, M. et al. in review. Compound effects of climate and fisheries fuel the jellyfish proliferation in the Mediterranean Sea. PNAS.

Molinero, J. C., Casini, M. and Buecher, E. 2008. The influence of the Atlantic and regional climate variability on the long-term changes in gelatinous carnivore populations in the northwestern Mediterranean. Limnology and Oceanography 53: 1456-1467.

Moore, J. K., Doney, S. C. and Lindsay, K. 2004. Upper ocean ecosystem dynamics and iron cycling in a global three-dimensional model. Global Biogeochemical Cycles 18: GB4028.

Moore, J. K., Doney, S. C., Kleypas, J.A., Glover, D. M., and Fung, I.Y. 2002. An intermediate complexity marine ecosystem model for the global domain. Deep-Sea Res. II, 49, 403-462.

Monniot, C. and Monniot, F. 1966. A benthic pyrosoma, *Pyrosoma benthica* n. sp. French Academy of Science 263: 368-370.

Morse, J. W. and Bender, L. M. 1990. Partition coefficients in calcite: Examination of factors influencing the validity of experimental results and their application to natural systems. Chemical Geology 82: 265-277.

Morse, J. W. Andersson, A. J. and Mackenzie, F. T. 2006. Initial responses of carbonate-rich shelf sediments to rising atmospheric pCO_2 and "ocean acidification": Role of high Mg-calcites. Geochimica etc Cosmochimica Acta 70: 5814-5830.

Morse, J. W. and Mackenzie, F. T. 1990. Geochemistry of sedimentary carbonates. Elsevier Science, Amsterdam

Moseley, H.N. 1880. Deep-sea dredging and life in the deep sea III. Nature 21: 591-593.

Moya, F., Ramos, A. and Manjon-Cabeza, M. E. 2003. Distribution and Ecology of *Ophionotus victoriae* Bell, 1902 (Ophiuroidea, Echinodermata) in the South Shetland Islands area (Antarctica). Boletin del Instituto Español de Oceanografia 19: 49-55.

Mucci, A. and Morse, J. W. 1987. The incorporation of Mg^{2+} and Sr^{2+} into calcite overgrowths: influences of growth rate and solution composition. Geochimica et Cosmochimica Acta 47: 217-233.

Mucci, A. 1983. The solubility of calcite and aragonite in seawater at various salinities temperatures, and one atmosphere total pressure. American Journal of Science 283: 780-799.

Müller, M. N., Beaufort, L., Bernard, O., Pedrotti, M. L., Talec, A. and Sciandra, A. 2012. Influence of CO_2 and nitrogen limitation on the coccolith volume of *Emiliania huxleyi* (Haptophyta). Biogeosciences Discussions 9: 4979-5010.

Müller, M. N., Kisakürek, B., Buhl, D., Gutperlet, R., Kolevica, A., Riebesell, U., Stoll, H. and Eisenhauer, A. 2011. Response of the coccolithophores *Emiliania huxleyi* and *Coccolithus braarudii* to changing Mg^{2+} and Ca^{2+} concentrations: Mg/Ca, Sr/Ca ratios and $\delta^{44/40}Ca$, $\delta^{26/24}Mg$ of coccolith calcite. Geochimica et Cosmochimica Acta 75: 2088-2102.

Müller, M. N., Schulz, K. G. and Riebesell, U. 2010. Effects of long-term high CO_2 exposure on two species of Coccolithophores. Biogeosciences 7: 1109-1116.
Müller, N. M. 2009. Calcification in coccolithophores: Effects of environmental conditions and palaeoproxy calibrations. Doctoral thesis, University of Kiel. pp. 154.

Müller, M. N., Antia, A. N. and Laroche, J. 2008. Influence of cell cycle phase on calcification in the coccolithophore Emiliania huxleyi. Limnology and Oceanography 53: 506-512.

Mullin, M. M. 2001. Plankton, Encyclopaedia of Ocean Sciences, 1st Edition 4: 2129-2194.

Murty S. J., Bett, B. J. and Gooday, A. J. 2009. Megafaunal responses to strong oxygen gradients on the Pakistan margin of the Arabian Sea. Deep Sea Research I 56: 472-487.

Myrberg, K., Ryabchenko, V., Isaev, A., Vankevich, R., Andrejev, O., Bendtsen, J., Erichsen, A., Funkqvist, L., Inkala, A., Neelov, I., Rasmus, K., Medina, M. R., Raudsepp, U., Passenko, J., Söderkvist, J., Sokolov, A., Kuosa, H., Anderson, T. R., Lehmann, A. and Skogen, M. 2010. Validation of three-dimensional hydrodynamic models of the Gulf of Finland. Boreal Environmental Research 15: 453-479.

Nesterenko, P. N. and Jones, P. 2007. Recent developments in the high-performance chelation ion chromatography of trace metals. Journal of Separation Science 30: 1773-1793.

Nicholas, D. J. D. and Nason, A. 1957. Determination of nitrate and nitrite. Methods in Enzymology 3: 982-984.

Niggl, W., Naumann, M. S., Struck, U., Manasrah, R. and Wild, C. 2010. Organic matter release by the benthic upside-down jellyfish *Cassiopea* sp. fuels pelagic food webs in coral reefs. Journal of Experimental Marine Biology and Ecology 384: 99-106.

Nisumaa, A-M., Pesant, S., Bellerby, R. G. J., Delille, B., Middelburg, J., Orr, J. C., Riebesell, U., Tyrrell, T., Wolf-Gladrow, D. and Gattuso, J-P. 2010. EPOCA/EUR-OCEANS data-mining compilation on the impacts of ocean acidification. Earth System Science Data Discussions 3: 109-130.

Okazaki, K., Dillaman, R. M. and Wilbur, K. M. 1981. Crystalline axes of the spine and test of the sea urchin *Strongylocentrotus purpuratus*: determination by crystal etching and decoration. Biological Bulletin 161: 402-415.

Orr, J. C., Fabry, V. J., Aumont, O., Bopp, L., Doney, S. C., Feely, R. A., Gnanadesikan, A., Gruber, N., Ishida, A., Joos, F., Key, R. M., Lindsay, K., Maier-Reimer, E., Matear, R., Monfray, P., Mouchet, A., Najjar, R. G., Plattner, G. K., Rodgers, K. B., Sabine, C. L.,

Sarmiento, J. L., Schlitzer, R., Slater, R. D., Totterdell, I. J., Weirig, M. F., Yamanaka, Y. and Yool, A. 2005. Anthropogenic ocean acidification over the twenty-first century and its impact on calcifying organisms. Nature 437: 681-686

Oschlies, A., Pahlow, M., Yool, A. and Matear, R. J. 2010. Climate engineering by artificial ocean upwelling - channelling the sorcerer's apprentice, Geophysical Research Letters 37: L04701.

Oschlies, A. and Garcon, V. 1999. An eddy-permitting coupled physical-biological model of the North Atlantic, I, Sensitivity to advection numerics and mixed layer physics. Global Biogeochemical Cycles 13: 135-160.

Ovreas, L., Bourne, D., Sandaa, R. A., Casamayor, E. O. Benlloch, S., Goddard, V., Smerdon, G., Heldal, M. and Thingstad, T. F. 2003. Response of bacterial and viral communities to nutrient manipulations in seawater mesocosms. Aquatic Microbial Ecology 31:109-121.

Paasche, E. 2002. A review of the coccolithophorid *Emiliania huxleyi* (Prymnesiophyceae), with particular reference to growth, coccolith formation, and calcification-photosynthesis interactions. Phycologia 40: 503-529.

Paasche, E. 2001. A review of the coccolithophorid Emiliania huxleyi (Prymnesiophyceae), with particular reference to growth, coccolith formation, and calcification-photosynthesis interactions. Phycologia 40: 503-529.

Paasche, E. 1998. Roles of nitrogen and phosphorus in coccolith formation in Emiliania huxleyi (Prymnesiophyceae). European Journal of Phycology 33: 33-42.

Paasche, E. 1964 A tracer study of the inorganic carbon uptake during coccolith formation and photosynthesis in the coccolithophid *Coccolithus huxleyi* (Prymnesiophycea). Physiologia Plantarum 3: 5-82.

Pak, D. K., Lea, D. W. and Kennett, J. P. 2004. Seasonal and interannual variation in Santa Bárbara Basin water temperatures observed in sediment trap foraminifera Mg/Ca. Geochemistry Geophysics Geosystems 5: Q12008.

Pakhomov, E. A., Fuentes, V., Schloss, I., Atencio, A. and Snal, G. B. 2003. Beaching of the tunicate *Salpa thompsoni* at high levels of suspended particulate matter in the Southern Ocean. Polar Biology 26: 427-431.

Paulmier, A., Ruiz-Pino, D. and Garcon, V. 2011. CO_2 maximum in the oxygen minimum zone (OMZ). Biogeosciences 8: 239-252.

Pauly, D., Graham, W. M., Libralato, S., Morissette, L. and Palomares, M. L. D. 2009. Jellyfish in ecosystems, online databases, and ecosystem models. Hydrobiology 616: 67-85.

Perkins, H., Kinder, T. and La Violette, P. 1990. The Atlantic inflow in the Western Alboran Sea. Journal of Physical Oceanography 20: 242-263.

Perissinotto, R. and Pakhomov, E. A. 1998. Contribution of salps to carbon flux of marginal ice zone of the Lazarev Sea, Southern Ocean. Marine Biology 131: 25-32.

Petterson, H., Gross, F. and Koczy, F. 1939. Large-scale plankton cultures. Göteborg's K Vetensk Vitterh Samh Handl Ser 6: 1-24.

Phillips, B., Kremer, P. and Madin, L. P. 2009. Defecation by *Salpa thompsoni* and its contribution to vertical flux in the Southern Ocean. Marine Biology 156: 455-467.

Pierrot, D., Lewis, E. and Wallace, D. W. R. 2006. MS Excel Program Developed for CO_2 System Calculations. ORNL/CDIAC-105a. Carbon Dioxide Information Analysis Center, Oak Ridge National Laboratory, U.S. Department of Energy, Oak Ridge, Tennessee.

Pilkey, O. H. and Hower, J. 1960. The effect of the environment on the concentration of skeletal magnesium and strontium in *Dendraster*. Journal of Geology 68: 203-214.

Pitt, K. A., Welsh, D. T. and Condon, R. H. 2009. Influence of jellyfish blooms on carbon, nitrogen, and phosphorus cycling and plankton production. Hydrobiologia 616: 133-149.

Pitt, K. A., Kingsford, M. J., Rissik, D. and Koop, K. 2007. Jellyfish modify the response of planktonic assemblages to nutrient pulses. 351: 1-13.

Ploberger, W. and Krämer, W. 1992. The local power of the CUSUM and CUSUM of squares tests. Ecometrics Theory 6: 335-347.

Ploug, H. and Grossart, H. P. 2000. Bacterial growth and grazing on diatom aggregates: Respiratory carbon turnover as a function of aggregate size and sinking velocity. Limnology and Oceanography 45: 1467-1475.

Ploug, H., Iversen, M. and Fischer, G. 2008. Ballast, sinking velocity, and apparent diffusivity within marine snow and zooplankton fecal pellets: Implication for substrate turnover by attached bacteria. Limnology and Oceanography 53: 1878-1886.

Plummer, L. N. and Mackenzie, F. T. 1974. Predicting mineral solubility from rate data. Application to the dissolution of magnesium calcites. American Journal of Science 274: 61-83.

Politi, Y., Batchelor, D. R., Zaslansky, P., Chmelka, B. F., Weaver, J. C., Sagi, I., Weiner, S. and Addadi, L. 2010. Role of magnesium ion in the stabilization of biogenic amorphous calcium carbonate: A Structure-Function Investigation. Chemical of Materials 22: 161-166.

Politi, Y., Arad, T., Klein, E., Weiner, S. and Addadi, L. 2004. Sea urchin spine calcite forms via a transient amorphous calcium carbonate phase. Science 306: 1161-1164

Porzio, L., Buia, M. C. and Hall-Spencer, J. M. 2011. Effects of ocean acidification on macroalgal communities. Journal of Experimental Marine Biology and Ecology 400: 278-287.

Powell, E. N., Brett, C. E., Parsons-Hubbard, K. M., Callender, W. R., Staff, G. M., Walker, S. E., Raymond, A. and Ashton-Alcox, K. A. 2011. The relationship of bionts and taphonomic processes in molluscan taphofacies formation on the continental shelf and slope: eight-year trends: Gulf of Mexico and Bahamas. Facies 57: 15-37.

Purcell, J. E. 2011. Jellyfish and ctenophore blooms coincide with human proliferations and environmental perturbations. Annual Review of Marine Science 4: 209-235.

Purcell, J. E., Uye, S-i. and Lo, W-T. 2007. Anthropogenic causes if jellyfish blooms and their direct consequences for humans: a review. Marine Ecology Progress Series 350: 153-174.

Purcell, J. E., Graham, W. M. and Dumont, H. 2001. Jellyfish blooms: ecological and societal importance. Kluwer Academic Publishers. Developments in Hydrobiology 155: 1-333.

Purcell, J. E. and Decker, M. B. 2005. Effects of climate on relative predation by scyphomedusae and ctenophores on copepods in Chesapeake Bay during 1987-2000. Limnology and Oceanography 50: 376-387.

Ra, K., Kitagawa, H. and Shiraiwa, Y. 2010. Mg isotopes and Mg/Ca values of coccoliths from cultured specimens of the species *Emiliania huxleyi* and *Gephyrocapsa oceanica*. Marine Micropaleontology 77: 119-124.

Raimbault, P., Diaz, F., Pouvesle, W. and Boudjellal, B. 1999. Simultaneous determination of particulate forms of carbon, nitrogen and phosphorus collected on filters using a semi-automatic wet-oxidation method. Marine Ecology Progress Series 180: 289-295.

Ramirez-Llodra, E., Company, J. B., Sarda, F. and Rotllant, G. 2009. Megabenthic diversity patterns and community structure of the Blanes submarine canyon and adjacent slope in the Northwestern Mediterranean: a human overprint? Marine Ecology 31: 167-182.

Ramirez-Llodra, E., Reid, W. D. K. and Billett, D. S. M. 2005. Long-term changes in reproductive patterns of the holothurian *Oneirophanta mutabilis* from the Porcupine Abyssal Plain. Marine Biology 146: 683-693.

Raup, D. M. 1966. The endoskeleton. In Boolootian, R. A. (ed.), Physiology of Echinodermata, Interscience, New York. 16: 379-395.

Raven, J., Caldeira, K., Elderfield, H., Hoegh-Guldberg, O., Liss, P., Riebesell, U., Shepherd, J., Turley, C. and Watson, A. 2005. Ocean Acidification due to Increasing Atmospheric Carbon Dioxide. Royal Society, London.

Raven, J. A. and De Michelis, M. I. 1980. Acid-base regulation during ammonium assimilation in *Hydrodietyon afrieanum.* Plant Cell and Environment 3: 299-311.

Raz, S., Weiner, S. and Addadi, L. 2000. Formation of high-magnesian calcites via an amorphous precursor phase: Possible biological implications. Advanced Materials 12: 38-42.

Redfield, A. 1934. On the proportions of organic derivatives in sea water and their relation to the composition of plankton. In Daniel, R. J. (ed.), James Johnstone Memorial Volume. University Press of Liverpool pp. 177-19.

Rees, H. L. and P. J. Dare. 1993. Sources of mortality and associated life-cycle traits of selected benthic species: a review. Fisheries Research Data Report N° 33. Directorate of Fisheries Research, Lowestoft.

Relini, G. 2000. Demersal trawl surveys in Italian seas: a short review. In Bertrand, J. A. and Relini, G. (eds.), Demersal Resources in the Mediterranean. Proceedings of the symposium held in Pisa, 18-21 March 1998. Actes de Colloques 26: 76-93.

Reid, E., Worthy, C. A., Probert, I., Ali, S. T., Love, J., Napier, J., Littlechild, J. A., Somerfield, P. J. and Allen, M. J. 2011. Coccolithophores: Functional Biodiversity, Enzymes and Bioprospecting. Marine Drugs 9: 586-602.

Reinke, M. 1987. On the Feeding and locomotory physiology of *Salpa thompsoni* and *Salpa fusiformis*. Reports on Polar Research, Bremerhaven 36: 1-89.

Reusch, T. B. H., Bolte, S., Sparwel, M., Moss, A. G. and Javidpour, J. 2010. Microsatellites reveal origin and genetic diversity of Eurasian invasions by one of the world's most notorious marine invader, *Mnemiopsis leidyi* (Ctenophora). Molecular Ecology 19: 2690-2699.

Reynolds, C. S. 1984. The Ecology of Freshwater Phytoplankton, Cambridge, Cambridge University Press.

Rhein, M., Dengler, M., Sültenfuss, J., Hummels, R., Kabus, S. H. and Bourles, B. 2010. Upwelling and associated heat flux in the equatorial Atlantic inferred from helium isotope disequilibrium. Journal of Geophysical Research 115: C08021.

Richardson, A. J., Bakun, A., Hays, G. C. and Gibbons, M. J. 2009. The jellyfish joyride, causes, consequences and management responses to a more gelatinous future. Trends in Ecology and Evolution 24: 312-322.

Rickaby, R. E. M., Henderiks, J. and Young, J. N. 2010. Perturbing phytoplankton: a tale of isotopic fractionation in two coccolithophore species. Climate of the Past Discussions 6: 257-294.

Ridgwell, A. J. and Schmidt, D. N. Past constraints on the vulnerability of marine calcifiers to massive CO_2 release. Nature Geoscience 3: 196-200.

Ridgwell, A., Schmidt, D. N., Turley, C., Brownlee, C., Maldonado, M. T., Tortell, P. and Young, J. R. 2009. From laboratory manipulations to Earth system models: scaling calcification impacts of ocean acidification. Biogeosciences 6: 2611-2623.

Ridgwell, A., Zondervan, I., Hargreaves, J., Bijma, J. and Lenton, T. 2007. Assessing the potential long term increase of oceanic fossil fuel CO_2 uptake due to CO_2-calcification feedback 4: 481-492.

Ridgwell, A. A. 2005. Mid Mesozoic Revolution in the regulation of ocean chemistry. Marine Geology 217 339-357.

Riebesell, U., Fabry, V. J., Hansson, L. and Gattuso, J-P. 2010. Guide to best practices for ocean acidification research and data reporting. Luxembourg: Office for Official Publications of the European Union.

Riebesell, U., Zondervan, I., Rost, B., Tortell, P., Zeebe, R. E. and Morel, F. 2000. Reduced calcification of marine plankton in response to increased atmospheric CO_2. Nature 407: 364-367.

Riebesell, U. 1992. The formation of large marine snow and its sustained residence in surface waters. Limnology and Oceanography 37: 63-76.

Riegman, R., Stolte, W., Noordeloos, A. A. M. and Slezak, D. 2000. Nutrient uptake and alkaline phosphatase (EC 3:1:3:1) activity of *Emiliania huxleyi* (Prymnesiophyceae) during growth under N and P limitation in continuous cultures. Journal of Phycology 36: 87-96.

Ries, J. B. 2011. Skeletal mineralogy in a high-CO_2 world. Journal of Experimental Marine Biology and Ecology 403: 54-64.

Ries, J. B. 2010. Geological and experimental evidence for secular variation in seawater Mg/Ca (calcite- aragonite seas) and its effects on marine biological calcification. Biogeosciences 7: 2795-2849.

Ries, J. B., Cohen, A. L. and McCorkle, D. C. 2009. Marine calcifiers exhibit mixed responses to CO_2-induced ocean acidification. Geology 37: 1131-1134.

Ries, J. B. 2009. The effects of secular variation in seawater Mg/Ca on marine biocalcification. Biogeosciences Discussions 6: 7325-7452.

Ries, J. B. 2004. Effect of ambient Mg/Ca ratio on Mg fractionation in calcareous marine invertebrates: a record of the oceanic Mg/Ca ratio over the Phanerozoic. Geology 32: 981-984.

Rigobello-Masini, M., Masini, J. C. and Aidar, E. 2006. The profiles of nitrate reductase and carbonic anhydrase activity in batch cultivation of the marine microalgae *Tetraselmis gracilis* growing under different aeration conditions. FEMS Microbiology Ecology 57: 18-25.

Robison, B. H., Reisenbichler, K. R. and Sherlock, R. E. 2005. Giant larvacean houses, rapid carbon transport to the deep-sea floor. Science 308: 1609-1611.

Rochelle-Newall, E., Delille, B., Frankignoulle, M., Gattuso, J. P., Jacquet, S., Riebesell, U., Terbruggen, A. and Zondervan, I. 2004. Chromophoric dissolved organic matter in experimental mesocosms maintained under different pCO_2 levels. Marine Ecology Progress Series 272: 25.31.

Rodolfo-Metalpa, R., Houlbreque, F., Tambutte, E., Boisson, E., Baggini, C., Patti, F. P., Jeffree, R., Fine, M., Foggo, A.,, Gattuso, J-P. and Hall-Spencer, J. M. 2011. Coral and mollusc resistance to ocean acidification adversely affected by warming. Nature Climate Change 1: 308-312.

Rodolfo-Metalpa, R., Martin, S., Ferrier-Pagès, C. and Gattuso, J-P. 2010. Response of the temperate coral *Cladocora caespitosa* to mid- and long-term exposure to pCO_2 and temperature levels projected for the year 2100 AD. Biogeosciences 7: 289-300.

Roe, H. S. J., Billett, D. S. M. and Lampitt, R. S. 1990. Benthic/midwater interactions on the Madeira Abyssal Plain; evidence for biological transport pathways. Progress in Oceanography 24: 127-140.

Roe, H. S. J., Angel, M. V., Badcock, J., Domanski, P., James, P. T., Pugh, P. R. and Thurston, M. H. 1984. The diel migrations and distributions within a mesopelagic community in the northeast Atlantic. Progress in Oceanograhy 13: 245-511.

Rose, J.M. and Caron, D. A. 2007. Does low temperature constrain the growth rate of heterotrophic protists? Evidence and implications for algal blooms in cold waters. Limnology and Oceanography 52: 886-895.

Rost, B., Riebesell, U., Burkhardt, S. and Sultemeyer, D. 2003. Carbon acquisition of bloom-forming marine phytoplankton, Limnology and Oceanography 48: 55-67.

Rowe, G. T. and Staresinic, N. 1979. Source of organic matter to the deep-sea benthos. Ambio Special Report 6: 19-23.

Roy, R. N., Roy, L. N., Lawson, M., Vogel, K. M., Porter-Moore, C., Davis, W., Millero, F. J. and Campbell, D. M. 1993. Determination of the ionization constants of carbonic acid in seawater. Marine Chemistry 44: 249-259.

Roux, M., Renard, M., Ameziane, N. and Emmanuel, L. 1995. Zoobathymetrie et composition chimique de la calcite des ossicules du pedoncule des crinoides. Académie des Sciences, Paris 321: 675-680.

Rude, P. D. and Aller, R. C. 1991. Fluorine mobility during early diagenesis of carbonate sediment: An indicator of mineral transformations. Geochimica et Cosmochimica Acta 55: 2491-2509.

Rue, E. L. and Bruland, K. W. 1997. The role of organic complexation on ambient iron chemistry in the equatorial Pacific Ocean and the response of a mesoscale iron addition experiment. Limnology and Oceanography 42: 901-910.

Ruhl, H. A., Ellena, J. A. and Smith, K. L. 2008. Connections between climate, food limitation, and carbon cycling in abyssal sediment communities. Proceedings of the National Academy of Sciences 105: 17006-17011.

Ruhl, H. A. 2008. Community change in the variable resource habitat of the abyssal northeast Pacific. Ecology 89: 991-1000.

Ruhl, H. A. 2007. Abundance and size distribution dynamics of abyssal epibenthic megafauna in the northeast Pacific. Ecology 88: 1250-1262.

Ruhl, H. A. and Smith, K. L. 2004. Shifts in deep-sea community structure linked to climate and food supply. Science 305: 513-515.

Russell, A. D., Hönisch, B., Spero, H. J. and Dea, D. W. 2004. Effects of seawater carbonate ion concentration and temperature on shell U, Mg, and Sr in cultured planktonic foraminifera. Geochimica et Cosmochimica Acta 68: 4347-4361.

Sabine, C. L., Feely, R. A., Gruber, N., Key, R. M., Lee, K., Bullister, J. L., Wanninkhof, R., Wong, C. S., Wallace, D. W. R., Tilbrook, B., Millero, F. J., Peng, T-H., Kozyr, A., Ono, R. and Rios, A. F. 2004. The oceanic sink for anthropogenic CO_2. Science 305: 367-371.

Sadekov, A. Y., Eggins, S. M., and De Deckker, P. 2005. Characterization of Mg/Ca distributions in planktonic foraminifera species by electron microprobe mapping, Geochemistry Geophysics Geosystems 6: Q12P06.

Sameoto, J. A., Ross, T. and Metaxas, A. 2010. The effect of flow on larval vertical distribution of the sea urchin, *Strongylocentrotus droebachiensis*. Journal of Experimental Marine Biology and Ecology 383: 156-163.

Sanchez, P., Demestre, M. and Martin, P. 2004. Characterisation of the discards generated by bottom trawling in the northwestern Mediterranean. Fisheries Research 67: 71-80.

Sarhan, T., Lafuente, J. S., Vargas, M., Vargas, J. M. and Plaza, F. 2000. Upwelling mechanisms in the northwestern Alboran Sea. Journal of Marine Systems 23: 317-331.

Sarmiento, J. L., Hughes, T. M. C., Stouffer, R. J. and Manabe, S. 1998. Stimulated response of the ocean carbon cycle to anthropogenic climate warming. Nature 393: 245-249.

Sarmiento, J. L., Dunne, J., Gnanadesikan, A., Key, R. M. and Matsumoto, K. and Slater, R. 2002. A new estimate of the CaCO3 to organic carbon export ratio. Global Biogeochemical Cycles 16: 1107.

Sartor, P., Sbrana, M. and Reale, B. 2003. Impact of the deep sea trawl fishery on demersal communities of the northern Tyrrhenian Sea (Western Mediterranean). Journal of the Northwest Atlantic Fishery Science 31: 275-284.

Schartau, M., Engel, A., Schröter, J., Thoms, S., Völker, C. and Wolf-Gladrow, D. 2007. Modeling carbon overconsumption and the formation of extracellular particulate organic carbon. Biogeosciences 4: 433-454.

Schiebel, R. 2002. Planktic foraminiferal sedimentation and the marine calcite budget. Global Biogeochemical cycles 16: 1065.

Schmittner, A., Oschlies, A., Matthews, H. D. and Galbraith, E. 2008. Future changes in climate, ocean circulation, ecosystems and biogeochemical cycling simulated for a business-as-usual CO_2 emission scenario until year 4000 AD. Global Biogeochemical Cycles 22: GB1013.

Schmittner, A., Latif, M. and Schneider, B. 2005. Model projections of the North Atlantic thermohaline circulation for the twenty-first century assessed by observations. Geophysical Research Letters 32: L23710.

Schulz, K. G., Barcelos e Ramos, J., Zeebe, R. E. and Riebesell, U. 2009. CO_2 perturbation experiments: similarities and differences between dissolved inorganic carbon and total alkalinity manipulations, Biogeosciences 6: 2145-2153.

Schulz, K. G., Riebesell, U., Bellerby, R. G. J., Biswas, H., Meyerhöfer, M., Müller, M. N., Egge, J. K., Nejstgaard, J. C., Neill, C., Wohlers, J. and Zöllner, E. 2008: Build-up and decline of organic matter during PeECE III. Biogeosciences 5: 707-718.

Sciandra, A., Harlay, J., Lefèvre, D., Lemée, R., Rimmelin, P., Denis, M. and Gattuso, J-P. 2003. Response of coccolithophorid *Emiliania huxleyi* to elevated partial pressure of CO_2 under nitrogen limitation. Marine Ecology Progress Series 26: 111-122.

Sempere, R., Yoro, S. C., van Wambeke, F. and Charriere, B. 2000. Microbial decomposition of large organic particles in the northwestern Mediterranean Sea: an experimental approach. Marine Ecology Progress Series 198: 61-72.

Send, U., Weller, R., Wallace, D., Chavez, F., Lampitt, R. S., Dickey, T., Honda, M., Nittis, K., Lukas, R., McPhaden, M. and Feely, R. A. 2010. OceanSITES. OceanObs'09, Venice, Italy, September 21-25.

Sett S. 2010. The combined effect of global warming and ocean acidification on the coccolithophore Gephyrocapsa oceanica carbon production and physiology. University of Kiel. Master Thesis.

Sett, S., Koch-Klavsen, S., Bach, L. T., Lebrato, M., Oschlies, A., Riebesell, U., and Schulz, K. G. in preparation. Temperature induced changes in sensitivity of organic and inorganic carbon production to ocean acidification in the coccolithophores *Emiliania huxleyi* and *Gephyrocapsa oceanica*.

Sewell, M. A. and Hofmann, G. E. 2011. Antarctic echinoids and climate change: a major impact on the brooding forms. Global Change Biology 17: 734-744.

Sexton, M. A., Hood, R. R., Sarkodee-adoo, J. and Liss, A. M. 2010. Response of *Chrysaora quinquecirrha* medusae to low temperature. Hydrobiologia 645: 125-133.

Seymour, J. E., Carrette, T. J. and Sutherland, P. A. 2004. Do box jellyfish sleep at night? Medical Journal of Australia 181: 706.

Sharp, J. H. 1974. Improved analysis for particulate organic carbon and nitrogen from seawater. Limnology and Oceanography 19: 984-989.

Shanks, A. L. and Trent, J. D 1980. Marine snow. Microscale nutrient patches. Limnology and Oceanography 24: 850-854.

Shi, D., Xu, Y. and Morel, F. M. M. 2009. Effect of the pH/pCO_2 control method on medium chemistry and phytoplankton growth. Biogeosciences 6: 1199-1207.

Siesser, W.G. 1977. Chemical composition of calcareous nannofossils. South African Journal of Science 73: 283.

Silverberg, N., Gagnon, J. M. and Lee, K. 1995. A benthic mesocosm facility for maintaining soft-bottom sediments. Netherlands Journal of Sea Research 34: 289-302.

Sikes, C. S., Roer, R. D.and Wilbur, K. M. 1980. Photosynthesis and coccolith formation: inorganic carbon sources and net inorganic reaction of deposition. Limnology and Oceanography 25: 248-261.

Small, L. F., Fowler, S. W. and Unlu, M. Y. 1979. Sinking rates of natural copepod fecal pellets. Marine Biology 51: 233-241.

Smayda, T. J. 1970. The suspension and sinking of phytoplankton in the sea. Oceanography and Marine Biology Annual Review 8: 353-414.

Smayda, T. J. 1969. Some measurements of the sinking rate of fecal pellets. Limnology and Oceanography 14: 621-625.

Smith, A. M. and Lawton, E. I. 2010. Growing up in the temperate zone: Age, growth, calcification and carbonate mineralogy of *Melicerita chathamensis* (Bryozoa) in southern New Zealand. Palaeogeography Palaeoclimatology Palaeoecology 298: 271-277.

Smith, C. R., De Leo, F. C., Bernardino, A. F., Sweetman, A. K. and Martinez-Arbizu, P. 2008. Abyssal food limitation, ecosystem structure and climate change. Trends in Ecology and Evolution 23: 518-528.

Smith, A. B. 2005. The echinoid directory (electronic publication). Available at http://www.nhm.ac.uk/palaeontology/echinoids.

Smith, C. R. and Baco, A. M. 2003. Ecology of whale falls at the deep-sea floor. Oceanography and Marine Biology Annual Review 41: 311-354.

Smith, D. C., Simon, M., Alldredge, A. L. and Azam, F. 1992. Intense hydrolytic enzyme activity on marine aggregates and implications for rapid particle dissolution. Nature 359: 139-142.

Smith, C. R., Kukert, H., Wheatcroft, R. A., Jumars, P. A. and Deming, J. W. 1989. Vent fauna on whale remains. Nature 341: 27-28.

Smith, S. V. 1972. Production of calcium carbonate on the mainland shelf of southern California. Limnology and Oceanography 17: 28-41.

Sokolova, M. N 1994. Euphausiid "dead body rain" as a source of food for abyssal benthos. Deep-Sea Research I 41: 741-746.
Sokolova, M. N. 1972. Trophic structure of deep-sea macrobenthos. Marine Biology 16: 1-12.

Solomonson, L. P. and Barber, M. J. 1990. Assimilatory nitrate reductase: functional properties and regulation. Annual Review of Plant Physiology and Plant Molecular Biology 41: 225-253.

Soltwedel, T., Bauerfeind, E., Bergmann, M., Budaeva, N., Hoste, E., Jaeckisch, N., von Juterzenka, K., Matthiessen, J., Mokievsky, V., Nothig, E-V., Queric, N-V., Sablotny, B., Sauter, E., Schewe, M., Urban-Malinga, B., Wegner, J., Wlodarska-Kowalczuk, M. and Klages, M. 2005. HAUSGARTEN: multidisciplinary investigations at a deep-sea, long-term observatory in the Arctic Ocean. Oceanography 18: 46-61.

Soltwedel, T., von Juterzenka, K., Premke, K. and Klages, M. 2003. What a lucky shot! Photographic evidence for a medium-sized natural food-fall at the deep seafloor. Oceanologica Acta 26: 5-6.

Sommer, U., Aberle, N., Engel, A., Hansen, T. and others. 2007. An indoor mesocosm system to study the effect of climate change on the late winter and spring succession of Baltic Sea phyto- and zooplankton. Oecologia 150: 655-667.

Sprinkle, J. 1973. Morphology and Evolution of Blastozoan Echinoderms. Museum of Comparative Zoology Special Publication, Harvard University, Cambridge.

Stanier, R. Y. and Smith, J. H. C. 1959. Carnegie Inst. Wash. Yearbook. 58. pp. 336.

Stanley, S. M., Ries, J. B. and Hardie, L. A. 2005. Seawater chemistry, coccolithophore population growth, and the origin of Cretaceous chalk. Geology 33: 593-596.

Staver, J. M. and Strathmann, R. R. 2002. Evolution of fast development of planktonic embryos to early swimming. Biological Bulletin 203: 58-69

Steinacher, M., Joos, F., Fr¨olicher, T. L., Plattner, G-K. and Doney, S. C. 2009. Imminent ocean acidification in the Arctic projected with the NCAR global coupled carbon cycle-climate model, Biogeosciences 6: 515-533.

Steinberg, D. K., Van Mooy, B. A. S., Buesseler, K. O., Boyd, P. W., Kobari, T. and Karl, D. M. 2007. Bacterial vs. zooplankton control of sinking particle flux in the ocean's twilight zone. Limnology and Oceanography 53: 1327-1338.

Stoll, H. M., Langer, G., Shimizu, N. and Kanamaru, K. 2012. B/Ca in coccoliths and relationship to calcification vesicle pH and dissolved inorganic carbon concentrations. Geochimica et Cosmochimica Acta 80: 143-157.

Stoll, H. M. and Shimizu, N. 2009. Micropicking of nannofossils in preparation for analysis by secondary ion mass spectrometry. Nature Protocols 4: 1038-1043.

Stoll, H. M., Shimizu, N., Archer, D. and Ziveri, P. 2007. Coccolithophore productivity response to greenhouse event of the Paleocene-Eocene Thermal Maximum. Earth and Planetary Science Letters 258: 192-206.

Stoll, H. M. and Ziveri, P. 2004. Coccolithophorid-based geochemical paleoproxies. In Thierstein, H. and Young, J. R. (eds.), Coccolithophores: From Molecular Processes to Global Impact. Springer Verlag Berlin Heidelberg, Germany. pp. 529-562.

Stoll, H. M., Klaas, C. M., Probert, I., Ruiz-Encinar, J. and Garcia Alonso, I. 2002. Calcification rate and temperature effects on Sr partitioning in coccoliths of multiple species of coccolithophorids in culture. Global and Planetary Change 34: 153-171.

Stoll, H. M., Ruiz-Encinar, J., Garcia Alonso, J. I., Rosenthal, Y., Probert, I. and Klaas C. 2001. A first look at paleotemperature prospects from Mg in coccolith carbonate: Cleaning techniques and culture measurements. Geochemistry Geophysics Geosystems 2.

Stoll, H. M. and Schrag, D. P. 2000. Coccolith Sr/Ca as a new indicator of coccolithophorid calcification and growth rate. Geochemistry Geophysics Geosystems 1: 1006.

Strathmann, R. R. 2007. Time and extent of ciliary response to particles in a non-filtering feeding mechanism. Biological Bulletin 212: 93-103

Staver, J. M. and Strathmann, R. R. 2002. Evolution of fast development of embryos to early swimming. Biological Bulletin 203: 58-69.

Strathmann, M. F. 1987. Reproduction and Development of Marine Invertebrates of the Northern Pacific Coast. University of Washington Press, Seattle, WA.

Strickland, J. D. H. and Terhune, L. B. D. 1961. The study of in-situ marine photosynthesis using a large plastic bag. Limnology and Oceanography 6: 93-96.

Sudo, R., Ohtake, H. and Aiba, S. 1978. Some ecological observation on the decomposition of periphytic algae and aquatic plants. Water Research 12: 179-184.

Sumich, J. L. and McCauley, J. E. 1972. Calcium-magnesium ratios in the test plates of *Allocentrotus fragilis*. Marine Chemistry 1: 55-59.

Sweetman, A. K. and Chapman, A. 2011. First observations of moribund jellyfish at the seafloor in a deep-sea fjord. Deep-Sea Research I 58: 1206-1211.

Sweetman, A. K. and Witte, U. 2008a. Response of an abyssal macrofaunal community to a phytodetrital pulse. Marine Ecology Progress Series 355: 73-84.

Sweetman, A. K. and Witte, U. 2008b. Macrofaunal response to phytodetritus in a bathyal Norwegian fjord. Deep Sea Research I 55: 1503-1514.

Takahashi, K., Saito, H., Kakehi, S. and Hidaka, K. 2010. Sapphirinid copepods as a predator of doliolids, their contribution to doliolids mortality and sinking flux. EOS Transactions AGU, 91, 26, Ocean Science Meeting. Abstract BO13A-08.

Takahashi, K., Saito, H., Kakehi, S. and Hidaka, K. 2010. Sapphirinid copepods as a predator of doliolids, their contribution to doliolids mortality and sinking flux. EOS Transactions AGU, 91, 26, Ocean Science Meeting. Abstract BO13A-08.

Takahashi, T., Broecker, W. S. and Bainbridge, A. E. 1979. The alkalinity and total carbon dioxide concentration in the world oceans. L.D.G.O. Contribution No. 3078.

Tanaka, T., Thingstad, T. F., Lovdal, T., Grossart, H. P., Larsen, A., Allgaier, M., Meyerhöfer, M., Schulz, K. G., Wohlers, J., Zöllner, E. and Riebesell, U. 2008. Availability of phosphate for phytoplankton and bacteria and of glucose for bacteria at different pCO_2 levels in a mesocosm study. Biogeosciences 5: 669-678.

Tang, D. and Morel, F. M. M. 2006. Distinguishing between cellular and Fe-oxide-associated trace elements in phytoplankton. Marine Chemistry 98: 18-30.

Taylor, A. R., Chrachri, A., Wheeler, G., Goddard, H. and Brownlee, C. 2011. A voltage-gated H^+ channel underlying pH homeostasis in calcifying coccolithophores. PLoS Biology 9: e1001085.

Tesoriero, A. J. and Pankow, J. F. 1996. Solid solution partitioning of Sr^{2+}, Ba^{2+}, and Cd^{2+} to calcite. Geochimica et Cosmochimica Acta 60: 1053-1063.

Thomas, H., Schiettecatte, L-S., Suykens, K., Koné, Y. J. M., Shadwick, E. H., Prowe, A. E. F., Bozec, Y., de Baar, H. J. W. and Borges, A. V. 2009. Enhanced ocean carbon storage from anaerobic alkalinity generation in coastal sediments. Biogeosciences 6: 267-274.

Thomas, C., Sun, Y., Naus, K., Lloyd, A. and Roux, S. J. 1999. Apyrase functions in plant phosphate nutrition and mobilizes phosphate from extracellular ATP. Plant Physiology 119: 543-552.

Thorstenson, D. C. and Plummer, L. N. 1977. Equilibrium criteria for two-component solids reacting with fixed composition in an aqueous phase. Example the magnesian calcites. American Journal of Science 277: 1203-1223.

Tinta, T., Malej, A., Kos, M. and Turk, V. 2010. Degradation of the Adriatic medusa Aurelia sp. by ambient bacteria. Hydrobiologia 645: 179-191.

Titelman, J., Riemann, L., Sornes, T. A., Nilsen, T., Griekspoor, P. and Bamstedt, U. 2006. Turnover of dead jellyfish, stimulation and retardation of microbial activity. Marine Ecology Progress Series 325: 43-58.

Trimborn, S., Langer G. and Rost, B. 2007. Effect of varying calcium concentrations and light intensities on calcification and photosynthesis in *Emiliania huxleyi*. Limnology and Oceanography 52: 2285-2293.

Trotter, J., Montagna, P., McCulloch, M., Silenzi, S., Reynaud, S., Mortimer, G., Martin, S., Ferrier-Pages, C., Gattusp, J-P. and Rodolfo-Metalpa, R. 2011. Quantifying the pH vital effects in the temperate zooxanthellate coral Cladocera caespitosa. Validation of the boron seawater pH proxy. Earth and Planetary Science Letters 303: 163-173.

Turner, J. T. 2002. Zooplankton faecal pellets, marine snow and sinking phytoplankton blooms. Aquatic Microbiology and Ecology 27: 57-102.

Turner, R. D. 1973. Wood-boring bivalves, opportunistic species in the deep sea. Science 180: 1377-1379.

Turon, X., Giribet, G., Lopez, S. and Palacin, C. 1995. Growth and populatin structure of Paracentrotus lividus (Echinodermata: Echinoidea) in two contrasting habitats. Marine Ecology Progress Series 122: 193-204.

Turpin, D. H. 1991. Effects of inorganic N availability on algal photosynthesis and carbon metabolism. Journal of Phycology 27: 14-20.

Tyrrell, T., Schneider, B., Charalampopoulou, A. and Riebesell, U. 2008. Coccolithophores and calcite saturation state in the Baltic and Black Seas. Biogeosciences 5: 485-494.

Tyrrell, T. and Merico, A. 2004. *Emiliania huxleyi*: bloom observations and the conditions that induce them. In Thierstein, H. R. and Young, J. R. (eds.), Coccolithophores from Molecular Processes to Global Impact Springer, Berlin, Heidelberg, Germany. pp. 75-97.

Tyrrell, T. and Zeebe, R. E. 2004. History of carbonate ion concentration over the last 100 million years. Geochimica et Cosmochimica Acta 68: 3521-3530.

Tyrrell, T. 1999.Oceanography - iron, nitrogen and phosphorus in the ocean - reply, Nature, 402: 372.

Tyler, P. A. 1988. Seasonality in the deep sea. Oceanography and Marine Biology Annual. Review 18: 125-153.

Ubaghs, G. 1975. Early Palaeozoic echinoderms. Annual Reviews of Earth and Planetary Sciences 3: 79-98.

Vander Putten, E., Dehairs, F., Keppens, E. and Baeyens, W. 2000. High resolution distribution of trace elements in the calcite shell layer of modern *Mytilus edulis*: environmental and biological controls. Geochimica et Cosmochimica Acta 64: 997-1011.

Vardaro, M. F., Ruhl, H. A. and Smith, K. L. 2009. Climate variation, carbon flux, and bioturbation in the abyssal North Pacific. Limnology and Oceanography 54: 2081-2088.

Vázquez-Cuervo, J., Armstrong, E. M., Casey, K. S., Evans, R., Kilpatrick, K. 2010. Comparison between the Pathfinder Versions 5.0 and 4.1 sea surface temperature datasets: A case study for high resolution. Journal of Climate 23: 1047-1059.

Velásquez, Z. R. 1997. Fitoplancton en el Mediterráneo noroccidental. Thesis Dissertation, Universidad Politécnica de Cataluña, Barcelona. pp. 271.

Venn, A. A., Tambutte, E., Lotto, S., Zoccola, D. and Allemand, S. 2009. Intracellular pH in symbiotic cnidarians. PNAS 106: 16574-16579.

Verardo, D., Froelich, P. and Mcintyre, A. 1990. Determination of organic carbon and nitrogen in marine sediments using the Carlo Erba NA-1500 Analyzer. Deep Sea Research 37: 157-165.

Verbeek, J. W. 1990. Late Quaternary calcareous nannoplankton biostratigraphy for the northern Atlantic Ocean. Meded. Rijks Geol. Dienst 44: 13-43.

Verling, E., Ruiz, G. M., Smith, L. D., Galil, B., Miller, A. W. and Murphy, K. R. 2005. Supply-side invasion ecology: characterizing propagule pressure in coastal ecosystems. Proceedings of the Royal Society B 272: 1249-1256.

Vetter, E. W. and Dayton, P. K. 1999. Organic enrichment by macrophyte detritus, and abundance patterns of megafaunal populations in submarine canyons. Marine Ecology Progress Series 186: 137-148.

Vetter, E. W. and Dayton, P. K. 1998. Macrofaunal communities within and adjacent to a detritus-rich submarine canyon system. Deep Sea Research II 45: 25-54.

Vinogradov, A. 1953. The elementary chemical composition of marine organisms. Yale University, New Haven.

Vogt, M., Steinke, M., Turner, S., Paulino, A., Meyerhöfer, M., Riebesell, U., LeQuere, C. and Liss, P. 2007. Dynamics of dimethylsulphoniopropionate and dimethylsulphide under different CO_2 concentrations during a mesocosm experiment. Biogeosciences Discussions 4: 3673-3699.

Volpe, G., Santoleri, R., Vellucci, V., Ribera d'Alcala, M., Marullo, S. and D'Ortenzio, F. 2007. The colour of the Mediterranean Sea: global versus regional bio-optical algorithms evaluation and implication for satellite chlorophyll estimates, Remote Sensing of Environment. 107: 625-638.

von Bodungen, B., von Bröckel, K., Smetacek, V. and Zeitzschel, B. 1976. The plankton tower. I. A structure to study water/sediment interactions in enclosed water columns. Marine Biology 34: 369-372.

Waldbusser, G. G., Steenson, R. A. and Green, M. A. 2011. Oyster shell dissolution rates in estuarine waters: effects of pH and shell legacy. Journal of Shellfish Research 30: 659-669.

Walsby, A. E. and Holland, D. P. 2006. Sinking velocities of phytoplankton measured on a stable density gradient by laser scanning. Journal of the Royal Society Interface 3: 429-439.

Walsby, A. E. and Xypolyta, A. 1977. The form resistance of chitan fibres attached to the cells of *Thalassiosira fluviatilis* Hustedt. British Phycological Journal 12: 215-223.

Walter, L. M. and Morse, J. W. 1985. The dissolution kinetics of shallow marine carbonates in seawater: A laboratory study: Geochimica et Cosmochimica Acta 49: 1503-1513.

Walter, L. M. and Morse, J. W. 1984. Reactive surface area of skeletal carbonate during dissolution: Effect of grain size: Journal of Sedimentary Petrology 54: 1081-1090.

Weber, J. N. 1973. Temperature dependence of magnesium in echinoid and asteroid skeletal calcite: a reinterpretation of its significance. Journal of Geology 81: 543.556.

Weber, J. N. 1969. The incorporation of magnesium into the skeletal calcites of echinoderms. American Journal of Science 267: 537-566.

Wefer, G. and Fischer, G. 1993. Seasonal patterns of vertical particle flux in equatorial and coastal upwelling areas of the eastern Atlantic. Deep Sea Research I 40: 1613-1645.

Weikert, H. and Godeaux, J. E. A. 2008. Thaliacean distribution and abundance in the northern part of the Levantine Sea (Crete and Cyprus) during the eastern Mediterranean climatic transient, and a comparison with the western Mediterranean basin Helgoland Marine Research 62: 377-387.

Weiner, S., Levi-Kalisman, Y., Raz, S. and Addadi, S. 2003. Biologically formed amorphous calcium carbonate. Connective Tissue Research 44: 214-218.

Weiss, R. F.1974. Solubility of helium and neon in water and seawater. Journal of Chemical and Engineering Data 16: 235-241.

Welschmeyer, N. A. 1994. Fluorometric analysis of chlorophyll a in presence of chlorophyll b and pheopigments. Limnology and Oceanography 39: 1985-1992.

West, E. J., Pitt, K. A., Welsh, D. T., Koop, K. and Rissik, D. 2009a. Top-down and bottom-up influences of jellyfish on primary productivity and planktonic assemblages. Limnology and Oceanography 54: 2058-2071.

West, E. J., Welsh, D. T. and Pitt, K. A. 2009b. Influence of decomposing jellyfish on sediment oxygen demand and nutrient dynamics. Hydrobiologia 616: 151-160.

Widdicombe, S., Dashfield, S. L., McNeill, C. L., Needham, H. R., Beesley, A., McEvoy A., Øxnevad S., Clarke K. R. and Berge J. A. 2009. Effects of CO_2 induced seawater acidification on infaunal diversity and sediment nutrient fluxes. Marine Ecology Progress Series 379: 59-75.

Wiebe, P. H., Madin, L. P., Haury, L. R., Harbison, G. R. and Philbin, L. M. 1979. Diel vertical migration by *Salpa aspera* and its potential for large-scale particulate organic matter transport to the deep-sea. Marine Biology 53: 249-255.

Wiebe, P. 2008. Response of coccolithophores to ocean acidification and ocean warming. Master thesis, University of Kiel, p 50.

Wigham, B. D., Tyler, P. A. and Billett, D. S. M. 2003. Reproductive biology of the abyssal holothurian *Amperima rosea*: an opportunistic response to variable flux of surface derived organic matter? Journal of the Marine Biology Association of the United Kingdom 83: 175-188.

Wilkins, M. E., Zimmernmann, M. and Weinberg, K. L. 1998. The 1995 Pacific West Coast bottom trawl survey of groundfish resources: estimates of distribution, abundance, and length and age composition. NOAA technical Memorandum NMFS-AFSC-89.

Wilkinson, B. H. 1979. Biomineralization, paleoceanography, and the evolution of calcareous marine organisms. Geology 7: 524-527.

Wilson, R. W., Millero, F. J., Taylor, J. R., Walsh, P. J., Christensen, V., Jennings, S. and Grosell, M. 2009. Contribution of fish to the marine inorganic carbon cycle. Science 323: 359-362.

Wilt, F. H. and Benson, S. C. 1988. Development of the endoskeletal spicule of the sea urchin embryo. In Varner, J. E. (ed.), Self-Assembling Architecture. New York. pp. 203-227.
Wingenter, O. W., Haase, K. B., Zeigler, M., Blake, D. R., Rowland, F. S., Sive, D. C., Paulino, A., Thyrhaug, R., Larsen, A., Schulz, K. G., Meyerhöfer, M., and Riebesell, U. 2007. Unexpected consequences of increasing CO_2 and ocean acidity on marine production of DMS and CH_2Cl I: Potential climate impacts. Geophysical Research Letters 34.

Witte, U., Aberte, N., Sand, M. and Wenzhofer, F. 2003. Rapid response of a deep-sea benthic community to POM enrichment, an *in situ* experimental study. Marine Ecology Progress Series 251: 27-36.

Wood, H. L., Spicer, J. I. and Widdicombe, S. 2008. Ocean acidification may increase calcification rates, but at a cost. Proceedings of the Royal Society B 275: 1767-1773.

Woosley, R. J., Milleron, F. J. and Grosell, M. 2012. The solubility of fish-produced high magnesium calcite in seawater. Journal of Geophysical Research 117: C04018.

Wootton, J. T., Pfister, C. A. and Forester, J. D. 2008. Dynamic patterns and ecological impacts of declining ocean pH in a high-resolution multi-year dataset. Proceedings of the National Academy of Sciences of the United States of America 105: 18848-18853

Wu, J. and Luther, G. W. 1995. Complexation of iron(III) by natural organic ligands in the Northwest Atlantic Ocean by a competitive ligand equilibration method and a kinetic approach. Marine Chemistry 50: 159-177.

Xia, J-R. and Gao K-S. 2005. Impacts of Elevated CO_2 Concentration on Biochemical Composition, Carbonic Anhydrase, and Nitrate Reductase Activity of Freshwater Green Algae. Journal of Integrative Plant Biology 47: 668-675.

Xu, Y., Boucher, J. M. and Morel, F. M. M. 2010. Expression and diversity of alkaline phosphatase EHAP1 in *Emiliania huxleyi* (Prymnesiophyceae). Journal of Phycology 46: 85-92.

Xu, Y., Wahlund, T. M., Feng, L., Shaked, Y. and Morel, F. M. M. 2006. A novel alkaline phosphatase in the coccolithophore *Emiliania huxleyi* (Prymnesiophyceae) and its regulation by phosphorus. Journal of Phycology 42: 835-844.

Yamada, N. and Suzumura, M. 2010. Effects of seawater acidification on hydrolytic enzyme activities. Journal of Oceanography 66: 233-241.

Yamamoto, J., Hirose, M., Ohtani, T., Sugimoto, K., Hirase, K., Shimamoto, N., Shimura, T., Honda, N., Fujimori, Y. and Mukai, T. 2008. Transportation of organic matter to the sea floor by carrion falls of the giant jellyfish *Nemopilema nomurai* in the Sea of Japan. Marine Biology 153: 311-317.

Yamamoto-Kawai, M., McLaughlin, F. A., Carmack, E. C., Nishino, S. and Shimada, K. 2009. Aragonite undersaturation in the Arctic Ocean: Effects of ocean acidification and sea ice melt. Science 326: 1098-1100.

Yoon, W. D., Kim, S. K. and Han, K. N. 2001. Morphology and sinking velocities of fecal pellets of copepod, molluscan, euphausiid, and salp taxa in the northeastern tropical Atlantic. Marine Biology 139: 923-928.
Young, G. A. and Hagadorn, J. W. 2010. The fossil record of cnidarian medusae. Paleoworld 19: 212-221 .

Young, J. R., Geisen, M., Cros, L., Kleijne, A., Sprengel, C., Probert, I. and Østergaard, J. B. 2003. A guide to extant coccolithophore taxonomy. Journal of Nannoplankton Research Special issue 1.

Young, C., Devin, M., Emson, R. and Tyler, P. 1998. Social behavior, reproduction and larval development in the deep-sea spantangoid urchin *Archaeopneustes hystrix*. In Mooi, R. and Telford, M. (eds.), Echinoderms: San Francisco. AA Balkema, Rotterdam, The Netherlands.

Yu, J., Elderfield, H., Greaves, M. and Day, J. 2007. Preferential dissolution of benthic foraminiferal calcite during laboratory reductive cleaning. Geochemistry Geophysics Geosystems 8: Q06016.

Zachos, J. C., Dickens, G. R. and Zeebe, R. E. 2008, An early Cenozoic perspective on greenhouse gas warming and carbon-cycle dynamics: Nature 451: 279-283.

Zachos, J., Pagani, M., Sloan, L., Thomas, E. and Billups, K. 2001, Trends, rhythms, and aberrations in global climate 65 Ma to present: Science 292: 686-693.

Zang, W., Dai, X., Jiang, M., Yao, Q., Cai, Y., Luo, C., Xu, G. and Ding, F. 2003. The influences of Mg^{2+}, Ca^{2+} and Mg^{2+}/Ca^{2+} ratio in mixed seawater on the emergence rate of *Penaeus japonicus* postlarva. Chinese Journal of Oceanology and Limnology 21: 78-85.

Zeldis, J., Davis, C. S., James, M. R., Ballara, S. L., Booth, W. E. and Chang, F. H. 1995. Salp grazing: effects on phytoplankton abundance, vertical distribution and taxonomic composition in a coastal habitat. Marine Ecology Progress Series 126: 267-283.

Ziveri, P., Broerse, A. T. C., van Hinte, J. E., Westbroek, P. and Honjo, S. 2000. The fate of coccoliths at 48°N, 21°W, NE Atlantic. Deep Sea Research 47: 1853-1875.
Zondervan, I., Rost, B. and Riebesell, U. 2002. Effect of CO_2 concentration on the PIC/POC ratio in the coccolithophore *Emiliania huxleyi* grown under light-limiting conditions and different day lengths. Journal of Experimental Marine Biology and Ecology 272: 55-70.

Zondervan, I., Zeebe, R. E., Rost, B. and Riebesell, U. 2001. Decreasing marine biogenic calcification: A negative feedback on rising atmospheric pCO_2. Global Biogeochemical Cycles 15: 507-516

Acknowledgements

I deeply thank the following academic individuals for advise, help, support, data sharing and contribution to this PhD thesis work: Prof. Andreas Oschlies, Dr. Debora-Iglesias Rodriguez, Ms. Sonia Blanco-Ameijeiras, Dr. Nadia Suarez-Bosche, Dr. Juan-Carlos Molinero, Dr. Joan E. Cartes, Dr. Marius N. Müller, Ms. Scarlett Sett, Mr. Roberto Benavides, Dr. Kai G. Schulz, Dr. Bethan M. Jones, Dr. Daniel O. B. Jones, Prof. Heather M. Stoll, Ms. Ana Mendez, Dr. Markus Pahlow, Prof. Justin B. Ries, Prof. Andreas J. Andersson, Dr. Pedro de Jesus Mendes, Dr. Kylie A. Pitt, Dr. Monica Rouco-Molina, Prof. Richard S. Lampitt, Dr. Miles Lamare, and Prof. James B. McClintock. Without them it would not be possible to present all this work.

I am grateful to the two funding bodies that allowed me to conduct this PhD and the numerous experiments, cruises and conferences I attended:

1) European Project on Ocean Acidification (EPOCA), which is funded from the European Community's Seventh Framework Programme (FP7/2007-2013) under grant agreement n° 211384. This project was the main funding for my PhD work under work package 9 to study elemental processes from experiments to models.

2) Kiel Cluster of Excellence “The Future Ocean” (project D1067/87: Does the “rise of slime” foster an oceanic “jelly carbon pump"?). This project allowed me to extend my research beyond ocean acidification to gelatinous zooplankton processes and organic carbon export

Last, but not least, the biggest amount of physicological and moral support came from my parents (Mariano and Emi), who are always for the good and bad times.

Erklärung

Here, I declare the following:

a) This doctoral degree dissertation, in form and content and except for advice given by the supervisor and other co-workers constitutes the applicant (Mario Lebrato) own work. Where applicable, I have specified the collaborative work that leaded to the chapters presented here ("Authors contributions" section).

(b) The work presented here has not been previously submitted to any other body in the course of an examination procedure or has been published or submitted for publication. I have clearly specified the chapters that have already been published in scientific journals, that are in press, in review, or pending submission.

(c) This work has been conducted in compliance with the German Research Foundation's (DFG) rules of good academic practice.

Kiel, _____ 2012